MODERN TRENDS IN

ACTIVATION ANALYSIS

U.S. DEPARTMENT OF COMMERCE

NATIONAL BUREAU OF STANDARDS

SPECIAL PUBLICATION 312, VOLUME II

MODERN TRENDS IN ACTIVATION ANALYSIS

Proceedings of the 1968 International Conference
held at the National Bureau of Standards
Gaithersburg, Maryland, October 7–11, 1968

James R. DeVoe, Editor
Philip D. LaFleur, Assistant Editor

Institute for Materials Research
Analytical Chemistry Division
National Bureau of Standards
Washington, D.C. 20234

Volume II of 2 Volumes

ABSTRACT

A conference on Modern Trends in Activation Analysis was held at the National Bureau of Standards, October 7–11, 1968. This volume contains texts of three plenary lectures, one on nuclear reactions, one on radiation detectors and data processing, and one on computation methods in activation analysis. Contributed papers, remarks by honored guests, and synopses of discussion sessions by chairmen are included. Topics covered include nuclear reactions in activation analysis, radiation detectors, data handling and processing, computation methods, error analysis, and information retrieval.

Key Words: Conference, activation analysis, nuclear reactions, neutron, charged particles, photons, radiation detectors, computation, data handling.

FOREWORD

The Analytical Chemistry Division of the NBS Institute for Materials Research provides a major national focal point for analytical chemistry through its continuing efforts to encourage meaningful analytical measurements, to exercise leadership in attacking analytical problems of the nation, and to fill in gaps in critical measurement competences. This Division consists at present of about 120 technical personnel encompassing some 57 different analytical competences from activation analysis and atomic absorption to vacuum fusion and x-ray spectroscopy. These competences are charged with the responsibility for research at the forefront of analysis as well as for an awareness of the practical sample, be it Standard Reference Material or service analysis.

One important mechanism by which the Division exercises leadership in the "state of the art" of a competence is that of sponsoring special conferences and symposia. Experts from around the world are invited to these conferences to summarize the present status of the many facets of a particular competence. In addition, contributed papers as well as comments of rapporteurs or summaries of panel discussions are often used to help better define this status.

The first such conference sponsored by the Division was a broad one on "Trace Characterization—Chemical and Physical" held October 3–7, 1966 at the new NBS Laboratories at Gaithersburg, Maryland. On June 12–13, 1967, a seminar on a more restricted topic, "Quantitative Electron Probe Microanalysis," was held in these same facilities. The hard-cover proceedings of each of these meetings are available from the Government Printing Office as NBS Monograph 100 and NBS Special Publication 298, respectively.

As a continuation of these definitive "state of the art" conferences, the Analytical Chemistry Division and the NBS Institute for Materials Research were very pleased to host the 1968 International Conference on Modern Trends in Activation Analysis. These volumes are the end product of the 1968 conference and contain the plenary lectures as well as condensations of the more than 150 papers submitted. We hope that the volumes will provide the reader, be he specialist or generalist, with a definitive, up-to-date picture of this very important field of activation analysis.

The excellent organization provided by James R. DeVoe, Philip D. LaFleur, and their many associates for this week-long conference made available a maximum amount of time for very substantive discussions in the broad field of activation analysis. Dr. DeVoe's tireless efforts in organizing and editing the papers for this conference provided the primary drive which resulted in an outstanding conference and in pertinent, up-to-the-minute proceedings. Special thanks are due Mrs. Rosemary Maddock whose continuing interest in, and awareness of, the rapidly changing techniques for literature publication have made possible the early issuance of the proceedings of all our conferences.

W. Wayne Meinke, *Chief*,
Analytical Chemistry Division,
Institute for Materials Research.

PREFACE

The third in a series of conferences on activation analysis, "The 1968 International Conference on Modern Trends in Activation Analysis," was held at the National Bureau of Standards, Gaithersburg, Maryland on October 7–11, 1968. The conference, which was sponsored jointly by the National Bureau of Standards, U.S. Atomic Energy Commission, International Atomic Energy Agency, and EURISTOP, European Communities Commission, was truly an international one with one-third of the attendees coming from thirty-two different foreign countries. The scope of the conference was comprehensive in the sense that fundamental studies were combined with as many applications as could be conveniently accommodated. It is an almost obvious fact that the field of activation analysis has grown to a point where such comprehensiveness will be very difficult to achieve in any future conference of five days' duration.

The format for the conference was designed to maximize efficiency in transmitting the large volume of information associated with this field. Authors were encouraged to make liberal use of figures and tables for the preparation of the condensations which appear in these proceedings. These condensations were then made available to the attendees one week prior to the beginning of the conference in a preprint booklet.

Although each condensation was carefully edited and the author's corrections have been made, questions resulting from the absence of the usual "refereeing system" may arise. All authors of condensations are encouraged to publish their work in greater detail in a formal scientific periodical of their choice.

Each day of the conference began with a "state of the art" plenary lecture on a major phase of the activation analysis technique. In order to provide complete coverage of the field, simultaneous sessions were required. The regrettable problem that the attendee faced in wanting to be in two places at once was alleviated to some degree by convening a plenary panel discussion at the end of each day in which all of the chairmen of the day's sessions provided a synopsis of the major points of discussion in their particular session. Synopses of these discussions appear in these proceedings.

The availability of highly efficient business machines when combined with the format for this conference, provided for rapid publication of the proceedings (which is a necessity if conference proceedings are to have any useful purpose). All of the papers were typed on a typewriter that was connected to a magnetic tape recorder. The typewritten copy was reproduced to create the preprint. Authors were asked to edit their

papers in the preprint. These corrections along with properly coded instructions were entered onto the previously recorded tape. This tape was then converted to a computer-compatible tape which was formatted to be processed through an automated typesetting system, with graphic-art quality, at the Government Printing Office. Since uncorrected parts remain unchanged on the tape, the author's correction of the preprint constituted editing of galley proofs which was essentially completed by the end of the conference! Such efficiency in documentation has resulted in proceedings which contain the invited plenary lectures, the submitted condensations of papers, and the synopses of discussions in the sessions, and these extend through two volumes. A "personnel register" of persons working in the field of activation analysis will be published separately.

The conference was most fortunate to be presented with addresses by the Honorary Chairman of the Conference, Professor Richard E. Wainerdi, Professor and Associate Dean, Texas A&M University, College Station, Texas, on October 8, 1968, and by the Honorary President of the Conference, Dr. Vincent P. Guinn, Manager and Technical Director, Activation Analysis Program, Gulf General Atomic Incorporated, San Diego, California.

Conducting a conference of this magnitude could not have been done without the assistance of many people within the National Bureau of Standards. Many of these are included in the list of committees in Appendix I.

Special thanks is given to Dr. Philip D. LaFleur, Assistant General Chairman and editor, who very capably handled all of the arrangements for conducting the conference with the assistance of the NBS Office of Technical Information and Publications. His help and that of his Activation Analysis Section in checking proofs are also greatly appreciated.

The automated document processing was the result of cooperation between many groups at NBS: Mr. Rubin Wagner and Mrs. Rebecca Morehouse, who coordinated the transition from our code to that usable at the Government Printing Office; Mr. J. D. Waggoner, Mr. R. Thompson, and Mr. William O'Neal, who wrote various parts of the computer programs used; and of greatest importance, Mrs. M. Oland and Mrs. J. Gossard who spent long days of continuous effort in typing to meet deadlines and in assembling the preprints and encoding them for computer processing. Thanks are also given to Mrs. Joy Shoemaker and Mr. Robert Boreni for preparing the many tables and figures. Particular appreciation is expressed to Mrs. Rosemary Maddock who provided overall coordination of the procedures and assembly of the various parts of the preprints and proceedings that resulted in the high quality of documents that are hereby published.

By no means of least importance was the support (financial and otherwise) given by the Division of Analytical Chemistry, Dr. W. Wayne Meinke, Chief.

<div align="right">James R. DeVoe.</div>

November 27, 1968

1968 International Conference on Modern Trends in Activation Analysis

General Chairman
JAMES R. DEVOE

Arrangements Chairman
PHILIP D. LAFLEUR

Program Committee Chairman
JAMES R. DEVOE

Plenary Session Speakers
FRANCESCO GIRARDI
RUSSELL L. HEATH
JULIEN HOSTE
J. M. A. LENIHAN
HERBERT P. YULE

Moderator of Panel Discussions
W. WAYNE MEINKE

Session Chairmen

SAADIA AMIEL
O. U. ANDERS
DOMINIQUE COMAR
CHARLES ENGELMANN
DEREK GIBBONS
HIROSHI HAMAGUCHI

ROBERT E. JERVIS
JEAN LAVERLOCHERE
GEORGE W. LEDDICOTTE
WILLIAM S. LYON
WERNER SCHULZE
JACK TROMBKA

D. E. WOOD

CONTENTS

Section 3. — Nuclear Reactions

NEUTRON, PHOTON, AND CHARGED PARTICLE REACTIONS FOR ACTIVATION ANALYSIS

CHAPTER 8. — USE OF CHARGED PARTICLES AND PHOTONS

CHAPTER 15. – ACCURACY, PRECISION AND STANDARDS

REMARKS BY HONORARY CHAIRMAN

Richard E. Wainerdi

Professor and Associate Dean
Activation Analysis Research Laboratory
Texas A&M University
College Station, Texas

Mr. Chairman, Ladies and Gentlemen:

It is a real pleasure to have this opportunity to make a few remarks to the 1968 International Conference: Modern Trends in Activation Analysis.

I am reminded at this time of the very amusing story, recently told to me by Dr. Albert Smales, which occurred shortly after World War II. At that time, in an effort to bring to the public, information about the new field of atomic energy, the government asked a very great scientist to travel around the country and make a series of scholarly lectures to describe the recent scientific developments in that field. Because of that scientist's high prestige, he was provided a government limousine and a chauffer. The meetings were very well attended because there was so much public interest in the field of atomic energy at that time. The scientist gave a brilliantly lucid, intelligent lecture which captivated his audience. The first time he gave the lecture he enjoyed giving it; it was well received, and he got a great thrill out of the interest of the audience. The second night the effort was a little bit tedious and the third night he was bored. So as he was riding onward to the fourth engagement he said to his chauffer, "John, you have been sitting in the audience listening to this speech three times. You've heard it over and over, and I'm really getting quite tired of giving it. Next time let me dress up as the chauffer and you give the speech. I'll sit out in the audience". The chauffer was a bit nervous about this proposal, but he finally agreed to it. The next evening the chauffer got up and word for word gave the address. But there was a problem. At the end of the lecture, the meeting was opened to questions. A difficult, technical question was asked of the chauffer. It was a question the answer to which he did not know. Being a resourceful man he said, "My dear sir, the question you have just asked is so trivial and so simple that even my chauffer can answer it." And he called on the scientist sitting in the audience to provide the answer. In a sense there is some question in my mind this afternoon as to whether I am the scientist

673

or the chauffer, but I am sure that any omissions or oversights that I might make now will be speedily corrected by others during the Conference.

I would like to make a few brief remarks on selected subjects which may have significance to our field, and which possibly may catalyze your thinking. First of all, I would like to talk about certain informational aspects of activation analysis. For 12 years, I have been operating a university activation analysis research program. During parts of that time, especially most recently, the academic involvement of the laboratory has been happily received by the academic community. There are, however, some very substantial problems in integrating a new, complex, expensive, methodology into the teaching of graduate science and engineering. For example, such problems include informing graduate students that this is an area in which they may choose to do a major part of their work, or conversely, informing graduate students that this is an area in which they may choose to do a minor part of their work using the method as an adjunct to some other route of investigation. It is also not a trivial matter to inform the rest of the campus research community — largely the research faculty — as to the capabilities and limitations of the method, about activation analysis facilities and their availability, and about how these other campus scientists might collaboratively work with these activation analysts in order to initiate mutually beneficial research programs. The problems of informing the campus research faculty are small, however, compared with the problems of informing the off-campus research-oriented scientific community. Rarely do off-campus people have time for formal courses, or short courses, or even for on-campus lectures and seminars. They have to be approached through off-campus lectures, technical writing and other means. I think it's interesting to cite a case in point. I was resently appointed to the visiting faculty of a neighboring, distinguished medical college. One of my first duties was to present a research seminar on activation analysis. It was well attended; there were about 150 physicians present, and the first thing I said at the beginning of the seminar was, "How many people in this room have ever heard of activation analysis?" Six people raised their hands, and I said, "Of the people who have raised their hand how many feel that they are conversant with the capabilities and limitations of this method in even a general sense?" Five of the hands went down. This is a faculty which is very well known; it is a place of distinguished scholarship and real interest in modern techniques in medicine. So, after all the articles and all the pamphlets and all the international conferences and all the things which have been written and said about activation analysis during the last 32 years, the great preponderance of practicing, research-oriented physicians at that college had no concept of what activation analysis was and how it might profitably be used in their work. On another occasion, I was walking in the hall at the medical school and ran into a physician

studying cystic fibrosis. His interest was to measure sodium. I could hardly believe it when he asked me: "Can activation analysis be used to measure sodium in biologic materials?" I was of course delighted to be asked that particular question. These examples strike me as evidence of a major challenge to those of us who hope to promote and develop the uses of this method. In this regard, I believe that in publicizing the technique, equal attention should be paid to both its great capabilities and its substantial limitations. Further, in addition to going to potential users with the technique describing its capabilities, its limitations, and its potentialities, one must carefully listen to the man with the problem and try to understand from him their objectives so research in the technique can be motivated towards the solution of real and practical problems.

A second topic which I would like to discuss involves the applications of activation analysis in developing countries. As you know, through the efforts of several large nations, nuclear reactors have been placed in almost every part of the world; and, in fact, in some of the most unlikely corners of the world. Many of these reactors are by no means being fully utilized for the scientific or economic development of the countries in which they are located. Very good uses of these reactors could involve agricultural, industrial and medical applications of activation analysis. The proceedings of the International Atomic Energy Agency meeting on "The Uses of Research Reactors" impresses one with the fact that a majority of the work done in all countries using research reactors already involves nuclear activation analysis, but much more can be done. And in this regard, Wayne Meinke has, for years, been discussing and promoting this particular aspect of international collaboration, and first mentioned it to me some years ago after one of his trips to see a number of overseas research reactors. I think this is an area to which we should all pay substantial attention. By bringing research participants into our laboratories from the developing countries we have a chance to assist them, not only in utilizing the reactors in or near their countries, but also in doing some positive good for their national economies and for the general field of nuclear activation analysis which benefits greatly by being useful anywhere. This must of course be followed up by continuing liaison with the participants and by a good deal of hard work on their part and on ours.

I would next like to speak to the field to which I devote much time. That is the matter of fund raising for research. My remarks are to some extent directed to the local system, with which I have had some experience, but they may be appropriate in other cases too. At the present time, I know of no agency of national government which has *any* external research support budget dedicated and earmarked for the development of nuclear activation analysis as a method. You may say this is perfectly fair, and that nuclear activation analysts should go out and compete with other

scientists for research dollars on the basis of individual research proposals. But, there are, in fact, dozens, or hundreds, if not thousands of other programs which *are* dedicated to specific areas of interest for which money is removed from agency external research support budgets before methodology in activation analysis can compete on *any* basis. These dedicated programs include food preservation by nuclear methods, reactor development and all sorts of other very important and useful projects ranging from the exploration of the moon to the building of artificial hearts. Each of these programs has been initiated and sold by its proponents. The point is that somewhere in the funding mechanism of government it does not seem too much to expect some money to be dedicated to research in a field which can do so much for the contemporary world, as was so lucidly described by Dr. John Lenihan this morning. A major recent report of the National Academy of Sciences describes the general lack of financial support for the whole field of chemistry in America, and I suspect that nuclear activation analysis suffers at the bottom of the chemistry heap along with the rest of analytical chemistry.

I am sure those of you who have experience in fund raising have sent your proposals to an agency and have had the proposals shuttled from group to group in a vain attempt to determine who is responsible for, or interested in, the particular kind of work you want to do in activation analysis methodology. And then, the proposal is, all too often, purely judged on the applicability of the method, with the included necessary basic methodology to make an application sound, often given comparatively little attention. I think frankly that this is one of the reasons there has been somewhat of a quietus in major advances in activation analysis methodology during recent years. There simply have not been available the extensive financial resources necessary to make important basic methodological advances. I think this is a very fertile area for cooperation among all the laboratories, groups and individuals interested in nuclear activation analysis, as a method, and I would like to propose to anyone interested in collaborating on this problem that we seek to acquaint the appropriate scientific federal officials with the potentialities which activation analysis has to offer, and I am very pleased to have a written version of Dr. Lenihan's talk which I would like to get some of them to read.

In conclusion, I would like to mention that in the program of this very fine meeting there is one small oversight. There is a kind reference to me in regard to the 1961 and 1965 meetings. In actual point of fact both of these meetings were organized collaboratively with my good friend, Derek Gibbons who served as co-chairman, co-organizer and co-promoter of both of them. The *imprimatur* of the International Atomic Energy Agency was kindly granted by the Agency to the conference as a

result of Dr. Gibbons' efforts. I would like to also cite Oscar Bizzell of the Division of Isotopes Development, U.S. Atomic Energy Commission, who also had the vision to back these conferences at their most early inception.

Ladies and Gentlemen, I thank you very much for your kind attention, and for the honor of addressing you.

REMARKS BY HONORARY PRESIDENT

THE CURRENT STATUS OF NEUTRON ACTIVATION ANALYSIS APPLICATIONS

Vincent P. Guinn

Technical Director, Activation Analysis Program
Gulf General Atomic Incorporated
San Diego, California

In its earlier years, and to a lesser extent even quite recently, neutron activation analysis (NAA) could be described as "a solution looking for a problem". Particularly at the high thermal-neutron fluxes available in nuclear reactors, it was recognized by early workers that the method offered great sensitivity for the determination of many elements, and hence ought to have many useful applications. However, until the early 1950's, the method was only utilized in a few laboratories in the world — those few that possessed research-type nuclear reactors, and in which there was an interest in exploring the possibilities of NAA. Progress was slow up to that time for another reason also — gamma-ray spectrometry, the basis for the modern instrumental form of the method, was not yet available, so analyses by NAA in almost all cases required tedious radiochemical separations and beta counting.

Starting about 1950, and continuing right up to the present, developments came in rapid succession that greatly improved the capabilities and utilization of the method. These were, in approximate order, the development of:

(1) the NaI(Tl) scintillation detector,

(2) the single-channel pulse-height analyzer,

(3) the 20-channel pulse-height analyzer (based upon discriminators),

(4) the amplitude-to-time-conversion multichannel pulse-height analyzer,

(5) a multi-element purely-instrumental method of performing NAA, based upon gamma-ray spectrometry,

(6) small Cockcroft-Walton (drift-tube and now sealed-tube) and Van de Graaff accelerators for thermal-neutron and fast-neutron NAA at moderate fluxes,

(7) an intrinsically-safe research-type nuclear reactor especially designed for efficient NAA work,

(8) computers and computer techniques for effective NAA data processing,

(9) commercial activation analysis service laboratories with extensive facilities, offering rapid, low-cost, high-sensitivity NAA on a routine and confidential basis,

(10) high-intensity reactor pulses for improved sensitivity for elements forming very short-lived induced activities,

(11) the high-resolution Ge(Li) detector, along with related 4096-channel pulse-height analyzers and fast magnetic-tape readouts,

(12) the Swedish automated radiochemical-separation apparatus,

(13) direct inter-laboratory data links by Teletype and

(14) ^{252}Cf spontaneous-fission neutron sources.

The purpose of this presentation is to give an assessment of the degree of useful application of the NAA technique, in its present stage of development, and in active competition with other methods of elemental analysis. The background for this assessment is largely the experience of the author's Activation Analysis Service group at Gulf General Atomic, since, in this work, the method is in very real competition with all other methods of analysis, in a great variety of fields (industry, medicine, agriculture, biology, oceanography, geochemistry, crime investigation, *etc.*) — and is performed for more than 600 different organizations (private companies, government laboratories, hospitals, universities, crime investigation laboratories, *etc.*).

I. Competition with Other Methods

Activation analysis is defined very simply as a nuclear method of elemental analysis — based upon induced nuclear reactions, and the detection, identification, and quantitation of the various induced radionuclides of interest. It is thus quite different from other methods of elemental analysis, which are based upon chemical reactions or electronic excitations, but not, *per se*, necessarily better than other methods. There are, of course, many different methods of elemental analysis, in addition to activation analysis: for example, wet chemistry, spectrophotometry, emission spectroscopy, atomic absorption, flame emission, polarography, x-ray emission, electron microprobe spectroscopy, and spark-source mass spectrometry. It is important to note that:

(1) each of these methods has important applications, in which it is the method of choice, and, as a corollary,

(2) no single method can be legitimately claimed to be the "best" method for all applications.

Even for a hypothetical laboratory that has available, on its own premises, each and every one of these methods, in a highly developed state, in the hands of highly experienced and capable personnel, it is still a problem to decide which method is the method of choice for any given application. The difficulty arises from the rather large number of variables

that one must consider in deciding upon the "best" method for a given application. Excluding the special requirements of *in-situ* analysis (such as *in-situ* analyses down bore holes, or of process streams), if one or more samples of a particular type (particular matrix) are to be quantitatively analyzed for one or more elements, at least these questions must be answered before one can reliably select an optimum method of analysis:

(1) What is the general composition of the matrix?

(2) Is the sample material very homogeneous, or rather heterogeneous?

(3) How much sample is available for analysis?

(4) Which particular element (or elements) is (or are) to be determined, or are all detectable elements to be determined?

(5) Is the element (or are the elements) of interest present at major $(1 - 100\%)$, minor $(0.01 - 1\%)$, trace $(1 - 100 \text{ ppm})$, or sub-trace $(<1 \text{ ppm})$ levels?

(6) What are the minimum precisions and absolute accuracies that are acceptable?

(7) Can the samples be consumed, or is a nondestructive analysis required?

(8) How soon are the analytical results needed?

(9) Is there an economical limitation that sets an upper limit to the allowable cost per analysis?

The attributes of high-flux thermal-neutron activation analysis (the most fully developed, most widely employed, and generally the most sensitive and useful form of the activation analysis method) can be considered in the light of the above nine questions:

(1) The method is applicable to almost any kind of solid or liquid (or even gaseous) matrix; where problems of neutron self-shielding, gamma-ray attenuation, or fast-neutron interferences occur, they can usually be suitably corrected for or minimized.

(2) and (3) The method has a wide dynamic range of acceptable sample sizes ($\sim$micrograms to grams), so representative samples of even rather heterogeneous materials can be employed by using large samples.

(4) At a thermal-neutron flux of 10^{13} n·cm^{-2}·sec^{-1}, and only 1-hour irradiation time, the method provides good sensitivity for most (75) of the elements of the periodic system (ranging from a low as 10^{-7} μg for a few elements, to a median of 10^{-3} μg, to as high as 10 μg—for a few rather insensitive elements); the method is readily applied as a single-element or as a multi-element method.

(5) It has a very wide dynamic range of quantitative application: from near the limit of detection, all the way up to a concentration of 100%.

(6) At levels sufficiently above the bare limits of detection (under the irradiation and counting conditions employed), precisions and absolute accuracies of about $\pm 2 - 3\%$ of the values are readily achieved, or, with much extra care, even $\pm 0.5 - 1\%$.

(7) The method can frequently be employed successfully in its purely-instrumental, nondestructive, form — based upon multichannel gamma-ray spectrometry of the activated sample; where the induced activity of interest is a pure β^- emitter, or where severe interferences from other induced activities occur, the sample must be destroyed, and radiochemical separations with carriers conducted before counting.

(8) If the element of interest forms a short-lived induced activity (with a half life in the range of seconds to minutes), or if rapid post-irradiation radiochemical separations are employed, results can be obtained within minutes, or within a few hours (respectively), after receipt of the samples; if one or more elements that form long-lived induced activities are to be determined nondestructively, it is sometimes necessary to allow the activated samples to decay for several days or weeks, after the end of the irradiation, before carrying out the final gamma-ray spectrometry measurements.

(9) In spite of the expensive nature of the equipment that is necessary in high-flux NAA work (typically, a \$200,000 to \$300,000 research-type nuclear reactor, and at least \$10,000 to \$30,000 worth of gamma-ray spectrometry apparatus), the real cost of many kinds of analyses can be quite reasonable ($\sim$\$10 – \$15 per sample, for one element, with a smaller increment for each additional element), if the sample analysis load is large, the reactor has a large sample capacity, and the analyses can be performed instrumentally.

Thus, high-flux NAA looks rather good in virtually all of these aspects. For multi-element determinations, it often turns out that no single method is ideal for all of the elements of interest, but rather a combined attack by two or three methods is optimum.

II. Some Good Examples of NAA Applications

There are many examples, in this author's opinion, in which NAA would appear to be the method of choice, but in which, in most laboratories, some other method of analysis is used instead. Usually, this situation is due to a lack of familiarity of those persons with the NAA method and its capabilities. Often, it is due to the lack of the requisite NAA facilities and trained personnel. In many cases, however, this lack is not a real barrier to the utilization of the method, as commercial activation analysis services — capable of supplying accurate and rapid results at low cost, on a completely confidential basis — are readily available. In fact, it was with the objective in mind of making high-flux NAA routinely and simply available to everyone that the author's Activation Analysis Service was instituted, in 1961. Other organizations also offer generally similar NAA services.

On the other hand, one notes in the literature many applications of NAA in which clearly some other method of elemental analysis could do a better job. Such applications usually are the result of efforts by NAA enthusiasts who are determined to demonstrate that the method can do most anything. This situation is by no means entirely bad. Every method has its dedicated, enthusiastic specialists. Such persons are very important, because they help develop each method to its maximum degree — thus enabling one to intercompare methods in their most fully developed form, relative to their usefulness in any particular application at hand. Even such enthusiasts (and the author is one of them, too), however, need always to keep in mind how his particular method compares with other competitive methods of analysis.

In the course of more than seven years service NAA work in the author's laboratory, for a great number of outside organizations of many kinds, a very wide variety of matrices have been analyzed for, *in toto,* almost every element in the periodic system, and from sub-ppb levels up to high percentage levels. Matrices analyzed to date include blood, urine, bone, teeth, hair, fingernails, other biological tissues, rocks, ores, minerals, metals, semiconductors, non-metals, inorganic chemicals, organic chemicals, plastics, solvents, foodstuffs, marijuana, other plant materials, soils, waters, glass, paint, bullet lead, paper, coal, petroleum, etc. Of all of these, it may be of interest to list and briefly describe just a few of these, to illustrate some of the NAA applications carried out in this Laboratory that appear to be particularly well suited to the NAA method, and that appear to be of considerable interest to many groups.

1. Fluorine in Treated Cloth. Several companies make certain fluorinated compounds that are used to treat cloth (especially cloth used in the furniture industry), to make it water-repellant and stain-repellant. They sell the treating compound, and license the treatment process, to many processing companies. The companies that make the compounds, and license the process, have experienced difficulties in that some processing companies are sometimes careless, or sometimes deliberately use a lower concentration of the rather expensive chemical than is prescribed. This practice usually results in cloth that is not adequately repellant, and sometimes results in lawsuits and bad publicity. One of the principal manufacturers now monitors the treated cloth produced by their licensees, taking spot samples and sending them to our laboratory for fluorine determinations. They also publicize the fact that they conduct such a monitoring program — thus inhibiting the likelihood of careless or deliberately sub-standard cloth processing. Large numbers of these determinations are carried out rapidly, routinely, and at low cost — via instrumental thermal-neutron activation analysis (at a thermal-neutron flux of 3×10^{12} $n \cdot cm^{-2} \cdot sec^{-1}$), detecting and measuring the

1.63 MeV gamma rays of 11.56-second ^{20}F. The fluorine levels are quite high (~1000 ppm), so other analytical methods could be used also — but NAA is preferred on the basis of low cost and good accuracy.

2. Fluorine in Hydrocarbons. In recent years, a number of petroleum companies have commenced use of a new (or modified) refining technique, involving HF. For various reasons, they must either regularly or periodically check the final product, to be sure that it does not contain more than a few hundredths of a ppm of fluorine. An analytical sensitivity of about 0.01 ppm F is needed. Our normal limit of detection for fluorine (instrumental, at a thermal-neutron flux of 3×10^{12} n · cm^{-2} · sec^{-1}, via 11.56-second ^{20}F) is not quite good enough, namely, about 0.1 ppm F. However, by pulsing the TRIGA Mark I reactor to a peak power of 1,000 Mw (giving a peak thermal-neutron flux, at the sample, of about 10^{16} n · cm^{-2} · sec^{-1}), the limit of detection for fluorine is improved to about 0.01 ppm F. (This same reactor-pulsing technique enables one also to attain sensitivities, in 1-gram examples, of about 0.001 ppm Li, 1 ppm B, and 0.1 ppm Pb, via detection of their very short-lived induced activities.)

3. Vanadium in Oil. This is a well-known application of NAA, and can be carried out in many instances satisfactorily with only the moderate thermal-neutron flux of a small accelerator ($\sim 10^8$ n · cm^{-2} sec^{-1}). Typically, vanadium occurs in crude oils at concentration ranging anywhere from 1 ppm V to almost 1,000 ppm V, depending upon the origin of the oil (in which it is present as natural metal porphyrins). In the refinery, vacuum flashing produces a distillate low in vanadium and suitable as a feedstock for catalytic cracking. The bottoms are concentrated in the relatively non-volatile metal porphyrins, including the vanadium porphyrins. If the vacuum-flashing operation is not well-controlled (e.g., if entrainment of non-volatile droplets occurs), the distillate will contain appreciable levels of vanadium and other metal porphyrins. These are quite injurious to the life of the fairly expensive (~$300/ton) cracking catalyst. Since a big "cat cracker" may contain as much as 1,000 tons of catalyst, early catalyst poisoning can be very expensive. Vanadium is one of the worst catalyst poisons, and also serves as a good indicator of carryover of other non-volatile metal porphyrins. Vanadium is easily determined by instrumental NAA, via a short irradiation and short counting period, detecting the 1.434 MeV gamma radiation of 3.75-minute ^{52}V. Vanadium levels down to about 1 ppm can be determined with a 10^8 n · cm^{-2} · sec^{-1} thermal-neutron flux and large samples (~10 cc). With the $10^{12} - 10^{13}$ n · cm^{-2} · sec^{-1} reactor flux, much lower vanadium levels (down to ~ 0.1 ppb) can be determined, or smaller samples and shorter irradiation and counting periods can be used.

4. Oxygen in Metals. This is a well-known, important, and widely-used application of NAA, using 14 MeV neutrons (neutrons produced by the ^{3}H(d,n) ^{4}He reaction, with a small deuteron accelerator and a tritium target). The activation reaction used is the ^{16}O(n,p) ^{16}N reaction, which has a Q value of -9.60 MeV, and an energy threshold, therefore, of 10.2 MeV. The product formed, 7.14-second ^{16}N, is unusual in that it emits extremely high-energy gamma rays (6.13 MeV in 69% of its disintegrations, 7.11 MeV in 5%). In the author's laboratory, thousands of samples (mostly metals) are analyzed for oxygen each year by this method, using 10^8–10^9 n·cm^{-2}·sec^{-1} fluxes of 14 MeV neutrons, a dual nitrogen-driven pneumatic-tube transfer system — so that sample and flux monitor are irradiated identically (both spinning), and a pair of 5-inch × 5-inch NaI(T1) detectors for counting of the sample. The limit of detection for oxygen in this system is about 30 μg, *i.e.,* 10 ppm O in a 3-gram sample, or 1 ppm O in a 30-gram sample. Because of the very short half life of ^{16}N, the analysis is rapid and purely-instrumental. Typically, 10-second irradiation, 2-second transfer, and 20-second counting periods are used. Machined cylindrical samples can be activated and counted with no sample container. Other low-oxygen metal samples are either irradiated and counted in specially-produced low-oxygen polyethylene vials, or are irradiated in one vial but automatically transferred to a fresh vial for counting. A density correction is applied to allow for the greater attenuation of ^{16}N gamma rays in metals of appreciable density than in the oxalic acid-graphite oxygen standard samples. In some cases, a small correction must be applied, to allow for the difference in 14 MeV neutron scattering between sample and standard.

Fluorine, if present, is a direct interference, since it forms the same ^{16}N product, *via* the ^{19}F(n,α)^{16}N reaction. Its contribution to the observed ^{16}N level can be computed and corrected for, if necessary, by determining the fluorine separately, *via* the ^{19}F(n,p)^{19}O or ^{19}F(n,2n)^{18}F fast-neutron reactions, or *via* the ^{19}F(n,γ)^{20}F thermal-neutron reaction. Oxygen-19 has a half life of 29.1 seconds, and emits 0.197 MeV and 1.37 MeV gamma rays; ^{18}F has a half life of 109.7 minutes, and is a pure positron emitter. In most kinds of samples (metals and other kinds), the amount of fluorine present is negligible, relative to the amount of oxygen, so such corrections are seldom needed.

Boron can provide a secondary interference, *via* the formation of ^{11}Be, from the ^{11}B(n,p)^{11}Be fast-neutron reaction. Beryllium-11 has a half life of 13.6 seconds, and emits four different gamma rays in the energy range of 4.67 MeV to 7.99 MeV in a total of 10.6% of its disintegrations. Since the ^{16}N formed is usually counted in the 4.5 – 7.5 MeV range, much of this ^{11}Be gamma radiation also contributes counts in this region of the pulse-height spectrum. However, in the author's system, it takes about 40 parts

of boron, by weight, to be equivalent to 1 part of oxygen, so a correction for boron is not necessary unless the sample contains more boron than oxygen. Where necessary, a correction is made by counting at several decay times, and resolving the data into the 7.14-second and 13.6-second half-life contributions.

5. **Mercury in Foodstuffs.** Mercury is a well-known and serious poison. It currently is designated as a "zero tolerance" element in foodstuffs, although there is some reason to believe that a practical tolerance level of around 0.01 ppm Hg would be reasonable — since many normal foodstuffs, not specifically contaminated with mercury from mercurial pesticides or other man-made sources, appear to contain mercury at levels ranging from about 0.001 ppm up to even 0.05 ppm. An important and dangerous source of mercury in grains is the illegal sale of mercury-treated seed grain (wheat, oats, *etc.*) for human consumption — usually mixed in with uncontaminated new-crop grain. Nowadays, most seed grain used in planting has been coated with one mercury compound or another, serving as a fungicide, to protect the seed from fungus attack while it is germinating in the soil. Such seed grain usually contains from 10 to 30 ppm Hg. A negligible amount of this mercury ends up in the new crop of grain — unless left-over seed grain is illegally dumped in with it.

In order to monitor grain for possible contamination by mercury, large numbers of samples must be analyzed — and for mercury levels down to at least as low as a few hundredths of a ppm. In the author's laboratory, this is done regularly by simultaneously irradiating as many as 39 large (7 cc bulk volume) samples for 30 minutes at a thermal-neutron flux of 2×10^{12} $n \cdot cm^{-2} \cdot sec^{-1}$, in the 40-tube rotary specimen rack of the TRIGA Mark I reactor, along with a 7 cc aqueous standard solution of Hg. Large samples are needed, because of the statistical problem of treated seed grains (containing $10 - 30$ ppm Hg) being mixed, usually, with a much larger number of ordinary grain seeds (~ 0.01 ppm Hg). After about a 48-hour decay period (to allow for sufficient decay of various shorter-lived induced activities, particularly, 14.96-hour ^{24}Na), the samples are each counted for 10 minutes on a Ge(Li) detector. The presence of mercury is shown by the appearance of the 77.6 keV gamma rays of 65-hour ^{197}Hg, and the ~ 69 keV K x-rays of its EC product, ^{197}Au. By this purely-instrumental technique, Hg can be unequivocally detected down to levels as low as about 0.05 ppm. If remaining interfering activities are removed by radiochemical separation of the ^{197}Hg, with Hg carrier, levels as low as 0.005 ppm Hg can be determined.

6. **Barium and Antimony in Gunshot Residues.** An important application of high-flux NAA in the field of crime investigation is that of determining the amounts of Ba and Sb on the backs of the hands of suspects in shooting cases (and of victims in questionable gunshot-suicide

cases). These two elements are present, in ~ milligram amounts, as added constituents of the primers of most cartridges. When a revolver or pistol is fired, small amounts of Ba (of the order of a microgram or a few micrograms) and Sb (of the order of several tenths of a microgram) are deposited on the back of the gunhand. A NAA method for the detection of such gunshot residues was developed in the author's laboratory several years ago, and is still being refined and improved. The technique involves the removal of any (invisible) particles from a selected area of the backs of the hands of suspects and victims by (1) coating the area with a thin layer of molten paraffin, (2) allowing the paraffin to solidify, (3) peeling off the paraffin, (4) placing the paraffin lift in a sample vial, (5) activating it in the reactor for 30 minutes at a thermal-neutron flux of 2×10^{12} n·cm^{-2}·sec^{-1}, (6) boiling the activated sample in dilute nitric acid, with Ba and Sb carriers, (7) radiochemically separating any 82.9-minute ^{139}Ba and 2.80-day ^{122}Sb present, and (8) counting the separated samples by NaI(Tl) gamma-ray spectrometry, using the 0.166 MeV photopeak of ^{139}Ba, and the 0.564 MeV photopeak of ^{122}Sb.

Special paraffin hand-sampling kits have been distributed to a large number of law enforcement agencies, and gunshot-residue samples taken from suspects and victims are regularly analyzed for such agencies through the Laboratory's non-profit Forensic Activation Analysis Service. Where necessary, the results are also presented in court, under the same non-profit Service. The method provides ample sensitivity for the detection and quantitative measurement of even tiny amounts of these two elements, and has become the only accepted method for the detection of gunshot residues. It has been applied successfully in many actual cases, and results have been presented, and accepted, in court on many occasions. The method is also used by the Treasury Department's activation analysis group and the FBI's activation analysis group — the other two qualified groups in the U.S. that regularly conduct forensic NAA examinations of evidence samples involved in criminal cases.

7. **Uranium in Ore Samples.** In the early uranium boom, only surface deposits rich in uranium were found by prospectors, and turned into uranium-producing mines. With the rapid growth of nuclear power, the demand for uranium has grown much more rapidly than was originally anticipated. As a result, many companies now conduct extensive exploratory programs to find new uranium deposits. Now, deeper deposits and deposits much leaner in uranium must be sought — ones even containing as little as 0.01% U. Thousands of samples are obtained by drilling, and these must be analyzed rapidly, accurately, and economically, for uranium levels as low as 0.01%.

Although a number of analytical methods can provide good values for uranium down to levels as low as 0.01%, one particular form of the NAA method appears to be outstanding for this purpose: the delayed-neutron

technique. This method is quite specific, very fast, nondestructive, accurate, and very sensitive. It is based upon the detection of delayed neutrons by a uranium-containing sample, following a short irradiation with thermal neutrons in the reactor. In the author's laboratory, a system developed recently by H. R. Lukens is employed. A small sample is activated for 20 seconds at a thermal-neutron flux of 3×10^{12} $\text{n·cm}^{-2}\text{·sec}^{-1}$, propelled in 0.5 second into a polyethylene moderator/BF_3 counters assembly, and the delayed neutrons counted by multichannel scaling for 30 seconds. Uranium-235 is the only naturally-occurring nuclide that is fissioned by thermal neutrons, so the technique is quite specific for uranium in ore samples. Even though natural uranium is only 0.720% ^{235}U, and less than 1% of the neutrons released in fission are from delayed-neutron emitters (having half lives of 0.18, 0.60, 2.7, 5.6, 22.0, and 55.6 seconds), the thermal-neutron fission cross section of ^{235}U is so large (582 barns) that even 0.001% U can be detected in a 0.2-gram sample. The BF_3 detection system is very sensitive to neutrons, but almost completely insensitive to the gamma rays and high-energy β^- particles emitted by other activated elements in ore samples. The method is completely independent of the presence of uranium radioactive-decay daughter products—an advantage over the direct counting procedure (on non-activated samples), which can give erroneous results if the uranium is not in radioactive equilibrium with its daughter products. Since the sample is also exposed to an appreciable fast-neutron flux, there is a small contribution from fast-neutron fissions of ^{238}U. This is of no consequence in ore samples, since this is still uranium. If, however, the sample should contain more thorium than uranium, a correction should be applied (based upon activation with, and without, cadmium shielding) to obtain an accurate value for the uranium content. This is because ^{232}Th is also fissionable by fast (> 1 MeV) neutrons, as is ^{238}U—but not by thermal neutrons.

8. Bromine in Foodstuffs. Another pesticide residue (besides Hg) that is of interest and concern in foodstuffs is bromine. This element can concentrate in (1) food crops grown in nematocide-treated soil, and (2) grains, and some other food products, that have been fumigated with methyl bromide. A very effective, and widely-used, nematocide is dibromochloropropane. When soil is fumigated with it, nematodes (small worms that attack the root systems of plants) are killed very efficiently. The compound gradually decomposes in the soil, releasing bromide ions that are picked up to some extent by the roots of the plants. A single moderate soil fumigation does not result in any serious amount of Br^- pickup by the plant, but excessive or repeated fumigations can result in Br^- levels in the edible parts of the plant that are in excess of FDA tolerance levels (typically, 50 ppm Br). Similarly, when grains in storage are fumigated with CH_3Br—to kill insects that would otherwise attack

and destroy the grain—a single moderate fumigation does not result in a serious Br⁻ pickup by the grain. However, excessive or repeated fumigations can result in Br levels above the tolerance level of 50 ppm Br. Grains and other foodstuffs containing more than the tolerance levels of Br are declared unfit for human consumption, and can be confiscated and destroyed by the FDA—or their illegal sale can be the basis for legal action.

In order to enforce such regulations, large numbers of samples need to be analyzed for bromine. At levels anywhere near 50 ppm Br, several methods of analysis are quite satisfactory, but instrumental NAA offers an excellent choice, because large numbers of samples can be processed with very little chemist's time per sample. In the author's laboratory, as many as a few hundred samples (in small vials, stacked in 39 of the 40 rotary specimen rack tubes of the TRIGA Mark I reactor) can be activated simultaneously, for 30 minutes at a thermal-neutron flux of 2×10^{12} n·cm^{-2}·sec^{-1}, along with aqueous Br⁻ standards. After about 48 hours decay, they are then counted for a few minutes each on a 3-inch × 3-inch NaI(Tl) gamma-ray spectrometer, or for about 15 minutes each on a large Ge(Li) gamma-ray spectrometer. The analysis is based upon the detection of the characteristic gamma rays of 35.34-hour ^{82}Br, and the measurement of one or more of these 0.554, 0.619, 0.698, 0.777, and 0.828 MeV gamma rays (appreciably overlapped in the NaI(Tl) spectra, but completely resolved from one another in the Ge(Li) spectra). The additional 1.044, 1.317, and 1.475 MeV gamma rays of ^{82}Br also show up, but are normally not used in the calculations. Under these conditions, Br levels as low as 0.1 ppm are usually detectable, instrumentally. Most plant materials normally contain anywhere from a few tenths of a ppm Br to a few ppm Br. Levels of about 10 ppm Br usually indicate the presence of Br⁻ pesticide residues.

9. Antimony in Bullet Lead. Another example in the field of crime investigation is the measurement of the Sb content of bullet-lead specimens involved in shooting cases. Some bullet lead contains no deliberately-added Sb, but only the 1−100 ppm Sb present as an impurity. Most manufacturers of bullet lead, however, add Sb to the lead, to increase its hardness. The levels added are usually in the range of from 0.3% Sb up to as high as 4.0% Sb, varying particularly from one manufacturer to another. Some manufacturers also add different amounts of Sb to the different kinds of bullets they produce (various types and calibers), and most have, at one time or another, changed the amount of Sb that they add. Thus, in shooting cases that involve bullets that are sufficiently mangled so that the usual ballistic microscope comparisons of rifle markings (striations) are not possible, or fragments of bullets, measurement of the Sb concentrations in the various samples can indicate whether some or all of the various specimens have different origins, or

whether some may have a common origin (same type, caliber, manufacturer).

The accurate determination of Sb in such specimens, in this range of concentrations, can be accomplished quite well by several analytical methods, but NAA is particularly attractive. A 10-50 mg sample is activated for 30 minutes in the reactor, at a thermal-neutron flux of 2×10^{12} n·cm^{-2}·sec^{-1}, then counted briefly on a NaI(Tl) or Ge(Li) gamma-ray spectrometer. The antimony content is calculated from the 0.564 MeV gamma-ray photopeak of 2.80-day ^{122}Sb. Determination of just the Sb content of such specimens is often sufficient. In other cases, it is necessary to look for, and measure, other elements — present in some bullet leads as additives (*e.g.*, As, Sn), or as impurities (*e.g.*, Al, Cu, Mn). In order to distinguish between the 0.559 MeV gamma rays of 26.4-hour ^{76}As, and the 0.564 MeV gamma rays of 2.80-day ^{122}Sb, a high-resolution Ge(Li) detector is needed — and works quite well.

10. Silver in Rainwater. A somewhat more academic application is that of determining < ppb levels of silver in rainwater and snow. This application is in connection with very interesting studies being conducted on cloud-seeding with AgI. Typical Ag$^+$ levels are so low that a pre-concentration step is employed, several hundred ml of water being passed through an ion-exchange resin, then eluted and the eluant evaporated to dryness on a thin film of plastic. This is folded up and placed in a small polyvial, ready for NAA. With extensive clean-room precautions and ultra-pure reagents, the Ag blank correction is extremely small. The silver content of each sample is determined by activating the sample for 48 seconds in the reactor pneumatic-tube position, at a thermal-neutron flux of 3×10^{12} n · cm^{-2}·sec^{-1}, rapidly transferring to a fresh vial, then counting with a NaI(Tl) gamma-ray spectrometer. Calculations are based upon the 0.658 MeV gamma-ray photopeak of 24.4-second ^{110}Ag.

11. Coding Elements. In various areas of interest (industrial counterfeiting, crime investigation, *etc.*) there is a need to be able to unambiguously identify a particular object or product — *via* some subtle method of tagging that is detected only with difficulty. Many industrial products are counterfeited, with well-known brand names illegally stamped on them. These are often sold at cut-rate prices, but sometimes are markedly inferior — or at least more variable in quality — than the legitimate product. This frequently leads to law suits against the legitimate manufacturers, who then must prove that the inferior product in question is actually not their own, even though their brand name is on it. Sometimes this is quite difficult to prove, unless some subtle method of tagging the product has been used by the manufacturer. Many tagging techniques have been tried out, and various ones are in use, but many of them are unsatisfactory because they are readily detected and, in turn, also counterfeited.

The author's laboratory several years ago undertook to develop a much more subtle product-coding technique, based upon subsequent identification by means of high-flux NAA. This has worked out well, and is now used regularly by two major producers of textile fibers — one of whom recently defended themselves against a half-million dollar lawsuit by showing that the textile fiber was not coded, and hence not their product, even though it had their name on it. A number of manufacturers of pharmaceuticals also have difficulties with counterfeiting of their products, and some are considering this same type of product-coding — if FDA approval can be obtained. There are similar possible applications of this technique in many other industries.

If coding of some particular product is desired, the procedure involved in the author's laboratory is to first carry out an extensive multi-element instrumental NAA survey of the material — employing gamma-ray spectrometry after different irradiation and decay times. In this way, various induced activities with half lives all the way from seconds to minutes, hours, days and months are appreciably generated and effectively detected. The computer programs then search all the data, identifying all statistically-significant photopeaks, and computing μg and ppm values for each detected element (by comparison with a library of data on the pure elements), along with the standard deviation of each value. The programs also compute a firm (3σ) upper limit for the concentration of each element that is not detectable, and then provide a readout for 65 elements. In a typical case, some $10-20$ of these will be detected elements, with measured concentration values, and the remaining $45-55$ undetected elements will be listed with their respective upper limits.

Some of the upper-limit values will be quite large (hundreds or thousands of ppm) — these are of little importance. However, typically, some 10 or 20 of the upper-limit values will be less than 1 ppm — some even as low as 0.001 ppm. These are of real use, since — from their very derivation — it follows that if the material were to be doped with even $10-20$ times as much of a given element as the upper-limit value, it would then clearly be detectable instrumentally. This means that one usually has a choice of quite a few elements that can be added at levels of only $0.01-0.1$ ppm, and yet be detectable by means of instrumental high-flux NAA. With such low levels (1) the cost of the added elements is negligible, (2) the levels are so low that their addition will not affect the physical or chemical properties of the material, and (3) the added elements will be present at such low levels that they cannot be detected by ordinary methods of analysis. With a number of elements to choose from, one has many possible combinations (of perhaps 3 elements) to work with. There still remains the job of choosing a suitable chemical

form of the tagging elements, and the point in the manufacturing process at which they are to be introduced.

12. Trace Elements in Hair. A very important forensic application of high-flux NAA is that of instrumentally characterizing even very small samples of hair, involved as evidence in criminal cases. The pioneering work of R. E. Jervis in Canada, further advanced by studies by A. K. Perkons in Canada, R. F. Coleman in England, L. C. Bate at ORNL, and the author's group, has shown that a total of 29 elements can be detected by this method in human head hair. No single sample (even as large as a gram) reveals all 29 elements, instrumentally, but if large samples from many persons are so analyzed, the total number of detected elements climbs to 29. It is found that (1) in general, persons vary widely from one another in their trace-element hair compositions, (2) the individual strands of hair on the head of any given individual also vary appreciably in elemental composition — but much less widely than the person-to-person variation, and (3) although some elements show appreciable element-element correlations, many show very little correlation with other elements.

In actual case work, one usually must examine individual strands of hair — sometimes even very short strands $(1 - 5$ cm$)$. In such cases, the total sample to be analyzed is thus typically only $20 - 200$ μg, and many of the elements are present only at levels of $1 - 100$ ppm — so a very sensitive method of analysis is obviously necessary. Even with such single strands, one is usually able to detect and measure some $6 - 10$ elements, sometimes more (and even $12 - 14$ with longer strands). There are many complications and possible pitfalls in the forensic NAA comparison of hair samples involved in actual cases (external contamination and its effective removal, time lapse between commission of a crime and apprehension of a suspect, distinction between dead hairs and growing hairs, *etc.*). However, under favorable circumstances, and with very careful work, this technique is very useful, and has become the most powerful one available to criminalists today for the determination (to various degrees of probability) of whether any two strands of head hair came from the same person, or from different persons. Such results have now been successfully introduced in U.S. courts in a number of cases. Earlier this year, H. L. Schlesinger, of the author's group, successfully presented NAA hair results in a California murder case — for the defense. In all 39 previous court cases (the first one being in March 1964) involving NAA results (on various kinds of evidence materials, including hair in some cases) presented in court by the Treasury Department group and the Gulf General Atomic group, the results were presented as part of the prosecution's case. In this first defense case, the defendant was acquitted.

This same general approach, that of trace-element characterization and matching of evidence specimens *via* instrumental high-flux NAA, is also applicable — and has been applied — to many other kinds of both natural and manufactured materials that occur in criminal cases, *e.g.*, marijuana, paint, glass, paper, *etc.*

13. Sodium in Fingernails. An extremely simple, but potentially quite important, application of NAA is that of assisting in the early diagnosis of cystic fibrosis (CF) in children — merely by determining the sodium content of fingernail or toenail clippings. As anyone who has ever employed NAA in studies of biological samples is very well aware, there is nothing much simpler than measuring the sodium content of such samples! With a reactor thermal-neutron flux, even a short irradiation of a fingernail or toenail sample weighing only a few milligrams is quite adequate for a quantitative instrumental determination. In a single 30-minute irradiation, several hundred such samples can be simultaneously activated, if desired, then briefly counted one at a time (using either the 1.369 MeV or 2.754 MeV gamma-ray photopeak counting rate of 14.96-hour ^{24}Na in the calculations).

The conventional clinical diagnostic test for CF is the so-called "sweat test". This requires that the child be brought into the clinic or hospital, be made to perspire profusely for a period of time under controlled conditions, the perspiration being absorbed in cotton, and the perspiration then analyzed for sodium (often, also for K and Cl) by means of flame emission. The work of A. L. Babb and G. L. Woodruff, and their co-workers, has shown that NAA determinations of sodium in nail clippings correlate very well with the sweat-test results. Normal children show a lower range of Na values in both perspiration and nails than do children who have cystic fibrosis. If their pioneering work is further confirmed and extended, the medical profession would clearly have available a simple testing procedure suitable for mass screening of infants soon after birth. Samples can be taken at home, and mailed in for analysis. Some NAA studies of the CF problem carried out in the author's group, in cooperation with the San Diego Naval Hospital, have agreed very well with the findings of Babb and Woodruff. There are some problems yet to be overcome: the proper taking of nail samples, their proper cleaning from external contamination, and determination of the relationship between Na content and age of the child — both normal children and those with CF.

14. Trace Elements in Blood. There is much interest at present in studying the potential biological roles of many hitherto unstudied trace elements in biological organisms, including man. As J.M.A. Lenihan has summarized so effectively:

(1) man is made up of 10 major, or structural, elements: O, C, H, N, Ca, P, K, S, Na, Cl — in descending order of abundance,

(2) 2 essential elements at trace levels: Mg, Fe,

(3) 7 known essential elements at sub-trace ($<$ 1 ppm) levels: Zn, Cu, Mn, Mo, I, Co, Se,

(4) 8 elements at sub-trace levels for which there is some indication that they are essential to the body: Cr, F, Ni, Si, V, Cd, Al, Sn, and

(5) undoubtedly, 49 other sub-trace elements.

Very little is known about these last 49 sub-trace elements. They occur in the earth; they are picked up at least to some degree by plants and thus get into the bodies of animals — including man. Many of these elements are present in man at such low concentrations that they have not yet even been detected in man. Others have been detected; but there is as yet little knowledge of their normal ranges of concentrations (whole-body, or in specific tissues, such as blood), let alone whether or not they perform any essential functions in the body, or whether abnormal concentrations are in any way related to any specific diseases. There thus exists a very large and important region of needed investigation.

Of course, it is especially at such sub-trace levels that high-flux NAA becomes increasingly the method of choice — in many instances even the only applicable method. Its great sensitivity for most elements, its very quantitative nature, and its freedom from contamination errors and blank corrections, make it the best choice for such studies. Although the advent of the high-resolution Ge(Li) detector has much improved the power of the instrumental form of the NAA method, one still, for most sub-trace elements of interest in biological studies, needs to resort to post-irradiation radiochemical separations with carriers. In this field, the development of the new Swedish automated radiochemical-separation apparatus — based upon the work of K. Samsahl and his colleagues — appears to be a significant step forward.

15. Rare-Earth Elements in Rocks, Minerals, and Ores. With the increasing interest in, and utilization of, certain of the rare-earth elements (*e.g.*, for color television), there is an increasing interest in the determination of these elements in rock, mineral, and ore samples. It is well known that many of the RE elements can be determined with tremendous sensitivity by high-flux NAA. In the author's laboratory, it has been found that a single RE group radiochemical separation, followed by Ge(Li) gamma-ray spectrometry, enables one to determine 12 of the RE elements in many samples (Ho and Tm being somewhat more difficult).

III. Summary

It is hoped that these fifteen examples of important applications of the NAA method — ones in which the method exhibits, in one way or another, an appreciable superiority over other analytical methods, will get across

one main point: NAA is not just an exotic method — it can be in many, many cases a very practical method, and, indeed, the method of choice. These 15 examples represent only a modest illustrative sampling of the much larger number of useful applications of the method that, time permitting, could be culled from the experience of the author's group. Even such an enlarged list of applications could, no doubt, in turn be enlarged further still if other applications from other laboratories were also included.

The 15 examples selected were also chosen in a way that would illustrate:

(1) some of the great variety of matrices to which the method is applicable (*e.g.*, cloth, petroleum, metals, foodstuffs, rocks and ores, rainwater, fibers, hair, marijuana, paint, glass, paper, fingernails, and blood),

(2) a few of the many elements that can be determined very effectively by the method (*e.g.*, F, V, O, Hg, Ba, Sb, U, Br, Ag, Na, and the rare-earth elements), and

(3) the various forms and variations of the method that find useful application (*e.g.*, thermal-neutron and fast-neutron activation, reactor and accelerator neutron sources, instrumental and radiochemical-separation procedures, NaI(Tl) and Ge(Li) detectors, single-element and multi-element procedures, determinations at all levels from sub-ppb to percentage levels).

IV. Acknowledgments

V. References

For those who may be interested in reading further about some of the techniques and applications described above, a short selected list of references is given below.

[1]   Graber, F. M. and Lukens, H. R., "A Sensitive and Accurate Activation Analysis Method for the Routine Determination of Fluorine", Trans. Amer. Nucl. Soc., 9, 590 (1966).

[2]   Yule, H. P. and Guinn, V. P., "Enhancement of Neutron Activation Analysis Sensitivities by Use of Reactor Pulses", in Radiochemical Methods of Analysis, Volume 2 (International Atomic Energy Agency, Vienna, 1964), 111.

[3]   Lukens, H. R., "A Neutron Activation Analysis Method for the Determination of Be, Li, B, F, and Pb", J. Radioanal. Chem. **1**, 349 (1968).

[4]   Guinn, V. P. and Wagner, C. D., "Instrumental Neutron Activation Analysis" Anal. Chem. **32**, 317 (1960).

[5]   Gulf General Atomic Activation Analysis Staff, "The Determination of Oxygen by Neutron Activation Analysis", Gulf General Atomic, San Diego (1968).

[6]   Guinn, V. P., Graber, F. M., and Fleishman, D. M., "Ge(Li) Gamma-Ray Spectrometry as a Pilot for NaI(Tl) Gamma-Ray Spectrometry", Talanta **15**, 1159 (1968).

[7]   Guinn, V. P., "The Determination of Traces of Barium and Antimony in Gunshot Residues by Activation Analysis", in the Proceedings of the First International Conference on Forensic Activation Analysis, edited by V. P. Guinn (Gulf General Atomic, San Diego, 1966), 161.

[8]   Guinn, V. P. and Potter, J. C., "Determination of Total Bromine Residues in Agricultural Crops by Instrumental Neutron Activation Analysis", J. Agri. and Food Chem. **10**, 232 (1962).

[9]   Guinn, V. P., "Neutron Activation Analysis of Foodstuffs for Pesticide Residues", World Review of Pest Control **3**, 138 (1964).

[10] Lukens, H. R. and Guinn, V. P., "Neutron Activation Analysis of Bullet Lead", Trans. Amer. Nucl. Soc. **10**, 66 (1967).

[11] Perkons, A. K., "Individualization of Human Head Hair", in the Proceedings of the First International Conference on Forensic Activation Analysis, edited by V. P. Guinn (Gulf General Atomic, San Diego, 1966), 221.

[12] Babb, A. L., Woodruff, G. L., *et al*, "The Use of Neutron Activation Analysis in the Early Diagnosis of Cystic Fibrosis in Children", Trans. Amer. Nucl. Soc. **9**, 591 (1966).

[13] Bethard, W. F., Olehy, D. A., and Schmitt, R. A., "The Use of Neutron Activation Analysis for the Quantitation of Selected Cations in Human Blood", in L'analyse par Radioactivation et Ses Applications aux Sciences Biologiques (in English), edited by D. Comar (Presses Universitaires de France, Paris, 1963), 379.

[14] Campero, A. and Lukens, H. R., "A New Co-Precipitation Method for the Activation Analysis Simultaneous Determination of Manganese, Copper, and Zinc in Blood Serum", Trans. Amer. Nucl. Soc. **8**, 333 (1965).

[15] Guinn, V. P., "The Determination of Traces of Se, V, Sr, and As in Biological Samples by Neutron Activation Analysis", in L'analyse par Radioactivation et Ses Applications aux Sciences Biologiques (in English) edited by D. Comar (Presses Universitaires de France, Paris, 1963), 69.

[16] Lenihan, J. M. A., "Trace Elements in Biomedical Research", Nucleonics **23**, (1) 50 (1965).

[17] Guinn, V. P., "Activation Analysis, with Particular Attention to the Detection of Stable Tracers", in Isotopes in Experimental Pharmacology, edited by L. J. Roth (University of Chicago Press, 1965), 23.

[18] Schmitt, R. A. and Smith, R. H., "Abundances of the Fourteen Rare-Earth Elements, Scandium and Yttrium in Meteoritic and Terrestrial Matter", Geochimica et Cosmochimica Acta **27**, 577 (1963).

[19] Lukens, H. R. and Graber, F. M., "The Neutron Activation Analysis Determination of Rare-Earth Elements in Silicate Ores", Trans. Amer. Nucl. Soc. **8**, 329 (1965).

[20]   Fleishman, D. M. and Lukens, H. R., "Instrumental Determination of Rare-Earth
         Elements by Activation Analysis", in the Proceedings of the Seventh Rare
         Earth Conference (Coronado, California, 1968), in press.
[21]   Guinn, V. P., "The Activation Analysis Laboratory of Gulf General Atomic", J.
         Radioanal. Chem. 1, 269 (1968).
[22]   Yule, H. P., Lukens, H. R., and Guinn, V. P., "Utilization of Reactor Fast Neutrons
         for Activation Analysis", Nucl. Instr. and Methods 33, 277 (1965).
[23]   Guinn, V. P., "Neutron Activation Analysis with Small Accelerators", in the
         Proceedings of the Conference on the Use of Small Accelerators for Teaching
         and Research, edited by J. L. Duggan (Oak Ridge, Tennessee, 1968, CONF-
         680411), 1.
[24]   Guinn, V. P., "Non-Biological Applications of Neutron Activation Analysis in
         Forensic Studies", chapter in Methods of Forensic Science. Volume 3, edited
         by A. S. Curry (Interscience Publishers, London, 1964), 47.
[25]   Bryan, D. E., Guinn, V. P., and Settle, D. M., "Activation Analysis of Biological
         Samples of Forensic Interest", in Nuclear Activation Techniques in the Life
         Sciences (International Atomic Energy Agency, Vienna, 1967), 681.
[26]   Guinn, V. P., "Activation Analysis in the Petroleum and Chemical Industry",
         chapter in Activation Analysis—Principles and Applications, edited by J. M.
         A. Lenihan and S. J. Thomson (Academic Press, New York 1965), 129.
[27]   Gulf General Atomic Activation Analysis Staff, "Activation Analysis Publications
         Prepared by the Activation Analysis Staff of GGA" (Gulf General Atomic, San
         Diego, 1968—a list of 144 GGA publications in this field).

NEUTRON, PHOTON AND CHARGED PARTICLE REACTIONS FOR ACTIVATION ANALYSIS

Plenary Lecture by J. Hoste

D. DE SOETE, R. GIJBELS AND J. HOSTE

Institute for Nuclear Sciences, Ghent University, Belgium

I. Introduction

In nuclear reactions applied to activation analysis two parameters are of fundamental importance: the cross section and the activating particle flux. Both are directly proportional to the induced activity and thus determine the sensitivity of the analysis. Beside these two parameters, one has also to take into account the type of induced reaction which will depend essentially on the type and energy of the applied particle.

At present neutron activation by means of a nuclear reactor or a neutron generator is by far the most common. However a number of analytical problems cannot be solved with these types of reactions so that rapidly increasing research efforts are applied in the field of photon and charged particle activation. The latter techniques are mainly concerned with trace analysis of low mass elements or surface analysis, although other applications are possible.

II. Neutron Induced Reactions

A. GENERAL PRINCIPLES

When a neutron collides with a nucleus three important types of interactions can occur: elastic scattering, inelastic scattering and nuclear reactions. In all of these cases the total charge ΣZ is constant, there is conservation of total energy, $E,$ and of total momentum, conservation of energy including, of course, change of mass. If the scattering is elastic, the kinetic energy is divided between the neutron and the nucleus. In fact it can be considered as an (n,n) reaction. In inelastic scattering the nucleus is left in an excited state and the reaction is represented by an (n,n') reaction. In nuclear reactions the neutron is captured forming a compound nucleus which emits photons in the case of radiative capture or elementary particles (*e.g.* a proton, α-particle, neutron, *etc.*). In some cases fission, fragmentation and spallation are possible.

In Table 1 the most occurring reactions are shown as a function of neutron energy. The reactions are given in decreasing order of probability.

Table 1. Interaction of neutrons with nuclei.

Neutron energy	Nuclear reactions with nuclei	
	$25 \leqslant A < 80$	$80 \leqslant A < 240$
0 – 1 keV	(n,n) (n,γ)	(n,γ) (n,n)
1 – 500 keV	(n,n) (n,γ)	(n,n) (n,γ)
0.5 – 10 MeV	(n,n) (n,n′) (n,p) (n,α)	(n,n) (n,n′) (n,p) (n,γ)
10 – 50 MeV	(n,2n) (n,n′) (n,n) (n,p)	(n,2n) (n,n′) (n,n) (n,p)
	(n,np) (n,2p) (n,α) . . .	(n,np) (n,2p) (n,α) . . .

B. Energy Considerations and Thresholds

Nuclear reactions are usually abbreviated as A(a,b)B, meaning that nucleus, A, reacts with particle, a, forming a product nucleus, B, while a particle (or photon), b, is emitted, liberating or absorbing an energy, Q. Obviously Q is defined as

$$Q = c^2 \left(\sum_{\text{initial}} m_i - \sum_{\text{product}} m_p \right) \tag{1}$$

or

$$Q(\text{MeV}) = 931 \left(\sum_i m_i - \sum_p m_p \right) \tag{2}$$

Depending on whether $Q > 0$ or < 0 the reaction is called exoergic or endoergic.

One has to keep in mind that even for exoergic reactions a certain amount of energy is needed to overcome the Coulomb barrier in order that the emission of positive particles can occur.

$$E_b = 1.44 \, \frac{Z_A Z_a}{R_A + R_a} \, \text{MeV} \tag{3}$$

$$R_A \sim 1.5 A^{1/3} \tag{4}$$

Z_A, Z_a = number of protons of, A, and a, resp.
R_A, R_a = radius of the respective nuclei expressed in Fermi units (10^{-13}cm).

For a neutron where $Z_a = 0$. no Coulomb barrier exists: hence. the capture of thermal neutrons is a favorable process.

The Coulomb barrier not only affects a charged particle reacting with the nucleus. but also charged particles leaving the nucleus. Thus for endoergic reactions where incident neutrons must have sufficient energy. there is a so-called threshold energy. E_T. This is not just a function of the calculated Q value. because part of the kinetic energy of the incident particle is used for the recoil of the compound nucleus hence:

$$E_T(\text{MeV}) = -Q(\text{MeV}) \frac{m_A + m_a}{m_A} \tag{5}$$

Example:

For $^{12}C(n,2n)^{11}C$

$$\sum_i m_i - \sum_p m_p = -931 \text{ MeV} \times 0.020098 = -18.71 \text{ MeV}$$

$$E_T = 18.71 \times \frac{13.0086654}{12.0000000} = 20.3 \text{ MeV}$$

For charged particles leaving the nucleus one must take into account the energy needed to overcome the Coulomb attraction.
Example:

For $^{52}Cr(n.p)^{52}V$

$$\sum_i m_i - \sum_p m_p = -931 \text{ MeV} \times 0.0034458 = -3.21 \text{ MeV}$$

and

$$E_T = 3.21 \times \frac{52.9491794}{51.940514} \text{ MeV} = 3.27 \text{ MeV}$$

whereas

$$E_b = \frac{1.4 \times 23 \times 1}{1.5 \times 52^{1/3} + 1.5 \times 1^{1/3}} \text{ MeV} = 4.7 \text{ MeV}$$

Similarly for $^{55}Mn(n.\alpha)^{52}V$ one finds

$$E_T = 0.65 \text{ MeV}$$

$$E_b = 8.3 \text{ MeV}$$

Thus with neutrons of an energy below 8 MeV. chromium could be determined from an (n.p) reaction without manganese interference.

Since reactor neutrons are not monoenergetic. their energy distribution must be considered. If the probability for a nuclear reaction as a function

of E is represented as $\sigma(E)$ and the fast neutron flux density per unit energy interval as $f(E)$, the reaction rate as a function of E is given by $f(E)\sigma(E)$ i.e. the response function (see Fig. 1). The total reaction rate is given by

$$\int_0^\infty \sigma(E)f(E)\,\mathrm{d}E \tag{6}$$

i.e. the area ABC.
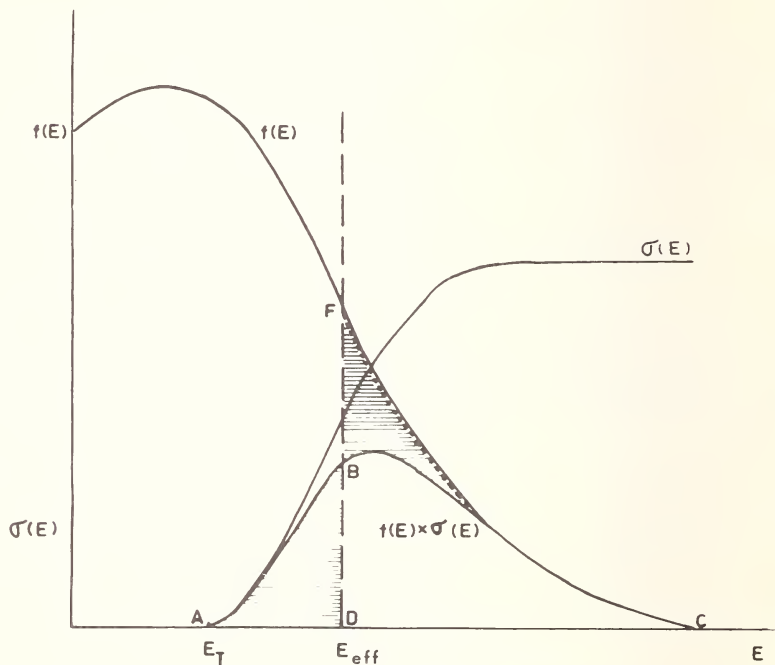
Figure 1.   Definition of effective threshold [1].

According to Hughes [1] an effective threshold E_{eff} is defined so that area ABC equals area DFC or area ABD equals area BFC. This means that all neutrons above E_{eff} are assumed to be equally effective, whereas below this energy the reaction does not occur:

$$E < E_{eff}\sigma(E) = 0$$

$$E \geqslant E_{eff}\sigma(E) = \sigma_{eff}$$

thus

$$\int_{E_T}^\infty \sigma(E)\,\mathrm{d}E = \sigma_{\mathrm{eff}} \int_{E_{\mathrm{eff}}}^\infty f(E)\,\mathrm{d}E \tag{7}$$

The difference, $E_{eff} - E_T$, is obviously a function of the charge of the nucleus and of the emitted particle as can be seen from Figure 2.

$E_{eff} - E_T$ (MeV) for (n,α) reactions
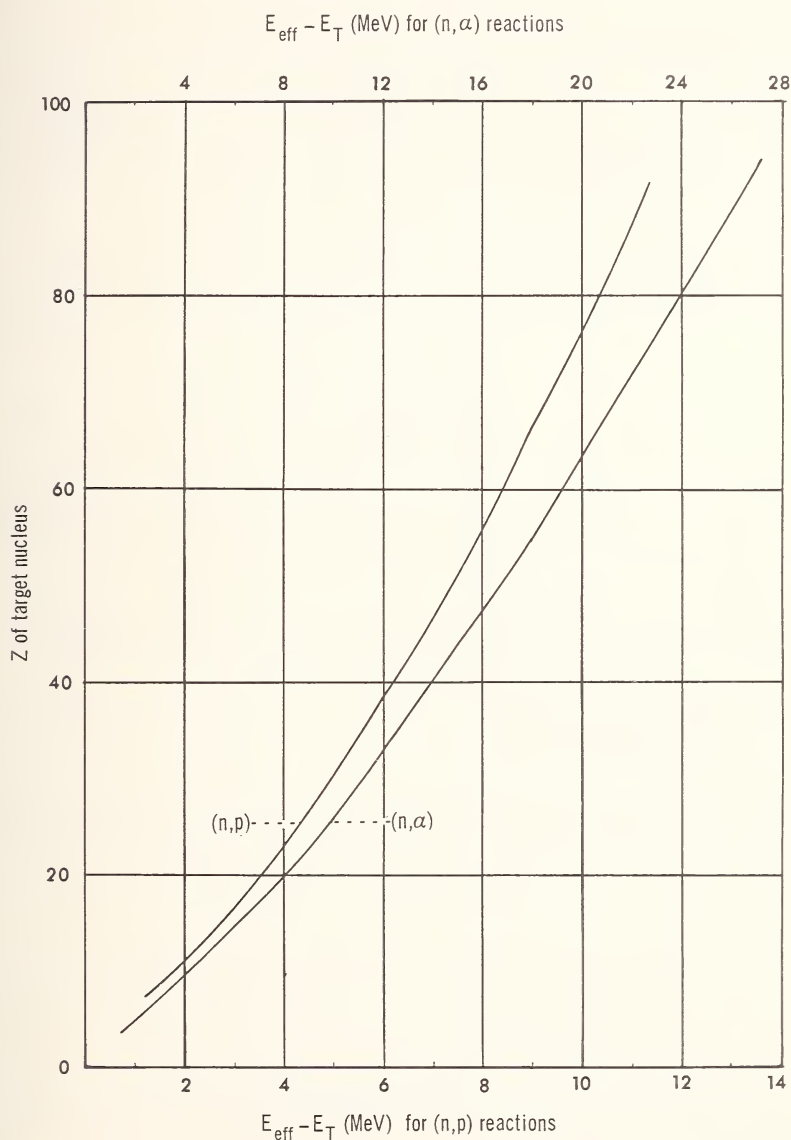
Figure 2. The quantity E_{eff}-E_T for (n,p) and (n,α) reactions as a function of the atomic number of the target nucleus taken from Hughes [1].

It must also be stated that some exoergic reactions as given in Table 2 are also called threshold reactions. This is due to the fact that although E_T

$< 0, E_{eff} > 0$. Equation (5) must then be replaced by

$$E_T(\text{MeV}) = -Q(\text{MeV}) \qquad (8)$$

Table 2. Examples of some exoergic threshold reactions.

	E_T (MeV)	E_{eff} (MeV)
$^{58}\text{Ni}(n,p)^{58}\text{Co}$	-0.64	$2.6 - 4.1$
$^{35}\text{Cl}(n,p)^{35}\text{S}$	-0.62	2.5
$^{64}\text{Zn}(n,p)^{64}\text{Cu}$	-0.21	$4.0 - 4.8$
$^{54}\text{Fe}(n,\alpha)^{51}\text{Cr}$	-0.87	9.1

C. Cross Sections

1. Definitions and Units

The probability of a nuclear reaction is expressed by the cross section. For a thin foil placed in a neutron beam one defines:

$$\sigma = \frac{\text{number of events of certain type per second per nucleus}}{\text{number of neutrons per cm}^2 \text{ per second}}$$

$$= \frac{\text{reaction rate}}{\text{neutron flux}} = \frac{R}{\Phi} \qquad (9)$$

If the neutrons have an angular distribution, the neutron flux, Φ, is best expressed as the product of neutron density times the neutron velocity:

$$n(\text{n}\cdot\text{cm}^{-3})\, v(\text{cm} \cdot \text{sec}^{-1}) \qquad (10)$$

Several types of events are actually possible as already mentioned above: photon-, proton-, α-particles, *etc.* emission, each with a certain probability and, thus, cross section. A number of definitions of types of cross sections are of practical importance in neutron activation analysis:

1. Thermal cross section: refers to neutrons having the most probable velocity, v_o, of the Maxwellian distribution at 20 °C, *i.e.* 2200 m·sec⁻¹ or an energy of 0.025 eV.

2. Reaction cross section: refers to all cases in which the neutron is not reemitted as for (n,γ), (n,p), (n,α) reactions.

3. Absorption cross section: reactions measured by observing the absorption of the neutron itself, for instance by the pile oscillator technique.

4. Atomic cross section: refers to a given element with the natural mixture of isotopes.

5. Isotopic cross section: refers to a given isotope.

6. Activation cross section: determined by means of the induced radioactivity and hence is an isotopic cross section. This cross section allows the calculation of the induced activity in activation analysis.

7. Total cross section: determined by transmission measurements. Obviously, it is the sum of the absorption and scatter cross sections

$$\sigma_T = \sigma_{abs} + \sigma_{scatter}$$

8. Macroscopic cross section: all cross sections given above refer to one nucleus, whereas the macroscopic one refers to the number of atoms N per cm^3:

$$\Sigma = \sigma N \tag{11}$$

If several types of nuclei are present, the macroscopic cross section is given by

$$\Sigma = \text{sum of } \sigma_i N_i \tag{12}$$

2. Neutron Cross Section Curves and Resonance Parameters

The cross sections are functions of neutron energy and are represented as curves and/or given as tables in excellent reference books [2,3]. Mostly the total cross section is given (σ_T) although others are sometimes explicitly plotted. Typical curves are given in Figure 3. Sometimes resonances occur at certain energies, E_o, having a total width Γ and partial widths Γ_γ, Γ_p, Γ_α, Γ_n. These are expressed in keV, eV or mV (mV = 10^{-3} eV). Typical examples are given in Table 3.

D. Reactor Neutrons Reaction Rates

1. Thermal and Epithermal Activation

Thermal neutrons have an average energy of 0.025 eV (velocity v_o = 2200 m/sec), whereas neutrons with energies between 0.1 and 1 eV are called epithermal. In the latter σ_T is often proportional to $E^{-1/2}$ or $1/v$ as appears from Figure 3. Absolute values for σ_T vary widely for each isotope, and no general rule can be given.

As already stated the reaction rate per target nucleus is given by

$$R = \sigma(E)\Phi(E) = \sigma(v)n(v)dv \tag{13}$$
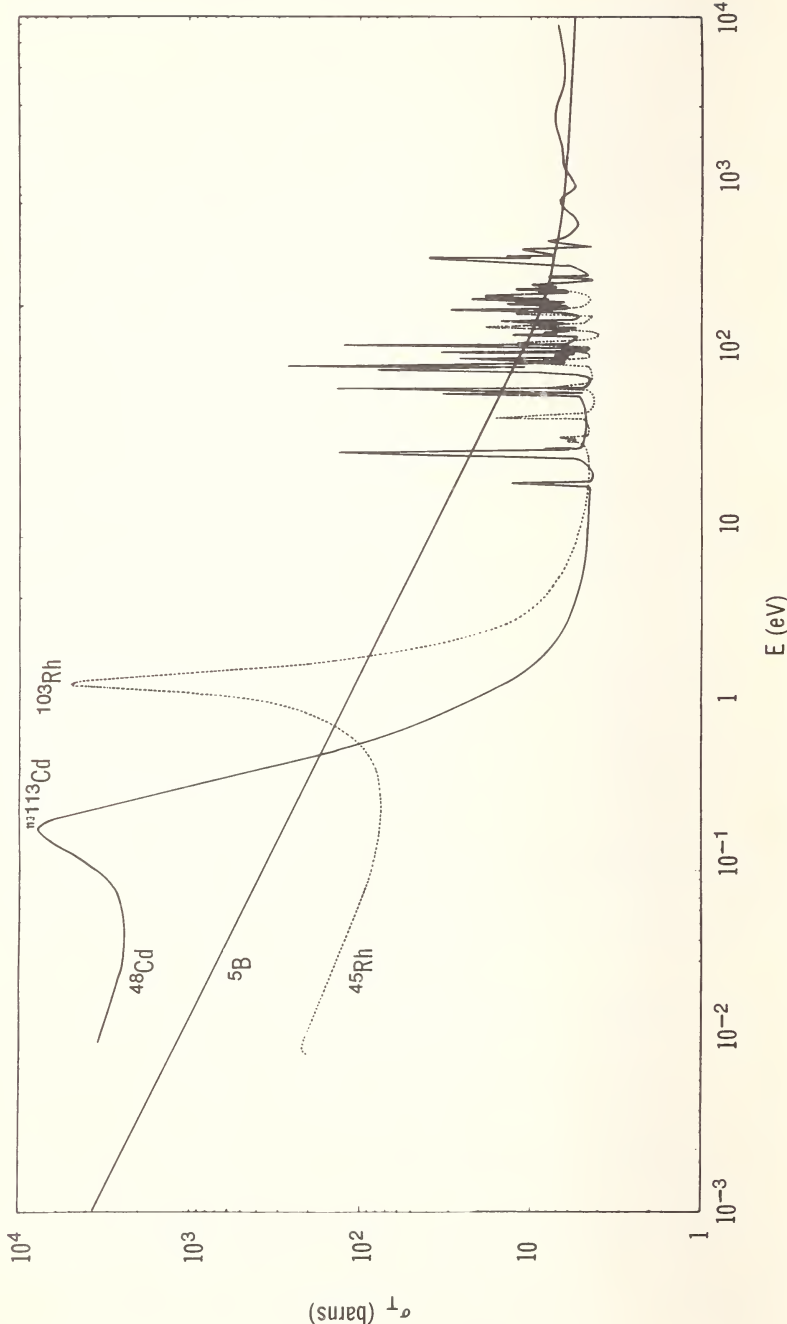
Figure 3.   Some typical forms of cross sections as a function of neutron energy.

Table 3. Examples of some characteristic resonance parameters.

Isotope	Resonance energy	Level width		Remark
^{181}Ta	0.433 ± 0.004 eV	Γ_γ =	30 ± 5 mV,	
		Γ_n =	0.12 ± 0.02 mV	
^{95}Mo	45.0 ± 0.6 eV	Γ_γ =	210 ± 60 mV;	
		Γ_n =	174 ± 10 mV	
^{6}Li	248 ± 4 keV	Γ =	90 ± 10 keV;	
		Γ_n =	60 ± 15 keV;	
		Γ_α =	30 ± 10 keV	
		$(\Gamma = \Gamma_n + \Gamma_\alpha$; $\Gamma_\gamma \approx 0)$		
^{10}B	530 ± 30 keV	Γ_n =	100 ± 20 keV	
	1860 ± 20 keV		450 ± 50 keV	
	2800 keV		300 keV	
	4100 keV		500 keV	E_r >> thermal energy
^{11}B	430 ± 10 keV	Γ_n =	40 ± 5 keV	
	1260 ± 20 keV		140 ± 20 keV	
	1780 ± 20 keV		60 ± 20 keV	
	2450 ± 20 keV		120 ± 40 keV	
	2580 ± 20 keV		60 ± 20 keV	
^{113}Cd	0.178 ± 0.002 eV	Γ_γ =	113 ± 5 mV	E_r epithermal energy
		$(\Gamma_n$ =	0.65 ± 0.02 mV)	$\Gamma \approx E_r$
^{103}Rh	1.260 ± 0.004 eV	Γ_γ =	115 ± 5 mV	E_r epithermal energy
		$(\Gamma_n$ =	0.76 ± 0.04 mV)	$\Gamma << E_r$

In a sample, where neutron attenuation is negligible the activation rate is:

$$R = \int_0^\infty n(v) \cdot \sigma(v) v \, dv \tag{14}$$

n(v) · dv = neutron density with a velocity between v and $v + dv$.
σ(v) = activation cross section for a neutron velocity

If σ is proportional to $1/v$

$$\sigma_{(v)} = \frac{\sigma_0 v_0}{v} \tag{15}$$

and

$$R = v_0\sigma_0 \int_0^\infty n(v)\,\mathrm{d}v = nv_0\sigma_0 \tag{16}$$

Thus equation (14) can be replaced by

$$R = nv_o\sigma_o = \Phi_o\sigma_o \tag{17}$$

where Φ_o is the conventional neutron flux.

2. Resonance Activation

According to a convention proposed by Høgdahl [4] reactor neutrons can be divided in those absorbed by a cadmium filter (energy from 0 to E_{Cd}) and in epicadmium neutrons, i.e. integrated from E_{Cd} to 1-2 MeV or infinite. Since the neutron energy is proportional to $1/E$, the epicadmium resonance integral at infinite dilution is given by:

$$I_x = \int_{ECd}^{2\mathrm{MeV}} \sigma_x(E)\,\frac{\mathrm{d}E}{E} \tag{18}$$

where x represents the type of nuclear reaction, E_{Cd} the cadmium cut-off.
    The latter depends on experimental conditions. The EANDC [5] recommends 0.55 eV whereas other authors [6-8] propose values as listed in Table 4. When resonance integrals are corrected for self-absorption they are indicated as effective resonance integrals, I_{eff}.

Table 4. Effective cadmium cut-off for $1/\nu$ absorbers (in eV) collimated neutron beam.

		Isotropic neutron flux density		
Cadmium thickness (mm)	Cut-off	Foil in cadmium sandwich	Small sample in spherical shell	Small sample in cylindrical shell
0.76	0.473	0.62	0.476	0.50
1.02	0.512	0.68	0.518	0.55
1.52	0.567	0.77	0.583	0.62

Obviously, the resonance integral, I_x, can be divided into two parts, respectively due to the resonance, I', and to the $1/v$ tail, $I_{1/v}$. It can be shown that for a cadmium cut-off value of 0.55 eV the $I_{1/v}$ equals 0.45 σ_o. Typical values of E_r, I', $I_{1/v}$ and σ_o for a number of important isotopes are listed in Table 5 [9].

Table 5. Resonance integral cross sections.

Nuclide	Half life formed	Resonance energy (eV)	I′ (barns)	I (1/v) (barns) a	I (1/v) (barns) b	I = I′ + I (1/v) (barns) a	I = I′ + I (1/v) (barns) b	σ_0 (barns)
^{115}In	54.2 m	1.457	2000 ± 300	60	68	2060 ± 300	2068 ± 300	166 ± 2
^{197}Au	2.70 d	4.906	1505 ± 20[a] 1507 ± 20[b]	38 ± 0.2	44 ± 0.2	1543 ± 20	1551 ± 20	98.8 ± 0.3
^{59}Co	5.26 y	132	50 ± 12	15	17	65 ± 12	67 ± 12	37.2 ± 1.5
^{65}Cu	5.1 m	227	1.2 ± 0.5	0.9	1	2.1 ± 0.5	2.2 ± 0.5	1.8 ± 0.4
^{55}Mn	2.58 h	337	6.0 ± 1.2	5.1	5.8	11.1 ± 1.2	11.8 ± 1.2	13.3 ± 0.2
^{63}Cu	12.8 h	580	2.4 ± 0.5	1.7	2	4.1 ± 0.5	4.4 ± 0.5	4.51 ± 0.23

[a] Cadmium cut-off energy 0.68 eV for a flat cylindrical cover with thickness of 1 mm in an isotropic flux density of neutrons.

[b] Cadmium cut-off energy 0.52 eV for a 1 mm cadmium cover in collimated beam of neutrons.

From the foregoing it is apparent that the reaction rate will be given by

$$R = n_{th}v_o\sigma_{th} + \Phi_e I \tag{19}$$

where:

n_{th} = neutron density for energies up to E_{Cd};
σ_{th} = σ_o if $1/v$ law is followed;
Φ_e = epithermal flux.

One can also write:

$$R = n_{th}v_o\sigma_{reactor} \tag{20}$$

where

$$\sigma_{reactor} = \sigma_o + (\Phi_e/\Phi_{th})I \tag{21}$$

where, Φ_{th}, is the conventional thermal flux. Thus the calculation of R is possible if Φ_{th} and Φ_e are known. The determination of these quantities is described below.

Extensive measured values of I are given by Drake [10].

E. Fast Neutron Activation

1. 14 MeV Neutrons

Since neutron generators based on the $T(d.n)\alpha$ reaction are of considerable interest and produce practically monoergetic neutrons of *ca.* 14 MeV. the cross sections for these particles will be considered before discussing fast neutron activation in a nuclear reactor. The latter is indeed

considerably more complex due to the continuous energy distribution of the neutrons.

As before, σ_T can be considered as a sum of σ_{el} and σ_{ne}:

$$\sigma_T = \sigma_{el} + \sigma_{ne} \tag{22}$$

where

$$\sigma_{ne} = \sigma(n,2n) + \sigma(n,p) + \sigma(n,\alpha) + \sigma(n,\gamma)... \tag{23}$$

The value of σ_T is given by

$$\sigma_T = 2\pi R^2 \tag{24}$$

and

$$R \approx 1.5 \times 10^{-13} A^{1/3} \tag{4}$$

Thus σ_T has a value between 1.5 and 6 barn ($\sigma_T^{1/2}$ is proportional with $A^{1/3}$). The value of σ_{ne} can be calculated from the following equation [11]:

$$\sigma_{ne}(14 \text{ MeV}) = \pi(0.12\, A^{1/3} + 0.21)^2 \tag{25}$$

At 14 MeV, the probability of a (n,γ) reaction is quite small though not always negligible. The most important reactions are due to (n,2n), (n,p) and (n,α) threshold reactions. The former is particularly favored and depends on the relative neutron excess in the nucleus.

The following empirical equations can be used for this reaction.
For $(N\text{-}Z)/A > 0.07$:

$$\log \sigma = 2.473 + 3.48\,(N\text{-}Z)/A \text{ (mb)} \tag{26}$$

For $(N\text{-}Z)/A < 0.07$:

$$\log \sigma = -0.341 + 42\,(N\text{-}Z)/A \text{ (mb)} \tag{27}$$

These relations are valid for odd-even and even-even nuclei. Experimental values can be found in different publications [12-14].

Empirical relations also allow the calculation of (n,p) and (n,α) reactions [15]:

$$\sigma_{n,p} = k(0.12A^{1/3} + 0.21)^2 \exp(-31.1\,[(N\text{-}Z)/A]) \tag{28}$$

where $k = 0.50$ for odd-even nuclei and 0.83 for even-odd or even-even nuclei.

$$\sigma_{n,\alpha} = k(0.12A^{1/3} + 0.21)^2 \exp(-37.8[(N-Z)/A]) \qquad (29)$$

where $k = 0.55$ for odd-even and 0.92 for even-even nuclei.

Experimental values for these cross sections can be found in the same references.

The reaction rate per atom is of course given by

$$R_{14\,MeV} = \Phi \, \sigma_{14\,MeV} \qquad (30)$$

2. Fast Reactor Neutrons

Different equations have been proposed to describe an unmoderated fission flux [16-18]

$$\Phi(E) = k_1 \exp(-E) \sinh \sqrt{2E} \qquad (31)$$

$$= k_2 \exp(-1.036E) \sinh \sqrt{2.29E} \qquad (32)$$

$$= k_3 \sqrt{E} \exp(-0.775E) \qquad (33)$$

For reactor irradiations one can consider that in many instances this fast neutron spectrum is little disturbed above 2 MeV.

The average cross section of threshold reactions in such a fast flux, f, is given by

$$\bar{\sigma}_f = \frac{\displaystyle\int_0^\infty f(E)\sigma(E)\,\mathrm{d}E}{\displaystyle\int_0^\infty f(E)\,\mathrm{d}E} \qquad (34)$$

where

$$\bar{\sigma}_f = \text{average cross section for fission neutrons;}$$
$$\sigma(E) = \text{cross section for neutrons of energy } E;$$
$$f(E) = \text{fission neutron flux of energy } E.$$

Hughes [2] was the first to describe a relation between $\bar{\sigma}_f$ and the fission integral, with $\bar{\sigma}_f$ normalized to a standard size nucleus. As more data became available considerable deviations were observed, so that Roy and Hawton [19] proposed another empirical relation between $\bar{\sigma}_f$ and E_{eff}, with $\bar{\sigma}_f$ normalized to a standard nucleus with $A = 125$. If in this way 25 $\bar{\sigma}_f/A^{2/3}$ is plotted versus E_{eff} for (n,p) reactions, two straight lines are obtained with different slopes for odd A or for even A nuclides.

For (n,α) reactions such a difference cannot be observed. The above relations allow a prediction of unknown $\bar{\sigma}_f$ values, although errors of a

factor of 10 are not exceptional. If for (n,2n) reactions 25 $\bar{\sigma}_f/A^{2/3}$ is plotted, not against E_{eff}, but *versus* E_T, a straight line is again obtained with no systematic difference between odd A and even A nuclides.

Recently (n,n') reactions from reactor irradiations were studied [20,21] and a number of (n,n') cross sections determined. Up to now no empirical relation has been proposed. Isomers which could be applied in activation analysis are given in Table 6.

Table 6. Production of isomers with measurable half—lives by inelastic neutron scattering.

Reaction	θ %	$T_{1/2}$	E_γ (keV)	Threshold E_T (keV)
^{103}Rh(n,n')^{103m}Rh	100	57.4 min	40	E_γ
^{109}Ag(n,n')^{109m}Ag	48.65	39.2 sec	87	E_γ
^{115}In(n,n')^{115m}In	95.77	4.5 h	335	E_γ
^{137}Ba(n,n')^{137m}Ba	11.32	2.6 min	661	660($E_{eff} \cong 1.9$) MeV
^{197}Au(n,n')^{197m}Au	100	7.4 sec	407, 277 + 130	407
^{199}Hg(n,n')^{199m}Hg	16.84	44 min	368 + 159	527
^{207}Pb(n,n')^{207m}Pb	22.6	0.9 sec	1060 + 565	1633
^{79}Br(n,n')^{79m}Br	50.52	4.8 sec		
^{89}Y(n,n')^{89m}Y	100	14 sec	913	913
^{193}Ir(n,n')^{193m}Ir	61.5	11.9 d	80	80
^{204}Pb(n,n')^{204m}Pb	1.48	68 min	912, 374, 899 (others)	2186

F. Determination of Neutron Fluxes

In most cases activation analyses are carried out by means of a simultaneously irradiated standard of the element being determined. This technique avoids the determination of the neutron flux, since one can assume that standard and sample receive the same integrated flux if adequate precautions are taken. In a number of cases, however, the knowledge of the neutron fluxes is highly desirable. Fast reactor neutrons can for instance cause interferences such as those illustrated in Table 7.

When a large number of elements has to be determined in a single matrix, the simultaneous irradiation of all the standards can be impossible due to the limited size of the irradiation capsule. In any case the measurement of numerous standards represents a long counting time. Application of a single comparator, as suggested by Girardi [22] offers an elegant solution to this problem. If however different irradiation places

Table 7. Interferences caused by fast neutron reactions.

Determination of	Interfering reaction
Iron in cobalt	$^{59}Co(n,p)^{59}Fe$
Phosphorus in sulfur	$^{32}S(n,p)^{32}P$
Copper in zinc	$^{64}Zn(n,p)^{64}Cu$
Sodium in aluminum	$^{27}Al(n,\alpha)^{24}Na$
Manganese in iron	$^{56}Fe(n,p)^{56}Mn$
Cobalt in nickel	$^{60}Ni(n,p)^{60}Co$
Scandium in titanium	$^{46}Ti(n,p)^{46}Sc$

are used, large errors can be made, especially for those elements having large resonance integrals that are different from the single comparator. A better solution would perhaps be to apply a double comparator so that more accurate values of thermal and resonance flux are obtained (see below).

1. Reactor, Thermal and Resonance Flux

As apparent from Figure 3, cadmium has a very large absorption cross section for neutrons with an energy below ca. 0.5 eV, due to the reaction $^{113}Cd(n,\gamma)^{114}Cd$. If a sample is irradiated under a cadmium foil of 0.7-1 mm, thermal neutrons are screened out and (n,γ) activation takes only place with "epicadmium" neutrons. From Table 4 it also appears that the "effective cut-off energy" depends on the thickness of the cadmium and on the geometry. The cadmium ratio (CR) is thus defined by:

$$CR = \frac{\text{activity without } Cd \text{ foil}}{\text{activity with } Cd \text{ foil}} = \frac{\phi_{th}\sigma_0 + \phi_e I}{\phi_e I} \qquad (35)$$

$$CR - 1 = \Phi_{th}\sigma_o/\Phi_e I \qquad (36)$$

where Φ_{th} and Φ_e represent the conventional neutron flux up to E_{cd} and the epicadmium flux above E_{cd}, respectively.

If σ_o and I are known the CR does not give directly the ratio of the fluxes unless a $1/v$ detector is used.
Indeed:

$$I = I' + 0.44\,\sigma_o \qquad (37)$$

This type of detectors however gives small activities under cadmium so that preference is given to detectors with resonance peaks such as gold.

silver, cobalt and others. These should be used as thin foils or even better as dilute alloys to avoid self-shielding effects. One should also consider that errors can occur from thermal and resonance flux perturbation due to the cadmium itself.

The cadmium ratio of a nuclide x can of course be expressed in terms of the CR of gold, cobalt or silver as standards:

$$CR_x = 1 + (CR_S - 1)(I_S\sigma_{o,x})/(\sigma_{o,S}I_x) \tag{38}$$

Values of σ_o and I for these detectors are given in Table 8.

Table 8. I and σ_0 values for the gold, cobalt and silver detectors.

Detector	σ_0 (barns)	I (barns)
^{197}Au(n,γ)^{198}Au	98.8	1551
^{59}Co(n,γ)^{60}Co	34.4	75
^{109}Ag(n,γ)^{110m}Ag	3.2	47.5

If cadmium is not used, thermal to epithermal flux ratios or even the absolute values of these fluxes can be obtained from an irradiation of two detectors:

$$R_1 = \Phi_{th}\sigma_{0_1} + \Phi_e I_1 \text{ for detector 1}$$

$$R_2 = \Phi_{th}\sigma_{0_2} + \Phi_e I_2 \text{ for detector 2}$$

and

$$\Phi_{th} = \frac{R_1 I_2 - R_2 I_1}{\sigma_{o_1}R_2 - \sigma_{0_2}I_1} \tag{39}$$

$$\Phi_e = \frac{R_2\sigma_{0_1} - R_1\sigma_{0_2}}{\sigma_{0_1}I_2 - \sigma_{0_2}I_2} \tag{40}$$

The thermal flux can of course also be obtained by irradiating a bare and Cd covered sample. The total rate is indeed given by:

$$R = R_{th} + R_e = \Phi_{th}\sigma_o + \Phi_e I \tag{41}$$

and the rate of the Cd covered sample by:

$$R_e = \Phi_e I \tag{42}$$

The net difference thus gives the thermal flux if σ_o is known.

Conventions other than the Høgdahl convention [4] described here can be followed [7,8,23,24].

It is also clear that the epicadmium flux, Φ_e, can be determined from equation (42). For numerical data the recommendations of the European-American Nuclear Data Committee [5] can be followed.

2. Reactor Fast Flux

The reactor fast flux is usually determined by means of the (n,p), (n,α), (n,2n) and even (n,n') threshold reactions. The flux can be calculated by absolute activity measurements from the equation

$$R = \overline{\Phi}_f \overline{\sigma}_f \tag{43}$$

where $\overline{\Phi}_f$ is the equivalent fission flux and $\overline{\sigma}_f$ the average cross section in a fission neutron spectrum. Useful threshold detectors are given in Table 9.

The most frequently used reaction is $^{32}S(n,p)^{32}P$, $\overline{\sigma} = 65$ mb. It is however desirable to use several detectors with different E_{eff} values. If the same $\overline{\Phi}_f$ is found, it can be concluded that the fast spectrum is a pure fission spectrum.

If the fast to thermal flux is constant one can also use a thermal flux monitor. A factor k is introduced for this purpose [19]:

$$k = \frac{\Phi}{\Phi_{\text{reactor}}} = \frac{\overline{\Phi}_f}{\Phi_{th}} = \frac{\sigma_{\text{reactor}}}{\overline{\sigma}_f} \tag{44}$$

All the above procedures obviously involve absolute counting techniques.

If only the ratio, Φ_f/Φ_{th}, is needed, one can apply a relative counting procedure by using the reaction $^{32}S(n,p)^{32}P$ as fast flux monitor and the reaction $^{31}P(n,\gamma)^{32}P$ as thermal flux monitor [25].

3. 14 MeV Neutron Flux from Generators

a.   **Flux Distribution.** As neutron generators have targets with effective diameters of 10 mm to 30 mm, it is obvious that large flux gradients arise at close proximity to the target. Many authors have determined the gradients on the central axis of the target. A typical gradient as a function of the distance, d, is represented in Figure 4 [26]. From this it appears that at close proximity, the flux varies as $1/d$; whereas it varies as $1/d^2$ at a larger distance.

Less attention has been paid to lateral flux gradients which are also very important as can be seen by reference to Figure 5 [27]. These lateral gradients are of course sharper at close target range. It is also interesting to note that for large diameter targets, the lateral gradient is sharper than for small ones, all other factors being equal.

Table 9. Threshold detectors for the determination of the equivalent fission flux.

Reaction	Absolute counting	Remark
$^{27}Al(n,\alpha)^{24}Na$ $T_{1/2} = 15.0$ hr $\bar{\sigma} = 0.61$ mb $E_T = 3.26$ MeV $E_{eff} = 7.3 - 8.8$ MeV	$E_{(\gamma 1)} = 1.368$ MeV (100%) $E_{(\gamma 2)} = 2.754$ MeV (100%) $\gamma - \gamma$ coincidence	Al must be very pure to avoid ^{24}Na contamination; irradiation under Cd to reduce (n,γ)
$^{32}S(n,p)^{32}P$ $T_{1/2} = 14.3$ d $\bar{\sigma} = 65$ mb $E_T = 0.96$ MeV $E_{eff} = 2.7 - 3$ MeV	pure β – emitter $E(\beta) = 1.7$ MeV (100%) Calibrated G–M tube; 4π – prop. counter; liquid scintillation counting	P–impurity must be checked with and with without Cd. Chemical form: $(NH_4)_2SO_4$. Chemical separation of ^{32}P activity.
$^{54}Fe(n,p)^{54}Mn$ $T_{1/2} = 303$ d $\bar{\sigma} = 53$ mb $E_T = 0.16$ MeV $E_{eff} = 3 - 5$ MeV	$E(\gamma) = 0.835$ MeV (100%) γ – spectrometry	Let ^{56}Mn from $^{56}Fe(n,p)$ decay $(T_{1/2} = 2.6$ hr). Eliminate ^{59}Fe activity from $^{58}Fe(n,\gamma)$ and possible ^{60}Co activity from Co-impurity by chemical separation Mn/Fe, Co or by γ – spectrometry $(^{59}Fe \ 1.13–1.31$ MeV; $^{60}Co : 1.17–1.33$ MeV). Or use iron depleted in ^{58}Fe and enriched in ^{54}Fe.
$^{58}Ni(n,p)^{58(m)}Co$ $T_{1/2} = \ \ 9.13$ hr (m) $\ \ \ \ \ \ \ 71.3$ d $\bar{\sigma} = 28$ mb (m) $\ \ \ \ \ \ \ 74$ mb $E_T = 0.62$ MeV	Special coincidence technique possible β^+ particles detected with coincidence selector using 2 scintillation probes for 0.511 MeV annihilation.	No chemical separation necessary. Ni must be pure to avoid ^{60}Co from Co-impurity Attention : burn-up of $^{58(m)}Co : \sigma_{th} = 1650$ b;

Table 9. Threshold detectors for the determination of the equivalent
          fission flux. (continued)

Reaction	Absolute counting	Remark
$E_{eff} = 2.6 - 5$ MeV	The 800 keV γ – quanta are detected with 3rd γ – detector. Coincidences between signals of 3rd detector and coincidence signals from the other 2 detectors are measured.	$\sigma_{th}(m) = 170,000$ b.
^{103}Rh(n, n')^{103m}Rh $T_{1/2} = 58.7$ min $\bar{\sigma} = 1093$ mb $E_{eff} = 0.6$ MeV	I.T.: 40 keV, large internal conversion gives 20 keV x-ray; special counting technique.	Interesting because of low E_{eff}. But: Ir-impurity (^{192}Ir, even for Cd-covered detector).
^{238}U(n, f) $\bar{\sigma} = 310$ mb $E_{eff} = 1.5$ MeV	– ^{140}La (daughter of ^{140}Ba, fission yield (5.7%) : $E_{(\gamma)} = 1.6$ MeV – ^{137}Cs (fission yield (6.1%) : $E_{(\gamma)}$: 0.663 MeV, well-known decay scheme γ – spectrometry.	Uranium depleted in ^{235}U (ca. 10 ppm ^{235}U)

b.   Flux Determination. In the "Texas convention" a copper target was
proposed as flux monitor, using the reaction ^{63}Cu(n,2n)^{62}Cu. The target
should have a purity of at least 99.9%, have a diameter of 1 or 2.5 cm,
have a thickness of 0.25 mm, be irradiated for 1 min and be measured in a
lucite sandwich after 1 min decay at a distance of 3 cm of a 3 in. $\times$ 3 in.
NaI(Tl) crystal. The absolute disintegration is measured according to
Heath [28]:

$$D = A_p/PCAB \qquad (45)$$

where

$D =$ disintegration rate;
$A_p =$ 511 keV photopeak area in counts/min minus
        contribution of bremsstrahlung of the 2.9 MeV β^-;
$C =$ detector efficiency for used source geometry;
$A =$ absorption correction;
$B =$ branching ratio of 0.511 annihilation radiation;
$P =$ experimental peak to total ratio.
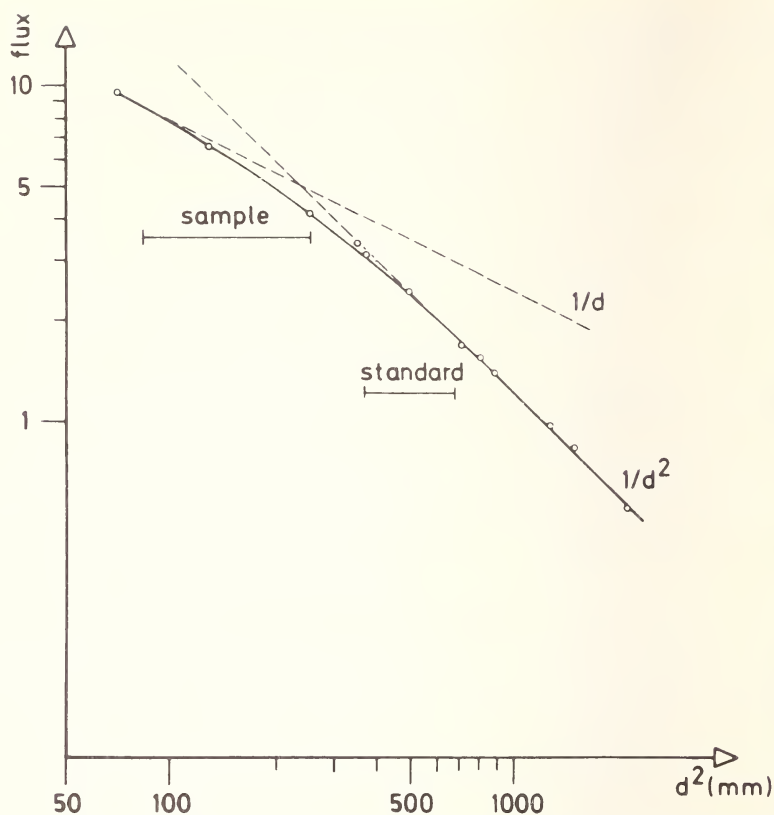
Figure 4.   Axial flux distribution as a function of the distance d, to the neutron generator target.
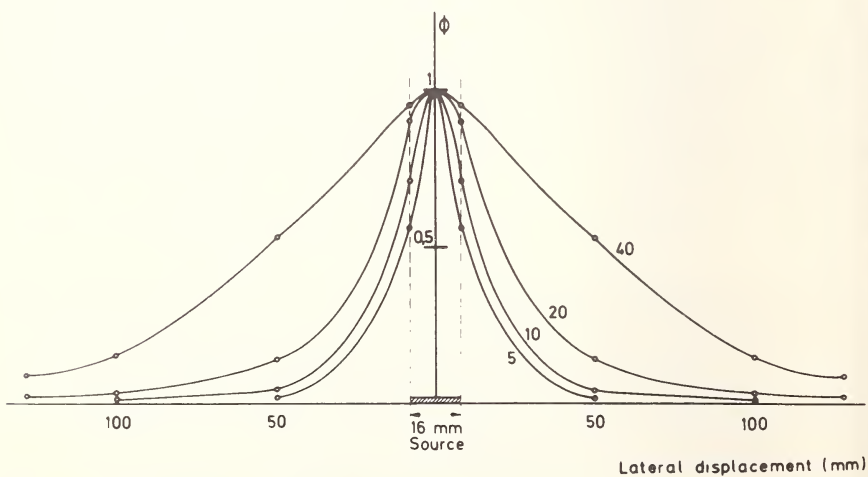
Figure 5.   Lateral flux distribution at different distances of the neutron generator target.

The value of $1/PCAB$, according to Heath [28] is 8.591 for a 1 cm and 8.703 for a 2.5 cm disc.

These values multiplied by A_p give the disintegration rate D and should be converted to decay time zero to yield the absolute disintegration rate D'. The flux is given by:

$$F = \frac{D'}{60\sigma N\theta[1 - \exp(0.693 t_b/T_{1/2})]} \tag{46}$$

$\sigma =$ 14 MeV cross section for the reaction $^{63}Cu(n,2n)^{62}Cu$ (560 mb);

$N =$ number of atoms $= 6.02 \times 10^{23} \times w/63.5$, where w is the copper weight in g;

$\theta =$ isotopic abundance of $^{63}Cu = 0.69$;

$t_b =$ irradiation time $= 1$ min;

$T_{1/2} =$ half life of $^{62}Cu = 10$ min.

An activity of 10^7 count·min^{-1}·g^{-1} of Cu corresponds to a flux 7.7×10^8 n·cm^{-2}·sec^{-1}.

III. Gamma Induced Reactions

A. TYPE OF REACTION

Although gamma induced reactions cannot be as easily treated as neutron induced ones, here also two parameters are of essential importance, namely the incident photon energy and the structure of the energy levels of the reacting nucleus. For systematic purposes, it is convenient to consider on the one hand (γ,γ') reactions, which give rise to isomeric states, and on the other hand gamma-particle reactions which give rise to nuclei different from the original one. The latter can further be divided into two groups: the (γ,n), $(\gamma,2n)$ . . ., reactions in which one or more neutrons are emitted, and those where charged particles are emitted, such as (γ,p), (γ,α), (γ,d), (γ,np), *etc.* In these cases the Coulomb barrier has obviously to be taken into account. In principle all the above reactions can be applied in activation analysis.

1. Gamma Particle Reactions

Gamma particle reactions can be produced by one of the following three processes:

1. The evaporation process in which the photon energy is entirely absorbed by the nucleus, distributed over all the nucleons, and followed by boil off of one or more particles.

2. The direct photon interaction process in which the entire energy is transferred to a single particle which is ejected.

3.   The quasi-deuteron effect resulting from the strong two body correlation in the nucleus. The high energy photon interacts with a neutron and a proton, colliding at high velocity, whereupon both particles are ejected.

The relative importance of these three processes as a function of photon energy, E_γ, and of the atomic number, Z, of the reacting nucleus is shown in Figure 6 [29]. For low Z nuclei direct interaction is the main
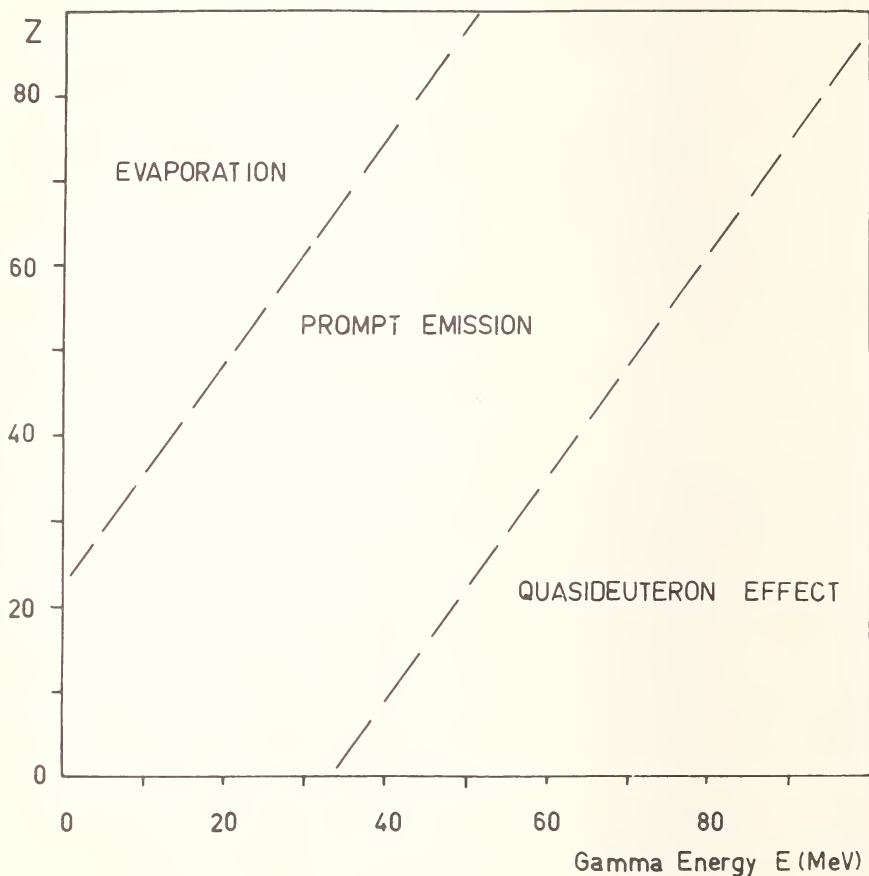
Figure 6.   Processes giving rise to gamma particle reactions as a function of Z and gamma energy.

process at low energy, whereas at higher energy competition occurs with the quasi-deuteron effect. With increasing Z, the probability that the energy will be distributed over all the nucleons increases. Hence competition occurs from the evaporation process which becomes more and more important. For medium and high Z nuclei, compound nucleus

formation competes with prompt particle emission, depending on the incident photon energy. In fact, the latter process is dominant at energies close to the giant resonance. At still higher energies even the quasi-deuteron effect can occur.

2. Gamma-gamma Reactions

When the incident photon has an energy higher than the first excited state of the target nucleus excitation can occur. The emitted prompt gamma carries the energy difference between the incident gamma and the energy of the first excited state of the nucleus. The latter returns to the ground state by emission of a gamma with an energy equal to the difference of the two levels. When the half life of the excited state is long enough to allow the counting of the products of deexcitation, application in activation analysis is possible [30]. Approximately 250 metastable states are known, with half lives between 10^{-10} sec and several years.

As a general rule one can state that metastable isomers with long half lives occur for nuclei with odd A numbers, *i.e.* before magic neutron or proton numbers [31]. They also follow Mattauch's rule [32,33], namely that isomers do not occur with even-even nuclei, that all nuclei with a spin of 9/2 in the ground state have a metastable state and that nuclei with a spin of 3/2 or 5/2 in the ground state have no metastable state.

B. REACTION THRESHOLDS

All gamma induced reactions are in fact threshold reactions. For (γ,n) reactions the threshold energies can be obtained from the mass difference method [34]. Usually the thresholds have a value of 7 to 18 MeV. They decrease with increasing atomic number. Two nuclei are known with unusually low thresholds:

$$^2H(\gamma,n)^1H \ E_{thr} = 2.23 \text{ MeV}$$

$$^9Be(\gamma,n)^8Be \ E_{thr} = 1.67 \text{ MeV}$$

In the case of charged particle emission, one has to take the Coulomb barrier into account, which increases rapidly with increasing Z as can be seen from Table 10. The emission of charged particles with high Z nuclei will for this reason be strongly hindered.

The threshold for the (γ,γ') reaction, on the other hand is only determined by the energy of the metastable state of the nucleus and is usually well below 10 MeV. Irradiation with photons with a maximum energy of 7 MeV for instance thus allows selective activation by the (γ,γ')

reaction without interference of gamma particle reactions. This technique also avoids neutron induced activity as the (γ,n) reaction does not occur.

Table 10. Thresholds in MeV for ^{16}O and ^{181}Ta

^{16}O	Coulomb	Δm	^{181}Ta	Coulomb	Δm
γ,n	—	15.6	γ,n	—	7.64
γ,p	2	12.1	γ,p	10.8	6.2
γ,α	3.6	7.15	γ,α	17	—

C. Reaction Cross Sections

The dominant feature in the interaction of photons with a nucleus is the giant resonance in the absorption process [35]. This phenomenon occurs with all nuclei and is a fundamental property of the nucleus. The corresponding cross sections depend on the structure of the energy levels in the nucleus.

With increasing energy nuclear levels broaden and are at the same time more closely spaced. Above the particle emission threshold, near 7 to 10 MeV, broadening increases until overlap finally occurs as is schematically shown in Figure 7. In medium and high A nuclei
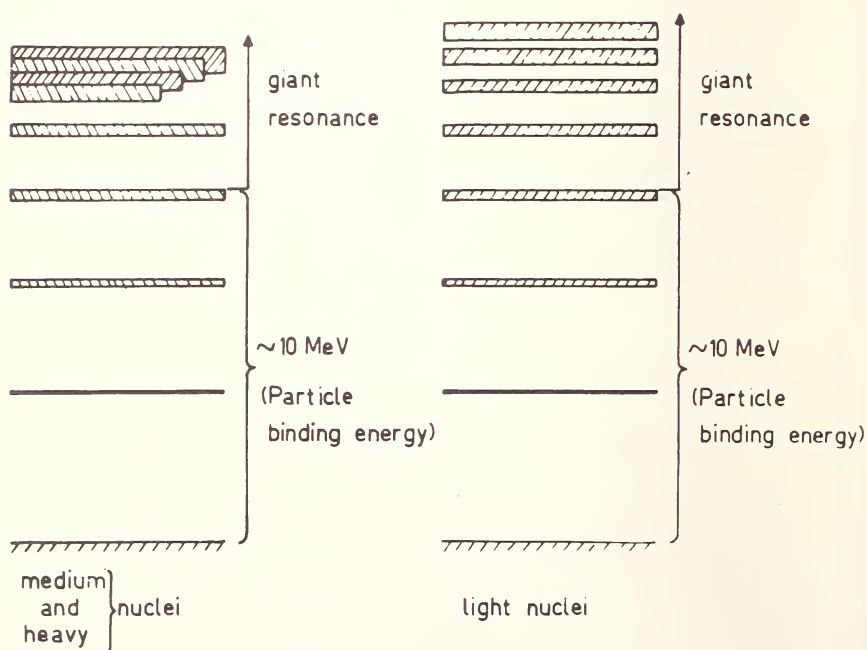
Figure 7. Schematic level structure in light, medium and heavy nuclei.

overlapping occurs in the giant resonance region, whereas for light nuclei the level structure persists throughout the giant resonance region and is lost only at much higher energies. For this reason, the giant resonance of light nuclei is only an envelope of the fine structure and is more strongly dependent on the particular properties of the nuclide. Therefore, reaction cross sections with very light nuclides (A between 2 and 20) must be treated individually.

For medium and heavy nuclei, where the complete overlap of the energy levels occurs at the giant resonance, the energy dependence of the cross section is defined by this resonance. The main parameters of this resonance represented schematically in Figure 8 are: E_m = energy at the
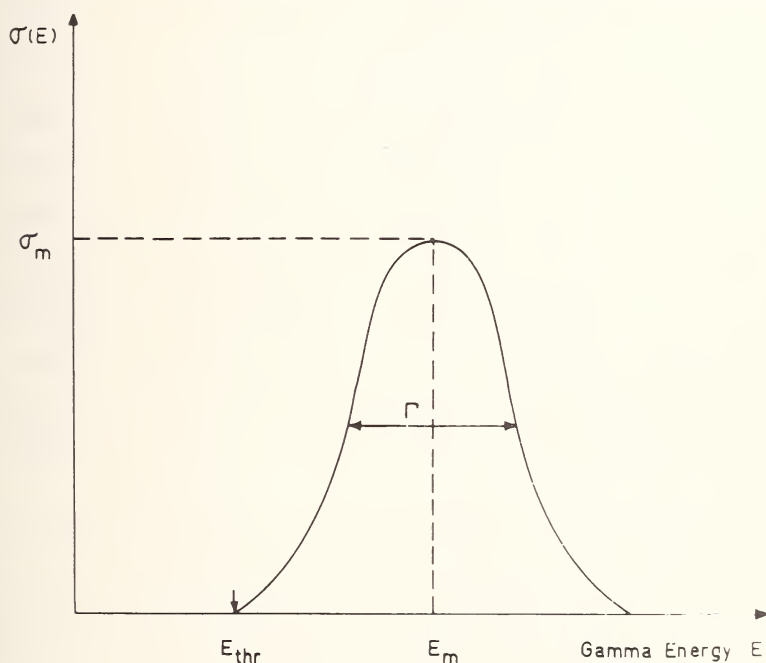
Figure 8.   Parameters defining the giant resonance.

maximum of the resonance (given by $E_m = 40.7\ A^{-0.20}$ [36]); σ_m = cross section at the resonance maximum; and Γ = width of the resonance at half peak height. For this type of nuclei the cross section as a function of photon energy can be approximated by a Lorentz shaped resonance line:

$$\sigma(E) = \sigma_m \frac{E^2\Gamma^2}{(E_m^2 - E^2) + E^2\Gamma^2}$$

where E represents the gamma-ray energy. Usually the value of Γ is

between 4 and 10 MeV depending on the nucleus. It reaches a minimum in the case of magic number nuclei.

As an example, the giant resonance cross section parameters for the (γ,n) reaction with a few elements are represented in Table 11 [36-37].

Table 11. Giant resonance cross section parameters for the (γ, n) reactions with some elements [36, 37].

Reaction	Threshold (MeV)	E_m (MeV)	σ_m (m barn)	Γ (MeV)	σ_{int} (MeV-barn)
$^{12}C(\gamma,n)^{11}C$	18.9	22.4	10.3	3.1	0.26
$^{14}N(\gamma,n)^{13}N$	10.5	22.5	15.3	3.2	0.061
$^{16}O(\gamma,n)^{15}O$	15.6	22.5	7.7	3.5	0.031
$^{19}F(\gamma,n)^{18}F$	10.4	22.2	11.5	5.6	0.077
$^{24}Mg(\gamma,n)^{23}Mg$	16.5	19.4	9.8	5.8	0.057
$^{28}Si(\gamma,n)^{27}Si$	17.1	20.5	21	3.5	0.075
$^{31}P(\gamma,n)^{30}P$	12.5	19	17	7.5	0.12
$^{32}S(\gamma,n)^{31}S$	15	20.5	13.6	6.3	0.086
$^{39}K(\gamma,n)^{38}K$	13	18.2	13.8	2.6	0.04
$^{40}Ca(\gamma,n)^{39}Ca$	15.8	19.3	15	4.2	0.065
$^{54}Fe(\gamma,n)^{53}Fe$	13.7	18.3	67	5.7	0.42

The values of σ_m and σ_{int} as a function of Z are represented in Figure 9 [38].

Splitting of the giant resonance can occur when dealing with greatly deformed nuclei (^{103}Rh, ^{113}In, ^{159}Tb, ^{181}Ta) due to the deviation of the nuclear shape from the spherical symmetry. This usually gives rise to two maxima which can be analyzed into two superimposed Lorentz lines. By integration of $\sigma(E)$ one obtains the integral cross section, σ_{int}, which is usually expressed in MeV-barn. This integral cross section is the sum of the various competing reaction cross sections and can be split into its constituent parts:

$$\sigma_{int} = \sigma_{\gamma,n} + \sigma_{\gamma,p} + \sigma_{\gamma,\alpha} \ldots$$

For low Z nuclides the (γ,n) and (γ,p) cross sections are of the same order of magnitude, the latter being even somewhat larger. However, with increasing Z, proton emission is more and more hindered by the Coulomb
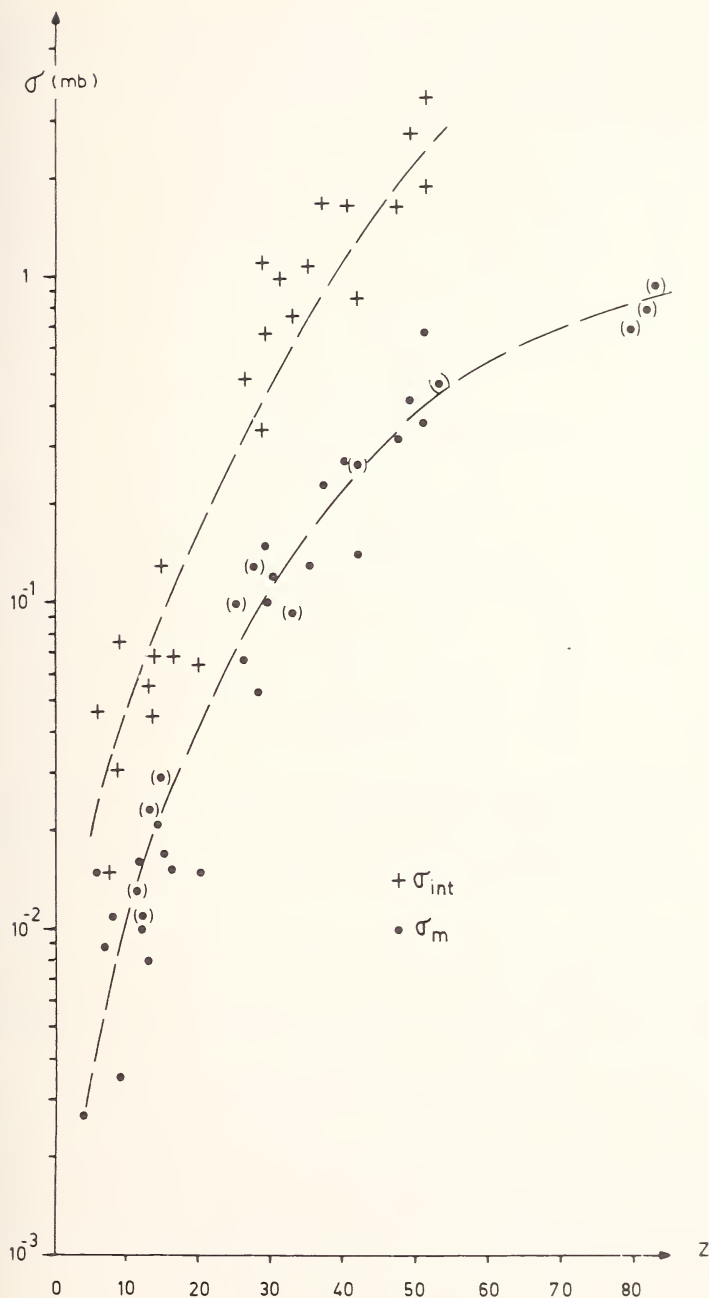
Figure 9. σ_{int} and σ_m for (γ, n) reactions as a function of Z. Values between brackets are atomic cross sections.

barrier, and consequently the cross section is small in comparison with the (γ,n) cross section. This is illustrated in Figure 10, where yields of (γ,n) and (γ,p) reactions are given as a function of Z [39,40].
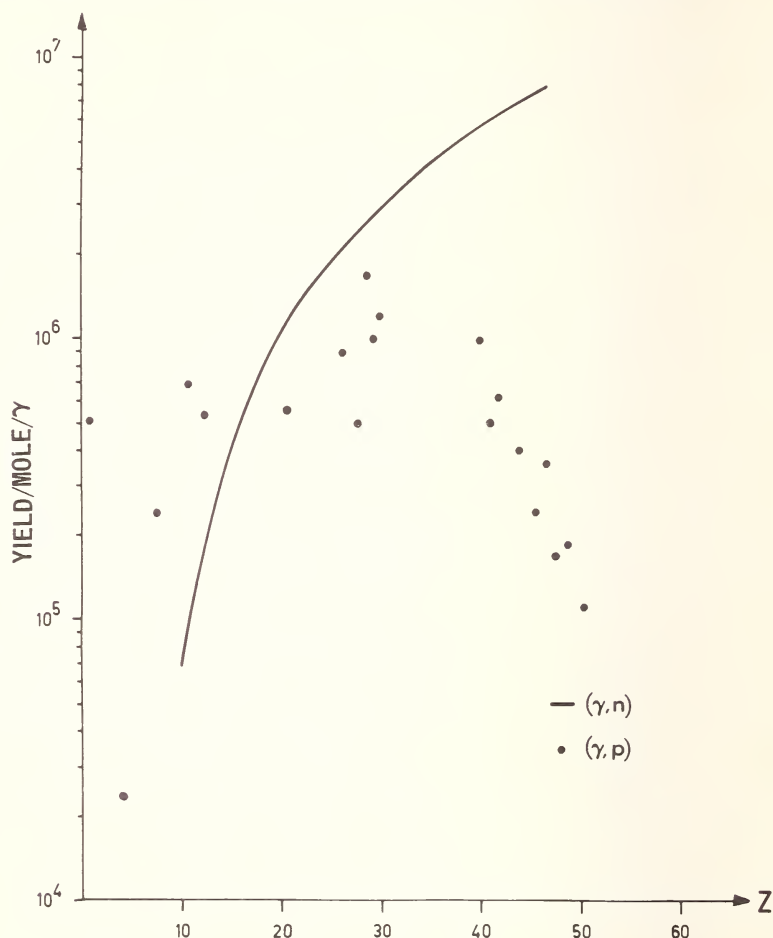
Figure 10.   Yields of (γ,n) and (γ,p) reactions as a function of Z.

It is obvious that for low Z nuclides both (γ,n) and (γ,p) reactions can be applied in activation analysis, whereas for high Z nuclides the (γ,n) reaction is the most widely applied. As an example, the different partial cross sections of ^{181}Ta as a function of gamma-ray energy, are given in Figure 11 [41,42].

Other types of reactions which have still smaller cross sections are of little practical use and will mainly have to be considered when studying interferences. The determination of carbon in metallic sodium by means of the reaction $^{12}C(\gamma,n)^{11}C$ ($E_{thr} = 18.9$ MeV) is for instance impossible
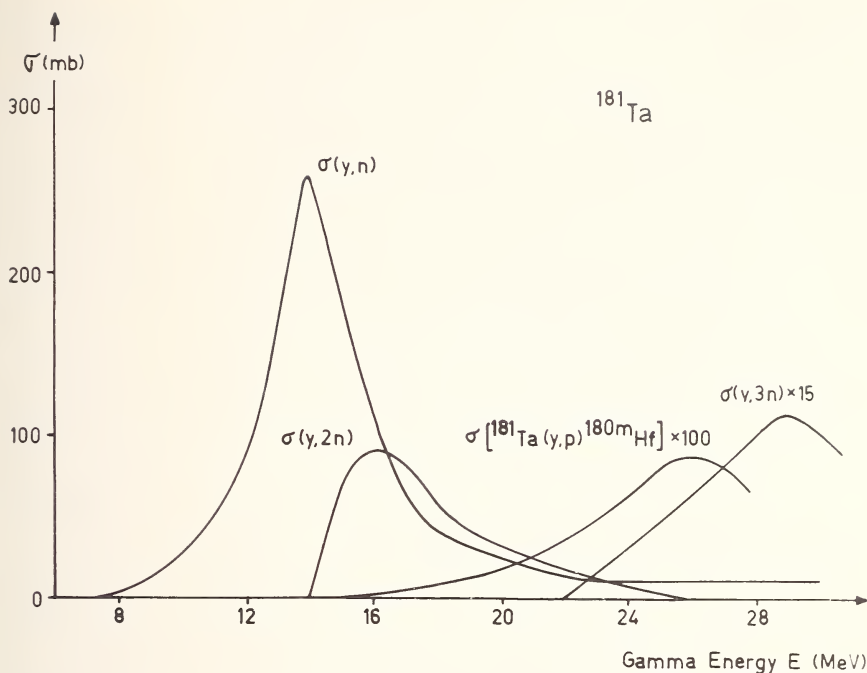
Figure 11. The partial cross section for ^{181}Ta.

without chemical separation due to the interfering reaction on the matrix ^{23}Na $(\gamma,n\alpha)^{18}$F $(E_{thr} = 20.9$ MeV$)$ [43]. Both ^{11}C and ^{18}F are pure positron emitters, and in spite of the large differences in half life (20 min and 110 min, respectively) the ^{11}C activity cannot be detected because of the large ^{18}F activity.

It is also obvious that the (γ,d) reaction will be more probable at low energies than the (γ,pn) and *vice versa* at high energies since particle emission dominates in the former case and the quasi-deuteron effect in the latter. This is illustrated in Figure 12, where (γ,d) and (γ,pn) cross sections for ^{64}Zn and ^{66}Zn are given as measured by Goldenberg and Marquez [44]. Excellent reviews of photonuclear cross sections are available [36,45].

Cross sections for (γ,γ') reactions show one or two maxima, or one maximum at low energy and a progressive increase towards the higher energies. In most cases the first occurs at about 9 MeV and the second one at about 18 MeV. The numerical values of these cross sections are rather low, of the order of millibarns in the most favorable cases. However since very high photon fluxes can be obtained in this energy region, activation analysis can theoretically be achieved with good sensitivity.
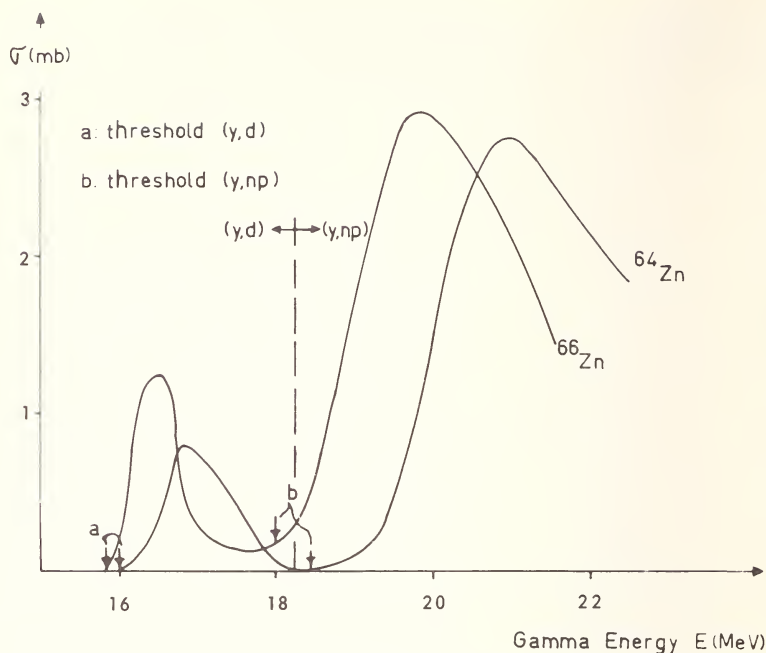
Figure 12.   The (γ,d) and (γ,pn) reaction cross sections for the isotopes ^{64}Zn and ^{66}Zn, as a function of gamma energy.

D. Photon Production

High energy photons are practically always produced by interaction of energetic electrons with matter which gives rise to a bremsstrahlung spectrum. Although any electron accelerator can be used for the purpose, the linear electron accelerator is by far the most adequate, since high intensities which are a requirement in trace activation analysis can be achieved.

One can estimate that an integrated electron beam of 100 μA produces a thick target photon yield between 10 and 30 MeV of 0.6×10^{14}, 2.0×10^{14} and 3.7×10^{14} photons·sec^{-1} for a corresponding electron energy of 20, 30 and 40 MeV, respectively. These high photon fluxes are even more important than in thermal neutron activation since cross sections are usually considerably smaller. Therefore an integrated current of more than 10 μA at energies up to 40 MeV is highly desirable.

The number of photons produced between a photon energy interval k and $k + dk$ is defined as the partial bremsstrahlung cross section, $d\sigma/dk$, and is given by the Bethe and Heitler equation [46,47]

$$\frac{d\sigma}{dk} \cdot dk = \Phi H \frac{dk}{k} \qquad (47)$$

$\Phi = 5.794 \left(\dfrac{Z}{100}\right)^2$ barn

$H =$ function of E, E' and of the screening parameter γ

$$\gamma = \frac{100\mu k}{E'EZ^{1/3}} \tag{48}$$

μ = electron rest energy;
E' = electron energy before reaction;
E = electron energy after reaction.

This cross section is valid for one single electron interacting with one nucleus. Multiplication by the number, N, nuclei/cm³ in the target yields the macroscopic cross section. Equation (47) describes a classical bremsstrahlung spectrum covering the energy region from zero to the incident electron energy (48).

However, electrons do not lose their energy by radiation only, but also by collision. Depending upon the Z of the target material and the electron energy one of the two processes dominates. Low Z targets give rise mainly to collision whereas in high Z targets radiation loss is predominant as can be seen from Figure 13 where both processes are given for
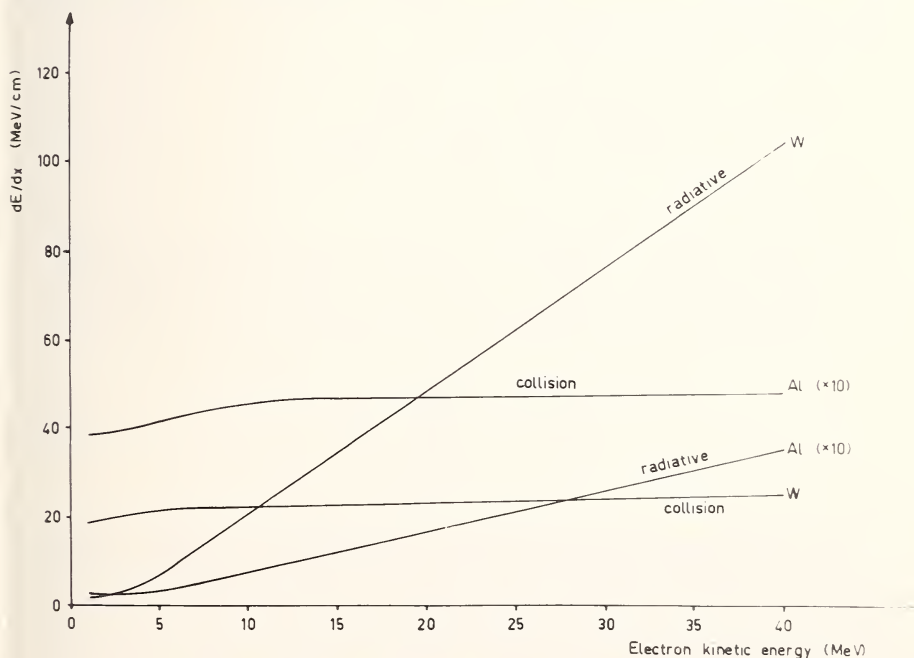
Figure 13. Energy loss by radiation and collision as a function of electron kinetic energy for Al(Z = 13) and W(Z = 74).

aluminum [40,41] and tungsten as a function of the incident electron energy.

For calculation purposes it is convenient to convert the target thickness dx in units of electron energy loss dE:

$$dx = \frac{dE}{\left(\dfrac{dE}{dx}\right)_{\text{tot}}} = \frac{dE}{\left(\dfrac{dE}{dx}\right)_{\text{rad}} + \left(\dfrac{dE}{dx}\right)_{\text{coll}}} \tag{49}$$

As a function of target thickness one can consider:

1.   thin targets which give rise to bremsstrahlung only as defined by equation (47). Their thickness is of the order of microns, so that the radiation is due mainly to a single interaction;

2.   intermediate targets with a thickness corresponding to a small fraction of the radiation length, the radiation length being defined as the thickness corresponding to a reduction of the electron beam intensity by a factor, e. These targets give rise to electron energy loss, however without complete absorption;

3.   thick targets with a thickness corresponding to several radiation lengths with complete electron absorption.

If for intermediate targets the thickness is expressed as energy loss, dE, the number of emitted photons, dn, in the energy range $k \pm dk/2$ per MeV total energy loss in the target is given by

$$\left(\frac{\partial^2 n}{\partial k \partial E}\right) dk dE = \frac{N d\sigma}{\left(\dfrac{dE}{dx}\right)_{\text{coll}} + \left(\dfrac{dE}{dx}\right)_{\text{rad}}} dE \tag{50}$$

If a thick target is considered as a sum of intermediate targets, integration of equation (50) over the whole target thickness gives the number of photons, dn per MeV interval of photon energy produced by the stopping of an electron with incident energy, E_o.

$$\frac{dn}{dk} = \int_{\mu + k}^{E_0} \frac{N d\sigma}{\left(\dfrac{dE}{dx}\right)_{\text{tot}}} dE \tag{51}$$

Thick target bremsstrahlung spectra as given by equation (51) are represented in Figure 14 for aluminum and tungsten targets and electron energies of 20 and 40 MeV. One should however be reminded that the above equation, described by Hansen and Fultz [43] are approximations since they neglect multiple electron scatter and photon absorption in the target.
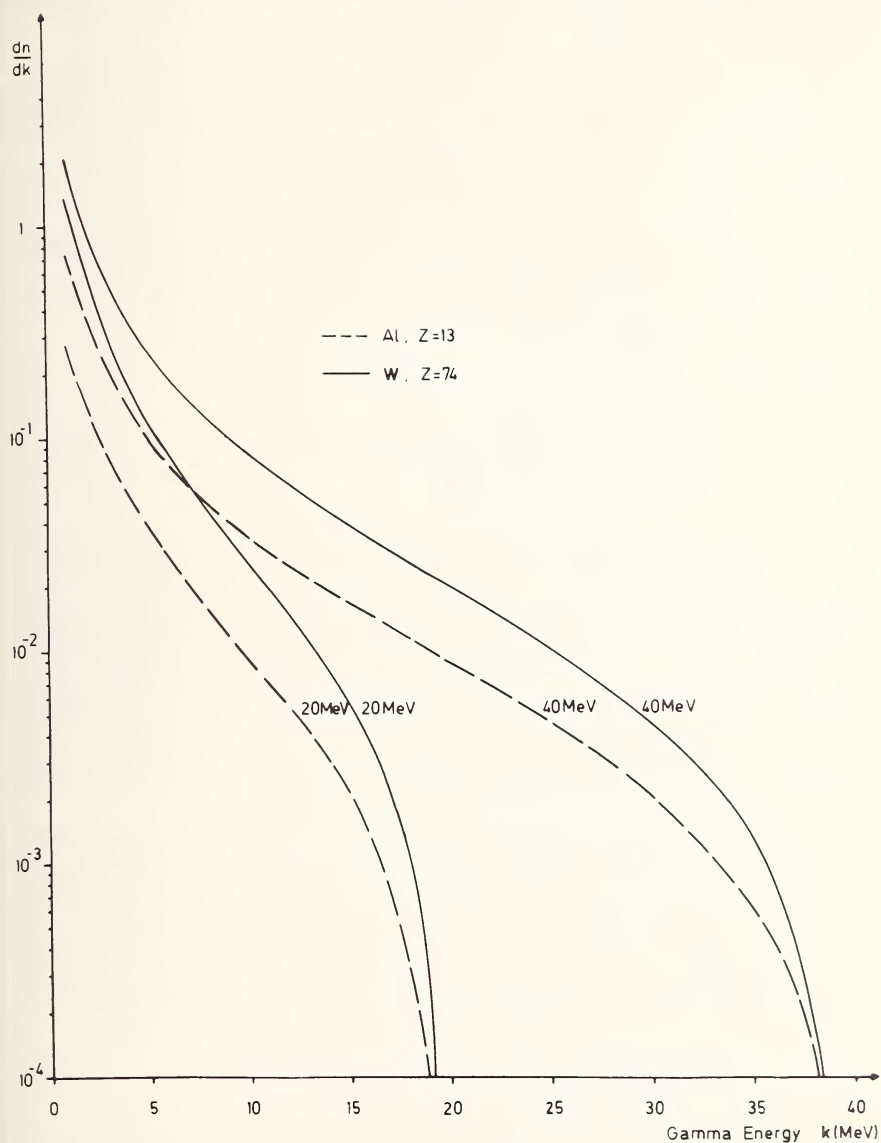
Figure 14. Bremsstrahlung spectrum in Al and W thick targets generated by the stopping of one electron with an energy of 20 and 40 MeV respectively.

An important feature of bremsstrahlung is its anisotropic character as the produced gamma-rays are peaked forward. The angular distribution is described by Schiff [49]:

$$\frac{I(\theta)}{I_0} = \frac{E_i\left(\dfrac{\theta^2}{2\beta x}\right)}{\ln\left(\dfrac{2\beta x E^2}{m^2 c^4}\right) - 0.5772} \tag{52}$$

$I_0 =$ intensity at 0° from the axis of the incident electron beam;
$I(\theta) =$ intensity at θ degrees from the axis;
$E_i =$ exponential integral;
$\beta = \left(\dfrac{9.2 Z e^2}{E}\right)^2 N$
$E =$ incident electron energy;
$N =$ number of target nuclei per cm³;
$x =$ target thickness in cm.

The angular distribution obtained by means of equation (52) for a tungsten point target of 0.325 cm thickness at a distance of 0.1 cm from the target and for different electron energies is given in Figure 15. From this figure it appears that the forward peaking increases with increasing energy. It is obvious that for activation analytical purposes a high photon flux is desirable and that no electron should reach the sample. This should be avoided to prevent intense heating and also to avoid the production of a bremsstrahlung spectrum of a different nature in the sample and reference.

It is clear that these two conditions can be achieved with a thick target of high Z, (e.g., W, Pt, Ta). It is moreover obvious that the thickness of these thick targets will depend upon the incident electron energy. In fact, for gamma-gamma reactions, an energy below 10 MeV will be used; whereas for gamma particle activation energies, not higher than 40 MeV are desirable since the giant resonance is usually located between 10 and 20 MeV.

E. REACTION RATES

The differential reaction rate $R(E)$ for a given gamma energy E is given by

$$R(E) = \sigma(E)\,\Phi(E) \tag{53}$$

Figure 16 represents the photon flux, $\Phi(E)$, and the cross section, $\sigma(E)$, as a function of photon energy, using an electron beam of energy, E_o. By
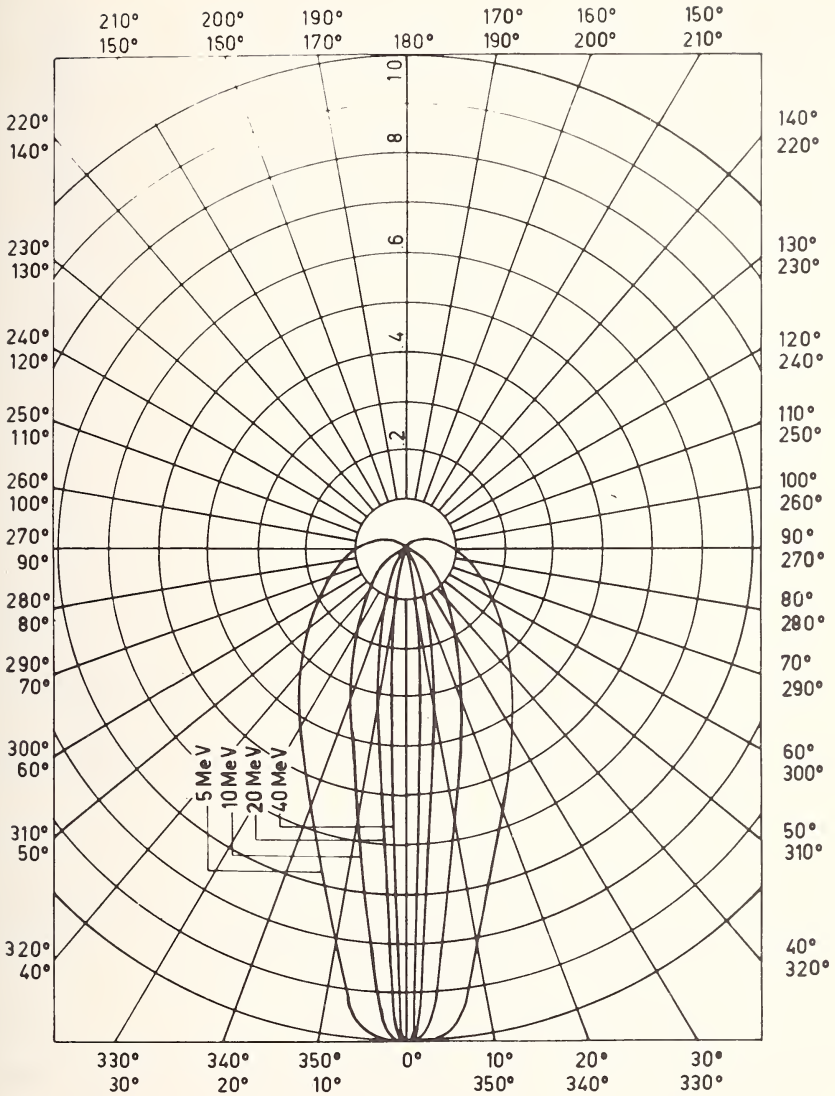
Figure 15. Angular distribution of the Bremsstrahlung at a distance of 0.1 cm of a W target of 0.325 cm thickness, for electrons of 5, 10, 20 and 40 MeV. The ratio of the numbers of photons emitted at an angle θ with the incident electron beam axis to the number of photons of $\theta = 0$ is given.

integrating equation (53) from zero to E_o one obtains the total reaction rate

$$R = \int_0^{E_0} \sigma(E)\Phi(E)\,\mathrm{d}E$$
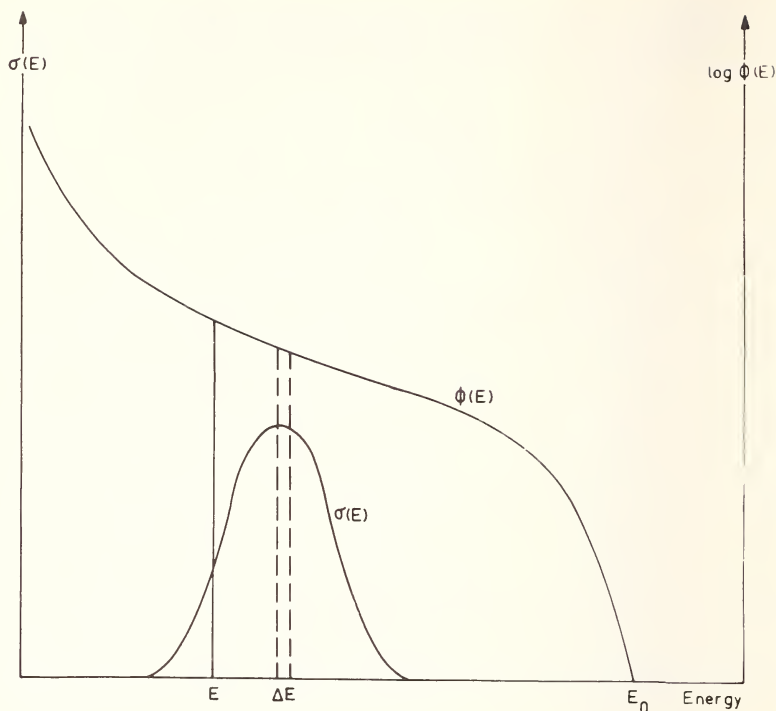
Figure 16.   Determination of the reaction rate from $\sigma(E)$ and $\Phi(E)$ as a function of the photon energy.

Since both $\sigma(E)$ and $\Phi(E)$ are complex functions of E, numerical integration has to be applied over energy intervals ΔE:

$$R = \Sigma\Delta\, \sigma(E)\Delta\Phi(E) \tag{54}$$

Even this approach gives only an approximate value of the induced activity in a sample since the precision on $\sigma(E)$ and $\Phi(E)$ is quite poor. Therefore, common use is made of activation curves which are obtained by absolute measurement of the induced activity in a given element as a function of electron energy. The normalization of the different measurements is performed by means of dosimetry. It is obvious that the obtained activities must be given for the same electron beam intensity.

Figure 17 gives some examples of the activation curves for the reactions $^{16}O(\gamma,n)^{15}O$; $^{14}N(\gamma,n)^{13}N$; $^{12}C(\gamma,n)^{11}C$ and $^{19}F(\gamma,n)^{18}F$ as reported by Engelmann [50]. From Figure 17 it is obvious that the choice of the electron energy can greatly influence the yield of reaction.
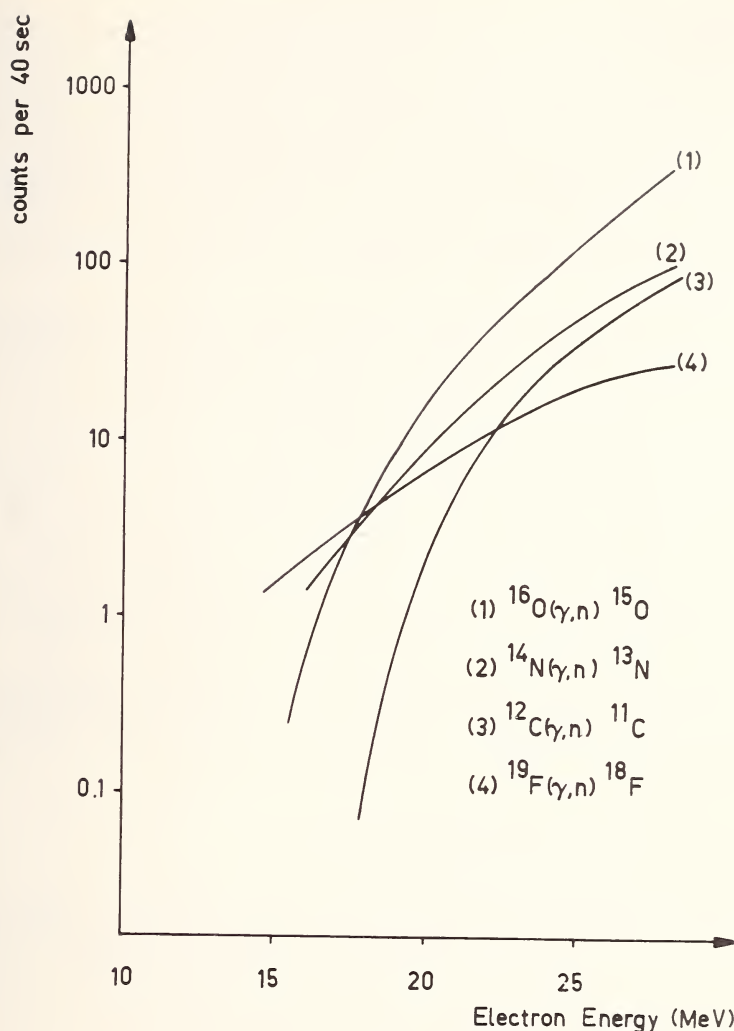
Figure 17.   Activation curves for O, N, C and F. The activities are given for a 1 μg sample and an integrated beam current of 50 μA.

F. Application in Activation Analysis

Photon activation has a number of advantages over neutron activation analysis. Elements not activated with thermal neutrons can be determined with high sensitivity, for instance the light elements C, N, O and certain medium and heavy elements as Fe, Pb. Photon activation has also the advantage of a variable maximum energy. This offers the possibility to enhance or depress certain reactions by adapting the electron energy to the threshold of the considered reactions as is shown.

Interferences can also be determined experimentally by multiple irradiation techniques at different electron energies. A striking example of this technique was given by Engelmann [50]. Both phosphorus and sulfur give rise to ^{30}P by a (γ,n) and a (γ,pn) reaction, respectively. This radioisotope is a positron emitter with a half life of 2.56 min and interferes with the measurement of ^{15}O produced by the reaction ^{16}O$(\gamma,n)^{15}$O which is also a pure positron emitter with a half life of 2.02 min. Three irradiations at three different energies allowed the determination of these interferences.

A further advantage of photon activation is that the great penetrability of the photons avoids self-shielding which can cause difficult problems in neutron activation of large samples with high cross section. However, for large samples, gamma absorption has also to be taken into account.

The major disadvantages due to photon activation are mainly related to the large gradients surrounding the target and to the type of induced nuclear reaction. Careful experimental techniques can correct for the former but neutron deficient isotopes, *i.e.* positron emitters are unavoidable in many cases. This makes gamma spectrometry unapplicable; so decay curve analysis and chemical separations are required.

Attention should also be paid to simultaneous neutron activation, due to appreciable neutron production from the (γ,n) reaction on sample and surrounding materials. A survey of possible reactions is given in Figure 18.

IV. Charged Particles

Although charged particle activation analysis was already applied by Seaborg *et al* in 1938, little attention was paid to this technique. This is probably due to the fact that with the advent of the nuclear reactor, intense neutron fluxes became available which solved many analytical problems in a far more simple way. Charged particle analysis is indeed considerably more complex than neutron and even photon activation analysis. Among the special problems encountered with this technique one can mention several types of simultaneously occuring nuclear reactions, limited range of the particles, and heating of the bombarded samples. In the case of low Z elements, however, neutron activation analysis has limited applicability and even photon activation cannot solve all of the analytical problems, for instance in the case of ultra high purity materials. Thus charged particle activation analysis can supplement these techniques or serve as an independent surface analysis technique where charged particles are particularly useful. Particularly after Markowitz and Mahony [51] drew the attention on the remarkable properties of ^{3}He
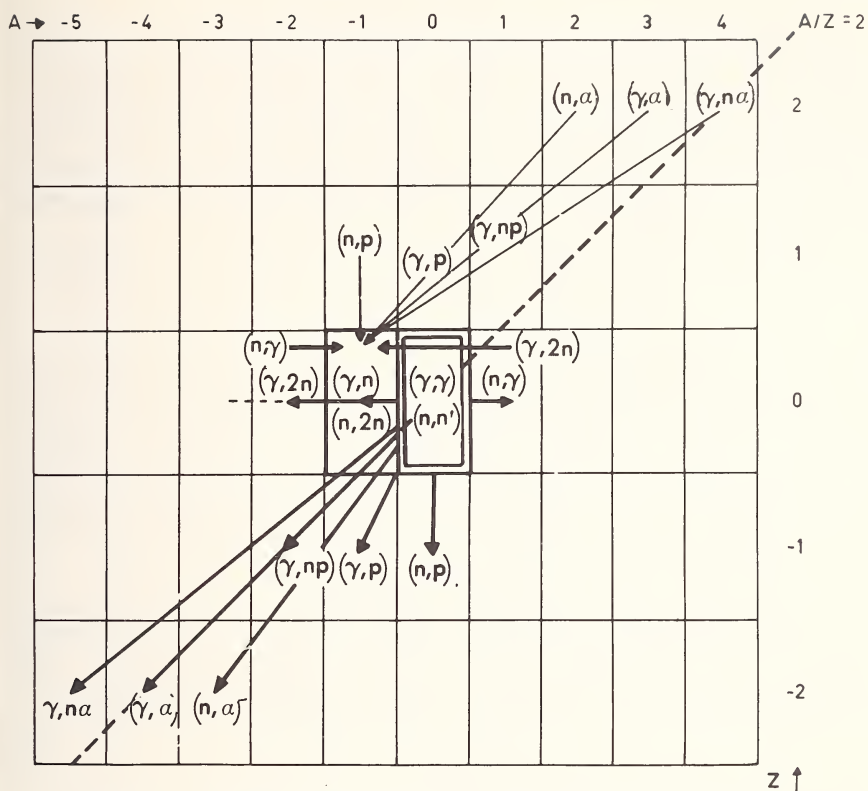
Figure 18.   Possible gamma reactions and neutron induced interferences.

activation, a large research effort was concentrated on charged particle activation. The successes obtained in this field appear clearly from the Proceedings of 2nd Conference on Activation Analysis with Charged Particles organized by Euratom in 1967 [52].

A. Type and Energy of the Particles

Until now charged particles applied in activation analysis were almost exclusively light ones, *i.e.* protons, deuterons, ^{3}He and ^{4}He. To overcome the Coulomb barrier and to obtain sufficiently high reaction rates, Albert [53] suggested that the following energies should be available: protons = 5 MeV to 25 MeV; deuterons = 5 MeV to 20 MeV; ^{3}He = 5 MeV to 20 MeV; and ^{4}He = 10 MeV to 45 MeV. Higher energies are indeed seldomly needed to achieve the desired type of analysis. One may even state that higher energies will be rather undesirable due to the complexity of the reactions. Commercial attempts have been made to achieve the above mentioned conditions by means of a small 30 inch isochronous cyclotron where accelerating protons, deuterons, helium-3 and 4 to 15

MeV, 8 MeV, 20 MeV and 16 MeV, respectively. Tritons have also been extensively studied and applied [54,55]. This charged particle analysis is of a unique type since the tritons are produced by thermal neutron irradiation of ^{6}Li. Thus, the recoil energy of these tritons have a fixed energy of 2.7 MeV which is high enough to induce some nuclear reactions over a short range as for instance the reaction ^{16}O(t,n)^{18}F applied to oxygen determinations.

B. Excitation Functions

The cross section of a charged particle reaction as a function of energy is more complex than for neutrons since one has to consider the Coulomb barrier. If one accepts the formation of the compound nucleus, de-excitation can take place according to different competing reactions, for example neutron, proton, and alpha emission. Each of these de-excitations occur with probabilities that depend on the energy available, and thus, on the Q value of the reaction.

Some general rules can be formulated; namely, that the emission probability decreases in the order neutron, proton and alpha particle. Whereas, the cross section for the compound nucleus formation, σ_{com}, can be represented by expressions derived by Konopinski and Bethe [56]

$$\sigma_{\text{com}} = \pi \lambda^2 \sum_{\ell=0}^{\infty} (2\ell + 1) P_e \xi_e \qquad (55)$$

where λ is the de Broglie wavelength, P_e the probability that an incident particle will reach the nuclear surface, ℓ its angular momentum, and ξ the probability that it will enter the nucleus.

The function $\sigma(E)$ is called an excitation function and is usually determined by the stacked foil technique. The particle energy is gradually degraded until it is finally completely stopped or reaches at least an energy below the threshold. Either absolute or relative measurements can be used. In the latter case, aluminum is often applied since its excitation functions together with the corresponding ranges are well known for a number of particles.

In classical experiments Ghoshal [57] determined reaction rates from helium-4 bombardments of ^{60}Ni and proton bombardments of ^{63}Cu as a function of energy. The results are represented in Figure 19. These experiments are important since the compound nucleus ^{64}Zn is the same for both particles. Figure 19 shows that the ratio of the (p,n):(p,2n):(p,3n) is the same as the ratio $(\alpha,n):(\alpha,2n):(\alpha,np)$ and is thus independent of the mode of formation of the compound nucleus. If the sum of the different partial cross sections is considered as a function of energy their sum yields the total cross section, σ_{com}.
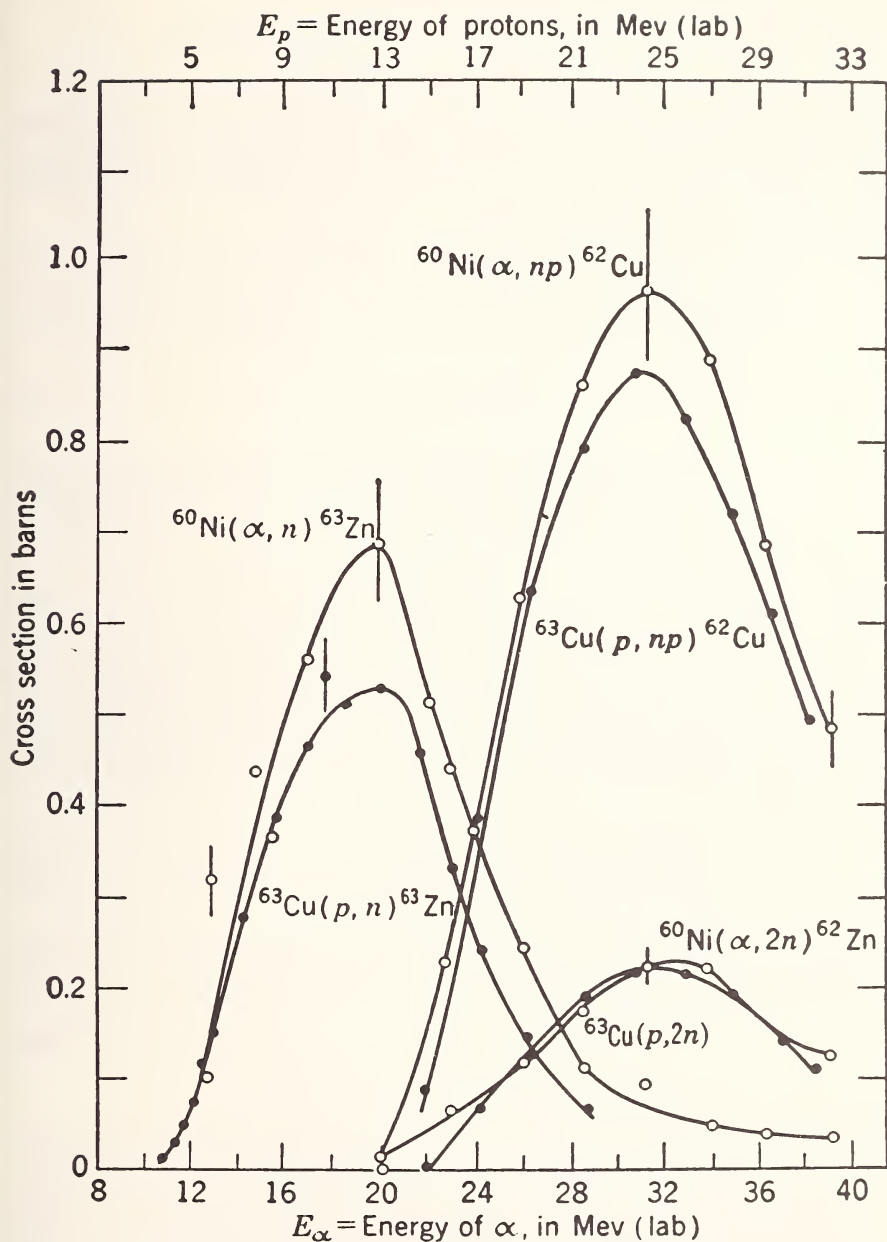
Figure 19. Excitation functions.

Numerical values derived from equation (55) are usually presented in tables or graphs [58]. In practice and more particularly in activation analysis, these curves can only serve to estimate orders of magnitude and obviously only experimental data can be used rigorously.

C. Flux and Range of Charged Particles

The determination of the flux of charged particles produced for instance from an accelerator can easily be computed from the beam intensity for example, measured by means of a Faraday cup. It can be shown that 1 μA is equivalent to 6.24×10^{12} particles per second for particles carrying one unit of charge.

If in neutron and photon activation, attenuation of the particle flux intensity is an unimportant source of errors, this is seldom the case in charged particle activation. The flux intensity attenuation is indeed given by

$$\Phi = \Phi_0 e^{-\sigma n x} \tag{56}$$

where σ is the microscopic cross section in cm^2, n is the number of target nuclides per cm^3 and x is the target thickness in cm. One can calculate that to reduce the flux intensity by one order of magnitude, σx should be approximately 50. Since cross sections have values of the order of 10 mb, flux intensity attenuation obviously is unimportant. If on the other hand range problems do not occur in neutron and photon analysis, the contrary of course occurs for charged particles. The knowledge of the energy loss per unit path length is particularly important since the cross section is also a function of energy, yielding the excitation curve. Bethe and Livingstone [59] have demonstrated that the energy loss dE per unit of path length dx is given by

$$-\frac{dE}{dx} = \frac{4\pi e^4 Z^2}{m_0 v^2} NZ \left[\ln \frac{2m_0 V^2}{I} - \ln (1 - \beta^2) - \beta^2 \right] \tag{57}$$

where I is the mean excitation and ionization potential. It can be approximated with the relation

$$I = kZ \tag{58}$$

where k is an empirical constant.

Usually the relative stopping power is determined versus aluminum and represents the ratio of the amount of standard material to the amount of material in question for equal energy loss. It is often expressed on a path length basis. The range of a charged particle is then of course equal to the total path length. For non-relativistic cases one can write:

$$E = 1/2 \ mv^2; \ dE = Mc\,dv \text{ and } dx = dr$$

then equation (57) becomes for $\beta^2 \ll 1$

$$dr = \frac{M}{Z^2} \frac{m_0}{4\pi e^4} \frac{1}{NZ} \frac{V^3 dV}{\ln (2m_0 V^2/I)} \tag{59}$$

By integration and from I values, ranges can be obtained for different charged particles.

For different particles of equal velocity one can also write:

$$\frac{R_{3He}}{R_\alpha} = \frac{(M/Z^2)_{3He}}{(M/Z^2)_\alpha} \approx \frac{3}{4} \tag{60}$$

$$\frac{R_d}{R_p} \approx 2 \quad \text{and} \quad \frac{R_t}{R_p} \approx 3 \tag{61}$$

where α, p, d, t refers to ^{4}He, ^{1}H, ^{2}H and ^{3}H, respectively.

On the other hand when an approximate range is desired the Bragg-Kleeman rule can be applied:

$$\frac{R_1}{R_0} = \frac{\rho_0 \sqrt{A_1}}{\rho_1 \sqrt{A_0}} \tag{62}$$

where ρ is the density and A the atomic weight.

Another point which can be considered in charged particle activation analysis is the nature and energy of the emitted particle. Like in the case of neutron activation analysis the prompt radiation can be a measure of the material under investigation, and the same is true for charged particle analysis, for instance by measuring gammas from Coulomb excitation or neutrons from the reaction product [60,61].

One should also keep in mind that when irradiating crystalline materials, the range of the charged particles is increased in what is called the channeling direction discussed extensively by Holm *et al* [62]. Straggling of the particle beam is also a phenomenon which has to be considered.

D. CALIBRATION TECHNIQUES

Since it is impractical to monitor accurately the particle flux during the irradiation of the sample, and since the particle range is a complex function of the nature of the irradiated material, calibration of the induced activity in a sample requires special attention in charged particle analysis. Albert [63] summarizes the different calibration procedures as those with spinning targets, internal standards, activation curves with "thin" standards and finally the average cross section.

If an unknown sample and a standard with similar composition are irradiated simultaneously under the same conditions of effective beam

surface in a spinning mechanism for instance in an external beam, direct and accurate results can be obtained. The major difficulties reside obviously in obtaining reliable standards and a sufficient beam intensity [64,65].

The use of an internal standard as recommended by Albert *et al* [66], and by Hoste *et al* [67] or a comparison with standards and flux normalization as recommended by Kuin [68], allows the use of the full beam intensity, but of course it is also limited by the fact that standards are required.

The average cross section method proposed by Ricci and Hahn, also makes use of a comparator, but since the defined $\bar{\sigma}$ is independent of the target material, the method is more absolute in character. The definition of average cross section is obtained as follows:

The number of disintegrations obtained from an irradiated target is given by

$$D = I_f n\sigma t \tag{63}$$

where

$I_f =$ number of charged particles per second;
$n =$ number of target nuclides, A, per mg of target;
$\sigma =$ cross section in cm^2 for the nuclear reaction $A \rightarrow B$;
$t =$ thickness of the target in mg/cm^2.

σ is of course a function of the particle energy.
If t is thicker than the range R, D is given by

$$D = I_f n \int_0^R \sigma_t \, dt \tag{64}$$

Considering the relation between the range R and the energy E of the charged particles:

$$R = \int_0^R dt = \int_E^0 \left(\frac{dt}{dE}\right) dE \tag{65}$$

one can write

$$\int_0^R \sigma_t \, dt = \int_E^0 \sigma_E \left(\frac{dt}{dE}\right) dE \tag{66}$$

In equation (66) σ_E represents the variation of the cross section with energy, *i.e.* the excitation function.

From the knowledge of the excitation function an average cross section $\bar{\sigma}'$ is defined as

$$\sigma' = \frac{\int_0^{R'} \sigma_t dt}{\int_0^{R'} dt} = \frac{\int_E^0 \sigma_E \left(\frac{dt}{dE}\right) dE}{\int_E^0 \left(\frac{dt}{dE}\right) dE} \tag{67}$$

dt/dE is similar to the negative reciprocal of equation (57) and can be simplified to

$$-\frac{dE}{dt} = \frac{k}{E} \ln \left(\frac{E}{I}\right) \tag{68}$$

In fact, equation (68) is not valid at zero energy but to E_o.
Thus:

$$R' = \int_E^{E_0} E \left(-k \ln \frac{E}{I}\right)^{-1} dE + \int_{E_0}^0 \left(\frac{dt}{dE}\right) dE \tag{69}$$

The second term of equation (69) is usually much smaller than the first one and can be reflected thus

$$\bar{\sigma}' = \frac{\int_E^{E_0} \sigma_E E \left(k \ln \frac{E}{I}\right)^{-1} dE}{\int_E^{E_0} E \left(k \ln \frac{E}{I}\right)^{-1} dE} \tag{70}$$

Since $k \ln \frac{E}{I}$ is approximately constant for a given target

$$\bar{\sigma}' = \frac{\int_E^{E_0} \sigma_E E dE}{\int_E^{E_0} E dE} \sim \frac{\int_E^0 \sigma_E dE}{\int_E^0 E dE} \tag{71}$$

and it is independent of the target material. Thus, equation (64) can be simplified to

$$D = I_f n \bar{\sigma}' \int_0^{R'} dt = I_f n \bar{\sigma}' R' \tag{72}$$

and the knowledge of $\bar{\sigma}'$ in one material allows the determination of the integral cross section, $\bar{\sigma}' R'$, for all materials and also for the application of the comparator technique.

In a more recent paper [69] the same authors redefined the thick target average cross section as

$$\bar{\sigma} = \frac{I}{R} \int_0^R \sigma_t \mathrm{d}t \tag{73}$$

where R is the total range instead of an effective range R'. It can be shown that

$$D = I_f n \bar{\sigma} R = I_f n \bar{\sigma}' R'$$

The equivalent thickness method, proposed by Engelmann [70,71] has the advantage of being experimental, thus being free of any approximation in its principle. No knowledge of the particle range is needed since it makes use of an experimentally determined value, the equivalent thickness, which is defined as follows:

$$D = I_f n \int_0^R \sigma_t \mathrm{d}t = I_f n \sigma_0 e \tag{74}$$

where the same symbols are used as in equation (63), e being the equivalent thickness. This is a fictive thickness over which a uniform activity would be distributed. The value, σ_o, is the cross section at the energy of the undegraded beam. The equivalent thickness is generally obtained from the activation curve, which is measured by sandwiching an increasing thickness of matrix material between two "thin" slices of standard material. The activities induced in the standards are always referred to the one which is closest to the beam. The activation curve could evidently also be obtained from the excitation function, and the range-energy relation of the particles, but since these values are known with rather poor precision, serious errors can occur.

Analysis by means of this technique can be performed in two ways [72]. A standard with negligible thickness d is placed before the sample in the particle beam. Writing equation (74) for the element to be determined in the sample, and in the standard, yields

$$\frac{D_X}{D_S} = \frac{I_{f_X} n_X \sigma_0 e_X}{I_{f_S} n_S \sigma_0 d} = \frac{n_X e_X}{n_S d} \tag{75}$$

where D_X and D_S represent the measured activities of the element X in sample and standard.

From equation (75) the concentration of the element X in the sample can be calculated as follows:

$$X_{\mathrm{ppm}} = \frac{D_X}{N_S S e_X} \tag{76}$$

where N_S is the specific activity per μg in the standard, and S represents the irradiated surface. The value of e_X is then expressed in g/cm^2.

Another possibility to perform an analysis, consists of using a thick sample and a thick standard which are irradiated with the same particle flux, *e.g.* by means of a rotating target device. Equation (74) can then be written as follows:

$$\frac{D_X}{D_S} = \frac{n_X e_X}{n_S e_S} \tag{77}$$

From which the concentration of X in the sample can be calculated if the values of e_X and e_S have been previously measured.

Comparing the equivalent thickness technique with the average cross section technique, it can be shown that:

$$e = \frac{\bar{\sigma}}{\sigma_0} R \quad \text{or} \quad e = \frac{\bar{\sigma}'}{\sigma_0} R' \tag{78}$$

Furthermore, comparing equivalent thicknesses and ranges for a given reaction in two materials, 1 and 2, one obtains:

$$\frac{e_1}{e_2} = \frac{R_1}{R_2} = \frac{R_1'}{R_2'} \tag{79}$$

This means that the value e/R and e/R' remains constant for a given energy of incident particles. This is clearly shown in Table 12 where these

Table 12. Equivalent thickness.

Element	e (g/cm^2)	R (g/cm^2)	R'(g/cm^2)	e/R	e/R'
Beryllium	0.120	0.1796	0.1350	0.668	0.889
Aluminum	0.135	0.2010	0.1497	0.671	0.901
Silicon	0.1305	0.1974	0.1467	0.661	0.889

ratios are represented for the reactions $^{16}O \rightarrow {}^{18}F$ with 44 MeV alpha particles in different matrices [72]. A survey of activation analyses, performed with charged particles is given in Table 13.

Table 13. Applications of charged particles.

Element determined	Reaction used	Matrix	Ref	Remarks
Oxygen	$^{16}O(^3He,p)^{18}F$ $^{16}O(^3He,n)^{18}Ne$ $\longrightarrow ^{18}F$	Th, Be	(73)	Interferences: $^{27}Al(^3He,3\alpha)^{18}F$ $^{23}Na(^3He,2\alpha)^{18}F$ $^{19}F(^3He,\alpha)^{18}F$
		Au, Si	(74)	
		Tb	(75)	
		$^{239}Pu - ^{241}Am$	(76)	
		Ge	(77)	
		Zr, Mo, Hf, W	(78)	
	$^{16}O(\alpha,d)^{18}F$	Zr, Mo, Hf, W	(78)	Interferences:
	$^{16}O(\alpha,pn)^{18}F$			$^{15}N(\alpha,n)^{18}F$
	$^{16}O(\alpha,2n)^{18}Ne$			$^{19}F(\alpha,\alpha n)^{18}F$
	$\longrightarrow ^{18}F$	Fe, Ni, Cr	(79)	$^{23}Na(\alpha,2\alpha n)^{18}F$
		Si	(80)	
	$^{18}O(p,n)^{18}F$	Be, Si	(81)	
Carbon	$^{12}C(^3He,\alpha)^{11}C$	Au, Si	(74)	
	$^{12}C(^3He,d)^{13}N$ $^{12}C(^3He,np)^{13}N$	Tb	(75)	
	$^{12}C(d,n)^{13}N$	Si	(82)	
		Fe	(83)	
Nitrogen	$^{14}N(p,\alpha)^{11}C$	silicon carbide	(86)	
		Be, Si	(85)	
	$^{14}N(d,n)^{15}O$	Be, Si	(84)	Interference: $^{16}O(d,t)^{15}O$
Boron	$^{11}B(p,n)^{11}C$	silicon carbide	(86)	
		Be, Si	(85)	
	$^{11}B(d,2n)^{11}C$ $^{10}B(d,n)^{11}C$	Be, Si	(84)	Interferences: $^{14}N(d,\alpha n)^{11}C$ $^{12}C(d,t)^{11}C$

Table 13. Applications of charged particles. (continued)

Element determined	Reaction used	Matrix	Ref	Remarks
Oxygen	$^{16}O(^3He,n)^{18}F$	powdered metals	(87)	^3H produced by $^6Li(n,\alpha)^3H$ reaction. Sample
		Be	(88)	is mixed with 7x its weight of LiF and irradiated in a nuclear reactor
Oxygen	$^{12}C(d,n)^{13}N$	gases	(89)	prompt neutron time of
Nitrogen	$^{14}N(d,n)^{15}O$			flight
Carbon	$^{16}O(d,n)^{17}F$			spectrometry

V. References

[1] Hughes, D. J., Pile Neutron Research, Addison-Wesley, Cambridge, Mass., 1953.
[2] Hughes, D. J., and Schwartz, R. B., "Neutron Cross Sections", U.S. Atomic Energy Commission, Rept. BNL-325, 2nd ed., 1958.
[3] Hughes, D. J., "Neutron Cross Sections", (Intern. Series Monographs on Nuclear Energy, Div. II, Vol. I) Pergamon Press, London, 1957.
[4] Høgdahl, O. T., "Neutron Absorption in Pile Neutron Activation Analysis", MMPP-226-1 (Dec. 1962).
[5] Goldstein, H., Harvey, J. A., Story, J. S., and Westcott, C. H., "Recommended Definitions for Resonance Integral Cross Sections", European-American Nuclear Data Committee, 12 Oct. (1962).
[6] Stoughton, R. W., and Halperin, J., Nucl. Sci. Eng. 6, 100 (1959).
[7] Westcott, C. H., Walker, W. H., and Alexander, T. K., Proc. Int. Conf., Geneva, 16, 70 (1958).
[8] Westcott, C. H., "Effective Cross Section Values for Well-moderated Thermal Reactor Spectra", AECL-1101, 1960.
[9] Beauge, R., "Sections Efficaces pour les Detecteurs de Neutrons par Activation Recommandees par le Groupe de Dosimetrie d'Euratom", Euratom 1963.
[10] Drake, M. K., Nucleonics 24, Aug. (1966) 108.
[11] Flerov, N. N., and Talyzin, V. M., J. Nucl. Energy 4, 529 (1957).
[12] Friedlander, G., and Kennedy, J. W., "Nuclear and Radiochemistry", Wiley & Sons, New York (1960).
[13] Schulze, W., "Fast Neutrons in Activation Analysis", 3e Congres International de Biologie de Saclay (Sept. 1963).
[14] Neuert, H., and Pollehn, M., "Tables of Cross Sections of Nuclear Reactions with Neutrons in the 14-15 MeV Energy Range", EUR-122e Brussels 1963.
[15] Baghurst, B. P., and Prestwood, R. J., "Inorg. Nucl. Chem. 23, 173 (1961).
[16] Watt, B. F., Phys. Rev. 87, 1037 (1952).
[17] Cranberg, L., et al, Phys. Rev. 103, 662 (1956).
[18] Leachman, R. B., Proc. Intern. Conf. on the Peaceful Uses of Atomic Energy, Geneva, Vol. II, 193 (1955).

[19]   Roy, J. C., and Hawton, J. J., "Tables of Estimated Cross Sections for (n,p), (n,α) and (n,2n) reactions in a Fission Neutron Spectrum", CRC-1003 (Dec. 1960).
[20]   Anders, O. U., Anal. Chem. **34**, 1678 (1962).
[21]   Kramer, H. H., Molinski, V. J., Tilbury, R. S., Wahl, W. N., and Stier, P. M., Report NYO-10, 174, Tuxedo, New York, Sept. 1963.
[22]   Girardi, F., Guzzi, G., Pauly, J., Anal. Chem. **37**, 9, 1085-1092 (1965).
[23]   Horowitz, J., and Tretiakoff, O., "Effective Cross Sections for Thermal Reactors", EANDS(E) 14, Oak Ridge Meeting (1960).
[24]   Nisle, R., "Neutron Dosimetry", Proceedings of a Symposium, Harwell, 10-14, Dec. 1962, IAEA, Vienna, 1963, Vol. I, p. 111.
[25]   De Neve, R., De Soete, D., and Hoste, J., Radiochim. Acta **5**, 188 (1966).
[26]   Hoste, J., De Soete, D., and Speecke, A., Euratom Report, EUR-3565e, Brussels (1967).
[27]   Op de Beeck, J., J. of Radioanal. Chem. **1**, 313-323 (1968).
[28]   Heath, R. L., "Scintillation Spectrometry Gamma-ray Spectrum Catalogue", Atomic Energy Division, Idaho Falls, Idaho, August 1964, Res. and Development Report IDO-16, 880 (Vol. I and II).
[29]   Hayward, E., NBS Rad. Phys. International Report, 21 August (1961).
[30]   Engelmann, C., and Jerome, D. Y., Euratom Report EUR-3896 d-f-e(1967).
[31]   Goldhaber, M., and Hill, R. D., Rev. Mod. Phys. **24**, 179 (1952).
[32]   Huntley, H. E., Nuclear Species, McMillan (1954), Chap. XI.
[33]   Goldhaber, M., and Sungar, A. W., Phys. Rev. **83**, No. 5, 906 (1951).
[34]   Howerton, R. J., Braff, D., Cahill, W. J., and Chazan, N., UCRL Report 14006 (1964).
[35]   Hayward, E., "Photonuclear Reactions", Scottish University's Summer School (1964).
[36]   Goryachev, B. I., Atomic Energy Review **2**, 71 (1964).
[37]   Ferguson, *et al*, Phys. Rev. **95**, No. 3 (1954).
[38]   Montalbetti, R., Katz, L., and Goldemberg, J., Phys. Rev. **91**, 659 (1953).
[39]   Mann, A. K., and Halperin, J., Phys. Rev. **82**, 733 (1951).
[40]   Price, G. A., and Kerst, D. W., Phys. Rev. **77**, 806 (1950).
[41]   Carver, J. H., and Turchinet, W., Proc. Phys. Soc. **71**, 613 (1958).
[42]   Carver, J. H., Taylor and Turchinetz, W., J. Phys. **13**, 617 (1960).
[43]   Lutz, G. J., and De Soete, D., Anal. Chem. **40**, 802 (1968).
[44]   Goldemberg, J., and Marquez, L., Nuclear Physics **7**, 202 (1958).
[45]   Photonuclear Data Index, NBS Miscellaneous Publications 277 (1966).
[46]   Bethe, H., and Heitler, W., Proc. Roy. Soc. (London) **A146**, 83 (1934).
[47]   Bethe, H., Proc. Cambridge Phys. Soc. **30**, 524 (1934).
[48]   Hansen, N. E., and Fultz, S., UCRL Report 6099 (1960).
[49]   Shiff, L. I., Phys. Rev. **70**, 87 (1946).
[50]   Engelmann, C., IAEA Conf. "Radiochem. Meth. of Anal.", Progress Report Vol. I, p. 341, Vienna (1965).
[51]   Markowitz, S. S., and Mahony, J. D., Anal. Chem. **34**, 329 (1962).
[52]   Proceedings of the 2nd Conference on Activation Analysis with Charged Particles. Liege (Belgium), Sept. 21-22, 1967. Publ. by the European Communities, EUR-3896 d-f-e, Brussels (1968).
[53]   Albert, P., Proc. of the 2nd Conference on Activation Analysis with Charged Particles, EUR-3896 d-f-e, p. 3-14 (1968).
[54]   Osmond, R. G., and Smales, A. A., Anal. Chim. Acta **10**, 117 (1954).
[55]   de Geoij, J. J. M., and Houtman, J. P. W., Proc. of the 2nd Conference on Activation Analysis with Charged Particles, EUR-3896 d-f-e, p. 293-318 (1968).

[56] Konopinski, E. J., and Bethe, H. A., Phys. Rev. **54**, 130 (1938).
[57] Ghoshal, S. N., Phys. Rev. **80**, 939 (1950).
[58] Shapiro, M. M., Phys. Rev. **90**, 171 (1953).
[59] Bethe, A. A., and Livingstone, M. S., Rev. Mod. Phys. **9**, 245 (1937).
[60] Peisach, M., and Pretorius, R., Anal. Chem. **39**, 650 (1967).
[61] Peisach, M., Proc. of the 2nd Conference on Activation Analysis with Charged Particles, EUR-3896 d-f-e, p. 65-102 (1968).
[62] Holm, R. M., Briscoe, W. L., Parker, J. L., Sanders, W. M., and Parker, S. H., Proc. of the 2nd Conference on Activation Analysis with Charged Particles, EUR-3896 d-f-e, p. 239-260 (1968).
[63] Albert, P., Proc. of the 2nd Conference on Activation Analysis with Charged Particles, EUR-3896 d-f-e, p. 10-13 (1968).
[64] Curie, J., J. Phys. Radium, **13**, 33 (1952).
[65] Kohn, A., and Doumere, J., J. Phys. Radium **16**, 649 (1955).
[66] Albert, P., Annales de Chimie, 13-1, 827 (1956).
[67] Hoste, J., Bull. Soc. Chim. Belge **72**, 761 (1963).
[68] Kuin, P. M., Proc. of the 2nd Conference on Activation Analysis with Charged Particles, EUR-3896 d-f-e, p. 31-44 (1968).
[69] Ricci, E., and Hahn, R. L., Anal. Chem. **39**, 794 (1967).
[70] Engelmann, C., CRAS **258**, 4279 (1964).
[71] Engelmann, C., "Radiochemical Methods of Analysis", Conf. IAEA, Salzburg, Vol. I, 405 (1965).
[72] Chevarier, N., Giroux, J., Duc, T. M., and Tousset, J., LYCEN/6714 (1967).
[73] Markowitz, S. S. and Mahony, J. D., Anal. Chem. **34** (3), 329 (1962).
[74] Markowitz, S. S. and Mahony, J. D., I.A.E.A. Symposium "Radiochemical Methods of Analysis", Proc. Vol. I, p. 419 (1964).
[75] Ryan, V., Green, J. L., and Löwenhaupt, E. H., U.S.A.E.C. Rpt UCRL-11618 (1964).
[76] Demildt, A. C., Anal. Chem. **35**, 1228 (1963).
[77] Holm, D. M., Briscoe, W. L., Parker, J. L., Sanders, W. M., and Parker, S. H., EURATOM Symposium "Practical Aspects of Activation Analysis with Charged Particles", Liège (Belgium), Proc. p. 239 (1967).
[78] Revel, G., and Albert, P., EURATOM Symposium "Practical Aspects of Activation Analysis with Charged Particles", Liège (Belgium), Proc. p. 261 (1967).
[79] Barrandon, J. N., Debrun, J. L., and Albert, P., EURATOM Symposium "Practical Aspects of Activation Analysis with Charged Particles", Liège (Belgium), Proc. p. 277 (1967).
[80] Albert, P., Modern Trends in Activation Analysis, College Station, Texas (U.S.A.), Proc. p. 78 (1961).
[81] Engelmann, C., I.A.E.A. Symposium "Radiochemical Methods of Analysis" Proc., Vol. I, p. 405 (1964).
[82] Schuster, E., and Wohlleren, K., EURATOM Symposium "Practical Aspects of Activation Analysis with Charged Particles", Liège (Belgium), Proc. p. 45 (1967).
[83] Albert, P., Chaudron, G., and Sue, P., Bull. Soc. Chim. France, 97 (1953).
[84] Engelmann, C., J. Appl. Rad. Isotopes, **18**, 569 (1967).
[85] Engelmann, C., and Cabane, G., Modern Trends in Activation Analysis, College Station, Texas, Proc. p. 331 (1965).
[86] EURATOM Symposium "Practical Aspects of Activation Analysis with Charged Particles", Liège (Belgium), Proc. p. 31 (1967).
[87] Osmund, R. H., and Smales, A. A., Anal. Chim. Acta **10**, 117 (1954).

[88]   de Goeij, J. J. M., and Houtman, J. P. W., EURATOM Symposium "Practical Aspects of Activation Analysis with Charged Particles", Liège (Belgium), Proc. p. 293 (1967).

[89]   Peisach, M., EURATOM Symposium "Practical Aspects of Activation Analysis with Charged Particles", Liège (Belgium), Proc. p. 65 (1967).

USE OF CHARGED PARTICLES AND PHOTONS

Synopsis of Discussions

CHARLES ENGELMANN, *Chairman*

Center for Nuclear Studies
Saclay, France

The principle results of the several papers presented in the two charged particle and photon activation analysis sessions and their discussion may be summarized as follows:

1. The calibration problem appears to be very important and difficult in activation analysis with charged particles. Only one method takes into account the several phenomena existing in this particular activation technique. This method is proposed by Rook *et al.* The authors assume that a well defined activation curve determined experimentally in a matrix can be transformed into the corresponding activation curve of any matrix by using a differential range-energy relationship. The fundamental results from the beam study by Duc *et al* agrees with this point of view. They are showing that the straggling is in first approximation similar for every matrix. Therefore, this method is probably the only one which can allow very precise measurements. Let us remember that this method is entirely experimental and takes into account the particular energy spread of the beam from the accelerator.

2. A very important study in connection with the use of charged particles in activation analysis of single crystals appears in a paper by Ricci. Ricci has studied the influence of channeling in customary ^{3}He activation analysis. From his paper it is pointed out that such effects cannot generally influence the customary methods. On the other hand, he concluded that it is apparent from his experience, that detailed studies of impurity locations by channeling will have to rely on complex equipment. Thus, no high sensitivity determination of light elements in single crystals may be feasible in the near future.

However, we must point out that some people are using this method, and they obtain some interesting results. Probably in a few years, many studies which use this particular technique will appear in the literature.

3. Some very interesting results concerning oxygen, carbon, and sulfur determinations are summarized by Albert *et al.* P. Albert's group has studied the interference of fluorine with oxygen determinations and the interference of beryllium and oxygen with carbon determinations up

to 30 MeV with ^{3}He and 55 MeV with ^{4}He. But the most important result concerns the possibility of sulfur determination by proton activation without interference. In fact, by all other activation methods, sulfur determination in the ppb range is very difficult because of the interference from phosphorus and chlorine.

In another paper the possibility of deuteron activation for the determination of oxygen is discussed. It appears that in comparison with ^{3}He and ^{4}He activation, deuterons are not too useful for this type of analysis. The interference from fluorine is too high and the sensitivity is much lower.

4. Charged particles at very low energies may also be used for the determination of oxygen and carbon present at the surface of metals. Triton activation appears to be a very good method for oxygen determination in the range of 100 to 10^{-3} μg/cm^2. ^{3}He activation can be used for the simultaneous determination of carbon and oxygen.

However, for very precise measurements precautions must be taken because the surface can be contaminated during the irradiation by the residual oxygen and carbon atoms in the accelerator volume. Also, in some cases where the beam intensity is very high (a few μA or more), the surface composition can be modified by evaporation or some other mechanism which is correlated with thermochemical or nuclear effects.

5. The papers presented in this second session show for the first time practical results concerning C, N and O determinations in the ppb range. This has been done by Dr. Nozaki's group using silicon, by Dr. Albert's group and by our own group using metals (e.g. iron, niobium, and germanium).

^{3}He and ^{4}He activation provide almost the same sensitivity, but the use of ^{3}He activation for the nondestructive analysis in a real solid material presents some difficulties because an inevitable fluctuation in the etching thickness causes variation and uncertainty in the final result.

When using these two particles, it must be pointed out that it is not possible to eliminate interference from fluorine by selection of the irradiation energy; however, this may be done by proton activation. Therefore, a preliminary fluorine determination must be done by another method such as photon activation analysis.

6. The simultaneous separation of nitrogen-13 and carbon-11 by a technique similar to inert gas fusion appears to be a very interesting method for carbon and nitrogen determination in pure metals by photon activation. The possibility of oxygen-15 separation by reduction fusion is also an important separation step in the activation analysis field.

7. In connection with photon activation, it must be pointed out that the beam monitoring problems are very important. The shift in the energy distribution does not allow the use of internal standards if standard and impurity to be determined in the sample do not have exactly the same

threshold and the same shape of excitation curve. In addition, heating of the sample in a photon flux produced by high electron beam intensity appears to be a serious problem.

It appears that in photon activation analysis, it is necessary to limit the maximum energy to about to 30 to 35 MeV because some interfering reactions exist at higher energies. For example, nitrogen and oxygen can cause uncertainty in the carbon determination and oxygen interferes with the nitrogen determination.

8. In general, photon activation is much easier to use for the determination of low concentrations of light elements than charged particles. It is important to remember that if charged particles are used, it is absolutely necessary that the impurity is homogeneously distributed in the sample. This is not necessary if photon activation is applied because the activation is more uniform in the sample when its thickness is adjusted in connection with the flux absorption as pointed out by G. Lutz. However, we must also take into account the flux distribution within the sample because the longitudinal and transverse gradient is as important as the photon absorption effect in heavy metals and much more important than absorption in medium and light weight metals.

9. A particular application of photon activation analysis is the use of (γ,γ') reaction as proposed by H. R. Lukens. This method appears to be very interesting and useful for the nondestructive determination of some elements in various matrices.

In conclusion, the standardization in charged particles and photon activation is certainly more difficult than in neutron activation. However, only charged particle and photon activation allow the determination of light elements at very low concentrations, e.g. in the ppb range, and these determinations appear to be absolutely necessary in connection with solid state and physical metallurgical studies.

Let us advise again that many interfering reactions exist in charged particle activation. Of course, in this case it is necessary to be very careful in reporting sensitivity. Only practical results obtained in the ppb range are able to confirm the desired light element sensitivity indicated above.

The experiences during the last few years have effectively shown that several interfering reactions result from the matrix. This is particularly the case for oxygen determinations in aluminum as related by Albert and in silicon as related by Tousset and Nozaki.

Photon activation analysis is more direct and reliable than charged particle analysis because it is always possible to eliminate interfering reactions through choice of the maximum beam energy.

STUDY OF A BEAM OF CHARGED PARTICLES; THEIR SLOWING DOWN, AND THEIR ENERGY DISTRIBUTION IN A THICK, COMPLEX TARGET FOR ACTIVATION ANALYSIS

Minh Duc Tran and Jean Tousset

Institut de Physique Nucleaire
Faculte des Sciences de Lyon
Lyon, France

I. Introduction

The application of excitation functions to charged particle activation analysis requires a knowledge of the parameters of the particular beam used and of the way in which these parameters change as the beam traverses the target material. We have developed methods which permit us to measure the energy and the resolution of a beam and to determine the loss of energy and of resolution (straggling) in a complex chemical compound for which one may fear that the tables give values that are too approximate. A mathematical treatment of the stopping power and energy distribution data provides a correction factor, K, which allows us to calculate the true excitation function and to convert this into an activation curve for a thick target.

II. Energy and Resolution of the Beam

A. External Beam

The energy of the external beam of the Lyon synchrocyclotron is determined from its range in aluminum [1]. The mean ranges are: $R_o = 291$ mg/cm² with alpha particles; $R_o = 572$ mg/cm² with deuterons. These correspond to energies of 54.4 and 27.0 MeV, respectively [2].

A scattering chamber (Figure 1) is used to measure the beam resolution. The current, i, passing through the coils of a bending magnet determines the fraction of the beam which enters this chamber, is scattered by a thin gold foil target and is analyzed by a surface barrier detector. By varying the value of i, we successively analyze the several fractions of the total beam (Figure 2). The full energy width at half maximum (FWHM) of the α-particle beam is 2.1 ±0.2 MeV; that of the deuteron beam is 1.0 ±0.1 MeV. If the beam is passed through a circular
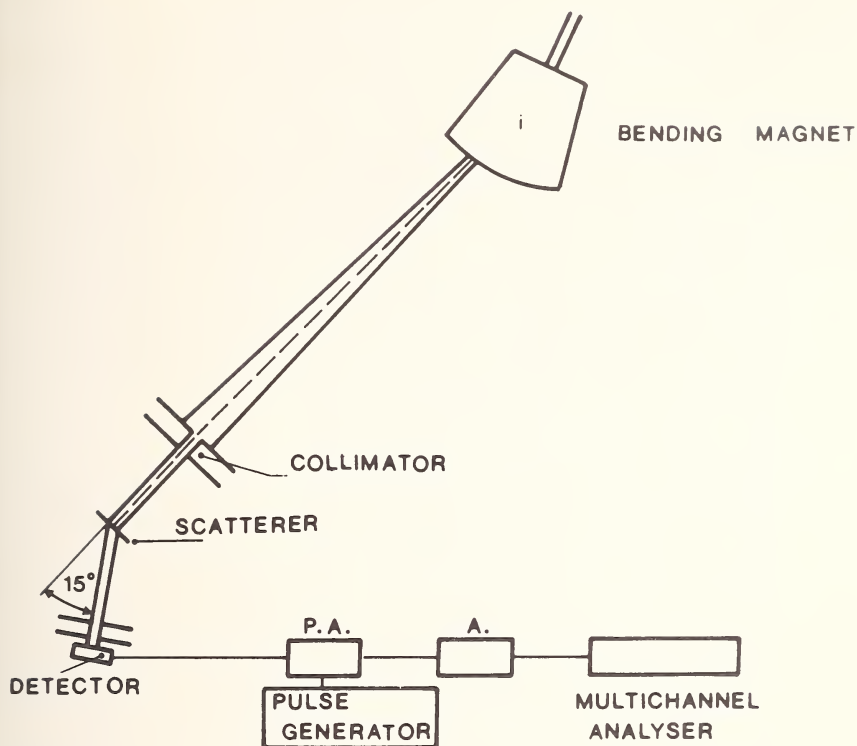
Figure 1.   Scattering chamber used for measuring the beam resolution. The values of the current, i, in the bending magnet determine the fractions of the beam admitted into the scattering chamber.

diaphragm of 1 cm diameter placed between the focusing and bending magnets, these values are reduced to 0.75 ±0.10 and 0.35 ±0.05 MeV, respectively [3].

B. Internal Beam

The internal beam was studied by an activation method based on the variation with energy of the ratio of (α,xn) or (d,xn) cross sections [4]. If one has measured energy sensitive cross section ratios by a previous experiment with a well defined external beam, he can determine the energy of the particles striking an internal target by measuring the ratios of the product formed in different parts of this internal target.

With the deuteron beam, we use the reactions on terbium (Figure 3). We placed the leading edge of the Tb foil just inside the cyclotron radius corresponding to maximum deuteron energy and measured the average
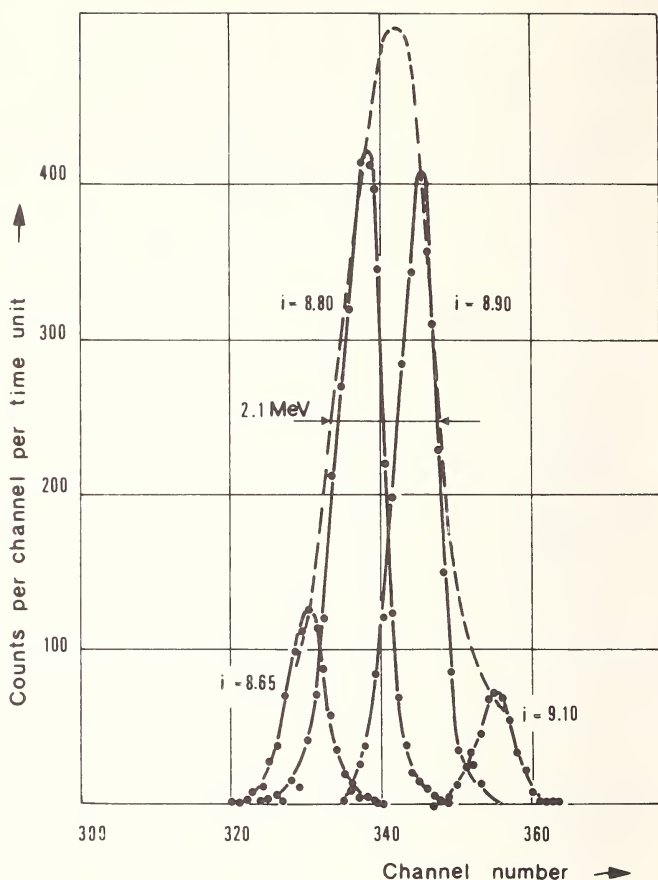
Figure 2.   Shift of the scattering peaks for different values of the current, *i*, in the bending magnet. The dotted line joining the peaks gives the beam resolution.

deuteron energy along the foil by cutting segments of the foil and analyzing product ratios. The mean energy of the deuterons varied between 22.5 and 23 MeV (Figure 4). With the alpha beam, the study made by means of (α,xn) reactions on gold [5] indicates an average energy of 44.5 MeV for the alphas striking an internal target at the maximum radius of irradiation.

These measured values are 20% below the theoretical values defined by the radius (28.5 MeV and 57 MeV). Because these mean energies vary very little along the length of the irradiated area, the specific activity in each target segment determines the beam current along the target. The decrease in activity is exponential, corresponding to:

$$I = I_o e^{-Kd}$$
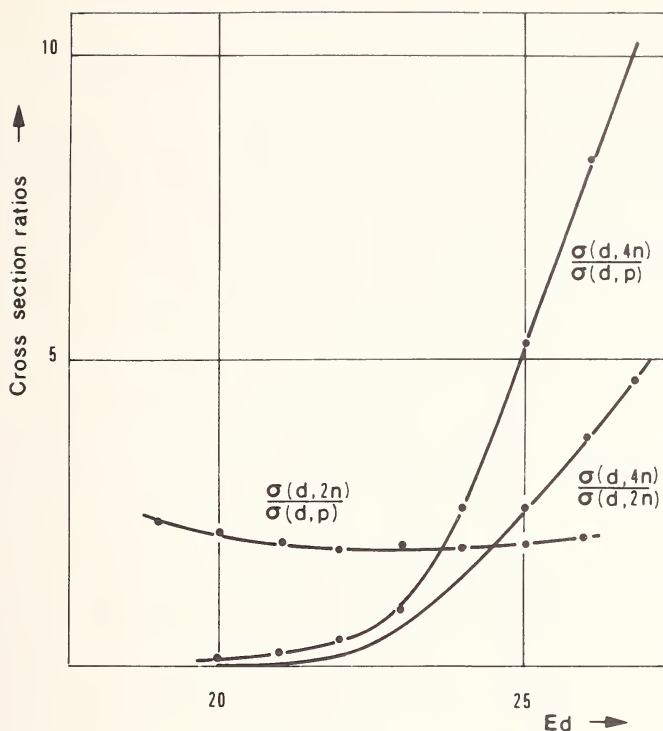
Figure 3. Cross section ratios for deuteron reactions about terbium, measured with the external beam.

where I_o is the beam flux at the leading edge and I the flux at distance d from the edge. Therefore we define $K = 0.693/d_{1/2}$ [4], where $d_{1/2}$ is the distance at which $I = I_o/2$. The small values of K found for the internal beam (Figures 5 and 6) of the Lyon synchrocyclotron show that the irradiated surface is very large.

III. Stopping Power and Energy Loss

The stopping power for a chemical compound is given by:

$$\left(\frac{\mathrm{d}E}{\mathrm{d}x}\right)_T = \sum_{i=1}^{n} N_i \left(\frac{\mathrm{d}E}{\mathrm{d}x}\right)_i$$

where N_i is the percentage by weight of each element of the compound and $\left(\frac{\mathrm{d}E}{\mathrm{d}x}\right)_i$ is the stopping power of the element. The range in the
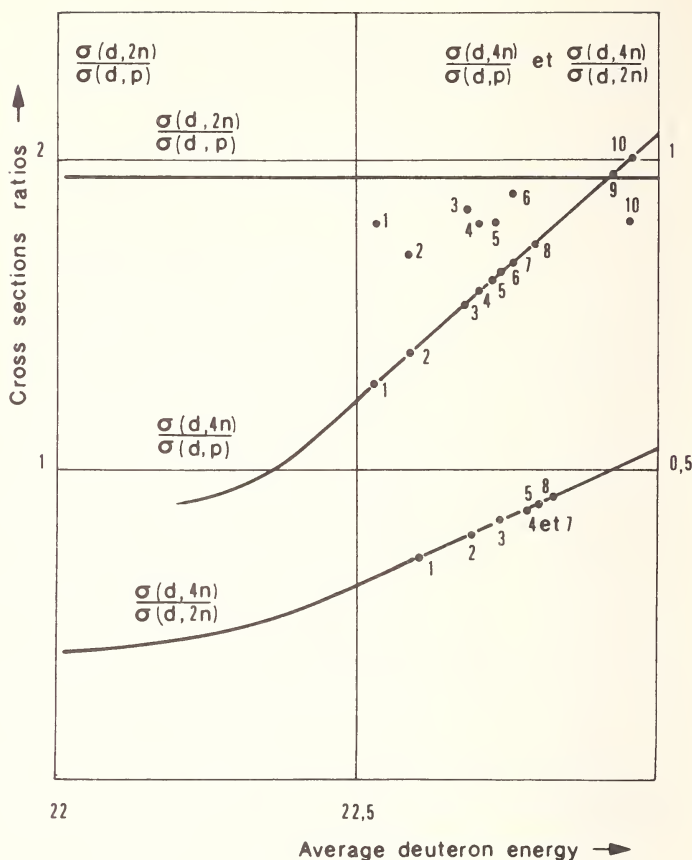
Figure 4.   Measurements of deuteron average energy upon an internal target. The points
            are the cross section ratios measured for different slices of the internal target
            plotted against the curves obtained with external beam. They give the energy of
            the particles striking each slice.

compound is also calculated from the individual ranges R_i in each
element:

$$\frac{1}{R_T} = \sum_{i=1}^{n} \frac{N_i}{R_i}$$

The experimental method is based on the direct measurement of deuteron
and alpha beam mean energy losses. We use the beam scattered by a thin
gold target with an interposed absorber [6]. The Figures 7 and 8 present
the experimental data of energy loss in Teflon and Mylar. The theoretical
curve is calculated from the data given by Williamson et al [2].
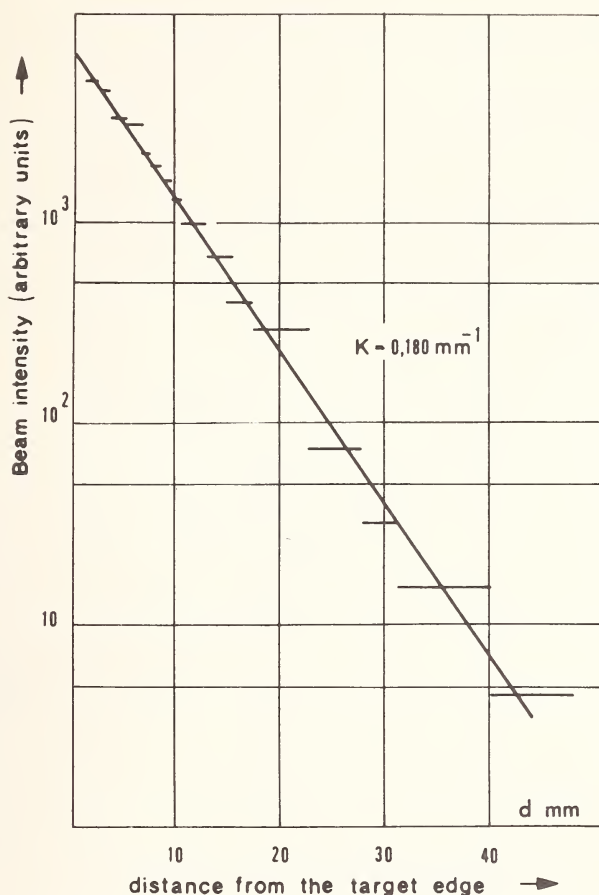
Figure 5. Variation of the beam intensity along the internal target for alpha irradiation.

The experimental stopping powers are determined by two measurements of energy losses, ΔE_1 and ΔE_2, for two close thicknesses e_1 and e_2:

$$\left(\frac{dE}{dx}\right)_E = \frac{\Delta E_1 - \Delta E_2}{e_1 - e_2}$$

with $E = E_0 - \dfrac{\Delta E_1 + \Delta E_2}{2}$ E_o is the initial energy.

The Figures 9 and 10 give values of stopping power in Teflon and Mylar.

IV. Straggling

The broadening of peaks when the beam traverses matter is due to the straggling phenomenon. Since the distributions can be fitted to Gaussian
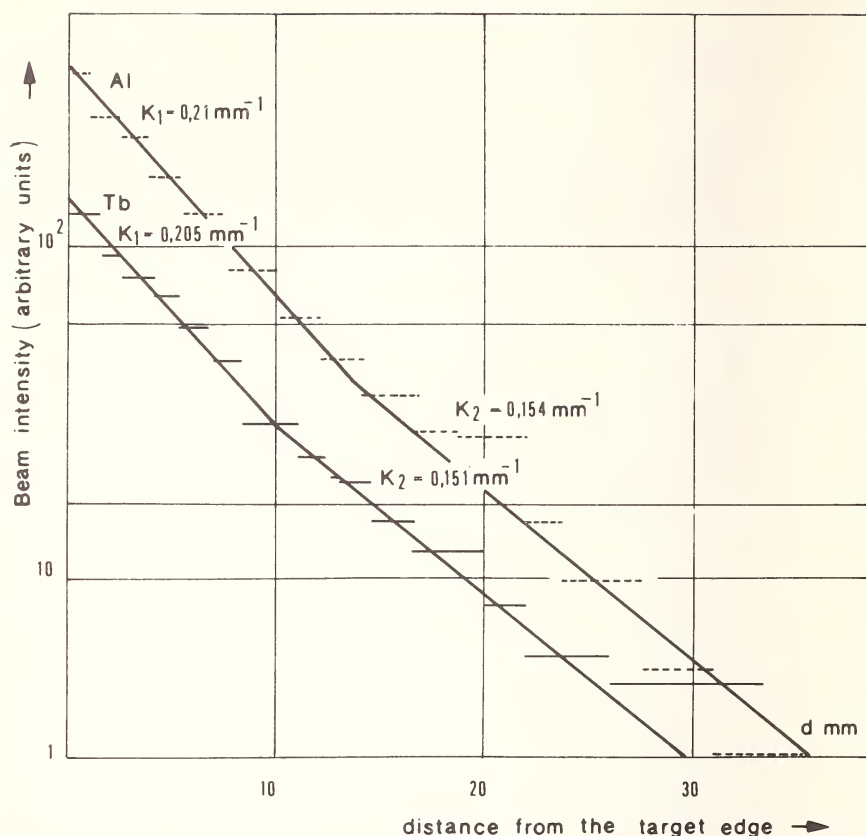
Figure 6.   Variation of the beam intensity along the internal target for deuteron irradiation.

distributions, the energy straggling may be obtained from the difference of the widths:

$$\Omega_s^2 = \Omega^2 - \Omega_0^2$$

We have measured Ω_s for Teflon and Mylar and have plotted these values with others found for some elements [3]. The values for Mylar and Teflon which are light elements compounds (H, C, O, F) are slightly smaller (Figure 11).

V.   Excitation Functions and Activation Curves

When a charged particle beam traverses a target containing n atoms per mg of thickness, l (expressed in mg per cm^2), the number of created atoms is given by the relation: ·

$$N = \Phi n \int_0^l \sigma_x \, \mathrm{d}x \qquad (1)$$
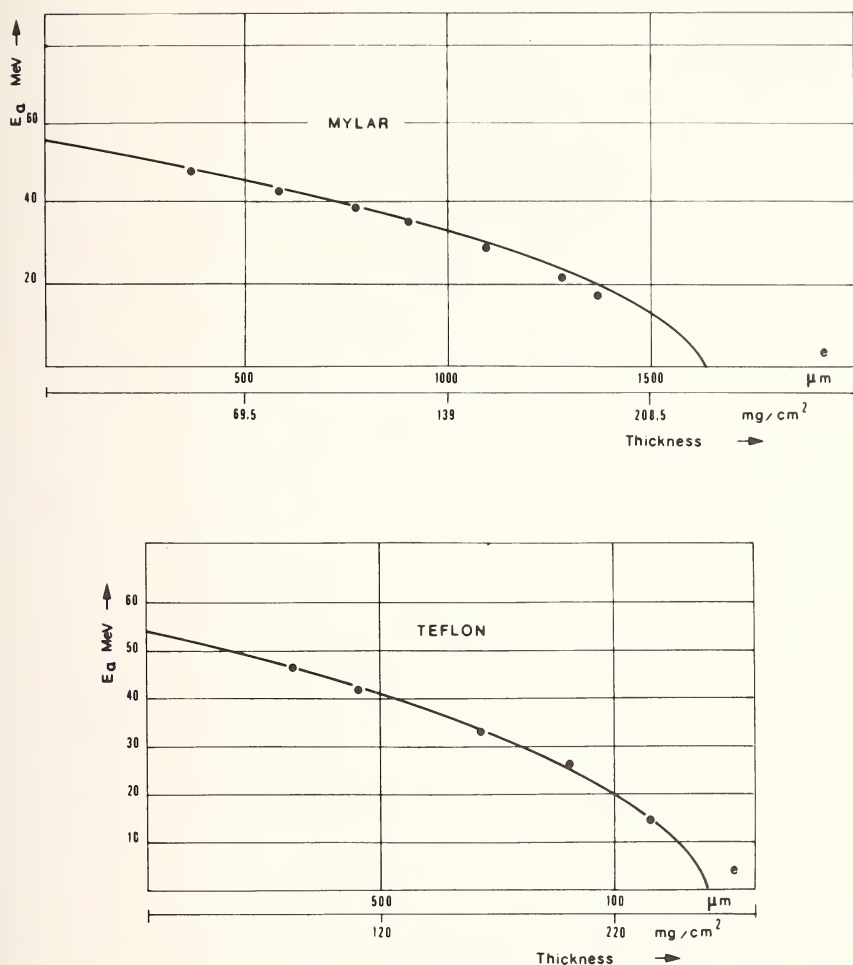
Figure 7. Energy losses in Mylar and Teflon for 54.4 MeV alphas. The theoretical curves are calculated according to the formula with weight percentage and ranges tables of Williamson *et al* [2].

Φ is the number of particles striking the target per second; σ_x is the value of the reaction cross section at the distance x. Experimentally, the integration of this relation leads to an activation curve defined by values of experimental cross sections:

$$N = \Phi \sigma_{\exp} n l \qquad (2)$$

In this integration [2] the beam energy loss through the target is not considered, nor is the energy distribution of the beam. At the distance, x,
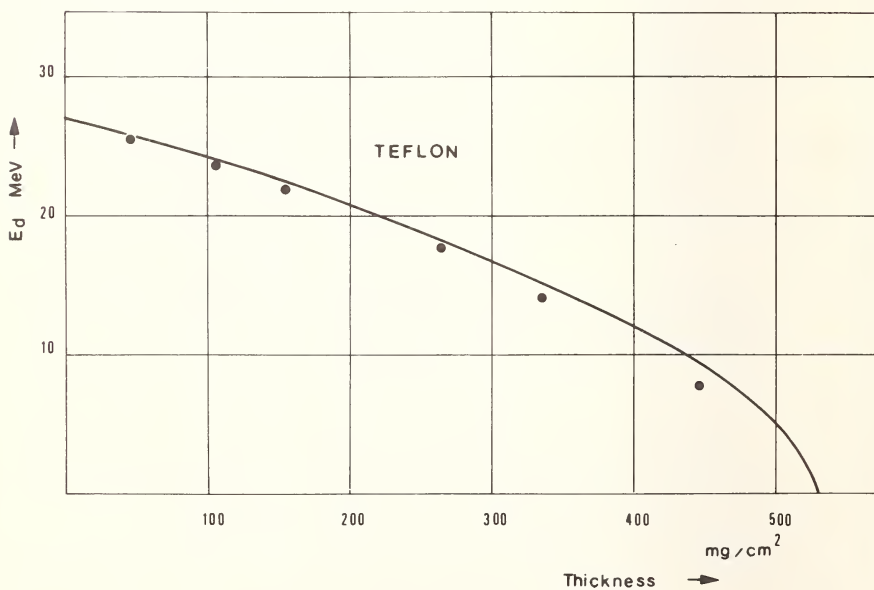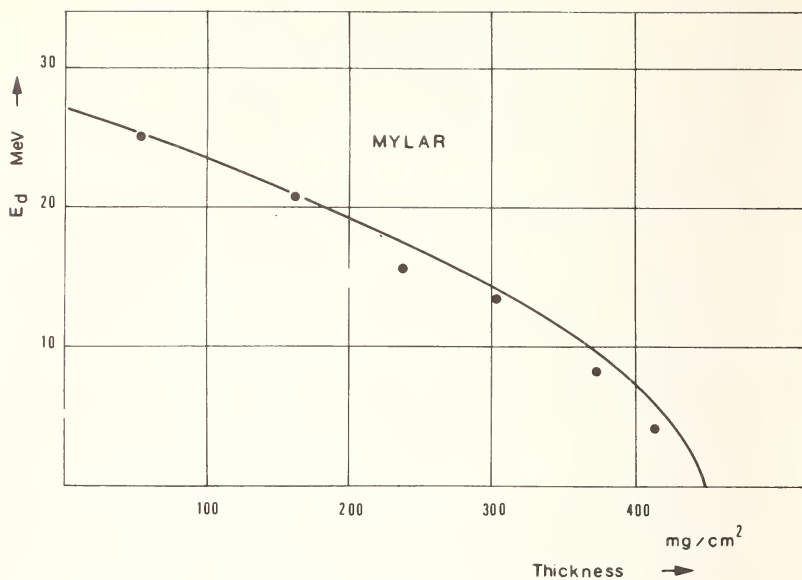
Figure 8.   Energy losses in Mylar and Teflon for 27 MeV deuterons.
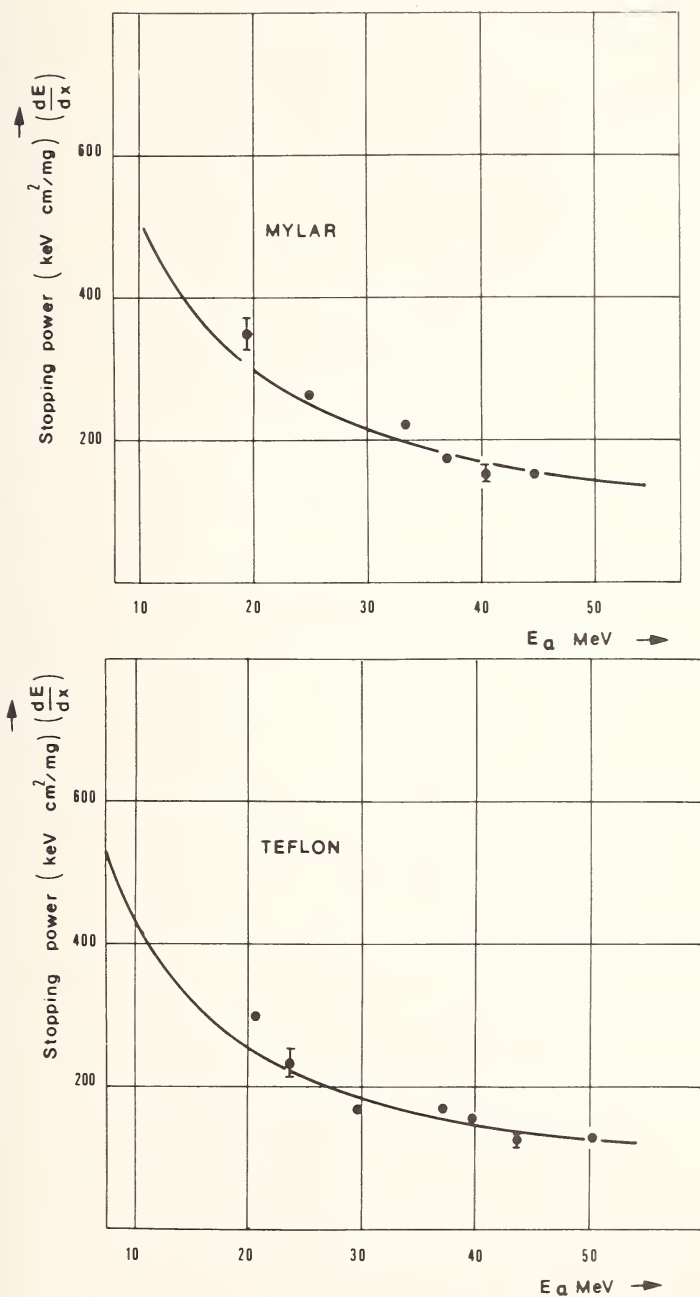
Figure 9.   Stopping powers for alphas in Mylar and Teflon. The theoretical curves are computed according to the formula with weight percentage and stopping powers tables of Williamson *et al* [2].
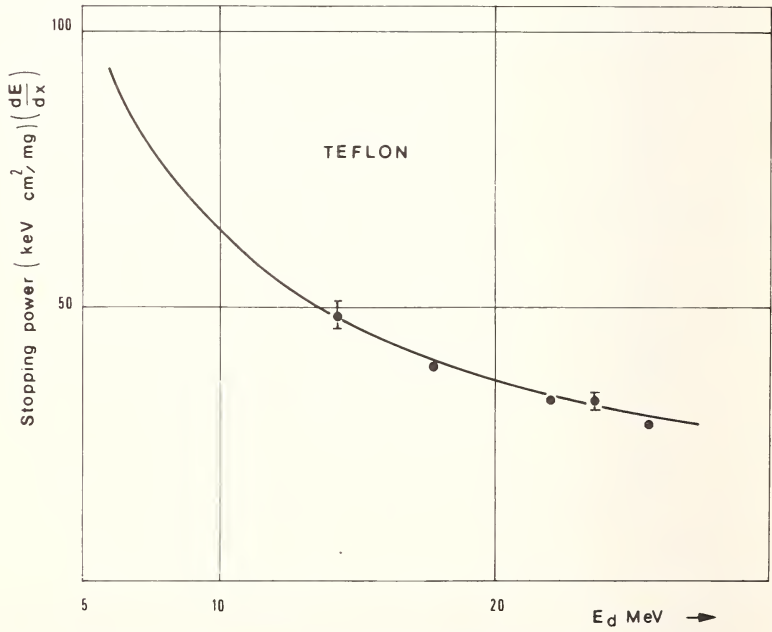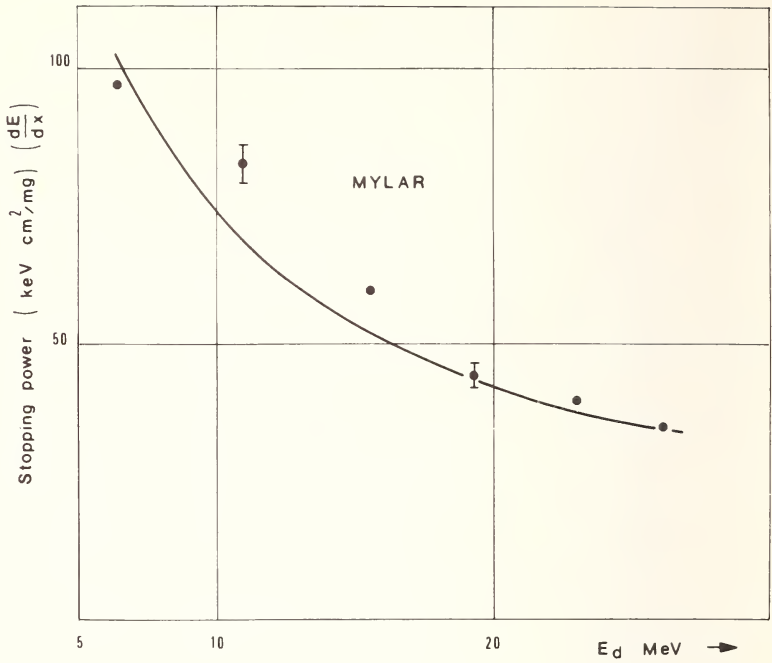
Figure 10.   Stopping powers for deuterons in Mylar and Teflon.
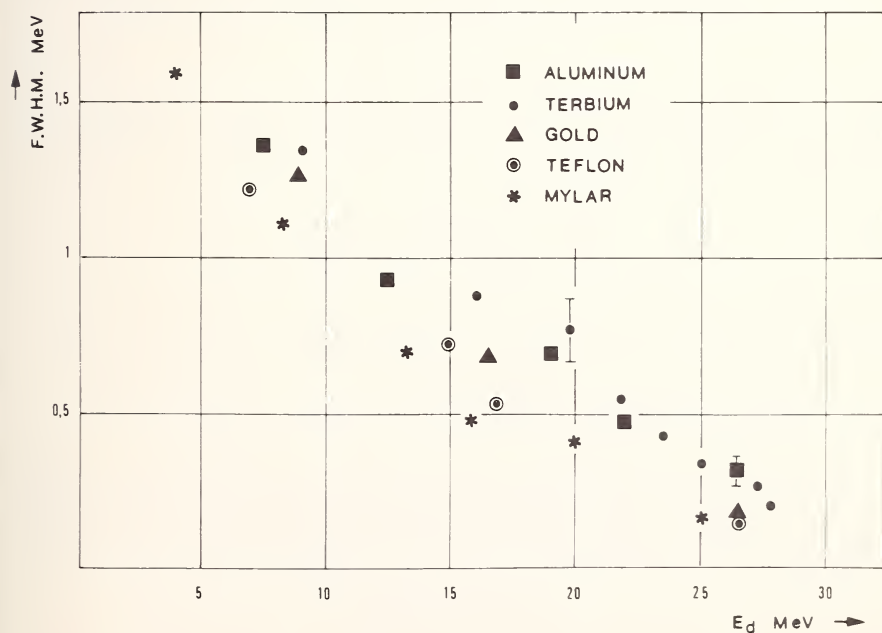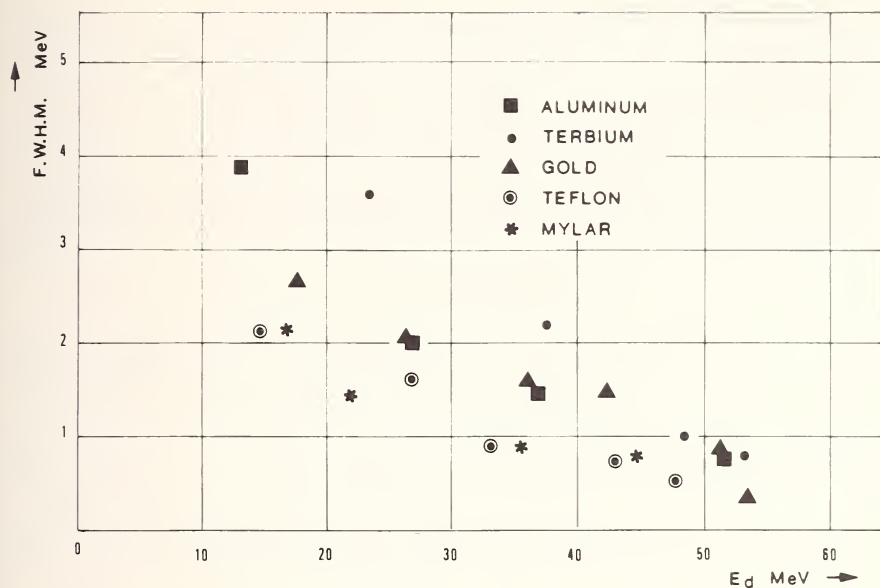
Figure 11.   Full width at half maximum due to straggling phenomenon versus the residual energy for 54.4 MeV alphas and 27 MeV deuterons.

the beam shows a Gaussian form energy distribution around the mean value $\bar{E}_x$ with a variance s^2.

$$P(E)\,dE = \frac{1}{s\sqrt{2\pi}}\,e^{-\frac{(E-\bar{E}_x)^2}{2s^2}}\,dE \tag{3}$$

σ_x then represents the mean value of cross sections, σ_E, corresponding to this distribution.

$$\sigma_x = (\bar{\sigma}_E)_x = \frac{\int_{-\infty}^{+\infty}\sigma_E P(E)\,dE}{\int_{-\infty}^{+\infty}P(E)\,dE} = \left[\int_{-\infty}^{+\infty}\sigma_E P(E)\,dE\right]_{\bar{E}_x} \tag{4}$$

The equation (1) is written now with the variable $\bar{E}_x$:

$$N = \Phi n \int_{\bar{E}_i}^{\bar{E}_f}\frac{dx}{d\bar{E}_x}\,d\bar{E}_x\left[\int_{-\infty}^{+\infty}\sigma_E P(E)dE\right]_{\bar{E}_x} \tag{5}$$

The borders $\bar{E}_i$ and $\bar{E}_f$ are the initial and final mean energy in the target. If s is assumed to be constant through the target, the integration of the expression [5] in the particular and most frequent case of an exponential variation of the excitation function around the reference σ_{E_R} gives

$$\sigma_E = \sigma_{E_R}e^{\alpha(E-E_R)}$$

and with the approximation of an energy loss inversely proportional to the energy

$$\frac{dE}{dx} = \frac{1}{aE}\text{ with }a = \frac{2l}{\bar{E}_f^2 - \bar{E}_i^2}$$

leads to a term correcting the values of experimental cross section, σ_{exp}:

$$\frac{\sigma_{\bar{E}_0}}{\sigma_{\exp}} = \frac{1}{e^{\alpha^2 s^2 2}}\frac{\alpha^2(\bar{E}_f^2 - \bar{E}_i^2)e^{\alpha\bar{E}_0}}{2[(\alpha\bar{E}_f - 1)e^{\alpha E_f} - (\alpha\bar{E}_i - 1)e^{\alpha E_i}]} \quad : \quad \bar{E}_0 = \frac{\bar{E}_i + \bar{E}_f}{2}$$

Our other paper [7] in this conference will show the application of this correction factor to the excitation function of deuteron induced reactions on oxygen and fluorine. This factor will be important only for large energy losses.

VI. Conclusion

We have established methods which permit us to define the parameters of a charged particle beam, *i.e.* energy and distribution, which are useful

for activation analysis. We have indeed pointed out that the average energy may change for the same synchrocyclotron between the different irradiation positions which theoretically should give the same energy. The values of energy loss in a light element compound can be calculated accurately enough with a weight percentage formula from tables. Elsewhere, we have introduced a term which connects excitation function and activation curves by taking into account energy loss and straggling data.

VII. References

[1] Suraqui, S., These Docteur Ingenieur, Universite Lyon (1967).
[2] Williamson. C. F., Boujot, J. P., and Picard, J., C.E.A R. 3042 (1966).
[3] Tran, Minh Duc, These Docteur Ingenieur, Universite Lyon (1968).
[4] Le Beyec. Y., Lefort, M., and Tarrago, Y., J. de Phys. **24**, 157A (1963).
[5] Chevarier, N., Giroux, J., Tran, Minh Duc, and Tousset, J., Bull. Soc. Chim. **8**, 2893 (1967).
[6] Tran, Minh Duc, Demeyer, A., Tousset, J., and Chery, R., J. de Phys. **29**, 129 (1968).
[7] Tran, Minh Duc, Chenaud, A., Giron, H., and Tousset, J. (See this volume, p. 811.)

RANGE TRANSFORMATION OF ACTIVATION CURVES AND THEIR APPLICATION TO QUANTITATIVE CHARGED PARTICLE ACTIVATION ANALYSIS

H. L. Rook, E. A. Schweikert, and R. E. Wainerdi

Activation Analysis Research Laboratory
Texas A & M University
College Station, Texas 77843

I. Introduction

In contrast to neutron and photon activation, where in most cases the activation cross section is assumed to be constant throughout the irradiated material, in charged particle activation analysis, the activation cross section varies continuously with the energy degradation of the bombarding particle in matter. Accordingly, a quantitative analytical procedure using charged particle activation must account for the nonuniform activation of a sample. Different possible solutions for quantitative analysis in charged particle activation analysis have been devised [1-5]. Their merits and limitations have been discussed by Chevarier *et al* [6], who have also shown the particular advantages of the "equivalent thickness" method proposed by Engelmann [5]. The principle and the features of this method have been discussed in detail elsewhere [5-8]. It need only be recalled here that this method is based on an experimentally established activation curve for a given nuclear reaction in a given matrix material.

When considering the application of charged particle activation for the determination of trace elements in a large variety of matrices using different nuclear reactions, the establishment of the corresponding activation curve for each analytical case becomes a tedious task.

A solution to this problem is presented in this study which shows that a complete, well defined activation curve, determined experimentally in a matrix, can be transformed into the corresponding activation curve of any matrix by using a differential range-energy relationship. An obvious advantage of this method is that since an activation curve for a given reaction need only be established once, more effort can be devoted to the curve to insure its quality. Subsequent quantitation will therefore rely on more precise "equivalent thickness" values which are derived from the activation curves. The construction of a synthetic activation curve from

an experimental one will be presented here using the activation curve for $^{16}O(\alpha,pn)^{18}F$ with α particles of 40 MeV.

II. Experimental

Mylar, mica and aluminum foils, in stacks thick enough to absorb the entire beam, were irradiated using the external beam of the 88 inch variable energy sector focused cyclotron at Texas A&M University. Thicknesses of the Mylar and aluminum foils were of 12.7 μm. The thickness of mica foils was determined individually by weighing on a micro-analytical balance and assuming a uniform surface (average thickness for a mica foil was ~10 μm)

Counting of the positron annihilation radiation of ^{18}F was performed on a gamma-gamma coincidence counting system coupled to an automatic sample changer. The foils were counted in sequence until a minimum of five counts per half life component present was obtained. The data coupled with the proper timing sequence were resolved into individual half life components and decay corrected to the time at the end of irradiation (t_o) using the least square computer routine developed by J. B. Cummings [9].

To obtain an activation curve, the specific activity at t_o for each foil was divided by that at 39.0 MeV, giving the activity ratio, ρ. The foils between 39.0 and 40.0 MeV being discarded due to recoil effects. Thus, an activation curve was obtained which gives the relative cross section as a function of thickness.

Experimentally determined activation curves for the $^{16}O(\alpha,pn)^{18}F$ reaction in a matrix of mica and Mylar were used to test the method of range transformation. Differential range-energy tables with a one MeV step function of energy were constructed for Mylar and mica from those published for pure elements by Williamson, Boujot, and Picard [10]. These were constructed by taking a weighted sum of the elemental ranges where the weighting factors used were the fractional chemical composition of the foils. The transformation between mica and Mylar was carried out by taking a thickness of Mylar, multiplying by the density to obtain a range, calculating the related energy from the range-energy table by linear interpolation. The energy in Mylar was equated to the energy in mica whereby the theoretical range in mica was calculated, again by linear interpolation, which was converted to a thickness of mica by dividing by the density. This range transformation was carried out for each point on the Mylar curve, giving as a result, an activation curve valid for a mica matrix which was experimentally determined using Mylar. This curve was compared with an activation curve experimentally determined in mica.

III. Results and Discussion

The range of a charged particle in matter is given by the expression

$$\int_0^E \frac{1}{dE/dx}$$

dE where dE/dx is the stopping power. Stopping powers have been tabulated in conjunction with energies and ranges in many tables. These values have generally been calculated from theoretical equations but are found to be valid within the limit of errors found among published experimental data [11].

The stopping power of a mixture or compound can be calculated from the sum of the fractional stopping powers of the individual components This simple relationship is not strictly valid for ranges since the range is the integral of the reciprocal of the stopping power. However, if differential range-energy tables are constructed for the compound or mixture from range-energy tables for pure elements, using the fractional composition, the ranges obtained are valid above 1 MeV. Below 1 MeV the errors are not serious since the cross sections are negligible for almost all the analytically important reactions due to coulombic considerations.

The validity of employing elemental range-energy tables to construct compound tables was tested by constructing, for Mylar, a range-energy
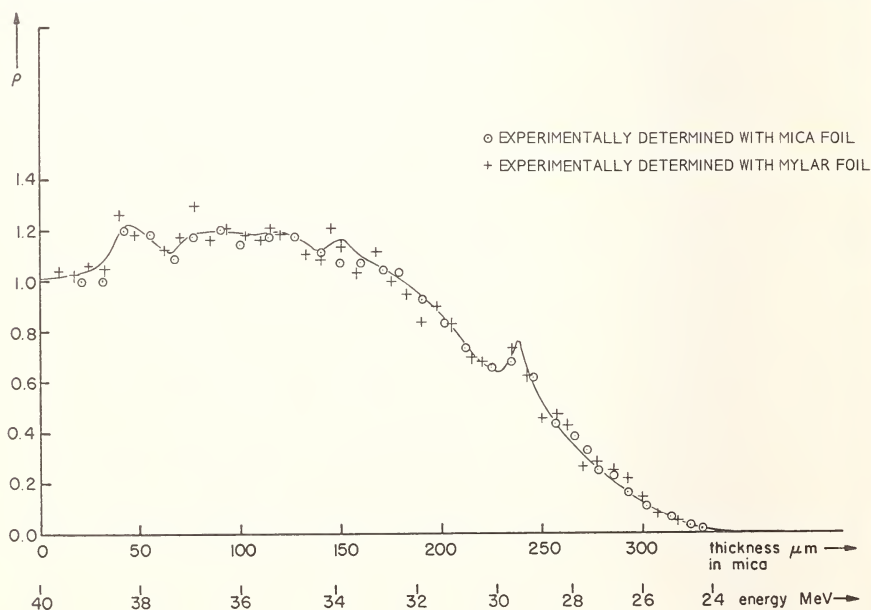
Figure 1.　Activation cross section *vs.* thickness for mica matrix: $^{16}O(\alpha,pn)^{18}F$.

table which was calculated by numeric integration of the reciprocal stopping powers. There was no significant discrepancy, for energies from 1 to 40 MeV, when energy intervals of 1 MeV were used.

The method of range transformation of activation curves was verified by constructing the activation curve for the $^{16}O(\alpha,pn)^{18}F$ reaction in a mica matrix from an activation curve experimentally determined in Mylar. This synthetic curve was compared to a curve experimentally determined in a mica matrix. As shown in Figure 1, there is excellent agreement between the activation curves.

A similar experimental curve on high purity aluminum foils, when compared to that of a synthetically constructed curve in aluminum, showed that besides the ^{18}F due to oxygen in the superficial Al_2O_3 layers of each foil, ^{18}F was also produced by a reaction apparently occurring on aluminum with α particles of $E \geqslant 33.4$ MeV. The interference due to aluminum was resolved and weight corrected as shown in Figures 2 and 3, respectively. This is in agreement with a similar observation made earlier by Albert [8].
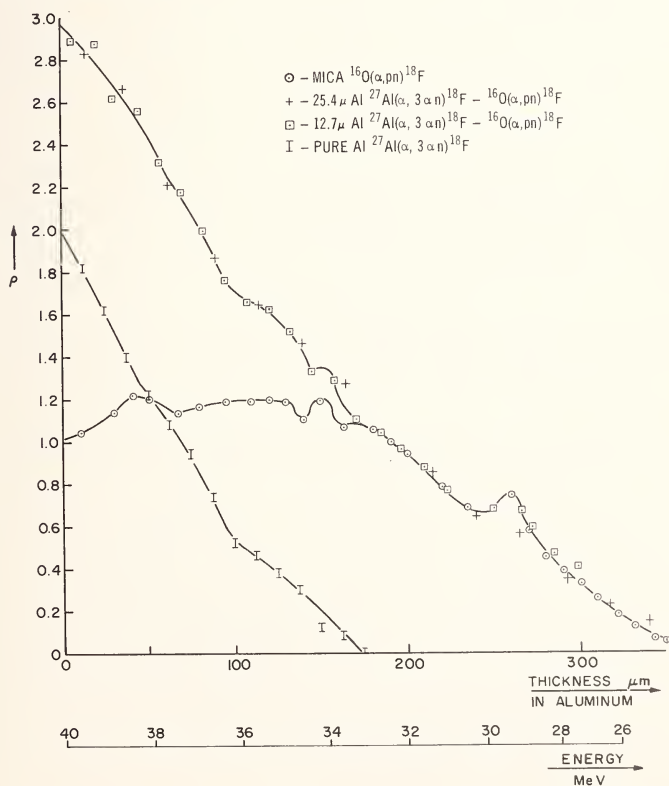
Figure 2. Interference due to aluminum on the reaction of $^{16}O(\alpha,pn)^{18}F$.
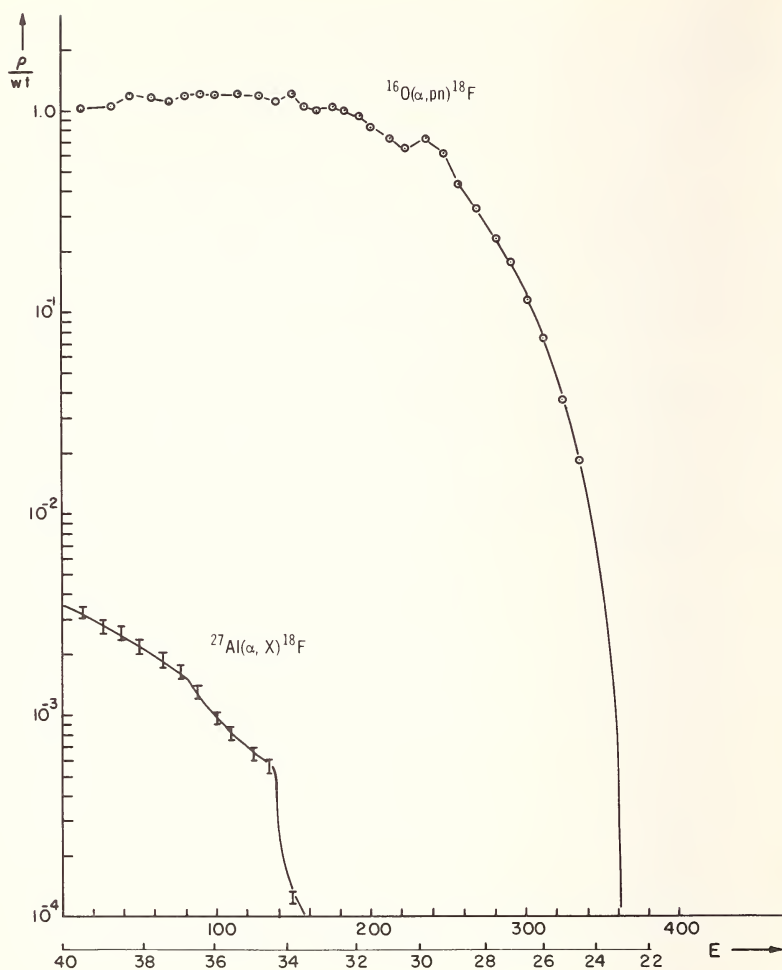
Figure 3.   Weight corrected aluminum interference on the reaction $^{16}O(\alpha,pn)^{18}F$.

Detailed activation curves can be constructed for any matrix of interest through the conversion of a single well defined experimental activation curve using differential range-energy tables calculated from those available on pure elements. Since the range transformation requires a point by point calculation of the corresponding thickness in the activation curves where there may be 200 or more points, the procedure lends itself readily to a computer calculation. A program is now being written which will construct the differential range-energy table for any desired compound matrix with up to 10 components.

As a result, the variations of the equivalent thickness from one matrix to another can be calculated directly. A further possibility is to establish

for a given matrix the equivalent thickness values as a function of any desired irradiation energy. This may be effected most efficiently again using a simple computer calculation. This capability is of particular interest when post-irradiation etching is carried out on samples. Using this procedure resultant sample thicknesses vary slightly among samples, thereby affecting the irradiation energy to be used for calculation.

Since only a few experimental activation curves and their associated equivalent thicknesses have been published to date and since these have been sparse in detail, the method of constructing activation curves in a variety of matrices of analytical interest from a precise experimentally determined curve should become a valuable aid in the practical application of quantitative determinations using charged particle activation analysis.

IV. Acknowledgment

V. References

[1] Albert, Ph., Sue, P., Chaudron, G., Bull. Soc. Chim. de France, **20/C**, 97 (1953).
[2] Markowitz, S. S., Mahony, J. D., Anal. Chem., **34**, 329 (1962).
[3] Ricci, E., Hahn, R. L., Strain, J. E., Dyer, F. F., Proc. 2nd Int. Conf. on Modern Trends in Activation Analysis, Texas A & M University, 200 (1965).
[4] Ricci, E., Hahn, R. L., Anal. Chem., **40**, 54 (1968).
[5] Engelmann, Ch., C.E.A. Report R/2559, (1964).
[6] Chevarier, N., Giroux, J., Tran. M. D., Tousset, J., Lycen Report 6714 (1967).
[7] Engelmann, Ch., "Radiochemical Methods of Analysis", Vol. I., IAEA Vienna, 405 (1964).
[8] Albert, Ph., Chimia (Aarau) **21**, 32 (1967).
[9] Cummings, J. B., BNL Report 6470.
[10] Williamson, C. F., Boujot, J. P., C.E.A. Report 3042 (1966).
[11] Northcliffe, L. C., Ann. Rev. of Nuclear Science, **13**, 67 (1963).

CONTRIBUTION TO ACTIVATION ANALYSIS BY CHARGED PARTICLES; DETERMINATION OF CARBON AND OXYGEN IN PURE METALS, POSSIBILITIES OF SULPHUR DETERMINATION

Jean-Luc Debrun, Jean-Noel Barrandon and Ph. Albert

CNRS - Centre d'Etudes de Chimie Metallurgique
Vitry, France

I. Introduction

We present here the results of the determination of oxygen in high purity iron, nickel and chromium samples by irradiation in ^{3}He and ^{4}He particles. The interference of fluorine has been studied up to 30 MeV with ^{3}He and 55 MeV with ^{4}He.

We are studying the possibility of carbon determination by means of the radioisotope ^{11}C, induced by nuclear reaction on carbon by ^{3}He and ^{4}He. Interferences of beryllium and oxygen have been experimentally measured up to 30 MeV with ^{3}He and 55 MeV with ^{4}He.

Finally, we will show that sensitive determination of sulphur can be performed by irradiation with the usual charged particles which lead to the radioisotope ^{34m}Cl. With ^{3}He and ^{4}He, interferences cannot be limited and are rather important. With deuterons, interferences can be limited, since we can limit the energy of the particles. For the same reason there are no interferences in the case of tritons and protons.

II. Recent Studies on the Determination of Oxygen and Carbon

A. Determination of Oxygen

The method has been sufficiently described by numerous authors and by ourselves [1-4], and we need not go into the principles and their realization here. We give in Table 1 some results on high purity metals achieved at the "Centre d'Etudes de Chimie Metallurgique" at Vitry. Some of the results given represent only the superior limits of the oxygen concentration, due to the fact that the beam was of too low intensity. It should be observed that the low superior limits obtained with ^{4}He have been confirmed through experiments with ^{3}He.

It is now well known that certain elements other than oxygen such as N, F, Na, Mg, Al and Si give ^{18}F by nuclear reaction with ^{4}He and even in

774

Table 1. Determination of oxygen in high purity chromium, nickel, and iron.

Chromium	O_2, ppm	Nickel	O_2, ppm	Iron	O_2, ppm
Annealed in argon + oxygen atmosphere	83–44–115 (oxide precipitation)	Melted in argon atmosphere	12 − 17	Zone melting in hydrogen (lime boat) I	3 − 4
Zone melting in hydrogen atmosphere (1 passage)	31–9–23–	Zone melting in hydrogen atmosphere (2 passages)	0.7 − 5 0.5[a]	Oxidized and reduced, zone melting in hydrogen (copper boat) II	< 0.5 (3 times) < 1 (3 times)
Zone melting in hydrogen atmosphere (3 passages)	9–3–12 5–11–4			Zone melting in hydrogen (copper boat) III	< 0.5 (3 times) < 1 (1 time) < 0.5[a] (2 times)
Melted in argon atmosphere and annealed in hydrogen 10 h at 1500 °C	11–12–22–16				
Melted in argon atmosphere and annealed in hydrogen 20 h at 1500 °C	< 1 < 1 < 1.5 < 1.5				

[a] ^{3}He irradiation (other results by ^{4}He)

some cases with ^{3}He, but it is also well known that with the exception of fluorine, the cross sections of these reactions are very low (at the energy we used). While interferences of N, Na, Mg, etc. do not exist, if we limit conveniently the energy of the particles, in the case of fluorine, interference exists at every energy. For these reasons we have studied the problem, and we present in Figures 1 and 2 the variation
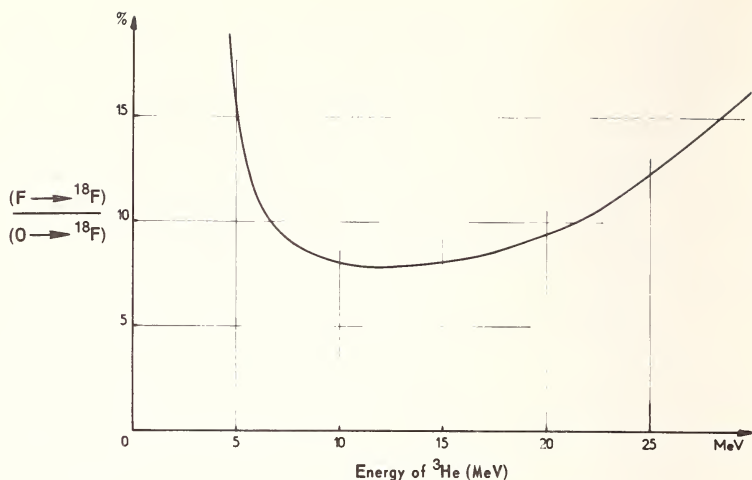
Figure 1. $(F \rightarrow {}^{18}F)/(O \rightarrow {}^{18}F)$ vs Energy of ^{3}He.
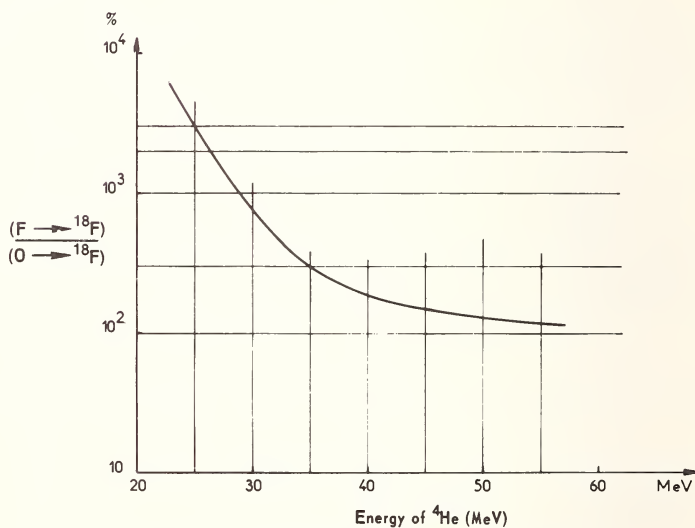
Figure 2. $(F \rightarrow {}^{18}F)/(O \rightarrow {}^{18}F)$ vs Energy of ^{4}He.

of $\dfrac{(F \rightarrow {}^{18}F)}{(O \rightarrow {}^{18}F)}$ in terms of energy. Obviously, it is impossible to determine traces of oxygen in elements such as Na, Mg, Al and Si beyond the thresholds of the interfering reactions leading to ^{18}F, and this limits the possibilities of the method. Finally, it should be notified that we applied the method of determination of oxygen by irradiation with ^{3}He and ^{4}He in the case of very pure metals in which N, Na, *etc.* are present in very small quantities, and in which F concentration is certainly much lower than the oxygen concentration.

B. STUDY OF CARBON DETERMINATION

Through reaction on carbon, ^{3}He and ^{4}He lead to the radioisotope ^{11}C and it is possible to detect 10^{-2} parts per million (ppm) of carbon if the intensity and the energy of the beam are sufficient. The elements Be, B, N and even O give ^{11}C. R. L. Hahn and E. Ricci [5] studied the case of Be and B up to 18 MeV with ^{3}He and S. S. Markowitz [6] the case of beryllium up to 31 MeV with ^{3}He. We studied the case of Be and O up to 30 MeV with ^{3}He and 55 MeV with ^{4}He. At first, it appears difficult to determine carbon by irradiation in ^{3}He and ^{4}He because of these interferences, but we observe as we did with oxygen, that concentrations of Be, B and N are very low in high purity metals. Oxygen and carbon are the main impurities of these metals. Since we can neglect oxygen interference under 11 MeV with ^{3}He and 33 MeV with ^{4}He, we believe that the determination of carbon by means of these two particles may have interesting applications (for instance, see Reference [7] and Figures 3-6).

III. Study of Sulphur Determination

Sulphur determination is of great importance in metallurgy. It is unfortunately very difficult to determine sulphur traces by radioactivation analysis either with thermal neutrons, with fast neutrons [8], and even with photons, because several elements interfere. For instance with thermal neutrons, 1 μg of chlorine gives by (n,p) reaction an activity of ^{35}S (on which sulphur determination is performed) about 50 times greater than that produced from 1 μg of sulphur by the (n,γ) reaction of ^{34}S. For convenience we shall write this as follows: $\dfrac{(Cl \rightarrow {}^{35}S)}{(S \rightarrow {}^{35}S)} \simeq 50$ [8]. With fast neutrons chlorine and phosphorus interfere. Determination of sulphur is performed with ^{32}P and it is experimentally found [8] that $\dfrac{(S \rightarrow {}^{32}P)}{(Cl \rightarrow {}^{32}P)} \simeq 4$ and $\dfrac{(S \rightarrow {}^{32}P)}{(P \rightarrow {}^{32}P)} \simeq 4-5$. When sulphur is determined by means of irradiation with photons, phosphorus interferes by the nuclear reaction ^{31}P $(\gamma,n)^{30}$P. Thus, we thought it could be interesting to determine sulphur by irradiation with charged particles. Of course, interferences exist in that case also, but since the energy of the particles can be limited, interferences become very small (deuterons) or do not exist (protons) on account of the different thresholds of the nuclear reactions for the different interfering elements. We said already, by former work from E. Schweikert in protons [9] that when irradiated with the usual charged particles, natural sulphur leads to ^{34m}Cl [$T_{1/2} = 32.4$ min, positron and gamma emitter (0.14 MeV)]. This radioisotope is interesting by reasons
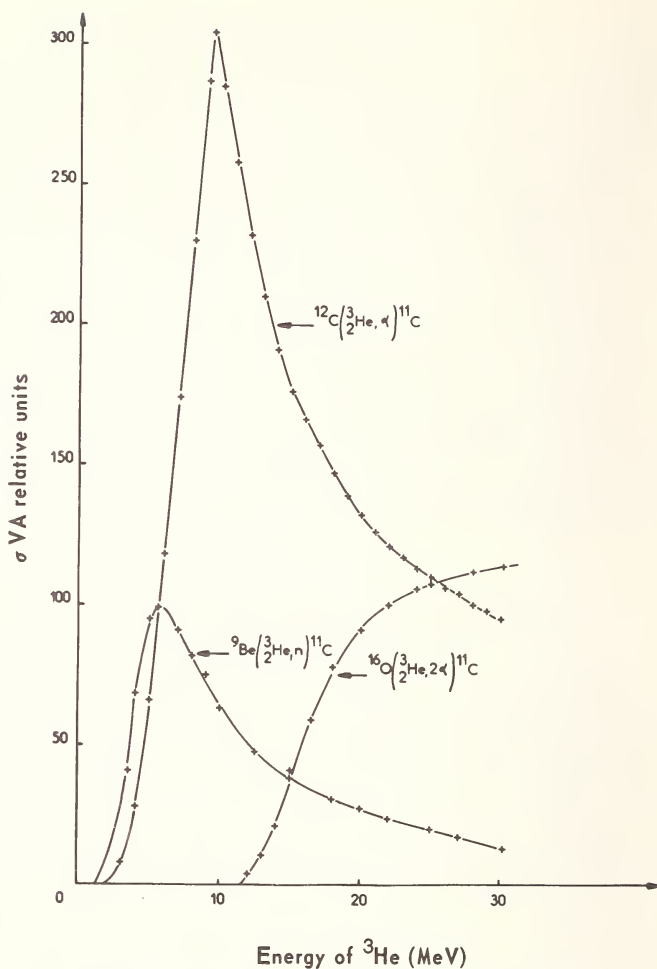
Figure 3.   Relative values of σ VA vs Energy of ^{3}He.

of its half life being neither too short nor too long, of its easily detected rays, and of its easy chemical separation.

1. Alpha Particles

We proved by measuring experimentally, that 5×10^{-3} ppm of sulphur in aluminum can be detected at 55 MeV when the intensity is 6 μA and
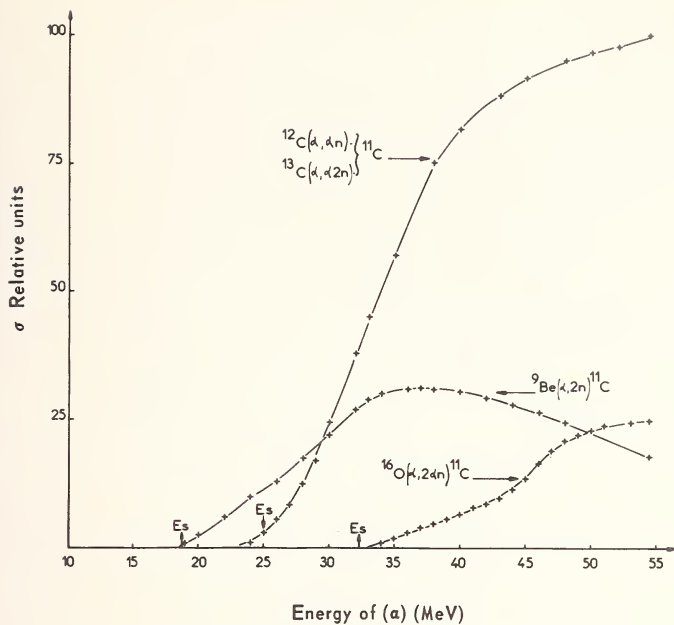
Figure 4.   Relative values (u-a) vs Energy of ⁴He.
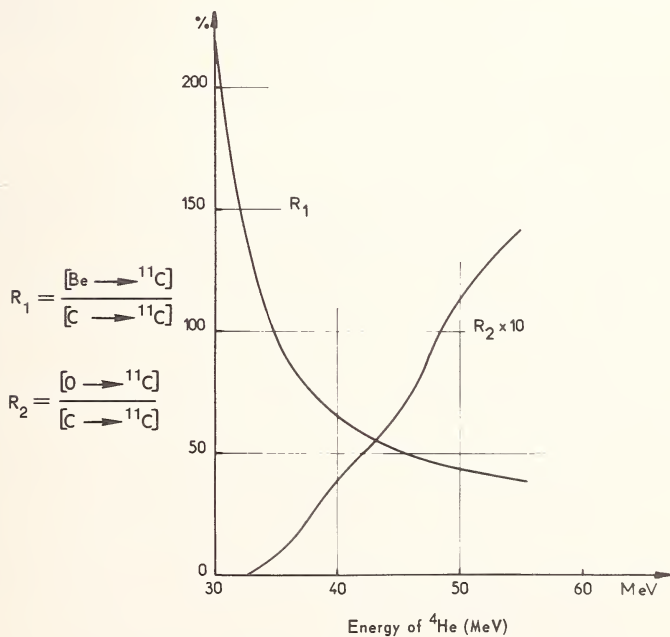
Figure 5. $R_1 = (Be \rightarrow {}^{11}C)/(C \rightarrow {}^{11}C)$ vs Energy of ⁴He; $R_2 = (O \rightarrow {}^{11}C)/(C \rightarrow {}^{11}C)$ vs Energy of ⁴He.

$$R_3 = \frac{[\text{Be} \longrightarrow {}^{11}\text{C}]}{[\text{C} \longrightarrow {}^{11}\text{C}]}$$
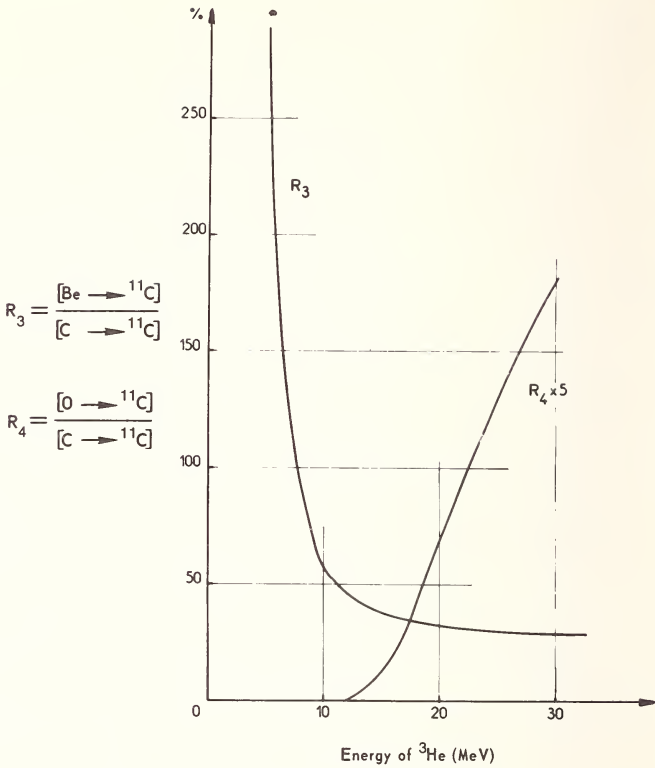
$$R_4 = \frac{[\text{O} \longrightarrow {}^{11}\text{C}]}{[\text{C} \longrightarrow {}^{11}\text{C}]}$$

Figure 6. $R_3 = (\text{Be} \to {}^{11}\text{C})/(\text{C} \to {}^{11}\text{C})$ vs Energy of ${}^{3}\text{He}$; $R_4 = (\text{O} \to {}^{11}\text{C})/(\text{C} \to {}^{11}\text{C})$ vs Energy of ${}^{3}\text{He}$.

when the irradiation lasts 30 min (Fig. 7). Phosphorous and chlorine interfere as we can see from the following reactions:

$${}^{32}\text{S}(\alpha, \text{d}){}^{34\text{m}}\text{Cl}$$ Threshold: 13.83 MeV

$${}^{31}\text{P}(\alpha, \text{n}){}^{34\text{m}}\text{Cl}$$ Threshold: 6.39 MeV

$${}^{35}\text{Cl}(\alpha, \alpha\text{n}){}^{34\text{m}}\text{Cl}$$ Threshold: 14.1 MeV

experimentally:

$$\frac{(S \to {}^{34m}Cl)}{(P \to {}^{34m}Cl)}$$ $E = 55$ MeV $E = 40$ MeV

                                          $1.5 - 2$ $1 - 1.5$

$$\frac{(S \to {}^{34m}Cl)}{(P \to {}^{34m}Cl)}$$ 5   7

We see that it is impossible to determine sulphur without interference, and this limits the use of ${}^{4}\text{He}$ in that case.
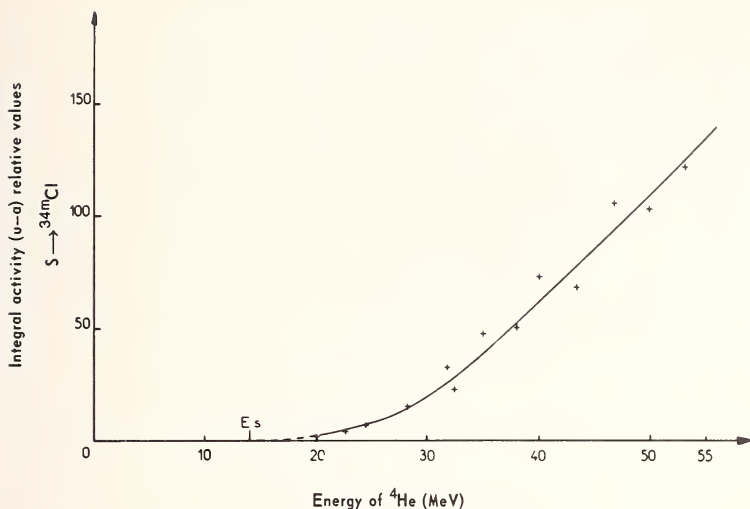
Figure 7.   Relative values (u-a) vs Energy of ^{4}He.

2. Deuterons

About 5×10^{-3} ppm of sulphur in aluminum can be detected at 27 MeV, if the intensity is 8 μA and if the irradiation lasts 30 min. Argon, chlorine and potassium may interfere by the reactions:

^{36}Ar(d, α)^{34m}Cl	Threshold:	0 MeV
^{35}Cl(d, t)^{34m}Cl	Threshold:	6.76 MeV
^{39}K(d, αt)^{34m}Cl	Threshold:	13.5 MeV
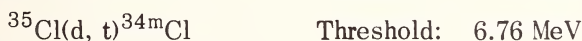
It may be expected that the argon interference will be very low. The ^{36}Ar percentage in natural argon is 0.34% and the argon percentage in air is about 1%. Finally, in our high purity metals, argon is certainly present at very low concentrations. Potassium irradiation gave no measurable amount of ^{34m}Cl. Chlorine interference begins at 6.76 MeV; at 13 MeV, R $= \dfrac{(Cl \rightarrow \,^{34m}Cl)}{(S \rightarrow \,^{34m}Cl)}$ is equal to 1 and at that energy we can detect 10^{-2} ppm of sulphur in aluminum. We show in Figures 8-10, the variation of R as a function of the deuteron energy.

3. Protons

The following reactions lead to ^{34m}Cl:

^{33}S(p, γ)^{34m}Cl	Threshold:	0 MeV
^{34}S(p, n)^{34m}Cl	Threshold:	6.5 MeV
^{35}Cl(p, d)^{34m}Cl	Threshold:	10.72 MeV
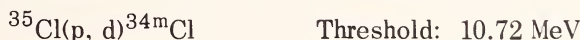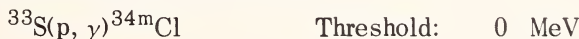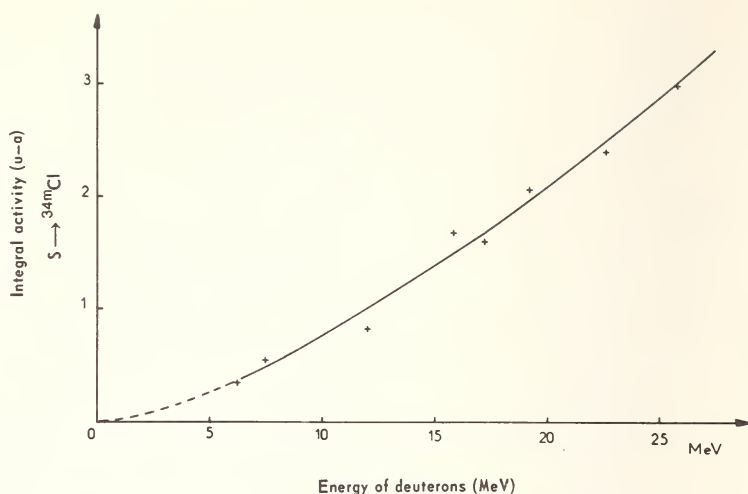
Figure 8.   Relative values (u-a) vs Energy of deuterons for S $\rightarrow$ ^{34m}Cl.
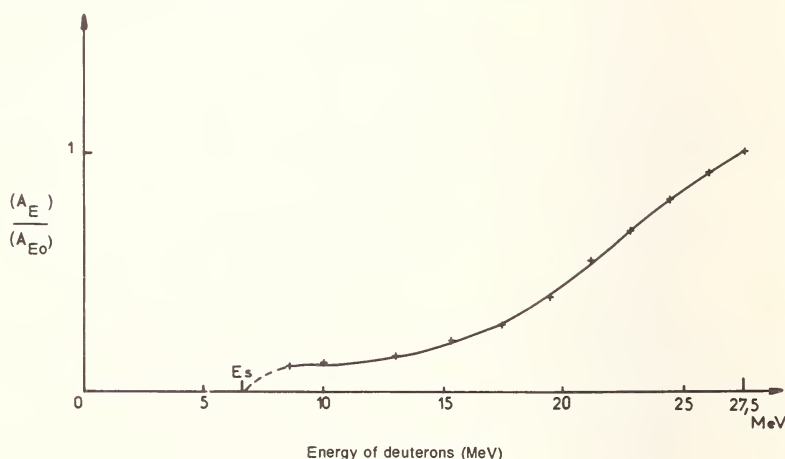
Figure 9.   Relative values A_E/A_{E_0} vs Energy of deuterons for chlorine.

If the proton energy is $\leqslant 10.72$ MeV, no interference exists. At that energy we measured that 2×10^{-2} ppm of sulphur in aluminum can be detected for an intensity of 4 μA for a 30 min irradiation (Figure 11). This is very important because it seems to be the only way (with ^{3}H) in radioactivation analysis to determine sulphur without any interference with such a sensitivity.

We made no experiments with ^{3}He and ^{3}H. Let us say that the case of ^{3}He seems to be very similar to the case of ^{4}He [10]. The study of the thresholds of nuclear reactions induced by tritons shows that it is
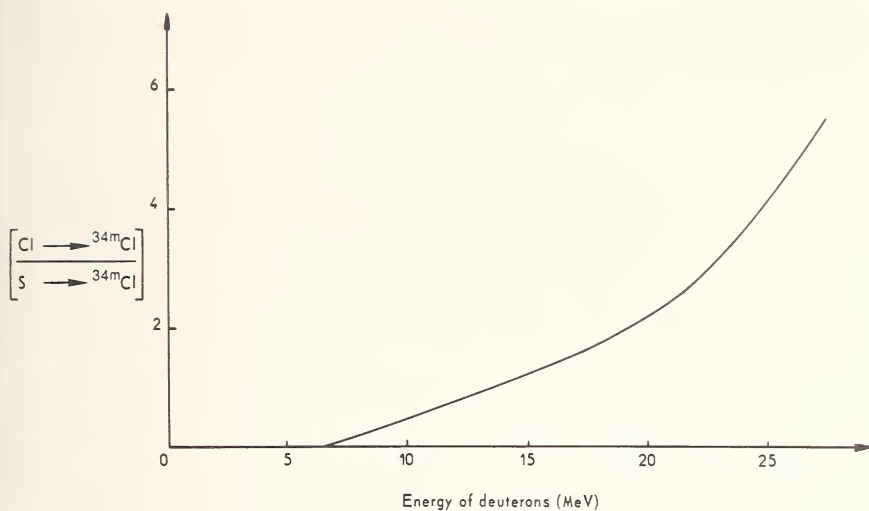
Figure 10. Relative contribution $(\text{Cl} \rightarrow {}^{34m}\text{Cl})/(\text{S} \rightarrow {}^{34m})$ vs Energy of deuterons.
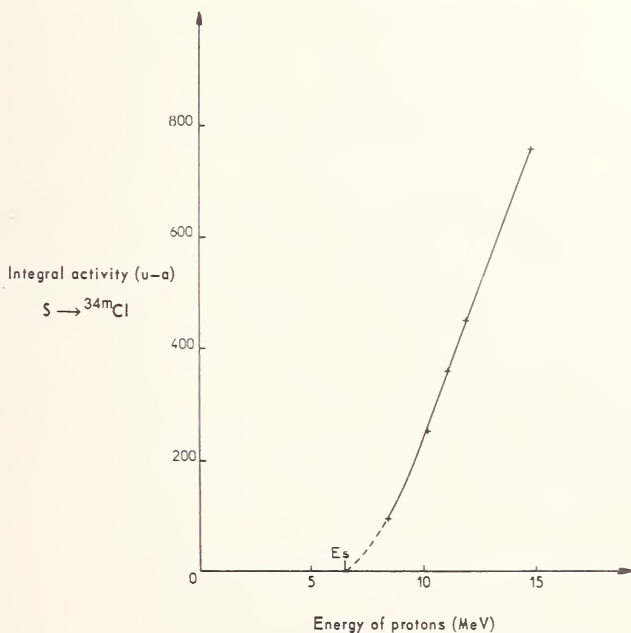
Figure 11. Relative values (u-a) for $\text{S} \rightarrow {}^{34m}\text{Cl}$ vs Energy of protons.

theoretically possible to determine sulphur without interference. if $E_{3H} \leqslant 13.74$ MeV, so that it appears to be the same as with protons. But let us take into account that the reaction is ${}^{32}\text{S}({}^{3}\text{H,n}){}^{34m}\text{Cl}$ instead of

$^{34}S(p,n)^{34m}Cl$, and that the sensitivity must be of course much better ($^{34}S = 4.22\%$, $^{32}S = 95\%$).

IV. Summary

In summary, ^{3}He and ^{4}He give almost the same results as the fast neutrons. Deuterons are more interesting because phosphorous interference does not exist. Finally, protons (and tritons) present exceptional interest because they allow us to determine sulphur without interference with all the advantages of activation analysis, *i.e.* great sensitivity and no pollution.

V. Acknowledgments

VI. References

[1]   Albert, P., These Juin 1955 — Annales de Chimie (1956), 13eme serie, 1-827.
[2]   Albert, P., Modern Trends in Activation Analysis, Texas A&M, College Station, Texas, 1961, p. 78.
[3]   Deyris, M., Revel, G., and Albert, P., Symposium on Trace Characterization Chemical and Physical, October, 1966, NBS, Gaithersburg, Md., and Albert, P., Chimia **21**, 32 (1967).
[4]   Barrandon, J. N., Debrun, J. L., and Albert, P., Second Meeting on Practical Aspects of Activation Analysis with Charged Particles and Gamma Photons, Liege, September, 1967, Proceedings Rep. EURATOM 3896, p. 277 (1968).
[5]   Hahn, R. L., and Ricci, E., Phys. Rev. **146**, 650-659 (1966).
[6]   Markowitz, S. S., and Hall, J. M., Bull. Am. Phys. Soc. 4-8, (1959).
[7]   Revel, G., and Albert, P., The Journal of Nuclear Materials **25**, 87 (1968); C.R. 265, Serie C., 1967, p. 1443.
[8]   Albert, P., Blouri, J., Cleyrergue, C., Deschamps, N., and Le Hericy, J., Journal of Radioanalytical Chemistry **1**, 297-311 (1968).
[9]   Schweikert, E., in Rapport de Mission de Ph. Albert. CECM-C.N.R.S., Eindhoven, Holland (1964).
[10] Ricci, E., and Hahn, R. L., Anal. Chem. **37**, 742-48 (1965); EURATOM 3896, p. 15 (1968).

INFLUENCE OF CHANNELING IN CUSTOMARY ³He ACTIVATION ANALYSIS

Enzo Ricci

Analytical Chemistry Division
Oak Ridge National Laboratory
Oak Ridge, Tennessee

I. Introduction

The channeling of energetic charged particles in crystals has been known and studied since 1963 [1]. This phenomenon, usually called "channeling effect", results when such particles enter a crystal with small angles either with respect to the lattice rows or to its planes; the ions suffer a number of small angle collisions with lattice atoms which tend to channel their paths inside the crystal. The channeling effect offers advantages and drawbacks to charged particle activation analysis. Very interesting uses of this effect to locate foreign atoms in crystals were discussed by Holm *et al* [2] and demonstrated by Eriksson *et al*[3]. A quantitative measure of the fraction of impurities located on different lattice rows or planes can be obtained by bombarding the crystal along different directions. On the other hand, the main disadvantage of channeling is that it causes parameters of a random nature, like particle range and reaction cross section, to vary in a rather complex fashion. Thus, when a crystal is irradiated in a channeling direction, the equations governing charged particle activation analysis [4,5] may not be expected to hold. The mathematical interpretation of the activation experiment may then become quite involved and uncertain.

When channeling is used to locate impurities in a crystal lattice, the sample is usually fixed to a remotely controlled goniometer which permits finding the channeling directions of the crystal by irradiation. It may be said that these experiments are rather sophisticated and by no means similar to customary charged particle activation. For example, prompt nuclear reaction products are usually measured rather than induced radioactivities. Moreover, part-per-billion determinations are ruled out because high intensity bombardments cannot be attempted on the uncooled samples. To make cooling possible the complexity of the goniometer must be increased beyond reasonable limits.

The ³He activation program at the Oak Ridge National Laboratory is aimed at achieving the outstanding sensitivities promised by this method. Therefore, the difficulties that channeling effects may cause in high

785

intensity customary ³He activation analysis are of great importance to us and deserve investigation. On the other hand, if these effects were apparent in usual charged particle activation, it might be possible to increase the sensitivity of the lattice impurity-locations techniques. Thus, experiments were carried out to study these points. Germanium crystals were used as targets because of the importance recently acquired by ³He activation analysis for oxygen in this metal [2,6]. A Ge single crystal ingot (shaped like a margarine stick) was cut into numerous slices perpendicularly to its 111 axis. Each of these slices was bombarded at a different angle and counted. To insure the validity of the results over a wide area in charged particle activation, the sophistication of the experiment was planned to be greater than that of ordinary bombardments such that observation of channeling effect could reasonably be expected. However, activation and radioactivity measurements were preferred to counting of prompt radiation or of particles from scattering processes because the former situation is the norm in activation analysis. Though nuclear reaction products from impurities (C and O) were observed, only products from Ge were taken into account because only its atoms constitute the lattice.

As a consequence of these experiments the purpose of this paper is to prove that channeling effects have no influence in most customary ³He activation analyses of crystals.

II. Experimental

The 111 axis of the Ge single crystal was found by x-ray diffraction before cutting the perpendicular slices with a diamond saw. The slices were 2 mm thick and their two flat faces were parallel within 0.001 in. A simple goniometer with 0.2° precision was constructed to hold the samples during irradiation. Figure 1 shows the goniometer in its vacuum chamber with a sample in irradiation position. A mirror of good optical quality is also shown mounted on the back of the sample holder (goniometer). The alignment of the 111 axis of the sample with the ³He beam was achieved by using this mirror and an external autocollimator. The irradiations were performed at the Oak Ridge Isochronous Cyclotron with a reasonably parallel ³He beam of 0.15 μA at 7.8 ± 0.2 MeV. The channeling critical angle for bombardment of Ge in these conditions is 0.56 ± 0.01 degrees. Thus, 18 samples were bombarded in sequence for 5 min each, at angle intervals smaller than 0.5 degrees. Each sample was etched a short time before irradiation, with a mixture of conc. 1 HF: 2 HNO_3 for 1 − 3 min. The bombardment angles (beam with respect to 111 axis) were: − 1.0, − 0.8, − 0.6, − 0.4, − 0.2, 0, 0.2, 0.4, 0.6, 0.8, 1.0, 4.0, 4.4, 4.8, 5.0, 5.2, 5.6, and 6.0 degrees. The alignment was checked frequently with the mirror and autocollimator.
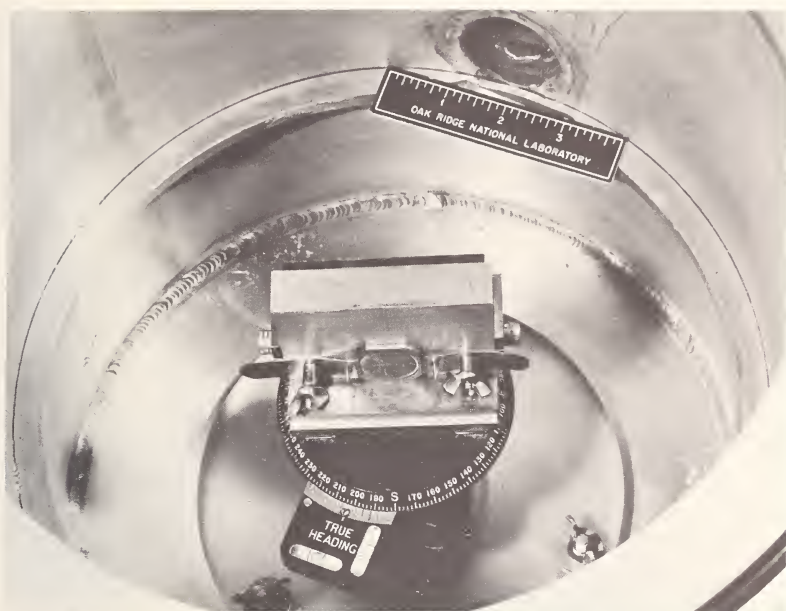
Figure 1. Goniometer in vacuum chamber with Ge sample in irradiation position. Also shown is mirror in back of sample holder and back hole of chamber, needed for alignment.

The decay of each sample was followed with a 3 in. × 3 in. NaI(Tl) detector and multichannel analyzer. One sample was irradiated for 20 min at 0.3 μA and counted with a Ge(Li) detector to determine the reaction products by gamma spectrometry. The nuclear reactions and products so observed were: $^{70}Ge(^3He,pn)^{71}As$, 62h, $^{70}Ge(^3He,p)^{72}As$, 26 h, and $^{72}Ge(^3He,2n)^{73}Se$, 7.1 hr. A long-lived residual activity, probably due to 18 d ^{74}As, was also present, as well as 20.5 min ^{11}C and 110 min ^{18}F from carbon and oxygen impurities, respectively [2,6]. On the basis of these half lives, least squares decay curve analysis of the gross gamma counts (to improve precision) was performed by using the CLSQ program [7] with the IBM 360/75 computer.

III. Results and Conclusions

Figures 2 and 3 are plots of product radioactivities vs. angle, at the end of a 5 min bombardment; the ^3He beam intensity has been normalized to 0.1 μA. The error marks correspond to the standard deviations resulting from the computer treatment of the data. From the charged particle activation equation [4,5] the radioactivity induced in a thick target is

proportional to the average cross section of the nuclear reaction involved and to the particle range. If any of these parameters were influenced by channeling in these experiments, Figures 2 and 3 would show structure, *i.e.*, departure from the horizontal (constant). However, these graphs show that within experimental error, the induced radioactivity is independent of irradiation angle. Clearly, despite the fact that this study was set up with a much higher degree of optical alignment than customary
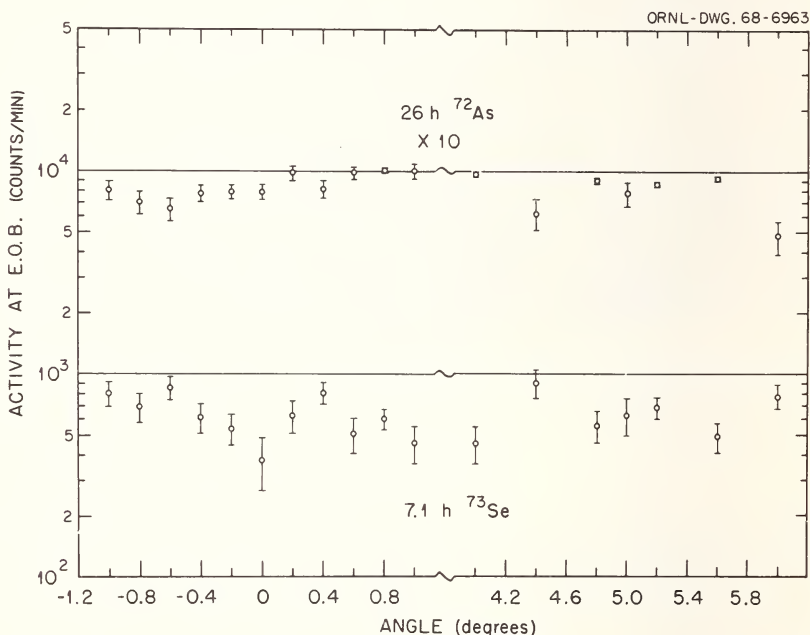
Figure 2.   Count rates of 26 h ^{72}As and 7.1 h ^{73}Se at end of bombardment (EOB) of Ge crystal vs. angle of beam with respect to 111 axis. Conditions: bombardment for 5 min with a 0.1 μA beam of 7.8 MeV ^{3}He particles; counting of gross gamma counts of sample on top of 1.3 cm lucite absorber lying on 3 in. $\times$ 3 in. NaI(Tl) detector.

charged particle activation analysis, its precision is not yet high enough for detecting channeling effects. Thus, we can safely conclude that such effects cannot generally influence the customary methods. This is particularly true because the critical channeling angle of 0.56° in these experiments is relatively broad in comparison with that corresponding to most activation bombardments. Measurements in the range 4.0−6.0 degrees, where channeling could not be expected, were made for comparison. It may be seen that they are consistent with the measurements in the channeling region within the precision of these experiments.

Since channeling effects cannot be observed in an experiment of medium sophistication as this one, it is apparent that fine studies of impurity locations by channeling [2,3] will have to rely on complex equipment for some time. Thus, no high sensitivity determinations of this type (requiring high currents) may be feasible in the near future.
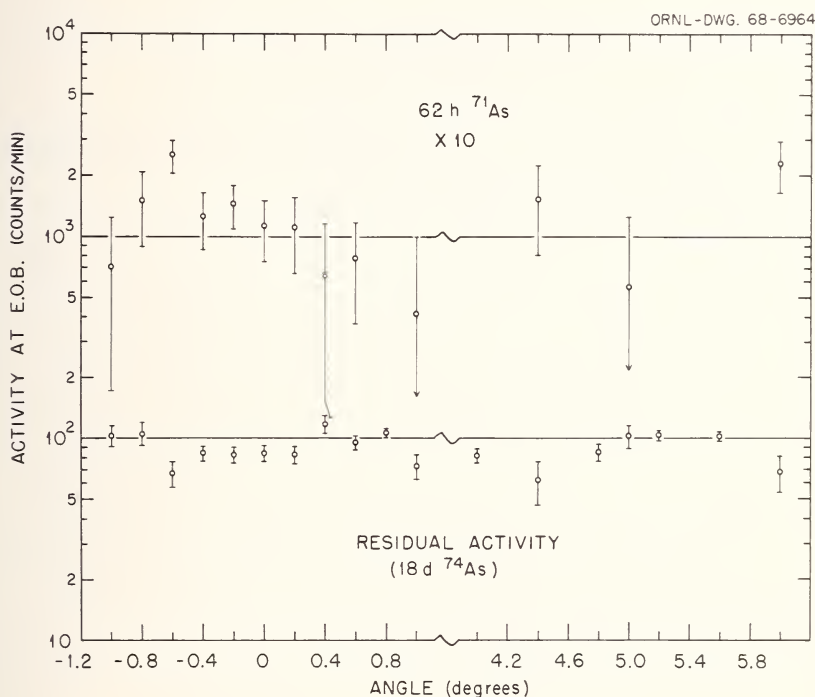
Figure 3.   Count rates of 62 h [71]As and long-lived tail of 18 d [74]As at end of bombardment (EOB) of Ge crystal vs. angle of beam with respect to 111 axis. Conditions: bombardment for 5 min with a $0.1 \mu A$ beam of 7.8 MeV [3]He particles; counting of gross gamma counts of sample on top of 1.3 cm lucite absorber lying on 3 in. $\times$ 3 in. NaI(Tl) detector.

IV. Acknowledgments

V. References

[1]   Datz, S., Erginsoy, C., Leibfried, G., and Lutz, H. O., Annual Review of Nuclear Science Vol. l7, E. Segre, Ed., Annual Reviews, Inc., Palo Alto, Calif., p. 129, 1967.

[2]   Holm, D. M., Briscoe, W. L., Parker, J. L., Sanders, W. M., and Parker, S. H., "Practical Aspects of Activation Analysis with Charged Particles, Proceedings of a Conference in Liege, Belgium, 1967, Euratom Rpt. EUR-3896 d-f-e, 1968, p. 239.

[3]   Eriksson, L., Davies, J. A., Denhartog, J., Matzke, H. J., and Whitton, J. L., Canadian Nuclear Technology 5, No. 6, 40 (Nov. – Dec. 1966).

[4]   Ricci, E., and Hahn, R. L., Anal. Chem. 37, 742 (1965).

[5]   Ricci, E., and Hahn, R. L., Anal. Chem. 39, 794 (1967).

[6]   Aleksandrova, G. I., Demidov, A. M., Kotelnikov, G. A., Plewakova, G. P., Suxov, G. V., Coporov, D. R., and Wmanenkova, G. I., Russian Rpt. IAE-1156, Institute of Atomic Energy, Moscow (1966).

[7]   Cumming, J. B., in U.S. Atomic Energy Commission Rept. NAS-NS 3107, 25 (1963),

SURFACE ANALYSIS OF GOLD AND PLATINUM DISKS BY ACTIVATION METHODS AND BY PROMPT RADIATION FROM NUCLEAR REACTIONS

James W. Butler and Eligius A. Wolicki

Nuclear Physics Division
U.S. Naval Research Laboratory
Washington, D.C.

In many experiments, contaminant-free surfaces of metals are highly desirable. The present paper is a report of methods for testing the surfaces of gold and platinum for carbon, oxygen, and aluminum contamination. Nuclear activation techniques and the measurement of prompt radiation from nuclear reactions were chosen as the testing methods because high sensitivity and specificity were required. Carbon and oxygen were detected through the ^{11}C ($T_{1/2} = 20$ min) and ^{18}F ($T_{1/2} = 110$ min) positron emitters produced by the ^{12}C(^{3}He,α)^{11}C and ^{16}O(^{3}He,p)^{18}F nuclear reactions, respectively. Aluminum contamination was measured by means of the prompt gamma radiation from the ^{27}Al(p,γ)^{28}Si reaction.

The details of the analysis procedures, such as the lengths of the bombarding times, varied during the course of the measurements; but a typical analysis procedure for carbon and oxygen is as follows:

A disk whose surface was to be analyzed was placed in the target position in the vacuum system of the NRL 5-MeV Van de Graaff accelerator. Within a few seconds after the disk was exposed to the vacuum, it was enclosed by a long tube kept at liquid-nitrogen temperature as illustrated in Figure 1. The purpose of this tube is to protect the target from condensable vacuum-system contaminants.
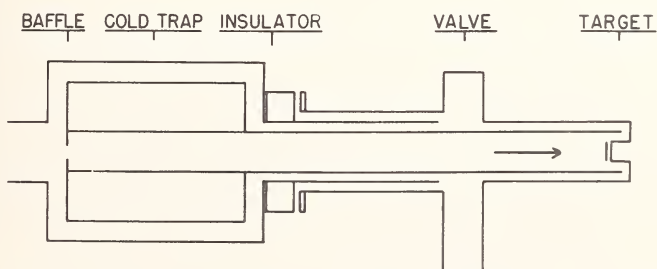
Figure 1. Target enclosed for a cold tube near liquid-nitrogen temperature for protection from accelerator vacuum-system vapors.

791

The disk target was bombarded by a beam of 4.5 MeV singly ionized ³He particles (about one to two microamperes) for about five minutes. The temperature of the target during bombardment is not known but probably was above 200 °C. After the bombardment the annihilation radiation from the positron activities in the disk was measured as a function of time with a 76 mm diam by 76 mm NaI(Tl) crystal detector.

The first disk to be so examined was a gold (99.999% Au) disk (9.0 mm diam by 1.2 mm) which had been polished by conventional methods utilizing levigated γ-Al$_2$O$_3$ polishing powder (0.3 μm maximum particle size) in distilled water on a cloth from which extractable organic materials had been removed. The gold disk was then analyzed for contaminants as described above. The decay curve exhibited both the ¹¹C 20 min half life and the ¹⁸F 110 min half life.

On the basis of the published cross section values of the ¹²C(³He,α)¹¹C and the ¹⁶O(³He,p)¹⁸F reactions [1] the counting rates were translated into amounts of contaminants (carbon and oxygen) on the gold surface. A convenient way of expressing these amounts is in terms of "atomic layers". As used herein, one *atomic layer* is defined to be that amount of elemental contaminant that would cover the face of the disk if one contaminant atom were attached to each "surface" metal atom. For gold the number of surface metal atoms per square centimeter was assumed to be 1.5×10^{15}.

The first gold disk tested contained about 7 atomic layers of carbon and 20 atomic layers of oxygen. The uncertainties in these and subsequent measurements of amounts of contaminants are roughly 30 percent. (More precise results could be obtained, but this precision was adequate for present purposes). Since these amounts of contaminants were unacceptably large for the particular application involved, several other cleaning procedures were attempted in an effort to obtain a contaminant-free surface.

Since a possible source of at least part of the oxygen contamination was Al$_2$O$_3$ powder embedded during the polishing process, the following test for aluminum was made. The NaI(Tl) crystal previously mentioned was used to detect the prompt gamma radiation when protons bombarded the gold disk. The pronounced resonance in the ²⁷Al(p,γ)²⁸Si reaction at 992 keV was detected with the above gold disk as the target. A comparison of the gamma-ray counting rate obtained from the gold disk with that obtained from an aluminum target of known thickness gave for the amount of aluminum on the gold disk, 9 atomic layers, implying that about 70 percent of the oxygen found above was in the form of Al$_2$O$_3$.

A thin layer of the gold surface was next removed with the use of a new dry file in an effort to remove the Al$_2$O$_3$ particles. No aluminum was found after this treatment. The sensitivity of the test was such that one

atomic layer could have been detected. (This sensitivity could have been improved if necessary by the use of a detector shield and a more intense bombarding beam). A second gold disk was machined in a jeweler's lathe with a clean dry cutting tool. This sample contained 21 atomic layers of carbon and 27 atomic layers of oxygen. The second gold disk was then heated in a platinum furnace with an air atmosphere to about 800 °C for half an hour after which it was inserted into the vacuum system. The disk was then bombarded by a beam of 2 MeV protons with about 6 watts input power for 15 min for the purpose of removing any contaminants that might have adhered to the disk during the few seconds before the cold tube enclosed the target. No positron annihilation was detectable *in situ* after the proton bombardment. Then the disk was bombarded by ^{3}He particles, and 3.5 atomic layers of carbon and 11 atomic layers of oxygen were found.

Several tests were made to ascertain whether contaminants were introduced by the accelerator vacuum system. Thus, a high purity platinum disk (12 mm diam by 0.03 mm) was cleaned in hot concentrated nitric acid for half an hour and then rinsed with doubly distilled water. A heating by proton bombardment as before, followed by activation by ^{3}He bombardment, revealed 8 atomic layers of carbon and 2 atomic layers of oxygen. The platinum disk was next heated in air in the platinum furnace to a temperature of about 1200 °C for one half hour. The sample was then heated by proton bombardment and activated by ^{3}He bombardment as before. The resulting decay curve clearly exhibited the 2-min ^{15}O activity from the ^{16}O(^{3}He,α)^{15}O reaction and the 110 min ^{18}F activity from the ^{16}O(^{3}He,p)^{18}F reaction. The ^{15}O and ^{18}F activities corresponded to 3 atomic layers of oxygen. The counting rate produced by 3 atomic layers of oxygen may be reasonably extrapolated to an ultimate sensitivity of $\sim 10^{-3}$ atomic layer.

No evidence was found for the 20-min ^{11}C activity from the ^{12}C(^{3}He,α)^{11}C reaction. It is estimated that $\sim 10^{-2}$ atomic layer of carbon could have been detected if such an amount had been present along with the 3 atomic layers of oxygen. (If *only* carbon contamination were present, then the detection sensitivity would have been $\sim 10^{-4}$ atomic layer). This apparent absence of carbon shows that it is possible to maintain a carbon-free target in an accelerator vacuum system when used with a surrounding cold tube as shown in Figure 1.

The authors wish to thank Dr. W. A. Zisman for bringing the problem to their attention and Mrs. M. K. Bernett for supplying some of the gold samples.

I. Reference

[1] Hahn, R. L., and Ricci, E., Phys. Rev. **146**, 650 (1966).

DETERMINATION OF OXYGEN PRESENT AT THE SURFACE OF METALS BY IRRADIATION WITH 2 MeV TRITONS

J.-N. Barrandon and Ph. Albert

CNRS - C.E.C.M.
Vitry, France

I. Introduction

In 1949 Smales [1] showed that it was possible to determine oxygen by the reaction: $^{16}O(^{3}H,n)^{18}F$; $Q = +$ 1.280 MeV. Many experiments were performed with the tritons produced by the reaction $^{6}Li(n,\alpha)^{3}H$ [2,3]. The cross section of this reaction is 910 barns with thermal neutrons. The maximum energy of the tritons is 2.74 MeV. It is not very interesting to obtain tritons by this method because: (1) The nondestructive determination of oxygen in most materials is impossible for the thermal neutrons give too much radioactivity. (2) The triton beam presents a spectrum of energies. Oxygen determination in the bulk of the sample is then very difficult. (3) It is impossible to determine oxygen on perfectly clean surfaces since the surfaces are polluted during irradiation by contact with lithium or lithium salts. Even in the most elaborate type of this method [3], it can be difficult to keep the surface free from contamination. Therefore, we studied the possibility of surface oxygen determination by means of tritons accelerated in a Van de Graaff accelerator.

II. Experimental Device

These experiments were performed in the vertical 3 MeV Van de Graaff of the "Centre de recherches Nucleaires" at Strasbourg. The ion source is fed by tritium diluted in helium in the ratio of 3/1000 in volume. In these conditions the accelerator gives an intensity of 0.2 μA with the beam analyzed and diaphragmed [4].

III. Excitation Function of the Reaction $^{16}O(^{3}H,n)^{18}F$

In the first experiments we studied the excitation function of the reaction $^{16}O(^{3}H,n)^{18}F$. Our experimental conditions have been described in a former publication [5] (Figures 1 and 2).
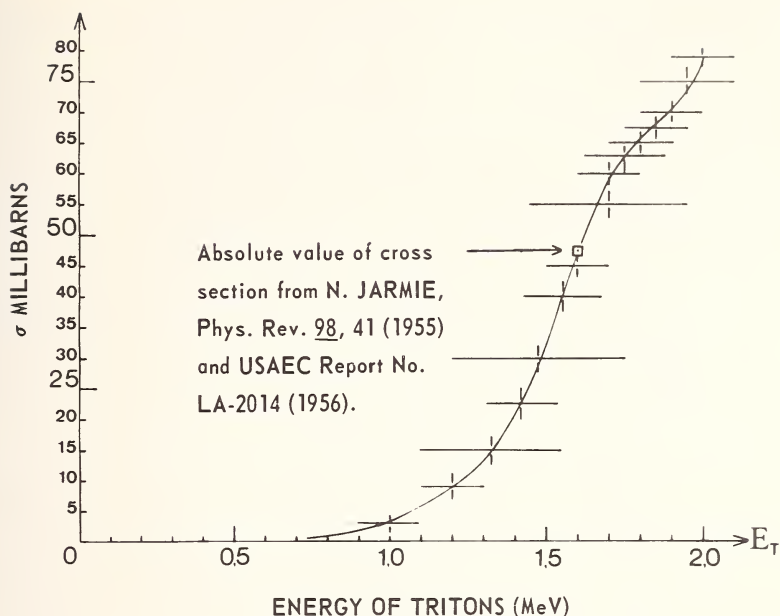
Figure 1.   Excitation function of $^{16}O(^3H,n)^{18}F$ reaction; 0.5 to 2 MeV.

IV. Standardization

We suppose there exists on the surface of the standards an oxide whose thickness is x_s, the thickness of the oxide film on the sample being Δx_e; Δx_e is supposed to be very small so that the energy of tritons is considered as constant through it. Consequently the cross section is considered as constant through Δx_e where we can write:

$$\sigma(E) = \sigma(E_0) + \left(\frac{d\sigma}{dE}\right)_{E_0} \Delta E = \sigma(E_0)\left[1 + \frac{d \log \sigma(E_0)}{dE}\Delta E\right]$$

It is necessary that:

$$\frac{d \log \sigma(E_0)}{dE}\Delta E \ll 1$$

The irradiation time being short compared to the half life of the radioisotope, ^{18}F, the activities at the end of the irradiation will be:

(1)   for the standard:

$$A_1 = Q_1 n_1 \int_0^{x_s} \sigma_x dx \tag{1}$$
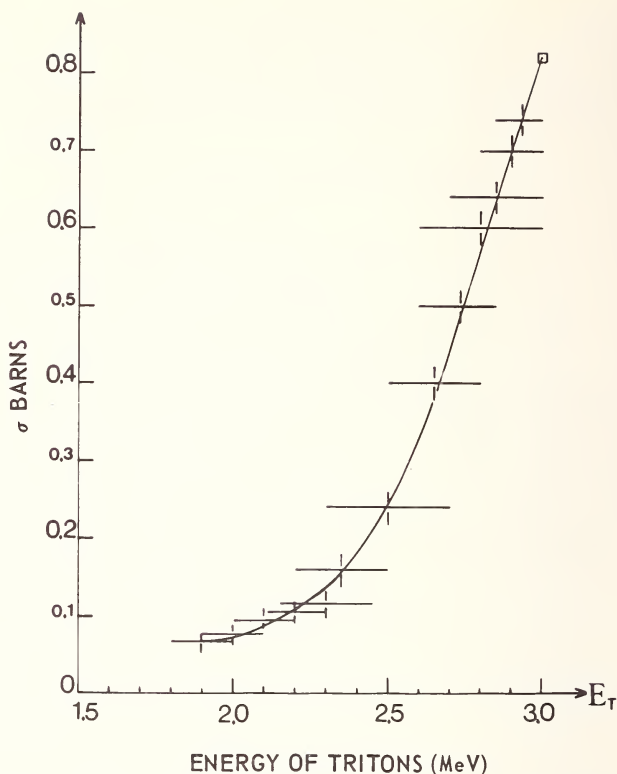
Figure 2.   Excitation function of $^{16}O(^3H,n)^{18}F$ reaction; 1.9 to 3 MeV.

(2)   for the sample:

$$A_2 = Q_2 n_2 \int_0^{\Delta x_e} \sigma_x dx \qquad (2)$$

A_1, $A_2 = $ ^{18}F activity for the standard and the sample

Q_1, $Q_2 = \int_0^t i dt$ given by the integrator

n_1, $n_2 = $ oxygen atoms per milligram

$\sigma_0 = \sigma(E_0) = $ cross section of the reaction if the energy of incident particles is E_o

$\sigma_x = \sigma(E_x) = $ cross section of the reaction at the energy, E_x, the range of the particles being x

Let us introduce the "equivalent thickness" [6] defined as follows:

$$e = \frac{\displaystyle\int_0^{x_s} \sigma_x \, \mathrm{d}x}{\sigma_0}$$

e = equivalent thickness in which the activity would be uniform as indicated (Figure 3).

We have: $A_1 = Q_1 n_1 \sigma e$ and $A_2 = Q_2 n_2 \sigma_0 \Delta x_e$

and:

$$\Delta x_e = \frac{e A_2 n_1 Q_1}{A_1 n_2 Q_2}$$
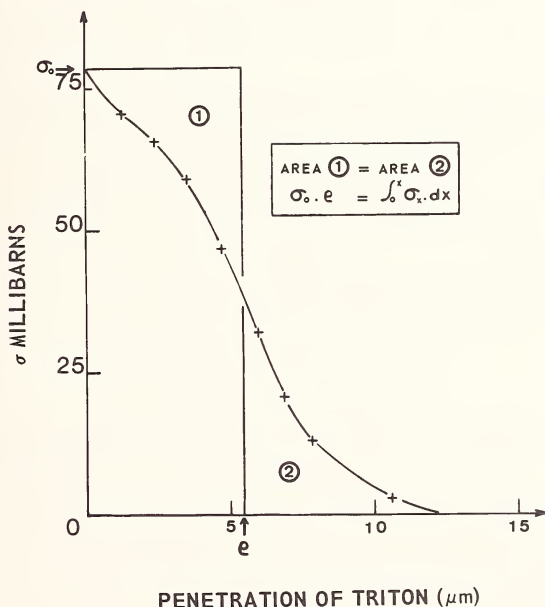
Figure 3. Determination of "equivalent thickness", e, for 2 MeV tritons. e in ZrO_2 is equal to 5.5 μm.

V. Choice of the Experimental Conditions

Our irradiations were performed at 2 MeV for the following reasons:

At this energy the cross section is sufficient to get a good sensitivity for the determination of the oxide films, and the interference of oxygen present in the subjacent metal can be neglected since (1) the oxygen

concentration in the bulk of our samples varies from 0.1 to 10 μg/g, (2) the cross section· of the reaction $^{16}O(^3H,n)^{18}F$ decreases strongly with the penetration of tritons, and (3) the range of 2 MeV tritons is very short.

For the 2 MeV tritons the variation of the cross section is 10% when the loss of energy is 0.1 MeV. The cross section can be considered constant and equal to σ_o through Δx_e.

VI.   Accuracy and Sensitivity of the Method

The relative error on Δx_e is equal to the sum of errors on each term of the formula for Δx_e. The absolute errors on e, n_1, n_2, A_1 and A_2 are easily known. On the other hand, the absolute errors on Q_1 and Q_2 cannot be easily estimated. These errors depend upon the checking of the current integrator and upon the secondary electrons coming from the target. Identical conditions of energy and measured current give the same rate of secondary electrons [7]. Using the current integrator as a check, the error is less than 1% on different experiments performed under these conditions.

Presently, under our experimental conditions, the accuracy on Δx_e is equal to 5%. Great sensitivity for the determination of surface oxygen is observed with 2 MeV tritons. If the irradiation lasts 10 min and if the intensity is 0.3 μA, 0.5 μg/ cm^2 of oxygen gives 2×10^3 counts per minute of ^{18}F. Therefore, 5×10^{-3} μg/cm^2 of oxygen can be detected if the counting lasts 10 minutes. In these conditions the error on counting is about 8% and the error on the determination is about 10%.

VII.   Results and Discussions

Our first studies were performed on pure zirconium and aluminum samples. In the case of zirconium we studied the variation of surface oxygen as a function of chemical and mechanical polishing. For this study we used very pure Van Arkel zirconium, in which the oxygen concentration varies from 5 to 20 μg/g. Results are given in Table 1.

We see (Table 1) that the least surface oxygen concentration 1.2 μg/cm^2 is found in the case of chemical polishing by HF 23 N:18%-HNO$_3$, 11 N:82%, but it must be said that this treatment leads now and then to results such as 1.9 μg/cm^2. So chemical polishing seems to give rather different results for identical samples. The variation of surface oxygen concentration with HF percentage and HNO$_3$ percentage must be studied. Aluminum has been polished in the following acid mixture: HNO$_3$ (11 N)− 5% : H$_3$PO$_4$ (d 1.7)−70% : H$_2$SO$_4$ (36 N)−25%; polishing lasts 30 min at 60 °C, and the samples are dried with compressed air after washing with distilled water (results are shown in

Table 1. Surface oxygen for zirconium samples.

	Treatment	Oxygen $(\mu g/cm^2)$	Trial number	Dispersion $(\mu g/cm^2)$
I	Initial treatment[a]	1.46	6	0.12
II	I annealed 1 h at 100 °C	1.6 − 1.74	2	
III	I chemically polished: HF (23 N) 18%	1.22	7	0.15
	HNO$_3$ (11 N) 82% dried with alcohol	1.90	3	0.13
IV	I polished like III but dried with acetone	2.15 − 2.30	2	
V	I mechanically polished and dried with acetone	5.8 − 6	2	

[a] The metal has been rolled, chemically polished in HF (23 N): 18% − HNO$_3$ (11 N): 82%, and annealed 1 hour at 950 °C, the pressure being 2.10^{-7} torr.

Table 2). Our results point out the influence of rolling and metal purity on surface oxygen.

Oxygen determination at the surface of aluminum and zirconium, are performed without chemical separation, since 2 MeV tritons do not induce any radioactivity interfering with the measure of ^{18}F radioactivity.

We know already that similar determinations can be performed in the case of pure nickel, iron, chromium and even industrial stainless steel. Since the determination is "nondestructive", surface oxygen concentration may be measured after different successive treatments.

The sensitivity of the method seems to be as good as the sensitivity using reaction ^{16}O (d,p)^{17}O[8]. When surface oxygen is determined for a sample in the bulk where oxygen concentration is high or if the thickness of the oxide film is higher than 0.1 μm, the proton peak is not symmetric. We think that in these two cases our method is more simple and the calculations more rapid. Moreover, our method allows us to estimate the radioactivity of ^{18}F due to the oxygen in the bulk of the metal by dissolving the oxide film.

Finally, we notice that while the proton peak of ^{16}O(dp)^{17}O is obscured by other reactions (for instance when the nitrogen concentration is high), nothing disturbs the measurement of ^{18}F radioactivity since the nuclear reactions ^{14}N(^{3}H,p)^{16}N and ^{14}N(^{3}H,2n)^{15}O lead to short half life radioisotopes (7.35 sec and 124 sec).

Table 2. Surface oxygen for aluminum samples.

Metal	Oxygen (μg/cm^2)	Trial number	Dispersion (μg/cm^2)	Oxide thickness (Al$_2$O$_3$) Å	Dispersion Å
I Double electrolysis (99.97%) industrially rolled	1.65	5	0.2	85	10
II I etched	1.1	5	0.15	58	8
III Simple electrolysis (99.7%) rolled at the laboratory and etched	0.9	5	0.1	47	5
IV Double electrolysis and high purity (99.998%) rolled at the laboratory and etched	0.48	6	0.08	25	4

VIII. Conclusion

In short, we described the first experiments that we performed for surface oxygen determination by means of radioactivation analysis. The excitation function of the reaction $^{16}O(^3H,n)^{18}F$ has been experimentally plotted from 0.5 to 3 MeV. 2 MeV tritons accelerated in a Van de Graaff offer good conditions for the determination of surface oxygen. It has been determined experimentally no chemical separation is necessary when the method is applied to aluminum, iron, chromium, nickel, and zirconium. The method enables us to measure surface oxygen in the range of 100 to $10^{-3}\,\mu$g/cm^2.

IX. Acknowledgment

X. References

[1]   Smales, A. A., Annal. Rep. Prog. Chem. **46,** 290 (1949).
[2]   Born, H. J., Angew. Chem. **72,** 559 (1960).
[3]   DeGoeij, J. J. N., Houtman, J. P. W., Modern Trends in Activation Analysis (1965),
        EURATOM Report 3896, 1968, p. 293.
[4]   Magnac-Vallette, D., J. Phys. Rad. **17** (1956).
[5]   Barrandon, J. N., and Albert, Ph., Revue de Physique Appliquee, Tome 3, Juin
        1968, pp. 111-115.
[6]   Engelmann, Ch., These C.N.A.M. (1964), Report C.E.A., (1964), No. R2559.
[7]   Gorodetzky, M. S., Bergdolt, A. M., Chevallier, A., Bres, M., and Armbruster, R.,
        Journal de Phys. **24,** 374 (1963).
[8]   Amsel, G., These annales de Physique **9,** 297 (1964). Amsel, G., and Samuel, D.,
        Analytical Chemistry **39,** 1689 (1967). Quaglia, L., Cuypers, M., Robaye, G., and
        Barrandon, J. N., Nuclear Instruments and Methods (to be published).

THE DETERMINATION OF STABLE CALCIUM ISOTOPES BY CHARGED PARTICLE IRRADIATION

Max Peisach and Rene Pretorius[1]

Southern Universities Nuclear Institute
P. O. Box 17, Faure, C.P.
South Africa

I. Introduction

Calcium is not only the fifth most abundant element in the earth's crust [1], it is also the most abundant metal in the human body, where it makes up about 1.5% of the body weight [2]. In many systems the role of calcium can best be studied by tracer techniques using either radioactive or stable isotopes but, in biomedical research, stable isotopes are preferred due to the reluctance of the medical profession to administer radioactive material to humans.

Because the heavier isotopes of calcium occur in such low concentrations in nature, preparations enriched in calcium-43, 46 or 48 are suitable for tracing purposes. Neutron activation methods have been used for determining calcium-48 [3-6] and calcium-46 [7], but these methods require a separate determination of total calcium content. No activation method for the isotopic determination of calcium-43 has previously been reported.

II. Experimental

A. Preparation of Samples and Standards

Calcium separated from biological material as oxalate or carbonate was dissolved in dilute hydrochloric acid and converted to calcium fluoride by evaporation with hydrofluoric acid in a platinum crucible. The calcium fluoride was evaporated in vacuum onto tantalum discs for proton or deuteron irradiation and on aluminium foils for alpha activation. Target thicknesses were approximately 1 mg/cm².

Standards were similarly prepared from enriched calcium isotopes as obtained from the Oak Ridge National Laboratory, U.S.A., and diluted with natural calcium to the required isotopic concentration.

---

[1] Presently at Activation Analysis Research Laboratory, Texas A&M University, College Station, Texas 77843.

B. Activation

Proton and deuteron activation was carried out with the 6 MeV Van de Graaff accelerator at the Southern Universities Nuclear Institute, and alpha activation at the cyclotron of the Council for Scientific and Industrial Research at Pretoria where energies up to about 32 MeV could be attained. Irradiations lasted up to 2 hours and beam currents between 2 and 5 μA were used.

Samples were mounted on a rotating target holder (Fig. 1), cooled by circulating water or air. Up to 12 samples were irradiated simultaneously. After irradiations, samples were analyzed either by gamma-ray spectrometry or gross gamma-ray counting, with a 3 in. × 3 in. NaI(Tl) scintillation detector. The enhanced resolution afforded by Ge(Li) detectors was not needed in this investigation.

C. Prompt Neutrons

The energy of the prompt neutrons emitted during irradiation was measured by the time-of-flight technique [8]. The neutron energy, E_n(MeV), may be obtained from the time (nanoseconds) taken by the neutron to traverse a fixed known distance d (meters), by the non-relativistic relationship;

$$E_n = \left(\frac{72.3 \times d}{t}\right)^2$$

Proton beams in pulses of 4 nsec duration, 400 nsec apart were obtained from the Van de Graaff accelerator. Targets were irradiated singly with average beam currents between 0.6 and 3.0 μA.

III. Results and Discussion

The determination of isotopic concentrations as described here is based on measuring a ratio of either activities or prompt neutron counts. It is thus unnecessary to determine the total calcium content separately. Furthermore, no yields, weights of targets, or irradiation fluxes need to be known.

Flux variation during irradiation would affect the activity ratios in samples irradiated singly. However, when the samples and standards are irradiated together, flux variations would only result in a calibration line with a different slope. In the case of prompt neutron measurement (see below), the flux variation during irradiation produces no effect because the decay of the product nuclides is not involved.
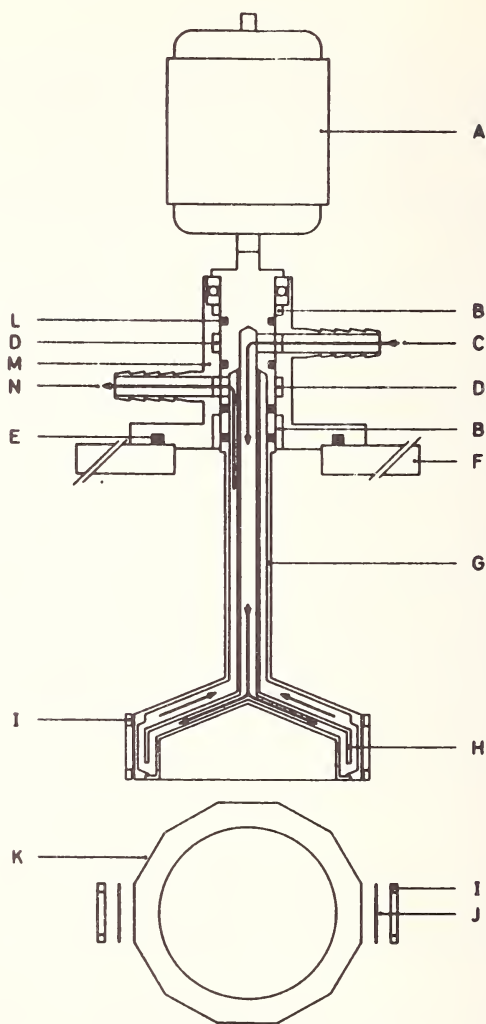
Figure 1.   Rotating target holder.

A.   Motor and gear box   H.   Cooling water stream guide
B.   Nylon bearings   I.   Target clamps
C.   Water inlet   J.   Target
D.   Water chamber   K.   Flats (12) for mounting targets
E.   Vacuum seal   L.   Water and vacuum seals
F.   Base plate   M.   Target holder support
G.   Rotating cooled target holder   N.   Water outlet

A.   PROTON ACTIVATION

Activation of calcium samples, with 4.75 MeV protons leads to the formation of 44 hour scandium-48 and 4 hour scandium-44 and 43, from

(p,n) reactions on calcium-48, 44 and 43, respectively. The ratio of the 44 to 4 hour activity gives a measure of the isotopic concentration of calcium-48. Activities from other calcium isotopes, fluorine, or from the tantalum backing do not interfere.

Scandium-44 activity does not form at proton energies below about 4.56 MeV and analysis of calcium-43 as tracer is possible at such energies [9]. Although at higher proton energies scandium-44 activity interferes with the determination of calcium-43, its formation is advantageous for the determination of calcium-48, as the precision with which the 4 hour activity representing total calcium is measured, is improved.

Table 1 shows some results for the determination of calcium-48 and 43 by proton activation at energies of 4.75 and 4.50 MeV, respectively. The relative standard deviation over the concentration range from natural

Table 1. The determination of calcium—43 and 48.

I Known concentration (atom %)	Activity ratio	Activity ratio per unit (atom %)	II Measured concentration (atom %)	Observed difference (II − I)
Calcium—48; Ep = 4.75 MeV [8]	(× 100)			
0.185	4.75	0.257	0.188	+ 0.003
0.192	4.83	0.252	0.191	− 0.001
0.375	9.32	0.249	0.369	− 0.006
0.825	21.57	0.262	0.854	+ 0.029
1.040	26.38	0.254	1.045	+ 0.005
1.370	33.15	0.242	1.313	− 0.057
Calcium—43; Ep = 4.50 MeV [9]	(× 1)			
0.145	1.97	9.13	0.149	+ 0.004
0.379	3.98	8.79	0.376	− 0.003
1.004	9.56	8.87	1.006	+ 0.002
1.769	16.41	8.91	1.780	+ 0.011
2.010	18.46	8.86	2.012	+ 0.002

Calcium—48: Relative standard deviation = ± 2.7%
          Mean error   = − 0.004 atom %

Calcium—43: Relative standard deviation = ± 3.2%
          Mean error   = + 0.003 atom %

abundance to about 2 atom % was ± 2.7% for calcium-48 and ± 3.2% for calcium-43.

B. DEUTERON ACTIVATION

When deuterons are used for activation, many radionuclides are produced from the stable isotopes of calcium. Of these, calcium-48 can be separately determined by measuring the high energy gamma rays of 8.8 minute calcium-49 formed by the reaction $^{48}Ca(d,p)^{49}Ca$. The 4 hour activity produced from calcium-42 and 43 served as a measure of total natural calcium and was determined by counting annihilation gamma rays [10].

A typical set of results for determining calcium-48 by deuteron activation is given in Table 2 where the activity ratio in column 2 represents the ratio of the 8.8 minute activity to the 4 hour activity. The relative standard deviation for the determination of calcium-48 concentrations ranging from natural (0.18%) to about 2 atom % was about ± 2%. The advantage of deuteron activation analysis over proton activation is its shorter duration because shorter-lived radionuclides are involved.

Table 2. Some determinations of calcium–48 by deuteron activation

I ^{48}Ca conc. known (atom %)	Activity ratio	Activity ratio per unit (atom %)	II ^{48}Ca conc. found (atom %)	Difference (II − I)	Relative error (%)
0.180	1.981	4.261	0.179	− 0.001	− 0.6
0.180	1.972	4.211	0.177	− 0.003	− 1.7
0.200	2.040	4.130	0.193	− 0.007	− 3.5
0.403	2.895	4.171	0.392	− 0.011	− 2.7
0.946	5.415	4.441	0.980	+ 0.034	+ 3.6
0.946	5.277	4.295	0.948	+ 0.002	+ 0.2
1.604	8.161	4.331	1.621	+ 0.017	+ 1.1
1.786	8.811	4.254	1.772	− 0.014	− 0.8

Number of samples in test series	= 16
Number of analyses in test series	= 25
Mean activity ratio per atom %	= 4.27 ± 0.09
Mean error	= − 0.0006 atom %
Relative standard error	= ± 2.03%
Slope of calibration line	= 4.286 per atom %
Intercept of calibration line; Activity ratio	= 1.214

C. ALPHA ACTIVATION

Alpha activation was found to be unsuitable for the determination of calcium tracers, because of the formation of intense activities of scandium-43 from the most abundant calcium isotope, calcium-40, by the reaction $^{40}Ca(\alpha,p)^{43}Sc$.

However, this reaction could well serve for the determination of calcium-40. The variation of the yield of scandium-43 activity, formed by the reaction $^{40}Ca(\alpha,p)^{43}Sc$, with alpha particle energy is shown in Figure 2 from which it can be seen that the most favorable energy at which total calcium could be determined would be at about 14 MeV.
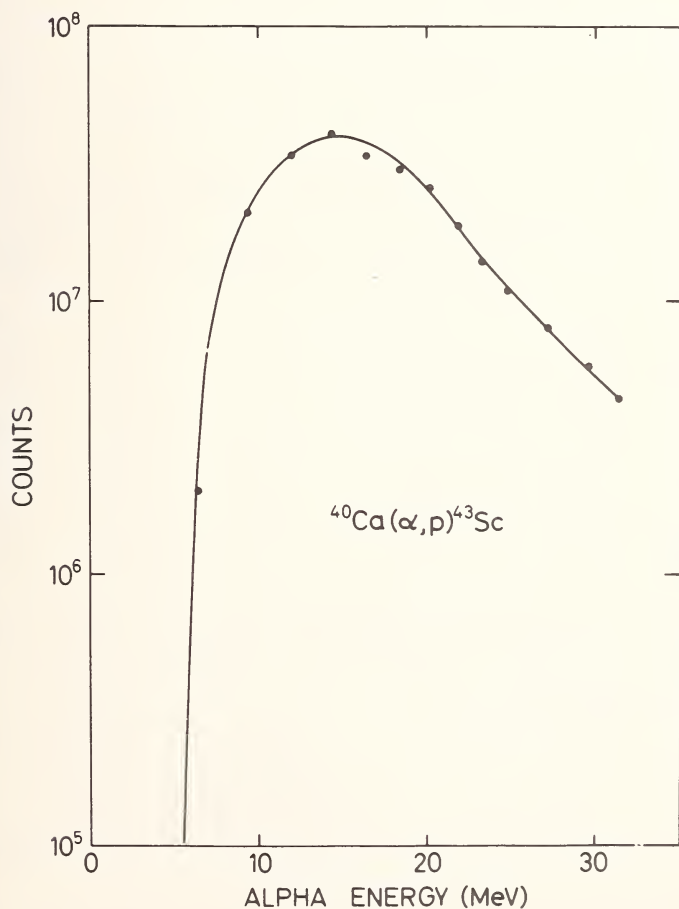
Figure 2. The variation of scandium-43 activity, formed by the reaction $^{40}Ca(\alpha,p)^{43}Sc$, vs. alpha irradiation energy.

D. Prompt Neutron Measurement

Time-of-flight spectra of neutrons emitted from calcium-43, calcium-48 and natural calcium targets irradiated with protons of 4.5 MeV are shown in Figure 3. At this bombarding energy neutrons from sources other than calcium-43 and calcium-48 could not be observed [11].

The net integrated counts of neutrons between 1.267 and 1.642 MeV (corresponding to the n_o and n_1 neutron groups from calcium-43 and
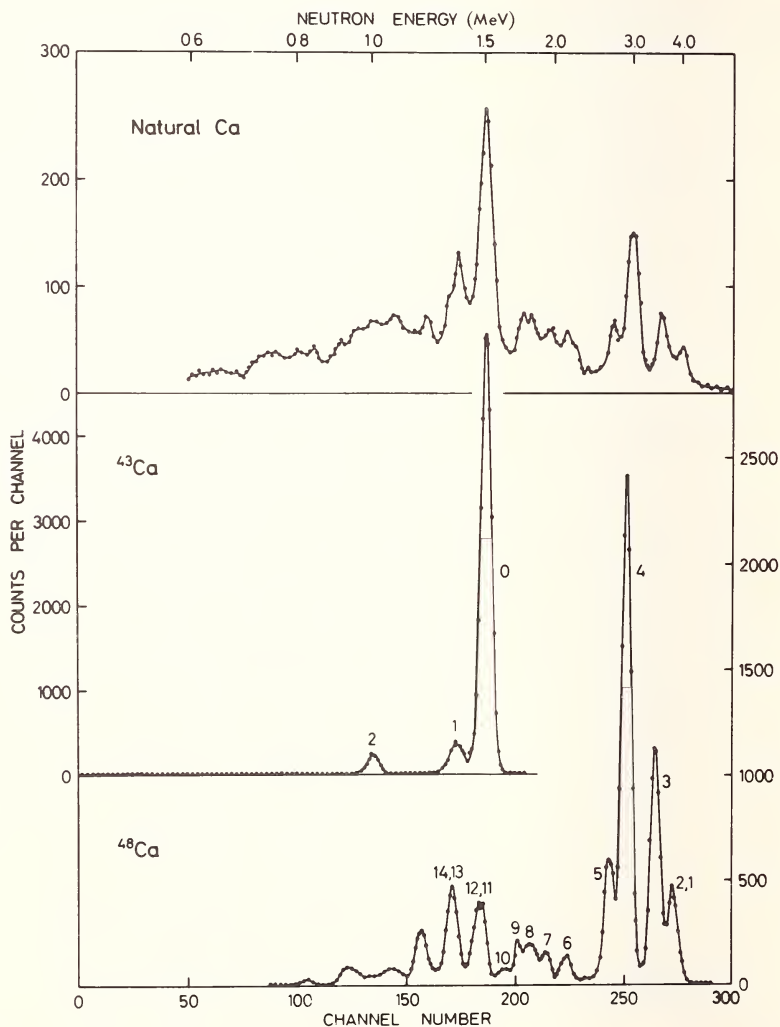
Figure 3.   Time-of-flight spectra of neutrons from (p,n) reactions on targets of natural-calcium and enriched ^{43}Ca and ^{48}Ca, Ep = 4.5 MeV, $\theta = 0°$; d = 2.991 meters [11].

including the n_{10} to n_{14} neutron groups from calcium-48, see Figure 3) is used as a measure of the calcium-43 concentration. The net integrated count from higher energy neutrons with energies between 2.416 and 4.151 MeV was used as a measure of calcium-48.

Results for the determination of calcium-43 are given in Table 3. The value in column 2 is the ratio of neutron counts representing calcium-43 to those representing calcium-48. A relative standard deviation of 4.34% was found for calcium-43 concentrations ranging from 0.145 (natural) to 2 atom of calcium-43 which represents total calcium, the internal ratio method is only applicable for comparatively low enrichments of calcium-48 up to about 0.4 atom ratio method. Although the time required to analyze a single sample by prompt neutron measurement is considerably shorter than by activation, the method cannot be applied to more than one sample at a time.

Table 3. Some determinations of calcium–43 by prompt neutron measurement.

I ^{43}Ca conc. known (atom %)	Neutron count ratio	Neutron count ratio per atom %	II ^{43}Ca conc. found (atom %)	Difference (II − I)	Relative error (%)
0.145	0.945	2.400	0.146	+ 0.001	+ 0.7
0.145	0.940	2.366	0.144	− 0.001	− 0.7
0.320	1.330	2.291	0.308	− 0.012	− 3.8
0.490	1.772	2.398	0.494	+ 0.004	+ 0.8
1.058	3.123	2.388	1.062	+ 0.004	+ 0.4
1.216	3.642	2.504	1.280	+ 0.064	+ 5.3
1.430	3.884	2.299	1.382	− 0.048	− 3.4
1.990	5.483	2.455	2.055	+ 0.065	+ 3.3

Number of samples in test series   = 15
Number of analyses in test series   = 24
Mean neutron count ratio per atom %   = 2.372
Mean error   = -0.0004 atom %
Relative standard error   = ± 4.34%
Slope of calibration line   = 2.378 per atom %
Intercept of calibration line;
    count ratio   = 0.597

IV. References

[1]   Holmes, A., "Principles of Physical Geology", Thomas Nelson and Sons Ltd.,
        London, 1964, p. 35.
[2]   Health Physics, Official Journal of the Health Physics Society 3, 146 (1960).
[3]   Junod, E., and Laverlochere, J., "Proceed. 3rd Intern. Coll. on Biology", Saclay
        1963.
[4]   Strelow, F. W. E., and Staerk, H., Anal. Chem. 35, 1154 (1963).
[5]   Amiel, S., and Juliano, J. O., Israel Atomic Energy Commission, Rept. IA-933
        (1964).
[6]   Corless, J. T., Anal. Chem. 38, 810 (1966).
[7]   Bethard, W. F., Schmitt, R. A., Olehy, D. A., Kaplan, S. A., Ling, S. M., Smith, R.
        H., and Dalle Molle, E., "Proceedings Symposium on Nuclear Activation
        Techniques in the Life Sciences", Amsterdam, 1967, p. 533.
[8]   Peisach, M., and Pretorius, R., Anal. Chem. 39, 650 (1967).
[9]   Brits, R. J. N., and Peisach, M., Unpublished data (1968).
[10] De Waal, T. J., Peisach, M., and Pretorius, R., Unpublished data (1968).
[11] McMurray, W. R., Peisach, M., Pretorius, R., van der Merwe, P., and van Heerden,
        I. J., Anal. Chem. 40, 226 (1968).

CROSS SECTIONS OF ^{18}F FORMATION BY DEUTERON BOMBARDMENT OF OXYGEN AND FLUORINE. APPLICATIONS TO OXYGEN ANALYSIS

Minh Duc Tran, A. Chenaud, H. Giron, and J. Tousset

Institut de Physique Nucleaire
Universite de Lyon
Lyon, France

I. Introduction

Interaction of oxygen with deuterons may produce three interesting radionuclides: ^{17}F, ^{13}N and ^{18}F. The ^{17}F formation has already been considered for analytical use by different authors [1-6]. This reaction is incontestably interesting but because of the too short period of ^{17}F the time required for the necessary cleaning of the sample and the possibility of radiochemical separation are limited. The ^{13}N production from oxygen has too little a probability compared to the parasite reaction ^{12}C(d,n)^{13}N and seems not to be promising for oxygen analysis. The ^{18}F formation already used by a few authors [7,8] occurring mainly by the reaction ^{18}O(d,2n)^{18}F (threshold energy 5.2 MeV) and also ^{17}O(d,n)^{18}F (exoergic) has been investigated here. Its analytical interference by the formation of ^{18}F from interaction of fluorine with deuterons (threshold energy 4 MeV) was estimated. Fluorine as an impurity is less often found together with oxygen than is carbon in pure materials; therefore, in spite of a ratio of cross sections most favorable for the reaction upon fluorine, we estimate this analytical study to be interesting. We have determined the excitation function to 27 MeV and pointed out from a certain energy, the interference of parasite spallation reactions producing ^{18}F from the matrice. One such reaction has been studied in aluminum. We confirm with other authors [9,10] the troublesome and often frequent existence of these reactions which we have already reported for alphas in silicon [11].

II. Excitation Functions

We use the 27 MeV deuteron beam delivered by the Lyon synchrocyclotron. The equipment employed chiefly the pneumatic transfer system for the irradiated sample has been described elsewhere [6,12]. The energy distributions of the particles at maximum energy, their slowing down, and the straggling due to energy loss fluctuations through

screens, standards and chemical compound targets, have been investigated in previous works [6,13-15]. The determination of the excitation functions in relative units is carried out by counting stacks of oxygen compounds in thin discs in which the stopping power is well known and measured.

The use of Mylar foils was very practical in spite of a high ^{13}N activity which requires a careful study of decay curves. The normalization is obtained by comparison with the well known $^{63}Cu(d,2n)^{63}Zn$ reaction which we have already used for the [17]F formation [6]. The excitation function is shown in Figure 1. In a quite identical manner the cross sections for the production of ^{18}F from ^{19}F are investigated with stacks of Teflon foils (Fig. 2). The importance of spallation reactions producing ^{18}F is estimated with stacks of aluminum discs whose surfaces are clean of
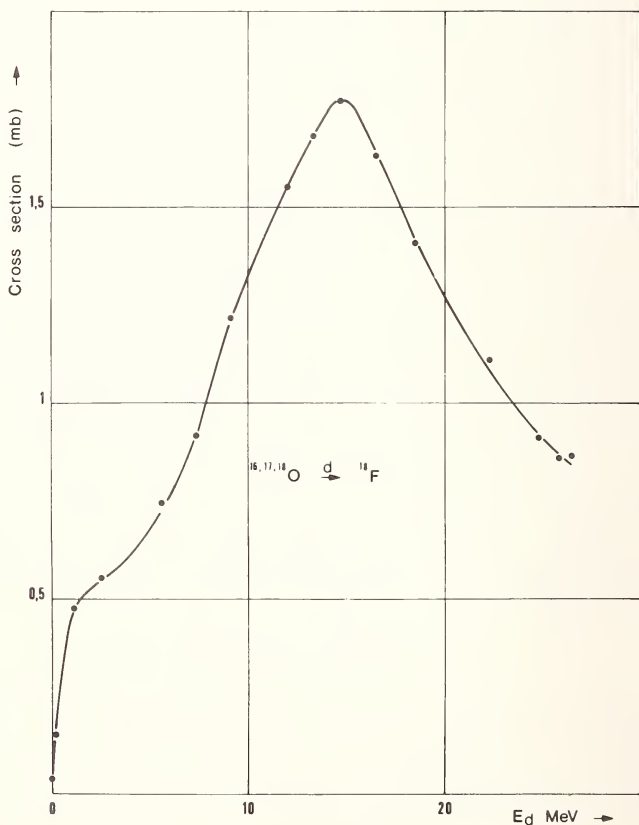
Figure 1.   Cross section of ^{18}F formation from deuteron reaction with oxygen. The correcting term K is very close to 1.
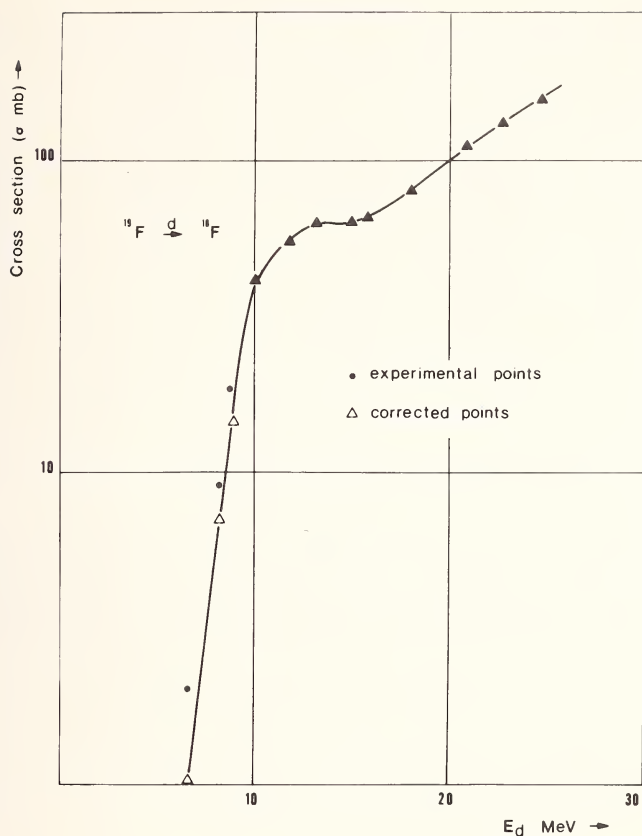
Figure 2. Cross sections of ^{18}F formation from deuteron reaction with fluorine.

their oxide coating before being counted. Figure 3 indicates the sharp rise from about 23 MeV of the interfering reaction.

In these activation curves for each experimental point which gives the mean value of cross section we have calculated the correction term introduced previously [15] for straggling and energy loss. The influence of this term is quite small except for large energy losses (Table 1); therefore, the activation curve or the excitation function can be used in either case for activation analysis.

III. Comparison of Oxygen and Fluorine Analysis Sensitivities

The saturation activities of two samples (A_1, A_2) of the same matrix containing respectively, n_1 and n_2, fluorine and oxygen atoms per
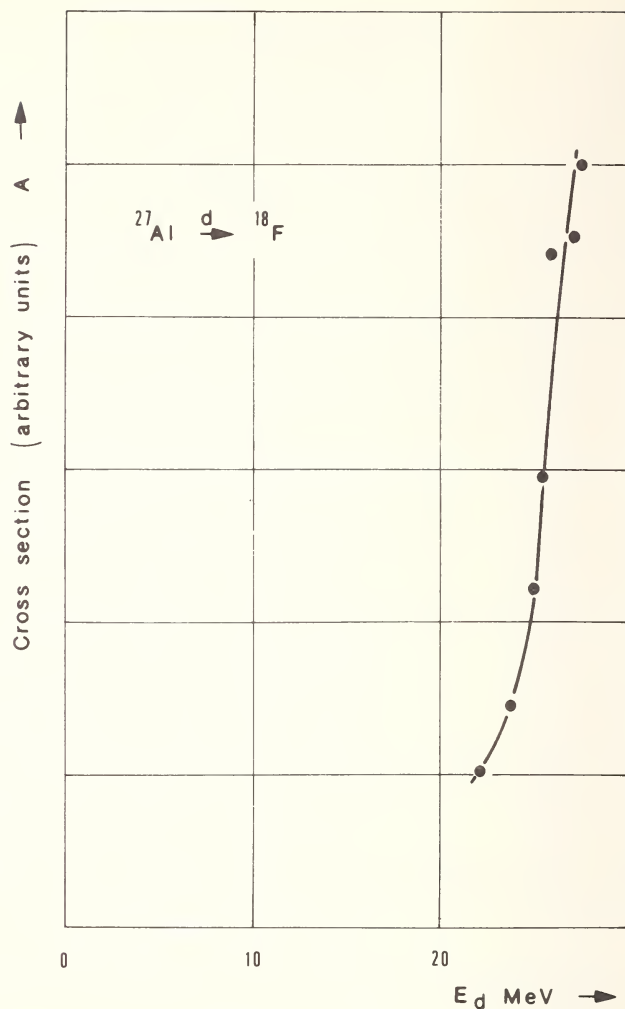
Figure 3.   Interfering reaction with aluminum producing ^{18}F from the 23 MeV
experimental threshold.

milligram, respectively and receiving I deuterons per second may be
expressed by [11,16,17].

$$A_1 = In_1\overline{\sigma}_1 R = In_1\sigma_{0_1}e_1$$

$$A_2 = In_2\overline{\sigma}_2 R = In_2\sigma_{0_2}e_2$$

$\overline{\sigma}$ and e represent the mean cross section (independent of the matrice) and
the equivalent thickness, respectively. σ_o is the cross section for the
considered reaction at the incident energy of the particles. R is the range
of the particles in the matrix.

Table 1. Correction factor k for ^{18}F formation cross sections from ^{19}F by deuteron bombardment of Teflon.

E MeV	ΔE MeV	S	α	k
6.6	0.8	0.617	1.37	0.67
8.3	0.4	0.574	1.27	0.78
8.9	0.3	0.553	1.20	0.77
10	0.5	0.531	0.24	1
15	0.6	0.404	0.026	1
20.8	0.5	0.255	0.099	1
24.7	0.5	0.148	0.074	1

The ratios of the activities from the same number of atoms:

$$\frac{A_1}{A_2} = \frac{\overline{\sigma_1}}{\overline{\sigma_2}} = \frac{\sigma_{0_1} e_1}{\sigma_{0_2} e_2}$$

defines the ratio of analysis sensitivities for the two elements in any matrix. They are represented in the Figure 4. The choice of the incident energy may limit the interference and even may suppress it.
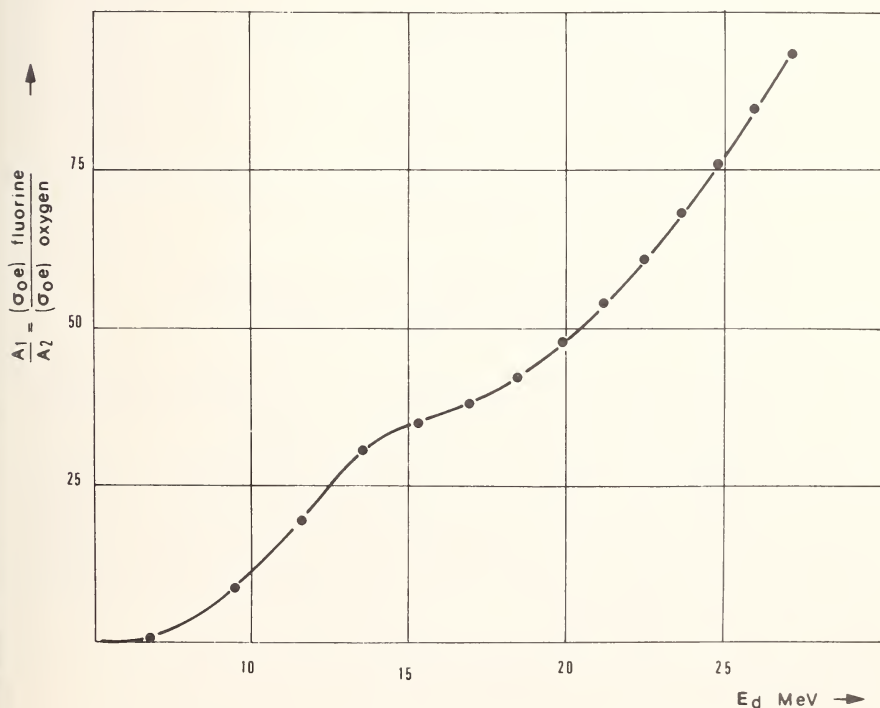
Figure 4. Oxygen and fluorine analysis sensitivity ratios versus deuteron energy.

The Figure 5 points out the variation of equivalent thicknesses in aluminum versus the particle energy.
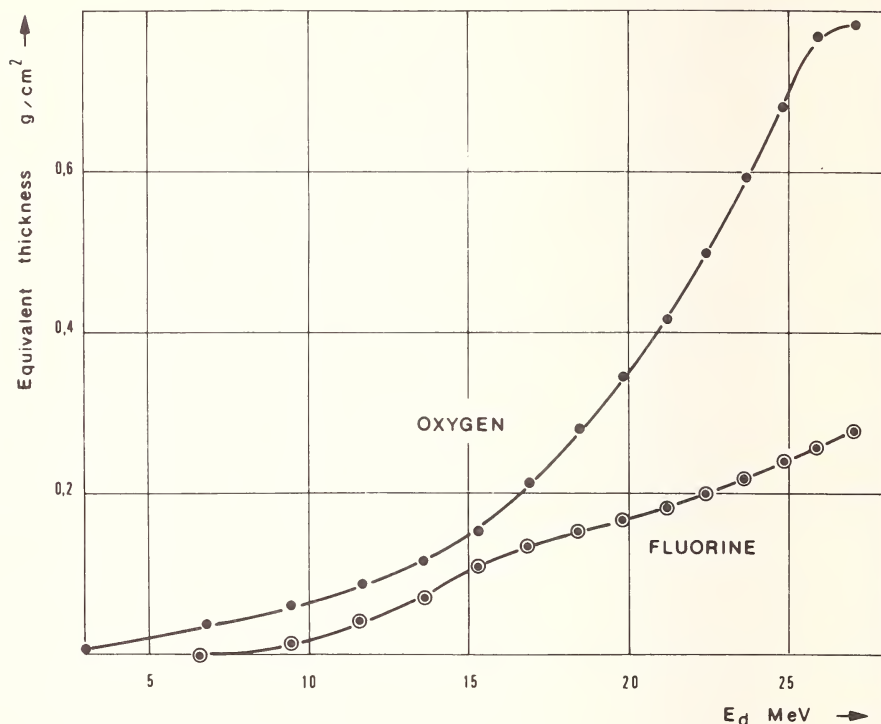
Figure 5.   Equivalent thicknesses in aluminum.

IV. Comparison of Oxygen Analysis Sensitivities
for Deuteron and Alpha Irradiations

It may be attempted to compare sensitivities of oxygen analysis by formation of ^{18}F for both deuteron and alpha irradiations with the same synchrocyclotron, *i.e.* the relation: $E_\alpha = 2E_d$ is satisfied.

This comparison in the general case of an undetermined matrix is theoretical, and it is assumed that the interference with fluorine for deuteron and the influence of parasitic reaction are negligible. With the same number of incident particles, the ratio of activities corresponding to the same number of atoms, is:

$$r = \frac{A_\alpha}{A_d} = \frac{\sigma_{0_\alpha} e_\alpha}{\sigma_{0_d} e_d}$$

for one given matrix.

This sensitivity ratio is practically independent of the matrix since with our previous assumptions $(E_\alpha = 2E_d)$:

$$R_d(E) = 2R_\alpha(2E)$$

and:

$$\frac{e_\alpha}{e'_\alpha} = \frac{R_\alpha}{R'_\alpha}$$

and also:

$$\frac{e_d}{e'_d} = \frac{R_d}{R'_d}$$

for two different matrices [11].

The value of r most favorable for alphas is found to be 50 with 54 MeV alphas and 27 MeV deuterons.

The curve of Figure 6 shows the variation of this ratio versus energy. It points out the advantage of deuteron activation in the case of small synchrocyclotrons $(E_d < 12 \text{ MeV})$:
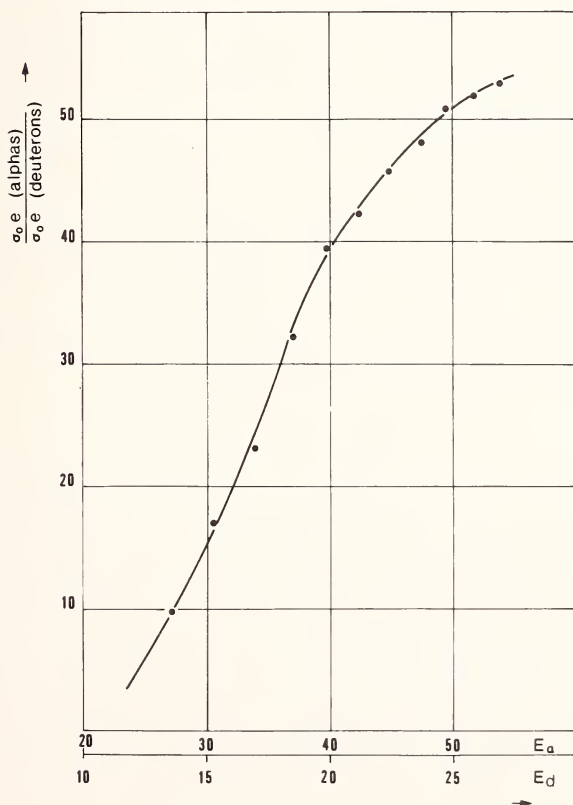
Figure 6. Ratio of sensitivities of oxygen analysis with deuterons and alphas.

V. Conclusion

The investigation of excitation functions of reactions producing ^{18}F from oxygen and fluorine has permitted us to determine precisely the reciprocal interference and its variation versus the deuteron energy.

A comparison of oxygen analysis by ^{18}F formation obtained with deuteron and alpha reactions has specified the choice of particle according to the energy.

VI. References

[1]   Amiel, S., and Peisach, M., Anal. Chem. **34**, 1305 (1962).

[2]   Blanc, A., Julliot, C., and Lanisiart, A., Bull. Inf. Science et Tech. 61 (1960).

[3]   Sippel, R. R., and Glover, E., Nucl. Instr. Meth. **9**, 37 (1960).

[4]   Sue, P., C.R.A.S. **242**, 770 (1956).

[5]   Hammar, L., and Forsen, S., J. Inorg. Nucl. Chem. **28**, 2111 (1966).

[6]   Lacroix, M. J., Tran, Minh Duc, and Tousset, J., Proc. of the 2nd Conf. on Practical Aspects of Activation Analysis with Charged Particles, Liege, Sept. 1967, EUR. 3896 d.f.e. 351 (1968).

[7]   Winchester, J. N., Report M.I.T., Cambridge, 39, Mass. (1960).

[8]   Moller, E., Nilsson, L., and Starfelt, N., Nucl. Instr. Meth. **50**, 280 (1967).

[9]   Barrandon, J. N., Debrun, J. L., and Albert, Ph., Proc. of the 2nd Conf. on Practical Aspects of Activation Analysis with Charged Particles, Liege, Sept. 1967, EUR. 3896 d.f.e., 277 (1968).

[10]   Deyris, M., These, Paris (1966).

[11]   Chevarier, N., Giroux, J., Tran, Minh Duc and Tousset, J., Bull. Soc. Chim. France **8**, 2893 (1967).

[12]   Martin, J., Tousset, J., Rev. Phys. **3**, 63 (1968).

[13]   Tran, Minh Duc, Demeyer, A., Tousset, J., and Chery, R., J. Phys. **29**, 129 (1968).

[14]   Tran, Minh Duc, These Doct. Ing., Lyon (1968).

[15]   Tran, Minh Duc, and Tousset, J. (See this volume, p. 754.)

[16]   Ricci, E., Hahn, R. L., Strain, J. E., Dyer, F. F., "Modern Trends in Activation Analysis", Texas A & M University, (1965).

[17]   Engelmann, Ch., Rapport C.E.A. R/2559, (1964).

EXAMPLES OF DETERMINATION OF LIGHT ELEMENTS IN VARIOUS HIGH PURITY MATERIALS, BY GAMMA PHOTON AND CHARGED PARTICLE ACTIVATION

Charles Engelmann, James Gosset, Monique Loeuillet, Alain Marschal, Pierre Ossart and Michele Boissier

Centre d'Etudes Nucleaires de Saclay
Departmente de Metallurgie
B.P. 2 — Gif S/Yvette (Essonne) - France

I. Introduction

The object of our paper is to present some of the results that we have obtained with the methods that have been employed in our laboratory for several years, relating mainly to the following analyses: (1) Nondestructive determination of oxygen in silicon by alpha and proton activation, in iron and niobium by ^{3}He activation. (2) Oxygen by gamma activation followed by a chemical separation of oxygen-15 by reducing fusion. (3) Carbon and nitrogen by gamma activation followed by a simultaneous separation of nitrogen-13 and carbon-11 by oxidizing fusion. (4) Nitrogen by proton activation. For some samples, the same element has been determined by two types of activation. The values showing the importance of some competitive reactions are given, mainly, those referring to the determination of carbon and nitrogen by photon activation and nitrogen by proton activation.

II. Experimental Procedure

A. STANDARDS

1. Charged Particles

The flux monitor placed in front of the sample is composed of a thin mica disk (from 5 to 10 μm) protected by a 25 μm pure aluminum wrapping, which collects the recoil nucleus to prevent the loss of radioactive nuclei by evaporation (Figure 1). For oxygen analysis by the following reactions, $^{16}O(\alpha,d)^{18}F$, $^{16}O(^3He,p)^{18}F$, and $^{18}O(p,n)^{18}F$ the ^{18}F activity induced in the mica is used. In the determination of nitrogen by proton activation, it is possible to use the activity of ^{18}F or ^{13}N from the reaction $^{16}O(p,\alpha)^{13}N$. To determine the amount of impurity, a standard and sample, both having a thickness larger than the range of the particle
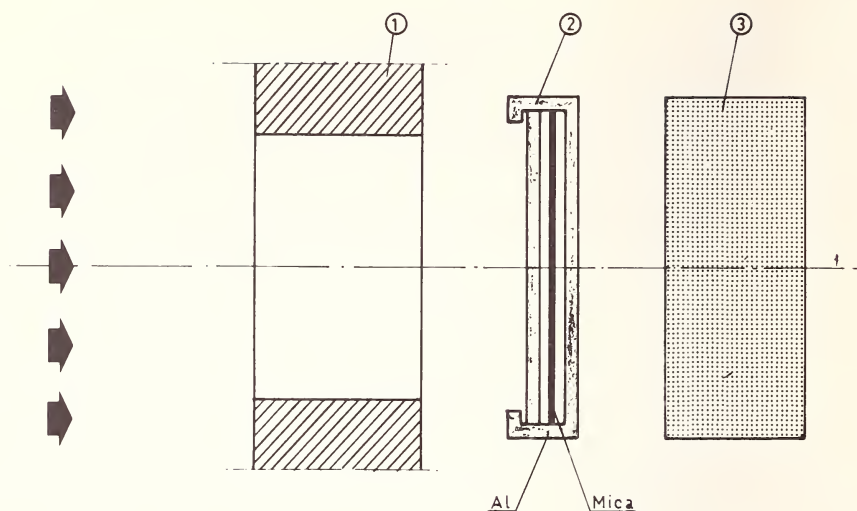
Figure 1. Relative disposal of the flux monitor and of the sample for charged particle activation.

are irradiated. After standardization of the counting rate to the activity of the flux monitor, the concentrations of impurity are calculated by the following equation [1].

$$\begin{array}{c}\text{concentration}\\\text{in}\\\text{the sample}\end{array} = \frac{\begin{array}{c}\text{activity in the}\\\text{sample}\end{array}}{\begin{array}{c}\text{activity in the}\\\text{standard}\end{array}} \times \frac{\begin{array}{c}\text{actual range}\\\text{standard}\end{array}}{\begin{array}{c}\text{actual range}\\\text{sample}\end{array}} \times \begin{array}{c}\text{concentration}\\\text{in}\\\text{the standard}\end{array} \qquad (1)$$

2. Gamma Photon

Standardization is easier. The weak absorption of gamma photons allows the simultaneous irradiation of a thick standard and sample so the calculation of the concentration is limited to a rule of three. It is necessary to take some precautions considering the existence of a transversal and longitudinal gradient of activation. A standard must be placed in front and behind the sample in the axis of the beam, the thickness of the whole being only a few millimeters. Standard and sample will have to be of the same radial shape.

B. Etching

After irradiation, the samples are systematically etched. The procedure depends upon the type of activation.

1. Charged Particles

The irradiated side of the sample is always damaged by the beam. We have observed that for certain materials, silicon, for example, the chemical etching at this place is considerably weakened and is very irregular. Therefore, it is necessary to remove the damaged layer by mechanical grinding before chemical etch in several solutions. For silicon, we use the mixture of HF, HNO_3, H_2SO_4, H_3PO_4 all being in equal proportions.

2. Gamma Photons

The chemical etching by itself is enough. The solution used depends on the nature of the analyzed material. Usually, the mixture HF-HNO_3 gives good results. As above the sample is etched by 3 solutions at least. In both cases of activation, the thickness removed is checked by weight or by micrometric measurement.

C. NONDESTRUCTIVE DETERMINATION OF OXYGEN

1. In Silicon

The main nuclear reactions to be considered are listed in Table 1. The incident energies are $\alpha = 42$ MeV and $p = 15$ MeV. The intensity of the beam is about 2 μA. The actual energies after etching, which must be considered in the determination of oxygen are given along with the results

Table 1. Nuclear reactions used for determination of oxygen by charged particle activation and main competitive reactions.

Nuclear reaction used for determination	Threshold (MeV)	Principal interfering reactions	Threshold (MeV)
$^{16}O(\alpha, d)^{18}F$	20.4	$^{15}N(\alpha, n)^{18}F$	8.1
		$^{19}F(\alpha, \alpha n)^{18}F$	12.6
		$^{28}Si(\alpha, ^{15}N)^{18}F$	22.8
		$^{29}Si(\alpha, ^{15}N)^{18}F$	23.3
		$^{30}Si(\alpha, ^{16}N)^{18}F$	28.6
$^{16}O(^3He, p)^{18}F$	$Q > 0$	$^{19}F(^3He, \alpha)^{18}F$	$Q > 0$
$^{18}O(p, n)^{18}F$	2.6	$^{19}F(p, d)^{18}F$	8.6
		$^{29}Si(p, ^{12}C)^{18}F$	15.5

in Table 2. For nitrogen considering its concentration is silicon and the isotopic abundance of nitrogen-15, the incidence of the competitive reaction is negligible. We have carried out analysis for fluorine by gamma photon activation. The concentrations were always much lower than 0.05 parts per million (ppm). Therefore the competitive reaction on fluorine is also negligible for the oxygen concentration determined. The reaction with the matrix by alpha activation has been reported by Tousset [2] at energies higher than the one we use. It does not seem that in our case this reaction is important for oxygen concentration larger than 10^{-7}.

Table 2.   Results of nondestructive determination of oxygen in silicon by α and p activation.

Silicon sample	α		p	
	· E (MeV)	ppm	E (MeV)	ppm
A	35	0.8		
	37	0.9	8.5	2.7
	38.5	1		
	38.5	2		
B	36.5	0.5		
	38.5	0.5		
	38.5	1		
C	37	3.5	9.5	1.8
	38.5	2.1		
D	36	1.2		
	39	3.3	14.2	4.6
	38.5	2.5		
E	35	0.2		
	38.5	0.5		
F	38.5	1.5		
	38.5	1.8		
G	38	3.3	14.2	1.8
	38.5	5.5		
	38.5	3		

2. In Iron and Niobium

Nuclear reactions are indicated in Table 1. Oxygen is much more activated than fluorine at the energy we use, at least 10 times more, so the influence of this halogen is negligible considering the very low concentration of this element in these samples. The incident energy of the ^{3}He particles is 14.7 MeV, the beam intensity is about 0.5 μA. The actual energy after etching and the results are given in Tables 3 and 4.

Table 3. Results of determination of oxygen, nitrogen, and carbon
in iron.[a]

Iron sample	Oxygen		Carbon	Nitrogen
	(γ, n)	^{3}He 6 MeV	(γ, n)	p 13 MeV
A	4		19	
	3.5		38	
B		2.2	0.4	0.15
		4.4	0.5	
		3.7		
C		1.8	10	0.04
		0.6	6	0.06

[a] All results are parts per million.

Table 4. Results of determination of oxygen, nitrogen, and carbon
in niobium.[a]

Niobium sample	Oxygen	Carbon	Nitrogen
	^{3}He 9.5 MeV	(γ, n)	(γ, n)
A	20	1.5	15
	15	1.2	
B	1	0.6	0.8
	0.6		
	2.9		

[a] All results are parts per million.

D. Determination of Oxygen by Gamma Photon Activation Followed by a Chemical Separation of Oxygen-15

The maximum energy of the photon beam is 35 MeV. The average intensity before conversion of the electrons is 50 μA. Oxygen-15 is produced by the reaction $^{16}O(\gamma, n)^{15}O$, threshold 15.7 MeV. Its half life is 2.1 minutes. This isotope is extracted by reduction fusion in inert gas atmosphere (helium, argon). The sample held in a graphite crucible is heated to temperature above 2000 °C by an induction furnace. The characteristics of the generator are 12 KW, 500 KHz. The oxides are reduced by carbon following the basic reaction $MO + C \rightarrow M + CO$.

The carbon monoxide carried by the gas stream is oxidized in carbon dioxide then trapped on "ascarite" (soda on asbestos) permanently placed between two counters NaI(Tl) size 80 mm × 100 mm. The heating lasts about 2 minutes. The carrier gas flow is a few liters per minute. The whole separation procedure is accomplished 5 minutes after the end of irradiation. Iron chips with a high oxygen concentration are melted with the sample. This bath has a double action; first, it helps the oxygen-15 extraction; secondly, the oxygen acts as a carrier. The diagram of Figure 2 shows the various parts of the apparatus.
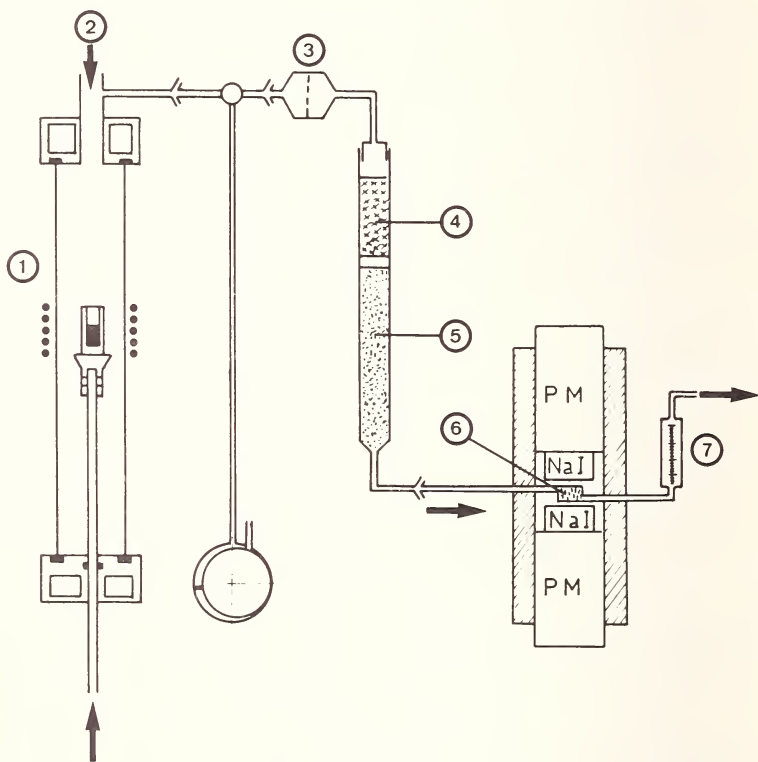
Figure 2.   Diagram of the apparatus used for separation of oxygen-15 by reduction fusion (1) induction furnace, (2) air lock for sample introduction (3) porous glass filter to remove particular matter (4) Schutze reagent (5) MnO_2 (6) "Ascarite" (7) flow meter.

Among the most likely competitive nuclear reactions we must point out $^{19}F(\gamma,tn)^{15}O$, threshold 27.4 MeV and $^{20}Ne(\gamma, \alpha n)^{15}O$, threshold 20.4 MeV. The second reaction which could be the more disturbing is negligible because of the chemical nature of the element. For the first one,

if one considers results obtained for the competitive reactions producing carbon-11 and nitrogen-13 at 35 MeV, it should be possible to neglect it for high purity metals.

E. Simultaneous Separation of Nitrogen-13 and Carbon-11 by Oxidizing Fusion

The maximum energy of the beam and its intensity are the same as above. After irradiation and etching, the sample is placed in a crucible containing from 20 to 30 g of the melting oxidizing mixture (87.5% $Pb_3O_4 - 12.5\%$ B_2O_3). By heating with an induction furnace, an oxidizing reaction is produced during which carbon and carbides give CO_2 and CO, nitrogen and nitrides give nitrogen and nitrogen oxides. The extracted gas is carried by a weak flow of helium (100 to 150 cm^3 per minute) and is passed successively through (Fig. 3) (1) silica wool and porous glass filter to remove particulate matter, (2) a 500 °C furnace which contains Cu to reduce nitrogen oxides to nitrogen and CuO which oxidizes CO, (3) MnO_2 which traps the halogens ^{78}Br, ^{18}F, and (4) Schutze reagent (I_2O_5 on silica gel) to oxidize the last traces of CO. Then the carrier gas contains only CO_2 and N_2. CO_2 is trapped on ascarite, N_2 on molecular sieve Linde
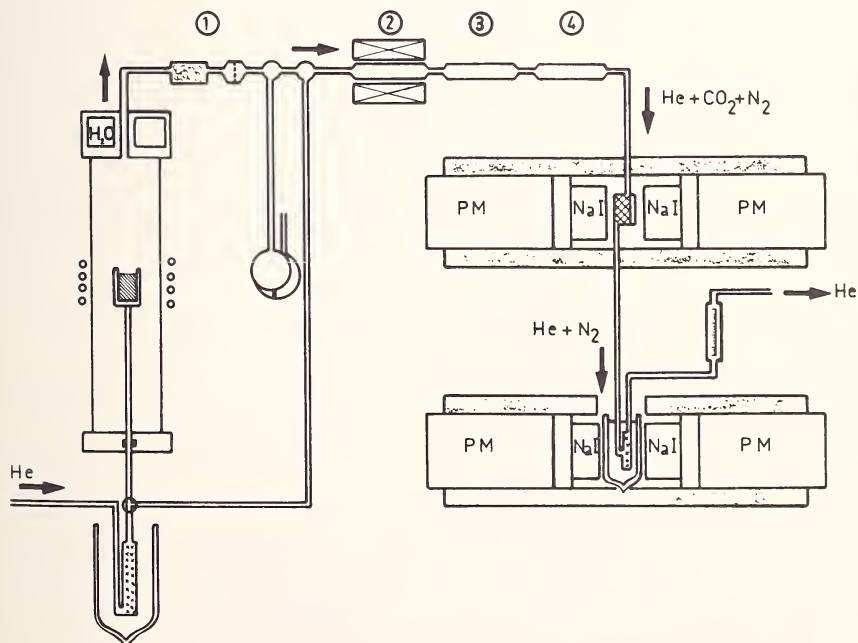
Figure 3.   Diagram of the apparatus used for simultaneous separation of nitrogen-13 and carbon-11 by oxidizing fusion.

5 Å cooled in liquid nitrogen. These two traps are permanently between two counters to measure the gamma annihilation of the β^+ emitted by ^{11}C and ^{13}N. The frequency of the induction furnace must be higher than 5 MHz to allow the coupling with the oxidizer. An output of 4 kW is sufficient. The reaction with the oxidizer begins at 700 °C only. About 1 g of iron chips with high carbon and nitrogen content is added as an igniter. Nonactive carbon and nitrogen act as carriers. The fusion lasts from 3 to 5 minutes. The extraction procedure is completed about 10 minutes after the end of the irradiation.

In Tables 3, 4, and 5 we give the results obtained by gamma activation to determine carbon and nitrogen and by proton activation to determine

Table 5. Various results of determination of nitrogen and carbon.[a]

Sample	Carbon	Nitrogen	
	(γ, n)	(γ, n)	p 13 MeV
Tantalum	0.8	6.8	1.1
	1.2	2.3	1.4
	1.3	4.5	1.6
			2.9
Ge A	0.07	5	
Ge B	0.7		
Ge C	<0.07	<0.1	

[a] All results are parts per million.

nitrogen. The nuclear reactions used and the main competitive reactions are listed in Table 6. Some values referring to the competitive reactions are given in Tables 7, 8 and 9.

Table 6. Nuclear reactions used for determination of nitrogen and carbon and main competitive reactions.

Nuclear reaction used for determination	Threshold (MeV)	Principal interfering reactions	Threshold (MeV)
$^{12}C(\gamma, n)^{11}C$	18.7	$^{14}N(\gamma, t)^{11}C$	22.7
		$^{16}O(\gamma, \alpha n)^{11}C$	26
$^{14}N(\gamma, n)^{13}N$	10.6	$^{16}O(\gamma, t)^{13}N$	25
$^{14}N(p, \alpha)^{11}C$	3.1	$^{11}B(p, n)^{11}C$	3

Table 7. Amounts of nitrogen and oxygen giving the same carbon—11 activity that 1 μg of carbon by gamma activation.

Electron beam energy (MeV)	μg of oxygen	μg of nitrogen
30	>6000	>2000
35	680	150
40	180	60
45	90	

Table 8. Amount of oxygen giving the same activity in nitrogen—13 that 1 μg of nitrogen by gamma activation.

Electron beam energy (MeV)	μg of oxygen
25	>2500
30	780
35	270
40	140
45	110

Table 9. Amount of boron giving the same activity in carbon—11 that 1 ppm of nitrogen by proton activation.

Energy of protons (MeV)	ppm of boron
6	0.13
8	0.4
10	0.5
14	1.2
18	2
20	2.5

In several samples of high purity polycrystalline silicon we tried to determine nitrogen and boron by proton activation. The energy after etching was 8.5 MeV. We have found that nitrogen and boron concentrations in the samples were lower than 10^{-3} parts per million (ppm). A 2 μA beam intensity was not sufficient to determine the exact concentration. For these two elements deuteron activation is more interesting [3].

III. Conclusion

All these results show that light element concentrations in certain materials are so low that only activation analysis by gamma photon and charged particles allow their determination. The lowest amounts determinable using these methods which depend on the type of activation and the intensity, are about 10^{-2} for gamma activation and 10^{-4} for charged particles [4]. The example of silicon, the results for nitrogen in pure iron (Table 3) and those for carbon in germanium (Table 5) show the necessity of such sensitivities.

IV. References

[1]   Chevarier, N., Giroux, J., Tran, Minh Duc, Tousset, J., Bull. Soc. Chim. de France **8,** August 1967.
[2]   Tousset, J., Private communication.
[3]   Engelmann, C., Int. J. of App. Rad. and Isotopes **18,** (1967).
[4]   Engelmann, C., Cabane, G., Proceedings International Conference (1965) "Modern Trends in Activation Analysis", College Station, Texas; Engelmann, C., Rapport C.E.A. 3307 (1967); Engelmann, C., Bull. Soc. Chim. de France **7,** (1967).

SELF-SHIELDING CORRECTIONS IN PHOTON ACTIVATION ANALYSIS

G. J. Lutz

National Bureau of Standards
Washington, D.C. 20234

I. Introduction

A general source of systematic error in activation analysis is the difference in absorption of the bombarding particles between sample and standard. This problem has been considered in thermal neutron [1-3] and 14 MeV neutron activation analysis [4]. The study described here was undertaken to evaluate the effect in high energy photon activation analysis.

Since the mean free path of the photons is large compared to the dimensions of the sample, one would expect a relationship of the type

$$\frac{f}{f_0} = \frac{A}{A_0} = e^{-t\Sigma\mu\rho}. \tag{1}$$

where

$f_0 =$ photon flux with zero attenuation (photons·cm^{-2}·sec^{-1})

$f =$ photon flux after attenuation (photons·cm^{-2}·sec^{-1})

$A_0 =$ specific activity of an element in the sample with zero attenuation

$A =$ specific activity of an element in the sample after attenuation.

$\Sigma\mu\rho =$ the sum over all elements in the sample of the product of the gamma ray attenuation coefficient and the density of each element (cm^{-1})

$t =$ thickness of the sample (cm)

A. SAMPLE THICKNESS

Since we will consider the average photon flux seen by a sample, the apparent sample thickness, t, would be expected to be one-half of the average distance traversed in the sample by the bombarding photons. The samples used in this laboratory are cylindrical in shape and have a diameter of 0.95 cm. The photon beam is perpendicular to the axis of the cylinder and this traverses a circular cross section of the sample. On the assumption that the sample is uniformly irradiated with a parallel beam,

the average path length of the photons in the sample would be the average length of parallel equally spaced chords of a circle. This is $0.785 \times$ diameter, and the expected apparent sample thickness is $0.785 \times$ radius.

B. Gamma-Ray Absorption Coefficients

Figure 1 shows in histogram form the energy dependence of bremsstrahlung, of the cross section of a typical photonuclear reaction, and of a typical gamma-ray absorption coefficient. Because of the energy dependence of the gamma-ray absorption coefficient, equation (1) must be modified to reflect the sum of contributions of each energy increment bin (taken here at one MeV). In addition each term in the sum must be weighted by the fraction of the total production of the reaction under consideration in that energy increment. With these modifications one obtains the expression

$$\frac{f}{f_0} = \frac{A}{A_0} = \sum^{\text{energy}} W_\epsilon e^{-t\Sigma\mu_\epsilon\rho} \tag{2}$$

where the weighting factor

$$W_\epsilon = \frac{\phi_\epsilon\sigma_\epsilon}{\sum^{\text{energy}}\phi_\epsilon\sigma_\epsilon}$$

The energy summation should be carried out from the threshold of the reaction to the electron energy. The summation in the exponential is still over elements in the sample.

For ease in computation and utilization of the correction factors to be obtained, we have considered an average energy and use equation (1) with the gamma ray absorption coefficients corresponding to this energy. A logical choice for the average energy is the energy of maximum cross section. Numerical values justifying this approximation will be considered in the discussion below.

II. Experimental

Samples of powders of MgO, PbO and carefully blended mixtures of the two compounds to give variations in photon absorption properties were used for the evaluation of the photon attenuation correction factors. The powdered samples were encapsulated into polyethylene vials of 0.95 cm inside diameter and 2.1 cm length. They were loaded a few hundred milligrams at a time and compacted with uniform pressure before the next addition. Care was taken that voids did not occur. Copper disks weighing about 100 mg were taped to each end of the vial as flux monitors and the vial was encapsulated in an aluminum rabbit. The irradiations were performed in the 45 degree facility of the NBS LINAC. The reactions induced in the samples were ^{25}Mg(γ,p)^{24}Na and ^{204}Pb(γ,n)^{203}Pb. The

RELATIVE FLUX

RELATIVE CROSS SECTION

GAMMA RAY
ATTENUATION COEFFICIENT

ENERGY (MeV)
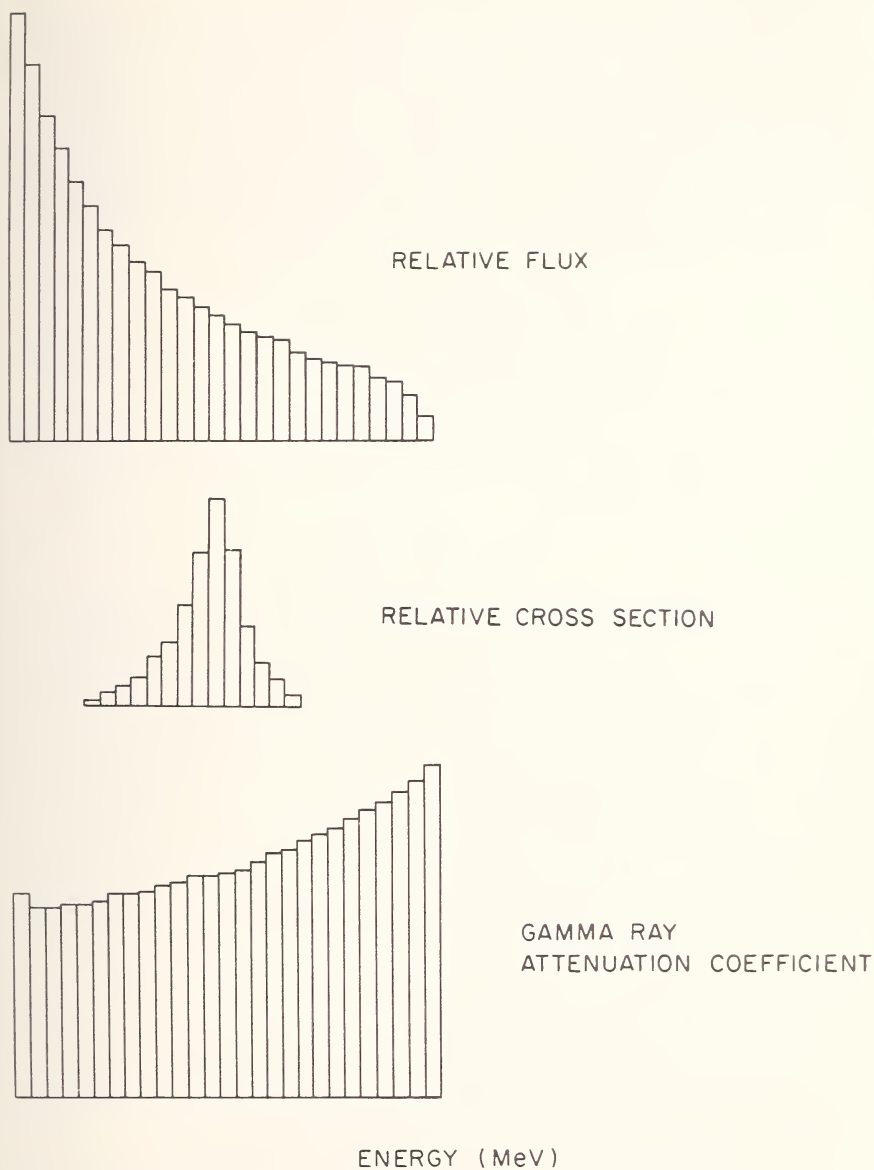
Figure 1. Typical energy relationship of photon flux, photonuclear cross section and gamma-ray attenuation coefficient.

electron energy was 35 MeV and the average beam current was about 20 μA. Irradiations of a few minutes gave quantities of radioactivity that were convenient for counting.

After irradiation, the samples were dissolved in a mixture of dilute nitric and acetic acids and diluted to a constant volume and configuration. As soon as possible after irradiation, the ^{24}Na was counted with a NaI detector and gamma ray spectrometer. The area under the 2.75 MeV gamma-ray peak was taken as a measure of the counting rate of the sample. After a delay of about a week to allow the ^{24}Na to decay, the 280 keV gamma ray of ^{203}Pb was similarly counted. The ^{64}Cu activity in the flux monitors was counted the day after irradiation.

III. Results and Discussion

The count rates per unit weight of magnesium and lead in each sample were calculated and corrected for decay and flux monitor.

Equation (1) was rewritten in logarithmic form using the mass absorption coefficients corresponding to the energy of maximum cross section yielding the equation

$$\ln A = \ln A_o - t\Sigma\mu\rho \tag{3}$$

Since the energy of maximum cross section for the lead and magnesium reactions are 14 and 21 MeV respectively, different values of the gamma ray absorption coefficients must be used and the data for each element treated separately.

The sum of the product of the gamma ray attenuation coefficient at the energy of maximum cross section and the volume density of the elements, $\Sigma\mu\rho$, was calculated for each sample. Values of μ were taken from Davisson [5]. The natural logarithm of specific activity of the element of each sample of a series was plotted against $\Sigma\mu\rho$ of the sample and the slope and intercept of the best fit straight line was calculated by the method of least squares. The negative of the numerical value of the slope of the line equals the apparent sample thickness.

The results of a typical series is shown in Figure 2. Table 1 shows values of the slope obtained from four series of determinations. For ease in utilizing the corrections, the data are normalized so that the intercept of the line corresponding to zero attenuation equals one, and the correction factors can be read directly for a desired value of $\Sigma\mu\rho$.

The weighted mean of the apparent sample thickness of the four series of determinations is 0.320 cm. This has a standard deviation of 0.020 cm. This is in reasonable agreement with the estimated value of $0.785 \times$ radius or 0.373 cm. With a measured value of sample thickness, it is now possible to test the validity of simplification of equation (2). The bremsstrahlung shape for electrons of 35 MeV energy and a tungsten target was generated from the Schiff equation [6]. The cross section of the ^{25}Mg$(\gamma,p)^{24}$Na and ^{204}Pb$(\gamma,n)^{203}$Pb reactions were taken from the
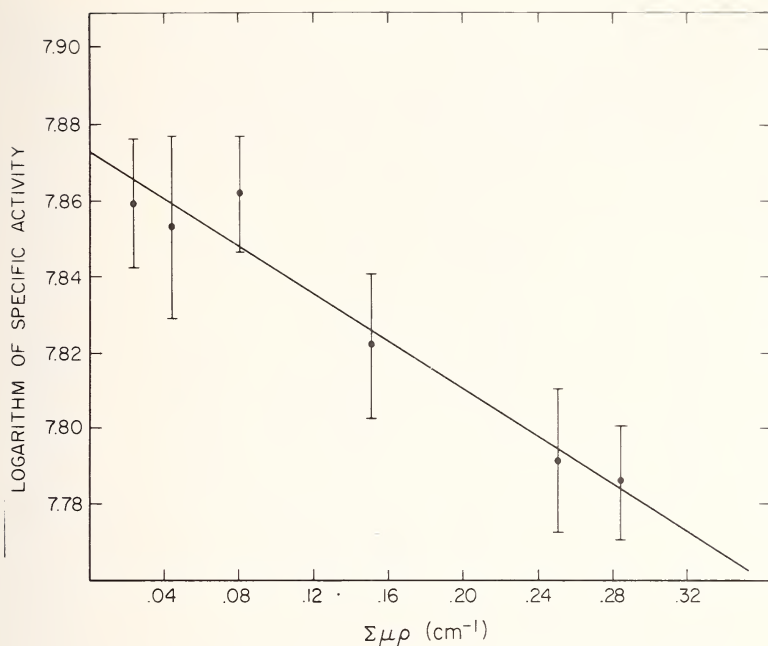
Figure 2. Relationship between logarithm of specific activity and $\Sigma\mu\rho$. Error flags represent standard deviation for four samples of $\Sigma\mu\rho$.

Table 1. Values of t, the apparent sample thickness.

Sample Series	No. of samples	t (sample thickness)	Standard deviation of t
Magnesium I	15	.309	.062
Magnesium II	31	.312	.034
Lead I	24	.358	.066
Lead II	17	.321	.076

Weighted average .320 ± .020

literature [7-8]. Equations (1) and (2) were solved for a variety of sample compositions. The experimentally determined value of t was used. In the solution of equation (2), summations were made in one MeV intervals from 8 to 20 MeV for the lead data and from 13 to 25 MeV for the magnesium data. Tabulated values of A/A_0 are shown in Table 2, and it

can be seen that the two expressions do not give significantly different results.

Table 2. Calculated values of $e^{-t\Sigma\mu\rho}$ and $\Sigma W_E e^{-t\Sigma\mu\rho}$.

Volume density of elements (g/cm^3)			$e^{-t\Sigma\mu\rho}$	$\Sigma W_E e^{-t\Sigma\mu\rho}$	$e^{-t\Sigma\mu\rho}$	$\Sigma W_E e^{-t\Sigma\mu_E\rho}$
Pb	O	Mg	Pb	Pb	Mg	Mg
5.682	.439	0	..9098	.9102	---	---
3.740	.479	.288	.9369	.9371	.9292	.9295
2.104	.469	.467	.9609	.9611	.9666	.9568
.957	.474	.609	.9778	.9781	.9763	.9763
.363	.497	.712	.9867	.9867	.9863	.9863
0	.485	.737	---	---	.9928	.9928

IV. References

[1]   Zweifel, P. F., Nucleonics **18,** (11) 174 (1960).
[2]   Reynolds, S. A., and Mullins, W. T., Int. J. Appl. Rad. Isotopes **14,** 421 (1963).
[3]   Hogdahl, O., Univ. of Michigan Report MMPP-226-1 (1962).
[4]   Nargolwalla, S. S., Crambes, M. R., and DeVoe, J. R., Anal. Chem. **40,** 666 (1968).
[5]   Davisson, C. M., in Alpha-, Beta- and Gamma-Ray Spectroscopy, Vol. 1, Kai Siegbahn, Ed., North Holland Publishing Company, Amsterdam, 1965, pp. 37-78.
[6]   Schiff, L. I., Phys. Rev. **83,** 252 (1961).
[7]   Katz, L., and Cameron, A. G. W., Phys. Rev. **84,** 1115 (1951).
[8]   Toms, M. E., and Stephens, W. G., Phys. Rev. **108,** 77 (1957).

PHOTON ACTIVATION ANALYSIS OF OXYGEN AND CARBON IN A EUTECTIC MIXTURE OF LEAD AND BISMUTH USING A LINAC

W. D. Mackintosh

Atomic Energy of Canada Ltd.
Ontario, Canada

R. E. Jervis

University of Toronto
Toronto, Canada

I. Introduction

Engelmann [1] and Schweikert and Albert [2] have described some specific examples and discussed further possibilities of using high energy bremsstrahlung beams for trace analyses. The reactions involved are $^{16}O(\gamma,n)^{15}O$, $T_{1/2} = 2.1$ min, and $^{12}C(\gamma,n)^{11}C$, $T_{1/2} = 20.3$ min. We have applied this method to the determination of oxygen and carbon in a eutectic mixture of lead and bismuth proposed as a spallation target material for an intense neutron generator (ING).

The samples were taken from a loop in which the mixture was circulated through mild steel, niobium and Zircaloy piping. The eutectic is not of high purity but fortunately free of those elements that could interfere with nondestructive determination of oxygen and carbon.

The features of this method of analysis that make it attractive for this application are these: (1) Bulk analysis of a 0.1 cm³ volume is obtained. Total oxygen contents are desired including that which may be chemically bound to other impurities occurring as discrete specks. Carbon is almost certain to exist as such. (2) Surface contamination problems are readily eliminated. The metal is soft and can be quickly scalped mechanically after irradiation. (3) Sufficient sensitivity is obtained. Samples normally contain 3 or more parts per million (ppm) oxygen and 20 or more ppm carbon. Such levels can be determined without chemical separation of the active products. (4) The eutectic has a low melting point and would generate cooling problems if irradiated with charged particles.

II. Experimental

A. Apparatus

The samples were irradiated with the University of Toronto Linac. The relevant parameters are tabulated below:

(1) Mean beam current $= 200 \, \mu A$

(2) Electron energy $= 30$ MeV

(3) Conversion target $=$ tantalum, 6 mm thick, rim-cooled with water

(4) Machine window to target distance $= 8$ cm

(5) Diameter of electron beam on target $= 2.5$ cm

(6) Target to sample distance $= 5$ cm

(7) Sample volume $= 0.1$ cm^3

(8) Sample container $=$ aluminum, air-cooled

(9) Pneumatic carrier travel time $= 20$ sec

The counting equipment consisted of two 2 in. NaI crystals opposed to each other. The amplified signals were passed through single channel analyzers set to accept a narrow band of pulses at 0.511 MeV. Both signals were then passed to a slow coincidence unit and the coincident events recorded on a scaler.

A mechanical device was used to shear off 0.5 mm from the sides and end of the sample after irradiation. This operation required only 10 sec.

B. Procedure

The intensity of the beam over the whole volume of the irradiation capsule was determined with copper monitors. Mylar, zirconia and tantalum foils, with known thicknesses of oxide on the surfaces, were tested as comparative standards. Two sizes of lead-bismuth samples were tried to determine the most suitable. Separate neutron activation experiments were done to determine the amount of phosphorous present since this could cause interference by production of the 2.6 min ^{30}P by the reaction ^{31}P$(\gamma,n)^{30}$P.

The procedure followed for the analysis of the eutectic mixture was:

(1) Irradiate a volume of 0.1 cm^3 lead-bismuth with comparative standards in close contact for 5 min.

(2) Shear the surfaces of the lead-bismuth.

(3) Count the samples and standards in identical geometry alternately. (The duration of the count was 30 sec; initially there was little interval between counting periods, but this was increased to several minutes after 20 min so that the next sample could be handled at the same time).

(4) The decay curve was unfolded and concentrations calculated by comparisons with the standards.

III. Results and Discussion

The preliminary experiments indicated that over a volume of 0.1 cm^3 the beam intensity was uniform, making a 1 g sample of the eutectic mixture the most suitable. Zirconia and Mylar foil proved to be the most suitable comparative standards for the oxygen and carbon respectively.

These standards indicated that at maximum beam intensity 154 counts per minute (cpm), μg were obtained from oxygen and 60 cpm/μg of carbon at the end of the irradiation.

The carbon content of samples analyzed ranged from 20 to 40 parts per million (ppm). The relative standard deviation arising from counting statistics was 15%. Triplicate samples cut from a single section of lead-bismuth solidified in part of the loop piping did not give good reproducibility. This is ascribed to inhomogeneity rather than lack of precision in the method, since carbon in these concentrations cannot be dissolved in the metal but must exist as discrete particles. It was deduced from the decay curves that sensitivities of 5 ppm could be achieved without lengthening the irradiation time.

The minimum amount of oxygen determined in the samples analyzed was 3 ± 2 ppm (standard deviation arising from counting statistics). Results for triplicate samples were 8, 12, and 7 ppm. If the samples were homogenous, a reproducibility of ± 3 ppm was indicated. The high carbon content of the eutectic samples limits the sensitivity to 3 ppm due to the uncertainty of subtracting out the carbon activity from the composite decay curve.

IV. Conclusions

Oxygen and carbon can be determined in a eutectic mixture of lead and bismuth with sensitivities of 3 and 5 ppm respectively.

V. References

[1] Engelmann, C., "Proceedings of a Symposium, Salzbourg", Radiochemical Methods of Analysis Vol. 1, I.A.E.A., 1964.
[2] Schweikert, E., and Albert, P., Ibid.

DETERMINATION OF CARBON IN HIGH PURITY IRON BY IRRADIATION IN PHOTONS

G. Revel, Th. Chaudron, J. L. DeBrun and Ph. Albert

CNRS - C.E.C.M.
Vitry, France

I. Introduction

The determination of carbon at low concentration in pure iron has been studied for many years in our laboratory [1-3]. Three years ago a new method using gaseous chromatography was developed [2]. This method is rapid and selective, enabling the performance of many determinations by means of it. Nevertheless, we maintain that activation analysis is preferable in the case of low concentrations. Activation analysis offers the following advantages: etching after irradiation prevents any surface pollutions; the carbon released by the walls of the apparatus and by the crucible does not introduce any error; finally, the losses by adsorption on the walls of the apparatus are considerably diminished by inactive carrier addition.

II. Experimental

Several nuclear reactions induced by different particles have been used for carbon determination in metallic samples [3]. The reaction we used is $^{12}C(\gamma,n)^{11}C$ [4]. The radioisotope ^{11}C is a β^+ emitter, and its half life is 20.4 min.

The sample (weight about 500 - 1000 mg and thickness about 1 - 2 mm) is placed between two standards. We irradiate this in the photon flux produced by an electron beam whose characteristics are 35 MeV and 50 μA mean intensity. Several materials have been tested as standards. Materials thermally unstable or of low melting point should be avoided. Homogeneous standards, exactly covering the surface of the sample, must be employed because the photon flux is heterogeneous. In short, energy variations lead us to use carbon itself as a standard. For these various reasons we used thin graphite sheets. Since our iron samples were very pure, the errors due to ^{11}C formation from other elements than carbon are negligible. Nevertheless, it would be preferable to irradiate at a lower energy with a higher electron intensity.

After irradiation the sample is etched in several acid solutions and weighed. Carbon is extracted by combustion and the resulting carbon dioxide is absorbed in soda asbestos.

III. Discussion

The radioactivity of ^{11}C is measured and compared to the radioactivity of the graphite standards. In general, the activity of the standards placed before and after the samples differ by a few percent, but in certain cases this difference may be as high as 20%. Our calculations are made using the mean activity of the two standards. Some results are presented in Table 1. In the case of pure iron prepared by successive phases of oxidation and reduction (O H iron), our results show a greater dispersion than the results given by chromatography. Nevertheless, the average concentration is the same. The two methods present the same dispersion when applied to industrial electrolytic iron due to the heterogeneity of this metal. On the other hand the concentrations found by chromatography in the case of very pure samples are higher than the concentrations found by radioactivation analysis. We think that this difference can be partly explained by the presence of absorbed carbon on the sample surface. Determination of surface carbon by irradiation with 635 keV deuterons [5] gave a measurement of 0.5 ± 0.1 $\mu g/cm^2$ of carbon on recently etched pure iron. This amount gives a blank of several parts per million (ppm) when carbon is determined by any other method than radioactivation and etching after irradiation.

It was verified by means of ^{11}C tracer that all carbon dioxide produced by combustion was stopped in soda asbestos. We can say that under our experimental conditions, errors from standardization and chemical separation influence the dispersion below the order of magnitude of the results. Our experiments on electrolytic iron show that carbon concentration is greatly diminished by simple melting. When the samples are refined in zone melting, then rolled and annealed in hydrogen, the carbon concentration is too low to be measured, even when 2×10^{-8} $\mu g/g$ can be detected. Similar results were found on industrial iron melted several minutes in a plasma torch working with a mixture of argon-hydrogen.

This method of carbon determination can be applied to other pure metals. Experiments have been already made with aluminum, magnesium, zirconium, molybdenum and chromium. It is necessary to study the process of combustion of the metal in these instances. The advantage of radioactivation analysis is that it is possible to add fluxes without taking any blank into account. For instance, the flux Pb_3O_4 : 87.5% - B_2O_3 : 12.5% used commonly for nitrogen determination [7] gives good results in the case of molybdenum, tungsten and nickel.

Table 1. Analysis of carbon in pure iron.

Samples	Carbon concentration (μg/g)	
	Photon activation	Gaseous chromatography
Pure industrial iron	120, 130, 114, 90, 99, 92	79, 90, 88, 88
Electrolytic industrial iron	57, 32, 31	55.5, 54.5, 54, 55.5, 49, 41, 39
Electrolytic industrial iron melted in hydrogen atmosphere	1.2, 1.9, 1.0, 0.9, 1.5, 2.0, 1.8, 1.2, 1.1, 0.9, 1.2, 1.4, 0.9	15.5, 18.5, 16.5, 16
O.H. iron refined by zone melting, rolled and annealed in hydrogen atmosphere	$\leq 0.12, \leq 0.12,$ $\leq 0.2^{a,c}, \leq 0.016,$ $\leq 0.012, \leq 0.026^{b,c}$	2.3, 5.7, 10, 4.4, 6
O.H. iron melted a few minutes in plasma torch [5] working with a mixture of argon-hydrogen	$\leq 0.2, \leq 0.15, \leq 0.10$	2, 2.5, 3

[a] One minute counting.

[b] Ten minute counting.

[c] Irradiation lasting ten minutes instead of twenty minutes.

IV. Acknowledgments

V. References

[1]   Moreau, L., Talbot, J., and Bourrat, J., Mem. Sci. Rev. Met. **50,** 775 (1953).

[2]   Durant, J. C., Chaudron, T., and Montuelle, J., Bull. Soc. Chim. Fr. 3, 109 (1965).

[3]   Albert, P., Chaudron, G., and Sue, P., Bull. Soc. Chim. Fr., 97 (1953); Albert, P., Annales de Chimie 8, 27 (1956); Albert, P., V° Colloque de Metallurgie - Les gaz dans les metaux, Presses Universitaires de France, 37 (1962).

[4] Revel, G., Chaudron, T., Debrun, J. L., and Albert, P., C. R. Acad. Sci. Paris **266,** 322 (1968).

[5] Barrandon, J. N., Debrun, J. L., Cuypers, M., Quaglia, L., and Robaye, G., C. R. Acad. Sci. Paris 1968 (a paraitre).

[6] Rondot, B., Antoniucci, P., Montuelle, J., and Chaudron, G., G. R. Acad. Sci. Paris **266,** 363 (1968).

[7] Boillot, P., Boulin, R., Jaudon, E., Chimie Analytique 1, 20 (1965).

CHARGED PARTICLE ACTIVATION ANALYSIS FOR CARBON, NITROGEN, AND OXYGEN IN SEMICONDUCTOR SILICON

Tadashi Nozaki

The Institute of Physical and Chemical Research
Yamato-machi, Saitama, Japan

Yoshifumi Yatsurugi, Nobuyuki Akiyama and Itaru Imai

Komatsu Electronic Metals Co., Ltd.
Hiratsuka, Kanagawa, Japan

I. Introduction

Although sufficient knowledge concerning concentrations and behaviors of carbon, nitrogen, and oxygen in semiconductor silicon have been necessitated in its industrial production and electronic research, reliable methods for their determination have not yet been fully developed. Using charged particle activation analysis we undertook to establish convenient processes for their quantitative determination and analyzed semiconductor silicons of various origins. In this paper, the processes are described and the results discussed.

II. Choice of Activation Conditions

Table 1 shows the nuclear reactions adopted in our present analyses and the possible interference reactions with their threshold energies. It also gives convenient incident particle energies which are selected in view of the excitation curves for the adopted reactions [1,2] and of some knowledge concerning the interference reactions.

Since any charged particle bombardment of silicon gives a high activity of ^{30}P, a chemical separation is required for measurement of the ^{11}C, ^{13}N, or ^{15}O. Because of difficulty of separating the ^{13}N, we did not adopt the $^{12}C(d,n)^{13}N$ reaction for determining carbon. For determining oxygen, although ^{3}He bombardment and alpha bombardment give almost the same sensitivity [3], we adopted the former because, in this case, an inevitable fluctuation and uncertainty in the incident particle energy and the etching thickness causes much less variation and uncertainty in the final result (see below).

842

Table 1. Activation reactions.

Element:	Carbon	Nitrogen	Oxygen
Reaction adopted:	$^{12}C(^{3}He, \alpha)^{11}C$	$^{14}N(p, \alpha)^{11}C$	$^{16}O(^{3}He, p)^{18}F$ $^{16}O(^{3}He, n)^{18}Ne \rightarrow {}^{18}F$
Interference reactions:	$^{9}Be(^{3}He, p)^{11}C$ [Exoth.]	$^{11}B(p, n)^{11}C$ [3.1]	$^{19}F(^{3}He, \alpha)^{18}F$ [Exoth.]
	$^{10}B(^{3}He, d)^{11}C$ [Exoth.]	$^{12}C(p, d)^{11}C$ [18.0]	$^{20}Ne(^{3}He, \alpha p)^{18}F$ [3.1]
	$^{14}N(^{3}He, \alpha d)^{11}C$ [10.2]		$^{20}Ne(^{3}He, \alpha n)^{18}Ne \rightarrow {}^{18}F$ [9.1]
	$^{16}O(^{3}He, 2\alpha)^{11}C$ [6.3]		$^{23}Na(^{3}He, 2\alpha)^{18}F$ [0.4]
	$^{28}Si(^{3}He, {}^{20}Ne)^{11}C$ [11.3]		$^{27}Al(^{3}He, 3\alpha)^{18}F$ [11.6]
			$^{29}Si(^{3}He, {}^{14}N)^{18}F$ [11.8]
Selected energy of bombardment:	15 MeV	12 MeV	15 MeV

Note: Brackets indicate threshold energy in MeV.

Although boron always interferes with the determinations of carbon and nitrogen by the adopted reactions, its concentration in semiconductor silicon can be known from the electrical property of the matrix. Beryllium concentration can safely be guessed quite closely from the production processes of semiconductor silicon. Thick target yields for the $^{16}O(^{3}He, 2\alpha)^{11}C$ reaction were measured for several incident ^{3}He energies: this interference was found to be insignificant for a ^{3}He energy under 15 MeV.

For the oxygen determination, fluorine always interferes. In view of the production processes of the matrix and the nuclear reaction mechanisms, the interferences due to the $^{23}Na(^{3}He,2\alpha)^{18}F$ and $^{27}Al(^{3}He,3\alpha)^{18}F$ can safely be guessed insignificant for the given ^{3}He energy.

We have ascertained occurrence of the $^{28}Si(^{3}He,{}^{20}Ne)^{11}C$ reaction, and show the observed excitation curve for the Si (natural) $+ {}^{3}He \rightarrow {}^{11}C$ reaction in Figure 1 with the calculated tunneling probabilities through the Coulomb barrier in the $^{31}S \rightarrow {}^{11}C + {}^{20}Ne$ reaction. Such kinds of fission of light elements would interfere seriously with the determination

of still lighter elements. Thus we propose such a selection of the bombarding particle energy that the calculated tunneling probability for any of the fissions of the matrix element should not exceed 10^{-10}.

III. Analytical Process

The process consists of the following six steps: bombardment, removal of surface contamination, chemical separation, activity measurement, carrier-recovery measurement, and calculation.

A sample disk (2.5 to 3 cm diameter, 0.5 to 1 mm in thickness) was bombarded with the charged particle beam (2 to 10 μA) from the cyclotron of the Institute of Physical and Chemical Research for 15 to 30 min. As to the activation standard for carbon, nitrogen, and oxygen, disks of graphite, nylon, and silica, respectively were covered with aluminum foils having thicknesses equivalent to the sample surface that will be
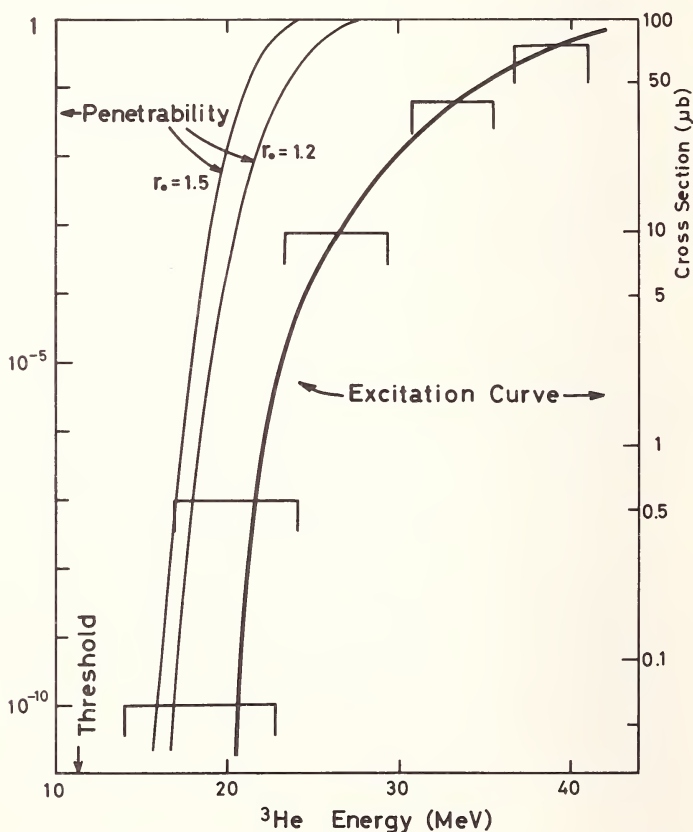
Figure 1.   Excitation curve for Si + ^{3}He → ^{11}C and penetrability for ^{31}Si → ^{11}C + ^{20}Ne.

removed, and were bombarded with lower fluxes and for shorter durations. Surface (20 to 25 μm thickness) of the bombarded silicon was etched off in a mixture of HNO_3 and HF [4,5].

We devised a convenient technique for separating the ^{11}C. Two bottles of flexible polyethylene were connected with a silicone rubber tube, one containing HF (15 ml) and KIO_4 (3 g) and the other containing NaOH (3 M 200 ml), $KMnO_4$ (1 g), and carrier Na_2CO_3 (0.3 M 10 ml). After air was squeezed out from both bottles, the sample was added to the former bottle; both bottles were stoppered to make a closed system, and then HNO_3 (5 ml) was added to the former bottle from a separatory funnel. The sample was decomposed within a few minutes. The contents of the two bottles then were mixed to give an alkaline solution, from which $^{11}CO_2$ was liberated and converted into $Ba^{11}CO_3$ for activity measurement. Including the etching the process required about 30 min.

For measurement of the ^{18}F, a chemical separation is necessary or at least preferred. The sample was dissolved in a NaOH solution containing carrier NaF, and the fluorine steam distilled and converted into $Pb^{18}FCl$. This process required about 1 h giving $Pb^{18}FCl$ for activity measurement in about 50% yield.

Annihilation radiations from the $Ba^{11}CO_3$, $Pb^{18}FCl$, and the bombarded standards were measured by a scintillation counter with a well-type crystal and a single channel analyzer to give satisfactory decay curves. Carrier recovery for the ^{11}C and ^{18}F were determined by an acid-alkali titration and a mercurimetric titration, respectively.

IV. Results

As low as 10 parts per billion (ppb) or even less concentration of carbon, nitrogen, and oxygen in semiconductor silicon proved to be able to be determined by the present methods. Table 2 shows a summary of the analytical results.

Carbon contents of polycrystalline silicon were found to vary according to the production methods but major parts of the carbon usually were removed after the single crystal formation. After repeated zone meltings of a single crystalline sample in vacuum, a part of the carbon had escaped into the atmosphere probably as CO and its remaining part was segregated towards the tail.

Commercial semiconductor silicon contained less than 20 ppb of nitrogen. Using silicons containing considerable quantities of nitrogen, we found that after a zone refining most part of the nitrogen had escaped into the atmosphere, and its remaining portion was segregated towards the tail.

Wide variations were observed in the oxygen content of semiconductor silicon. The content appeared to vary according to the conditions in the single crystal formation than as a result of the chemical purification

Table 2. Analytical results.

Element		Carbon	Nitrogen	Oxygen
Concentration (ppb)	Range	20 — 600	< 20	30 — 10000
	Most often observed	around 100	Several	A few hundred
Behavior in zone—melting	Segregation	Significant towards tail	Significant towards tail	Not clear
	Interaction with atmosphere	Escapes into	Escapes into	Either enters from or escapes into

methods. Zone melting in vacuum usually made the oxygen content much lower but sometimes in argon it was higher.

V. References

[1]   Hahn, R. L., and Ricci, E., Phys. Rev. **146**, 650 (1964); (see references in this paper).
[2]   Nozaki, T., Okuo, T., Akutsu, H.. and Furukawa, M., Bull. Chem. Soc. Japan **39**, 2685 (1966).
[3]   Nozaki, T., Tanaka, Y., Shimamura, A., and Karasawa, T., Intern. J. Appl. Radiation Isotopes **19**, 27 (1968).
[4]   Saito, K., Nozaki, T., Tanaka, S., Furukawa, M., and Cheng, H., ibid **14**, 357 (1963).
[5]   Aleksandrova, G. I., Demidov, A. M., Kotel'nikov, G. A., Pleshakova, G. P., Sukhov, G. V., Choporov, D. Ya., and Shmanenkova, G. I., At. Energ. **23**, 106 (1967).

^{7}Be AS A DOSIMETER DURING PHOTON ACTIVATION OF IODINE

J. A. Cardarelli, E. S. Dell and B. A. Burrows

Boston V.A. Hospital, Boston, Massachusetts
Yale Accelerator, New Haven, Connecticut

I. Introduction

Recently it has been shown that ^{126}I could be produced from ^{127}I by photon activation. The reaction is ^{127}I$(\gamma,n)^{126}$I. ^{126}I has a $T_{1/2}$ of 13.3 days with gamma rays of 0.386 MeV and 0.650 MeV [1]. It was also shown that this procedure could be accomplished in the presence of impurities by using proper spectroscopic pulse-height analysis. However, one of the problems first encountered by this work was that of poor beam dosimetry. After a few experiments we were able to correct this problem by employing a method of rotating the samples in front of the beam [2]. At first we decided to measure the beam dosimetry by employing internal dosimeters of each sample. This procedure caused problems in chemical separation and transfer of samples from the irradiated vessels. Later it became evident that the sample vessels themselves could be used as dosimeters. When using glass test tubes for our samples, we demonstrated equal dosimetry in each tube by measuring the always present sodium peaks. However, we still had the problem of quantitatively transferring the samples to nonirradiated vials. Subsequently, we tried to irradiate in plastic test tubes which contained much smaller amounts of sodium; but because of the intense heat close to the tungsten converter at the end of the accelerator, (Natick accelerator with energy up to 30 MeV), we were not able to employ these tubes. Therefore, we considered using an accelerator of higher current or yield. This lead us to the Yale U. accelerator with an energy of 40-50 MeV. Although we placed the samples about 1 meter away from the target, the dose rate with this accelerator was much higher, and we were able to irradiate for twice as long. However, because of this higher energy we encountered a further "complication". From the irradiated materials, we obtained a long half life isotope of beryllium: ^{7}Be, $T_{1/2} = 53$ days [3]. At first we felt this would be a detriment to our iodine analysis since the photopeak of ^{7}Be is 0.48 MeV, but we were able to use this peak as an accurate dosimeter without adding any other dosimeter to our samples. We removed the samples from the irradiated plastic tubes and transferred them to a nonirradiated vessel

847

and immediately the presence of beryllium diminished. We then carried on the following experiments using plastic test tubes.

II. Experiment

First we irradiated duplicate samples of potassium iodide solutions with concentrations from 100 μg to 1000 μg of iodide. These duplicates showed a variation of 5% or less. The linearity was excellent: $\pm 1\%$ variation. See Figure 1. These samples were not transferred from the plastic tubes. We measured the ^{126}I using the 0.650 MeV photopeak in the presence of the beryllium. Simultaneously, we measured the ^{7}Be 0.48 MeV photopeak and found it to be consistent with less than 4% total variation. See Table 1. It must be pointed out that in this particular experiment we added an unusually large amount of iodine to our samples to test whether it was possible to measure the iodine in the presence of the ^{7}Be photopeak without transferring the samples to a nonirradiated vessel.

Our next experiment involved the measurement of inulin, which is used to measure body fluid spaces. This compound has been tagged with radioactive iodine ^{131}I measured either in the urine or in the blood. However, the radiation from the ^{131}I tag might cause breakdown of the
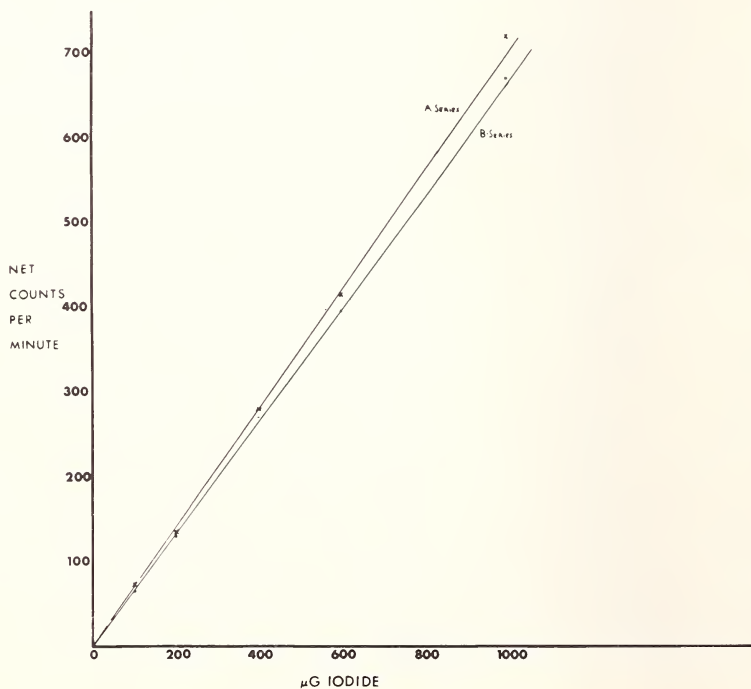
Figure 1.   KI standards *vs* radioactivity.

Table 1. Constancy of ^{7}Be counts in the presence of changing concentrations of iodide.[a]

	Iodide content of sample (μg)	^{7}Be net c/m	Average net c/m
(A)	100	2170 2150	2160
(B)	100	2133 2160	2146
(A)	200	2142 2120	2131
(B)	200	2148 2085	2116
(A)	400	2208 2145	2175
(B)	400	2244 2145	2195
(A)	600	2190 2100	2145
(B)	600	2203 2205	2204
(A)	1000	2233 2165	2199
(B)	1000	2200 2180	2190
			21661

Mean count/min (c/m) = 2166

Total variation = 4%

---

[a] ^{7}Be photopeak at 0.48 MeV integrated between 0.350 MeV and 0.540 MeV. Data taken 6/13/67.

polysaccharide molecule itself. Therefore, we considered the possibility of tagging the compound with "cold" iodine and then irradiating the blood or urine samples for measurement by our photon activation method. Since our technique had been established for potassium iodide standards, we anticipated no problem in performing this. Using inulin tagged with nonradioactive iodine we prepared samples in plastic tubes having four different concentrations of the compound, but with the same total volume of 8 ml. We had previously determined that this volume was well within the spread of the photon beam. The binding capacity of iodine to the inulin can vary depending upon the technique employed to prepare the compound. We knew only that the theoretical yield for our iodinated inulin was estimated to be 10%. We prepared duplicate potassium iodide samples containing 20 μg and 100 μg iodide as standards for quantitating the inulin iodide.

After our standard irradiation we measured the samples as before. We found that we had a very small amount of ^{126}I and we were unable to measure it in the presence of the proportionately large amount of ^{7}Be. We then transferred the samples to non-irradiated vessels and counted them. Our data showed that we had a variation of 6% or less. See Figure 2. We determined that approximately 0.25% iodine had been bound to the inulin compound. See Table 2. Our future experiments will include enough iodinated inulin so that we can measure the iodine in the presence of the ^{7}Be photopeak and reduce the possibility of transfer error.
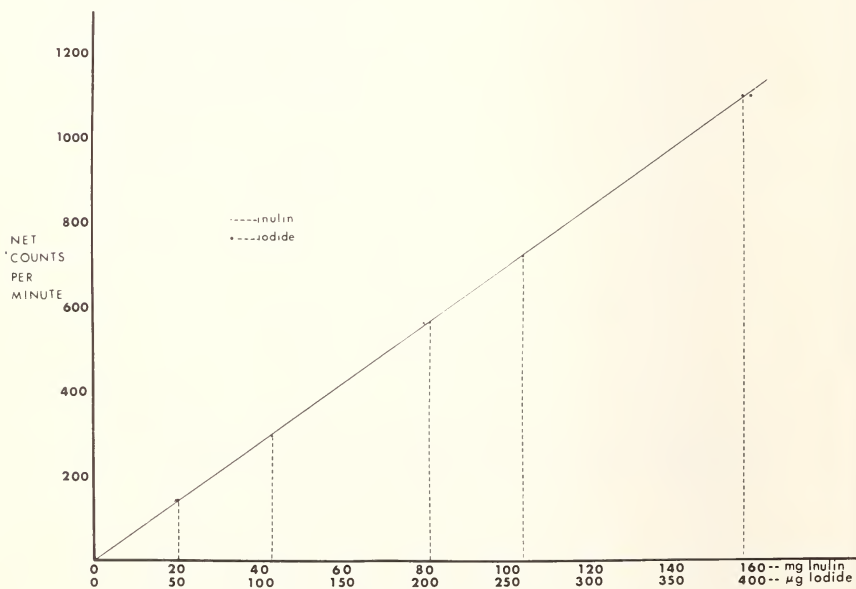
Figure 2.   Linearity of ^{126}I for a relative amount of iodinated inulin.

Table 2. Comparison of ^{126}I in iodinated inulin with potassium iodide solutions.[a]

Sample	^{126}I net c/m	Average net c/m	Amount of iodide bound (μg)	Percent of iodide bound
Inulin 20 mg	143.5			
	143.8	143.7	51	0.255
Inulin 40 mg	298.0	298.0	107	0.268
Inulin 80 mg (A)	579.1			
	552.0	565.0	203	0.254
Inulin 80 mg (B)	559.0			
	593.0	576.0	206	0.258
Inulin 160 mg	1125.0			
	1081.0	1103.0	395	0.247
KI 20 μg I$^-$ (A)	55.2			
		56.4	20	
KI 20 μg I$^-$ (B)	57.7			
KI 100 μg I$^-$ (A)	282.2			
		280.1	100	
KI 100 μg I$^-$ (B)	278.1			

[a] ^{126}I photopeak of 0.65 MeV integrated between 0.500 MeV and 0.750 MeV.

III. Discussion

We were not convinced at this writing whether the ^{7}Be came from the oxygen content of the plastic tubes or from the water and inulin samples, or if it was formed from some other element such as lithium, boron, or carbon. After transfer from the irradiated tubes, the ^{7}Be count of the samples diminished to less than 1% of the original count.

There seem to be two possibilities in regard to the plastic tubes. Either there is an element present in them which is not present in the samples or the concentration of an element common to both, is one hundred times greater in the plastic tubes.

IV. Conclusions

Using our rotation method of photon activation, the ^{7}Be photopeak of 0.48 MeV showed a uniform dosimetry within 4%. Potassium iodide

samples (100-1000 μg iodide) counted in the presence of ^{7}Be showed variation within the duplicates of less than 5% and linearity of $\pm$1% deviation.

Our experiments with iodinated inulin showed that samples containing 100 μg iodide can be analyzed with 4% variation in the presence of the beryllium peak without transferring samples to nonirradiated vessels. Even after transferring of samples to nonirradiated vessels we were able to show excellent linearity with variations of less than 6%.

We have shown that the ^{7}Be photopeak of 0.48 MeV can be used as an accurate dosimeter for measuring the uniformity of the radiation flux to the samples.

V. References

[1]   Mulvey, P. F., Jr., Cardarelli, J. A., *et al*, Jour. of Nucl. Med. **7**, 603-611 (1966).
[2]   Rocco, G. G., Garzon, O. L., and Cali, J. P., Int. Jour. of Applied Rad. and Isotopes **17**, 433 (1966).
[3]   Aumann, Von D. C., Radiochimica Acta **7**, 64-71 (1967).
[4]   Bowen, H. J. M., and Gibbons, D. M., Radioactivation Analysis, Oxford Univ. Press, 1963.
[5]   Lyon, W. S., Jr., Guide to Activation Analysis, D. Van Nostrand Co., Inc., New York, 1964.
[6]   Koch, R. C., Activation Analysis Handbook, Academic Press, New York, 1960.
[7]   Engelmann, C., Analyse Par Activation Aux Photons γ, Rapport CEA-R3307 Centre D'Etudes Nucleaires De Saclay, December, 1967.
[8]   DiNapoli, V., et al, Il Nuovo Cimento, Senis X **55B**, 95-106 (May, 1968).

SOME RECENTLY DETERMINED PHOTONUCLEAR REACTION YIELDS AND CROSS SECTIONS FOR FORMATION OF SEVERAL ISOMERS

H. R. Lukens

Gulf General Atomic Incorporated
San Diego, California

I. Introduction

Photonuclear activation analysis has been carried out with the use of the Gulf General Atomic Linacs for the determination of a number of elements in various matrices over the past several years. A modest but continuing research effort has been carried out over this time to provide back-up photonuclear reaction yield data for irradiations carried out with various bremsstrahlung energy maxima, and much of the resulting yield information has been published [1,2]. In this paper, some more recently determined yield values are presented.

In particular, yield values of radionuclides produced by the irradiation of Sr, Y, Ce, Pr, Nd, Er, and Au with 15 MeV (max) bremsstrahlung are presented. Also, cross sections for the formation of some metastable isomers by photonuclear excitation are presented.

II. Experimental

A. Apparatus and Reagents

Known amounts of strontium, yttrium, barium, cerium, praseodymium, neodymium, erbium, and gold were each sealed in separate polyethylene vials. The pneumatic tube position of the three-stage Gulf General Atomic Linac was used in the irradiation of the samples (sample directly in front of water-cooled beam converter). A 1.5 mm thick tungsten converter cooled with water was used to convert the electron beam to bremsstrahlung. These apparatus have been previously described [1].

A 3-inch diameter by 3-inch long NaI(Tl) detector coupled to a 400 channel pulse height analyzer was used to measure the radioactivity of irradiated samples. A one-half inch lucite disc was placed on the detector to suppress the measurement of beta particles.

B. Procedure

The Linac was operated with a 15 MeV electron beam. The peak pulse current was 400 mA, the pulse repetition rate was 180 pulses per second,

and each pulse was of 4.5 μsec duration. Thus, the electron beam power was 4.8 kW. Samples were delivered by compressed air to the sample irradiation position, irradiated for one minute, then returned by compressed air to the counting station.

The irradiated samples were counted in pulse height analysis mode to obtain gamma-ray spectra of the induced radioactivity. Each sample was counted several times in order to obtain half life data, also.

III. Results and Discussion

A. RESULTS

Yield values obtained from the experimental data are given in Table 1. The yield values are given for a 60 minute irradiation, in order to more fairly represent the yields of the relatively longer-lived radionuclides obtainable with longer irradiations. Obviously, the yields given for species having half lives of less than several minutes can be obtained with much shorter irradiations.

Table 1. Photoactivation yields from one hour irradiations with Bremsstrahlung from a converted 15 MeV, 4.8 kW electron beam.

Target Element	Product nuclide	Half life		Gamma-ray energy, (MeV)	Experimental yield[a]	Defined limit of detection (μg)[b]
Sr	^{85m}Sr	70	min	0.231	8.2×10^6	1
	^{87m}Sr	2.83 h		0.388	3.1×10^7	0.3
Y	^{89m}Y	16.1	sec	0.91	2.4×10^7	40
Ce	^{139m}Ce	54	sec	0.746	1.66×10^8	6
Pr	^{140}Pr	3.39 min		0.511 (β^+)	2.7×10^9	0.04
Nd	^{141m}Nd	64	sec	0.755	2.5×10^7	4
Er	^{167m}Er	2.3	sec	0.208	1.5×10^8	7
Au	^{197m}Au	7.2	sec	0.279	1.1×10^8	9

[a] Photopeak cpm per gram of target element.

[b] Limits of detection based upon the experimental photopeak cpm/g values and the minimum detectable photopeak cpm criteria (as a function of half life) given by Buchanan [3].

B. Discussion

The yields given in Table 1 demonstrate that the various elements examined can be determined with fairly good sensitivity by photonuclear activation analysis using 15 MeV (max) bremsstrahlung. The sensitivities for Pr and Sr are seen to be quite good ($<1 \mu$g); those for Ce, Nd, Er, and Au good (4-9 μg); and that for Y only fair (40 μg).

Among the product species examined, ^{89m}Y and ^{197m}Au are of special interest because they are metastable isomers of stable nuclides that can be produced from the target elements (Y and Au, respectively) only by photonuclear excitation. With these two elements, the absence in each case of a stable nuclide of one higher mass number precludes the possibility of a contributing (γ,n) reaction. ^{87m}Sr and ^{167m}Er are formed by both the (γ,γ') and (γ,n) reactions. The other radionuclide products listed in Table 1 are formed only by the (γ,n) reaction.

Table 2. Photoexcitation cross sections.

Isomer	Half life, seconds	Formation cross sections, in μb, using Bremsstrahlung of indicated $E_{(max)}$ [a]			
		3 MeV	6 MeV	8 MeV	15 MeV
^{73m}Ge	0.53		8	9	
^{77m}Se	17.5	0.2	1	3	
^{79m}Br	4.8		0.3	0.5	
^{89m}Y	16.1	0.02	0.06	0.2	10
^{107m}Ag	44.3				
^{109m}Ag	39.2	0.1	1	5	
^{137m}Ba	153	0.02	0.4	1	
^{167m}Er	2.3	0.3	9	9	
^{179m}Hf	18.6	3	3	3	
^{183m}W	5.3		0.2	0.7	
^{191m}Ir	4.9	0.9	4	7	
^{197m}Au	7.2	0.07	4	5	38

[a] 3 MeV values derived from data given in Ref. [4], and 6 MeV and 8 MeV values derived from data given in Ref. [2].

Since yields of ^{89m}Y and ^{197m}Au, as well as yields of metastable isomers of other stable nuclides from photoexcitation with lower energy bremsstrahlung (6 and 8 MeV [2] and 3 MeV [4]), had been previously determined, it was of interest to examine their formation cross sections as a function of energy. Hence, the shapes and intensities of bremsstrahlung spectra were calculated.

The fractional power conversion, C, of electron beam to bremsstrahlung, was obtained from the relation: $C = 4 \times 10^{-4}$ ZE. Primary bremsstrahlung intensities, I, as a function of energy, E, were computed from: $dI/dE = K(E_{max} - E)$. The attenuation of bremsstrahlung in each energy interval by the thick converter was computed, and the forward bias of bremsstrahlung as a function of energy was allowed for by calculating the fraction of the beam in the forward 10° cone, F_{10}, with the relationship: $F_{10} = 0.01188 \, \ln(E^2)$. Finally, the bremsstrahlung intensities as a function of energy in the forward 10° cone were converted to photons per cm^2 per second at the target position.

Cross sections for the formation of metastable isomers by direct photoexcitation of stable nuclides were computed with respect to the combined intensity of all photons above the energy level of the metastable state. Results are given in Table 2. The strong indication of broad excitation levels of ^{89}Y and ^{197}Au above 8 MeV can be seen.

IV. References

[1] Andersen, G. H., Guinn, V. P., Lukens, H. R., and Settle, D. M., in "Nuclear Activation Techniques in the Life Sciences" Int'l. Atomic Energy Agency, Vienna, 1967, p. 99.

[2] Lukens, H. R., Graber, F. M., and Perry, K. I., Trans. Amer. Nucl. Soc. **10,** 90 (1967).

[3] Buchanan, J. D., in "Proceedings of the 1961 International Conference on Modern Trends in Activation Analysis", Texas A&M University, College Station, Texas, 1961, p. 72.

[4] Lukens, H. R., Otvos, J. W., and Wagner, C. D., Int'l. J. Applied Rad. and Isotopes **11,** 30 (1961).

USE OF "FAST" NEUTRONS

Synopsis of Discussions

JEAN LAVERLOCHERE, *Chairman*

Activation Analysis Group
Center for Nuclear Studies
Grenoble, France

This session concerned activation analysis with neutron energies higher than those called "thermal energies". A lot of research has already been done in this field (*e.g.* for ten years or more), and the most frequent applications have been accomplished with 14 MeV neutrons and fission fluxes produced by small accelerators and light water reactors, resp.

In fact, this session has been devoted more to fast neutron production than to fast neutron applications.

Two papers have been presented in the field of 14 MeV and 2.8 MeV neutron activation analysis using the 200 kV accelerator located at the National Bureau of Standards.

One of these papers concerns the well-known but very difficult, precise, and accurate determination of trace oxygen with 14 MeV neutrons. Dr. Nargolwalla presented recent improvements for eliminating the blank. He uses a new "flow-through" container that is made of polyethylene and is usable for solid samples, in order to reduce the capsule blank. Then he eliminates the need to encapsulate the samples in a nitrogen atmosphere. He also presented attenuation effects — correction factors as a function of the sample diameter. These effects are of the order of 11% for a 12 mm diameter steel rod. This technique allows determination with a relative standard deviation of about 5% in the range of fifty parts per million of oxygen.

Another very interesting paper has been presented on chlorine and iodine determination in photographic emulsions by using ^{37}S (with 14 MeV neutron irradiation) and ^{126}I (2.8 MeV neutron irradiation), resp. In this case, attenuation effects could cause an additional maximum relative error of 0.5%. It appears that this application needs higher fluxes to be unquestionably better than other instrumental methods. This remark leads us to the neutron production about which six papers have been presented in this session.

Several points can be raised from these papers, and the discussion summarizes the present state of the art of fast neutron production and use in the case of accelerators.

1.   Neutron yields: With cyclotrons, 100 μA, 7.5 MeV deuteron beam gives a total neutron output of 10^{12} n/sec. Five times more neutrons can be obtained with 16 MeV deuterons and 14 MeV protons when using a beryllium target. With 20 MeV helium-3 beam, lower yields are obtained (about 40 times less than with 16 MeV deuterons). From the standpoint of high neutron yield, the Be target is the best one.

A linear accelerator (LINAC) gives 10^{13} n/sec total output with a 150 microampere and 35 MeV direct beam with a tantalum target. Beryllium targets give considerably lower yields than the high Z elements, but a combination of high and low Z elements might be the best target in the future from the standpoint of photon and neutron production.

Sealed-off neutron tubes with tritiated targets, give 10^{11} n/sec output and one can expect 10^{12} n/sec within the next few years. An output of several times 10^{11} n/sec has been already obtained but only for short durations.

Results have been presented concerning flux measurements with the Texas convention by J. D. L. H. Wood. Using a 1 cm diameter copper disc (0.175 g) he measured a normalized activity of 4.6×10^7 dis/min/g at a distance of 5 mm from the tritiated layer and of 2.9×10^7 dis/min/g at a distance of 12 mm.

2.   Life of the Target: From this point of view, massive metal targets such as beryllium or tantalum give a real advantage to the neutron production with a cyclotron or linear accelerator. However, sealed tubes have now reached such a level that it appears, in this case, that the target problem is no more the limiting factor. They can be used for example, for at least 100 hours with an output of 10^{11} n/sec or at least 1000 hours with an output of 10^{10} n/sec. Thick targets, 25 mg/cm^2, of tritiated layer for example, show a yield decay of less than 10% after 100 hours running, and of less than 15% after 500 hours.

3.   Neutron cost: Only a little information has been presented on this point: about \$20 per hour for a small cyclotron, and about four times greater for a 60 MeV LINAC. In this last case, it is interesting to point out that photon and neutron irradiation can be done simultaneously with different samples, since the axis of the maximum yield of gamma and neutron beams are placed at an angle of 90% to each other.

4.   Applications: Fast neutron fluxes produced by cyclotrons and linear accelerators offer new possibilities for reduction of interferences because of the possibility of energy variation, and for sensitivity improvement because of the high energy of the neutrons for such elements as carbon, fluorine, oxygen and silicon.

Three on-line units are installed for routine analysis in industrial production in the world. An example occurs in Belgium where a unit is providing 2000 oxygen determinations per week in a steel plant.

Capability for silicon determination at the level of about 3% has been recently added to this unit, and requires about 10 minutes to be performed.

One has estimated that a total of about 40 to 50 small accelerators are used in the world for activation analysis research in private industries and research organizations.

SPECTRUM, YIELD AND USE OF FAST NEUTRONS PRODUCED BY 20 MeV HELIUM-3 IONS, 14 MeV PROTONS AND 7.5 MeV DEUTERONS ON A THICK BERYLLIUM TARGET

E. Bruninx

Philips Research Laboratories
N. V. Philips' Gloeilampenfabrieken
Eindhoven, Netherlands

I. Introduction

Spectroscopy of fast neutrons is in most cases a lengthy procedure. The efficiency of the various types of spectrometers is in almost all cases low. For activation analysis a high resolution is not required. Flux determinations must be available in a simple form. Two procedures are described for the determination of fast neutron yields. One of these techniques allows the measurement of the fast neutron spectrum. The fast neutrons produced by 7.5 MeV deuterons, 14 MeV protons and 20 MeV helium-3 ions on a beryllium target are examined by these two techniques. The advantages and disadvantages of these neutrons for activation analysis are described.

II. Experimental

A. Accelerator

We have used the AVF prototype cyclotron as a source for 20 MeV helium-3 ions, 14 MeV protons, and 7.5 MeV deuterons. The extracted beam was used in all experiments. A thick beryllium target was employed for the neutron production.

B. Method of Threshold Detectors [1, 2]

By this method we can determine both the fast neutron spectrum and the fast neutron flux.

A sandwich of indium, silicon, aluminum, copper and carbon foils is irradiated in the fast neutron beam (at 0° angle with respect to the charged particle beam and perpendicular to this direction at a distance of 5-10 cm).

By means of calibrated counters we determined the absolute disintegration rates of the various nuclides formed in the sandwich

detector foils. Each of these absolute activities are then fitted to the formula:

$$A_i = M_{T,i} K \int_0^{E_{\max}} \sigma_i(E) E^\nu \exp\left(-\frac{E}{\epsilon}\right) dE \qquad (1)$$

where

$A_i =$ absolute disintegration rate and corrected for finite length of bombardment.

$M_{T,i} =$ number of target atoms

$K =$ a constant

$\sigma_i(E) =$ cross section for a given nuclear reaction $e.g.\,^{28}$Si (n,p) ^{28}Al, at a given neutron energy. E.

$E_{\max} =$ maximum energy of the neutrons, for a given charged particle and target.

$\nu, \epsilon =$ two parameters whose optimal value is to be determined.

Once the optimal values of ν and ϵ are known it is easy to calculate the average cross section

$$\bar{\sigma} = \frac{\int_0^{E_{\max}} \sigma(E) E^\nu \exp\left(-\frac{E}{\epsilon}\right) dE}{\int_0^{E_{\max}} E^\nu \exp\left(-\frac{E}{\epsilon}\right) dE} \qquad (2)$$

The fast neutron flux, ϕ, is then obtained from standard equations.

The total (4π) neutron yield Y, in (n·sec^{-1}·μA^{-1}) can be computed if we know the angular distribution of the emitted fast neutrons.

This distribution is easily obtained from a series of foils irradiated simultaneously at different angles, at a given distance from the target.

C. CADMIUM SHIELDED PARAFFIN-INDIUM DETECTOR [3]

This method does not give any indication about the neutron spectrum; only fluxes or total yields can be obtained.

The detector (see Fig. 1) consists of a cadmium box (15.7 cm × 15.7 cm × 15.7 cm). Inside the box, two identical half paraffin spheres (7.5 cm radius) can be placed. In the center of the flat face of one of these spheres, an indium foil fits into a shallow depression. All thermal neutrons are absorbed in the cadmium shield (0.8 mm). Fast neutrons are thermalized and activate the indium via the reaction ^{115}In(n,γ)^{116m}In.

The same detector is irradiated with a calibrated Am-Be neutron source $(2.5 \times 10^6$ n/sec, 4π geometry). By comparing the activities of the indium foil, the total fast neutron flux (or yield) can be obtained.
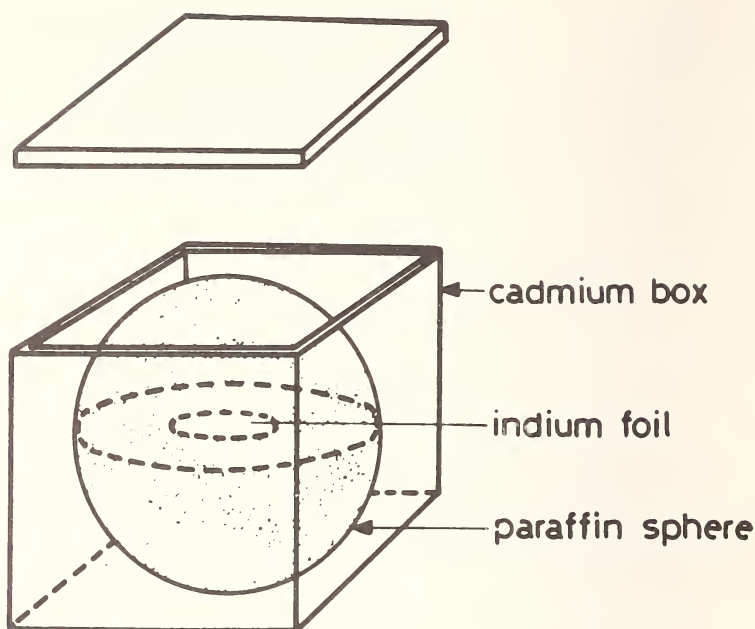
Figure 1.   Cadmium shielded paraffin detector.

III. Results and Discussion

A. RESULTS

1. Neutron Spectra

The values of ν, ϵ, the average energy, and the maximum energy for the neutrons produced by 20 MeV helium-3 ions, 14 MeV protons and 7.5 MeV deuterons are shown in Table 1. [Abbreviated in the following as n(20 MeV ^{3}He), n(14 MeV p), n(7.5 MeV d), respectively]. All quoted

Table 1. Experimental values for ν, ϵ, E_{av}, and E_{max}.

Incident particle	ν	ϵ	$E_{av}(=\nu \times \epsilon)$ (MeV)	E_{max} (MeV)	Number of determinations
20 MeV ^{3}He	1.96 ± 0.18	2.67 ± 0.24	$5.2^4 \pm 0.6^7$	27.0	7
14 MeV p	1.13 ± 0.09	0.94 ± 0.04	$1.0^6 \pm 0.1$	15.9	2
7.5 MeV d	3.14	0.61	1.9	11.8	1

errors are standard deviations. The differential spectra are shown in Figure 2a. The percentage of all neutrons above a certain energy is, however, more useful in activation analysis. This is represented in Figure 2b, together with the threshold of the different nuclear reactions used in the determination of ν and ϵ.
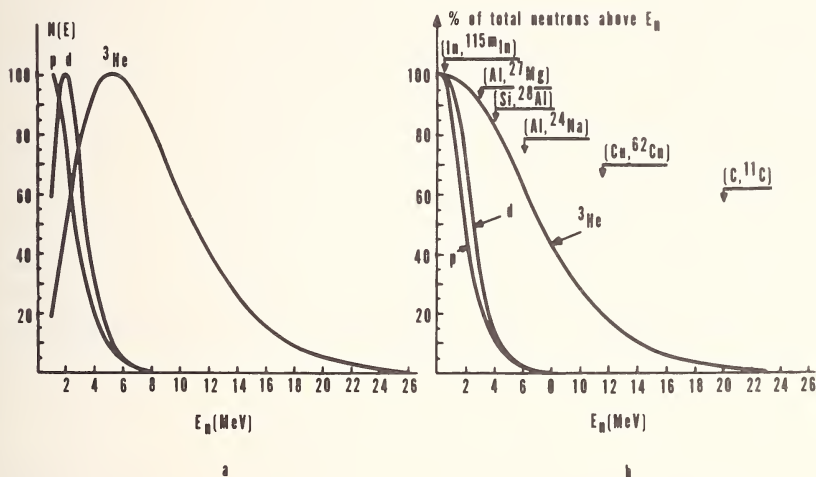
Figure 2. a. Differential neutron spectra for n(20 MeV ^{3}He). n(14 MeV p) and n(7.5 MeV d).
b. Percentage of neutrons above a given energy E.

2. Angular Distribution

Figure 3b,c,d shows the angular distribution, $F(\theta)$, for all three types of fast neutrons (*i.e.* the flux at a given angle θ relative to the flux at 0°). For a more practical use we have calculated for different angles:

$$N(\theta) = \frac{\int_0^\theta \sin(\theta)F(\theta)\,d\theta}{\int_0^\pi \sin(\theta)F(\theta)\,d\theta} \times 100 \qquad (3)$$

$N(\theta)$ is thus the percentage of neutrons emitted within a cone of half opening θ, or through a surface S (see Fig. 3a).

3. Yields

Total yields obtained by both methods (threshold detector and paraffin sphere) are shown in Table 2. The angular distribution is taken into account and all values are expressed as $n \cdot sec^{-1} \cdot \mu A^{-1}$ with 4π geometry.
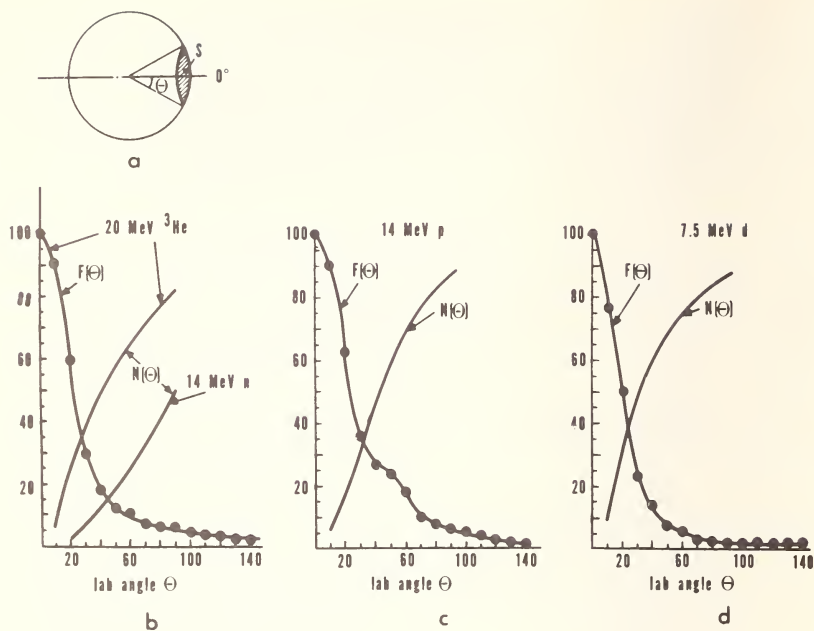
Figure 3. a. Definition of θ and S. b. Angular distribution for n(20 MeV ^{3}He). c. Angular distribution for n(14 MeV p). d. Angular distribution for n(7.5 MeV d).

Table 2. Experimental total neutron yields obtained by the threshold detector method and by the cadmium shielded paraffin sphere in n/(sec · μ A) 4 π geometry.

Distance (cm)	n(20 MeV ^{3}He)	n(14 MeV p)	n(7.5 MeV d)
		Threshold detectors	
4.75	0.9×10^9		
7.0	2.0×10^9	6.2×10^{10}	1.4×10^{10}
9.5	1.3×10^9	5.8×10^{10}	
	1.1×10^9		
Average	$(1.3 \pm 0.5) \times 10^9$	$(6.0 \pm 0.7) \times 10^{10}$	1.4×10^{10}
		Paraffin sphere	
33.8	$(9.5 \pm 2.1) \times 10^9$	$- -$	2.2×10^{10}

B. Discussion

1. Neutron Spectra

The low energy spectra (such as from 14 MeV protons or 7.5 MeV deuterons can best be compared with a fission neutron type spectrum. The average energies and the maximum energies of the neutrons are very roughly the same. Therefore, activation cross sections for these spectra are comparable to those for fission neutrons.

n(20 MeV ^{3}He) have a quite different character; their maximum energy lies around 25 MeV. This is a direct consequence of the high Q-value for the reaction, ^{9}Be(^{3}He,n)^{11}C. The advantages of the high energy neutron spectrum are partly set-off by the lower neutron yields. The proposed shape of the spectrum [eq. (1)] represents fairly well the major part of the experimental data at 0°. The high energy tail of the spectrum is underestimated for all three types of neutrons. Another source of incertitude is the value of the cross sections used in the evaluation of ν and ϵ.

2. Angular Distribution

The strong forward peaking of the emitted neutrons is one of the big assets of cyclotron produced neutrons. No particles are wasted in directions that are of no interest to the analyst. At 0° almost a factor 10 is gained in comparison to 14 MeV neutrons (d,t) (for a given total neutron output). There is evidence that neutrons of lower energy are emitted more isotropically.

3. Total Yield

Total yields measured by the threshold detector method are invariably lower than those obtained from the shielded paraffin box. The shape of the neutron spectrum may be partly responsible for this effect, but the main cause of this discrepancy seems to be the different shape of the angular distribution of neutrons of lower energy. Since the shielded paraffin box is essentially an integrating device (such as the manganese bath), these effects will be more pronounced than for the threshold detector method. Further work is in progress to confirm these points. The main advantage of the shielded paraffin box lies in its extreme simplicity. The response of the box is virtually identical for a wide range of neutron energies. Once the box is calibrated with a neutron source of known disintegration rate, only relative activity measurements are needed and no cross sections are required.

4. Applications in Activation Analysis

To obtain an idea of the order of magnitude of the induced activities, we have calculated the average cross section for a number of nuclear reactions [see eq. (2)]. These calculations were done for n(20 MeV ^{3}He) and n(14 MeV p). Assuming identical irradiation times, decay times, counters, counter efficiencies and counting times, we then computed for a given type of neutrons — the product $\sigma\phi$. This product for a given neutron source was then compared to the value for 14 MeV n(d,t). In other words, the ratio of the induced activities was calculated

$$R = \frac{^{(\bar\sigma\phi)}n(20 \text{ MeV } ^3\text{He})}{^{(\sigma\phi)}14 \text{ MeV n(d,T)}} \tag{4}$$

The flux at a distance of 2 cm was calculated from experimental data. All the results have been assembled in Table 3. In general, the induced activities are considerably higher than those obtained from 14 MeV neutron generators. The influence of the neutron spectrum on the threshold of a nuclear reaction shows clearly in case of n(14 MeV p) for the reactions with ^{12}C, ^{16}O and ^{63}Cu; the cross sections are virtually zero.

Table 3. Comparison of cross sections and induced activities for 14 MeV n(dT), n(14 MeV p) and n(20 MeV ^{3}He).[a]

Nuclear reaction	14 MeV n(dT)	n(14 MeV p)	n(20 MeV ^{3}He)	R n(14 MeV p)	R n(20 MeV ^{3}He)
^{12}C(n, 2n)^{11}C	0	0	0.05	0	
^{16}O(n, p)^{16}N	39	0	6.9	0	3.5
^{19}F(n, α)^{16}N	21	8.6	55	102	53
^{27}Al(n, p)^{27}Mg	27	2.8	52	9	14
^{27}Al(n, α)^{24}Na	116	0.24	40	0.5	7
^{28}Si(n, α)^{28}Al	340	5.7	208	4.2	12
^{63}Cu(n, 2n)^{62}Cu	620	0	96	0	3
^{115}In(n,n′)$^{115\text{m}}$In	68	200	255	760	73
⌀ at 2 cm in n·cm^{-2}·sec^{-1}	2×10^9	5×10^{11}[b]	4×10^{10}[b]		

[a] Cross section in millibarns.

[b] Assuming a beam intensity of 100 μA on a beryllium target.

The reaction on In (a typically low energy reaction) has on the contrary a much larger cross section.

n(20 MeV ^{3}He) is an interesting source for the activation of carbon, although the induced activities are small.

In conclusion, we can say that the variability of neutron energy presents a number of attractive aspects in activation analysis.

IV. References

[1]   Heertje, I., Aten, A. H. W., Jr., Physica 30, 478 (1964).
[2]   Bruninx, E., Crombeen, J., Symposium on Accelerator Target Designed for the Production of Neutrons, Euratom EUR 3895 d-f-e, Liege (1967).
[3]   Stephens, L. D., Smith, A. R., U.S. Atomic Energy Commission Report, UCRL 8418 (1958).

THE PRODUCTION OF FAST NEUTRONS BY SMALL CYCLOTRONS

A. A. Fleischer

The Cyclotron Corporation
950 Gilman Street
Berkeley, California 94710

I. Introduction

The availability of compact, relatively inexpensive cyclotrons offers an attractive alternative to the commonly used 14 MeV neutron generator for the production of high fluxes of fast neutrons. The high extracted beam current of energetic charged particles from the cyclotron can be used with a variety of solid and gaseous targets to produce neutrons with energies from thermal to 40 MeV and with source strengths greater than 10^{12} n/sec. The forward directed distribution of neutron flux and the possibility of removing the neutron producing targets from the cyclotron also offer unique possibilities for the collimation and motion of the neutron beam with respect to a fixed irradiation area.

II. Energy and Yield Calculations

The energy and angular distribution of neutrons produced in charged-particle reactions will be determined from the "Q equation" [1,2] for nuclear reactions, where Q is the nuclear disintegration energy for the reaction. If the total kinetic energy of the products exceeds that of the input particles, then Q is positive, and the reaction is called exoergic. A typical exoergic reaction is the (d,t) reaction used to produce 14 MeV neutrons.

Endoergic reactions have a negative Q, and the incident particle must bring a corresponding excess of kinetic energy into the reaction to make it occur. In endoergic reactions, the minimum energy at which the reactions will occur is called the threshold energy.

The data in Table 1 were derived by using the Q equation to calculate the energy characteristics of neutron producing reactions involving the several nuclei.

The number of new nuclides produced or particles emitted during a nuclear reaction is proportional to the number of bombarding particles and to the number of target atoms involved in the reaction, or equal to:

$$\sigma N_p N_t \tag{1}$$

Table 1. Fast neutron production by the model CS–15 cyclotron.

Reaction	Threshold (MeV)	Maximum neutron energy (MeV)
$^{32}S(p, n)^{32}Cl$	14.20	0.5
$^{4}He(d, n)^{5}Li$	6.30	1.0
$^{4}He(^{3}He, n)^{6}Be$	16.00	3.5
$^{58}Ni(p, n)^{58}Cu$	9.44	5.5
$^{12}C(d, n)^{13}N$	0.33	7.0
$^{27}Al(p, n)^{27}Si$	5.80	9.0
$D(d, n)^{3}He$	—	10.6
$^{9}Be(d, n)^{10}B$	—	12.0
$^{7}Li(p, n)^{7}Be$	—	13.3
$^{16}O(^{3}He, n)^{18}Ne$	—	15.5
$^{6}Li(^{3}He, n)^{8}Be$	—	16.5
$^{12}C(^{3}He, n)^{11}O$	—	18.5
$^{7}Li(d, n)^{8}Be$	—	22.0
$^{3}H(d, n)^{4}He$	—	25.0
$^{9}Be(^{3}He, n)^{11}C$	—	32.0

where N_P is the number of particles of energy E incident upon the target each second, and N_t is the total number of target atoms per unit area of target. The proportionality constant σ is called the reaction cross section, has the units of area, and is a function of the particle energy. The relationship between σ and E is also known as the "excitation function".

For a target thickness large compared to the range of the incident particles, the number of new nuclides produced per second is given by

$$dP = \sigma N_p N_t dx = \sigma N_p \left(\frac{\rho N_A}{A} \right) dx \qquad (2)$$

where ρ is the density of the target material, N_o Avogadro's number, and A the gram-atomic weight of the target. The cross section is usually

expressed in units of 10^{-24} cm² which is denoted a "barn". Equation 2 can also be expressed in the form

$$dP = \sigma N_p \left(\frac{\rho N_A}{A}\right)\left(\frac{dx}{dE}\right) dE = \sigma N_p \left(\frac{\rho N_A}{A}\right)\left(\frac{dE}{dx}\right)^{-1} dE \qquad (3)$$

The term dE/dx is the "stopping power" and represents the energy lost by the incident charged particle as it passes through the target material.

Thus the total yield or production rate in nuclides per second is given by

$$P = N_p \left(\frac{N_A}{A}\right) \int_{E_{threshold}}^{E_{max}} \frac{\sigma(E)\,dE}{\left[\dfrac{1}{\rho}\dfrac{dE}{dx}\right]} \qquad (4)$$

The excitation function $\sigma(E)$ has been measured for a number of reactions which produce fast neutrons [1-9]. The data shown in Table 2 were calculated using Equation 4 and compared against yields measured by using a series of activation foils with thresholds from thermal to 20 MeV.

III. Compact Cyclotrons

The Cyclotron Corporation of Berkeley, California, offers two compact cyclotrons which should be excellent sources of high energy, high flux neutrons. The characteristics of these cyclotrons are listed in Table 3, and Figure 1 is a picture of the Model CS-15 cyclotron. This is an extremely compact AVF cyclotron which weighs only 15 tons, occupies a floor space of about 63 square feet, and can easily be accommodated in a 20 foot shielded room. Actual experience with this cyclotron indicates that it can be operated and maintained by one technician with no previous cyclotron experience. Operating expenses, sewer, and water requirements are minimal, and both the CS–15 and CS–22 models can be manufactured, installed, tested, and accepted at the investigator's site in less than one year.

Table 2. Fast neutron data.

Reaction	Incident particle energy (MeV)	Maximum neutron energy (MeV)	Average neutron energy (MeV)	Neutron[a] production rate (n/sec)	Flux at 100 cm $n \cdot cm^{-2} \cdot sec^{-1}$	Dose rate[b] at 100 cm (rads/min)
	7.5	12.0	4.0	1×10^{12}	1×10^8	30.0
$^9Be(d, n)^{10}B$	11.5	16.0	5.5	3×10^{12}	3×10^8	90.0
	16.0	20.0	6.75	5×10^{12}	5×10^8	150.0[c]
	7.5	22.0	8.0	2×10^{11}	2×10^7	6.0
$^7Li(d, n)^8Be$	11.5	26.0	10.0	3×10^{11}	3×10^7	9.0
	16.0	30.0	12.0	4×10^{11}	4×10^7	15.0
	0.6	14.6	14.0	5×10^{10}	4×10^5	0.12
	0.6	14.6	14.0	5×10^{12}[d]	4×10^7	12.0
$^3H(d, n)^4He$	7.5	24.7	18.0	2.1×10^{11}	4.4×10^7	13.2
	11.5	29.0	20.0	3.4×10^{11}	7.2×10^7	21.5
$^3H(p, n)^3He$	15.0	14.0	8.0	1.35×10^{12}	8.5×10^7	25.0
	22.0	21.0	10.0	1.6×10^{12}	1×10^8	30.0
$^9Be(^3He, n)^{11}C$	20.0	32.0	8.0	1×10^{11}	2.2×10^7	6.6
	30.0	44.0	10.0	2.2×10^{11}	4.6×10^7	13.8
$^{12}C(^3He, n)^{12}O$	20.0	18.0	12.0	4×10^{10}	8.4×10^6	2.6
	30.0	25.0	15.0	8×10^{10}	1.7×10^7	5.2

[a] For 100 μA beam current.

[b] 2×10^8 n $\cdot$ cm^{-2} $\cdot$ min^{-1} = rad/min.

[c] Measured value of 50 rads/min for 20 microampere beam current which equals 250 rads/min for 100 microampere current. At Hammersmith Hospital, London, England.

[d] Beam current of 10 milliamperes.

Table 3. Characteristics of compact cyclotrons.

Particles:	Model CS–15			Model CS–22		
protons	15	MeV		22	MeV	
deuterons		7.5 MeV			11.5 MeV	
helium–3	20	MeV		30	MeV	

Extracted beam currents:

Guaranteed 50 microamps for all particles;
Design aim 100 microamps for all particles.

Minimum extracted beam

spot size: Less than 2 cm in diameter.

Size	W	D	H	W	D	H
cyclotron	9	7	7	10.5	10	11
power supplies	6	5	6	6	5	6
control console	4	5	4	4	5	4

Weights (Lbs.)
cyclotron	30,000	50,000
power supplies	4,000	4,000
control console	1,250	1,250

Power	175 kW	225 kW

Cooling water	30 gallons per minute	40 gallons per minute

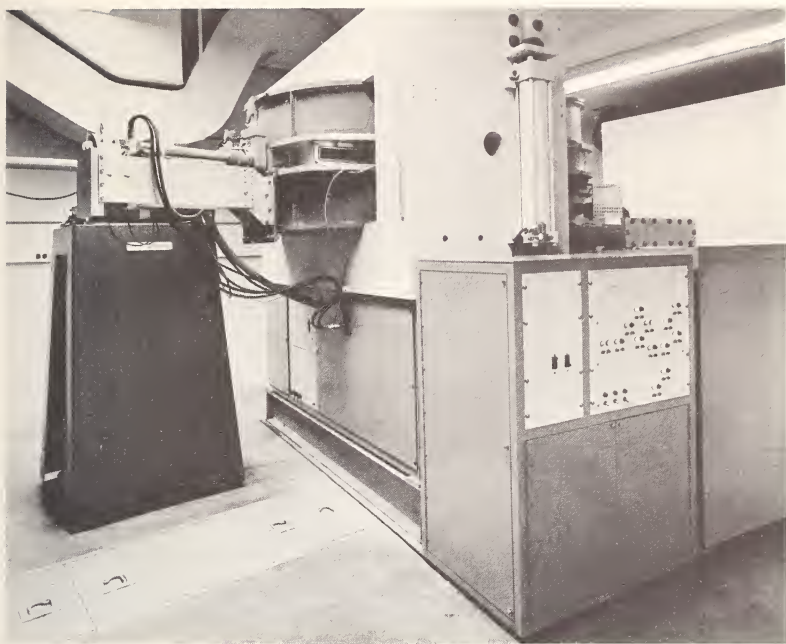| Cost	Approximately $300,000 installed.	Approximately $400,000 installed.

Figure 1.   Model GS–15 cyclotron.

IV. References

[1]   Marion, J., and Fowler, J., Eds., Fast Neutron Physics, Part 1, Interscience, New York, 1960.
[2]   Phillips, G., Marion, J., and Rissor, J., Eds. Progress in Fast Neutron Physics, University of Chicago Press, Chicago, 1963.
[3]   Bryant, *et al* Nuclear Physics **53,** 97 (1968).
[4]   Flynn and Rosen, Phys. Rev. **153,** 1228 (1967).
[5]   Hanson, *et al* Rev. Mod. Physics **21,** 635 (1949).
[6]   Cohen and Falk, Phys. Rev. **84,** 173 (1951).
[7]   Bryant, *et al,* "Excitation Functions of Reactions of 7 to 24 MeV ^{3}He Ions with $^{63,\ 65}$Cu", Phys. Rev. **130,** 1512 (1963).
[8]   Manley, J., "^{12}C(^{3}He,n)^{14}O Reaction at 19, 22, and 25 MeV", Phys. Rev. **130,** 1475 (1963).
[9]   Hahn, R., and Ricci, E., "Interactions of ^{3}He Particles with ^{9}Be, ^{12}C, ^{16}O and ^{19}F", Phys. Rev. **146,** 650 (1966).

USE OF A 60 MeV LINAC FOR FAST AND VARIABLE ENERGY NEUTRON ACTIVATION ANALYSIS

Peter E. Wilkniss

Naval Research Laboratory
Washington, D.C. 20390

I. Introduction

In recent years considerable interest has been shown by activation analysts in the use of photon activation analysis. Activation is accomplished by irradiation of the sample with a high energy bremsstrahlung beam obtained from an electron linear accelerator. The high energy bremsstrahlung is produced by the interaction of an electron beam of appropriate energy with a high Z element converter, for instance, tantalum. These high Z elements have considerable cross sections for photoneutron production. Under optimum conditions a total yield of approximately 10^{13} n/sec can be expected from a converter. This seemed to warrant investigation of the possible use of such a photoneutron source in fast neutron activation analysis. We have studied the bremsstrahlung distribution obtained from a converter, as well as the angular distribution of the photoneutrons, their energy spectrum and their intensity. Examples are given for activities obtainable with the fast neutron flux. The possibility of variable energy neutron activation analysis is demonstrated by the determination of fluorine according to $^{19}F(n,\alpha)^{16}N$ in the presence of large amounts of oxygen without interference by the reaction $^{16}O(n,p)^{16}N$.

II. Experimental

A. APPARATUS AND MATERIALS

The Naval Research Laboratory (NRL) 60 MeV Linac was used. Experiments were conducted using two different beams. One was the straight through beam which was not analyzed with respect to energy and whose current was about 145 μA. The other beam was deflected 45° and analyzed to $\pm 3\%$ of the electron energy, with currents up to 80 μA.

Two types of converters were used. One was a copper box containing 9.76 g/cm^2 tantalum equivalent to about 1.6 radiation lengths. This converter is routinely used for photon activation analysis at NRL [1].

874

The other converter was especially designed for neutron production at the Rensselaer Polytechnic Institute, Troy, N.Y. It contains 56 g/cm² of gold plated tungsten representing about 9.1 radiation lengths. A copy of this source was loaned to NRL by Dr. Evans Hayward, Linac Division, National Bureau of Standards, Washington, D. C., and was used for the experiments. A pneumatic transfer system and sample rotator [2] were used to facilitate sample irradiations.

A 3 in. × 3 in. NaI(Tl) scintillation crystal and 512-channel analyzer were used to count all activities, except ^{16}N, for which a 5 in. × 6 in. NaI(Tl) scintillation crystal was employed. The energy interval for the registration of ^{16}N gamma rays was set from 4.5 to 7 MeV.

B. Procedure

1. Intensity Measurements

Aluminum squares were positioned around the converters to measure angular distribution and intensity of the neutrons with respect to the electron-bremsstrahlung beam axis. The neutron flux above 2 MeV was measured with ^{27}Al(n,p)^{27}Mg and that above 6 MeV with ^{27}Al(n,α)^{24}Na. Relative neutron intensities were measured at 45°, 90° and 135° from the beam axis. The bremsstrahlung intensity distribution was measured in the same way as the neutron intensity by exposing Teflon squares together with the aluminum and by counting of ^{18}F obtained from ^{19}F(γ,n)^{18}F. Sample irradiations were performed at 90° with respect to the electron-bremsstrahlung beam axis by properly positioning the rotator of the pneumatic transfer system with respect to the converter.

III. Results and Discussion

A. Results

1. Angular Distribution of Neutrons

Neutron intensities were measured at 45°, 90° and 135° from the electron-bremsstrahlung beam axis. For the tantalum converter thickness of 1.6 radiation lengths, the neutron distribution is nearly isotropic. For the tungsten converter thickness of 9.3 radiation lengths, the relative neutron intensities are 1 at 45°, 1.65 at 90°, and 2.54 at 135°.

2. Angular Distribution of Bremsstrahlung

The relative bremsstrahlung intensities were measured for the 1.6 radiation length tantalum converter. They are 100 for 0° (the beam axis), 1 for 45°, 0.1 for 90° and 0.07 for 135°.

3. Energy Spectra of the Neutrons

The ratio of the neutron flux above 2 MeV to that above 6 MeV was found to be isotropic for both converters at 22 MeV electron beam energy. The ratio was 10 for the tantalum converter of 1.6 radiation lengths and 14 for the tungsten converter of 9.3 radiation lengths.

4. Absolute Neutron Intensities

For the 1.6 radiation length converter, the neutron flux above 2 MeV was determined to be 3×10^9 n·cm^{-2}·sec^{-1} at 30 MeV electron team energy and 80 μA beam current on the beam axis. For the 9.3 radiation length converter a neutron flux above 2 MeV of 2×10^9n · cm^{-2} · sec^{-1} was obtained for an electron beam of 35 MeV and 145 μA beam current.

5. Count Rates Obtained from Activation of Different Elements

Results are given in Table 1. They are for the irradiation of 1 g of the given element for one half life at 35 MeV using the 9.3 radiation length converter and a beam current of 145 μA. The count rates are those corrected for decay back to the end of bombardment at the gamma photopeak energy indicated for the radionuclides produced.

Table 1. Count rates obtained at end of bombardment.[a]

Element	Reaction	Eγ (MeV)	Count rate (counts/minute)
O	^{16}O(n, p)^{16}N	4.5 – 7.0	6×10^4
F	^{19}F(n, α)^{16}N	4.5 – 7.0	3×10^6
Mg	^{26}Mg(n, γ)^{27}Mg	0.83	2×10^5
Mg	^{24}Mg(n, p)^{24}Na	2.75	6×10^5
Al	^{27}Al(n, γ)^{28}Al	1.78	4×10^5
Al	^{27}Al(n, p)^{27}Mg	0.83	1×10^6
Al	^{27}Al(n, α)^{24}Na	2.75	1×10^5
P	^{31}P(n, α)^{28}Al	1.78	3×10^6

[a] Radionuclides produced in the irradiation of 1 g of the element indicated.

The irradiation times are equal to one half life of the product nuclide, energy 35 MeV, converter 9.3 radiation length, beam current 145 μA.

6. Variable Energy Neutron Activation Analysis

For the experiments the 1.6 radiation length tantalum converter was used, and the samples were placed at 90° from the analyzed electron-bremsstrahlung beam axis. The irradiation of water and Teflon samples in this position showed that the reaction $^{19}F(n,\alpha)^{16}N$ is produced by the photoneutron flux in the Teflon samples while $^{16}O(n,p)^{16}N$ is not observed in the water samples provided the electron beam energy does not exceed 22 MeV. It is important to use a beam analyzed with respect to electron energy within fairly small limits, in our case $\pm 3\%$.

B. Discussion

The angular distribution of bremsstrahlung from a converter is strongly peaked forward and rapidly falls off with increasing angle from the beam axis. The angular distribution of photoneutrons is nearly isotropic for the 1.6 radiation length converter, and is peaked backward ($>90°$) for the 9.3 radiation length converter. This makes it possible to use a photoneutron source for fast neutron activation analysis with minimum interference from photonuclear reactions if the sample is placed at an angle of 90° or larger with respect to the electron-bremsstrahlung beam axis.

The counting rates given in Table 1 show that sensitivity obtainable under the experimental conditions described, permits minor constituent analysis rather than trace analysis. Under controlled experimental conditions a photoneutron source can be used for variable energy neutron activation analysis as demonstrated using the classical example of the interference-free determination of fluorine by $^{19}F(n,\alpha)^{16}N$ in the presence of a large excess of oxygen. The practical importance of this is implied by the determination of fluorine at the 0.1% level in samples of geochemical interest. It is to be noted that the nondestructive determination of fluorine according to $^{19}F(n,\alpha)^{16}N$ using photoneutrons can be carried out simultaneously with the very sensitive photoactivation of fluorine using $^{19}F(\gamma,n)^{18}F$, because the samples are placed at different angles from the converter. This greatly enhances the economical aspects of photon activation analysis and makes a wide variety of samples with varying fluorine contents, such as marine geochemical samples, susceptible to activation analysis with the Linac.

The highest neutron fluxes obtained in our experiments were around $3 \times 10^9 \text{n} \cdot \text{cm}^{-2} \cdot \text{sec}^{-1}$. A flux of $10^{10} \text{ n} \cdot \text{cm}^{-2} \cdot \text{sec}^{-1}$ can definitely be obtained by using higher beam currents and specially designed photoneutron sources. This will raise the obtainable sensitivity to permit trace analysis. The shape of the neutron energy spectrum is such that nuclear reactions which do not have an appreciable cross section below 6 MeV are not very useful for photoneutron activation analysis. An advantage of a

photoneutron source is that radionuclides with fairly long half lives can be used for activation analysis especially when it is possible to ride "piggy-back" along with other long-term experiments, such as in nuclear physics.

IV. References

[1]   Wilkniss, P., and Linnenbom, V. J., Proc. 2nd Conf. Practical Aspects of Activation
       Analysis with Charged Particles, Liege, Belgium, Sept. 21-22, 1967, p. 147.
[2]   Wilkniss, P., Hoover, J. I., and Leighton, R. E., Nucl. Instr. Meth. **56,** 120 (1967).

BLANK CONSIDERATIONS IN 14 MeV NEUTRON ACTIVATION ANALYSIS FOR TRACE OXYGEN

S. S. Nargolwalla, E. P. Przybylowicz[1], J. E. Suddueth, and S. L. Birkhead

National Bureau of Standards
Washington, D.C. 20234

I. Introduction

The accuracy of trace oxygen determination by 14 MeV neutron activation analysis can be seriously affected if the oxygen contribution from the container is significant. If the count from the blank is merely subtracted from the total sample-in-container count, errors as large as 100% may be introduced. Solutions by other workers [1-5] are specific to the individual systems being used and are not of general applicability.

Using a general purpose activation analysis facility, an attempt has been made to provide a generalized solution to the problem. In our previous approach [5] leak problems, associated with the encapsulation technique for loading steel samples in polyethylene containers under a nitrogen atmosphere, introduced imprecision in about 20% of the experiments. The present technique gives consideration to the sample-in-container geometry and any attenuation effects which may arise during irradiation and counting. The application of this method does not presuppose the availability of low-oxygen containers, but can be used in any analysis where the blank problem is considered to be significant.

This study contributes to the state-of-the-art in the following ways: a) determination of the attenuation of the activity from the container by samples of different diameters, b) definition of a geometrical model which quantitatively expresses the observed attenuation by the samples, and c) design of a "flow-through" container for solid samples which reduces the capsule blank contribution and eliminates the need to encapsulate samples in a nitrogen atmosphere provided the propelling gas in the pneumatic system is dry nitrogen.

The solution of these blank problems considerably improves the reliability of the 14 MeV neutron activation technique for the precise and accurate determination of trace oxygen.

---

[1] Research associate from Eastman Kodak Company, Rochester, New York.

II. Experimental

A. Equipment

The facility at NBS consists of a 2.5 mA beam current Cockcroft-Walton neutron generator, a dual-sample pneumatic system with a rotating sample assembly [5], a sequence programmer, and a detector system of two 4 in. by 3 in. NaI(Tl) detectors coupled to a 400 channel pulse-height analyzer. For a quantitative study it was necessary that a container be constructed of a material with macro amounts of oxygen, *viz.* Nylon (*ca.* 12% oxygen) identical to the polyethylene vials normally used. The samples were steel rods (Table 1) containing small amounts of oxygen (<0.5%) relative to the Nylon container.

Table 1. Steel rods used in attenuation studies.

Steel	Rod length (in.)	Rod diameter (in.)	Approximate total oxygen content[a] (μg)
Ingot iron	1.95	1/8	1450
Vacuum melted	1.95	1/4	280
Stainless	1.95	3/8	1000
Stainless	1.95	1/2	1500

[a] The Nylon container contained approximately 500 mg of oxygen.

The "flow-through" container was a two dram polyethylene capsule, perforated by 5/16 in. diameter holes (Figure 1) so that nitrogen could flow freely around the sample during transfer. Consequently the void volume is free of oxygen.

B. Procedure

Verification of the experiment was done by comparing results using the previous technique [6] with those obtained with the "flow-through" container. The effectiveness of the perforated container was evident in the reproducibility of the blank determinations and the determination of oxygen in seven rods of valve steel using both methods.

Using sequential counting, the empty Nylon container and one of polyethylene filled with benzoic acid were irradiated and then counted

with the Nylon container first. Photons in the energy region 4.8 to 8.0 MeV were counted. Replicate determinations on the steel rods described in Table 1 were made. Comparing the activity of the loaded Nylon container to that of the empty container gave a measure of the attenuation of the oxygen activity in the container by the steel rod.

III. Results and Discussion

A. ATTENUATION EFFECTS

A geometrical model was developed to calculate the magnitude of attenuation of oxygen activity for all sample diameters. The experimentally determined attenuation of the container activity is given in Table 2 and Figure 2. Previous work [5] has shown that neutron shielding and gamma-ray self-absorption can be expressed in terms of the generalized exponential absorption law

$$f/f_0 = e^{-\epsilon d} \tag{1}$$

where

> f = effective neutron flux (n · cm^{-2} · sec^{-1}) or gamma intensity (photons per second)
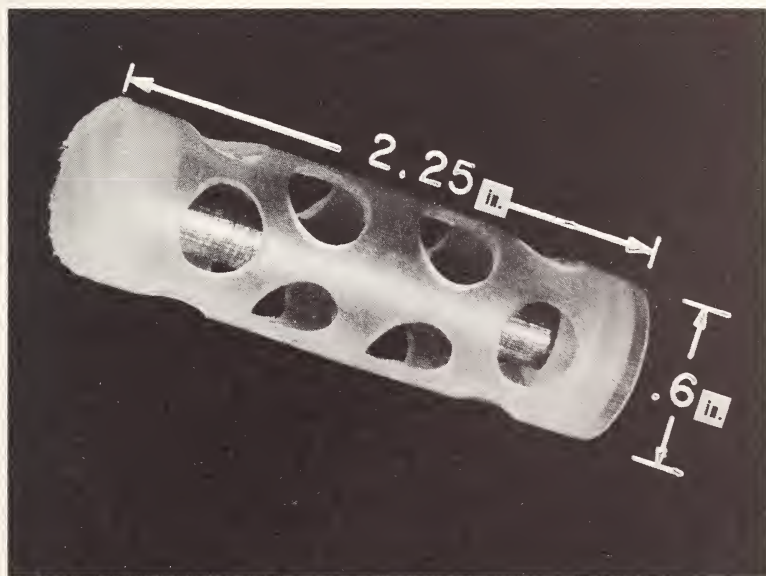

Figure 1. "Flow Through" container.

Table 2.   Comparison of experimental and calculated total attenuation
           correction factors.

| Steel rod diameter (in.) | Calculated total attenuation correction factor | | Experimental attenuation[a] |
	Point source	Parallel beam	Correction factor
1/8	0.9924	0.9928	0.9997 ± .0092
1/4	0.9694	0.9711	0.9714 ± .0091
3/8	0.9294	0.9330	0.9378 ± .0085
1/2	0.8666	0.8726	0.8862 ± .0089

[a] Results are the weighted means of 8 determinations, with weights equal to the reciprocal of the estimated variances where the estimated variances are based on Poisson counting statistics and propagation of error formulas. The errors are the standard errors of the weighted means.

$\epsilon =$ the proportionality constant in the differential expression $(df/dd = -\epsilon f)$, cm^{-1}, where d is the thickness.

$f_0 =$ unattenuated neutron flux (n·cm^{-2}·sec^{-1}) or gamma intensity (photons per second)

The measured activity, C_m, of a sample is related to the total possible activity, C_t, by:

$$C_m = C_t(e^{-\mu_0 Y} \times e^{-\Sigma_R X}) \qquad (2)$$

where

$\mu_0 =$ total linear gamma-ray absorption coefficient (cm^{-1})

$Y =$ gamma-ray attenuated sample thickness (cm)

$\Sigma_R =$ total neutron macroscopic removal cross section (cm^{-1})

$X =$ neutron attenuated sample thickness (cm)

When sample matrices differ, the exponential product may differ and C_t must be calculated and used in the comparison. As sample diameter decreases so does the slope of the correction curve which gives a direct measure of the effective attenuated sample thickness.

Applied to oxygen in sample containers several precautions must be observed. The oxygen is presumed to be uniformly distributed, but for individual atoms the attenuation differs depending on their position. The
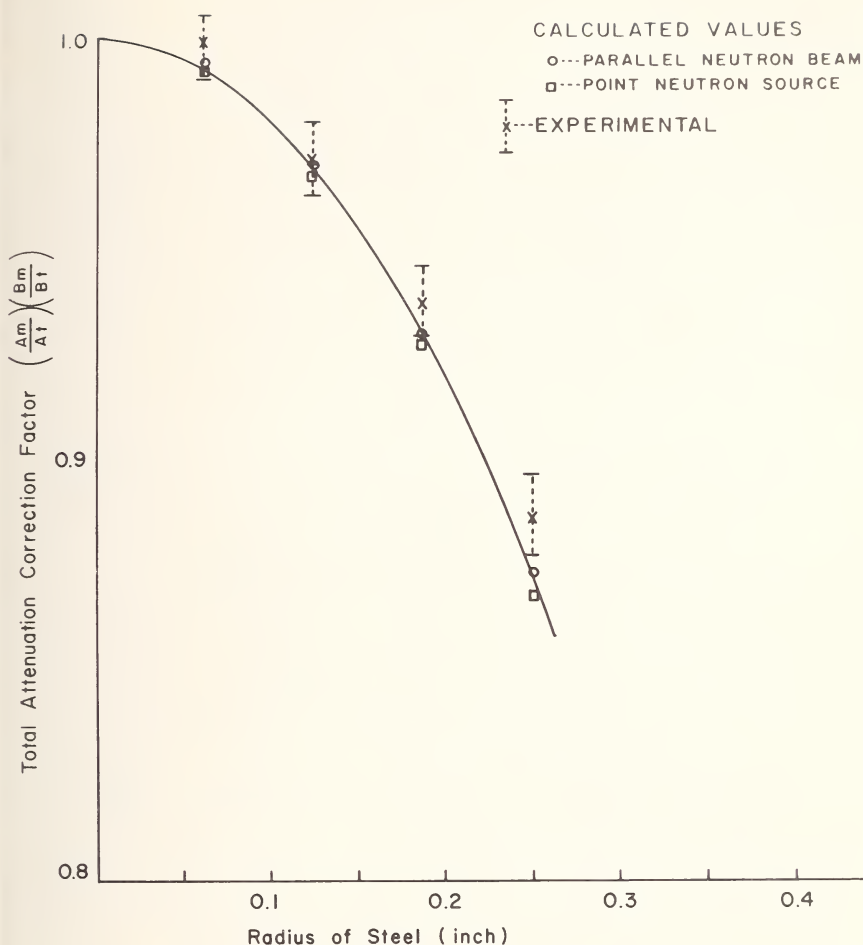
Figure 2.   Dependence of attenuation correction factor on radius of steel.

experimental curves [5] average out those differences for the entire sample for different diameters.

For attenuation of ^{16}N geometrical corrections must be made because, (a) oxygen is only in the container walls, and (b) sample diameter is less than the container diameter. The oxygen in the container walls will on the average be shadowed by a full container one-half of the time. As the sample diameter decreases the sample shadow is decreased. Geometrical corrections are based on two models, neutron and gamma-ray absorption neglecting "end effects" (Figs. 3, 4 and 5). The neutron beam is considered as a point source (Figure 3) and a parallel source beam (Fig. 4), the actual beam being best described as a non-uniform disc source.
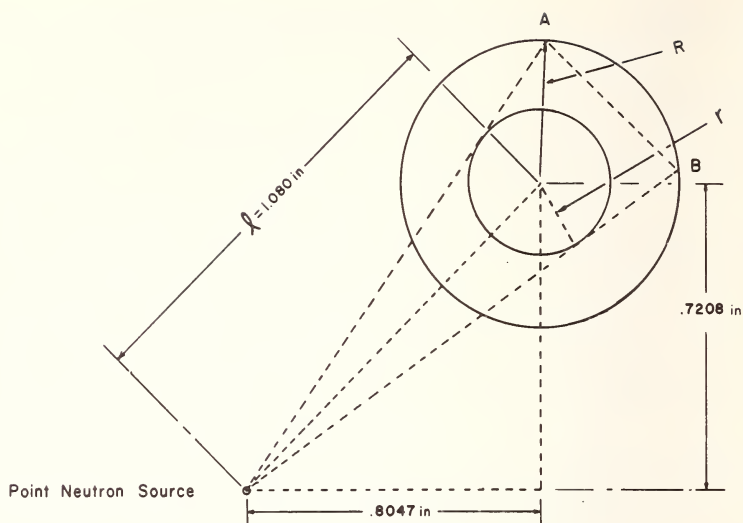
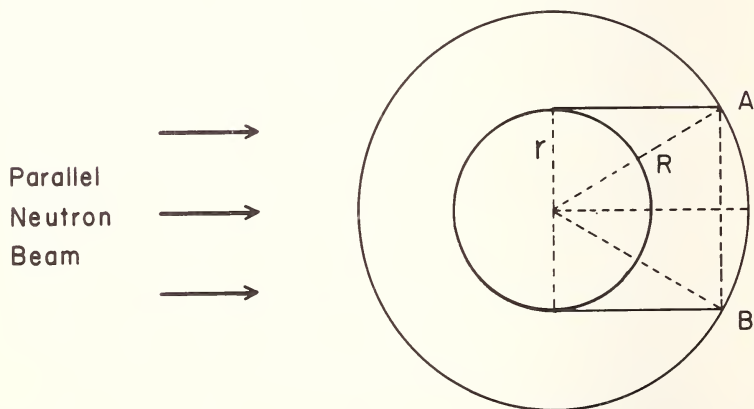Figure 3.   Geometric model: neutron point source.

Figure 4.   Geometric model: neutron parallel beam.

For neutron attenuation (Figs. 3 and 4), only a portion (arc AB) of the container is attenuated. The total activity induced is:

$$A_m = A_t \left[e^{-\Sigma_R X} \left(\frac{\text{arc } AB}{2\pi R} \right) + e^{-\Sigma'_R X'} \left(1 - \frac{\text{arc } AB}{2\pi R} \right) \right] \qquad (3)$$

where

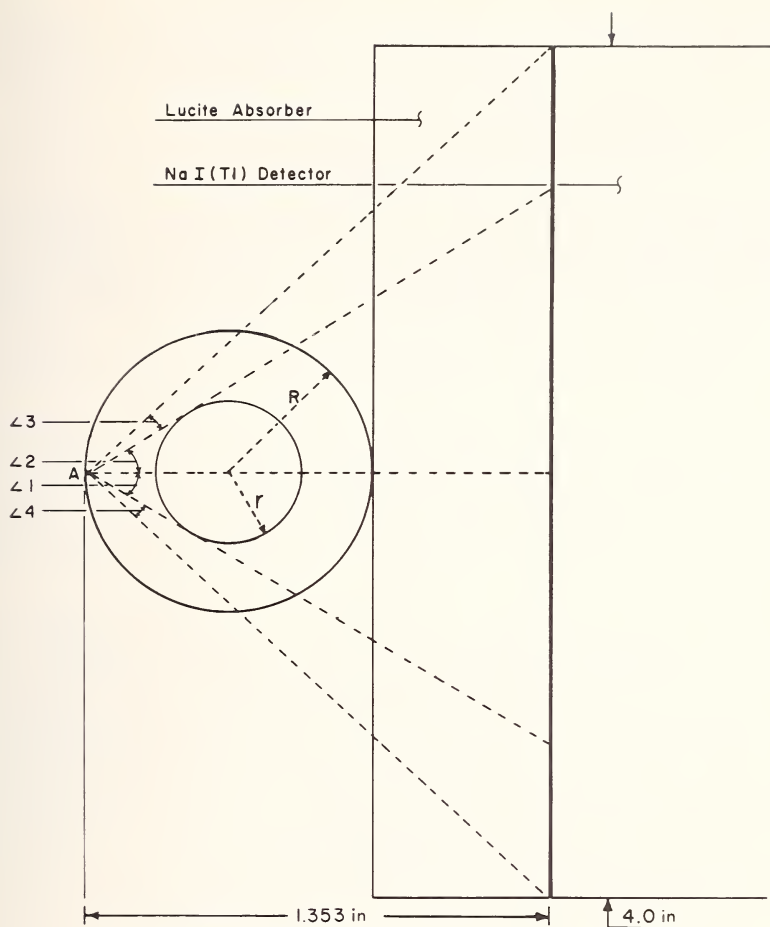$A_t =$ theoretical amount of activity with an unattenuated neutron beam

Figure 5. Geometric model: gamma attenuation.

$\Sigma_R =$ total sample macroscopic removal cross section, (cm^{-1})
$X =$ attenuated sample thickness, (cm)

(Σ_R' and X' being the same parameters for nitrogen in the container, where $e^{-\Sigma_R'X'}$ is taken as unity).

Neglecting end effects, calculations based on a two dimensional model show that the shadowed areas are:

$$\text{Point source: } 2R[\sin^{-1}(r/R) + \sin^{-1}(r/1)] \tag{4}$$

$$\text{Parallel beam: } 2R\sin^{-1}(r/R) \tag{5}$$

where

$R =$ inside container radius
$r =$ radius of sample
$l =$ distance from container to the point source

Attenuation by the sample is only through the angle defined by the sample (see Fig. 5). The activity at point A is attenuated through the angle $[1+2+3+4]$ for a full capsule. For a sample, the activity will be attenuated only through the angle $[1+2]$. The fractional angle $\dfrac{[1+2]}{[1+2+3+4]}$ is that portion of the total angle through which ^{16}N activity in the container is attenuated, and $1 - \dfrac{[1+2]}{[1+2+3+4]}$ represents the angle through which there is no attenuation (i.e., $e^{-\mu_0 Y}$ in equation 2 is unity). For a sample diameter smaller than the container's internal diameter, the measured activity, B_m, is related to the unattenuated activity, B_t, by:

$$B_m = B_t \left[\frac{\angle[1+2]}{\angle[1+2+3+4]} \times e^{-\mu_0 Y} + \left(1 - \frac{\angle[1+2]}{\angle[1+2+3+4]} \right) \right] \qquad (6)$$

The product (A_m/A_t) (B_m/B_t), represents the total neutron and gamma attenuation properly corrected for geometry. Blank oxygen may only be subtracted directly when (a) the blank is low compared to the sample (ca. 2%) or (b) when the sample diameter/ container diameter ratio is $<1:4$.
In all other cases the following procedure may be used:
1. Irradiate and measure the oxygen in an empty container.
2. Irradiate and measure the oxygen in a sample container.
3. Oxygen in sample $= [H - I] - [J - I] \left(\dfrac{A_m}{A_t} \right) \left(\dfrac{B_m}{B_t} \right)$

where

$H =$ oxygen in sample + container (gross counts)
$I =$ environmental background, counts
$J =$ oxygen in container, counts

The use of the "flow-through" container obviates the need for encapsulation of the sample in nitrogen. A comparison for the two techniques is reflected in the results shown in Table 3. The large fluctuations observed using the old technique is indicative of the magnitude of errors involved. The marked improvement with the "flow-through" container is obvious. The procedures described form a basis of a very precise analytical measurement. With these improvements in

attenuation corrections, the 14 MeV technique compares favorably with other instrumental methods of analysis for oxygen.

Table 3. Results: oxygen analysis on valve steel
(1/4 in. diameter rods).[a]

Rod No.	Uncorrected for attenuation of blank container[b]	Corrected for attenuation of blank container[c]	Corrected for attenuation of blank using "flow–through" container[d]
1	50 ± 4	94 ± 5	58 ± 5
2	30 ± 4	158 ± 9	61 ± 5
3	34 ± 4	83 ± 6	51 ± 5
4	44 ± 4	92 ± 8	55 ± 5
5	22 ± 5	77 ± 6	63 ± 5
6	33 ± 4	84 ± 6	66 ± 5
7	28 ± 5	82 ± 7	66 ± 5

[a] Concentrations (ppm) are the weighted means of 8 determinations on each rod, with weights equal to the reciprocal of the estimated variances where the estimated variances are based on Poisson counting statistics and propagation of error formulas. The errors are the standard errors of the weighted means.

[b] Nitrogen encapsulation method using standard capsule.

[c] Nitrogen encapsulation method using standard capsule, corrected for attenuation for 1/4 in. steel rod (Table 2).

[d] "Flow–through" container encapsulation corrected for attenuation for 1/4 in. steel rod (Table 2).

IV. References

[1] Anders, O. U., and Briden, D. W., Anal. Chem. **36**, 287 (1964).
[2] Coleman, R. F., Iron Steel Inst. (London) Spec Report **68**, (1960).
[3] Broadhead, K. G., and Heady, H. H., Anal. Chem. **37**, 759 (1965).
[4] Priest, H. F., Private communication.
[5] Nargolwalla, S. S., Crambes, M. R., and DeVoe, J. R., Anal. Chem. **40**, 666 (1968).
[6] Lundgren, F. A., and Nargolwalla, S. S., Anal. Chem. **40**, 672 (1968).

ACTIVATION ANALYSIS OF CHLORIDE AND IODIDE IN PHOTOGRAPHIC EMULSIONS USING 14.7 AND 2.8 MeV NEUTRONS

E. P. Przybylowicz[1], Gilbert W. Smith,
J. E. Suddueth and S. S. Nargolwalla

National Bureau of Standards
Washington, D.C. 20234

I. Introduction

Since the primary light sensitive properties of a photographic emulsion are determined by the composition of the silver halide component, there exists a need to have accurate and rapid methods of analysis for the halides in this matrix. Several methods have been applied to this problem, however, none of these provide the desired speed, coupled with acceptable accuracy.

The purpose of the present study was to examine the potentialities of a nondestructive neutron activation technique for this analysis. It was expected that in contradistinction to the x-ray emission technique, matrix problems would be considerably reduced with the higher energy gamma rays and therefore the analysis would be less dependent upon the composition of the matrix.

A survey of the literature has indicated a number of thermal neutron activation methods for the analysis of halogens in mixtures which involve radiochemical separation of the individual halides after reactor activation [1-3]. This approach is not attractive for routine use in an industrial situation where the speed of an analysis is often a prime consideration.

Several reports are available on the use of small neutron generators for halogen analysis, however only one deals with the problem of nondestructive analysis of mixed halides. Broadhead and Shanks [4] used 2.8 MeV neutrons for the determination of bromine in sodium chloride utilizing the reaction $^{79}Br(n,n'\gamma)^{79m}Br$. The lower detection limit for bromine was about 0.2 percent.

The presence of nitrogen in the gelatin of the emulsion precludes the analytical utilization of many of the isotopes produced by activation with 14.7 MeV neutrons because of the strong positron annihilation peak at 0.51 MeV from $^{14}N(n,2n)^{13}N$ and the resulting Compton and

---

[1]Research Associate, Eastman Kodak Company, Rochester, New York.

bremsstrahlung radiations at lower energies. With this limitation, there are only two isotopes which can be used for the measurement of chlorine — ^{34m}Cl and ^{37}S. Since the cross section for the latter was ten times larger, it was chosen for further study.

The measurement of iodide in this matrix with 14.7 MeV neutrons is not straightforward with present technology. ^{126}I produces useful radiations at 0.67 MeV, however, this is seriously interfered with by ^{108}Ag, ^{80}Br, ^{78}As, ^{106}Rh and the Compton continuum from ^{37}S and ^{34m}Cl. Thus activation with 2.8 MeV neutrons was investigated for the measurement of iodide. The 2.8 MeV neutron energy is below the threshold energy required for activation of nitrogen and oxygen, thus one is no longer limited to the use of gamma energies above the annihilation radiation (0.5 MeV). The 0.44 MeV photopeak of ^{128}I is useful for analytical measurements provided the production rates of ^{108}Ag, ^{110}Ag, and ^{80}Br are small in comparison with that for ^{128}I. This study experimentally demonstrated this to be the case, although no specific measurement of cross sections was made.

In this investigation we were not directly concerned with the measurement of bromide, since it is usually a major constituent and its concentration can be obtained by difference once the other halides and the silver have been determined. Thus, the focus of the work reported here centered around the development of calibration data for the nondestructive measurement of iodide in silver iodide-silver bromide emulsions, and chloride in silver chloride-silver bromide emulsions.

II. Experimental

A. Equipment

The fast neutron activation facility at the National Bureau of Standards consists of a Cockcroft-Walton generator rated at 2.5 mA beam current and a dual sample pneumatic system with a rotating sample assembly previously described [5,6]. In these experiments, the average flux at the sample position was estimated to be 5×10^8 n·cm^{-2}·sec^{-1} for 14.7 MeV neutrons and 1×10^6 n·cm^{-2}·sec^{-1} for 2.8 MeV neutrons.

B. Chemicals

All chemicals used in these experiments were either reagent grade or, in the case of the organic compounds, Eastman White Label chemicals. The calibration curves were obtained using fine grain photographic emulsions which had been previously analyzed for their composition. These consisted of individual emulsions of each silver halide suspended in gelatin.

C. Sample Preparation

Emulsions containing different levels of iodide and chloride in silver bromide were prepared by weighing out varying amounts of the emulsions in screw cap bottles and melting the mixtures by immersing the bottles for 1 hour in 50 to 60 °C water contained in an ultrasonic stirrer. Samples were placed in our standard 2 dram plastic vials (2 1/4 inch long × 5/8 inch in diameter) for irradiation and counting. The emulsion samples weighed about 9 grams.

III. Results and Discussion

A. Determination of Chloride in Silver Chloride-Silver Bromide Emulsions

Chlorine was measured by irradiating the sample, along with a flux monitor which was a full capsule of chlorobenzoic acid, in the dual sample irradiation assembly. The pair was irradiated for 2 minutes at full beam (2.5 mA) and allowed to decay for 2 minutes. The sample was then counted for 10 minutes followed by a 5 minute decay. Finally, the flux monitor was counted for 10 minutes. The energy interval from 2.69 to 2.75 MeV was used as a measure of bremsstrahlung from the sample whereas the chlorine peak was integrated from 2.75 to 3.30 MeV for both sample and flux monitor.

The results of the series of calibration experiments are shown in Figure 1. Four determinations were used to establish each point on the calibration curve. A weighted mean was calculated for each point along with the propagated statistical error. The error limits shown on the calibration points are weighted 1σ values; the line is a least squares fit to the points shown using the Gram-Schmidt Orthonormalization calculation.

Using this line, two different chloride containing emulsions were analyzed. The results of these analyses are shown in Table 1, along with results obtained by a chemical analysis of these emulsions. The agreement between the chemical method and the activation method is good.

B. Determination of Iodide in Silver Iodide-Silver Bromide Emulsions

Iodine was measured by irradiating the sample along with a capsule of ammonium iodide as a flux monitor. The timing sequence included a 30 minute irradiation, 1 minute decay, 30 minute sample count, 1 minute decay and a 5 minute flux monitor count. The pulses integrated for the
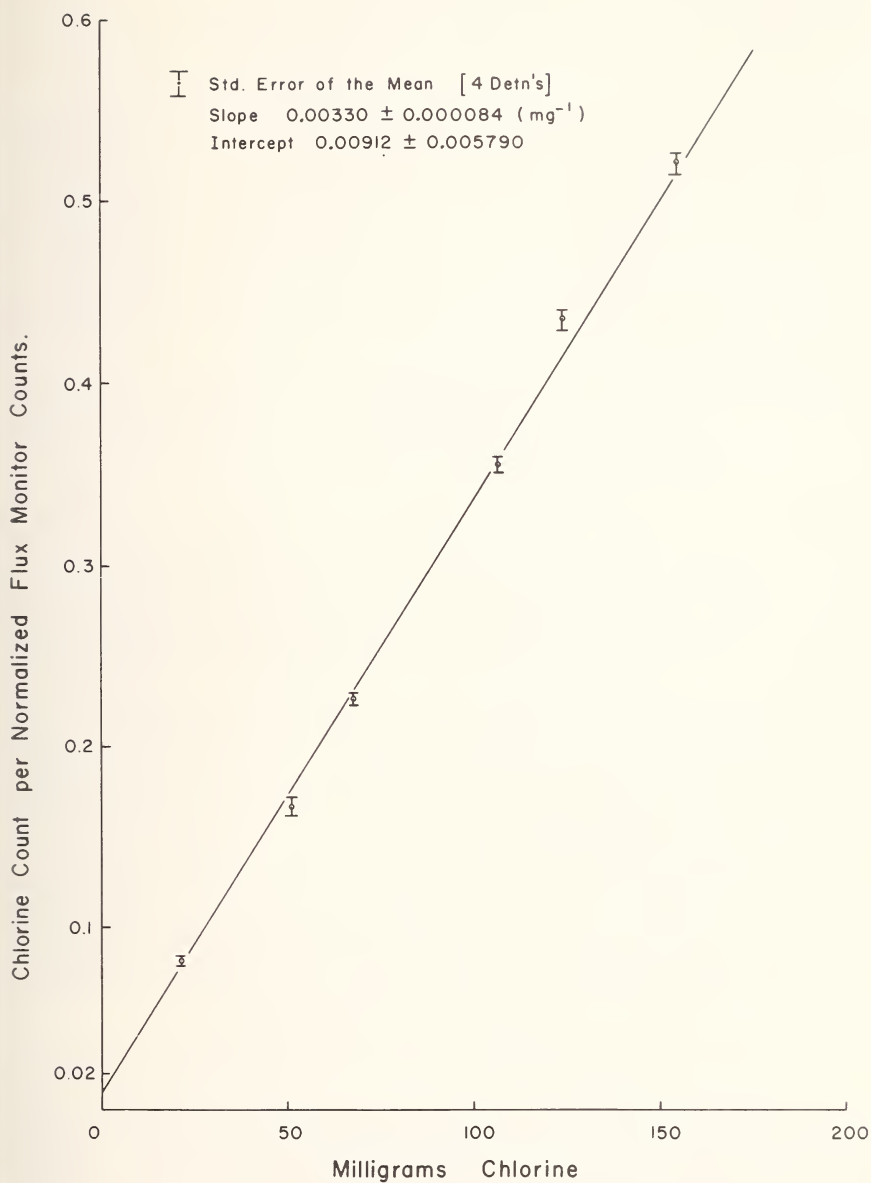
Figure 1. Chlorine calibration curve.

Table 1. Results of analyses on emulsions.

| Emulsions | Analysis | Milligrams of halogen | |
		Coulometric value[a]	Activation value[a]
A	iodine	16.7 ± 1.5	18.8 ± 2.5
B	iodine	29.6 ± 1.4	29.8 ± 2.5
C	iodine	44.8 ± 1.4	45.9 ± 2.5
D	chlorine	76.4 ± 0.4	76.4 ± 2.7
E	chlorine	75.6 ± 0.2	75.8 ± 2.7

[a] Results are the weighted means of replicate determinations. The errors are the weighted mean standard errors of the weighted means. Three replicates were run in the coulometric analysis; duplicates were run via the activation analysis method.

measurement of iodine were from 0.4 to 0.5 MeV. Correction for bremsstrahlung contribution was made by measuring the counts in the energy interval between 0.58 and 0.67 MeV and then using a measured ratio on pure bromide to correct for its contribution in the 0.4 to 0.5 MeV region.

The calibration curve for iodide is shown in Figure 2. Two determinations, statistically weighted, were used to establish each point on the calibration curve. The error limits shown on the curve are weighted 1σ and the line is a least squares fit. The error of the slope is less than 0.5% (relative) which is considered excellent for this analysis.

Results for the analysis of three silver iodide-silver bromide emulsions are given in Table 1, along with chemical analyses on these same emulsions. The relative standard errors (1σ) for both methods overlap for each sample indicating that results by the two methods, for the number of determinations made, are statistically indistinguishable.

C. NEUTRON ATTENUATION AND SAMPLE SELF ABSORPTION EFFECTS

It has been recognized [5] that neutron attenuation and gamma-ray self absorption effects must be corrected for in order to obtain accurate results in neutron activation analysis. Calculations show that the maximum error which will result if no attenuation corrections are made in these analyses is about 0.5%.

IV. Conclusion

A nondestructive neutron activation technique for the analysis of chloride and iodide in a silver bromide matrix is described. The method
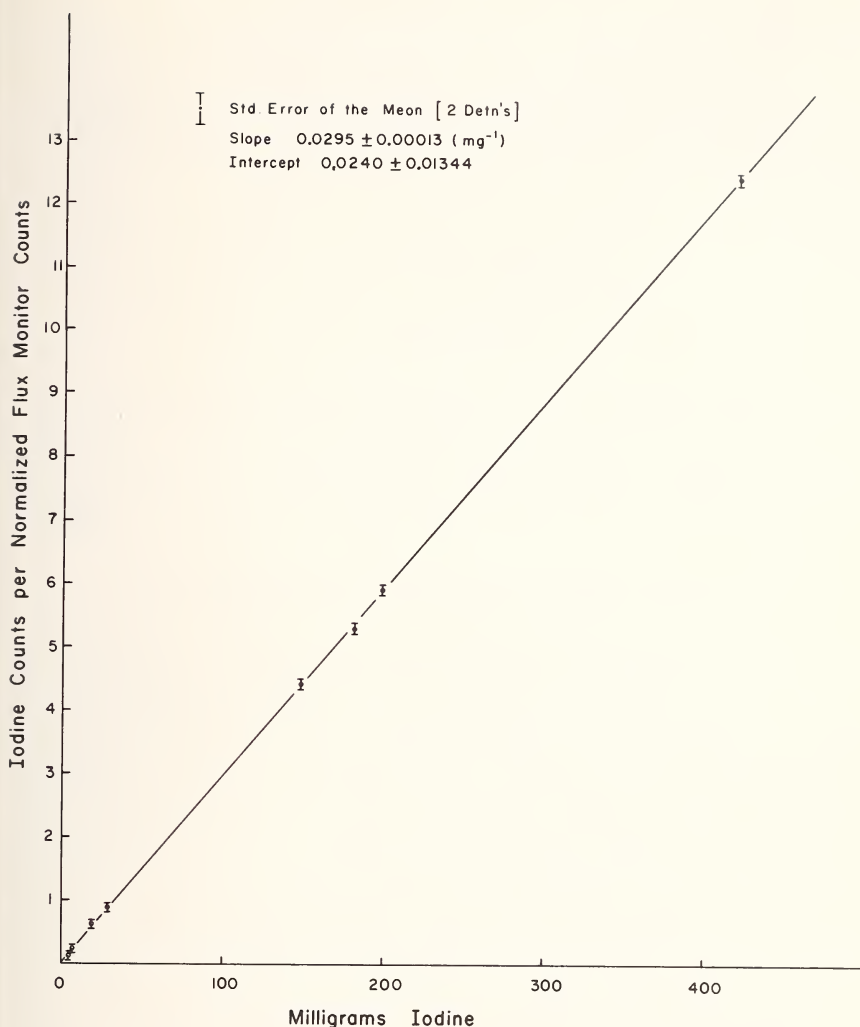
Figure 2. Iodine calibration curve.

offers an attractive alternate for the determination of iodide and chloride in silver halide mixtures since it has the potential for providing rapid analyses with reasonably good precision and accuracy. With an order of magnitude increase in neutron flux, the method would be unquestionably superior to other instrumental methods for the halides.

V. References

[1] Duce, R. A., Wasson, J. T., Winchester, J.W., and Burns, F., J. Geophys. Res. 68, 3943 (1963).

[2]   Belkas, E. P., and Souliotis, A. G., Analyst **91,** 199 (1966).
[3]   Goles, G. G., Greenland, L. P. and Jerome, D. Y., Geochimica et Cosmochimica
        Acta **31,** 1771 (1967).
[4]   Broadhead, K. G., and Shanks, D. E., Int. J. Appl. Rad. and Isotopes **18,** 279 (1967).
[5]   Nargolwalla, S. S., Crambes, M. R., and DeVoe, J. R., Anal. Chem. **40,** 666 (1968).
[6]   Lundgren, F. A., and Nargolwalla, S. S., Anal. Chem. **40,** 672 (1968).

LONG TERM OPERATING EXPERIENCE WITH HIGH YIELD, SEALED TUBE NEUTRON GENERATORS

P. L. Jessen

*Kaman Nuclear
Colorado Springs, Colorado*

I. Introduction

The operating history of a number of sealed (nonpumped) neutron generators indicates that laboratory life tests are valid indicators of expected use life. These tests also confirm the early indications that adequate lifetime would exist to permit practical routine activation analysis.

II. Laboratory Life Tests of Type A-3043 Accelerators

The A-3043 accelerator utilizes a single lens gap and a Penning ion source. It operates on a mixture of deuterium and tritium gas as is typical of nonpumped accelerators. The power supply control console system, which is used to drive the accelerator, is referred to as a Type A-710. It is designed to provide a continuous neutron yield of greater than 10^{10} n/sec. Three accelerators were tested for neutron yield as a function of total operating hours. The operation in all three cases was essentially continuous. The only interruptions were brought about by laboratory electrical power failures and inadvertent opening of the personnel safety interlocks for the systems. Figure 1 shows neutron yield *versus* operating time. The neutron yield was measured by copper activation. The test for two of the accelerators was terminated at approximately 65 hours. You will note that the yield at this time was still greater than one-half of the initial yield. These two units had not yet reached the "half life" that is frequently used as end of life for the targets in drift tube machines. The tests were terminated, however, because of limited shielding facilities and the desire to obtain life test data on a number of tubes to insure that the data obtained were representative. It can be seen that the third of these accelerators was life tested to approximately 87 hours, at which point the yield was approximately 40 percent of initial. The yield does not decrease because of depletion of the target as might be expected. Rather, the voltage which the tube will reliably withstand decreases, which forces a reduction in the total accelerating voltage at which the tube is operated if

reliable operation is required. Since the neutron yield is a strong function of the total accelerating voltage, this reduction in voltage is accompanied by a reduction in yield. The reduction in voltage hold-off capability is caused by metallizing of the glass envelope. This metallizing occurs because the lens design for this tube is a so-called unshielded one. A small number of the ions in the beam are scattered out of the beam by collision with neutral gas atoms. These ions will, in turn, collide with the lens elements, causing a low rate sputtering of the lens material. This sputtered lens material deposits on the glass envelope walls. A redesign of the lens system is presently being investigated.
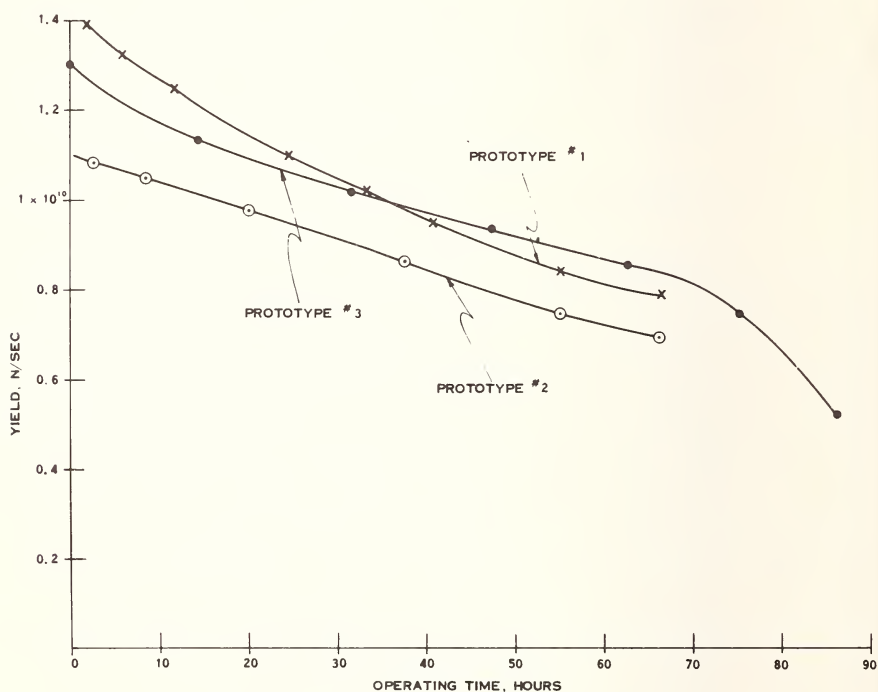

Figure 1.   Yield *vs* time for three A-3043 tubes.

III. Life History of the Type A-3043 Tubes in Actual Use

Some case histories are tabulated below indicating to the extent that data were available the service history of several of these tubes. It will be noted that these data are consistent with the laboratory test data. It is not possible in all cases to obtain good data from the user; as a consequence, only a few of the cases which exist are presented here. Case No. 3 undoubtedly represents the most meaningful data, since the customer

maintained excellent records of the neutron yield throughout the entire operating period. You will note that only two tubes were required for an operating period of six months, in which the equipment was operated on the average for 48 hours each week. This represents a very acceptable level of maintenance, particularly in comparison with the maintenance that would have been required with a typical drift-tube generator installation.

Table of A–3043 accelerator use histories.

Case No.	1st tube	2nd tube
1	Operating at 74 h, yield at 9×10^9, 14 months	
2	Replaced at 66 h, yield 1.1×10^{10}, broken, 3.7 months	Operating at 34 h, yield 1.2×10^{10}, 2.3 months
3	Replaced at 87 h, yield 6×10^9, 3.4 months	Operating at 127 h, yield 8×10^9, 2.8 months
4	Replaced at 117 h, yield 7×10^9, 8.3 months	Operating at 27 h, yield 1.2×10^{10}, 2.2 months

IV. A-3045 Laboratory Tests

The A-3045 accelerator utilizes a Penning ion source and a two-gap lens. The lens gap near the source is shielded, since the majority of beam scattering and associated sputtering of lens metal will occur there.

Case No. 1 Customer History
A–3045 Tube

1st Tube	2nd Tube
Replaced @ 95 h, pressure unstable, yield 8.5×10^{10} 4–1/2 months	Operating @ 19 h, yield 1.1×10^{11} 1.6 months

Three of the tests were conducted in a laboratory prototype control system. The fourth test (367 hours) was conducted in a production version of the control system. The design yield capability was the same for the two systems. Neutron yield was measured by both copper activation and a continuously recording system. This system consisted of a moderated LiF detector, a rate meter, and a pen recorder.

Yield *versus* operating time is shown for four of these accelerators in Figure 2. These accelerators were installed in the Kaman A-711 neutron generator system which has an initial neutron yield capability of greater than 10^{11} n/sec. It will be noted that two of these life tests were also terminated at approximately 100 hours, as a result of a shortage of shielding facilities. In one case you will note that the tube operated for approximately 123 hours at yields above 10^{11} n/sec, at which time the yield was intentionally lowered to approximately 2×10^{10} n/sec, since this is an adequate yield for many activation analysis applications. It was desired to determine the effects on lifetime of reduced yield operation. The maximum yield was measured several times during the reduced yield operation, as indicated by the X's above the curve. This was done to simulate the user who may not require full neutron yield for most applications, but would have infrequent need for full yield. This test was terminated at 367 hours. As in the A-3043 accelerators, the maximum voltage hold-off capability was decreasing.
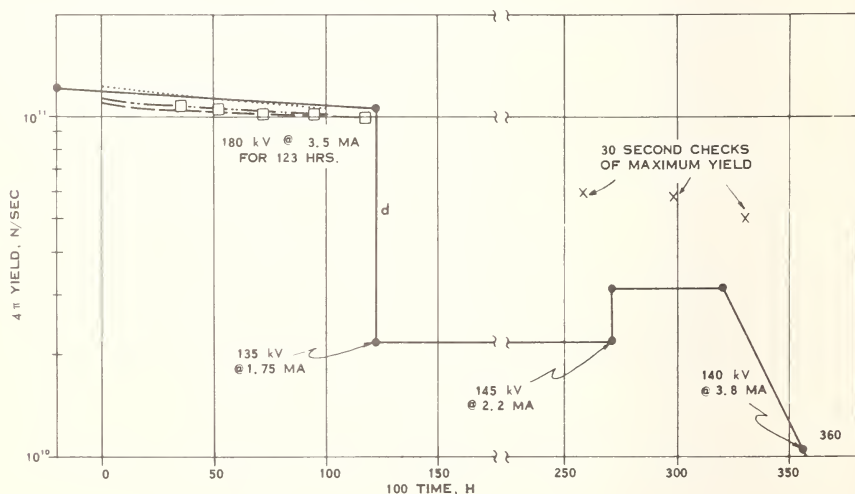

Figure 2.   Life test of type A-3045 tubes for A-711 neutron generator full reduced yield.

V. Customer Case History

The A-711 is a relatively new system and, while a number of these are presently in the field, only one has been in the field for a sufficient period

and has had sufficiently good records kept to provide a good case history of use. The data for that system are shown in the following table. Again, the data are consistent with the laboratory life test data.

VI. Conclusions

These data indicate that laboratory life tests simulate actual customer use sufficiently well to allow accurate prediction of accelerator lifetimes that may be expected in the field. They also indicate that operating periods of a few months may be expected under conditions of relatively high use before changing of the accelerator tube is required.

A 10^{11} NEUTRONS PER SECOND TUBE FOR ACTIVATION ANALYSIS

D. W. Downton and J. D. L. H. Wood

Services Electronics Research Laboratory
Baldock, Herts., England

I. Introduction

An adequate controllable neutron output coupled with long life, reliability and ease of operation are essential requirements of an activation analysis system for routine use. If 14 MeV neutrons are to fulfill their potential role in activation analysis, this specification must be met. To attain this objective sealed-off tubes utilizing the deuterium-tritium reaction have been made with outputs of 10^{11} neutrons per second. Such tubes operate at 120 kV with a beam of 12 mA and sustain the neutron output level for a period in excess of 100 hours with less than 10% degradation of yield.

II. Requirements for Long-Lived 14 MeV Neutron Source

The achievement of 10^{11}, 14 MeV neutrons per second for long periods from a conventional accelerator is thwarted by target difficulties. In such a system deuterium gas is ionized in a high pressure region and from this discharge an ion beam is extracted and accelerated through a low pressure region, maintained by a differential pumping system, on to a tritium loaded target. Various workers have assessed useful target half lives to be of the order of a few hours for outputs of 10^{11} neutrons per second [1-7]. This fall is due to a rapid dilution of the tritium by deuterium from the ion beam and is a severe limitation as far as a practical analysis system is concerned since degradation commences immediately. This effect may clearly be overcome by use of a deuterium-tritium mixture provided lowering of the initial neutron level is acceptable. However, in a continuously pumped system the excessive quantity of radioactive tritium necessary presents severe problems of safety and cost.

Sealed-off neutron tubes in which ion source and accelerating gap are at uniform pressure have the advantage of being able to use the gas mixture in both ion source and target so that a continuous circulation of gas occurs with proportions of deuterium and tritium maintained constant in ion source and target.

In 1965 we described the L-tube operating on this principle at a level of 10^{10} neutrons per second for a life of 100 hours [8-9]. Since then further development at this laboratory has extended this performance to 10^{11} neutrons per second with a similar long life.

III. The P-Tube — 10^{11} Neutrons Per Second

This tube is illustrated schematically in Figure 1. Gas pressure is controlled by a titanium replenisher and monitored by a pirani gauge. The plasma is excited in the ion source by an external r.f. oscillator and intensified by an external axial magnetic field. The ion beam is formed by an extractor electrode operating at -5 kV with respect to the ion source using an electrode system adapted from that of Thonemann and Harrison [10]. The ions are subsequently accelerated to 120 keV through an aperture in a suppressor electrode on to the target which comprises an erbium layer evaporated on a molybdenum substrate. Any secondary electrons formed at the target by the ion beam are suppressed, but those formed by ion-gas collisions in the accelerating region are accelerated back down the beam where they are collected by the cooled electron collector.

The tube itself is of glass and metal construction 5.5 cm diameter and 40 cm long. In use the tube is mounted in an oil-filled container to prevent external high voltage breakdown. The main operating parameters of the tube are summarized in Table 1.
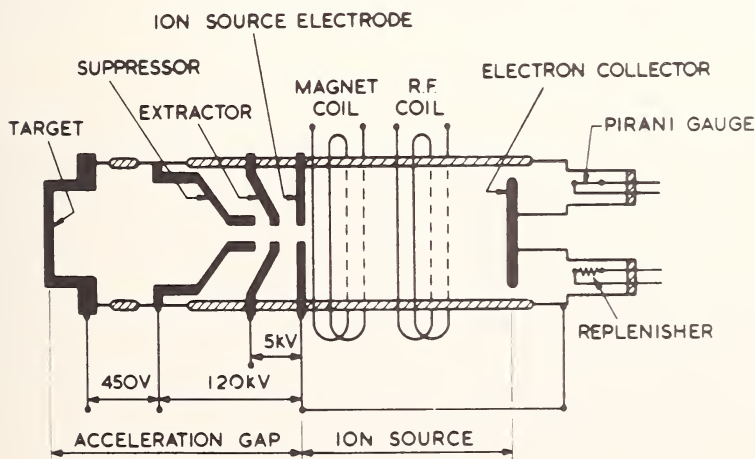

Figure 1.   P-tube schematic.

Table 1. Typical P—tube operating parameters.

Gas pressure	15 millitorr
Ion source power	500 W
Ion source oscillator frequency	14 MHz
Magnetic field	100 G
Extractor voltage	5 kV
Acceleration voltage	120 kV
Beam current	12 mA
Suppression voltage	450 V
Neutron output (4π)	10^{11} neutrons/sec
Useful target diameter	28 mm

A. LIFE TEST PERFORMANCE

Over ten tubes have been tested during development with an average life of 120 hours and the total running experience is over 1500 hours. The most recent results are illustrated in Figure 2 and compared with earlier results from the L- tube [9-12].

Extension of useful life has been achieved by use of targets up to twenty times thicker than the conventional target [13-14]. With the thin targets, output is seen to fall away during life due to gradual sputtering away of the target evaporated film. This fall from a thin target is some hundred times slower than the dilution effect described earlier. With the thicker targets now in use, a life at 10^{11} neutrons per second of several hundred hours is achieved. By 100 hours output has fallen by less than 10% of the initial value.

B. USE OF THE TUBE FOR ACTIVATION ANALYSIS

During development the tubes were operated with the target at high voltage with respect to ground. This however is not suitable for all activation analysis purposes where ready access to the target is desirable. In the most recent form of container the target is located near the surface and is operated at ground potential. Virtually a 2π geometry is available for samples, which can be placed within 4 mm of the neutron producing surface. The intervening material comprises the target coolant system. This container is some 31 cm in diameter and length 95 cm. It is a hermetically sealed unit and can be readily replaced with another container by its simple plug and socket connections.

High activation analysis sensitivities can be achieved, e.g. in analysis for oxygen using the $^{16}O(n,p)^{16}N$ reaction and a 35 second irradiation
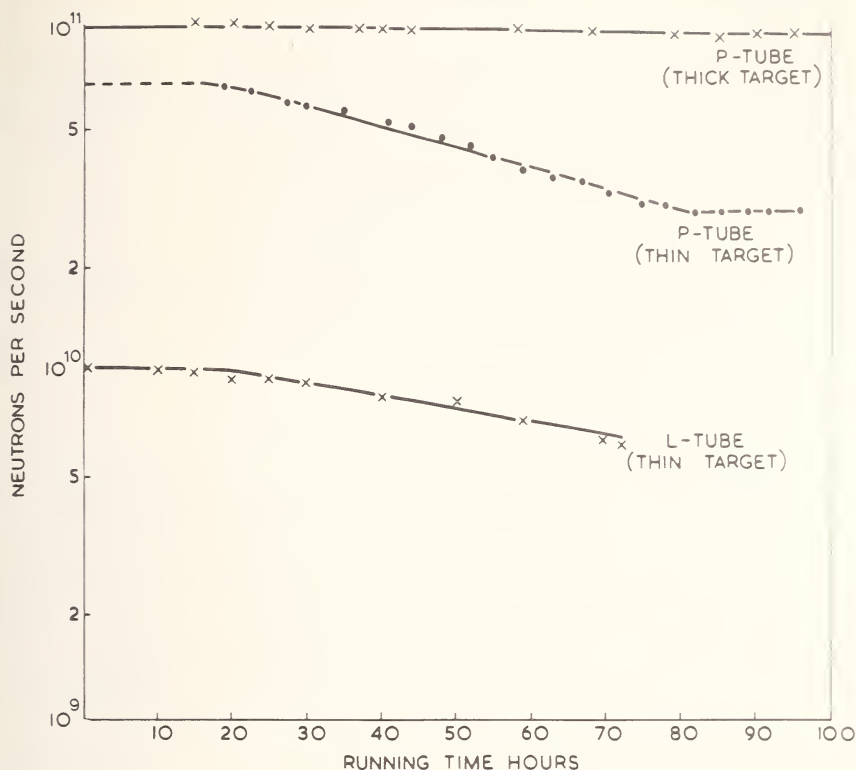
Figure 2.   Life test performance.

period followed by 2 second cool and 20 second count period, a sensitivity figure of 5,220 counts per milligram of oxygen is recorded using two 3 in. × 3 in. sodium iodide crystals. This figure was obtained from a 10 gram steel sample 16 mm diameter and is over five times greater than previously quoted values [11].

The exploitation of 14 MeV neutrons in activation analysis has awaited development of a source of this sort. This sealed-off tube with an output of 10^{11} neutrons per second for more than 100 hours in a form suitable for laboratory and industrial use is now established. It is very reliable, can be operated by unskilled staff, or, if fully automatic operation is required, it may be allowed to run unattended. As an example, up to 75% time utilization has been achieved in a 24 hour period.

IV. Acknowledgments

V. References

[1]   Dubus, M. M., Proc. Accelerator Targets Designed for Production of Neutrons, Grenoble 1965. Euratom Report EUR 2641 d, f, e, pp. 231-239.
[2]   Morgan, M. I. L., Euratom EUR 2641 d. f. e, pp. 239-263.
[3]   Perkin, M. J. L., Euratom EUR 2641 d, f, e, p. 91
[4]   Hollister, M. H., Euratom EUR 2641 d, f, e, p. 174.
[5]   Broerse, J. J., and Barendsen, C. E., Nature **206,** 208 (1965).
[6]   Coon, J. H., Fast Neutron Physics, Marion and Fowler, Eds., Interscience, N.Y., 1960, pp. 694, 699.
[7]   Booth, R., 1.E.E.E. Transactions on Nuclear Science, June 1967, pp. 938-942.
[8]   Wood, J. D. L. H., and Downton, D. W., Proc. Modern Trends in Activation Analysis, Texas, 1965, pp. 175-181.
[9]   Bounden, J. E., Lomer, P. D., and Wood, J. D. L. H., Proc. Modern Trends in Activation Analysis, Texas, 1965, pp. 182-185.
[10] Thonemann, P. C., and Harrison, E. R., A.E.R.E. Report GP/R1190, 1953.
[11] Stoll, N., Wagner, A., and Goedert, L., Euratom EUR 3161, f, Vol. II.
[12] Bounden, J. E., Lomer, P. D., and Wood, J. D. L. H., Nucl. Inst. and Meth. **33,** 283-288 (1965).
[13] Lomer, P. D., Euratom EUR 2641, d, f, e, pp. 147-156.
[14] Hillier, M., Lomer, P. D., Stark, D. S., and Wood, J. D. L. H., Euratom EUR 3895 d, f, e, 1967, pp. 125-145.

A HIGH OUTPUT SEALED-OFF NEUTRON TUBE WITH HIGH RELIABILITY AND LONG LIFE

O. Reifenschweiler

Philips Research Laboratories
N. V. Philips' Gloeilampenfabrieken
Eindhoven, The Netherlands

I. Introduction

Neutron generators working with the $^3H(d,n)^4He$ reaction are very suitable sources for activation analysis because they can be constructed in simple and compact versions. The conventional continuously pumped accelerator sources of this kind, however, have the drawback that the target into which the tritium is absorbed has a limited life. In spite of world-wide efforts [1] it has not yet been possible to find a basic solution to this problem which has so far prevented the large-scale use of these neutron generators, especially in industry.

In sealed-off neutron tubes the development of which presents a big step forward in the direction of even simpler and more compact accelerator neutron sources, a fundamental solution to this problem could be found in a self- loading target. The essential problem in the realization of such sealed-off neutron tubes were first solved in our laboratories. As early as 1937 Penning [2] had shown that in principle it is possible to operate an ion source and an accelerating system at the same gas pressure. In 1957 we described in a paper presented to the German Physicists meeting [3], a sealed-off neutron tube with a gas regulating device and using an essential improvement of the Penning principle. We thus realized for the first time a neutron tube with a usable neutron output and usable tube life. In 1960 we introduced the self loading target [4] with which extremely long life at a constant high output could be obtained in principle and which has since that time been utilized also by other designers of sealed-off neutron tubes. However, the longest operational lives reported so far for tubes with outputs of 10^{10} n/sec and more are only in the region of 100 hours [5-7], which limits general application.

The purpose of this paper is to describe a neutron tube with an output ranging from several times 10^{10} n/sec up to about 10^{11} n/sec with very good reliability and a life of more than 1000 hours.

II. Generation and Acceleration of Ions

Figure 1a shows the design of the tube. The ions are generated in a Penning ion source. This ion source is kept at a positive potential of 150 to 200 kV. The accelerating electrode is placed under the ion source. It is maintained at a potential of a few hundred volts negative against a diaphragm located above the target. In this way acceleration of secondary electrons formed at the target towards the ion source is prevented (secondary electron trap). The accelerated ions enter the accelerating electrode in a slim divergent beam and strike the target at the end of the tube. The diameter of the beam at the target is between 3 and 4 cm.
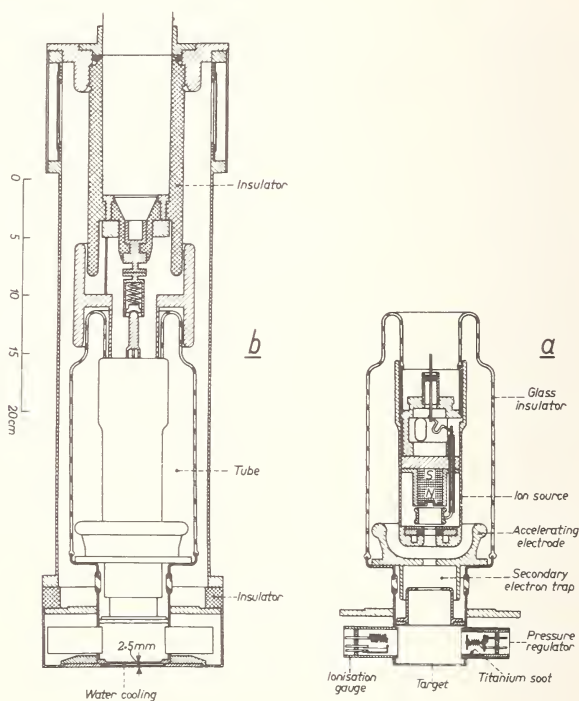
Figure 1.   (a) Sectional drawing of the neutron tubes, (b) the tube in its shield.

Special studies were carried out in order to obtain the optimum design of the accelerating system. The special shape of the accelerating electrode prevents deposition of sputtered metal atoms on the insulating glass walls. Such a metal deposition would result in a life limitation of the tube. A careful choice of the materials and surface preparation of the accelerating electrode proved to be essential.

III. The Target

The accelerated ions hit the target where neutrons are released. For attaining a long life, use is made of the drive-in target (self-loading target) [4]. With the conventional tritium targets the tritium absorbed in an exothermal hydrogen absorber is driven out by the deuteron beam. With the drive-in target an equal mixture of tritium and deuterium ions is driven into a thin layer of an exothermal hydrogen absorber. Up to now we use titanium. Once established, the state of saturation of the deuterium-tritium mixture in the target maintains itself throughout the life of the tube, and there is no drop in the neutron yield. A more extensive description of this self-loading target can be found in reference [8].

The next life-limiting factor after avoidance of the drive-out process of the tritium in conventional targets is the sputtering of the hydrogen absorbing material under ion bombardment. However, the experience gained so far with the tube described in this paper shows that with outputs of several times 10^{10} n/sec, this factor is not evident during 1000 hours of operation.

IV. Pressure Regulator

A special hydrogen pressure regulator is used for regulating and stabilizing the gas pressure inside the tube. Its working principle has been described earlier [9], but a new construction is employed (see Figure 1a).

Titanium is deposited by vaporization in an argon atmosphere onto the inner wall of a metal cylinder as an extremely fine powder (titanium soot). The titanium particles have a diameter of about 100 A giving a total superficial area of a few square meters. After the titanium soot has been made to absorb the deuterium-tritium mixture, the gas pressure inside the tube can be adjusted by heating the metal cylinder to a certain temperature.

In the new construction the metal cylinder which is able to be heated is enclosed in a second cylinder which is at the same time the outer wall of the tube. The space between the two cylinders is very narrow. This construction results in a quick response to temperature and thus pressure adjustment.

Thanks to the large superficial area of the titanium, this pressure regulator has an excellent getter action which is very important for high reliability and long life of the tube.

V. The Tube in its Shield

For simple and convenient application the tube is enclosed in a shield consisting of a metal cylinder with a maximum diameter of 15 cm and a

length of about 65 cm, as shown in Figure 1b. The insulation between tube and shield is maintained by oil. The accelerating voltage and the ion source voltage are supplied by a coaxial high tension cable led in at one end of the shield.   The connections for the pressure regulator, the ionization gauge, and the negative voltage for the secondary electron trap are located at the target end. The target, which is grounded, is water cooled. The distance between the neutron producing titanium layer and the outside of the target is only 2.5 mm, so that a high usable neutron flux is obtained.

This compact and robust version of the neutron tube in its shield attached to a high voltage cable is eminently suitable for application in activation analysis since in many cases simple and cheap shielding will be adequate.

VI. Performance of the Tube

The tube works at a gas pressure between several times 10^{-4} and several times 10^{-3} mm Hg depending upon the desired ion current.

Up till now we have worked with experimental tubes with target currents up to 5 mA, accelerating voltages up to 200 kV and with neutron outputs up to 3.5×10^{11} n/sec.

In the first instance, however, the tube was intended for application with outputs of several times 10^{10} n/sec providing high reliability and long life. To this end life and reliability tests were undertaken at such an output to investigate whether any life or reliability limiting factors would be revealed up to 1000 hours.
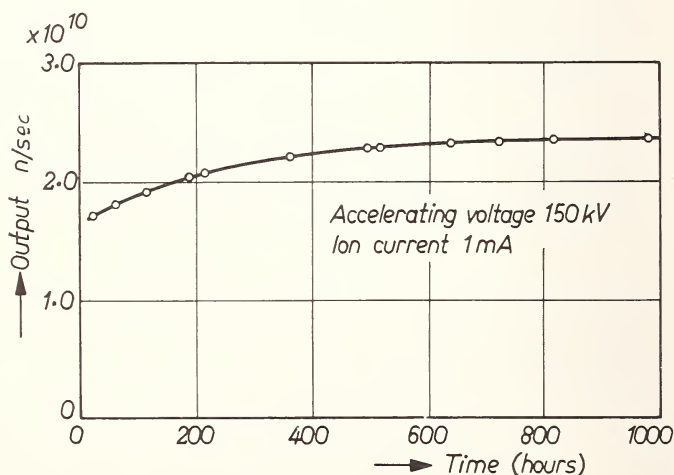

Figure 2.   Neutron output as a function of operation time.

In a life test with a tube taken from the production line we worked with an accelerating voltage of 150 kV and a target current of 1 mA; the output was 2×10^{10} n/sec, the neutron flux at the surface of the target was 10^9 n·cm^{-2}·sec^{-1}, and at a distance of 2 cm from the target 4×10^8 n·cm^{-2}·sec^{-1}.

The reliability was excellent. An impression of it may be gained from the fact that it was possible to operate the tube day and night as well as over the weekends without any supervision whatsoever. To accomplish this the target current was stabilized automatically by operating the pressure regulator via an electronic control system. The neutron output was measured continuously and recorded.

Figure 2 shows the neutron output as a function of operation time. The output first rises somewhat and then remains constant throughout the life test. At the termination of the 1000 hours experiment, reliability and neutron output showed no decrease. The tube is still operational today.

VII. Conclusions

These and further experiments have demonstrated that the described neutron tube has a reliability and life at an output of several times 10^{10} n/sec equal to those of comparable electron tubes. It therefore fulfills the requirements necessary for industrial application.

An automatic activation analysis system for such industrial applications comprising our neutron tube with feeding and control equipment, automated rabbit system and counting equipment has been developed and applied by Tertoolen. To the present it is used successfully to solve the following analytical problems: oxygen in steel; oxygen in zircaloy; oxygen in organic materials; silicon in solutions with high zirconium concentrations; phosphorus in organic material; sodium in mercury; rare earths in yttrium oxide; hafnium in zircaloy; phosphorus in the presence of silicon. This work will be published by Tertoolen elsewhere [10].

The development work is continued first of all with the intention of establishing conditions for operation with outputs of 10^{11} n/sec with a reliability and life required for large scale use.

The results of a feasibility study show that with such sealed-off neutron tubes, outputs of several times 10^{12} n/sec with a life of at least some hundreds of hours are possible.

VIII. References

[1]   Proceedings of the Symposia "Accelerator Targets deigned for the Production of Neutrons", Liege, 1964, Grenoble, 1965 and Liege, 1967, EURATOM reports EUR 1815, EUR 2641 and EUR 3895.

[2]   Penning, F. M., and Moubis, J. H. A., Physica 4, 1190 (1937).

[3]   Reifenschweiler, O., and van Dorsten, A. C., Phys. Verh. Mosbach **8,** 163 (1957).
[4]   Reifenschweiler, O., Nucleonics **18,** No. 12, 69 (1960).
[5]   Bounden, J. E., Lomer, P. D., and Wood, J. D. L. H., Proc. 1965 Int. Conf. "Modern Trends in Activation Analysis", College Station, Texas, 182 (1965).
[6]   Hillier, M., Lomer, P. D., Stark, D. S., and Wood, J.D.L.H., Proc. Symposium "Accelerator Targets Designed for the Production of Neutrons", Liege, 1967, EURATOM report EUR 3895, 125 (1967).
[7]   Jessen, P. L., Proc. Symposium "Accelerator Targets Designed for the Production of Neutrons", Liege, 1967, EURATOM report EUR 3895, 147 (1967).
[8]   Reifenschweiler, O., Philips Res. Reports **16,** 401 (1961).
[9]   Reifenschweiler, O., Rev. Sci. Instr. **35,** 456 (1964). See also Phys. Verh. VDPG **9,** 181 (1967).
[10] Tertoolen, J. F. W., "Industrial Activation Analysis with 14 MeV Neutrons", to be published.

UNIQUE METHODS

Synopsis of Discussions

SAADIA AMIEL, *Chairman*

Israel Atomic Energy Commission
Yavne, Israel

By the title of the session one may have expected presentations of unique methods; yet, in some instances it is not possible to distinguish between the papers of this session and some papers scattered throughout other sessions, which do have the same "unique" features in general terms.

Two major aspects stood out in this session: on-line analysis and cyclic or shuttle-rabbit analysis. On-line or on-stream analysis is a product of the increasing need for continuous nondestructive analysis posed to the analyst by modern industry. The elimination of human intervention in the course of the process and analysis which makes them completely instrumental, facilitates automation of industrial process control through processed informational feedback. This type of analysis, to my opinion poses a major challenge to the nuclear analyst, especially when dealing with complex matrices and where minor and trace constituents with great precisions are in question. Some important aspects of such methods were brought up in this session.

A point far more important than just semantics is the definition of "on-line" analytical methods. There may be some ambiguity in the interpretation of the on-line aspect; does only a direct measurement of reaction fragments and radiations meet the definition, or does it embrace also analysis of induced radioactivities? The latter involves a certain delay in measurement (as short or as long a delay as it may be) in an uninterfered-with dynamic system, either between the intervals of irradiation bursts or under continuous irradiation conditions by measuring the activities downstream away from the irradiation position. From the practical point of view, both may be defined as "on-line" methods considering the speed of informational supply and noninterference with the dynamics and function of the process.

Cyclic or shuttle-rabbit techniques indicate, as done by some authors, the analytical usefulness of very short-lived radioactivities which in many cases do offer specificity and speed when nondestructive analysis is needed. Careful programming and predetermination of analysis steps and

timing are of great importance in order to obtain specificity and satisfactory sensitivity. Pulsing a beam, circulating a conveyer, or shuttling rabbits are representative techniques.

Since the feature of analysis speed with different interpretations was brought up in this session some distinctions should be made. One visualizes a case where the irradiation and measurement are accomplished in a short time while, in another case, one refers to the total time spent on the analysis which may be very short, irrespective of whether the measurement is done with a substantial delay after irradiation. In either case, speed should be evaluated and thence, defined by the purpose that the analysis serves and by the speed criterion set by it. The diversity of approaches to this question proved the point.

A different topic presented in this session containing a feature somewhat unique with respect to many other reports which mainly discussed radioactivity measurements in this meeting, is analysis by charged particle spectrometry occurring simultaneously with the irradiation. This technique offers advantages for surface analysis.

Of a limited scope but of great value is the very specific and sensitive method of determining uranium or rather fissionable elements by visually counting fission tracks. Of great advantage (unique to this method) is the possibility not only of determining the content but also the location of the uranium for example within a microscopical scale in the sample.

The announcement of the availability of intense neutron sources of ^{252}Cf offers another very useful tool which is complementary with those presently in possession and use for activation analysts. It is expected that if such sources will indeed be available to a great many investigators, many new applications of such sources will be reported in the coming few years.

ON-STREAM ACTIVATION ANALYSIS USING SAMPLE RECIRCULATION

J. B. Ashe, P. F. Berry and J. R. Rhodes [1]

Texas Nuclear Corporation, Austin, Texas

I. Introduction

In recirculation activation analysis the sample is recycled between a continuously emitting neutron source and a shielded detector, which measures the radioactivity of the sample continuously throughout the analysis period. The main application considered here is to on-stream analysis, when a fluid is circulated in a closed loop.

For given values of neutron flux, detector efficiency, analysis time and volume flow rate, significant gains in detected signal are obtained, compared with the standard "open loop" method of on-stream activation analysis, particularly in the case of isotopes with half lives long compared with the recirculation time. An essential fundamental is that the radioactivity should not decay appreciably between activation and counting, nor between counting and re-activation. An important practical aspect is that the residence time in both the activation and counting cells can be short compared with the half life of the induced activity, and so flow rates can be easily made high enough to keep aqueous ore slurries in suspension. This is not so with open loop activation; particularly with isotopes with half lives longer than a few minutes when a compromise must be reached between achieving a long residence time in the activation cell and prevention of the slurry from settling out.

To our knowledge Starnes [1] first proposed a recirculation system, although others have studied continuous activation analysis effectively in open loop condition [2]. Keepin [3] and others, for example, Givens, Mills and Caldwell [4] have studied various forms of "cyclic activation". In one form, a discrete, stationary sample is activated by a pulsed neutron source and the radioactivity counted by a pulsed detector that is switched on when the source is off, and vice versa. Although the mathematics describing this form of cyclic activation is closely similar to the theory presented below, the two techniques are not the same and have different areas of application.

913

II. Theory

A. Total Count and Gain Factor

Figure 1 shows a schematic of the loop used in this work. The detector count, C_n, after a total of n cycles can be shown to be

$$C_n = S_o n G \tag{1}$$

where G is the gain factor over the signal obtained in open loop conditions (for the same total analysis time t), and S_o is the activation factor for a single cycle.

$$S_0 = k \frac{NV}{\lambda} (1 - e^{-\lambda t_a}) e^{-\lambda t_d} (1 - e^{-\lambda t_c}) \tag{2}$$

where

$k =$ a constant which is the product of the effective neutron flux in the activation cell, the cross section for production of the radiation to be detected, and the detector efficiency including geometrical factors

$N =$ number of nuclei per cm^3 that can undergo the specified reaction

$\lambda =$ the decay constant of the induced activity (sec^{-1})

$t_a =$ the effective time in the activation cell (sec)

$t_d =$ the effective delay time (sec)

$t_c =$ the effective time in the count cell (sec)

$V =$ the volume of the loop (cm^3).

$$G = \frac{1}{1 - e^{-\lambda T}} \left[1 - \frac{e^{-\lambda T}(1 - e^{-\lambda t})}{n(1 - e^{-\lambda T})} \right] \tag{3}$$

where T is the time for one cycle.

Figure 2 shows G plotted as a function of λT for various values of n. For half lives short compared with the recirculation time the gain factor tends to unity. For a half life equal to the recirculation time ($\lambda T = 0.693$), the gain factor tends to two. For half lives long compared with the recirculation time, the gain factor increases with the number of cycles. Thus:

$$G_{\lambda T \to 0} = \frac{n+1}{2}$$

For example, in the case of the reaction $^{56}Fe(n,p)^{56}Mn$ (half life, 2.58 hours), the total count obtained in a measurement time of 30 minutes is
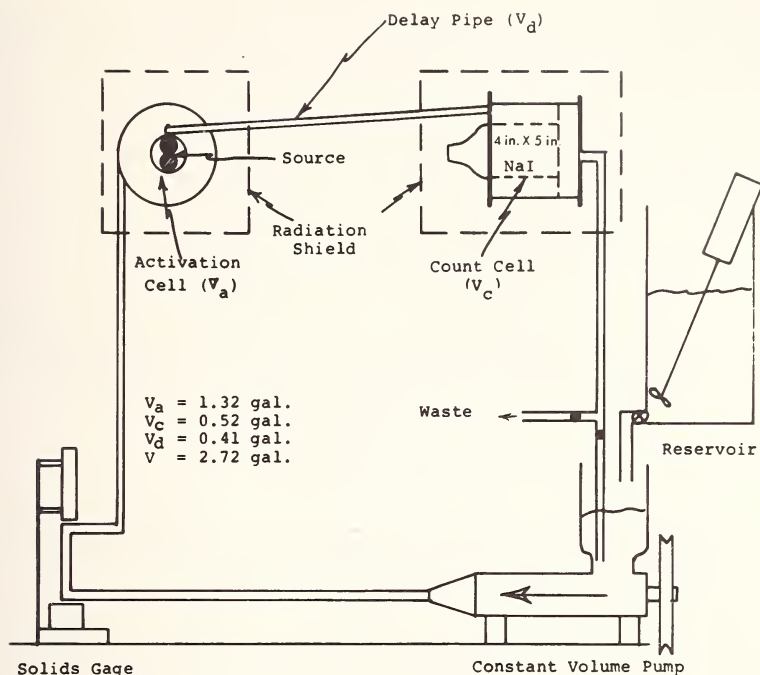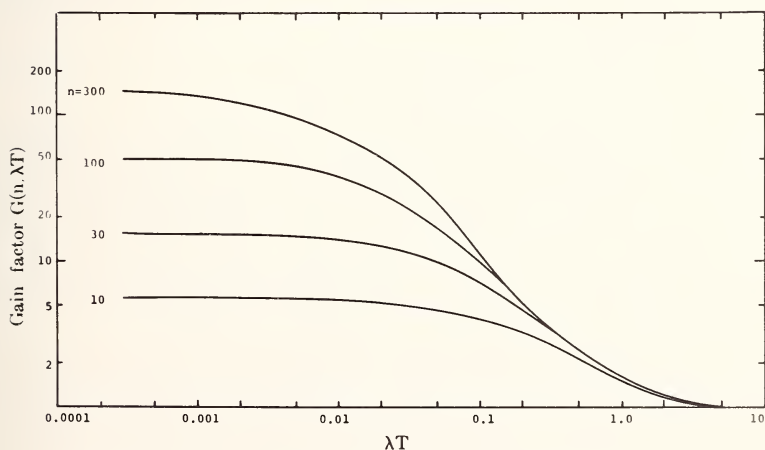
Figure 1.   Experimental activation loop (schematic).

Figure 2.   Gain factor as a function of λT for different values of n.

about 15 times greater in a recirculating loop with a period of 1 minute than in an open loop at the same volume flow rate.

Equations (1) and (3) are only strictly true for large n since we have neglected second order effects due to partial activation of the contents of

the activation cell in the first cycle and also the incomplete passage of material through the count cell at the end of each cycle.

B.   COUNT RATE AND FLOW RATE

The average count rate at a time, t, can be expressed as:

$$I_t = \frac{\text{Total count in the n'th cycle}}{T} = \frac{S_0}{T}\left(\frac{1 - e^{-n\lambda T}}{1 - e^{-\lambda T}}\right) \qquad (4)$$

Thus after an initial linear increase with time the average count rate reaches a steady value for a particular flow rate, $Q \ cm^3/\text{sec}$, given by

$$I_\infty = \frac{kN(1 - e^{-\lambda t_a})e^{-\lambda t_d}(1 - e^{-\lambda t_c})}{\lambda(1 - e^{-\lambda T})}Q \qquad (5)$$

For half lives long compared with the recirculation time, the steady count rate is independent of flow rate and is proportional to

$$\frac{t_a t_c}{T} = \frac{V_a V_c}{V}$$

For short half lives it is sometimes possible to choose the loop parameters so that the curve of equilibrium count rate against flow rate exhibits a broad maximum [1].

III.   Experimental

A taconite ore sample containing approximately 60% Fe and 5% Si was circulated as an aqueous slurry in the loop shown diagrammatically in Figure 1 at a flow rate of 1 gal/min, first, under open loop conditions and secondly, in the closed loop arrangement. The solids content was monitored by means of a gamma-ray transmission gauge and remained constant at a 30% w/w solids throughout the experiment. The neutron source was ^{239}Pu/Be of total output 2×10^7n/sec.

Figure 3 shows gamma-ray spectra obtained after 30 minute analysis times. Table 1 shows the experimental net counts obtained in the 0.845 MeV and 1.77 MeV gamma-ray peaks from Fe and Si activation, respectively, after correcting for background, the Compton continuum from high energy radiation, and a small contribution from Fe in the Si peak[1]. Also shown in Table 1 are the calculated and experimental gain factors for closed loop compared with open loop conditions. The agreement is seen to be excellent.

---

[1]The silicon is activated by the reaction ^{28}Si(n,p)^{28}Al, half life = 2.3 minutes.
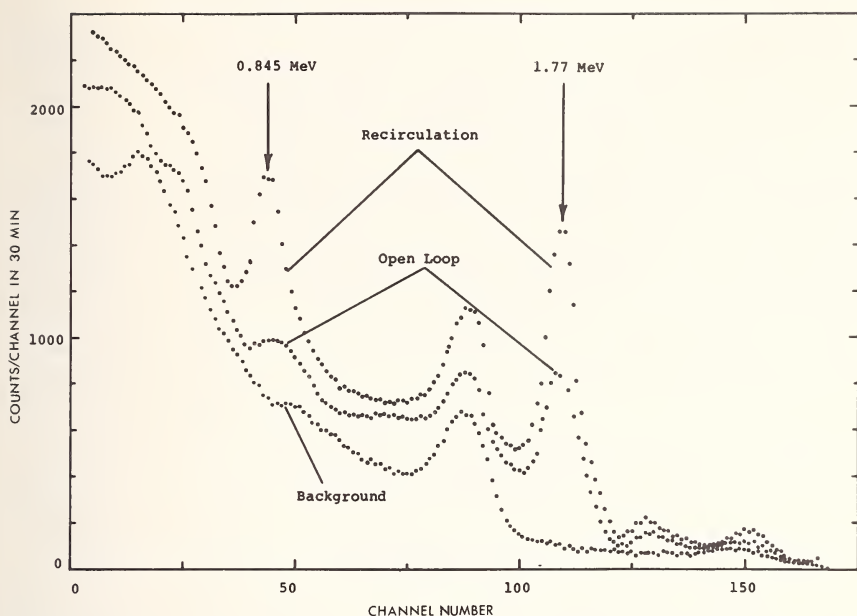
Figure 3. Gamma-ray spectra of taconite ore sample, activated using open loop and recirculation conditions (analysis time 30 min).

Table 1. Experimental and calculated gain factors for iron and silicon activation using closed loop and open loop conditions.

Energy of peak (MeV)	Net counts		Gain factor	
	Open loop	Closed loop	Experimental	Calculated
0.845	1290	7,300	5.65 ± 0.5	5.65
1.77	8800	13,400	$1.53 \pm .05$	1.68

[a] Flow rate, 1 gal/min; analysis time, 30 min.

IV. References

[1]   Starnes, P. E., U.S. Patent Appl. No. 628644 (1966).
[2]   Rhodes, J. R., Proceedings of 8th Japan Conf. on Radioisotopes, Tokyo (1967).
[3]   Keepin, G. R., LAMS-2215 (1958).
[4]   Givens, W. W., Mills, W. R. Jr., and Caldwell, R. L., (see this volume, p. 929.)

FAST NEUTRON CONTINUOUS ACTIVATION ANALYSIS OF DILUTE SOLUTIONS

R. E. Jervis and H. Al-Shahristani

*Department of Chemical Engineering
and Applied Chemistry
University of Toronto
Toronto, Canada*

S. S. Nargolwalla

*National Bureau of Standards
Washington, D.C. 20234*

I. Introduction

Continuous activation analysis for components at very low concentrations in flowing liquids can be accomplished rapidly. Since process variables can be adjusted promptly in response to any transients observed such monitoring promises to be of great value in process control and automation.

Activation of the specie(s) of interest can be done by exposing the liquid to any of a variety of radioisotopic or accelerator neutron sources yielding from 10^8 to 10^{11} neutrons per second. Measurement of the gamma component of induced radiation following the neutron activation is the most feasible approach for liquid systems, although in certain applications to assay of streams containing fissile uranium or thorium, delayed neutron counting may also be done.

Similar to normal activation analysis, the selectivity of the method can be enhanced by suitable adjustment of the relative irradiation, decay and counting times. In flow activation, an optimal arrangement of the dwell periods of a sufficiently large liquid volume in the irradiation zone, in the tubes carrying the fluid to the radiation detector *viz.* the decay zone and in the detector vicinity can result in sensitivities and specificity much superior to the more usual activation procedure.

II. Experimental

Flow activation studies were made in three aqueous systems: trace fluoride, vanadium and uranium. Fast neutron activation was used

918

throughout, but gamma counting was done in the first two cases and delayed neutron counting in the last.

A.   EQUIPMENT

Suitable liquid irradiation cells were located adjacent to the neutron source and the dilute solutions to be analyzed were pumped through openings in the biological shield around the source, through the cell and out again to a counting assembly within a relatively short time. Fast neutron activation was carried out both with 14 MeV neutrons produced by a Model 9900 Texas Nuclear neutron generator and also with evaporation (γ,n) neutrons of 1 to 4 MeV produced by the electron beam of a 35 MeV Vickers linear accelerator.

A series of irradiation cells of different geometry were positioned adjacent to or surrounding the neutron source. An attempt was made in the design of the cells (see Figures 1 to 4) to provide the same neutron flux exposure for each succeeding liquid volume element flowing through the cell and to minimize "channeling". This was particularly important when a twin-stream cell was used to allow for simultaneous activation and counting of the solution for analysis and a calibration solution of known concentration. In some experiments it was found feasible to resort to a single stream arrangement, and a reentrant cell was designed so as to utilize a large solid angle surrounding the source and also of a shape that would provide for laminar fluid flow conditions at most of the flow rates used. The dimensions of the cells in all cases were chosen to allow a sufficiently large solution volume to be effectively activated.
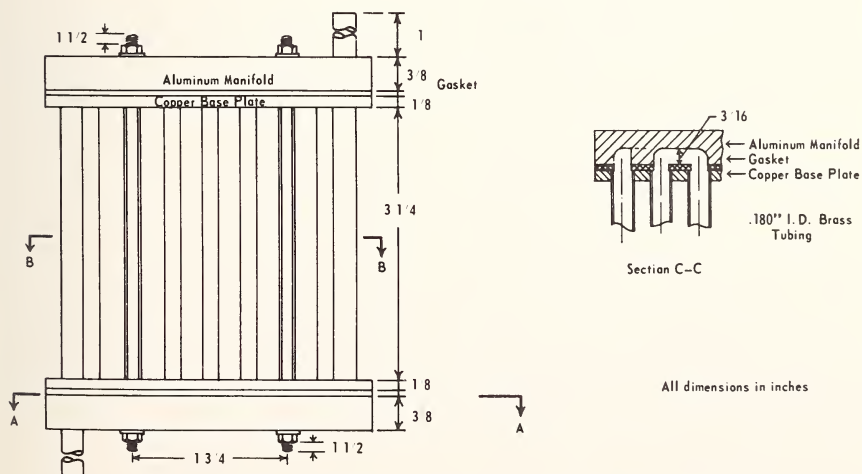
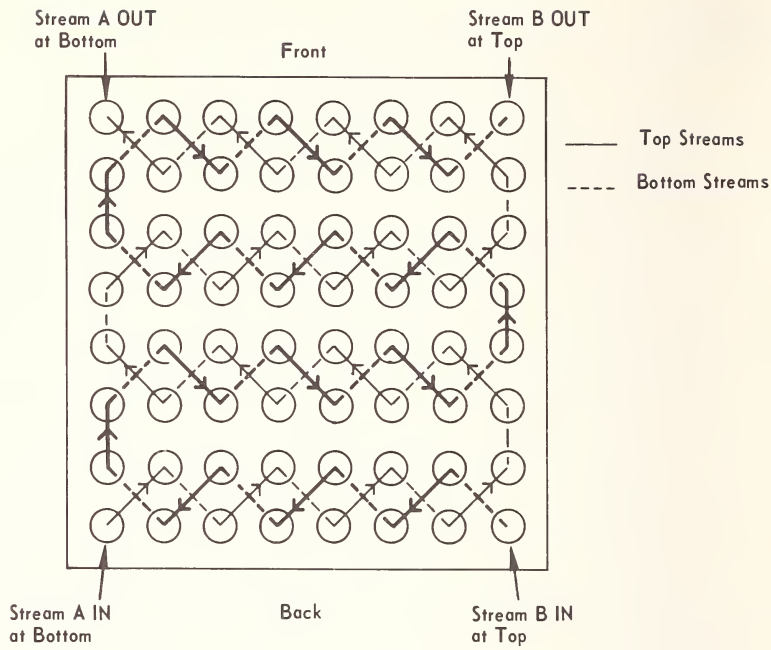Figure 1.   Twin-stream liquid irradiation assembly.
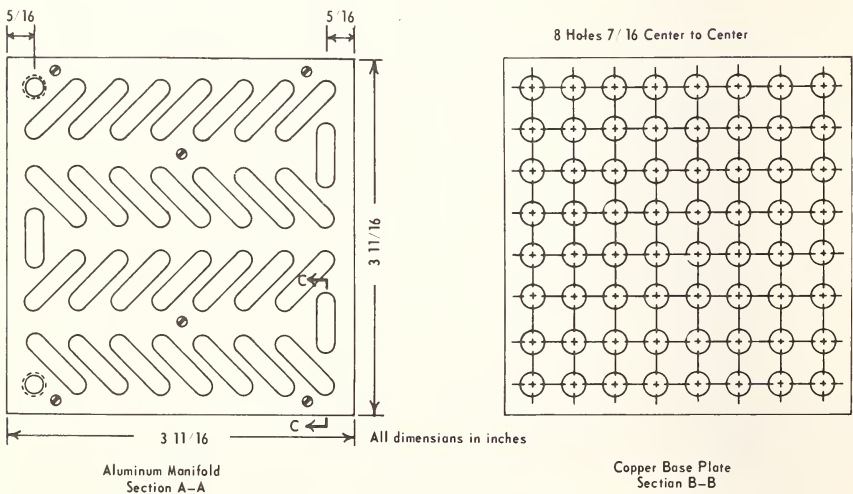
Figure 2. Flow-path, twin-stream assembly.

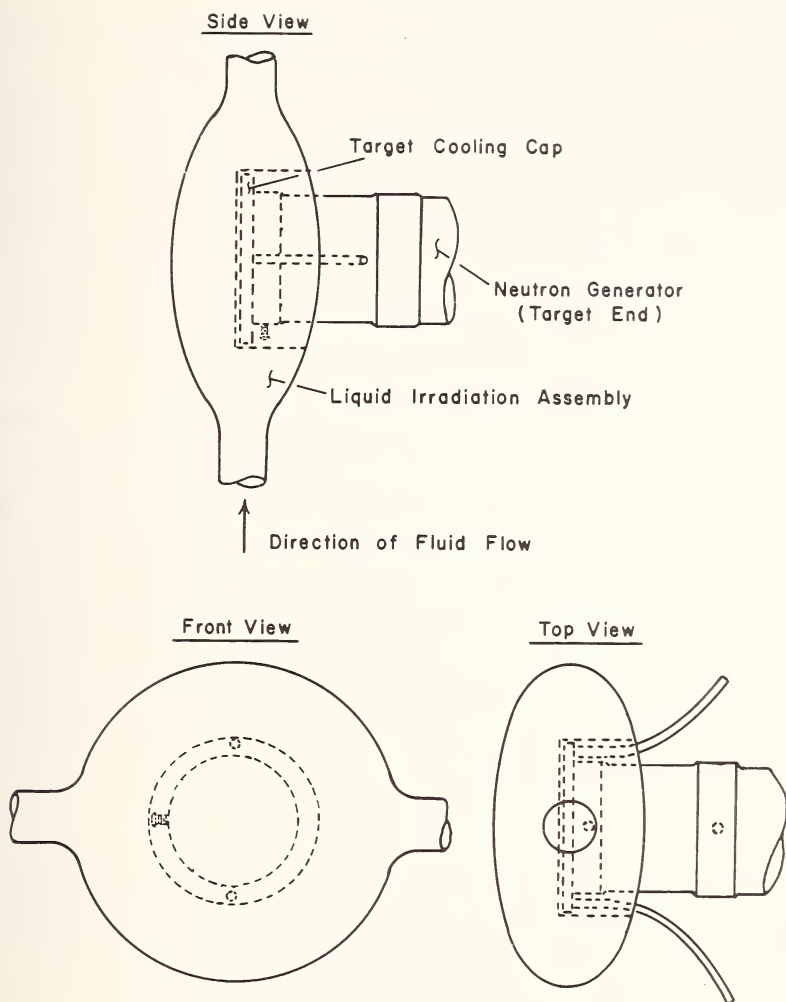Figure 3. Plan view, twin-stream assembly.

Figure 4.   Single cell irradiation assembly.

B.   PROCEDURE

A computer analysis was performed of the optimal ratios of the effective irradiation/decay/counting times which corresponded to the relative volumes of the three sections of the flow system. Any alteration in the system flow rate did not change these ratios, the residence times of a volume element in each part of the system was the only parameter affected. This optimization took into account a knowledge of the major interfering nuclides, and once the dimensions of the irradiation and therefore its volume were fixed, the liquid volumes of the transfer system

and the counting cell were adjusted to provide the optimal volume ratio of 1:8:1 used in much of this study.

Radiation measurement of the activated stream(s) was done either with a NaI gamma detector or a BF_3 neutron counter. Twin scintillation detectors in identical shields were used in the experiments with both unknown and calibration streams. A sufficient (optimal) residence time in the detector system was achieved by surrounding the detector(s) with a coil of tubing through which the liquid flowed. Additional nuclide discrimination as well as background reduction was provided by setting a single channel analyzer to include only the 0.2 and 0.32 MeV photopeaks of ^{19}O and ^{51}Ti nuclides produced through fast neutron activation of fluorine and vanadium, respectively.

Synthetic dilute solutions of from approximately 1 part per million (ppm) to greater than 100 ppm in fluoride, vanadium and uranium were placed in a 20 liter reservoir and pumped continuously through the apparatus at flow rates which varied from 100 to 400 cm³/min. The activity of the stream was either measured continuously with a count-rate meter or by integrating gamma counts over a short period of time when the most sensitive analyses were required. Corrections were made for the background in the detector with the neutron source in the "turned-on" mode. The extent of interference under optimal residence-time conditions was evaluated by flowing pure solvent and solutions of possible interfering elements such as Si, Al, Mg, Na, N, Cl and carbonaceous materials through the apparatus under the same conditions.

III. Results and Discussion

The nuclear reactions used in these analyses and the optimal flow conditions are listed in Table 1. In each case the conditions established experimentally confirmed the predictions of the computer analyses of the nuclear and flow parameters of the systems.

Table 1. Experimental evaluation of flow conditions.

Element	Nuclear reaction	Irradiation cell vol. (ml)	Flow-rate (ml/min)	Irradiation time (sec)	Decay time (sec)	Counting time (sec)	Interfering nuclide
Fluorine	$^{19}F(n, p)^{19}O$ 29 sec	72 (each twin stream)	224	20	160	20	^{16}N (7 sec)
Vanadium	$^{51}V(n, p)^{51}Ti$ 5.8 min	850	232	220	220	90	^{16}N (7 sec)
Uranium	$^{238}U(n, fission)$	850	850	60	50	120	^{17}N (4 sec) − neutron emitter
(thorium)	55 sec + 22 sec neutron emitters						

A high degree of discrimination was obtained in the measurement of the ^{19}O activity resulting from trace fluoride in water in the presence of copious ^{16}N activity (from oxygen) by allowing sufficient decay before the solution reached the detector zone (Figure 5). For the most sensitive fluoride analyses at a few ppm, correction had to be applied for the 10 minute ^{13}N component evaluated by activating pure water in the system. Fluoride analysis by flow activation was carried out over the
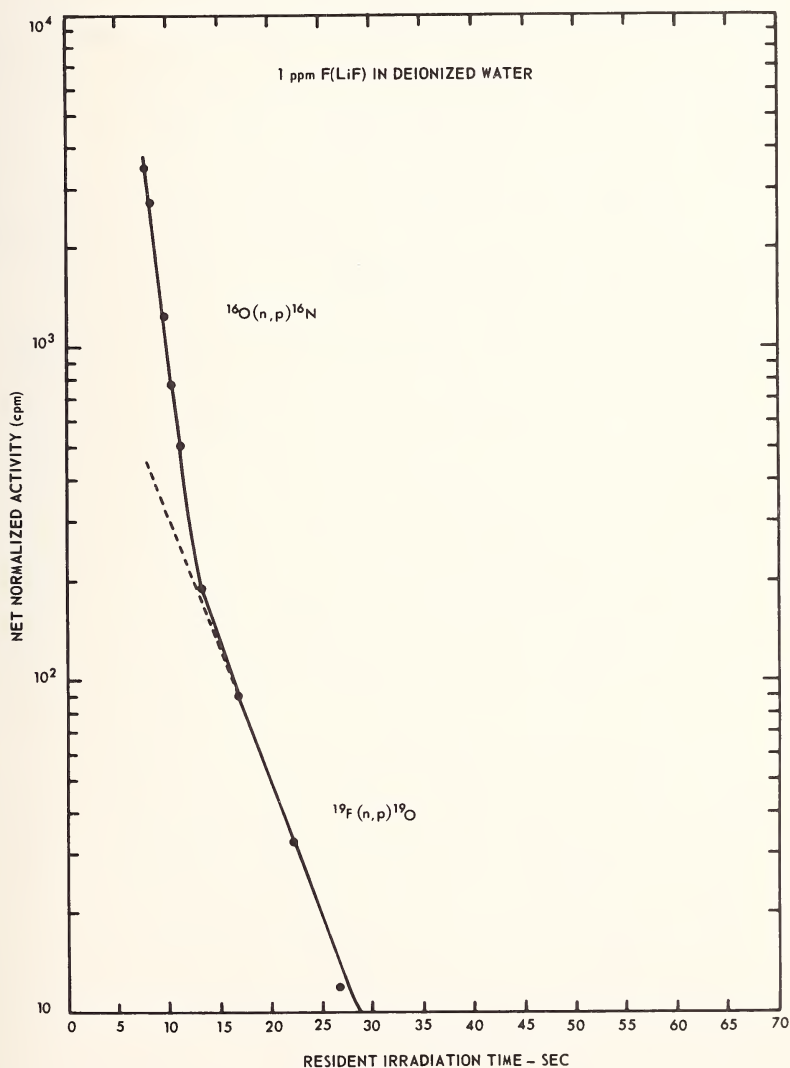
Figure 5. Fluoride activity vs. residence irradiation time. Net activity normalized to 50,000 neutron cpm and corrected for $^{16}O(p,\alpha)^{13}N$.

concentration range 0.2 to 100 ppm with a typical precision of 5 to 10% (Figure 6). It was established that negligible interference in fluoride analysis was caused by interfering elements commonly found in domestic or natural waters unless their concentration reached abnormally high values, greater than 100 and even 1000 ppm for some elements.

The sensitivity for the analysis of vanadium and uranium in dilute aqueous solutions was found to be of the order of a few parts per million when fast fluxes of 10^{10} and greater were used.

It was concluded that the twin-stream, twin-detector arrangement can be replaced by the single cell system provided a suitable neutron flux monitoring system with a response proportional to any flux variations across the irradiation cell was available. The single cell system considerably improves sensitivity of measurement, and for process control where extreme precision is not required its use is preferred. Using portable neutron sources, the flow activation technique shows good application to on-stream analyses in a number of industries involved in environmental control and water pollution.
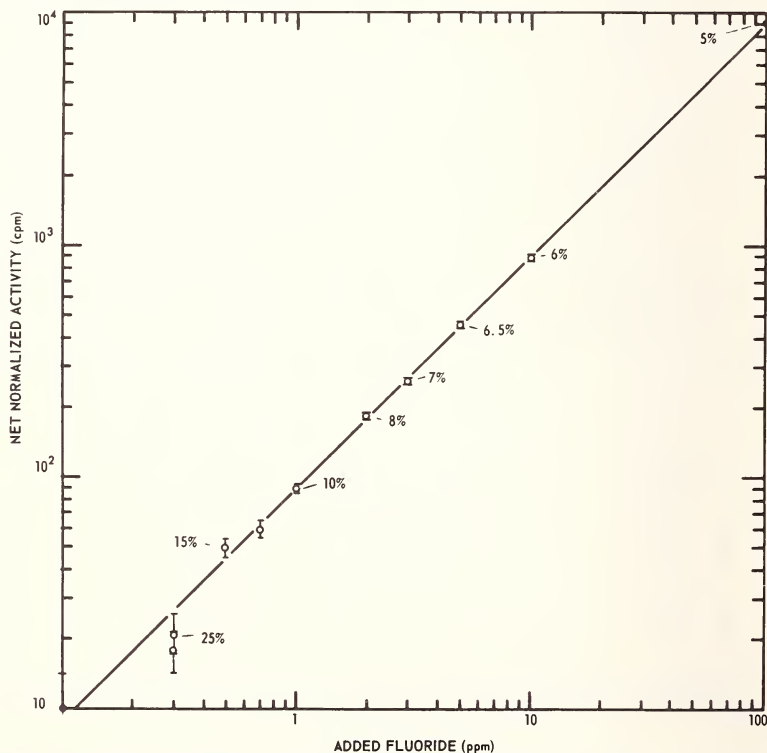
Figure 6.   Fluoride calibration curve. Comparison technique. Standard-5 ppm F as LiF. % = Reproducibility of flow experiments. All net counts are normalized to 50,000 neutron c.p.m. Flow rate: 40% of maximum.

USE OF VERY SHORT-LIVED NUCLIDES IN NONDESTRUCTIVE ACTIVATION ANALYSIS WITH A FAST SHUTTLE RABBIT

M. Wiernik and S. Amiel

Soreq Nuclear Research Centre
Yavne, Israel

I. Introduction

The apparent disadvantage of using short-lived nuclides ($T_{1/2} \sim 0.02$ to ~ 2 sec) for activation analysis, *viz,* their very rapid decay, can in many instances be reversed into an advantage when a very short irradiation and a rapid transfer from the irradiation position to the detector is possible. The rapidly decaying gamma-ray spectrum can be recorded by two consecutive measurements, in which the result of the second measurement is subtracted from the first one. The spectrum of the radioactivities present in the sample and which decay is small within the elapsed time will be nearly cancelled out, while the rapidly decaying spectrum will stand out clearly when appropriate irradiation and counting times are taken. Of prime importance in such an arrangement is the very precise timing and reproducible positioning of samples at irradiation and counting. To increase sensitivity, a system is needed by which repetitive irradiations and measurements can be made, *viz,* a shuttle rabbit, functioning at a predetermined cycle of: irradiation – transfer to counter – 1st measurement – 2nd measurement – subtraction – data storage – transfer to irradiation position.

The usefulness of very short-lived nuclides for activation analysis with reactor neutrons may be emphasized in cases where a short-lived nuclide is the only radioactive specie produced from the element in question and which can be assayed without chemical separation. Another case is the analysis of a sample which irradiation results in a multitude of radioactivities and a complex gamma-ray spectrum; a very short-lived radioisotope of the sought element may offer then a satisfactory solution, and the interference of the complex matrix of activities can be minimized to facilitate the analysis. The degree of interference by other activities present in the sample will decrease since their half lives are longer than of the one in question.

So far radionuclides with half lives shorter than a second which have been used in activation analysis, were used in conjunction with a pulsed reactor [1,2] which produces a very intense pulse of neutrons (equivalent to 1000 MW) resulting in a favored build-up of very short-lived activities.

The present work is aimed at exploring the usefulness of subsecond half life radionuclides in activation analysis using a steady-state operating reactor, a shuttle rabbit and NaI(Tl) scintillation spectrometry. The special problems of such a study are corrections due to rapidly decaying spectra, deadtime variations, and sensitivities in the presense of different possible interferences.

II. Experimental

The 0.8 sec [207m]Pb isotope was taken as a representative starting case in this study. Lead assay by radioactivation is rather difficult, since the only practical (n,γ) product for analysis is 3.3 hour [209]Pb which has a very low cross section and decays purely by beta emission. The use of [207m]Pb was briefly mentioned recently as part of a feasibility study of utilizing a pulsed reactor for activation analysis [3].

Our experimental facility consists of a pneumatic shuttle rabbit installed at a beam tube of the IRR-1 reactor [4]. The rabbit and the counting assembly are operated by a programmer. The transit time of the rabbit from the irradiation to the counting position is ~0.1 sec. Gamma-ray spectra are taken by a 3 in. × 3 in. NaI(Tl) scintillation spectrometer connected to a 400 channel analyzer. A typical experimental cycle consists of a 3 sec irradiation, 0.1 sec for transfer to counter, while counting starts 0.2 to 0.6 sec after the end of irradiation and lasts for 2.4 sec; spectrum then stored and another measurement at a subtract mode is taken for 2.4 sec, starting ~0.2 sec (or longer if required); information printed out or stored for accumulation of more data from more cycles. After a 10-20 sec delay (for "cooling") a second cycle starts. The gamma-ray spectrum of lead irradiated at such condition consists of only two peaks, both due to [207m]Pb, a major 0.57 MeV peak and a lower one of 1.06 MeV. The area under the 0.57 MeV peak is used for assay of the lead in the irradiated samples.

III. Results and Discussion

The 0.57 MeV activity of [207m]Pb obtained with different standards irradiated at a flux of ~ 5 × 10^{12}n · cm^{−2} · sec^{−1} was ~ 1400 counts per sec per mg (cps/mg) lead at the end of a 3 sec irradiation. This activity was found to be proportional to the lead content after dead time corrections were made [5]. Table 1 presents results of different lead containing samples analyzed in one-cycle runs.

Table 1. Assay of lead by counting ^{207}Pb^m.[a]

Sample	Sample weight (mg)	Lead concentration (%)	
		Present analysis	Chemical assay
solder	5.81	43.6	46.5[b]
	13.76	47.8	
	30.13	43.5	
lead glass	3.92	80.4	73.1[c]
	12.98	75.0	
	26.08	67.7	
	40.77	68.2	
Galena (PbS)	10.03	85.5	86.6[d]

[a] Each result obtained in a one–cycle run and compared to a calibrated standard.

[b] Gravimetric assay of $PbCrO_4$.

[c] Calculated lead content in $PbSO_3$.

[d] Calculated lead content in PbS.

   The precision of the procedure was checked by recycling a standard. When a sample of high lead activity was measured and the statistical error of the counts was kept below 1%, the precision (σ) of a 5-cycle run was 3 to 4%. The is mainly due to irreproducibility in the positioning at the irradiation end where the neutron flux gradient is known to be quite appreciable.

   Although recycling improves the statistics when low lead concentration is in question, it may also decrease the precision of the analysis due to background and dead time built up. Examples will be presented.

   Radionuclides produced by (n,γ) reactions with half lives of the same order as that of ^{207m}Pb and with a similar gamma-ray energy may interfere with the analysis. 0.7 sec ^{38m}Cl with a gamma ray of 0.66 MeV is of special concern. If chlorine is present, the 1.06 MeV gamma-ray of ^{207m}Pb may be used for the analysis (though resulting in a decrease of sensitivity by a factor of ~4). Fission products may pose a more difficult problem when uranium is present. The use of high resolution Ge(Li) spectrometry or resolving decay curves into individual components when counting in a multi-scaler mode may then be necessary.

   Results of experiments with low lead concentrations to check accuracy and sensitivity in presence of interferences will be presented. The use of other short-lived isotopes and isomers is also explored and preliminary results will be reported.

IV. References

[1] Lukens, H. R., Yule, H. P., and Guinn, V. P., Nucl. Inst. Meth. **33,** 273 (1965).

[2] Yule, H. P., and Guinn, V. P., in Radiochemical Mehtods of Analysis, Vol. II, 111,
      IAEA, Vienna (1965).

[3] Lukens, H. R., and MacKenzie, J. K., Trans. Am. Nucl. Soc., **10,** 85 (1967).

[4] Cuttler, J. M., Catz, A., and Amiel, S., Israel AEC Rep. IA-1128, 67 (1966).

[5] Wiernik, M., and Amiel, S., "Dead Time Corrections in Measuring Very Short Lived
      Radionuclides", Israel AEC report, in preparation.

CYCLIC ACTIVATION ANALYSIS [1]

W. W. Givens, W. R. Mills, Jr. and R. L. Caldwell

Mobil Research and Development Corporation
Field Research Laboratory
Dallas, Texas

I. Introduction

Cyclic activation analysis is the name given to a technique which utilizes very efficiently a low output, pulsed source of 14 MeV neutrons and cyclic counting of induced activities. This technique was suggested by Caldwell *et al* [1] as a part of a combination neutron experiment for remote elemental analysis of lunar and planetary surfaces. This technique differs from the technique of repeated mechanical cycling a sample between the irradiating source and the detector, a technique which is limited by sample transfer times to activities with minimum half lives of a few seconds. The main differences between cyclic activation as described here and the technique of mechanical sample transfer are that in cyclic activation (a) the sample in most applications of the method is fixed with respect to both the irradiating source and the detector (b) "cycling" is electronic rather than mechanical and hence very efficient, and (c) activities with half lives down to a few milliseconds may be utilized for analytical purposes.

A limited study of cyclic activation by Mills and Givens [2] which utilized a low output 14 MeV pulsed neutron source and cyclic counting of gamma rays from activities induced in large rock models of granite and basalt showed that analysis based upon very short-lived activities appeared feasible. In particular, the study showed that oxygen analysis based upon the $^{16}O(n,p)^{16}N$ reaction was greatly enhanced compared to the conventional method and that magnesium analysis based upon the 20 millisecond half life isomeric level of ^{24}Na is a possible alternative to the conventional method which utilizes the longer 15 hour half life activity of ^{24}Na.

This paper deals with the mathematical analysis of cyclic activation, additional experimental studies, and application of this technique to specific analysis problems.

929

II. Cyclic Activation Theory and Analysis

The basic quantity of cyclic activation analysis is the cumulative detector response to radiations from induced activities for n consecutive bombard-wait-count cycles. Consider the timing diagram shown in Figure 1 which illustrates a bombard-wait-count cycle with arbitrary bombard,
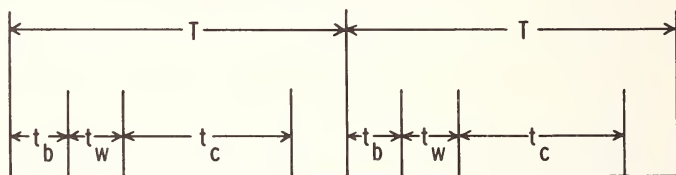
t_b - duration of neutron burst

t_w - waiting period

t_c - counting period

T - time between neutron bursts; $T \geq t_b + t_w + t_c$

Figure 1.   Timing diagram for cyclic activation analysis.

wait, and count periods of duration t_b, t_w, and t_c respectively, and which is repeated with a period $T \geq t_b + t_w + t_c$. The amount of induced activity at the end of the first neutron burst is

$$A_1 = Nf\sigma(1 - e^{-\lambda t_b}) \tag{1}$$

and the activity at the end of the first waiting period t_w is

$$A_{11} = Nf\sigma(1 - e^{-\lambda t_b})e^{-\lambda t_w}. \tag{2}$$

The detector response for the first counting period t_c is

$$D_1 = A_{11}\epsilon \int_0^{t_c} e^{-\lambda t}\mathrm{d}t = \frac{Nf\sigma\epsilon}{\lambda}(1 - e^{-\lambda t_b})(e^{-\lambda t_w})(1 - e^{-\lambda t_c}). \tag{3}$$

It is easily shown that during the nth counting period t_c that the detector response is

$$Dn = \frac{Nf\sigma\epsilon}{\lambda}(1 - e^{-\lambda t_b})(e^{-\lambda t_w})(1 - e^{-\lambda t_c})\left(\frac{1 - e^{-n\lambda T}}{1 - e^{-\lambda T}}\right). \tag{4}$$

The cumulative detector response for n successive bombardment, wait, and counting periods is easily shown to be

$$D_T = \sum_{n'=1}^{n} Dn'$$

$$= \frac{Nf\sigma\epsilon}{\lambda} (1 - e^{-\lambda t_b})(e^{-\lambda t_w})(1 - e^{-\lambda t_c}) \left[\frac{n}{(1 - e^{-\lambda T})} - \frac{e^{-\lambda T}(1 - e^{-n\lambda T})}{(1 - e^{-\lambda T})^2} \right] \quad (5)$$

where D_n, is given by Equation (4) and

N = the number of nuclei in a sample which can undergo a given reaction

f = the neutron flux ($\text{n·cm}^{-2}\text{·sec}^{-1}$),

σ = the reaction cross section,

λ = the decay constant of the radioactivity produced,

ϵ = the efficiency of the radiation detector including geometry factors,

t_b = the bombardment burst duration,

t_w = an arbitrary waiting period,

t_c = an arbitrary counting period,

T = the period of repetition ($T \geq t_b + t_w + t_c$), and

n = the total number of successive bombard-wait-count cycles.

Equation (5) gives the basic relationship for cyclic activation analysis. The detector response may be maximized by a proper selection of the parameters in Equation (5). For example, the detector response is maximum for a given λ and T when $t_w = 0$ and $t_b = t_c = T/2$. For a given λ there is also an optimum period T. Figure 2 shows the detector response for two radioactivities with different half lives as a function of the period T with $t_w = 0$, $t_b = t_c = T/2$ and the total time $t_t = nT =$ six half lives. The maximum response occurs at a period $T = 2.4$ half lives for each radioactivity. The maximum can also be found analytically; however, the plots show two additional and very significant features: (1) a rapidly decreasing response for $T > 2.4$ half lives, and (2) a maximum decrease of only about 12 percent for $T \ll 2.4$ half lives.

Cyclic activation analysis is best suited to utilize activities with half lives too short for the conventional method However, activities with half lives of several minutes are also useful. Figure 3 shows the theoretical detector response *versus* total experiment time for cyclic and conventional activation analysis for Si based on the 2.3 minute half life [28]Al activity. Beyond about 800 seconds total time, the detector response from cyclic activation increases almost linearly with time, whereas the response from conventional activation reaches some maximum but smaller value.

$$D = \left(1 - e^{-\frac{\lambda T}{2}}\right)^2 \left(\frac{1}{1 - e^{-\lambda T}}\right) \left[n - e^{-\lambda T} \frac{\left(1 - e^{-6\lambda T_{\frac{1}{2}}}\right)}{\left(1 - e^{-\lambda T}\right)} \right]$$

$$n = \frac{6 T_{\frac{1}{2}}}{T}$$
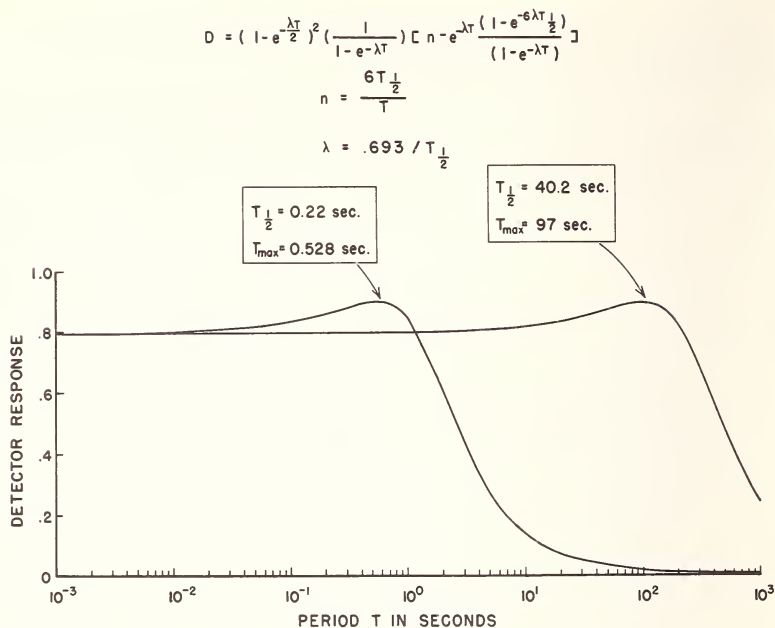
$$\lambda = .693 / T_{\frac{1}{2}}$$

Figure 2.   Detector response for cyclic activation analysis in arbitrary units versus cycle period.

In general, activation analysis is made for several elements in a sample and several radioactive species with different half lives will be produced. The detector response for cyclic and conventional analysis of a hypothetical sample yielding, for illustrative purposes, activities with half lives from 2.5 seconds to 9.73 minutes is shown in Table 1. The total

Table 1.   Hypothetical sample: copper, silicon, sodium, oxygen, and and indium.

Reaction	$T_{1/2}$	λ	Figures of merit Conventional	Cyclic
^{63}Cu(n, 2n)^{62}Cu	9.73 min	0.00119	0.7789	0.8253
^{28}Si(n, p)^{28}Al	2.3 min	0.0050	0.9998	4.254
^{23}Na(n, p)^{23}Ne	40.2 sec	0.0172	1.000	15.24
^{16}O(n, p)^{16}N	7.14 sec	0.0943	1.000	84.1
^{114}In(n, n'γ)^{114}In	2.6 sec	0.28	1.000	238

Note: Total experiment time, 3600 sec; conventional — irradiate 1800 sec; cyclic — period 6 sec; irradiate 3 sec; count, 3 sec; cycles, 600.
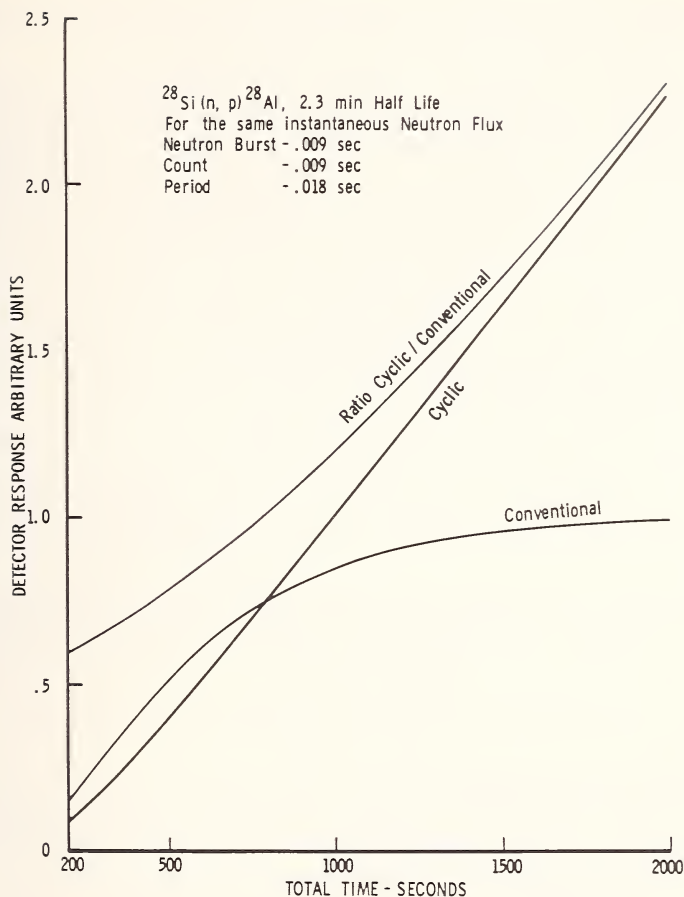
Figure 3. Theoretical comparison of conventional and cyclic activation analysis for silicon; cyclic conditions as shown; conventional conditions — irradiation count one-half total experiment time.

experiment time for a mixture of activities is dictated by the longest half life activity and the period, T, in cyclic activation by the shortest half life activity. The detector response for cyclic activation analysis is slightly greater for even the longest-lived activity and is greatly enhanced for the shorter-lived activities.

III. Cyclic Activation Experiments

Cyclic activation experiments have been performed to: 1. verify the theoretical detector response given by Equation (5). 2. investigate the ^{24}Na 20 millisecond isomeric activity as a possible basis for Mg analysis.

and 3. determine what elements commonly found in earth rocks might be subject to analysis by the cyclic activation method.

The validity of Equation (5) has been verified experimentally by measuring the ratio of the cyclic activation detector response to the conventional activation detector response. This quantity is calculated from Equations (3) and (5) with times appropriate to the conventional activation experiment substituted in Equation (3). Experimental ratios were determined from gamma-ray pulse-height spectra obtained by cyclic and conventional activation of a pure SiO_2 sandstone. The same sandstone sample, total experiment time, total neutrons, and geometry were used to obtain the cyclic and conventional activation gamma-ray spectra shown in Figure 4. For these experimental conditions the ratio of the counts in the cyclic activation spectrum from 4.5 to 6.3 MeV and under the 1.78 MeV peak to the corresponding counts in the conventional spectrum gave values for comparison to the theoretical ratios for both the $^{28}Si(n,p)^{28}Al$ and $^{16}O(n,p)^{16}N$ activities. The measured ratios are in good agreement with those predicted by the formulated cyclic activation theory.

Gamma-ray spectra from cyclic activation of metallic Mg and Al are shown in Figure 5. The spectra show the 473 keV gamma ray from the
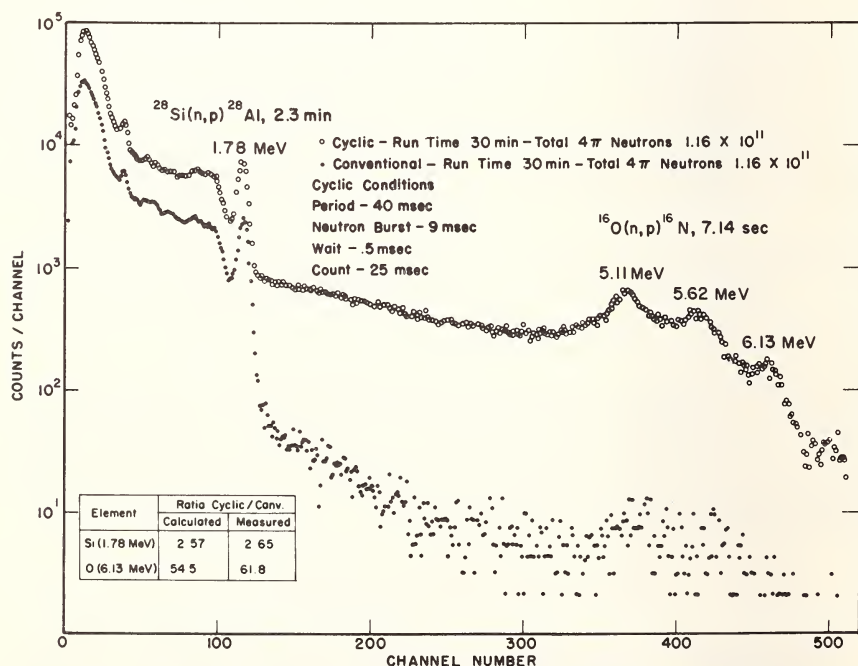
Figure 4.   Comparison of cyclic and conventional activation of Si and O in a pure sandstone (SiO_2).
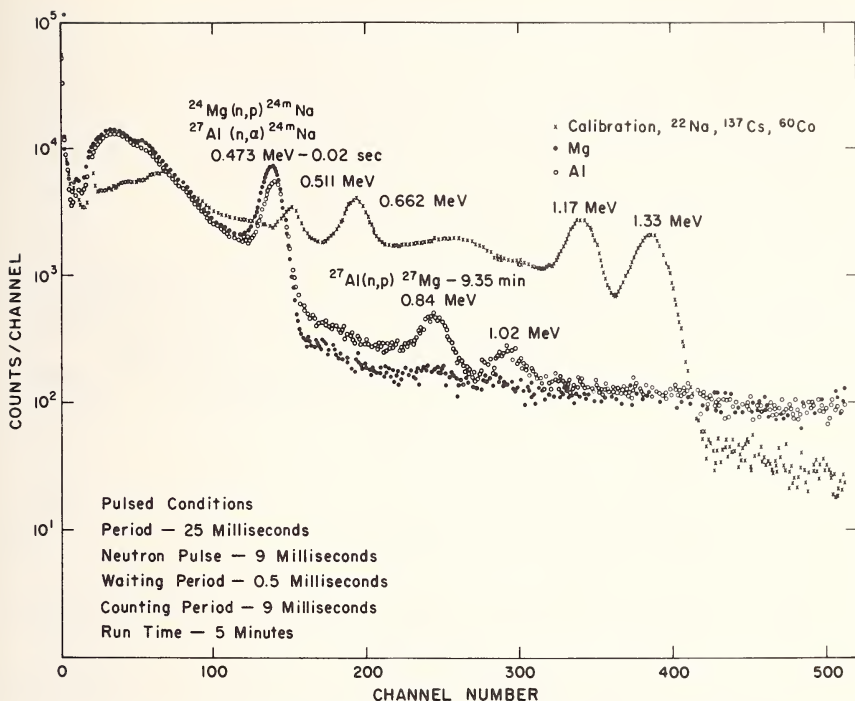
Figure 5.   Cyclic activation gamma-ray spectra from Al and Mg.

^{24}Mg(n,p)^{24m}Na and ^{27}Al(n,α)^{24m}Na reactions and the 1.01 and 0.84 MeV gamma rays from the ^{27}Al(n,p)^{27}Mg reaction. Mg analysis on the basis of the 473 keV gamma ray from isomeric ^{24}Na necessitates a correction for any Al contribution. An independent determination of Al based upon the 1.01 and 0.84 MeV gamma rays from the ^{27}Al(n,p)^{27}Mg reaction could be the basis for such a correction.

Gamma-ray spectra produced by cyclic activation and 14 MeV neutrons from granite and basalt are shown in Figures 6 and 7. The spectra in these figures show prominent gamma rays from the ^{28}Si(n,p)^{28}Al and ^{16}O(n,p)^{16}N reactions and the ^{24}Mg (n,p)^{24m}Na and ^{27}Al(n,α)^{24m}Na reactions producing isomeric ^{24}Na. The relative intensities of the gamma rays shown in Figure 7 are in good qualitative agreement with the known Si, Al, and Mg content of the basalt and granite. These spectra suggest that cyclic activation is applicable to elemental analysis of rock samples.

IV.   Summary and Conclusions

Cyclic activation analysis is ideally suited to utilize very short-lived activities for analytical purposes. Process control of ores and *in situ*
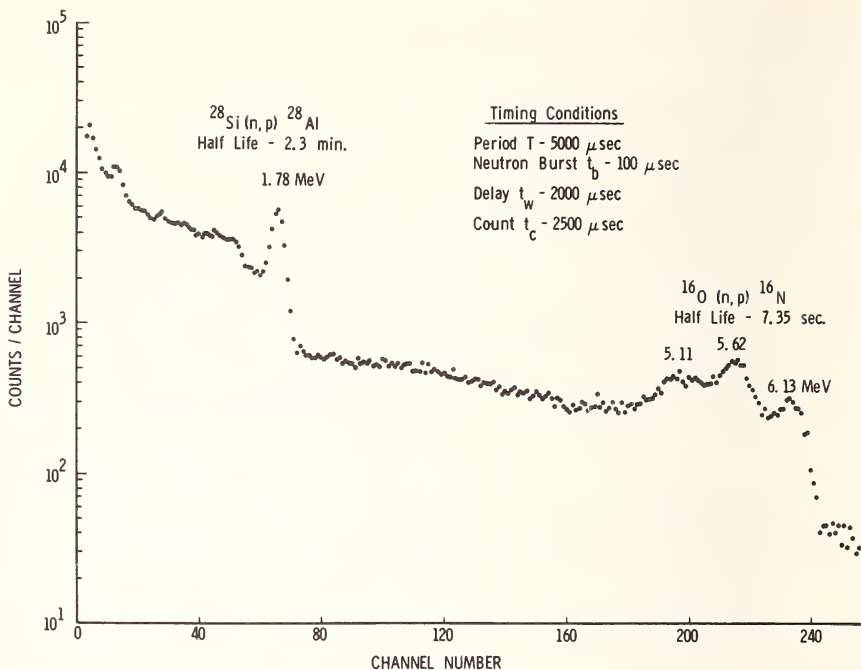
Figure 6. Cyclic activation gamma-ray spectrum from granite, neutrons per burst $= 3.4 \times 10^4$, total 4π neutrons $= 1.2 \times 10^{10}$.
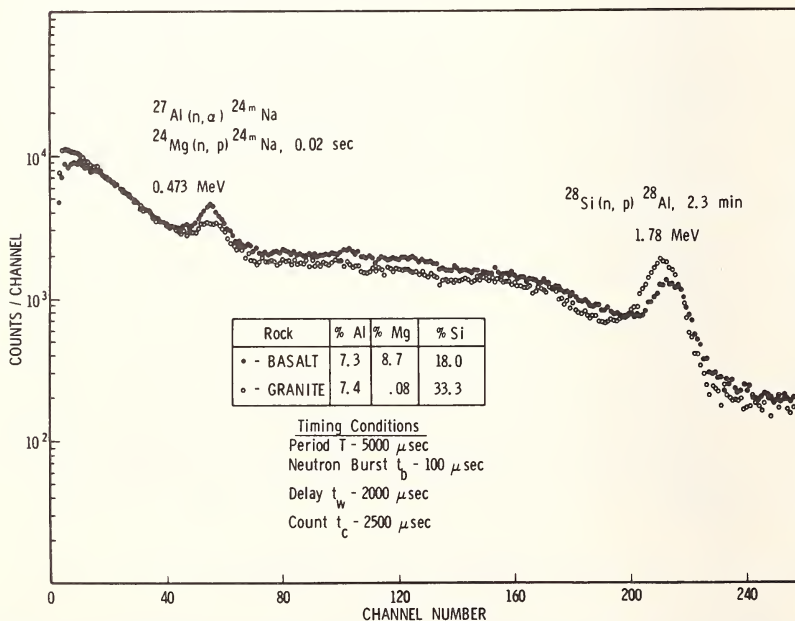
Figure 7. Cyclic activation gamma-ray spectra from granite and basalt, neutrons per burst $= 3.4 \times 10^4$, total 4π neutrons $= 1.2 \times 10^{10}$ per spectrum.

analysis of geological structures are likely areas where a low-output pulsed-neutron source and cyclic activation can be utilized to good advantage. Additional experiments need to be performed to determine the utility of cyclic activation to the analysis of small samples and in making quantitative measurements on an absolute basis.

V. References

[1] Caldwell, R. L., Mills, W. R., Jr., Allen, L. S., Bell, P. R., and Heath, R. L., Science **152,** 457 (1966).
[2] Mills, W. R., Jr. and Givens, W. W., "Neutron Die-Away Experiment For Lunar And Planetary Surface Analysis", July 26, 1966 to March 26, 1967, Phase 1 Final Report For NASA, Mobil Oil Corporation.

AN ANALOG COMPUTER CONTROLLED GAMMA-RAY SPECTROMETER FOR COMPARATIVE ACTIVATION ANALYSIS

P. C. Jurs and T. L. Isenhour

Department of Chemistry
University of Washington
Seattle, Washington 98105

I. Introduction

Because of its excellent sensitivity for many elements activation analysis has become widely used in trace analysis. A recent book by W. S. Lyon [1] lists 444 references to applications of activation analysis in metallurgical, geological, biochemical and medical research. Sensitivity values for 69 interference free elements range from 50 μg to 10^{-6} μg [2]. In practice, however, the analyst is rarely confronted with samples in which only one element becomes radioactive. Hence, the limit of sensitivity is frequently based on the ability to resolve the gamma radiation of a desired radioisotope from a mixture. The accuracy of the analysis is thereby directly related to the ability to resolve the component of interest.

Presently, the maximum accuracy is obtained by the comparative method in which a standard and an unknown are simultaneously irradiated. The two gamma-ray spectra are measured and compared to determine the concentration of the desired component in the mixture. Various computer programs have been written to "unscramble" mixed gamma-ray spectra [3]. In the more sophisticated schemes several spectra are taken over a time interval and combined to approximate decay curves. These must then be compared to standard spectra with various calibration and correction procedures. In the ultimate extreme of being able to record instantaneously each individual gamma ray and its time of occurrence, this method would produce the maximum theoretical accuracy. However, the instrumental time limitations of recording and reading out data do not presently permit this approach. Hence, the accuracy is restricted by the fact that spectra must be recorded in time blocks, a limitation which becomes increasingly severe with shorter half life.

II. Experimental

This paper describes an apparatus designed to perform real time comparative activation analysis. The instrument directly compares the gamma-ray spectrum from a standard and a mixed unknown to determine the weight of the desired species in the unknown sample. The instrument operates by subtracting a certain fraction of the sample activity from the unknown. If the correct fraction is subtracted, the spectrum of the mixture appears to contain no component from the sought species. In order to accomplish this, gamma rays are measured in two energy ranges, the first characteristic of the sought species, and the second characteristic of the interferences. If the correct fraction of the standard source is being subtracted from the mixture, the same effective half life is measured in each energy range of the unknown spectrum.

Figure 1 gives hypothetical gamma-ray spectra of a mixed unknown and a standard. These would be produced by simultaneous irradiation, thereby avoiding differences in flux, irradiation time, *etc.*, as in the accepted comparative technique. D_1 and D_2 are the energy ranges measured, and a fraction of the standard spectrum is subtracted from the mixed spectrum. The net count rates are compared and differentiated giving a value proportional to the difference in their apparent half lives. A zero value indicates that the correct fraction is being subtracted. Feed back drives the instrument to the correct setting. This null point method of directly comparing an unknown to a standard produces the highest accuracy in many analytical instruments.

A block diagram of the apparatus is given in Figure 2. Detectors 1 and 2 are matched in gain and resolution. Small variations are eliminated by adjusting the high voltages and the gains in the mixer amplifier. Only a fraction of the pulses from detector 2 are passed by the linear gate which is driven by the variable frequency oscillator. The signals are mixed in the mixer amplifier and further amplified in the main amplifier to guarantee identical amplification. The output of the main amplifier is sent to two
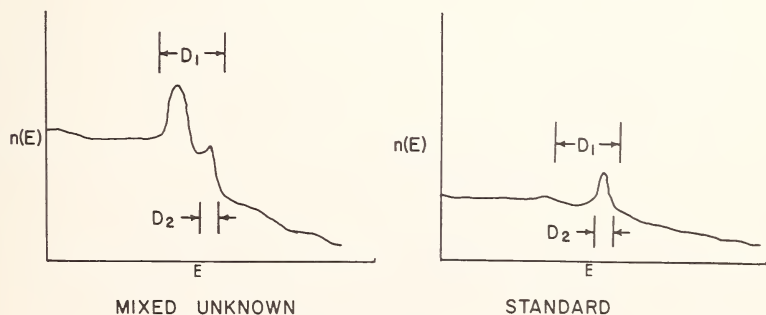

Figure 1.   Standard and unknown spectra.

separate single channel analyzers which select ranges D_1 and D_2. Coincidence units gated from detector 2 and operating in conjunction with differential rate meters, produce analog voltages representing the difference in count rate of the two detectors in each energy range. The next stage gives the derivative of a logarithmic ratio of these signals, thereby giving the difference of the effective half lives of the two energy ranges being observed. The sign and magnitude of the derivative indicate the adjustment necessary in the linear gate to give the correct value. Hence the output of the differentiator is used to drive a variable frequency oscillator to control the linear gate. A zero output from the differentiator indicates a correct setting of the linear gate and thereby, the weight ratio of the sample to the unknown.

The overall result of this rather elaborate method of comparing two spectra is that the decay information is used throughout the radioactive
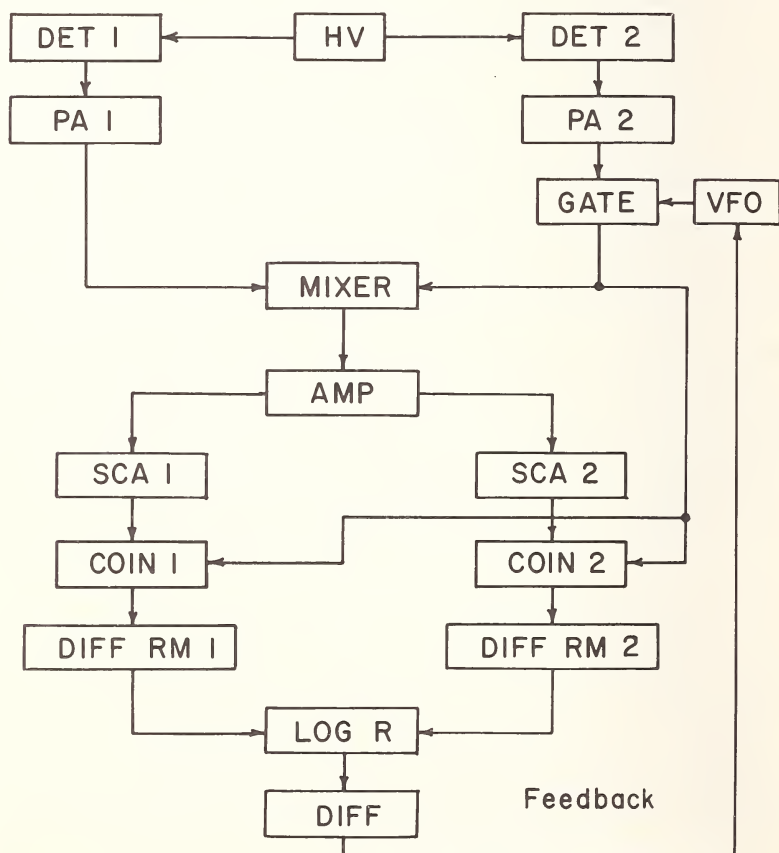
Figure 2.   Block diagram of spectrometer.

life of the sample. By conventional methods using only digital electronics, read out time causes more and more information to be lost as the half life becomes shorter.

III. Results and Discussion

Effective operation of the instrument involves optimizing several parameters, particularly the window settings of the single channel analyzers, the time constants of the differential rate meters and the frequency response of the derivative unit. The instrument has been tested with several analyses based on relatively short half life nuclides resulting from fast neutron reactions. Optimization has been approached by both mathematical analysis and experimental trial. The most effective instrumental conditions along with illustrative analyses will be discussed.

IV. References

[1]   Lyon, W. S., "Guide to Activation Analysis," Van Nostrand, Princeton, New Jersey, 1964.
[2]   Guinn, V. P., Lukens, H. R., Jr. "Trace Analysis: Physical Methods," Morrison, G. H., Ed., John Wiley, New York, 1965.
[3]   O'Kelley, G. D., Ed., "Application of Computers to Nuclear and Radiochemistry," U.S. Atomic Energy Commission, Monograph NAS-NS 3107, 1963.

DETERMINATION OF TRACE QUANTITIES
OF URANIUM IN BIOLOGICAL MATERIALS
BY THE NUCLEAR TRACK TECHNIQUE

B. Stephen Carpenter

National Bureau of Standards
Analytical Chemistry Division
Washington, D.C. 20234

I.   Introduction

Fission occurs in the isotopes of natural uranium when it is exposed to radiations of the proper type and energy [1,2]. Among such radiations are thermal neutrons and bremsstrahlung photons. If an insulating material is placed in intimate contact with the uranium, the recoiling fission fragments which enter the absorber will leave atomically and electronically disturbed regions along their paths. This type of radiation damage occurs because the ionization density produced along the fission-fragment track is greater than the critical ionization density for the absorber. The fission tracks can be made optically visible by etching in a suitable solution. The tracking technique has been described in a series of papers by Fleischer, Price, Walker and other authors using several absorbing materials as detectors [3-7]. These authors have used the technique in a variety of studies for the purpose of dating of geological samples and for detecting trace quantities of uranium in minerals, micas, and glass [8-10].

In the above-mentioned work, this technique was successfully employed in determining trace quantities of uranium in geological and metallurgical samples, [11,12]. At the National Bureau of Standards it was thought that the method could be applied to determine the uranium content of biological standard reference materials. In the above cited work, uranium was either determined or detected only on the surface of the materials without destroying the material. However, with biological materials the surface analysis is not feasible because of the porous nature of the organic matrix and the odd shape and size of the sample. Accordingly, biological materials must be prepared in solution form for analysis, thus providing a more uniform geometry for irradiation with the further advantage of reducing the bulk sample by several orders of magnitude.

In principle, any insulating material could be used to record fission fragment tracks, but because interfering nuclear reactions are possible,

e.g. $^{10}B(n, \alpha)^7Li$ selectivity of the recording medium is essential. For this application, the material selected must be insensitive to alpha particles, high energy protons and recoil neutrons and record only fission fragment tracks. In a series of experiments, Fleischer, Price and Walker [8,9] found that Lexan (a polycarbonate, $C_{16}H_{18}O_3$) has the relatively high critical ionization density required to act selectively in the desired manner.

II.   Experimental

There are plans at NBS to certify three biological Standard Reference Materials for trace elements: blood, tissue and a botanical leaf sample. Of these materials, blood, plasma, and dried leaves, were used in this study. Each sample was freeze-dried to remove most of the water, then ashed at a low temperature in an oxygen atmosphere using a low temperature dry asher. Finally, the residue was digested in nitric acid, filtered, and diluted to a known volume. Carefully controlled drops of sample solution, delivered from a micropipette, were placed on Lexan slides, 20 mm wide × 40 mm long × 0.25 mm thick. The solutions were evaporated to dryness on a laminar flow clean bench. Standard samples containing known amounts of uranium were mounted on Lexan detectors in an identical manner, in order to establish for specific irradiation conditions the relationship between the number of tracks observed and the weight of uranium present.

In order to prevent external contamination, the slides were packaged in polyethylene envelopes. After samples and standards were wrapped in plastic, they were exposed to a thermal neutron flux at the Naval Research Laboratory's swimming pool-type reactor for five minutes in an approximate flux of 3.5×10^{11} $n \cdot cm^{-2} \cdot sec^{-1}$. After irradiation the Lexan slides were etched in 6.5 N NaOH at $40° \pm 2$ °C for 45 minutes [8]. Following the etching step the fission tracks produced from the ^{235}U were counted with an optical microscope. The tracks observed in the case of the actual samples were compared with the number of tracks produced by the standards that are irradiated under the same conditions in order to determine the amount of uranium present.

NBS certified 950-A Uranium Oxide, U_3O_8, was used as a stock standard. The U_3O_8 was digested in nitric acid to convert the oxide to $UO_2(NO_3)_2$. Then the solution was diluted to a specified volume with distilled water. Various known volumes of the prepared stock solution were spotted on Lexan slides in order to determine the relation of the number of tracks to the amount of uranium irradiated. The relation was found to be linear. Standard, samples and reagent blanks were irradiated simultaneously, then etched and counted. The purpose of the reagent blanks was to determine the contribution of uranium in the reagents which

were used in the sample solutions. The preparation of these slides was identical to that of the standards and the samples. From the reagent blank it was possible to determine the contamination level that the reagents and Lexan slides contribute for each irradiation. The blank slides were found to contain an average of eight fission tracks, corresponding to 1.0×10^{-11} grams of uranium.

Trace amounts of uranium also can be determined by counting the fission tracks induced by photons. In this case, the fission fragments are produced from the ^{238}U atoms. The samples and standards can be prepared in an analogous manner to that utilized for thermal neutron irradiation.   In a preliminary study standards were irradiated for five minutes in the NBS Linear Accelerator (LINAC). The photons used to induce fission were produced from an accelerated electron beam with a maximum energy of 35 MeV that bombarded a tungsten converter. The LINAC was operated at an integrated beam current of 20 microamperes. The fission tracks produced by the fragments from ^{238}U were developed and counted. The average weight of uranium per fission track was found to be 7.7×10^{-11} grams.

III.   Results

The analyses of uranium in blood gave an average value of 86.1 parts per billion (ppb), with a standard deviation of 5.6 ppb (based on 21 determinations). The standard deviation is considered to be satisfactory in view of the very small quantity of uranium in the samples. The average value obtained is in poor agreement with Newman's [14] values of 14 ppb, and in serious disagreement with Hoffman's [15] value of 0.1 ppb. Newman and Hoffman utilized the method of fluorescence spectrometry, and their results are based on only one or two determinations.

The average value of the uranium content of mammalian plasma was found to be 60.5 ± 12.0 ppb. The results exhibit considerably more scatter than the determinations for blood, and the reason for this is not known. The precision of 20%, however, is considered acceptable in the concentration range of the measurements.

IV.   References

[1]   Fleischer, R. L., Price, P. B., Walker, R. M., Science 149, 383 (1965).
[2]   Price, P. B., and Walker, R. M., J. Appl. Phys. 33, 3407 (1962).
[3]   Fleischer, R. L., and Price, P. B., Geochimica et Cosmochimica Acta 28, 1704 (1964).
[4]   Fleischer, R. L., and Price, P. B., J. Appl. Phys. 34, 2903 (1963).
[5]   Fleischer, R. L., and Price, P. B., Science 140, 1221 (1963).
[6]   Walker, R. M., Price, P. B., and Fleischer, R. L., Appl. Phys. Letters 3, 28 (1963).
[7]   Debeauvais, M., Maurette, M., Mory, J., and Walker, R. M., Int. J. Appl. Radiation and Isotopes 15, 289 (1964).

[8]   Fleischer, R. L., Price, P. B., Walker, R. M., and Hubbard, E. L., Phys. Rev. 133, A1443 (1964).

[9]   Fleischer, R. L., Price, P. B., and Walker, R.M., New Scientist 378, 406 (1964).

[10]   Silk, E. C. H., and Barnes, R. S., Phil. Mag. 4, 970 (1959).

[11]   Fleischer, R. L., Price, P. B., and Walker, R. M., Nuclear Science and Engineering 22, 153 (1965).

[12]   Price, P. B., and Walker, R. M., Appl. Phys. Letters 2, 23 (1963).

[13]   Bowen, H. J. M., United Kingdom Atomic Energy Authority Research Group Report, AERE-24196 (1963).

[14]   Hoffman, J., Biochem. Z. 313, 377 (1943).

[15]   Newman, W. F., Nat. Nucl. Energy Ser. VI. I, II, 701 (1949).

SURFACE ANALYSIS OF MEDIUM WEIGHT ELEMENTS BY PROMPT CHARGED PARTICLE SPECTROMETRY

Colenso Olivier [1] and Max Peisach

Southern Universities Nuclear Institute
P.O. Box 17, Faure, C.P.
South Africa

I. Introduction

The limited penetration of charged particles with energies of a few MeV makes them suitable for the analysis of surface layers. Use has already been made of this property for the determination of surface concentrations of elements by the spectroscopy of elastically scattered charged particles [1-5]. Such methods have the advantage that small bombarding currents and short irradiations are sufficient for the analysis because charged particle scattering cross sections are usually large compared with reaction cross sections. However, the application is limited to the cases where the targets are light elements or the elements have widely differing mass numbers because the differential change of the energy of the scattered particle with the mass of the scatterer decreases with increasing target mass number [6]. In particular the method is of little use for the analysis of thick targets of the medium weight elements where both the surface element and the thick support have mass numbers between 50 and 70.

When charged particles induce nuclear reactions in surface layers the prompt charged particle products can best serve for an analytical method to determine surface concentrations because the energy of the product particle at the detector is determined not only by the energy of the bombarding particle and the nuclear reaction concerned, but also by the amount of energy lost by the bombarding particle in the target material before the nuclear reaction occurs and by the energy lost by the product particle between the points of its formation and detection. If prompt neutrons are measured, only energy lost in the first part of the path is likely to play a role in depth resolution. In this investigation the method using prompt protons from (d,p) reactions was evaluated for the determination of nickel films on copper and chromium films on nickel.

---

[1] Present address: Department of Chemistry, University of Stellenbosch, Stellenbosch, C.P., South Africa. This work forms part of the doctoral thesis to be submitted to the University of Stellenbosch by C. O. and is published with permission.

II. Experimental

A. Preparation of Standards

Standard thicknesses of nickel on copper and tantalum, of copper on tantalum and of chromium on nickel and tantalum were prepared by electroplating and weighing. Surface film thicknesses ranging from 10 to 5000 μg/cm^2 were used. These targets were irradiated in a 75-cm scattering chamber with a current of 0.5 to 1 μA of deuterons of 3.5 MeV obtained from the Van de Graaff accelerator of the Southern Universities Nuclear Institute.

B. Measurement

The energy of the protons formed by (d,p) reactions on the target and emitted at an angle, θ, to the bombarding beam were measured with a silicon semiconductor detector with a depletion layer of 700 μm and a resolution of less than 45 keV. This detector could measure protons up to 7 MeV. Since all the (d,p) reactions concerned were highly exoergic, in most cases the protons were produced with energies in excess of the range over which the available detector could be used. It was thus necessary to reduce the energy of the protons by covering the detector surface with a gold absorber of a suitable thickness. This absorber also served to eliminate relatively large fluxes of scattered deuterons. The appropriate thickness of absorber required for a detector was calculated from the known stopping power for protons [7]. A typical pair of curves showing the effect of gold thickness on the range of proton energies that could be measured with a detector capable of measuring up to 6 MeV protons, is shown as an example in Figure 1.

III. Results and Discussion

A. Energy Spectra of Prompt Protons

Typical spectra obtained from thin films of Cr, Ni and Cu on tantalum backings and of the protons from the backing itself are shown in Figure 2. The proton groups, p$_i$, refer to the ith excited state in which the product nuclide was formed, and the nuclide labelled in the figure refers to the target nuclide.

A common feature of the spectra in Figure 2 is the large extent to which the energy of each proton group had been broadened by the use of the absorber. However, the resolution was still sufficient to distinguish each target element.
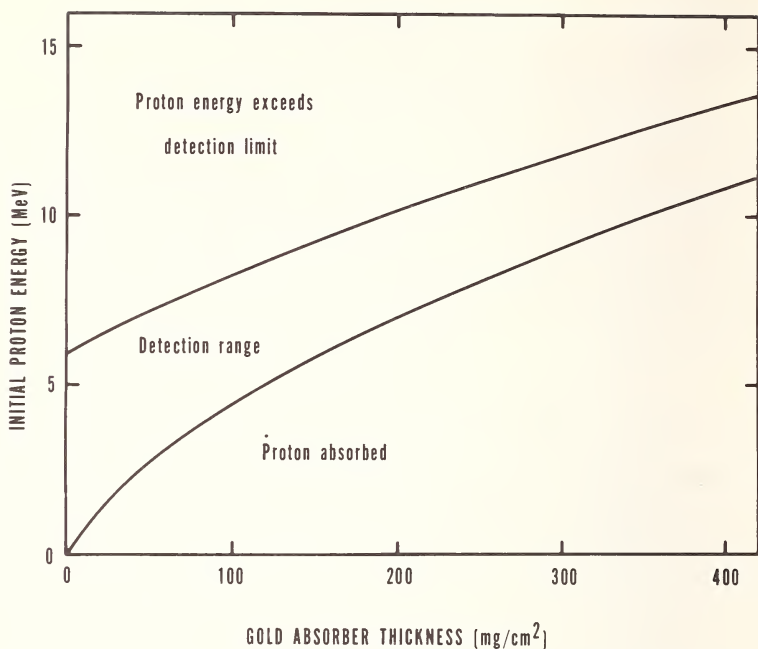
Figure 1.   The effect of absorber thickness on the proton energy range that could be measured with a silicon semiconductor detector capable of measuring up to 6 MeV protons.

Tantalum backings were used because the Coulomb barrier for such a heavy element ($Z = 73$) was large. The cross section of the (d,p) reaction at 3.5 MeV was expected to be so small that prompt protons from it would be undetectable. This was not quite the case (see Figure 2).

The high energy peak from protons of the reaction $^{53}Cr(d,p_o)$ was observed, but was not included in Figure 2 for the sake of uniformity. The high abundance of chromium-52 and the comparatively large cross section of the reaction $^{52}Cr(d,p_o)$ gave rise to a prominent peak characteristic of this element and suitable for use for analytical purposes.

The energy spectrum obtained from nickel shows peaks which could be ascribed to protons from the two most abundant isotopes of reactions leading to the ground states and the first few excited levels. The peak marked Z is from reactions leading to higher levels which were not resolved.

No characteristic peak was found in the prompt proton spectrum of copper. The two unresolved peaks are due to protons from reactions leading to a large number of relatively closely spaced excitation states. The energy corresponding to the point X, refers to the maximum proton energy obtainable from ^{63}Cu under the conditions of the experiment, and Y to the corresponding energy for ^{65}Cu.
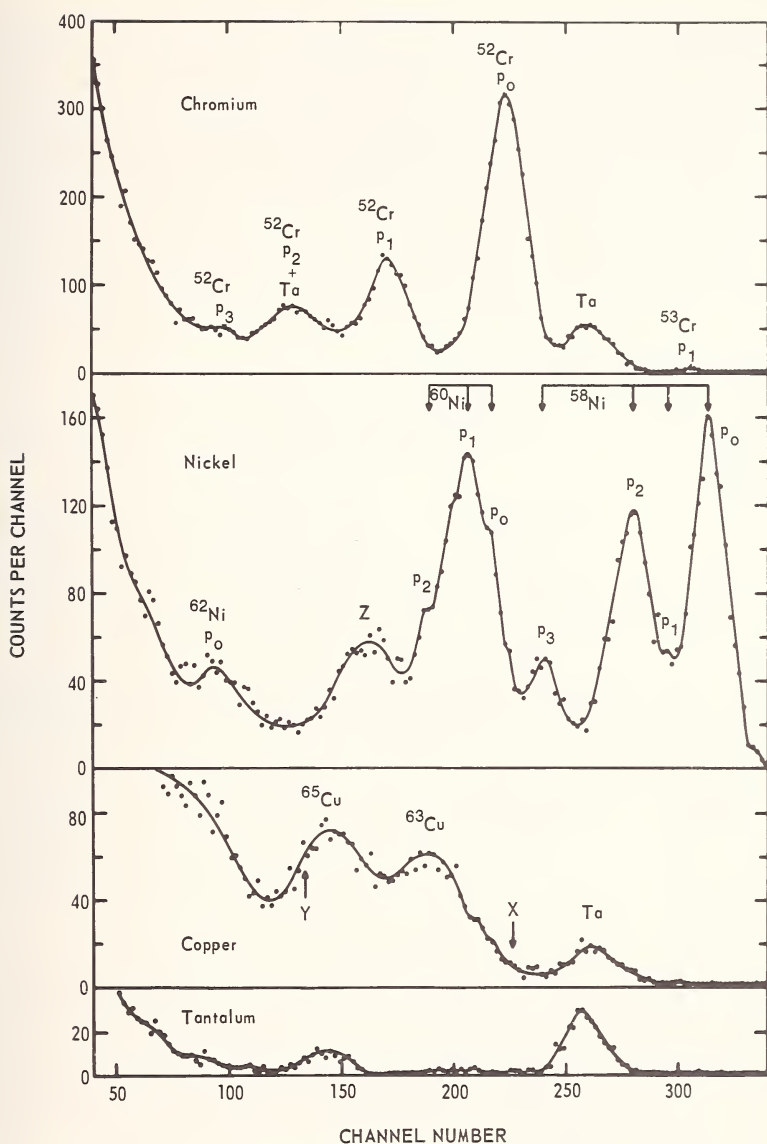
Figure 2.   Energy spectra of prompt protons obtained from the deuteron irradiation of thin
            layers of chromium, nickel and copper on tantalum.

B. ANALYSES

The analysis of surface nickel on copper was of prime concern. A typical spectrum obtained from a film of nickel, about 300 μg/cm^2 thick on copper is shown in Figure 3. The peaks due to protons from nickel can readily be distinguished from those of copper. A measure of the nickel

thickness was obtained by integrating the counts over the "observed" proton energy range from 4.86 to 6.30 MeV, corresponding to "initial" proton energies between 9.36 and 10.32 MeV.

The calibration showing the variation of proton counts with nickel thickness is shown in Figure 4. The curve reflects the decreased yield
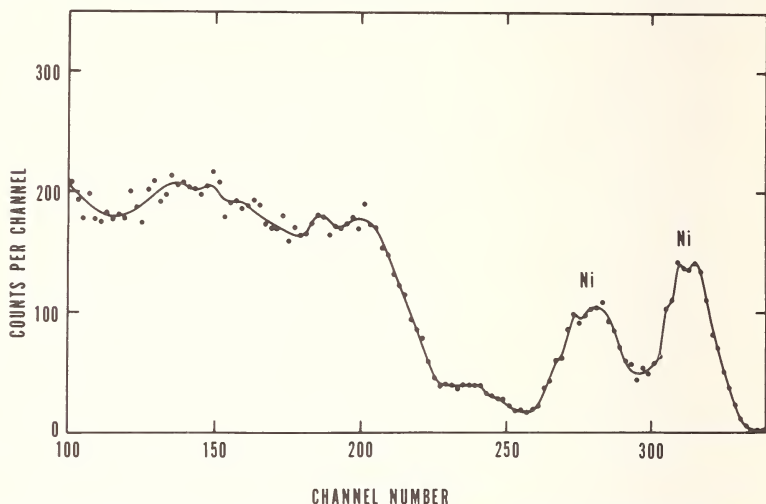
Figure 3. Energy spectrum of prompt protons obtained from a deposit of nickel on a copper backing irradiated with deuterons. $\theta=60°$, $E_d=3.5$ MeV, Au absorber $=196$ mg/cm².
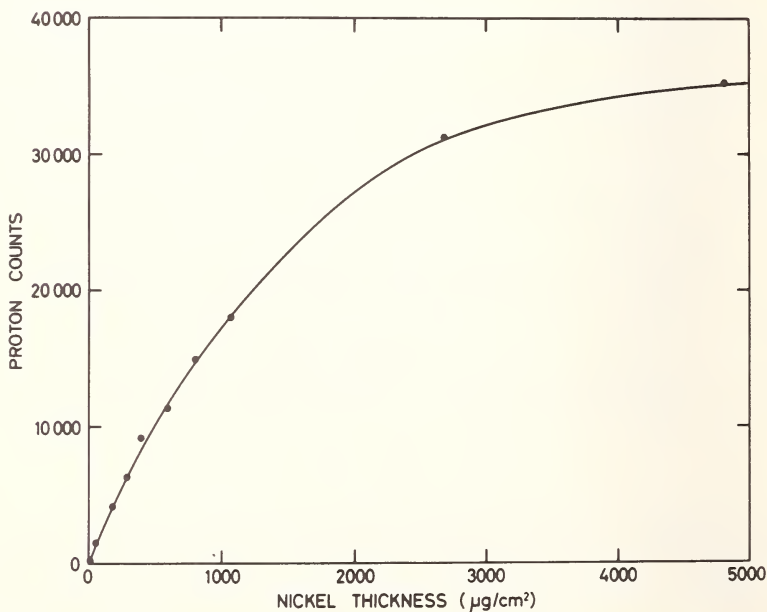
Figure 4. The variation of proton counts for nickel vs. nickel thickness.

obtained for thick films caused by the decrease in the cross section of the reaction with decreasing deuteron energy. However, it can be assumed that the calibration is linear up to 100 μg/cm². Results of a typical series carried out over this thickness region are listed in Table 1. The standard error was ±2.2 μg/cm² over the whole region. This corresponds to a relative standard error of 2.2% for films of about 100 μg/cm², but the relative error increases for thinner films. With a bombarding deuteron beam of 3 mm² area used in this investigation and with a target inclined at 30° to the beam, the precision attained is equivalent to a relative standard error of ±2.2% on 24 μg of nickel.

Table 1. Some determinations of nickel films on copper by prompt proton counting.

Known nickel thickness (μg/cm²)	Integrated proton counts per unit beam current	Measured nickel thickness (μg/cm²)	Error[a] (μg/cm²)
13.3	250	13.4	+ 0.1
17.8	418	20.6	+ 2.8
28.5	566	26.8	− 1.7
37.4	797	36.7	− 0.7
58.7	1233	55.2	− 3.5
76.5	1796	79.1	+ 2.6
97.8	2242	98.0	+ 0.2

[a] Standard error = ± 2.2 μg/cm²

The determination of chromium on nickel is made possible by the fact that the peak due to p_o protons from chromium-52 is so prominent (see Figure 5). By curve stripping this peak can be resolved from the peaks representing nickel. The calibration giving the variation of proton counts with chromium thickness is similar to that obtained for nickel.
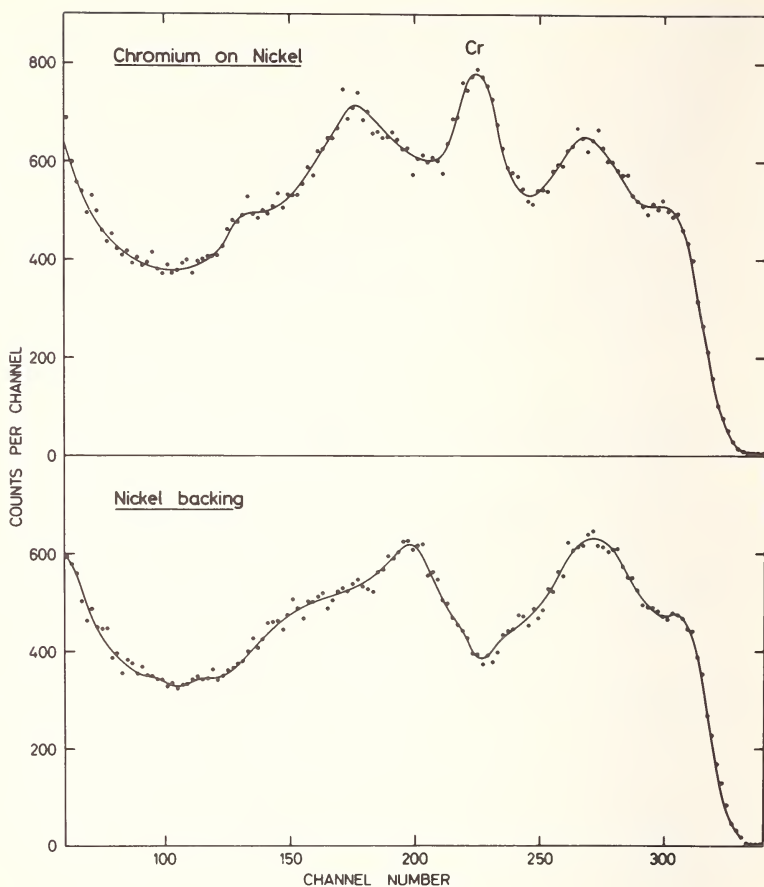
Figure 5. Energy spectrum of prompt protons from a thin chromium film on nickel compared with that obtained from the nickel backing. Chromium thickness = 160 θg/cm² (0.22 μm); $\theta = 60°$, $E_d = 3.5$ MeV, Au absorber = 196 mg/cm².

IV. References

[1]   Rubin, S., Passel, T. O., and Bailey, L., Anal. Chem. **29,** 736 (1957).

[2]   Peisach, M., and Poole, D. O., J. S. Afr. Chem. Inst. **18,** 61 (1965).

[3]   Peisach, M., and Poole, D. O., Anal. Chem. **38,** 1345 (1966).

[4]   Patterson, J. H., Turkevich, A. L., and Franzgrote, E., J. Geophys. Res. **70,** 1311 (1965).

[5]   Anders, O. U., Anal. Chem. **38,** 1442 (1966).

[6]   Peisach, M., Poole, D. O. and Rohm, H. F., Talanta **14,** 187 (1967).

[7]   Williamson, C. F., Boujot, J.-P., and Picard, J., Report CEA-R3042 (1966).

CALIFORNIUM-252: A NEW NEUTRON SOURCE FOR ACTIVATION ANALYSIS[1]

W. C. Reinig and A. G. Evans

Savannah River Laboratory
E. I. du Pont de Nemours and Co.
Aiken, South Carolina 29801

I. Introduction

This paper describes the characteristics of ^{252}Cf, a new neutron source. Californium is now available in limited quantities; larger amounts will be available in the next few years for extensive application in neutron activation analysis.

Since Seaborg and Livingood published the first American paper on activation analysis in 1938, isotopic sources, nuclear reactors, and accelerators have been used as neutron sources for activation analysis. Although the principle of activation analysis was discovered by von Hevesy with isotopic sources, such low intensity sources as those used by von Hevesy are now used mainly to demonstrate the concept of the activation technique. ^{252}Cf with its high neutron yield, however, is a potential source in many activation analysis applications.

II. Discussion

A gram of ^{252}Cf emits 2.34×10^{12} neutrons per second by spontaneous fission. Other isotopic neutron sources inefficiently produce neutrons by the reaction of alpha or gamma decay radiation from the radioisotope with a light element such as beryllium. A typical α,n source emits 1 neutron per 10^4 alpha disintegrations; in contrast, ^{252}Cf emits 1 neutron per 8.5 alpha disintegrations. A comparison of the yield of 1-curie neutron sources, Table 1, indicates that the emission rate from ^{252}Cf is 300 times higher than from any of the other radionuclide sources. The neutron spectrum of ^{252}Cf (Figure 1) is approximately the same as the spectrum of ^{235}U fission neutrons.

The advantages of ^{252}Cf become even more evident where intense neutron sources are required. Isotopic neutron sources that emit greater than 10^9 neutrons per second are rarely used for activation analysis

---

[1] The information contained in this article was developed during the course of work under Contract AT(07-2)-1 with the U.S. Atomic Energy Commission.

Table 1. Yield of 1—curie isotopic neutron sources.

Source	Type	Average neutron energy	Yield, n/sec
^{124}Sb–Be	γ, n	24 keV	1.6×10^6
^{239}Pu–Be	α, n	4.5 MeV	2.0×10^6
^{241}Am–Be	α, n	4 MeV	2.0×10^6
^{210}Po–Be	α, n	4.3 MeV	2.5×10^6
^{238}Pu–Be	α, n	4 MeV	2.8×10^6
^{244}Cm–Be	α, n	4 MeV	3×10^6
^{242}Cm–Be	α, n	4 MeV	4×10^6
^{226}Ra–Be	α, n	3.6 MeV	1.5×10^7
^{252}Cf	Spontaneous Fission	2.3 MeV	4.4×10^9

because of their cost, half life, volume, gamma emission, or heat emission. On the other hand ^{252}Cf is a practical high yield source.

The costs of neutron sources with emission rates of 5×10^{10} neutrons per second, such as may be required for activation analysis, are compared in Table 2. At a cost of \$$10^6$ per gram, which is an order of magnitude
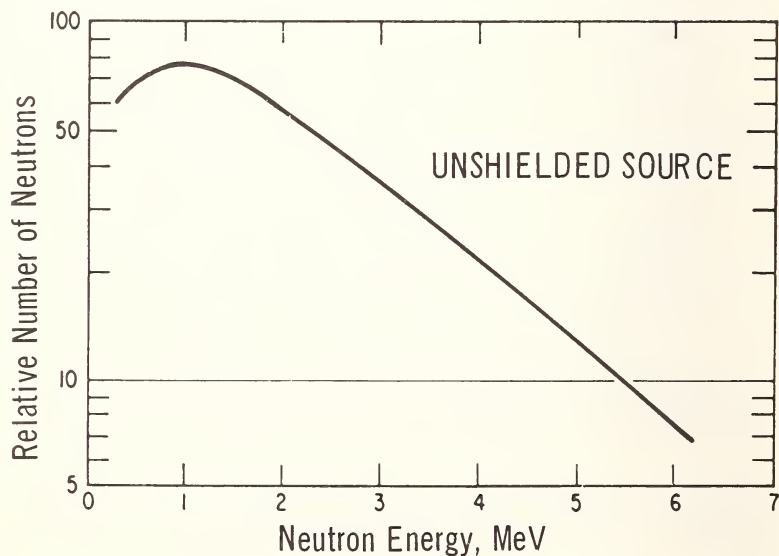
Figure 1.   Neutron Spectrum of ^{252}Cf.

estimate of the cost over the next ten years, the ^{252}Cf neutron source offers the most favorable combination of initial investment plus yearly replenishment costs of any isotopic neutron source. The costs listed in this table are based on the cost of the radionuclide only and do not include fabrication or shipping. Because a ^{252}Cf neutron source requires no target material, fabrication costs would be generally less than for other sources. Shipping charges associated with replenishing short lived sources, such as ^{124}Sb-Be, would significantly increase their costs. ^{239}Pu-Be is not listed in the table because the amount required exceeds the critical mass; ^{226}Ra-Be is omitted because insufficient radium would be available to make this intense source, and if it were, would cost 5×10^7 (based on present radium prices).

Other characteristics of isotopic neutron sources, which affect their practicality when yields of 5×10^{10} neutrons per second are required, are compared in Table 3. The volume of the sources includes only the radionuclide and target material. In designing capsules for α,n sources,

Table 2. Cost of intense neutron sources.

Source	Cost per 5×10^{10} n/sec[a]
^{242}Cm–Be	$ 10,000[b]
^{210}Po–Be	20,000[c]
^{252}Cf	20,000[d]
^{124}Sb–Be	25,000 [3]
^{244}Cm–Be	280,000[e]
^{238}Pu–Be	310,000[f]
^{241}Am–Be	1,500,000[g]

[a] Cost of radionuclide only.

[b] Based on $2,000/g. [1]

[c] Based on $4,300/g. [2]

[d] Based on 10^6/g. Very preliminary estimates indicate cost might range from 10^5 to 5×10^6/g depending on the scale of production.

[e] Based on $1400/g. [2]

[f] Based on $280/g. [2]

[g] Based on $200/g. [1]

Table 3. Characteristics of isotopic neutron sources.[a]

Source	Half life		Gamma dose rate r/hr at 1 meter	Heat generation watts	Volume[b] cm^3
^{124}Sb–Be	60	d	4.5×10^4	20	200
^{210}Po–Be	138	d	2.0	640	200
^{242}Cm–Be	163	d	0.3	600	2
^{252}Cf	2.65	y	2.9	0.8	<1
^{244}Cm–Be	18.1	y	0.2	600	70
^{238}Pu–Be	89	y	0.4	550	350
^{241}Am–Be	458	y	2.5	750	2.2×10^4

[a] Normalized to 5×10^{10} neutrons per second.

[b] Not including void space for helium from α decay.

consideration must be given to the accumulation of helium from alpha decay. A ^{242}Cm-Be source initially emitting 5×10^{10} neutrons per second produces a total of 470 cm³ of helium; in contrast, a ^{252}Cf source with the same neutron emission rate generates 2 cm³ helium. The volume of the capsule of α,n sources must be large enough to accommodate the helium.

Some of the α,n sources would require additional high conductivity metal to provide adequate surface area for heat dissipation to prevent damage when handled in air. This would also increase their volume. For example, to decrease its temperature to a safe level, the ^{242}Cm-Be source could be embedded in a cylinder of high conductivity metal, 10 cm in diameter and 10 cm in height, with fins added to double the surface area. Sources with large heat sinks have disadvantages. The effective neutron flux is decreased because the sample to be activated cannot be placed close to the source, in addition, some neutrons are absorbed in the mantle material.

Californium-252 sources can also be compared with accelerators. Certain differences favor ^{252}Cf for specific activation analysis applications: lack of maintenance as opposed to continual servicing for accelerators; the dependable and continuous neutron emission of ^{252}Cf of predictable intensity in contrast with the intermittent mode of operation for an accelerator and the supplementary measurements required to determine emission rate; and the less elaborate and cheaper shielding for an irradiation facility housing a californium source. ^{252}Cf is a practical source for activation analysis in hostile or remote environments because it is not affected by the rigors of transportation and does not require

cooling water or electrical power. However, ^{252}Cf may not be practical for applications where it is necessary to have a rapidly pulsed source, or where higher energy neutrons are required. The cost per neutron, based on capital investment, from an accelerator is about the same as that from californium if a continuous source of neutrons is not required. Where a continuous source is needed, ^{252}Cf is expected to be cheaper. Operating costs are much less for a californium source than for an accelerator. To summarize, both californium and accelerators have specific uses that favor one or the other. The choice of the proper source for activation analysis necessitates an evaluation of the individual requirements of each application.

When there is a large scale program to produce ^{252}Cf, the cost would be reduced substantially. Under this condition, californium would offer advantages over conventional reactor sources in size, simplicity, and efficiency for activation analysis [4]. The neutron flux (thermal or fast) in the core of a 100 kW reactor is approximately 10^{12} n·cm^{-2}·sec^{-1}. An array of intense ^{252}Cf sources can provide the same spectrum and flux. A 100 kW (thermal) reactor facility costs about $500,000, with an annual operating expense of $100,000. An array of ^{252}Cf sources would not require 1) the elaborate preparation to obtain approval for reactor construction and operation, 2) a separate building, 3) control rods and instrumentation, 4) cooling system, 5) fuel charging and discharging apparatus, 6) containment, or 7) operating personnel. The cost of the californium facility would be primarily the price of the source.

III.   Conclusions

Californium-252 is a valuable new neutron source for activation analysis. The cost of this radionuclide and the relatively simple shielding it requires indicate its promise for analytical, forensic, hospital, and university laboratories. The high neutron yield from minute sources and their transportability makes ^{252}Cf practical for mineral exploration and geophysical studies in remote environments on land, undersea, or extra-terrestrial. Where a continuous, dependable, high neutron flux is required, such as for industrial process control, ^{252}Cf has unique advantages over other sources.

IV.   References

[1]   Rohrman, C. A., in Proceedings of Conference on Isotopic Power Development, USAEC Report TID-7698, Part I (1964).

[2]   Overbeck, W. P., in Proceedings of Symposium on Large Scale Production and Applications of Radioisotopes, USAEC Report DP-1066, Volume 1 (1966).

[3]   Hennelly, E. J., Nucleonics 19, 3, 124 (1961).

[4]   Stetson, R. L., Nucleonics 24, 11, 44 (1966).

GAMMA-RAY SPECTROMETRY AND AUTOMATED DATA SYSTEMS FOR ACTIVATION ANALYSIS

Plenary Lecture by R. L. HEATH

National Reactor Testing Station
Idaho Falls, Idaho

I. Introduction

Over the past several years the development of the lithium-ion drifted detector and associated low noise electronics has had a considerable impact on experimental photon spectrometry. Although these devices offer energy resolution at least an order of magnitude better than was possible with NaI scintillation detectors, optimum performance has been difficult to achieve. The use of Ge(Li) spectrometers, pioneered in nuclear physics laboratories, involved the use of cryogenic techniques and sophisticated electronics. A number of recent developments in this area include large volume detectors which offer improved detection efficiency, improved resolution as a result of better preamplifier design, reduction of spectral distortion at high counting rates using specialized electronic pulse conditioning systems, and increased sensitivity for the analysis of complex gamma-ray spectra by simplification of the pulse height response of the spectrometers through the use of specialized detector systems which reject pulses in the unwanted continuum of the pulse height distribution. All of these improvements make the use of high resolution Ge(Li) spectrometers appear quite attractive for many applications in the field of activation analysis. The purpose of this review is to provide a capsule view of the state-of-the-art in high resolution photon spectrometry, to discuss in some detail the concepts of each element of a modern pulse height analysis system for general laboratory use in high resolution applications, and to present the role of digital computer based systems for data acquisition and on-line analysis. An introduction to the pertinent literature in this area is included, along with some background to supplement the many excellent papers illustrating applications of high resolution spectrometry which will follow.

The development of the solid state detector has somewhat paralleled the development of pulse height analysis techniques developed for use

with NaI(Tl) scintillation spectrometry. In 1951, McKay [1] first reported the use of a grown p-n junction diode to detect alpha particles. Mayer and Gossick [2] fabricated small area germanium surface-barrier diodes in 1951 which were operated at room temperature with rather poor energy resolution characteristics. Beginning in 1956, the first significant contribution was made by Walter and Dabbs [3] who began a series of experiments with germanium surface-barrier diodes operated at liquid nitrogen temperatures to obtain improved noise characteristics. These early experiments with germanium devices were followed by the rapid development of improved Si devices for high resolution charged particle spectrometry. The use of these early surface-barrier devices was largely confined to charged particle spectrometry because of their limited sensitive volume.

To clarify this point let us consider briefly the nature of the junction counter. The p-n junction device may be thought of as a solid state ionization chamber. If one applies a back-bias across a p-n junction, a small volume near the junction will be swept clear of charge carriers. An ionizing particle which enters this volume will then produce electron-hole pairs which may be collected at the electrodes of the diode. Typically, the depth in these early junction devices of the so-called depletion layer did not exceed a millimeter. Consideration of electron ranges in silicon made these devices unusable as gamma-ray spectrometers. More recently, surface-barrier devices have been made which can sustain sufficiently high electric fields to provide a depletion layer of several millimeters [4].

In 1960 Pell [5] demonstrated that lithium ions could be used to compensate for the presence of acceptor impurities in semiconductor materials. Using this technique, lithium ions are used to create a P-I-N structure such as shown in Figure 1. These devices are fabricated by diffusing lithium into the surface of an ingot of p-type Si or Ge, forming an n-type region on one surface. A bias voltage is then applied to the ingot at elevated temperature causing the lithium ions to drift through the p-type material. During this process, an equilibrium condition is established where lithium ions pair with atoms of the doping material (gallium or indium in the case of p-type germanium) creating a region with intrinsic properties. The term intrinsic implies that charge carriers will have a very long lifetime with all recombination processes reduced to a negligible level. Under reverse bias, the charge carriers can then be collected from this region, resulting in the production of a solid-state ionization chamber with appreciable volume. Using the best available single crystal germanium material, P-I-N structures have now been fabricated with intrinsic regions up to 2 centimeters in depth. Since the mobility of lithium ions in germanium is not negligible at room temperature, such devices, once fabricated, must be maintained at dry ice temperature or below to preserve the structure. This is not true of Si(Li) devices which can be

n$^+$ Layer

Electron Motion

+

Lithium-Drifted Intrinsic Region
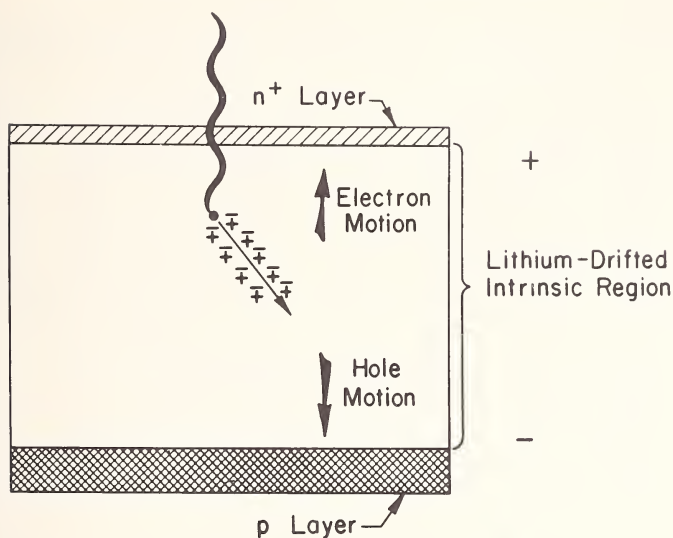
Hole Motion

−

p Layer

Figure 1.   Illustration of P-I-N planar structure of lithium-ion drifted germanium detector.

stored at room temperature for extended periods. A description of early work on the application of Ge(Li) devices to gamma- ray spectrometry is reported in references [6-8].

As described above, intrinsic regions with depths up to 2 cm have been successfully fabricated. Due to difficulties in obtaining germanium of sufficient quality, it has not been possible to drift devices with intrinsic regions much in excess of 1 cm which exhibit charge collection properties required for high resolution performance. To overcome this limitation and yet produce large volume devices, Tavendale [9] first proposed the coaxial configuration shown in Figure 2. This type of structure provides a large central volume of intrinsic material. The major limitations of this drift configuration are related to the radial field distribution which results from the geometry of the device. Because the field gradient will vary as 1/R, where R is the radius of the cylinder, the time required to collect the charge carriers following an ionizing event will depend on the source of production of the hole-electron pairs within the intrinsic volume. This results in a "time jitter" problem which is somewhat troublesome in coincidence applications. This problem is much less severe in the true coaxial detector than in the so-called five-sided device.

II.   Spectrometer Performance

Prior to any detailed discussion of the elements of a lithium-ion drifted germanium gamma-ray spectrometer, let us first examine a few examples of the performance of high resolution systems. The development of low
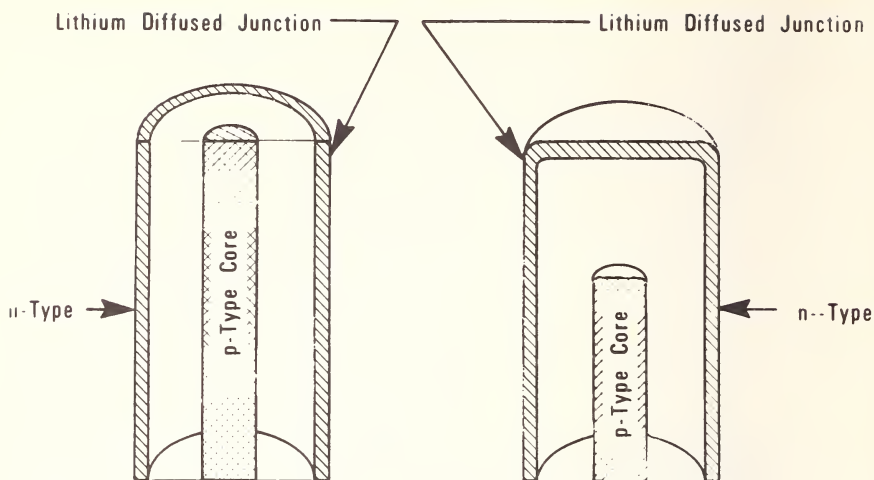
Figure 2.   Coaxial P-I-N configurations used to produce large-volume Ge(Li) detectors.

noise pulse amplifying systems which employ field-effect transistors operating in the liquid nitrogen temperature range has made it possible to achieve energy resolution approaching the statistical limits imposed by the variance in the number of hole-electron pairs created in the sensitive volume of the detector. Figures 3-7 are pulse height spectra obtained with systems employing lithium-drifted detectors and cryogenic FET preamplifiers. Other elements of a high resolution spectrometer include a low noise linear pulse amplifier (TC-200) and a 4096 or 8192 channel analog-to-digital converter (ADC). Figure 3 is a pulse-height spectrum obtained with a lithium-ion drifted silicon detector mounted in a cryostat with an FET preamplifier. These data represent the low energy photon spectrum emitted by the radioisotope ^{57}Co. This radioisotope decays by electron capture, giving rise to Fe x-rays and a nuclear gamma ray with an energy of 14.4 keV. We observe that the K_α and K_β Fe x-rays are resolved. The measured resolution in this energy region (full width at half maximum) is 420 eV. The noise contribution of the electronic system was 370 eV, as indicated by the measured width for pulse generator pulses inserted into the input of the preamplifier during the measurement. Quite recently, improvements in the noise performance of FET's has made it possible to obtain a resolution for the Fe K x-ray of 250 eV full width at half maximum (FWHM).

Figure 4 shows the pulse-amplitude spectrum of gamma rays emitted in the decay of 200 day ^{153}Gd. As indicated, the measured resolution of the 0.103 MeV gamma ray is 750 eV, while the contribution from amplifier
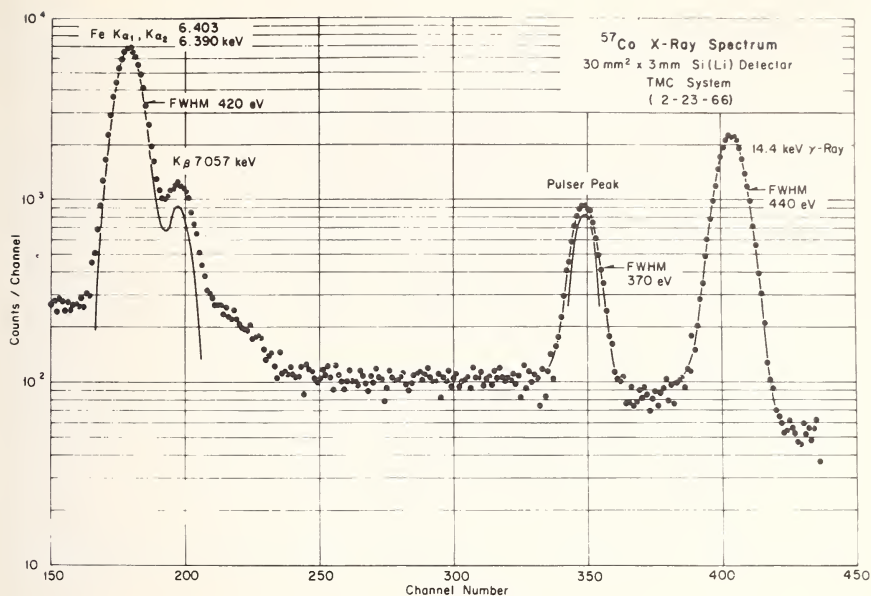
Figure 3.   Pulse-height distribution representing the low-energy photon spectrum from the decay of ^{57}Co. Spectrum shows Fe K_α and K_β x-rays resolved. Energy resolution in this energy region is 400 eV (FWHM). Spectrum obtained with Si(Li) detector.
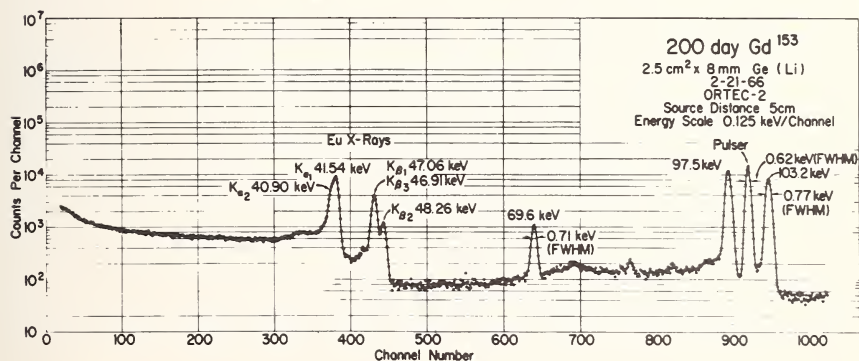
Figure 4.   Gamma-ray spectrum of radiation emitted in the decay of ^{153}Gd obtained with Ge(Li) spectrometer. Energy resolution at 103 keV is 750 eV (FWHM).

noise is 620 eV as indicated by the pulser peak. Figure 5 represents the spectrum of gamma rays emitted in the decay of ^{88}Y. This nuclide emits gamma rays of 898.00 ± 0.04 and 1836.08 ± 0.05 MeV. A measured resolution of 2.26 keV is indicated for the photoline of the high energy gamma ray. The resolution at this energy (0.012%) exceeds that presently
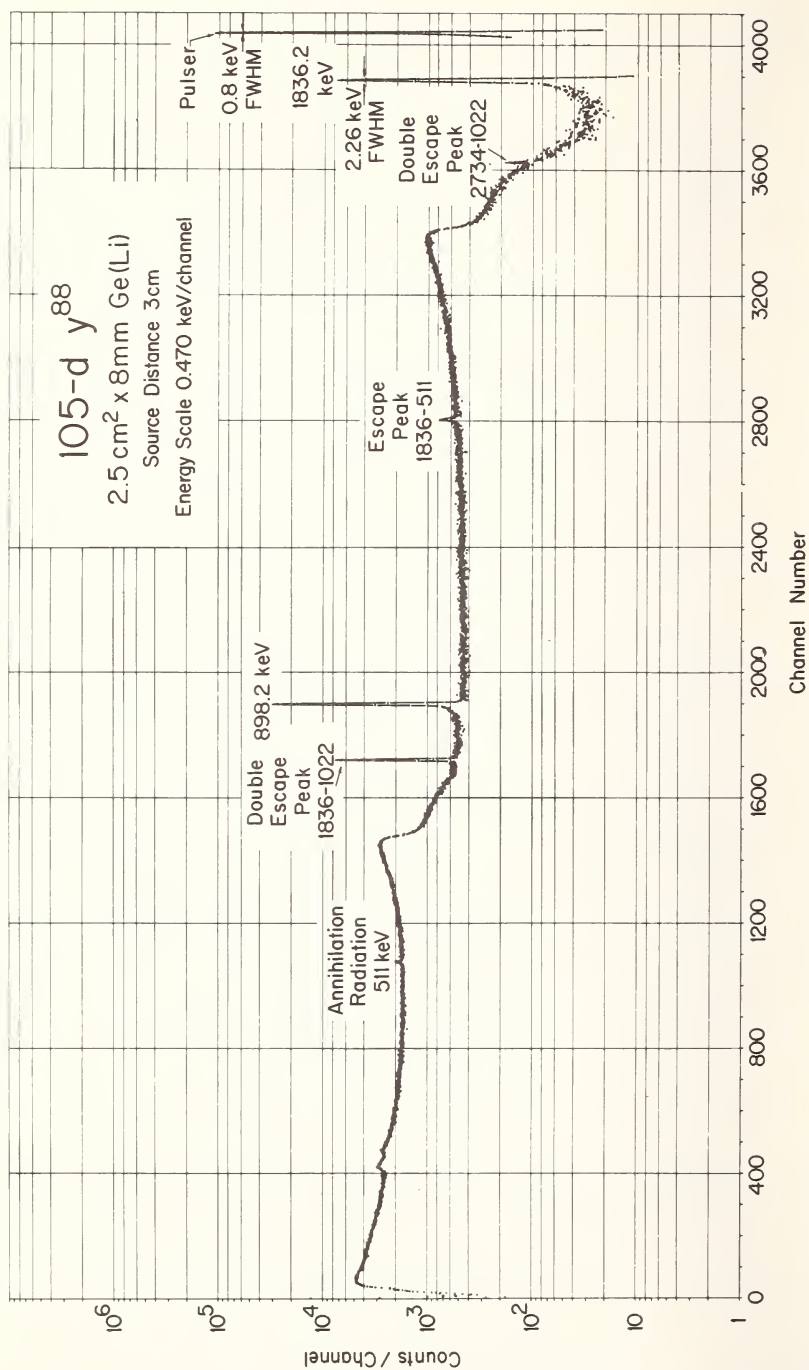
Figure 5.   Gamma-ray spectrum of radiation emitted in the decay of [88]Y. Resolution of the full-energy peak from the 1.83 MeV gamma ray is 2.26 keV (FWHM).

achieved by any other method for the measurement of gamma-ray energy spectra.

Figure 6 is a pulse height spectrum of capture radiation from the reaction $S(n,\gamma)$, using a small Ge(Li) detector. In this measurement an energy range up to 7 MeV was covered. As indicated in the figure, a measured resolution of 4.76 keV (FWHM) was obtained for the 4.399 MeV peak. Measurements of this type represent a severe test of the stability and high rate performance of a system since the presence of the large continuum of pulses in the spectrum requires operation of the pulse height analysis system at rates up to 10,000 pulses per second for periods of 24 hours or longer. These data were obtained with a laboratory system incorporating many of the refinements to be discussed in later sections, but did not employ digital gain or zero stabilization.

Figure 7, which is presented in four parts (a,b,c,d) has been included to provide some appreciation for the problems encountered in the application of a high resolution system to the measurement of complex gamma-ray spectra. This figure presents four (4) spectra representing the gamma rays emitted by gross fission products as a function of decay time following the irradiation of ^{235}U in the MTR reactor for a period of 13 days. The analysis of such spectra is a routine requirement in the surveillance of reactor coolant streams to determine the nature of radioactive waste streams which might be released to the biosphere. Examination of these spectra indicates the presence of over 150 gamma rays emitted in the decay of 40 radioactive fission product isotopes. The magnitude of the analysis problem, to obtain both quantitative and qualitative results, should provide some indication of the current interest in automated data processing techniques which will be discussed in some detail in a later section.

As indicated by these examples, the nuclear spectroscopist is interested in applying the techniques of high resolution gamma-ray spectrometry to the measurement of photon spectra from 1 keV to 10 MeV. To provide some insight into the magnitude of the electronics problem, let us consider the requirements for a pulse height analyzer system which is capable of utilizing the resolution of these detectors for measurements over this energy range. To properly analyze a pulse height distribution with no loss of resolution due to finite channel-width corrections and with adequate information for least squares data analysis, a given peak must have a minimum of 5 channels spanning one resolution width (FWHM). Table 1 shows the number of channels required to meet this condition for gamma rays up to 10 MeV. This assumes the measurement of a complete energy spectrum (no threshold amplifier). Examination of this table shows that a minimum of 4096 channels is required to span an energy range from zero to 2 MeV. Even this is somewhat misleading, for the improved energy resolution at low energies (e.g. 100 keV) would require a channel width of
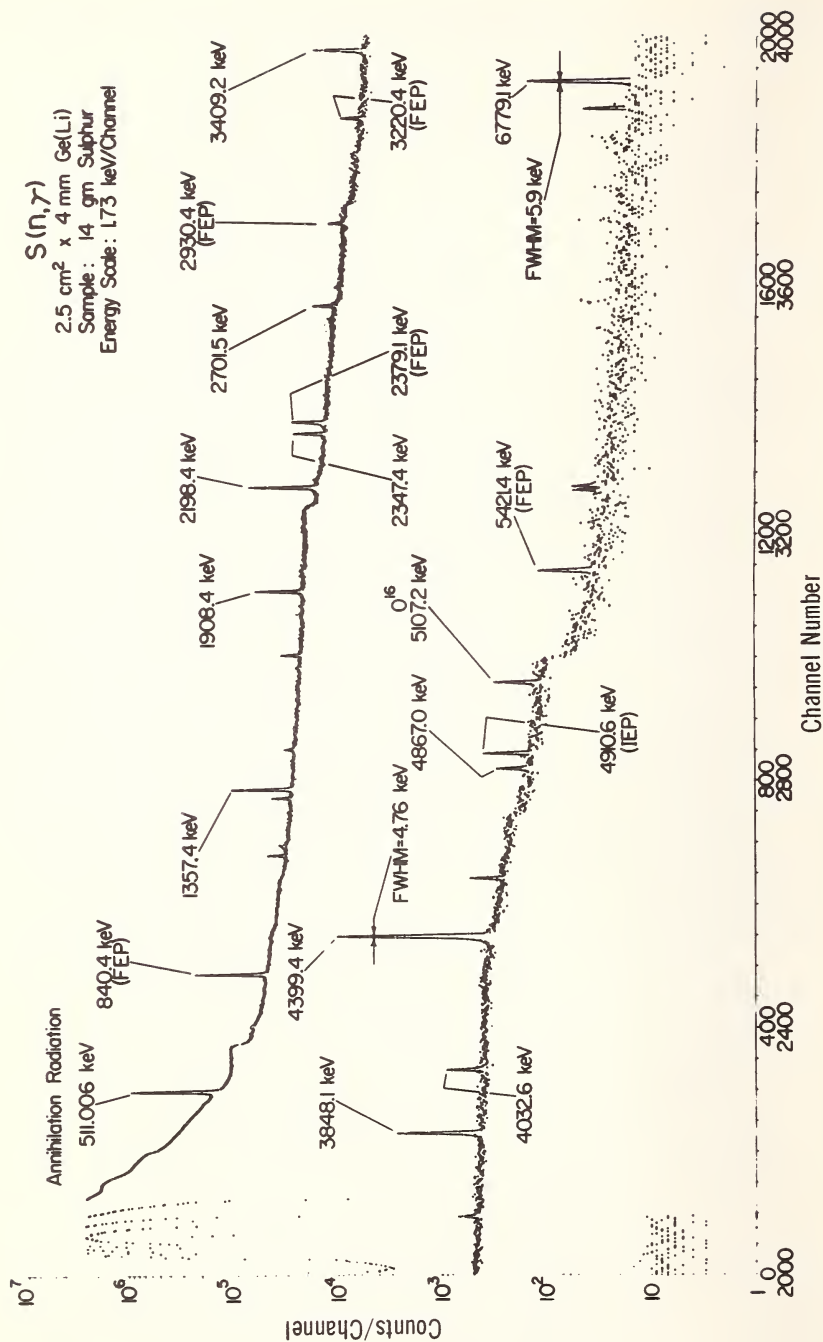
Figure 6. Gamma-ray spectrum of capture radiation from the S(n,γ) reaction. Indicated energy resolution for the pair peak at 4399.4 keV is 4.76 keV (FWHM).
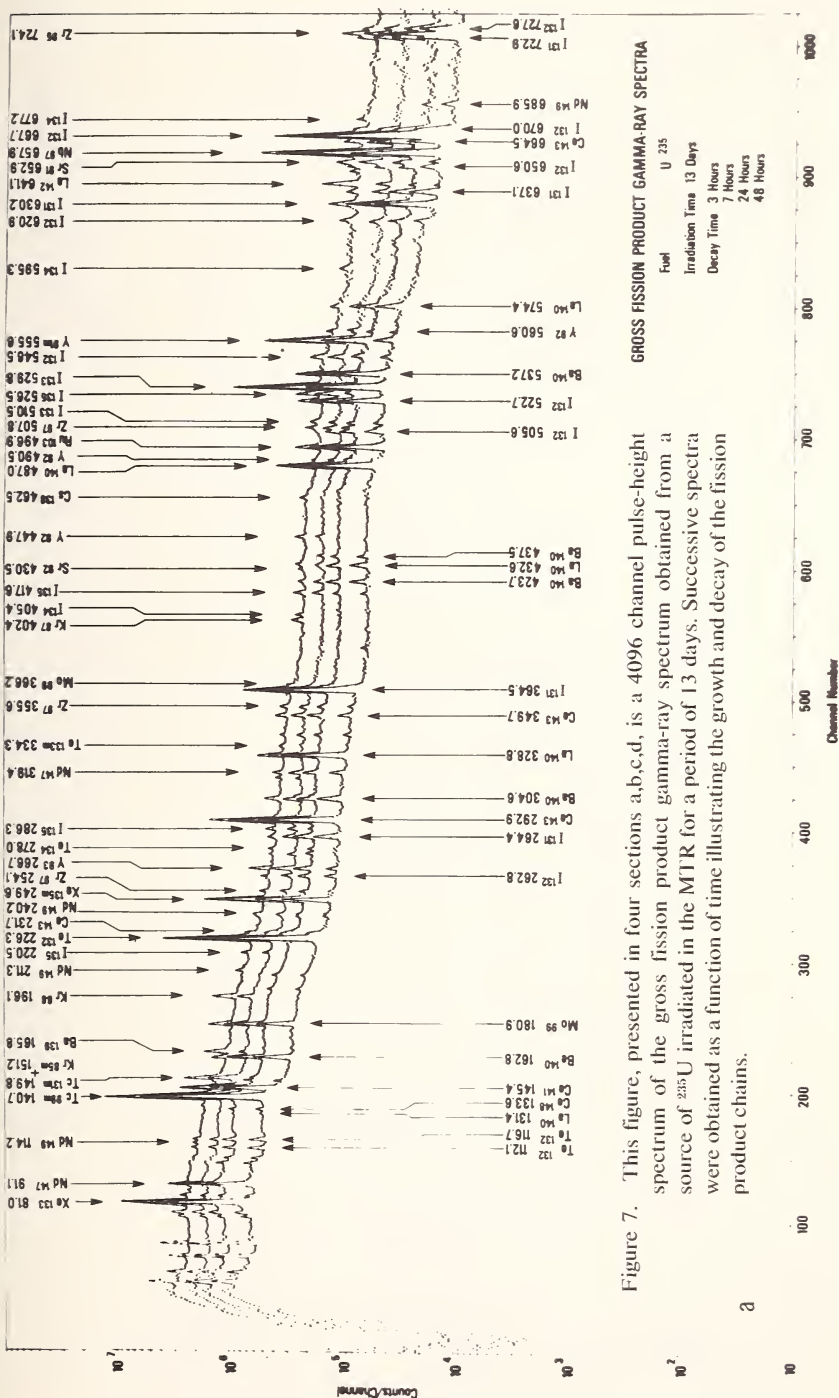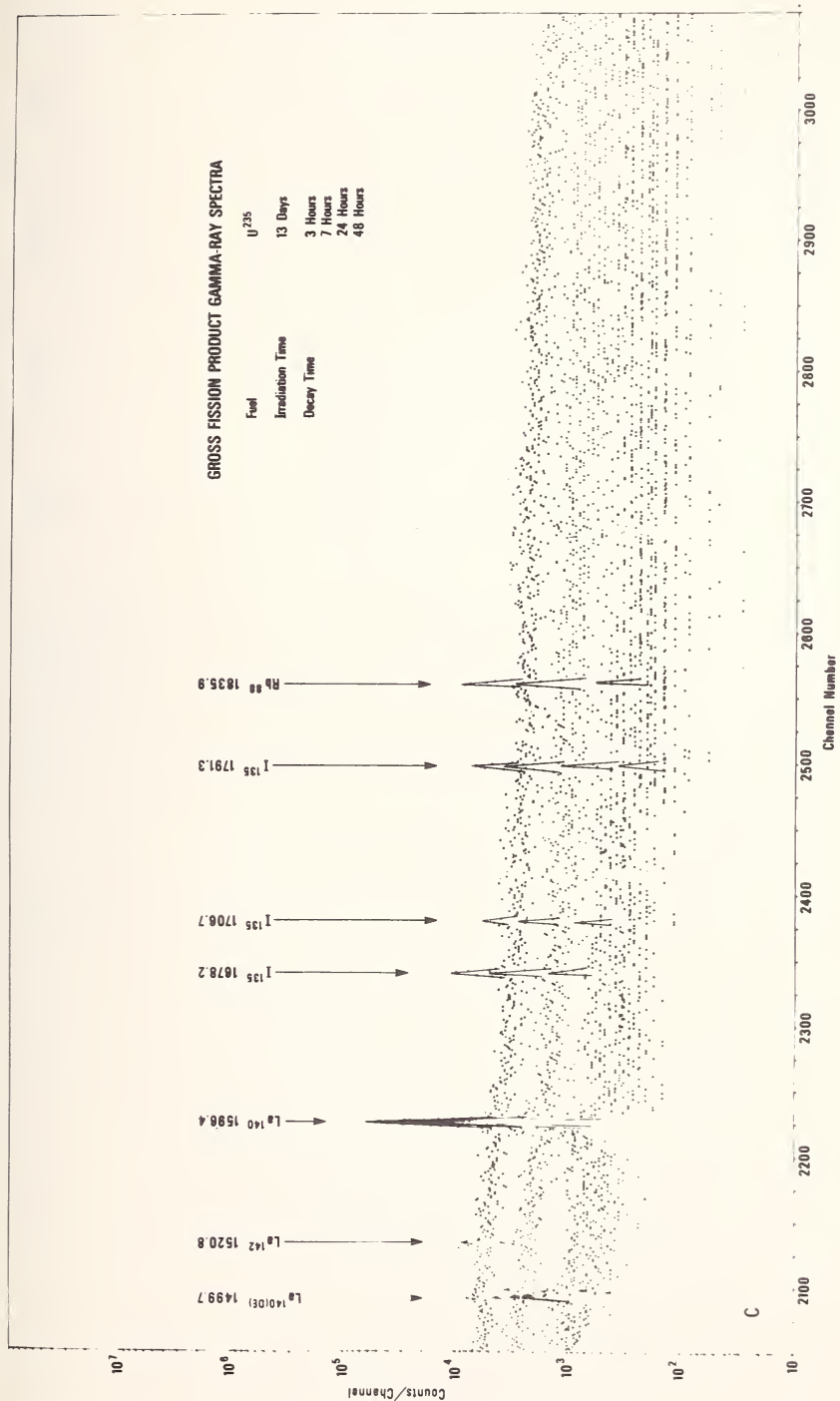
Figure 7. This figure, presented in four sections a,b,c,d, is a 4096 channel pulse-height spectrum of the gross fission product gamma-ray spectrum obtained from a source of ^{235}U irradiated in the MTR for a period of 13 days. Successive spectra were obtained as a function of time illustrating the growth and decay of the fission product chains.

GROSS FISSION PRODUCT GAMMA-RAY SPECTRA

Fuel   U²³⁵
Irradiation Time   13 Days
Decay Time   3 Hours
                    7 Hours
                    24 Hours
                    48 Hours

GROSS FISSION PRODUCT GAMMA-RAY SPECTRA

Fuel   U²³⁵
Irradiation Time   13 Days
Decay Time   3 Hours
                      7 Hours
                      24 Hours
                      48 Hours

GROSS FISSION PRODUCT GAMMA-RAY SPECTRA

	U^{235}
Fuel	
Irradiation Time	13 Days
Decay Time	3 Hours
	7 Hours
	24 Hours
	48 Hours

La^{140} 2521.7

La^{142} 2397.9
Kr^{88} 2391.6

d

Channel Number

Counts/Channel
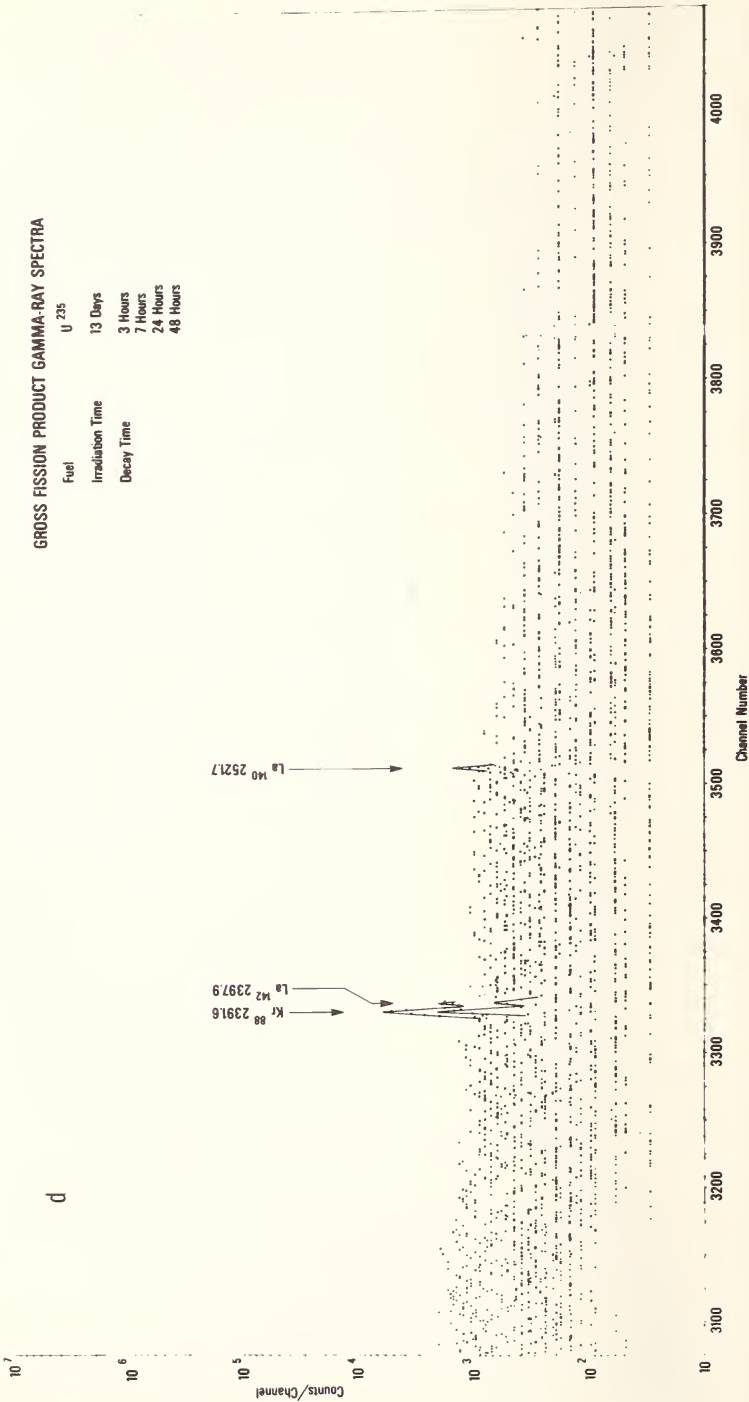
Table 1. Channel width (keV) to provide 5 channels
spanning peak (FWHM).

E_γ (MeV)	Channel width (keV)	Number of channels required (0 threshold)
0.05	0.14	360
0.10	0.15	670
0.30	0.20	1,500
0.60	0.27	2,200
1.00	0.34	3,000
2.00	0.46	4,300
3.00	0.58	5,200
5.00	0.73	6,800
8.00	0.92	8,600
10.00	1.00	10,000

0.15 keV vs 0.46 keV for a 2 MeV gamma ray. Thus, to maintain a minimum of 5 channels (FWHM) for gamma rays from 0.1 to 2.0 MeV would require 12,000 channels of equal width. This would indicate that a compromise must be made in order to keep the data acquisition problem within reasonable bounds. For example, we are presently using 8192 channel ADC's for capture gamma-ray spectra, covering an energy range of 0.1 to 10 MeV.

In order to achieve the quality of performance in a high resolution Ge(Li) spectrometer as illustrated by the preceding examples, a number of sophisticated electronic refinements are required. Figure 8 is a block diagram representing the electronic elements of a high performance pulse height analysis system. The addition of pulse conditioning circuitry to such systems is required to minimize deficiencies in the detectors and electronic pulse handling circuitry in a conventional system. Each of these elements will be discussed in the following sections with a brief explanation of the nature of the electronic problems which result in deterioration of resolution at high counting rates.

Summarizing at this point, it should be indicated that the experimental achievement of energy resolution of this magnitude with pulse- amplitude measurement equipment is somewhat remarkable when one considers the complexity of the electronic systems employed. To measure pulse-amplitude with a precision of the order of less than one part in 10^4 requires extreme stability in all electronic elements of the system. We will attempt in the following section to describe the elements of present-day laboratory systems and their relationship to the problems encountered in

BLOCK DIAGRAM

HIGH PERFORMANCE Ge(Li) SPECTROMETER
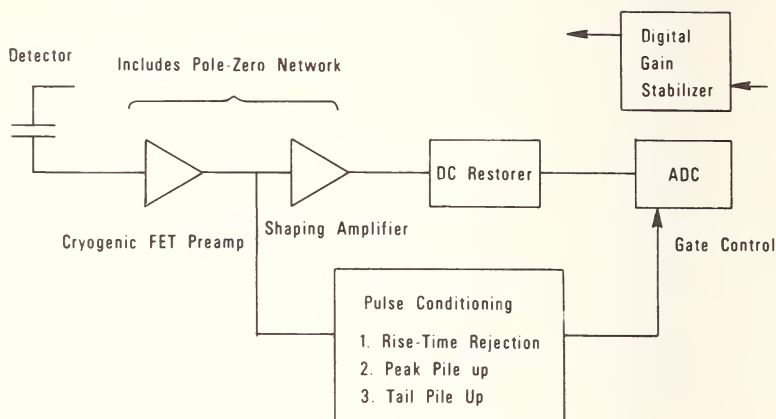
Figure 8. Block diagram of a high performance Ge(Li) spectrometer illustrating the types of specialized electronics required to obtain optimum performance in a high resolution system.

applying these techniques to experimental measurements in the field of activation analysis.

A. Detector Resolution

The observed experimental width of a monoenergetic electron line resulting from interaction of a gamma ray in the intrinsic region of a solid state detector by the photoelectric or pair-production process, is determined by a number of factors. The most important of these are: (1) statistical variance in the number of hole-electron pairs. (2) noise contribution of the detector, *i.e.*, leakage current, charge collection problems from trapping and variation in charge collection time. (3) electronic noise contribution from the input stages of the pulse amplifier system. (4) performance of the filter networks in the pulse shaping section of the amplifier. (5) accuracy of the analog-to-digital converter used to measure amplitude (time jitter in ramp-type ADC's). (6) time-dependent stability of amplifier and analog-to-digital converter. (7) rate dependent effects.

Of these, the basic limitation in resolution is imposed by the statistical variance in the production of hole-electron pairs, within the intrinsic volume of the detector.

In germanium, on the average, 2.98 eV of energy is required to produce an electron-hole pair. Following the production of a high energy electron in the detector, energy is lost either by the production of electron-hole pairs or processes which result in optical photon collisions. Since the sharing of this energy between these two competing modes is statistical in nature we must speak of an average number of electron-hole pairs resulting from the loss of a given amount of energy in the detector. It is customary to express the experimental resolution of a detector in the following manner:

$$\text{FWHM(keV)} = 2.355(FE\epsilon)^{1/2} \tag{1}$$

where E is the energy of the electron in keV, ϵ is the average energy to create an electron-hole pair, and F is the Fano factor, which is related to the yield or fractional amount of total energy absorbed which results in the production of electron-hole pairs [10]. It should be mentioned that solid-state devices have the distinct advantage that only 3 eV are required to produce a hole-electron pair vs 30 eV for gas counters.

From the expression above, we see that a prediction of the limit placed on energy resolution by fundamental statistical considerations requires a knowledge of the Fano factor. The experimental determination of this quantity is difficult. To a first approximation, it may be determined experimentally by removing the contribution due to all noise sources in the system. At low energies, the statistical spread attributable to the detector is small compared with all other noise sources. At high energies, the determination is limited by charge collection problems in the detector and limitations on the stability of the electronic system. Figure 9 is a plot of experimentally measured energy resolution for two low capacity germanium detectors—(1) 2.5 cm² × 4 mm and (2) 2.5 cm² × 8 mm. The field established by the detector bias used is indicated on the figure. Experimental values for energy resolution (FWHM) are indicated by the closed circles. To obtain an estimate of the detector line width, the contribution from all other factors contributing to the observed line width was assumed to be given by the observed width of a pulser measured simultaneously with the source. The 8 mm detector was operated with a cooled-FET preamplifier which contributed a noise level of approximately 0.63 keV (FWHM). A gradual increase in the measured width of the pulser line with increasing energy is observed which is attributed to pile-up problems and finite window width effects. The resulting line width for the two detectors after removal of the contribution from system noise is shown by the open circles (4 mm detector) and the symbol "x" for the 8 mm detector. Also plotted for comparison are two solid curves representing the expected line width for Fano factor values of 0.20 and 0.15. The data points agree favorably with a value of 0.15. Comparison of these curves with the experimental values for energy
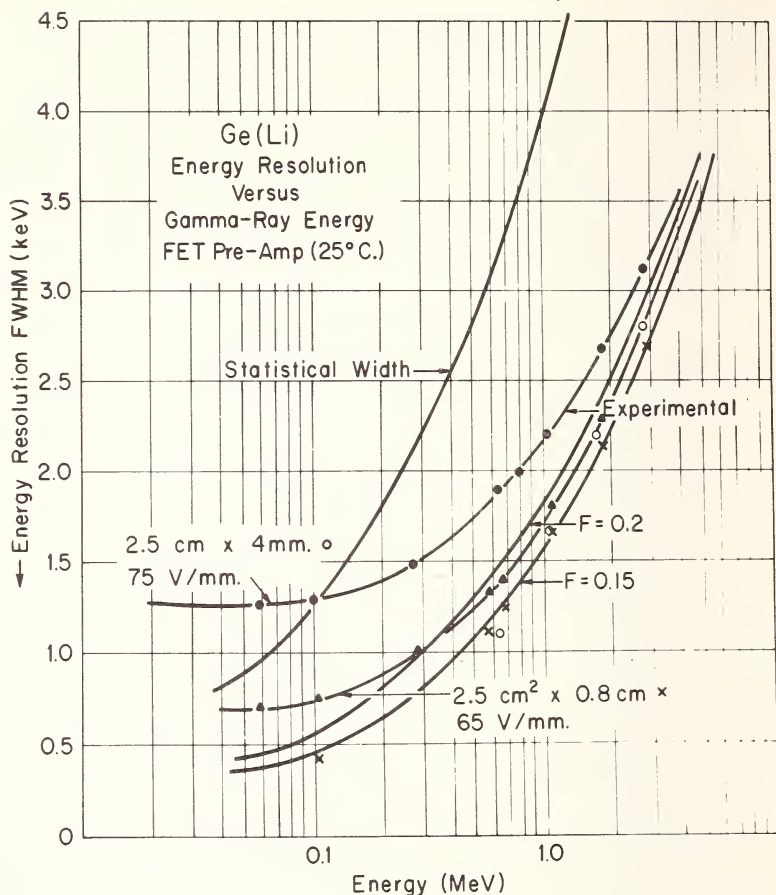
Figure 9.   Plot of energy resolution of a high resolution Ge(Li) spectrometer as a function
            of gamma-ray energy to illustrate the theoretical limit on resolution imposed by
            detector statistics.

resolution indicates that the resolution at low energies is limited largely by
preamplifier noise. The results of similar measurements for Si(Li)
detectors are shown in Figure 10.

B.   CHARGE COLLECTION PROBLEMS

To this point in the discussion, we have considered only the basic
limitation on energy resolution imposed by statistical considerations in
the production of hole-electron pairs within the intrinsic volume of the
detector. As mentioned in the previous section, there are other sources of
difficulty arising in the detector itself, which may affect system resolution.
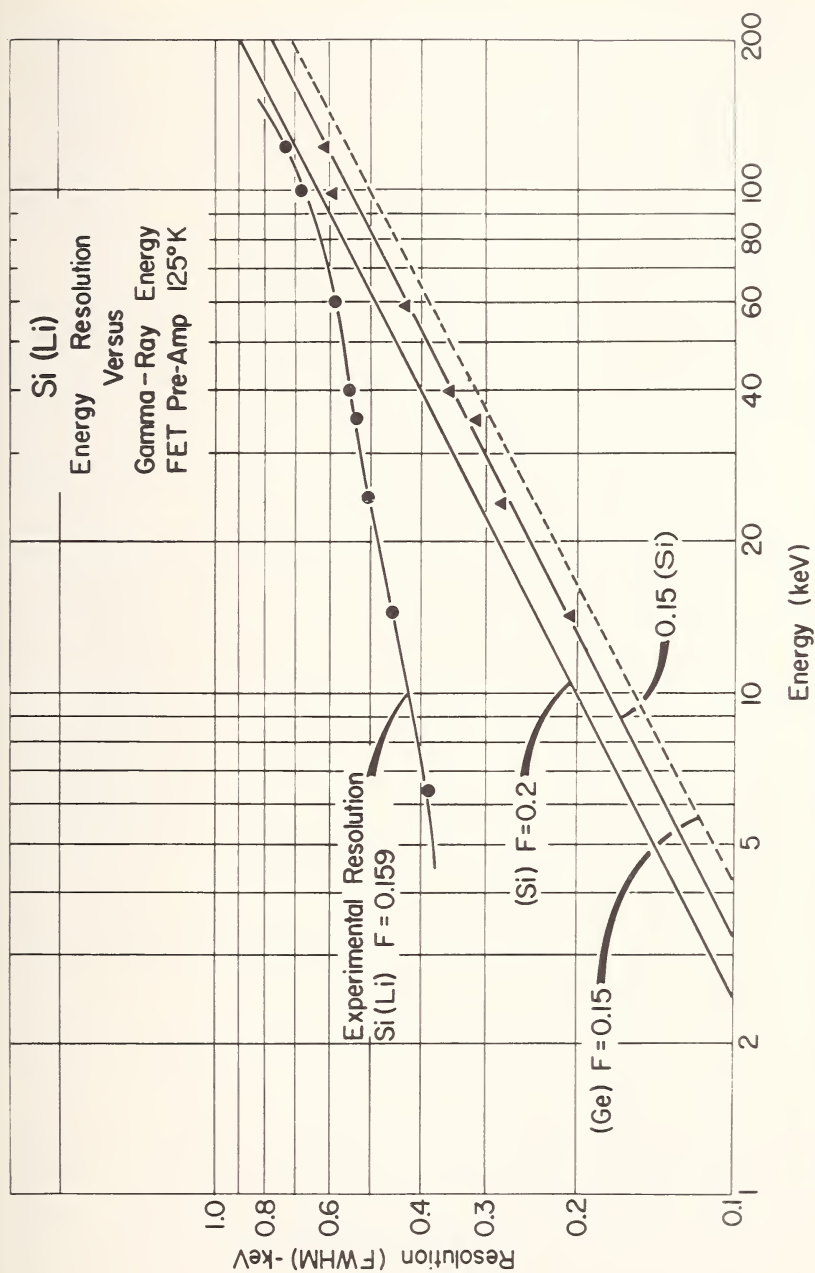
Figure 10. Resolution vs energy for Si(Li) system indicating experimental determination of the Fano factor for Si.

By far the most serious problem in present day devices is related to charge collection problems. Any phenomenon occurring within the detector sensitive volume which results in less than total charge collection within the resolving time of the pulse handling system, will produce a pulse whose amplitude is less than a true representation of the total energy lost within the intrinsic volume of the detector. The principle manifestation of such effects results in an asymmetrical peak shape such as shown in Figure 11. This plot shows the effect on the shape of a photoelectric peak as a function of bias voltage impressed across the diode detector. While this phenomenon is not completely understood, we can propose two major types of processes which contribute to peak "tailing" in semiconductor devices: (1) Regions of low field within the detector or other phenomena which extend the charge collection time to a point where it compares with the integration time constant of the amplifier shaping networks. In this case, complete integration of such an event does not occur and an "amplitude deficit" results. (2) Localized regions may exist within the intrinsic volume of the detector where charge "trapping" may occur. If the density of such regions is low, then only a small fraction of the total number of events occurring in the detector will produce less than total charge. In fact, a specialized case of extended charge collection time for events which lose energy near the junctions of P-I-N structures is the basis for rise-time rejection systems to eliminate unwanted pulses. This type of system will be discussed in detail in a later section. It is known that this effect is related to total depleted volume and applied field. For this reason it is necessary to operate most large volume devices at bias levels from 1500 to 3000 V. It should be mentioned that the magnitude of this effect (*i.e.* amount of asymmetry) is a function of gamma-ray energy. As will be pointed out in later sections, peak asymmetry may also result from deficiencies in the electronic system which degrade system performance as a function of counting rate. The most serious results of peak "tailing" are loss of resolution and a complicated functional form required to represent the peak shape. The latter greatly complicates the problem of analyzing pulse height spectra using curve fitting procedures.

Another important example of charge collection problems is found in the use of Si(Li) devices for high energy electron spectroscopy. Figure 12 presents data obtained by Prather and Cline of our laboratory on the resolution of Si(Li) detectors for electrons and x-rays as a function of detector operating temperature. Examination of these data indicates that the optimum operating temperature of these devices varies quite widely with temperature. While the nature of this phenomenon is not presently understood, it is assumed that charge collection problems in Si(Li) devices are involved. Fortunately, such effects are not considered to be important in Ge(Li) detectors.
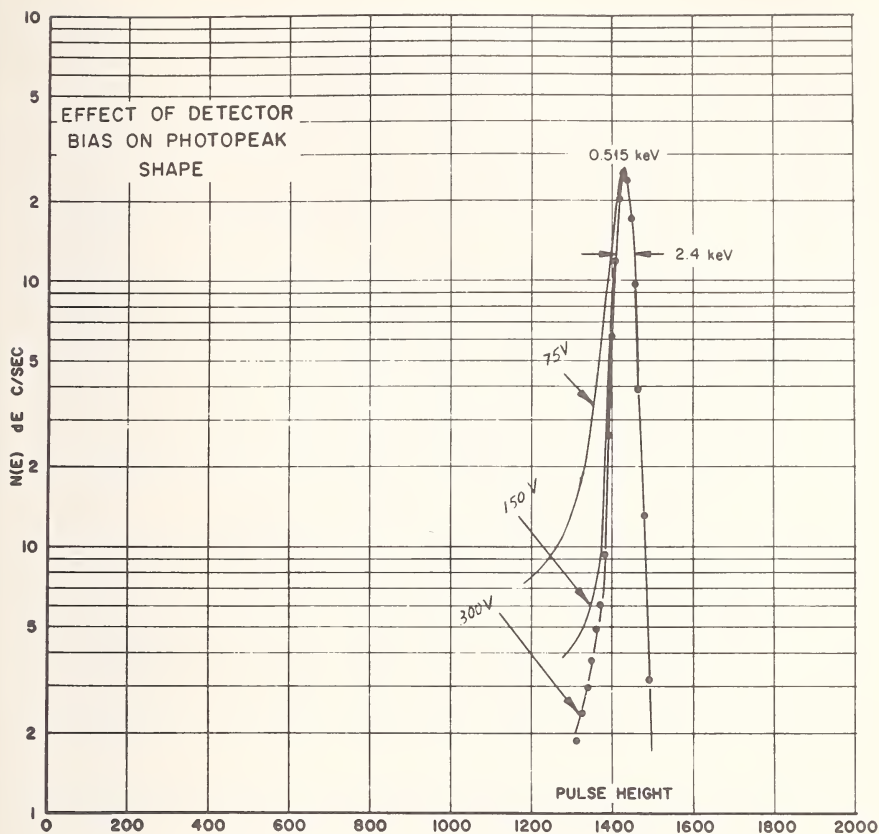
Figure 11. Effect of detector bias voltage on line shape of Ge(Li) spectrometer. This is used to illustrate the "tailing" phenomenon which is related to charge collection problems in these detectors.

C. Detector Response Verses Volume

Before we leave the discussion of inherent properties and limitations imposed by the detector devices, some attention should be given to the basic processes giving rise to the observed pulse height distribution. The information of major interest in a pulse height distribution is the energies and intensities of monoenergetic photons emitted from a source which have interacted within the sensitive volume of the detector by one of the three primary processes: (a) photoelectric, (b) Compton scattering, or (c) pair production. The sharp peaks in these spectra result primarily from single photoelectric or pair events or any multiple series of events arising from a single primary photon which result in total energy loss of that
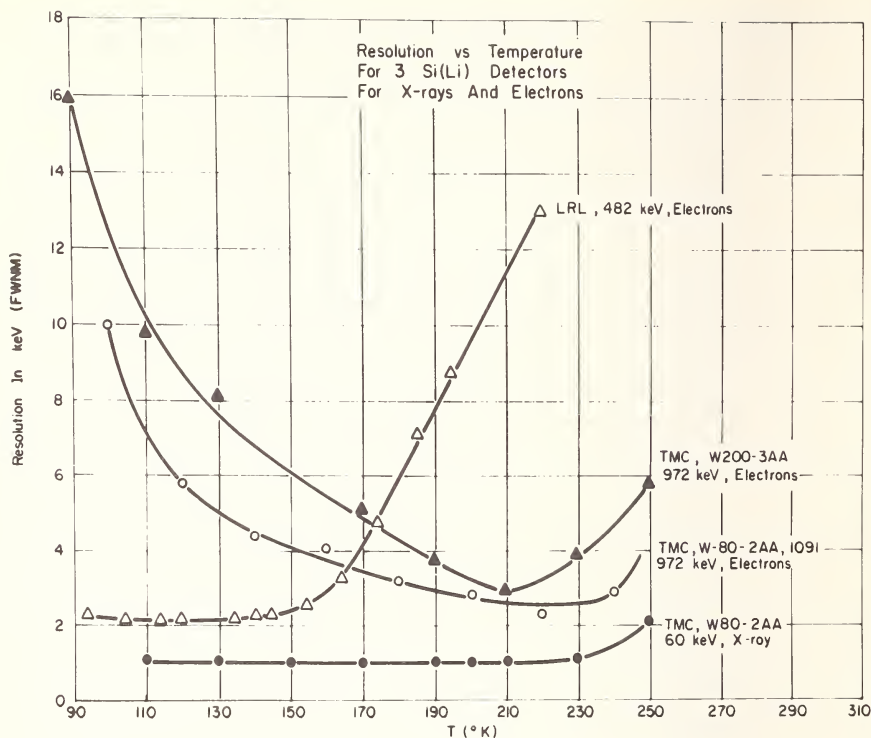
Figure 12.   A plot of resolution vs operating temperature for several Si(Li) detectors. The variation in performances of these devices is thought to result from charge collection problems due to "trapping" at low temperatures.

photon within the intrinsic volume of the detector. In very small devices it is to be expected that the probability for multiple events will be quite small, thus the efficiency of such detectors as a function of photon energy will be nearly proportional to the cross sections for primary interactions by one of the processes mentioned above. As the volume of the detector increases, the probability for multiple processes (*e.g.* a Compton event followed by photoelectric interaction of the scattered photon) will increase. From an experimental point of view, the information of interest (*i.e.* energy and intensity) is contained in the sharp peaks superimposed on a continuum. Thus a description of the performance of a spectrometer might be termed a signal-to-noise problem. In describing the response of NaI(Tl) scintillation spectrometers to monoenergetic radiation, a term was used which was called the peak-to-total ratio, which was defined as the ratio of the number of events in the full-energy peak to the number of events in the entire pulse height distribution which resulted from interactions of primary gamma rays emitted by a source. This ratio may be used to give a measure of the information content in a pulse height

distribution. An additional "figure of merit" which can be useful in the evaluation of detector performance may be obtained by dividing the peak-to-total ratio by the detector resolution to provide a means of including the inherent improvement in signal-to-background from improved instrumental resolution. Table 2 [30] presents a comparison of some of these quantities for a number of detectors. Data are presented for resolution, peak-to-total ratio and the figure of merit for 661 keV gamma rays using both cryogenic and room-temperature preamplifiers. It is interesting to compare, for example, the values for the figure of merit for a small high resolution detector employing a cryogenic preamplifier (3.5) with that of a large 35 cm³ coaxial device using a room-temperature

Table 2. Table of peak/total ratios, energy resolution (FWHM) and (peak/total)/(FWHM) at 662 keV for a number of detectors.

Detector	Detector capacitance pf	Peak/total ratio ($\times 10^{-2}$) ^{137}Cs	Resolution (FWHM) (keV)[a]		(Peak/total)/(FWHM) ($\times 10^{-2}$)	
			Cooled P.A. ^{137}Cs	Room temp P.A. ^{137}Cs	Cooled P.A. ^{137}Cs	Room temp P.A. ^{137}Cs
2.5 cm²×8 mm (2.0 cc)	4.4	4.9	1.41	1.73	3.5	2.8
4.9 cm²×4 mm (2.0 cc)	17.2	3.3	1.58	1.98	2.1	1.7
4.9 cm² × 8 mm (3.9 cc)	8.6	4.3	1.48	1.81	2.9	2.4
6.4 cm² × 8 mm (5.1 cc)	11.3	5.3	1.53	1.88	3.5	2.8
10.2 cm² × 8 mm (8.2 cc)	18.0	5.7	1.59	2.00	3.6	2.8
6.6 cm²×12 mm (7.9 cc)	7.8	7.1	1.46	1.80	4.9	3.9
3–cm long, 2.6–cm diam, ~8.5–mm drift open–ended coax (12 cc)	~ 30	8.3	1.72	2.21	4.8	3.7
2.8–cm long, 4–cm diam, 12–mm, 5–sided drift, coax (~35 cc)	~ 20	9.1	1.61	2.04	5.6	4.5

[a] Resolution as calculated using data presented in paper by K. F. Smith et al., IEEE Transactions on Nuclear Science, Volume NS–13, No. 3, 468 (1966). The assumptions were made that the Fano factor for Ge is 0.15 and that internal preamplifiers have an additional 3 pf and external preamplifiers have an additional 10 pf stray capacitance due to the detector lead wire.

preamplifier (4.5). Thus, we note the relationship between resolution and peak-to-total ratio.

As a practical illustration of the differences in the basis response of detectors as a function of sensitive volume, let us observe Figure 13. In this figure we have plotted the spectra of gamma rays emitted in the decay of 1.4 h ^{142}La, which exhibits a large number of transitions ranging up to 3.8 MeV, obtained with a 2.5 cm^2 × 8 mm detector employing a cryogenic preamplifier and a large 35 cm^3 coaxial detector using a room temperature preamplifier. The resolution of these two systems at 100 keV was 750 eV and 1.7 keV (FWHM), respectively. The most obvious difference between the two spectra is the increased sensitivity of the large volume device to high energy gamma rays. More important to an understanding of the effects of a larger volume is to examine the ratio of double escape pair peaks to the full energy peaks. For example, observe the triplet structure at about 1350 keV. We see that the intensity ratio of these three peaks has been drastically altered. The double escape peak of the 2397.7 keV gamma ray which was the most prominent of the triplet in the small device has been considerably reduced in intensity in the larger detector. In contrast, the full energy peak for this gamma ray has been enhanced. This results from the large increase in the probability for multiple events in the larger volume detector. In this case, the two annihilation quanta emitted in the pair process have an appreciable probability of interacting with total energy loss within the sensitive volume of the larger device.

III. Electronic Systems

A. Low Noise Preamplifiers

As previously indicated, if we assume that all of the charge produced in the intrinsic volume of the detector is collected, the basic limitation on energy resolution may be attributed to the statistical fluctuations discussed above. As indicated in the two figures just described, the practical limit in the low energy region results from electrical noise sources in the amplifier systems, while at higher energies the limit is imposed by other deficiences in the pulse-amplitude measurement system. The low noise amplifier systems employed with these detectors basically consist of a charge-sensitive preamplifier and a linear pulse amplifier which incorporates a frequency selective filter (pulse shaping network) which selects a frequency bandpass for optimum signal-to-noise ratio. Perhaps the most important development in the area of electronic circuitry which has contributed to high resolution gamma-ray spectrometry has been the application of the field-effect transistor (FET)
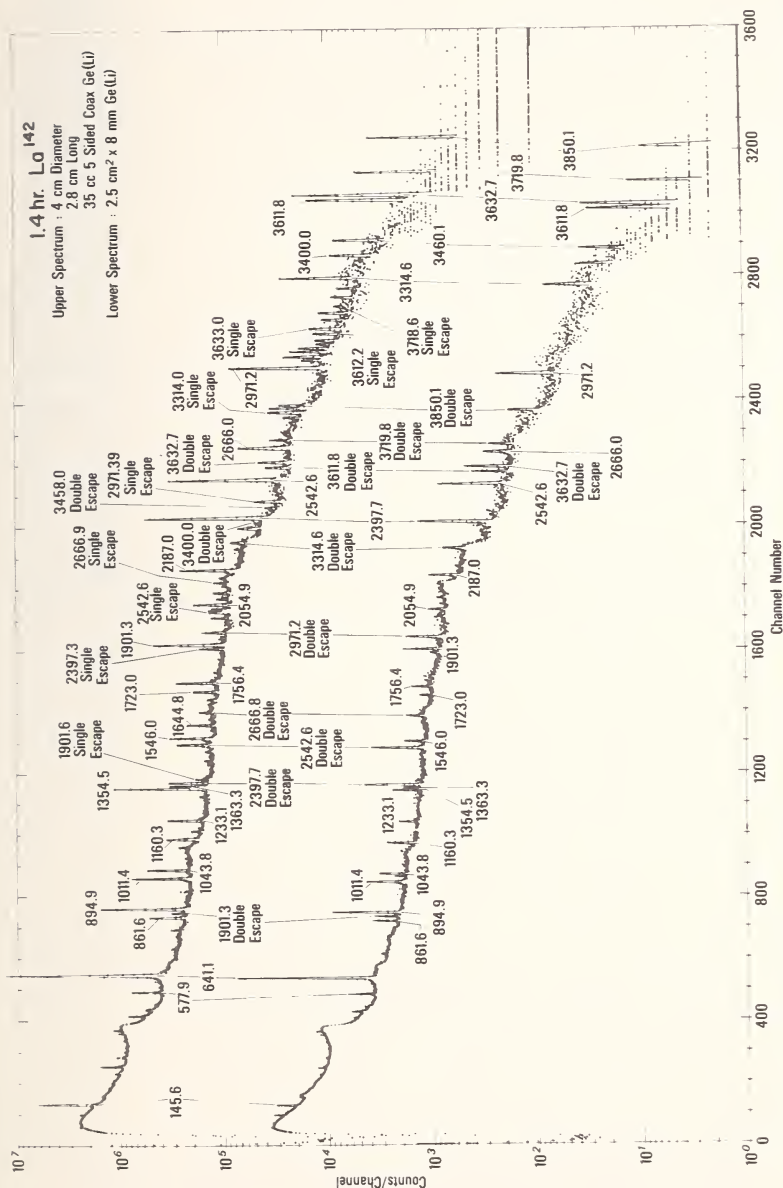
Figure 13. Gamma-ray spectra of ^{142}La. Upper spectrum was obtained with a large (35 cm^3) five-sided coaxial detector. The lower spectrum was obtained using a 2.5 cm^2 × 8 mm planar detector. The major effect observed is the large increase in efficiency for high-energy gamma rays.

as the input amplifying element in low noise preamplifiers. Although a detailed treatment of the design criteria for low noise amplifiers is beyond the scope of this summary, it is felt that the important characteristics of the preamplifier should be discussed. In 1965 Nybakken [11], Elad [12], and Radeka [13] demonstrated the superiority of the FET over vacuum tubes for low noise applications. An improved preamplifier was reported by Smith and Cline [14] which utilized paralleled FETs operated at 130 °K to obtain the performance illustrated in the experimental spectra shown in the preceding figures. A schematic of this preamplifier is shown in Figure 14. This preamplifier employs type 2N 3823 FETs as the first and second stages of a charge-sensitive feedback loop. The feedback capacitor used has a value of 0.5 pF. Paralleling of FETs is possible in this configuration to achieve improved noise performance with high capacity large volume detectors. Figure 15 illustrates the performance of this preamplifer as a function of FET operating temperature for one FET and four (4) paralleled FETs in the first stage. As indicated, the best noise performance was obtained at a case temperature of 140 °K. At this temperature the g_m of the devices increases by a factor of 2.5 producing a considerable improvement in the noise performance for large input capacity.

To the experimenter the most important parameter influencing the noise performance of an FET preamplifier is the magnitude of the
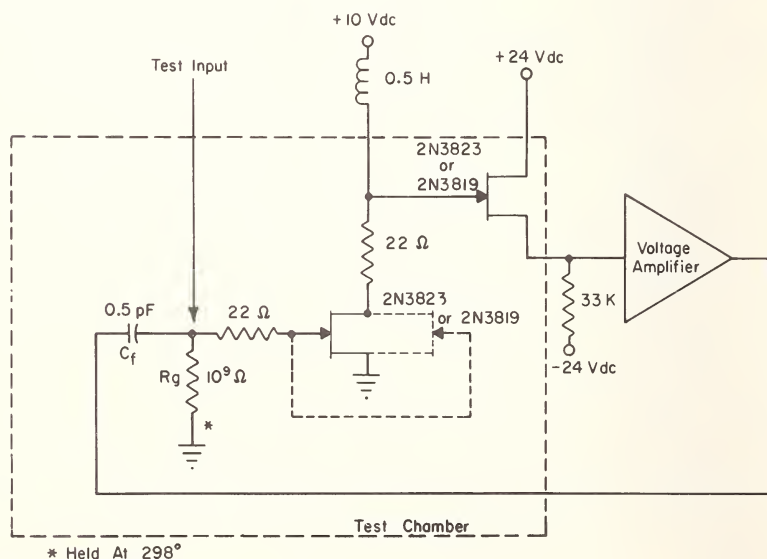
Figure 14. Schematic diagram of cryogenic FET preamplifier used with Ge(Li) spectrometers.
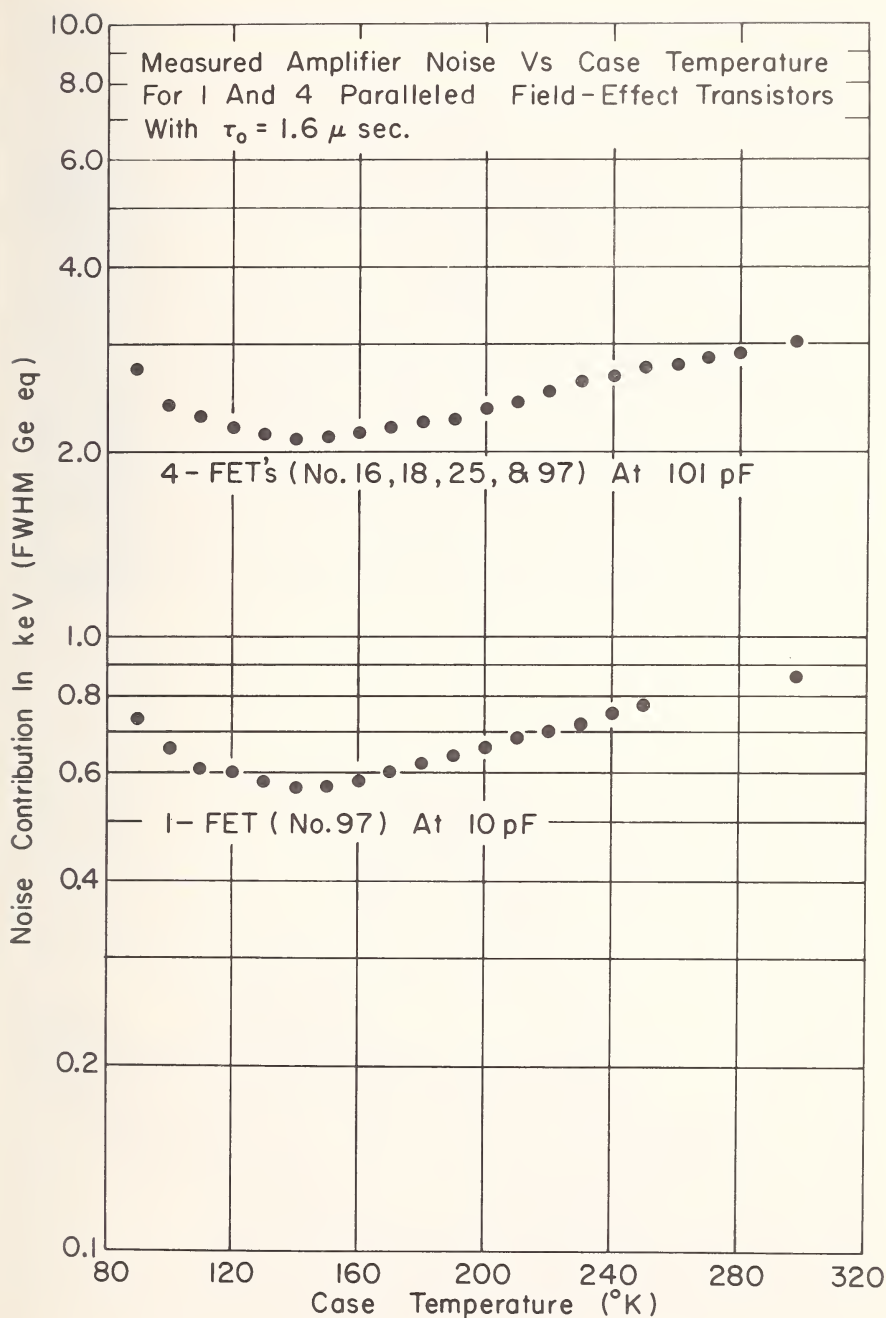
Figure 15.   Measured amplifier noise vs FET case temperature for 1 and 4 paralleled field-effect transistors employed in cryogenic preamplifier.

external capacitance represented by the detector placed across the input of the preamplifier input stage. Figure 16 shows a plot of the noise contribution of the preamplifier versus total capacitance at single RC integrating and differentiating time constants of 1.6 microseconds. Note that each of the curves starts at $C_T = nC_\sigma$, the minumum theoretical total capacitance. In practice this starting point is impossible to achieve because of stray capacity to ground introduced by the addition of the gate resistor, R, and the feedback capacitor, C_f.

In normal operation, the front section of the preamplifier is built into a liquid nitrogen cooled cryostat as shown in Figure 17. This figure shows the components of the preamplifier first stages in an exploded view. All components are mounted coaxially around a copper rod which is immersed in a container of liquid nitrogen. The detector is mounted on the end of the rod and covered by the white Teflon cap which is shown at the extreme right. A completed cryostat with detector and cryogenic preamplifer is shown in Figure 18. The FET is maintained at the optimum operating temperature (140 °K) by means of a heat leak to the outer wall of the vacuum chamber. The completed assembly is evacuated and the vacuum maintained by cryogenic pumping with molecular sieve.
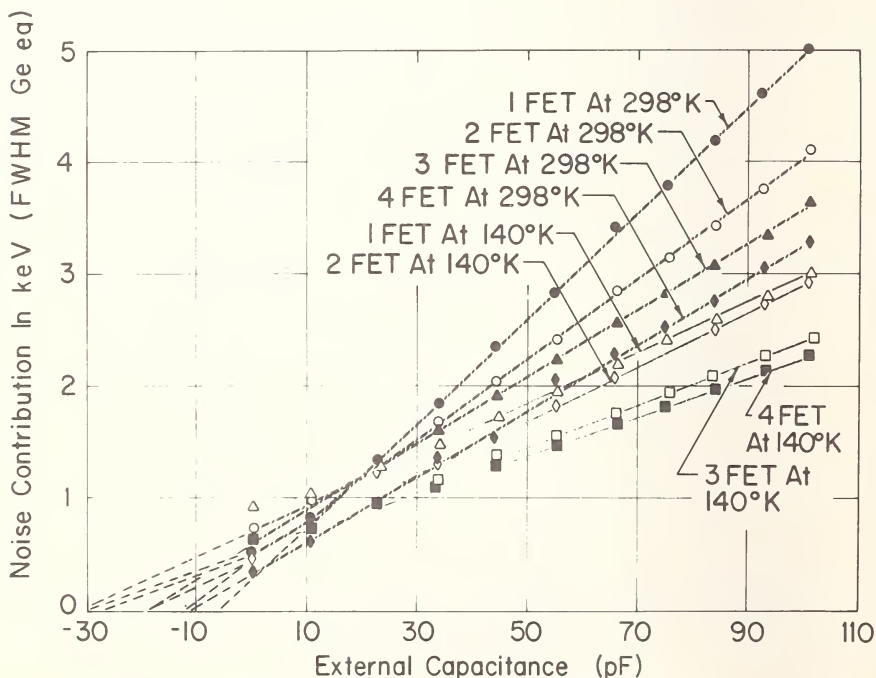
Figure 16.   Measured amplifier noise vs external capacitance for 1, 2, 3 and 4 paralleled field-effect transistors at 298 and 140 °K.
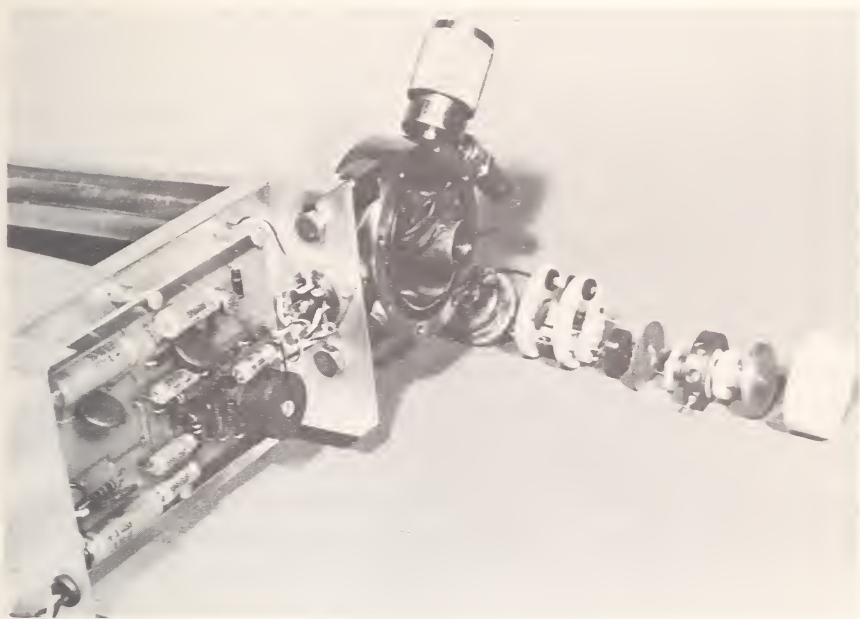
Figure 17. Exploded view of preamplifier assembly in cryostat. Cleanliness and mechanical rigidity are of utmost importance to low noise performance of these systems.

Figure 18. View of assembled cryogenic FET preamplifier with lithium-ion drifted detector mounted.

In the use of cryogenic preamplifiers, the inherent low noise characteristics of these systems impose stringent requirements on mechanical design. Considerable attention must be given to the mounting of all components to prevent mechanical movement or stress on electrical connections. The two major sources of noise input which are microphonic in nature are (1) modulation of the noise level due to changes in input capacity (major source-detector-FET lead wire) or piezoelectric effects in the detector devices, and (2) signal injection which is predominantly low frequency in character. This latter noise source may be component related. This requires careful selection of resistors and capacitors for low temperature operation.

One further comment should be made relative to the detector-preamplifier arrangement. There is some advantage to be gained if one uses DC rather than AC coupling of the detector to the preamplifier input. In the AC connection, there exist two factors which result in reduced signal-to-noise ratio: (a) an additional stray capacitance to ground caused by the distributed capacitance to ground, and (b) a division of the input signal between C_c and the input capacitance of the FET. Both of these problems result in a degradation in the resolution, particularly for low capacity detectors. Both can be eliminated in the DC arrangement.

B. Amplifier

The major requirement of an amplifier for use with germanium detectors. is that a choice of proper shaping networks are included to achieve the best signal-to-noise ratio. This subject has been discussed in detail by Goulding [4] and by Fairstein and Hahn [15]. Additional design criteria of importance are overshoot as related to pile-up problems, amplifier gain stability, and amplifier noise as related to the noise level at the output of the preamplifier. To meet the requirements for a spectrometer system which incorporates a cooled FET preamplifier and a 4096 channel ADC, a linear pulse amplifier must have the following minimum specifications:

Noise — noise should be less than 1 microvolt rms when referred to the amplifier input (for 1.6 microsecond shaping time constants — singly differentiated).

Gain stability — amplifier gain stability should be better than 1 part in $10^5/°C$ (0.001%). This requirement would produce no observable broadening in a 10 MeV photopeak measured under ambient laboratory conditions.

Amplifier gain — 1000 (max.)

C. Analog-to-Digital Converter

The analog-to-digital converter is by far the most important element of any pulse height analysis system. When one considers that a minimum of

4096 channels are required to utilize the resolution obtainable with Ge(Li) devices, the requirements for precision and stability in ADCs is exceedingly stringent. Most current 12 and 13 bit ADCs operate over a pulse amplitude range of from zero to 10 volts, with many ramps operating over a range of 5 volts or less. The digitizing rates in current models range from 20 to 100 megacycles. This requires that rise times of all logic signals involved in the start and stop of the time-conversion process be quite fast. In order to achieve the performance required for high resolution pulse height spectrometry, the criteria of interest in defining ADC performance characteristics are differential and integral linearity, zero and ramp stability, and the precision of the window edges which we choose to describe by the concept of the window profile [16]. If we are to achieve the levels of precision required, it is necessary to be able to measure these quantities using specialized techniques. For this reason considerable effort has been expended at our laboratory to develop techniques for the calibration and study of the operating characteristics of pulse height analysis systems. The technique presently in use [17, 18] is based upon the use of a digital processor incorporating a computer-controlled pulse generator. A schematic representation of this system is shown in Figure 19. The analog-to-digital converter under study is interfaced to a PDP-8 computer. The digital processor is equipped with a teletypewriter, oscilloscope display, and a 17 bit relay-operated voltage divider. The 17 bit relay tree makes it possible to dial a voltage level with 17 bit accuracy under control of a computer program. The resulting voltage, derived from a stable reference supply, is impressed on the charging capacitor of a conventional mercury-relay pulse generator. As
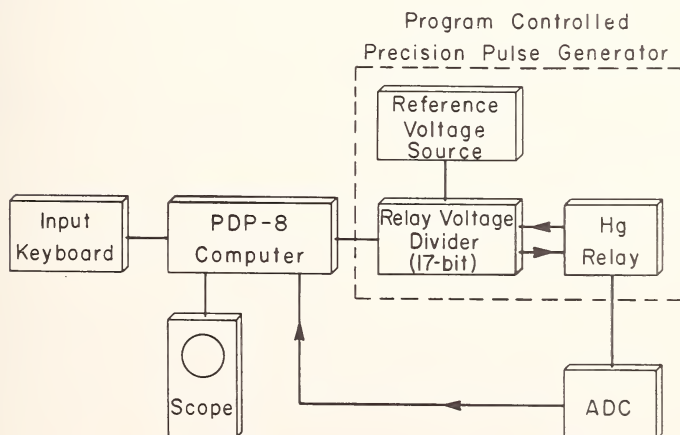
Figure 19.   Block diagram of computer system used to measure linearity and stability of high resolution amplifier-ADC systems.

shown in Figure 20, a DC amplifier is used to isolate the voltage divider from the charging capacitor to insure that the charging time constant does not affect the linearity of the pulse generator. The relay-operated divider used was obtained from Jouli and has a quoted specification of ± 5 parts per million over a temperature range of ± 5 °C from ambient. The reference supply is 10 volts. The settling time is of the order of several milliseconds. Relays have mercury-wetted contacts.

Experience with these precision dividers has indicated that thermal EMF problems are a major contributor to instability. It has been necessary to use special relays which minimize thermal EMF problems through careful use of materials in contact structures. Special solder must also be used in all connections within the divider. With these special precautions it has been possible to achieve long-term stabilities in these pulser systems of a few parts per million over a normal laboratory ambient temperature range.

The details of the procedure used to measure the integral linearity and stability of a system using a computer controlled pulse generator are described in detail in reference [19]; however, we will briefly describe the procedure that is used. Figure 21 will serve to define integral linearity. To measure integral nonlinearity for a system, two pulser amplitudes P_3 and P_4 are made to correspond to two channel locations C_3 and C_4 by adjustment of the ADC zero bias level. To define channel position with sufficient accuracy, these channel positions correspond to a channel boundary. The coordinates P_3,C_3 and P_4,C_4 then define the zero intercept and slope for the channel number *vs* pulse amplitude scale. Any deviation from linearity will then be represented by points falling off the straight line. For the purpose of such measurements we arbitrarily define the two tie points to be about 1/4 and 3/4 of full scale on the ADC. The computer

Computer Controlled Pulser
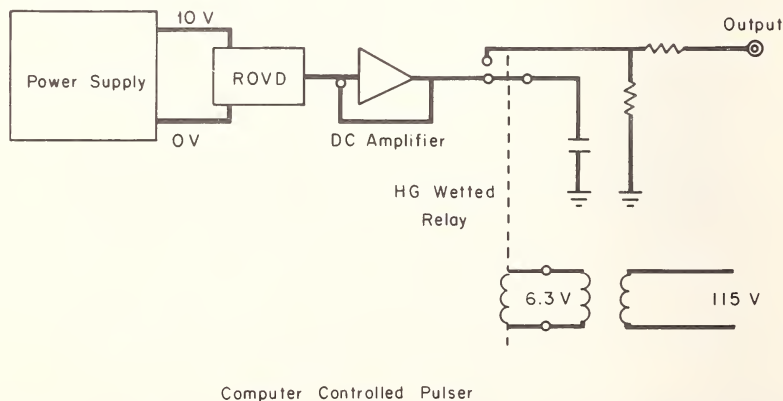
Figure 20.   Schematic diagram of computer-controlled pulse generator.
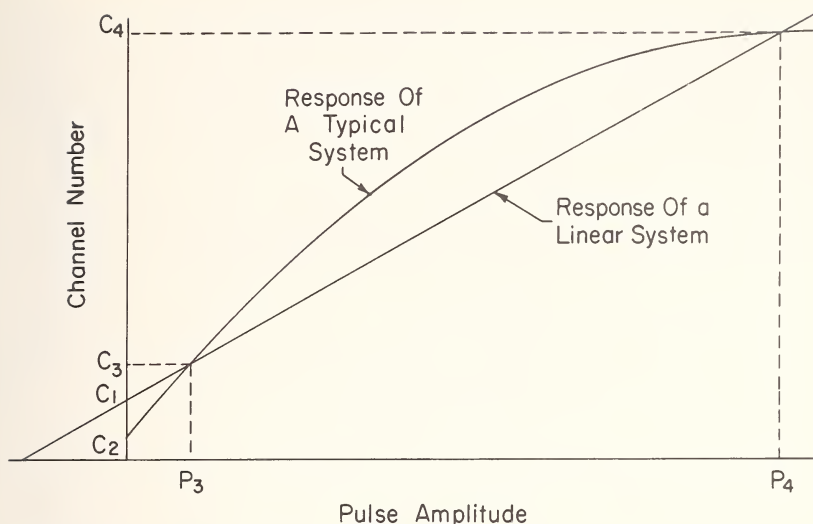
Figure 21. Convention used to define integral linearity of pulse-height analysis systems.

program controlling the amplitude of the pulse generator then adjusts the amplitude until *equal numbers of pulses* are stored in *the two adjacent channels* which represent the high tie point. By reference to a channel edge, it is possible to define a point on the channel number scale to ± 0.05 channel. This adjustment is made by first calculating an approximate slope to get a conversion factor between channel number and the 17 bit scale of the relay operated voltage divider. The amplitude is then adjusted in an iterative fashion with decreasing values of voltage change as the desired amplitude is approached. Once this condition is fulfilled, the channel boundary corresponding to the lower tie point is found and the two amplitudes used to calculate an effective slope and zero intercept for the system. To check for possible drift in the system, each determination of slope and intercept is followed by a check of the upper tie point. If the observed drift is less than a preset value (normally 0.1 channel for a 12 bit ADC) the measurement is accepted. Once the slope and intercept have been determined, the amplitude corresponding to a preselected channel boundary is then determined, and the high tie point again checked for drift. If drift has occurred, a new slope and intercept are measured and the point checked again. If no drift has occurred, the pulse amplitude corresponding to the desired channel boundary is stored by the computer. This procedure is then repeated for a number of points over the range of the ADC and the deviation of each measured point from true linearity is computed and a correction curve typed out on the teletype. To illustrate the precision that may be achieved with this technique, Figure 22 shows the results of a linearity measurement made on an exceptional 12 bit

ADC. Examination of these data indicates that the maximum deviation in integral linearity for this ADC does not exceed $\pm$ 0.2 channel over a major portion of the channel range. If a number of repeated runs are made on the same ADC, the deviation from the mean for a given point is estimated to be $\pm$ 0.05 channel.
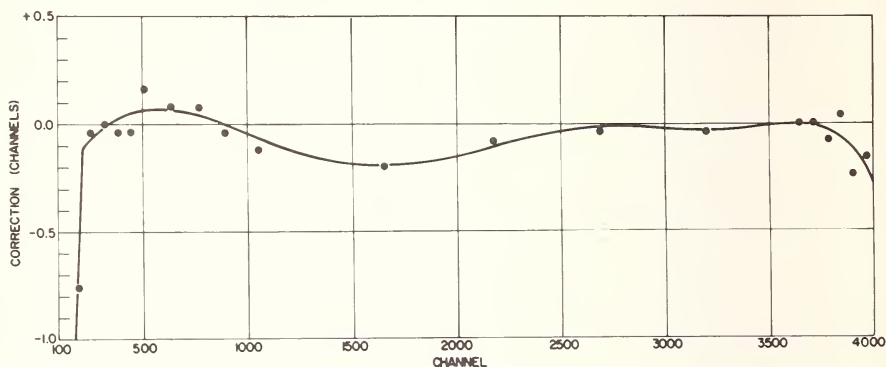
Figure 22.   Measured integral linearity of 4096 channel laboratory system.

It might be well at this point to stress that the magnitude of the deviation from linearity is not nearly as important as its reproducibility. The limiting factor being the accuracy with which the linearity curve can be determined. Using the computer system to measure integral linearity makes it possible to achieve a level of precision, independent of system drift, which could not be achieved using manual techniques. Normally, a complete linearity curve may be determined (average of five or more complete runs) in several hours with no operator attention required.

The computer controlled pulse generator can also be used to determine system stability by measuring the drift in ADC zero and slope as a function of time, temperature, etc. Results obtained for measurements on two commercial ADCs are shown in Figures 23 and 24. In these measurements the pulser was fed into the input of the preamplifier and the system gain and zero intercept measured as a function of time. These systems were being operated in a temperature controlled environment so that temperature drift would be minimized. In each figure, deviation in system gain in units of parts per 10^5 and shift in zero (channels) are plotted against time. The results shown in Figure 23 are those for the ADC system referred to in Figure 22. The gain of the system is seen to vary more or less randomly, with average excursions of 5 parts in 10^5. The zero was observed to vary by less than 0.2 channels, with rather discontinuous jumps observed. A number of ADCs have been observed
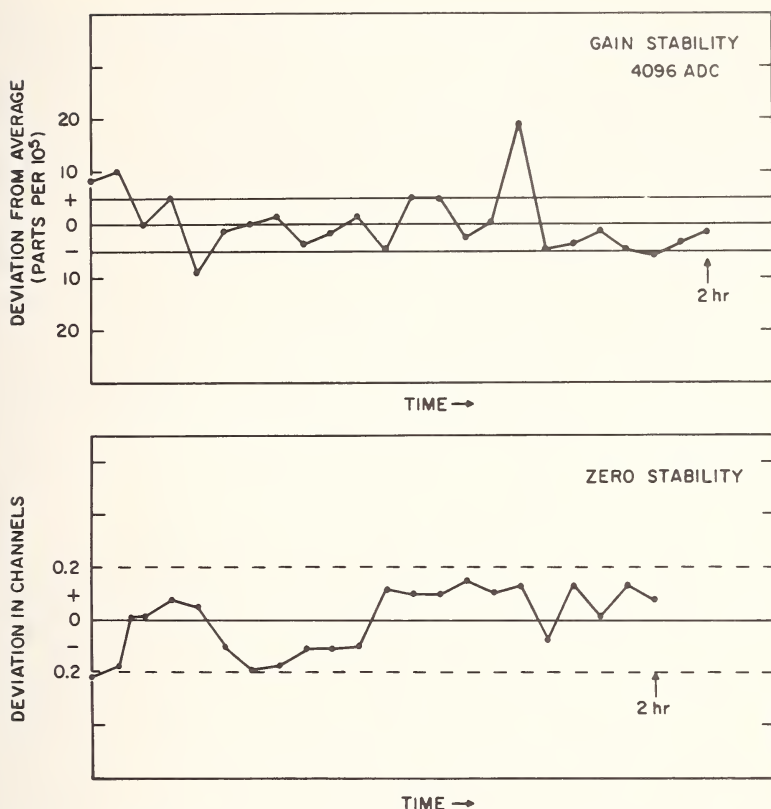
Figure 23. Measurement of zero and gain stability of 4096 channel system — "good" ADC.

to exhibit this phenomenon, which has been successfully reduced by heat-sinking critical elements in the ADC circuitry.

In Figure 24 we see results obtained from a more typical ADC. Over a period of 4 hours, the gain is observed to vary more or less in a random fashion with a gradual drift downward. The envelope would indicate a short-term drift of the order to 20 to 30 parts in 10^5. The zero is also varying considerably more than was indicated for the previous ADC, indicating excursions as high as one channel. Such a system would require digital stabilization for many applications. These data are presented to indicate the order of stability to be expected with currently available ADCs. To achieve the inherent capabilities of a Ge(Li) system, one would hope for stability in gain and zero of the order of 1 to 2 parts in 10^5.

Before we leave the subject of measuring system stability and linearity several points should be made. The basic assumption that must be made in this method is that the pulse generator is a resonable substitute for a
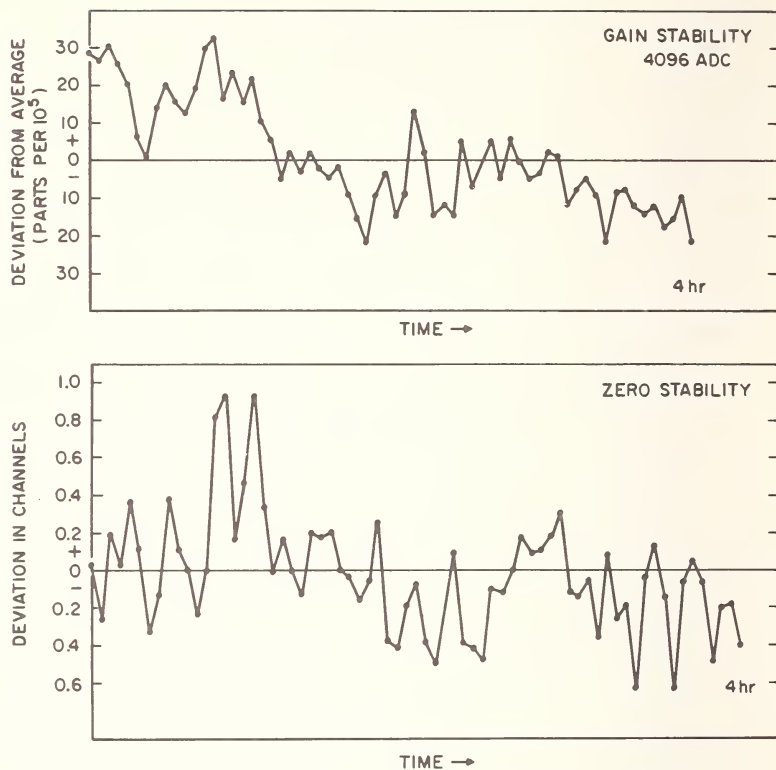
Figure 24. Measurement of zero and gain stability of 4096 channel system—"typical" performance.

detector. The second point is that all elements of the system may contribute to the observed linearity and stability. We have made an attempt to isolate observed effects in preamplifiers, amplifiers, and ADCs. With the limited data available at this point it is felt that well designed linear amplifiers (*e.g.* TC-200) and FET preamplifiers do not represent the major source of nonlinearity and system drift. As shown in Figures 23 and 24, zero drift is the major stability problem in the ADCs when operated in a temperature controlled laboratory environment. It should be stressed that all of the data presented were obtained with no digital gain stabilization. We have observed slight changes in linearity with changes in amplifier gain, pulse polarity, and shaping time constant.

A measure of the precision of an ADC may be obtained by the determination of the "sharpness" of the channel edges. The presence of abnormal jitter in the decision process due to digital noise or other problems inherent in the pulse height-to-time conversion method may

introduce appreciable degradation in the quality of a pulse amplitude spectrum. To obtain a measure of the accuracy of a ADC in this respect the computer controlled pulse generator may also be employed. In such a measurement the computer controlled pulser is programmed to make a measurement of pulse amplitude distributions by successively increasing the pulser amplitude in increments of 0.1 channel. A plot of these data will then provide an indication of the "shape" of successive channels and the degree of overlap between adjacent channels. The results of such a measurement for a 4096 channel ADC are shown in Figure 25. In such a representation, the channel width is defined by the cross-over point at 50% of peak amplitude. For a good system, essentially 100% of the counts will lie in one channel over 50% of the width of that channel. It should be stressed that the data shown in this figure were obtained by inserting the pulser output into the input of the pulse amplifier, thus, these results indicate true instrumental resolution.

D. DIGITAL STABILIZATION

As was previously mentioned, the stability of gain and zero in a pulse amplitude analysis system is most important to satisfactory performance of high resolution systems. The performance of the system described above was obtained under controlled laboratory conditions with the ambient temperature normally controlled to within $\pm$ 2 °C. Under these conditions, temperature drifts in electronic components, reference voltages, etc., are minimized. When equipment is to be operated under less stringent levels of environmental control, or when experimental limitations require exceptionally long measurement times, some means of gain and zero stabilization is in order. Most commercial analyzers are now available with electronic accessories which provide for some measure of control over these variables. The most successful of these, the digital stabilizer, is illustrated in concept by Figure 26. The digital stabilizer employs the principle of servo-control to stablize the effective zero and/or ramp slope of the analyzer system. In using such a system the error signal for control is derived by stabilizing the position of a peak in the pulse height spectrum. This is accomplished in the following manner: observing the illustration in the upper portion of the figure, a peak in an experimental spectrum is represented. Two "digital windows" are established on the lower and upper sides of the control peak bounded in this illustration by channels n through m, designated as digital window 1, and m + 1 through o, designated as digital window 2. The channel boundaries of these digital windows are selectable by diode restriction gates connected to the address register of the ADC. In this manner, all pulses which fall into channels bounded by the lower digital window are fed to an up-down scaler in an additive mode (*i.e.* these pulses will add to the current total in the scaler). In a like manner all pulses falling in the
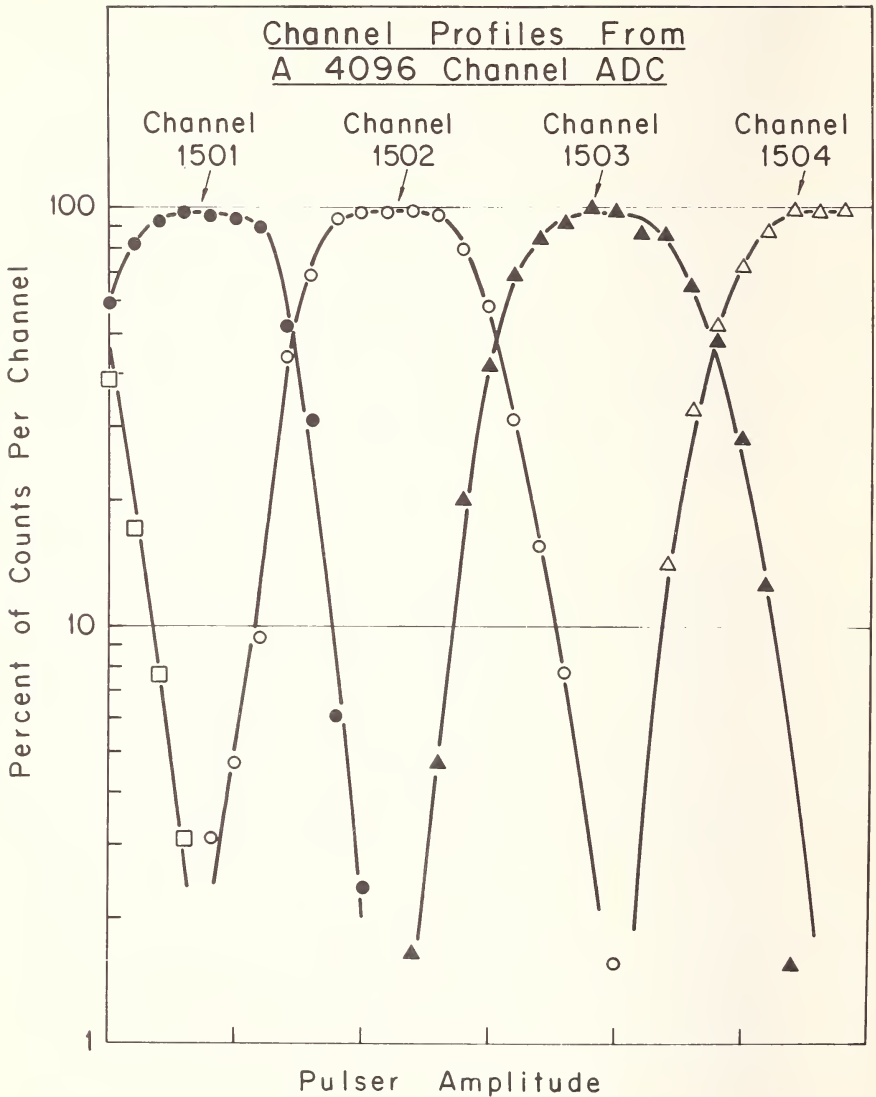
Figure 25.   Channel profile for 4096 channel ADC to illustrate stability of 12-bit ADC.

channels bounded by the upper window will subtract from the total in the up-down scaler. Thus the total (plus or minus) in the scaler at any time provides a digital value which is a measure of the shift in peak position, or the required correction. This digital value is then converted to an analog error signal by one of a number of schemes and this is in turn applied to the zero reference or ramp slope circuitry to correct for the observed shift in peak position. Such systems are moderately successful under adverse
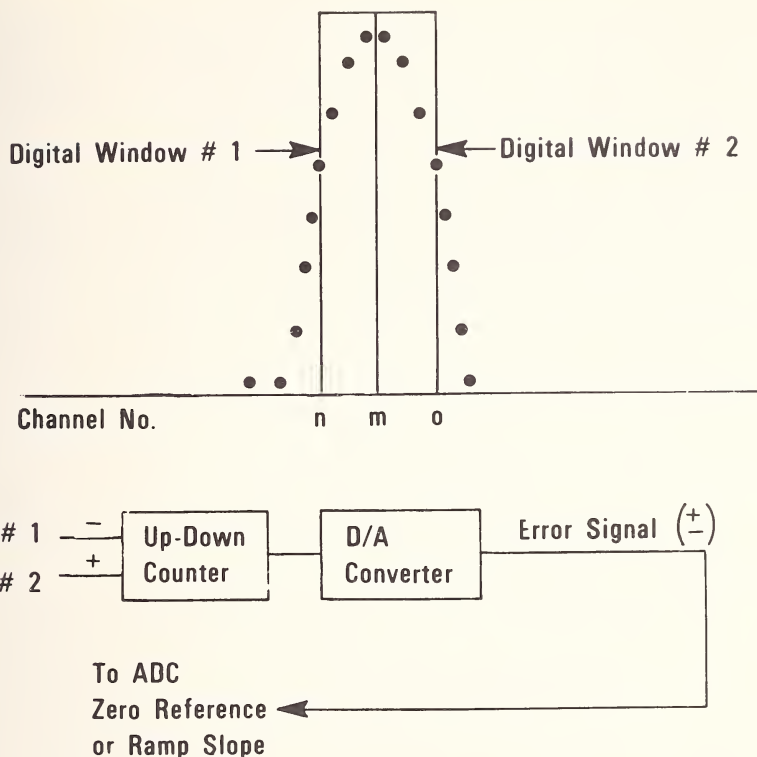
DIGITAL STABILIZER

Figure 26. Illustration of the concept of digital stabilization of gain and zero of pulse analyzer systems.

conditions and will provide control to ±0.1%. Difficulties encountered in the use of such systems include the requirement that a suitable peak exist in the spectrum for control, statistical considerations at low counting rates, and some deterioration in system resolution as a result of the normal overshoot in the servo principle.

E. PROBLEMS AT HIGH COUNTING RATES

In the use of high resolution spectrometers, experimental conditions are frequently far from ideal for optimum performance of the electronic systems employed. Perhaps the most difficult class of problems are those which result when high counting rates are encountered. Without the use of special precautions, operation at high counting rates will result in serious shifts of zero and system gain and degradation of resolution. Most

of these observed effects are the result of fluctuations in the zero reference baseline at the input of the analog-to-digital converter, produced by random fluctuations. To provide some insight into these effects and the nature of the specialized circuitry employed to correct these problems, let us examine part (a) of Figure 27. To achieve optimum signal-to-noise ratio in high resolution systems, a monopolar pulse shape with RC equal integration and differentiation time constants is generally employed [15]. As indicated in Figure 27(a) the output pulse shape from such a filter network will exhibit a more-or-less Gaussian shape with equal rise and fall times. Following the pulse there will be a negative undershoot with a long recovery time constant (generally several hundred microseconds). At low counting rates, the pulse will have returned to the original baseline and will have no influence on succeeding events. If, however, at high rates, another pulse (indicated by the dotted line) occurs, the negative tail of the preceding pulse will result in a reduced amplitude measurement by the ADC. At reasonable rates (a few thousand pulses per second) the net effect of this will be an asymmetry of peaks as indicated at the far right of the figure.

A circuit technique, first proposed by Knowlin and Blankenship [19], which has been termed "pole-zero cancellation", has been developed which quite effectively reduces the undershoot from a monopolar pulse. The net effect of pole-zero cancellation is shown in Figure 27(b). Here we see that the undershoot returns quickly to the original baseline, thus pulses following will be unaffected. It should be pointed out that pole-zero cancellation must be accomplished on the complete preamplifier-amplifier system to be effective. The use of such networks in low noise amplifier systems is now quite common, and if adjusted properly in combination with a given detector, will provide considerable reduction in spectrum degradation from undershoot at moderate counting rates.

At high counting rates (in excess of 5000 counts/sec), we still have problems from fluctuations in the baseline as shown in Figure 27(c). In this figure, we have reduced the time scale to show the long-term character of the baseline shift. As a result of residual charge on coupling capacitors within the AC coupled amplifier system, the baseline will vary in a random manner producing a net negative shift in the zero reference and a general broadening of peaks in the spectrum as indicated on the right side of the figure. This effect can be reduced by the use of DC baseline restoring circuitry. The schematic diagram of a simple DC restorer developed by Robinson [20] is illustrated in Figure 28. Other, more sophisticated circuits have been described by Chase and Poulo [21] and Gere and Miller [22]. The action of these circuits is to remove the random fluctuations in the zero reference level by means of the diode arrangement shown in Figure 28. It should be stated that the input time constant on the restorer must be optimized for best performance at high
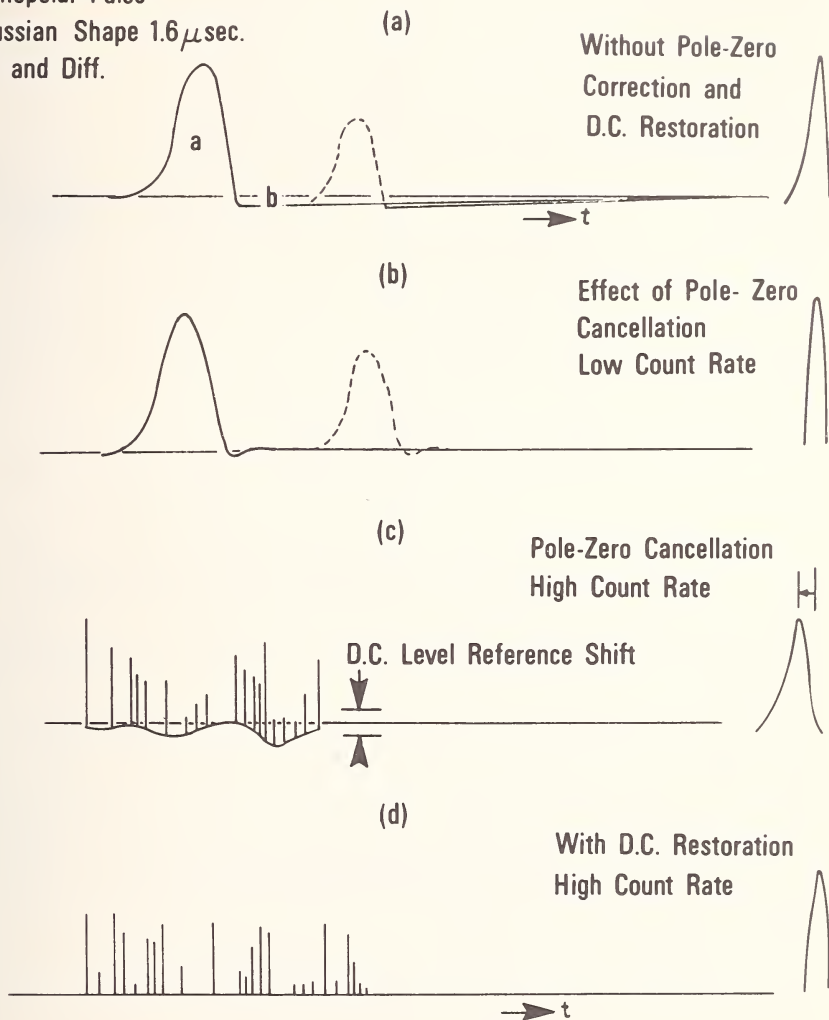
Monopolar Pulse
Gaussian Shape 1.6 μ sec.
Int. and Diff.

(a)

Without Pole-Zero
Correction and
D.C. Restoration

a

b

t

(b)

Effect of Pole- Zero
Cancellation
Low Count Rate

(c)

Pole-Zero Cancellation
High Count Rate

D.C. Level Reference Shift

(d)

With D.C. Restoration
High Count Rate

t

Figure 27. This figure presents the nature of the problems which result in distortion of peaks as a function of input signal rate (a) system without pole-zero cancellation and D.C. restoration, (b) system with pole-zero cancellation networks in amplifier at low input rate, (c) system at high count rate with no D.C. restoration, and (d) system at high input rates with both pole-zero and D.C. restorer circuits optimized.

rates. The net effect of this will be that the restorer will restore on noise and a small loss in resolution at low rates will result. The most recent DC restorers have switch selection of this time constant to permit selection of the best operating conditions for a given experiment. The result of restoring action, properly optimized, is illustrated in Figure 27(d). Here
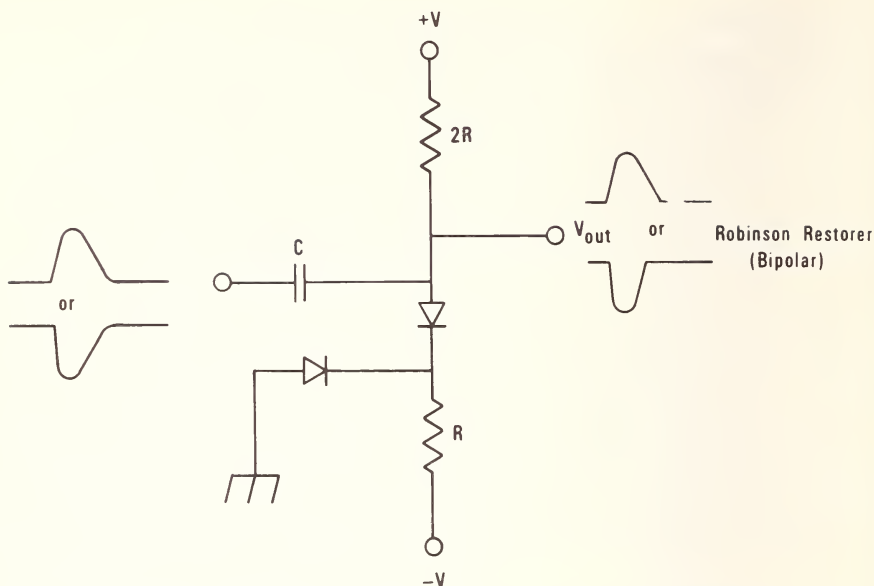
Figure 28.   Schematic diagram of Robinson-type D.C. restorer circuit.

we see that the zero reference baseline has been maintained at a constant level and the degradation seen without the restorer has been largely removed.

To provide experimental verification of these principles, Figure 29 summarizes the results of studies made on the performance of a laboratory Ge(Li) spectrometer as a function of input counting rate. The spectrometer consisted of a 2.5 cm^2 × 8 mm Ge(Li) detector mounted in a cryostat with a cooled FET preamplifier, a TC 200 linear amplifier modified to incorporate first order pole-zero cancellation, and a 12 bit ADC (Nuclear Data Model ND-161). The input of the ADC included a simple Robinson restorer circuit with optimized time constant. Results are presented for two cases: (1) without pole-zero cancellation and (2) with pole-zero cancellation. The gain was adjusted to place the 1.332 MeV peak of ^{60}Co in channel 3750. Although the peaks have been normalized to fall in the same channel, in no case did the peak position change by more than 1 channel below 5000 counts/sec and 3 channels at 35,000 counts/sec.

Observing the data on the right side of the figure, a series of measurements was made over a count rate range of 1000 to 18,000 counts/sec. As the count rate is increased, the peak is observed to broaden from 1.88 keV (FWHM) to 3.58 keV at 18,000 counts/sec. The broadening on the low-energy side is attributed to undershoot and the high energy tail to pile-up effects. When the pole-zero correction circuitry is included, the deterioration of peak width is seen to be materially

EFFECT OF PULSE RATE
ON ENERGY RESOLUTION
WITH AND WITHOUT
POLE – ZERO CORRECTION

2.5 cm² X 8mm Ge (Li)
TC-200 (1.6 μsec)
NRTS Cooled Preamp.
ND-161 (16 mc)
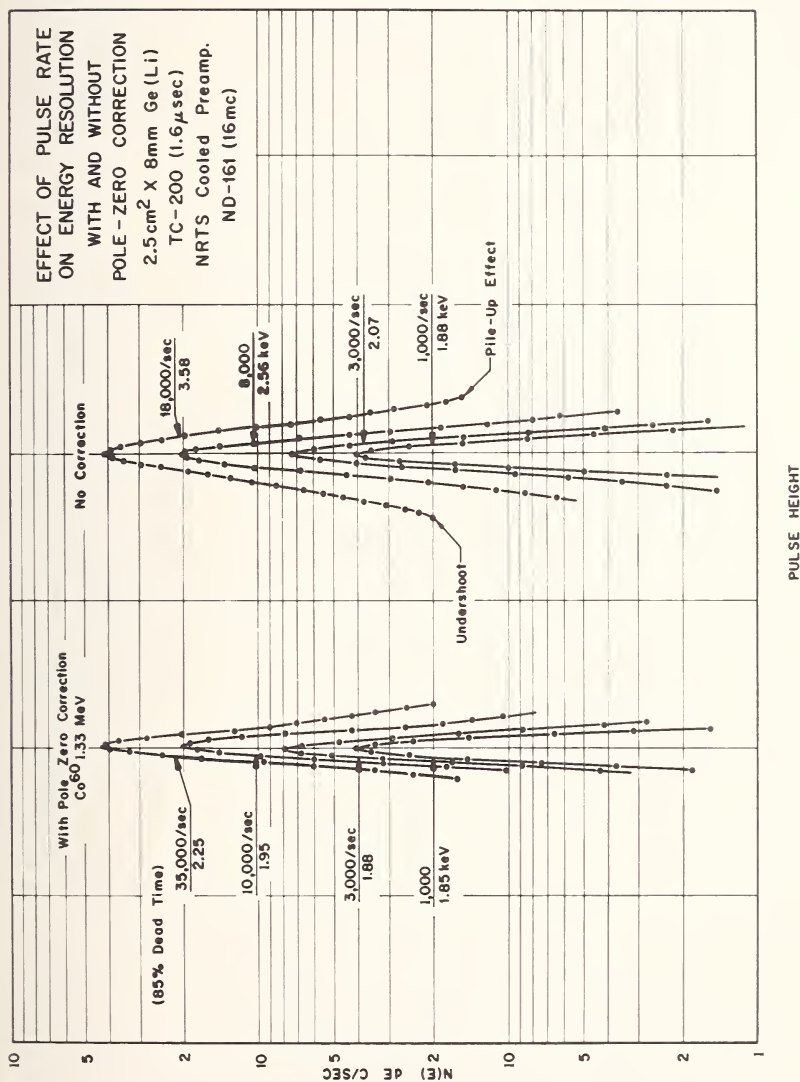
Figure 29. Series of measurements showing effect of pulse rate on energy resolution of Ge(Li) spectrometer system. Results are shown with and without pole-zero correction and optimized D.C. restorer.

reduced. The increase in peak width of approximately 20% (1.85 to 2.25 keV) over a count rate range up to 35,000 counts/sec is considered to be quite acceptable. It should be emphasized that that magnitude of the peak broadening due to rate effects should be independent of system resolution, so that if these measurements had been made on a system with appreciably worse resolution, the observed rate effect would be proportionally less. We would conclude from these results that the use of pole-zero cancellation techniques and DC restorers provide an effective means of reducing count rate degradation over a respectable range in input rate.

F. Pile-up Effects at High Rates

If we observe the performance of the system indicated in Figure 29 at high rates, we see some asymmetry remaining on the high side of the peak, even with baseline restoration. This results from pile-up effects which are so termed to describe the result of two pulses arriving at the input of the ADC within a very short time. To simplify a discussion of these effects it is most convenient to divide such effects into two classes: (a) peak pile up, which occurs when two pulses arrive within the time that the linear gate on the input of the analog-to-digital converter is open, thus yielding a stored pulse amplitude which is related to the sum of the two pulses, and (b) tail pile up, which results from a situation where the ADC has completed a conversion, stored the result in memory and reset the ADC. If the tail of a preceding pulse is present at the input of the linear gate and a second pulse arrives, the linear gate then opens and the resultant amplitude will again be related to the sum of the tail of the preceding pulse and the new pulse.

Tail pile-up effects are normally reduced by including in the ADC input circuitry an "inspection circuit" which requires that the reference baseline be identically zero before a new pulse can be digitized. In this manner, a fixed dead time is introduced which insures that pulses which are to be considered for conversion must have been preceded and followed by a fixed time period during which no event occurred.

Peak pile-up is generally handled by specialized external circuitry which incorporates fast differentiating networks which inspect short intervals of time and determine whether or not two pulses have occurred during the time an ADC conversion has been requested. If this is the case, a reject signal will be generated and the event rejected by the ADC.

G. Pulse Shape Discrimination

In the discussion of charge collection problems in detectors in an earlier section, it was mentioned that many events which occur within the

intrinsic volume of the detector do not produce an amount of charge which truly represents the energy of the particle produced within the sensitive volume of the device. Such events include the following: (1) events which lose some hole-electron pairs to trapping or competitive processes within the detector, (2) events which produce energetic electrons whose range exceeds their path length within the intrinsic volume, and (3) events which produce some pairs in regions of low field, resulting in a slow component to the charge collection current pulse arriving at the input to the filter network in the pulse amplifier. Because of the finite integration time of the filter network, the resultant pulse amplitude will be less than that required for a true representation of collected charge. It is this latter class of events which lend themselves to electronic rejection schemes. Studies of this problem have been made by Cline and Johnson [23] which have led to the development of rise time rejection systems for specialized applications. A study of the distribution of pulse rise time for a 5 cm² × 8 mm planar device using 2.76 MeV gamma rays indicated that about 15% of the pulses in the Compton distribution exhibited a slow component in the rise time. This results principally from the large probability that electrons will escape the intrinsic region of the detector, and lose some of their charge in the regions near the junctions. It has been demonstrated by Sakai [24] that charge produced in these regions will exhibit an abnormally long collection time.

A block diagram of the rise time rejection system developed by Cline and Johnson is shown in Figure 30. In this system, output pulses from the preamplifer are inspected and a pulse developed whose amplitude is proportional to the time for the leading edge of the pulse to reach a maximum, thus measuring effective rise time. This is accomplished with zero-crossing pick-off circuitry and a time-to-amplitude converter. Appropriate signals are then generated to reject pulses which exhibit long rise times.

Figure 31 illustrates the performance of this system. In this figure we have plotted the spectrum of capture gamma rays from the Fe(n,γ), reaction obtained with a small Ge(Li) detector, with and without rise time rejection. This is an extreme case, where large numbers of high energy electrons are being created within the intrinsic volume with a high probability of escape with less than full energy loss. The marked reduction in the unwanted continuum serves as a dramatic demonstration of the value of a rejection system.

H. ADVANCED SPECTROMETER SYSTEMS

In the preceding sections we have briefly discussed a large number of complications which must be understood and treated to obtain optimum performance from a high resolution Ge(Li) system for general

Figure 30. Block diagram of pulse rise-time rejection system employed to improve quality of spectra by elimination of events which lead to the escape of electrons from the intrinsic volume of the detector.
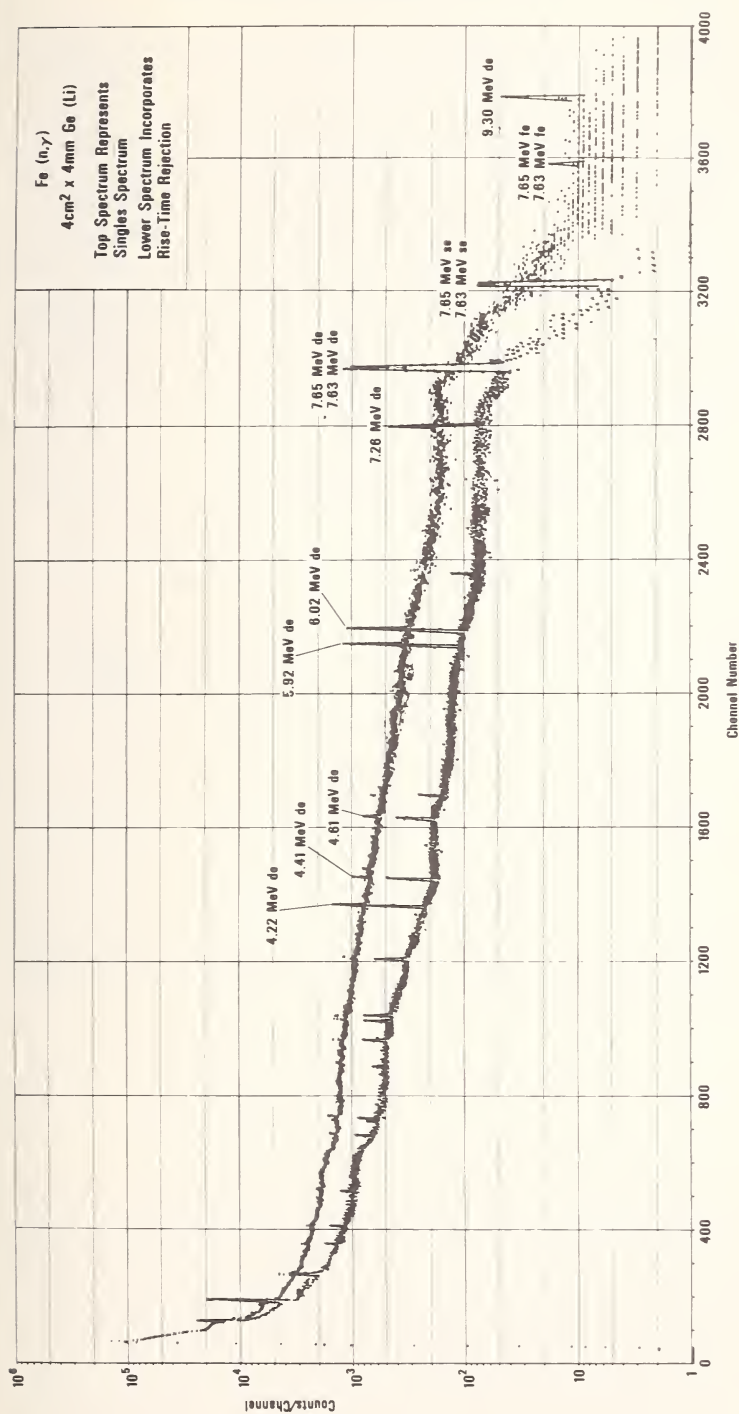
Figure 31. Gamma-ray spectrum of Fe(n,γ) reaction with and without rise-time rejection circuitry employed in the spectrometer. The reduction in the intensity of the background continuum results from the elimination of events which produce electrons which lose energy in the region of the p and n junctions.

applications. Recently we have placed in operation an advanced system which incorporated effective means of handling all of these problems. This system, developed by L. O. Johnson and the author [25], is presented in block form in Figure 32. The system, which is entirely DC coupled, incorporates peak and tail pile-up rejection circuitry with provision for the addition of rise time rejection if required. The use of DC coupling results in excellent performance at high counting rates. Using this system with a source of ^{60}Co, less than a 15% increase in resolution was observed at counting rates in excess of 50,000 counts/sec. Under these conditions, the shift in zero references was less than 1 part in 10,000. This system has the advantage of simplicity and a minimum of necessary adjustments which are related to experimental conditions.
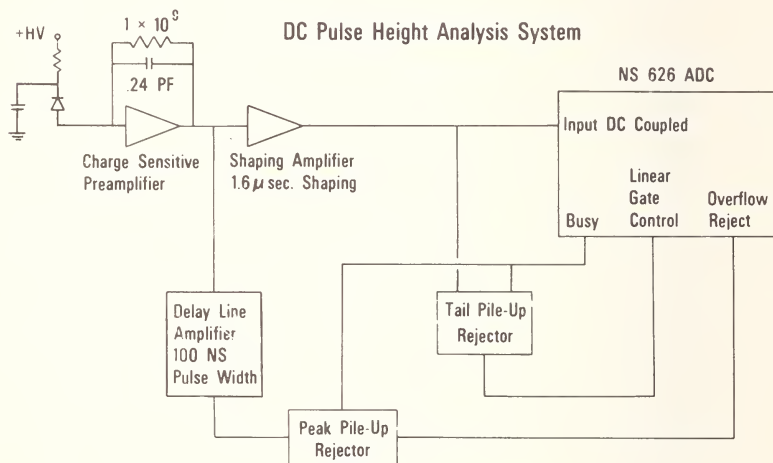
Figure 32.   Block diagram of completely D.C. coupled electronic system designed for high resolution spectrometry at high counting rates. System employs both peak and tail pile-up rejection circuitry.

IV.   Data Handling

A.   Energy Measurements

To provide some insight into the importance of the characteristics of a pulse height analysis system in the precision measurement of energies and the analysis of pulse height spectra, let us consider the techniques employed for precision energy measurement using Ge(Li) spectrometers. Although the amount of charge collected within the intrinsic volume of the detector is proportional to the energy of photons which interact and lose all of their energy in this volume, we have no convenient way of measuring this charge directly and relating it to observed pulse height.

For this reason the usual technique is to calibrate the energy scale of the spectrometer with gamma-ray reference standards whose energies have been measured by other techniques. The technique is illustrated by Figure 33. The vertical lines represent photoelectric or "full-energy" peaks in a pulse height spectrum. As shown, an unknown line is measured simultaneously with several lines of known energy and the energy scale is then determined from the median positions of the peaks on the pulse height scale by suitable curve fitting techniques [26], interpolating to obtain the energy of the unknown line. The precision which can be attained using this technique is limited first by the precision of the reference standards that are available. Secondly, by the precision with which one can locate the median position of the peaks of interest and establish an accurately known pulse height *vs* energy scale. For energy measurement with a precision in the range of one part in 10^4, the major limitations are related to the precision with which one can measure the
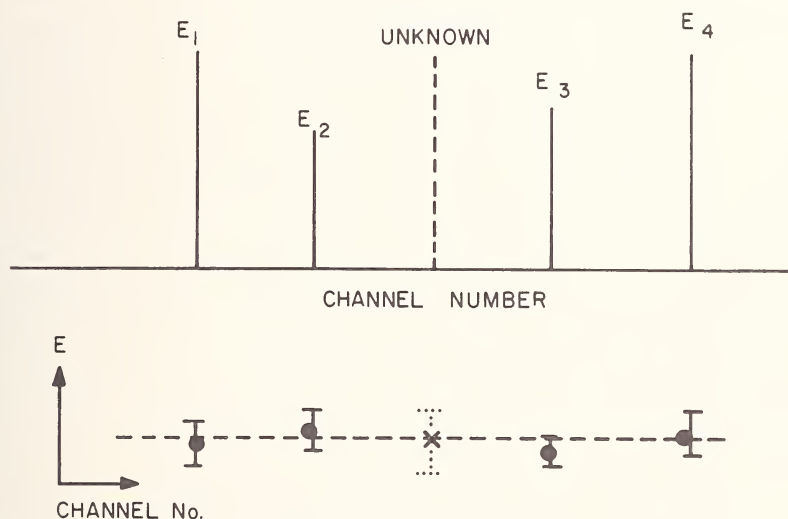
Figure 33. Illustration of procedure for measurement of gamma-ray energies using internal calibration reference standards.

linearity and stability of the pulse analysis system. The techniques which have been developed for this purpose have been described in earlier sections. Using these techniques it is felt that the linearity of an analyzer system can be measured to about 0.05 channel. If one assumes that it is also possible to measure the median position of a peak to ± 0.05 channel, using suitable least squares techniques, this implies that the relative position of two peaks could be determined to about ± 0.07 channel, excluding any systematic error. This corresponds to a precision approaching 10 eV for a 0.1 keV/channel energy scale.

Let us now examine some examples of the results obtained by applying these techniques. Table 3 presents a list of energy values for secondary standards presently in use at our laboratory. As indicated in the references at the bottom of the table, many of these values were measured using Ge(Li) spectrometers.

In order to provide a better indication of the potential of Ge(Li) spectrometers for precision energy measurements, R. G. Helmer of our laboratory has recently made a series of energy measurements on the gamma rays emitted in the decay of [182]Ta [27]. For gamma-ray transitions in the decay of [182]Ta below 270 keV, Seppi et al [28] have reported very precise energies based upon bent crystal diffraction spectrometer measurements. The quoted uncertainties range from 0.001 to 0.013 keV. In contrast, the high energy transitions (> 800 keV) have been reported with precisions of about 0.2 to 1.0 keV.

In this series of measurements, the transitions above 900 keV were measured with a Ge(Li) spectrometer. Gamma-ray spectra of [182]Ta were measured together with various calibration sources. The results of two measurements are shown in Table 4. The analysis of these spectra were carried out with a nonlinear least squares computer routine [26], which fits a Gaussian to the contribution above the continuum in the pulse height spectrum. From the positions of the peaks obtained with this program and the energies of the calibration lines, a quadratic fit is made. From this function, the energies of the unknown lines are then obtained.

In Table 4 the results of this analysis are indicated. The calibration lines used are listed first, showing a comparison between the reported energies of Seppi and energy values obtained from the fitting procedure. Of particular interest are the experimental results shown under "all other lines". These lines which were measured by Seppi but not included as calibration lines in the fitting procedure may be used as an indication of systematic error in the experimental method. Examination of the right hand column indicates excellent agreement with the bent crystal values with realistic errors in the order of 10 eV. Although these results might be termed a "best case" experiment, we would propose that it serves to establish the potential of the Ge(Li) spectrometer for precision energy measurements. Observation of the results for the high energy transitions in [182]Ta indicate that we are largely limited by the errors in energy standards used for the measurements. At the present time, attempts are being made to improve this situation by using cascade gamma rays to bootstrap precise bent crystal values up to the 1 MeV region.

B. FIELD INCREMENT EFFECT

An effect, basic to the energy loss mechanism within solid state detectors, which can introduce error in the calibration and determination of precision energies has recently been quantitatively verified by the

Table 3. Secondary gamma—ray energy standards.

Isotope	Energy (keV)	Isotope	Energy (keV)
^{241}Am	59.536 ± 0.001[a]	^{207}Bi	569.674 ± 0.02[b]
^{133}Ba	80.997 ± 0.008[b]		1063.614 ± 0.04[b]
^{109}Cd	88.036 ± 0.008[b]	^{228}Th	583.139 ± 0.023[g]
^{75}Se	96.731 ± 0.007[b]		2614.611 ± 0.060[g]
	121.113 ± 0.010[b]	^{124}Sb	602.712 ± 0.025[b]
	135.998 ± 0.010[b]		1690.991 ± 0.050[b]
	198.600 ± 0.020[b]	^{137}Cs	661.630 ± 0.03[b]
	264.648 ± 0.015[b]	^{95}Nb	765.83 ± 0.07[d]
	279.522 ± 0.012[b]	^{54}Mn	834.795 ± 0.04[d]
	303.892 ± 0.020[b]	^{46}Sc	889.25 ± 0.07[d]
	400.641 ± 0.015[b]		1120.50 ± 0.07[d]
^{153}Gd	97.430 ± 0.005[b]	^{88}Y	898.00 ± 0.03[d]
	103.178 ± 0.003[c]		1836.075 ± 0.050[d]
^{57}Co	122.060 ± 0.010[b]	^{65}Zn	1115.51 ± 0.07[d]
	136.471 ± 0.010[b]	^{60}Co	1173.226 ± 0.040[h]
^{141}Ce	145.443 ± 0.006[e]		1332.483 ± 0.046[h]
^{139}Ba	165.854 ± 0.011[e]	^{22}Na	1274.52 ± 0.07[d]
^{203}Hg	279.190 ± 0.007[b]	^{24}Na	1368.650 ± 0.040[g]
^{51}Cr	320.080 ± 0.013[e]		2754.11 ± 0.06[g]
^{198}Au	411.795 ± 0.009[f]	^{140}La	1596.22 ± 0.05[g]
^{7}Be	477.575 ± 0.02[b]		
^{85}Sr	513.998 ± 0.02[d]		

[a] R. W. Jewell et al., Nucl. Instr. and Meth. **62**, 68 (1968).

[b] R. C. Greenwood, R. J. Gehrke and R. G. Helmer (to be published).

[c] O. W. Schuldt, Z. Phys. **170**, 465 (1962).

[d] W. W. Black and R. L. Heath, Nucl. Phys. **A90**, 650 (1967).

[e] J. J. Reidy and M. L. Weidenbeck (private communication).

[f] G. Murray, R. L. Graham and J. Geiger, Nucl. Phys. **63**, 353 (1965)

[g] A. Taylor and R. L. Heath (to be published).

[h] G. Murray, R. L. Graham and J. Geiger, Nucl. Phys. **45**, 177 (1963).

ACTIVATION ANALYSIS

Table 4. Energies determined from ^{182}Ta spectra.

Gamma ray energies (keV)

Isotope	Seppi et al. and others	1st run		2nd run		Average	
		$--$ calibration lines $--$					
^{182}Ta	$152.441 \pm .003$[a]	152.438	$-.003$[b]	152.437	.004[b]		
	$156.386 \pm .003$	156.383	$-.003$				
	$179.394 \pm .004$	179.406	.012				
	$222.114 \pm .004$	222.106	$-.008$	222.109	.005		
	$264.079 \pm .009$			264.098	.023		
^{198}Au	$411.795 \pm .009$			411.784	.011		
^{207}Bi	$569.620 \pm .060$	569.668	.048	569.674	.054		
^{137}Ca	$661.590 \pm .080$	661.617	.027	661.626	.036		
^{207}Bi	1063.630 ± 070	1063.622	$-.008$	1063.638	$-.008$		
^{60}Co	$1173.230 \pm .040$	1173.202	$-.028$	1173.202	$-.028$		
	$1332.480 \pm .050$	1332.509	.029	1332.510	.030		
		$--$ all other lines $--$					
^{182}Ta	$156.386 \pm .003$[a]	156.386	.013	156.376	.016[c]	156.382	.010
	$179.394 \pm .004$	179.404	.016	179.409	.011	179.407	.009
	$198.356 \pm .005$	198.337	.019[c]	198.363	.018	198.354	.011
	$229.327 \pm .013$	229.325	.014	229.335	.017	229.320	.009
	$264.075 \pm .009$	264.088	.017				
				927.903	.095		
		1001.699	.072	1001.632	.049	1001.654[d]	.041[e]
				1113.050	.110		
		1121.214	.022	1121.223	.027	1121.218	.022
		1157.385	.086	1157.329	.085	1157.357	.086
		1188.972	.024	1188.986	.030	1188.978	.024
		1221.361	.024	1221.341	.032	1221.354	.024
		1230.989	.028	1230.973	.036	1230.982	.028
		1257.401	.064	1257.401	.048	1257.401	.064
		1273.664	.085	1273.650	.068	1273.657	.085
		1289.142	.048	1289.111	.046	1289.126	.048
		1342.765	.149	1342.721	.154	1342.743	.149
				1373.638	.139		

[a] Uncertainties quoted by authors.

[b] Differences between value computed by least–squares program and input value.

[c] Uncertainty computed by GAUSS ($\equiv \sigma$).

[d] Weighted average $= \dfrac{w_1 E_1 + w_2 E_2}{w_1 + w_2}$ where $w = \dfrac{1}{\sigma^2}$.

[e] Computed uncertainty in average $= \sigma_2 \sqrt{\dfrac{w_2}{w_1 + w_2}}$.

author. If we consider, for example, a planar detector, with photons directed normal to the surface, electrons created within the intrinsic volume of the detector will be under the influence of the electric field within the detector created by the diode bias. In fairly deep-drift devices the bias voltage may be in excess of 2000 volts. Thus, depending upon the direction of travel of the high speed electrons produced as a result of interaction of a photon within the detector and the direction of the field impressed across the diode, the electron will interact with this field with a resultant gain or loss of energy. This will result in the collection of a total amount of charge which is in error by the magnitude of what we have termed the "field increment". To study the magnitude of this effect, a series of measurements have been made as a function of gamma-ray energy with the photons entering the detector both normal to and parallel to the electric field. To establish a reference, internal calibration lines were measured simultaneously with the gamma ray of interest.

The results of such measurements on a 5 cm² × 8 mm planar detector which normally operates with a bias of 2000 V are presented in Figure 34.
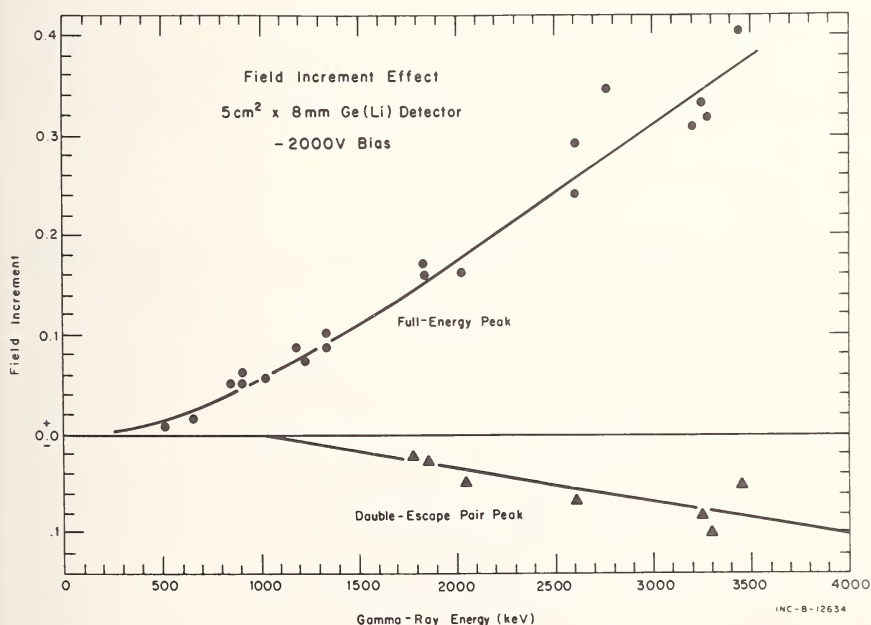
Figure 34. Experimental determination of the "Field Increment" resulting from the interaction of primary electrons with the detector field.

Here we have plotted the "Field Increment" (keV) *vs* photon energy for full energy peaks (circles) and double-escape pair peaks (triangles). The most interesting facet of these results is that the shift of pair peaks and full

energy peaks are opposite in sign. As might be expected, the magnitude of the effect is proportional to gamma-ray energy indicating that the vector of electron travel parallel to the field increases with electron range. The negative shift of the peaks which results from the collection of charge from positron-electron pairs is most interesting. One might expect, since the charge on these two particles are opposite in sign, that the net effect of interaction with the field within the detector would be zero. The fact that the positron interaction appears to dominate may be explained on the basis of differences in the interaction of positrons and electrons with matter. The range of positrons is experimentally determined to be longer than that for electrons of the same energy. This is attributed to differences in the small angle scattering cross sections for the two types of particles.

If we consider the implications of this effect, several conclusions may be drawn. If one is attempting to calibrate an energy scale, the frequently used method of establishing the scale by differences between pair and full energy peaks will produce an appreciable error. In the use of planar detectors, one can adopt the practice of making measurements with the source mounted so that photons will enter the detector normal to the field. Experience has shown that this approach is quite satisfactory in precision energy measurements where this effect should be minimized. It should be stated that there are other implications of this effect, particularly in large coaxial detectors which will be the subject of a publication at a later date.

C.   Detector Efficiency

Quantitative analysis of pulse height spectra obtained with Ge(Li) spectrometers requires a knowledge of the efficiency of the detector as a function of photon energy and source-detector geometry. Unlike the case of NaI(Tl) scintillation detectors where it was possible to calculate detection efficiencies with a high degree of precision [29], this is not so for Ge(Li) devices. Because of their small volume the number of events which interact with total energy loss is a function of the properties of the detector. It is also difficult to measure the volume of the intrinsic region of these devices with any precision. For this reason, the only method which is currently feasible for the determination of detection efficiencies for these spectrometers is by secondary calibration techniques using calibrated sources of monoenergetic radiation to establish an efficiency vs energy curve.

To provide some indication of the effect of detector area, thickness, and total volume on detection efficiency, some of the results recently reported by Cline [30] are presented in Figures 36-39. Prior to the presentation of these data, it should be stated that corrections for losses due to random coincidence summing are much more important with Ge(Li) detectors than they were with NaI spectrometers. Since the resolving time is much

greater due to the long integration and differentiation times required for optimum noise performance of the amplifiers, the magnitude of these losses is much greater. The results of experimentally determined counting losses for a high resolution system are presented in Figure 35.

Fractional Counting Losses Due to Random Pulse Pile-up
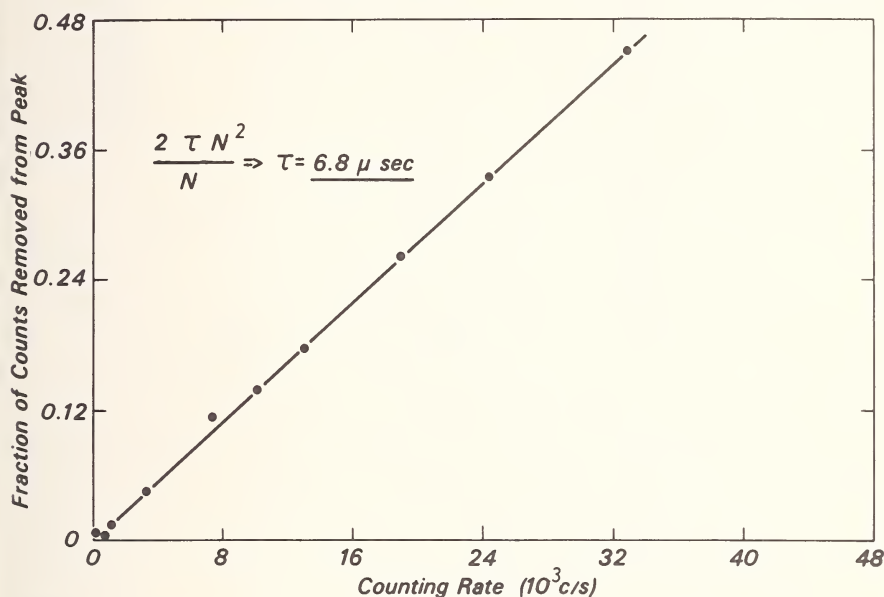
Figure 35.   Experimental determination of counting losses resulting from random peak pile-up effects as a function of counting rate.

The series of measurements presented in the following figures were made using point sources located 10 cm from the surface of the intrinsic volume of the detector. The detector was located in the cryostat by x-ray photography. Efficiency measurements for gamma-ray energies up to 2.76 MeV were made with radioactive sources calibrated with a 3 in. × 3 in. NaI(Tl) scintillation spectrometer using the techniques described in reference 29. Above 2.76 MeV, efficiency measurements were made using neutron capture gamma-ray sources. The principle standard was capture gamma rays from the $^{14}N(n,\gamma)$ reaction whose energies and intensities have been measured with considerable precision by Motz [31] using a Compton spectrometer. A summary of the energies and intensities used is given in Table 5. Normalization of the high energy data was made with radioactive sources.

Figure 36 presents full energy peak efficiencies for gamma-ray energies up to 11 MeV for three detectors with constant drift depth and varying area. Figure 37 indicates the absolute double-escape peak efficiencies for

Table 5. Table of high–energy gamma rays.

Reaction	E_γ (MeV)	I_γ (γ/100 captures)	Reaction	E_γ (MeV)
^{14}N(n,γ)	3.53	9	Fe(n,γ)	5.92
	3.68	23		6.02
	4.51	16		7.28
	5.27	32		7.63
	5.30	21		7.64
	5.53	21		8.89
	5.56	11		
	6.32	18	^{9}Be(n,γ)	3.37
	7.30	9		3.44
	8.31	4		6.81
	9.15	1.4		
	10.83	14	^{27}Al(n,γ)	7.72
^{1}H(n,γ)	2.223	441	Ni(n,γ)	5.31
				5.82
^{23}Na(n,γ)	3.59			6.84
	3.98			7.54
	6.40			7.82
				8.53
S(n,γ)	2.38			9.00
	2.93			
	3.22			
	4.87			
	5.42			

the same three detectors. Figure 38 presents data on the full energy peak efficiency for two large volume planar devices and two coaxial drift detectors, the largest having a reported volume of 35 cm³. Figure 39 shows values for the double-escape peak efficiencies for the same devices. Observing these data we may draw several important conclusions. The double-escape peak efficiency is seen to rise with the pair cross section to a maximum around 5 or 6 MeV and then to decrease as the probability for escape of long range electrons increases.

The principle reason for presenting these data is to provide a guide to aid in the selection of detectors for particular experimental applications.
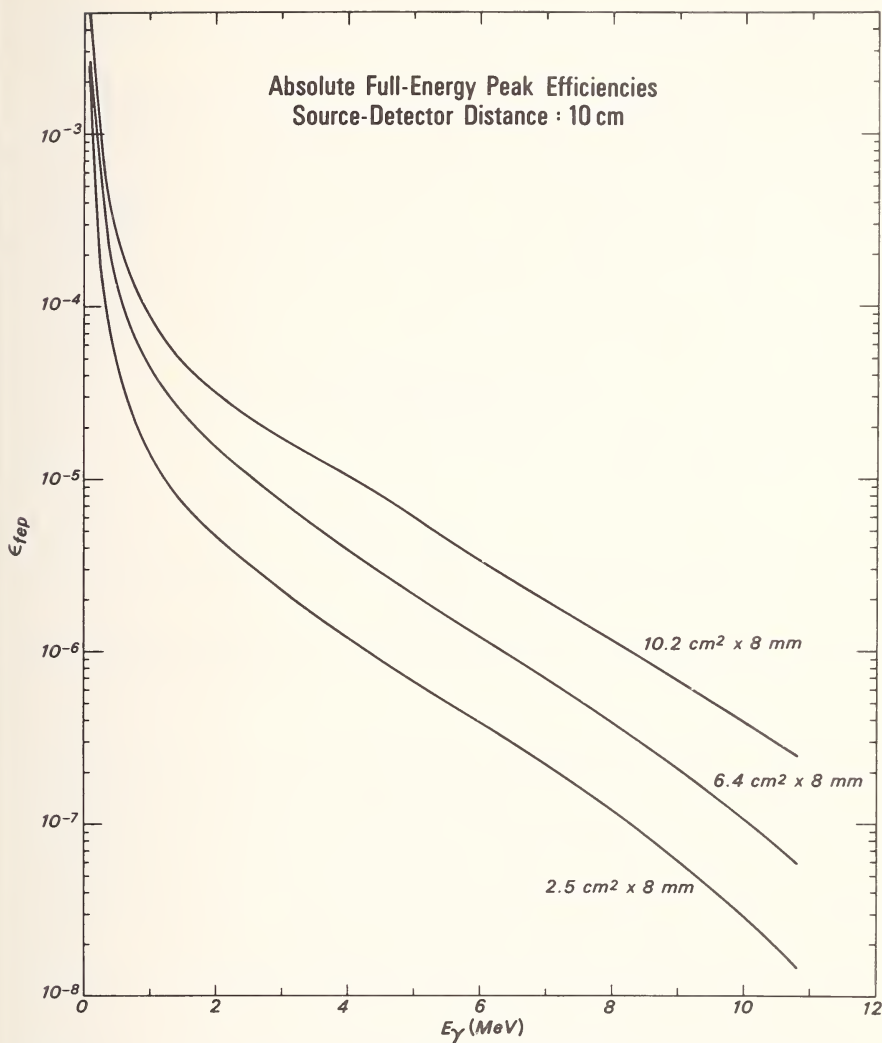
Figure 36.   Absolute full-energy peak efficiencies of Ge(Li) planar detectors of varying
          area for constant drift depth.

V.   Specialized Spectrometer Systems

A.   COMPTON ANNULUS SPECTROMETER

At the present time, considerable attention is being given to the
development of specialized detector systems to improve the performance
of Ge(Li) spectrometers for the analysis of complex gamma-ray spectra
as evidenced by the number of papers on this subject submitted to this
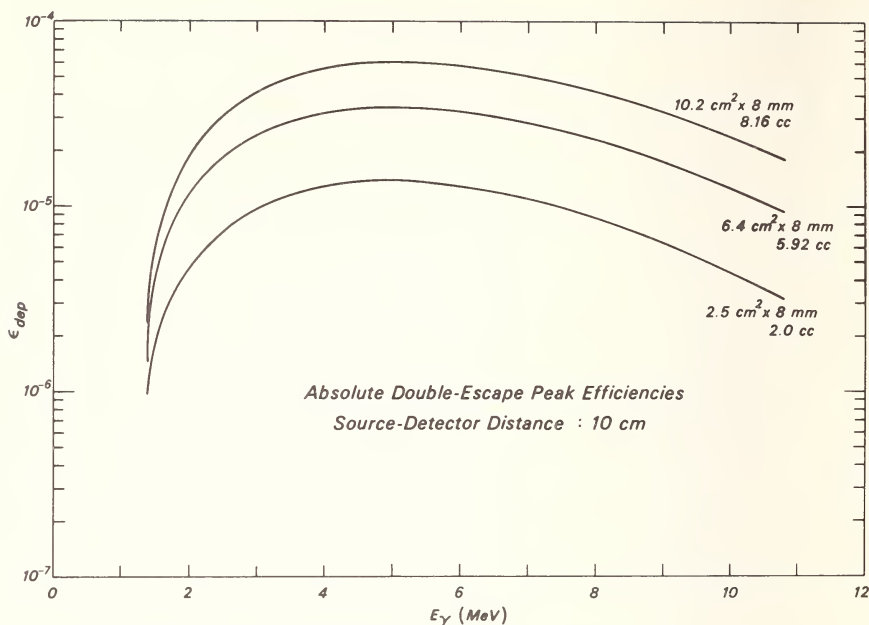
Figure 37.   Absolute double-escape pair peak efficiency of planar detectors in preceding
          figure.

conference. Figure 40 is a detailed drawing of a gamma-ray spectrometer
employing an 8 in. diam. × 12 in. sodium iodide scintillation detector as an
annulus for the rejection of Compton electrons in a gamma-ray spectrum.
As shown in the lower left hand corner of the figure, the arrangement
employs a germanium detector which is surrounded by an annulus of
sodium iodide. The gamma rays are collimated into the central Ge(Li)
spectrometer. In this configuration, if a Compton event occurs in the
central detector, the scattered Compton photon will have a reasonable
probability of being detected in the large NaI detector surrounding the
Ge(Li) spectrometer. If the two detectors are operated in coincidence,
such events can be identified and rejected in the final analysis by the pulse
height analyzer.
    The result of this method of operation is illustrated by Figure 41. In this
figure, pulse height spectra resulting from the measurement of ^{24}Na
gamma rays, obtained with a Ge(Li) spectrometer with and without a
NaI(Tl) annulus, are shown for comparison. Examination of these two
curves indicates the nature of the result of rejecting Compton events by
the sodium iodide annulus detector. The full energy peaks have been
considerably enhanced, while the pair peaks are reduced in amplitude as a
result of detection of the 0.511 MeV annihilation quanta in the annulus.
The full energy peaks result from events which leave the total energy of
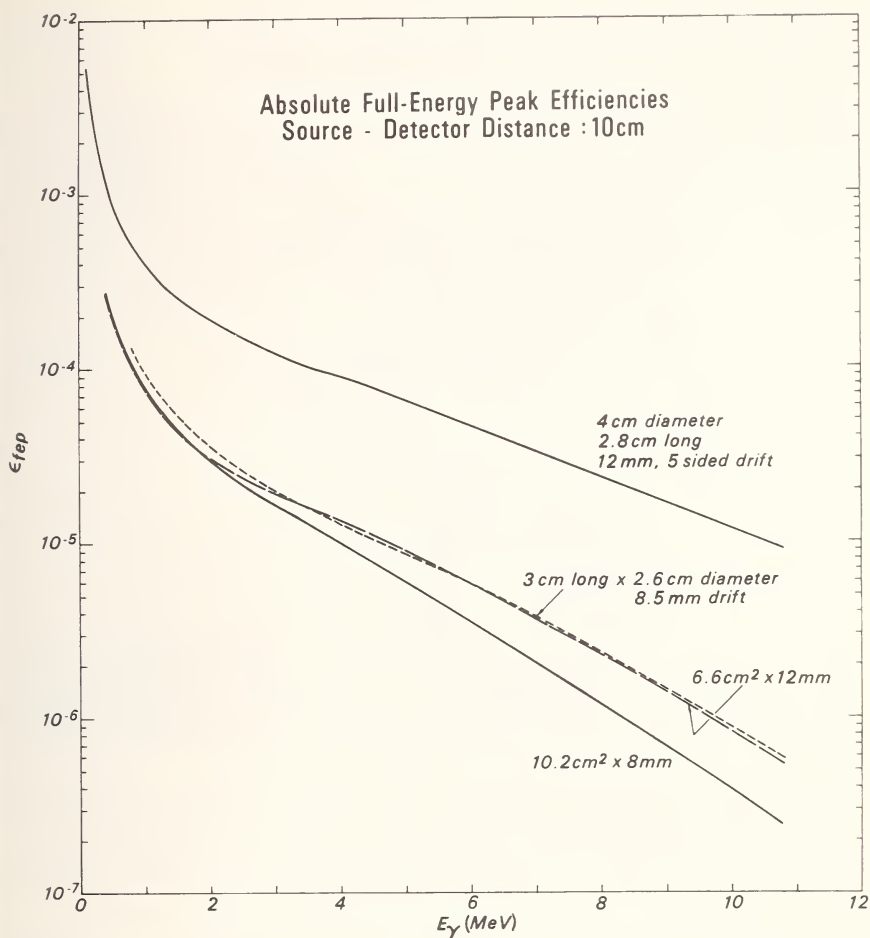
Figure 38. Absolute full-energy peak efficiencies vs E_γ for Ge(Li) detectors as a function of volume.

the gamma ray in the central detector. The continuous distribution of pulses down to zero energy results from Compton events and represents information which only serves to complicate the shape of the observed pulse height distribution. If this continuous distribution of pulses could be eliminated, our ability to recover information from a complex spectrum would be greatly enhanced. It is expected that this principal can be refined to produce a further reduction in the Compton continuum by a factor of ten. This would considerably improve our ability to analyze complex spectra.

To illustrate the importance of the technique in the analysis of complex spectra let us observe the spectra shown in Figure 42. In this figure we have plotted the gross fission product gamma-ray spectrum resulting from
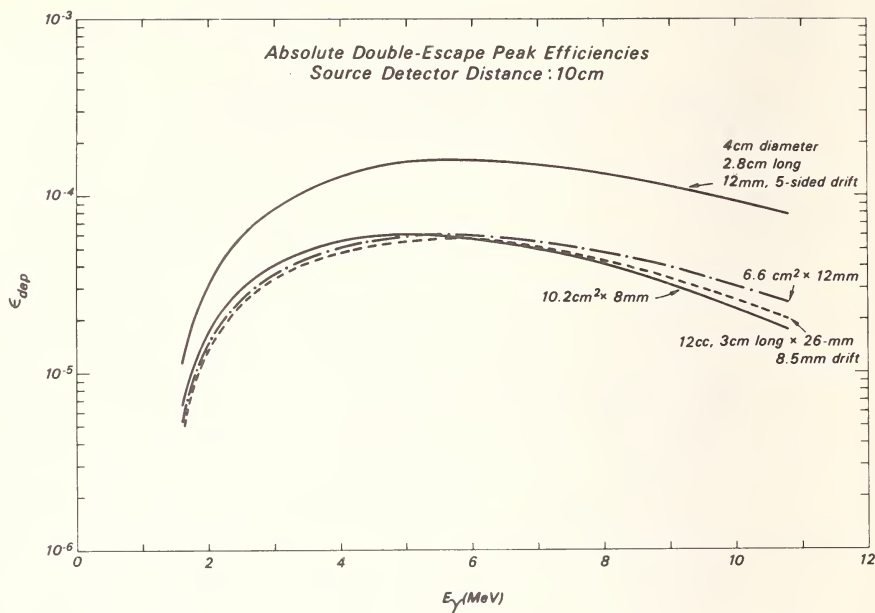
Figure 39. Absolute double-escape pair peak efficiency for detectors in preceding figure.

an 8 h irradiation of ^{235}U with a decay of 17 days following removal from the reactor. The two spectra compare results obtained with and without the use of a Compton rejection mantle. Close inspection of these two spectra shows that considerable additional detail is apparent in the lower curve. To illustrate the enhancement, the lower curve is labeled only with those peaks which were not detectable without the Compton rejection mantle.

B. COMPTON SUMMING SPECTROMETER

Recently a Ge(Li) version of the Compton summing spectrometer first proposed by Hoogenboom for NaI systems in 1958 [32] has been investigated in many forms. A version presently in use at our laboratory is shown in Figure 43. In this configuration, gamma rays enter through a collimator, passing through the hole in an annular Ge(Li) detector to interact in a planar detector. The principle of operation of the Compton summing spectrometer is as follows: A restriction to what approximates a line response is achieved by requiring that a Compton event occur in the planar device. If this event results in large angle scattering of the secondary photon, the probability that the low energy scattered secondary gamma ray will be detected in the annular detector is large. The output from the two detectors is then summed, with a coincidence requirement imposed, so that only such events will be stored in the
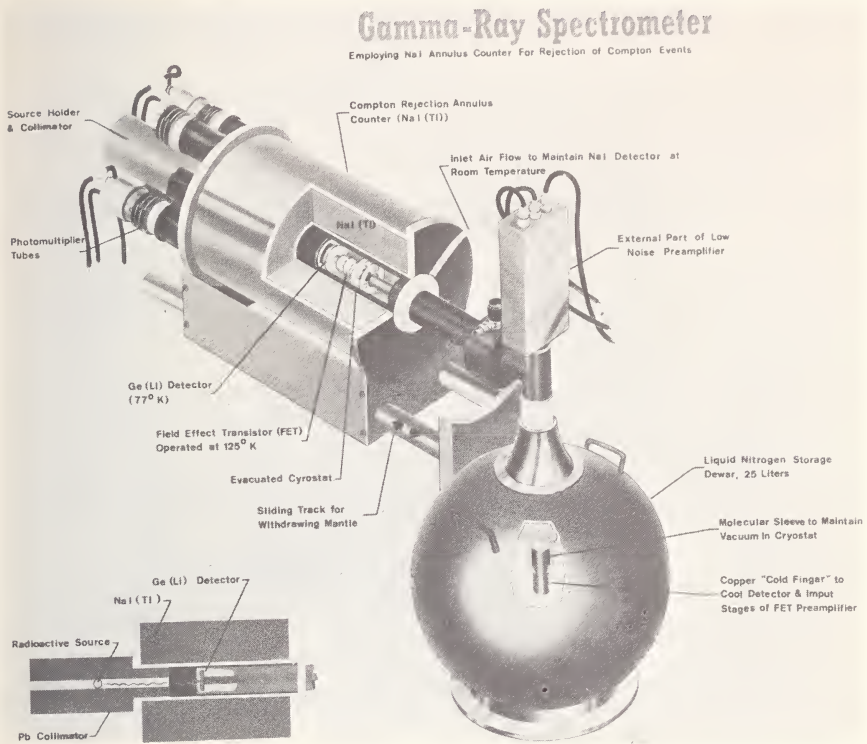
Figure 40.   Gamma-ray spectrometer system employing a lithium-ion drifted Ge detector surrounded with an annulus of sodium iodide. A collimated beam of gamma rays enter the central detector. Scattered gamma rays resulting from Compton processes in the central detector are rejected by coincidence circuitry if the scattered photon is detected in the NaI annulus detector.

analyzer memory. Preliminary experience with such systems indicates that suppression of the continuum of Compton pulses can surpass that of any other system. Major disadvantages of such systems are low detection efficiency and complicated electronics.

VI.   Automated Data Systems

A.   Data Acquisition

This section is intended to provide some background and vocabulary to supplement the discussions of the application of digital processors to problems in the acquisition and analysis of experimental data. The interest in automated techniques for the analysis and acquisition of pulse height data has been greatly enhanced by the development of Ge(Li) detectors and small, relatively inexpensive digital processors. As
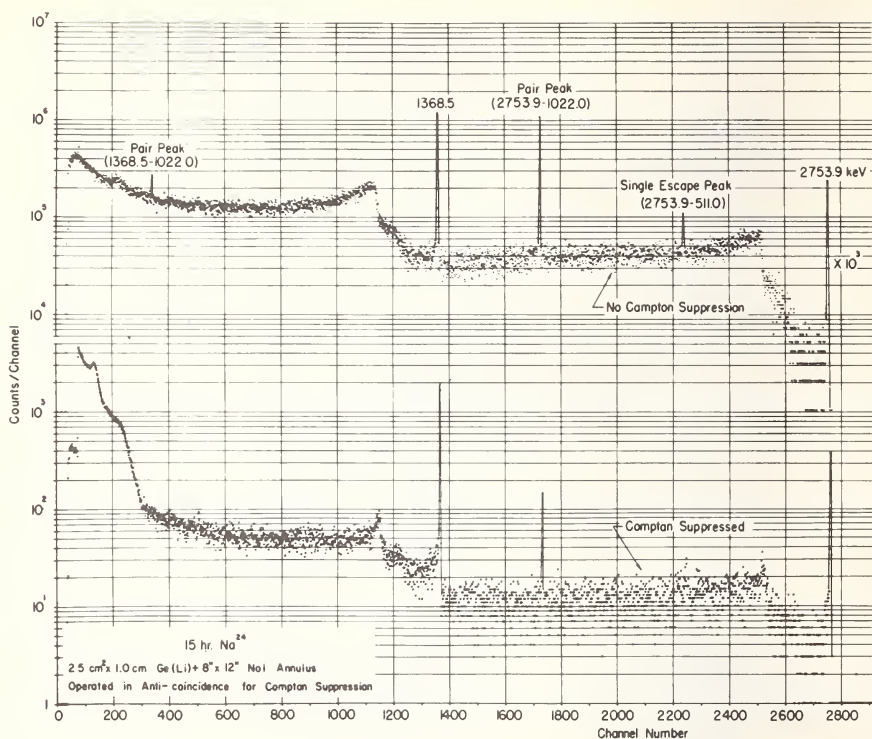
Figure 41.   Pulse-height spectrum of radiation emitted by a ²⁴Na source. The two pulse-
              height spectra illustrate the effect upon the shape of the spectrum produced by the
              Compton suppression technique.

spectrometer systems grow more complex, requiring many decisions as a result of the use of pulse conditioning circuitry, multiparameter measurements, *etc.*, the use of digital processors for the acquisition of pulse height data appears more attractive. Now that 4096 channel ADCs have come into general use for Ge(Li) spectrometers, users of these devices have come to appreciate the problems inherent in handling the volumes of data which these instruments can produce. In an effort to reduce this problem to manageable proportions we and other laboratories have expended considerable effort directed toward the development of on-line techniques for the analysis of pulse height data using the variety of peripheral devices which one now has at his command. In particular, we have directed our efforts to the utilization of graphic techniques incorporating the use of large display oscilloscopes, light pens, and function keyboards.

As an example, Figure 44 is a photograph of a computer data system built around a small digital processor (DEC PDP-8). This system incorporates magnetic tape, a large area CRT display oscilloscope,
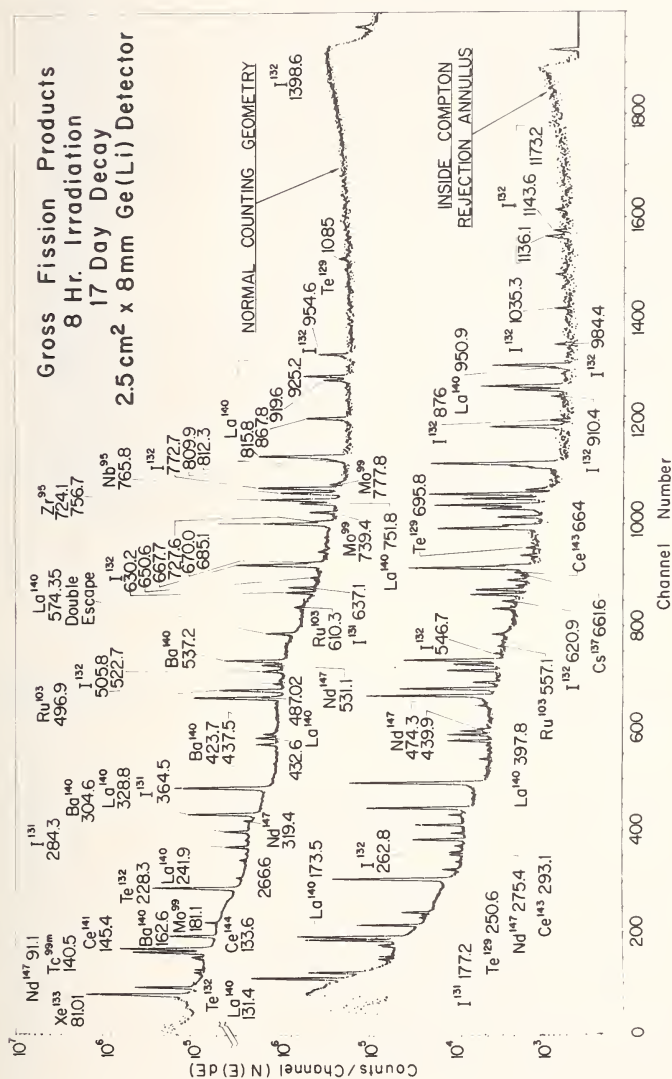
Figure 42. Pulse-height spectrum representing the gamma-ray spectrum of gross fission products with and without the use of a Compton suppression annulus detector system. Only peaks identified in lower spectrum which were not apparent without the rejection system are labeled.
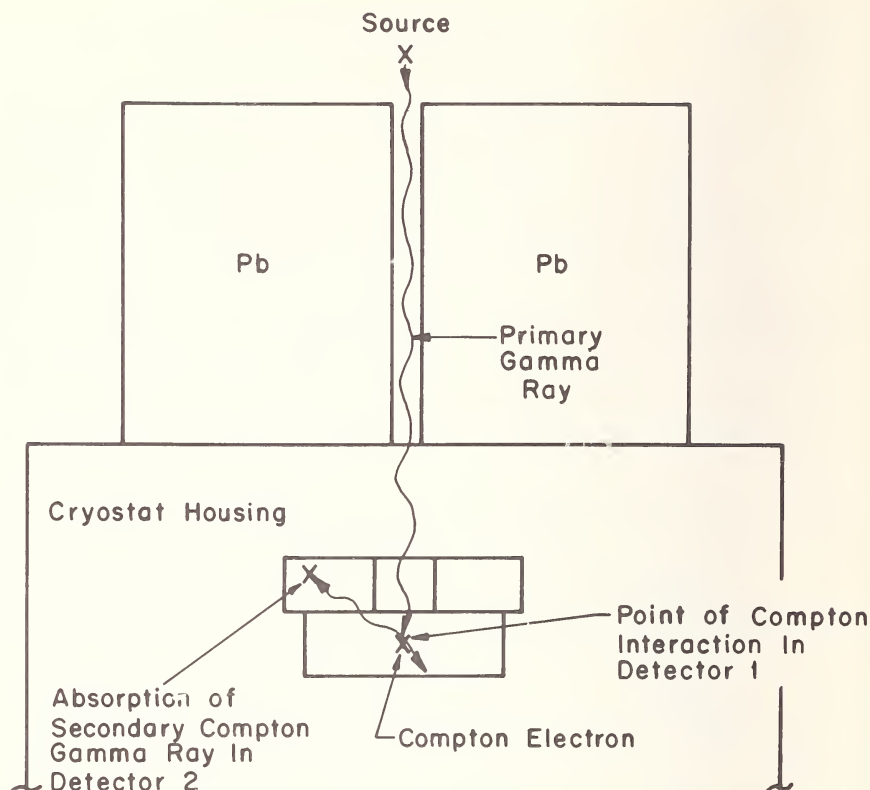
Figure 43. Schematic representation of the configuration of a Compton-summing spectrometer employing two Ge(Li) detectors.

function keyboard, and light pen. This system has been employed to develop techniques for the analysis of 4096 channel pulse height spectra to obtain gamma-ray energies and intensities through the use of man-machine interaction with a graphical system [33,34]. More recently a larger system, shown in Figure 45, has been employed to expand this capability. This system employs a DEC PDP-9 processor with a large magnetic drum mass storage unit, magnetic tape and a processor-controlled display system with light pen and function keyboard. This system has also been used to develop data file and retrieval systems to aid the experimenter in the analysis of data.

B. ADC INTERFACE

In the use of a digital processor for the acquisition of pulse-amplitude data, the major difference from a normal "hard-wired" pulse analyzer lies in the ability of the processor to handle information provided by the
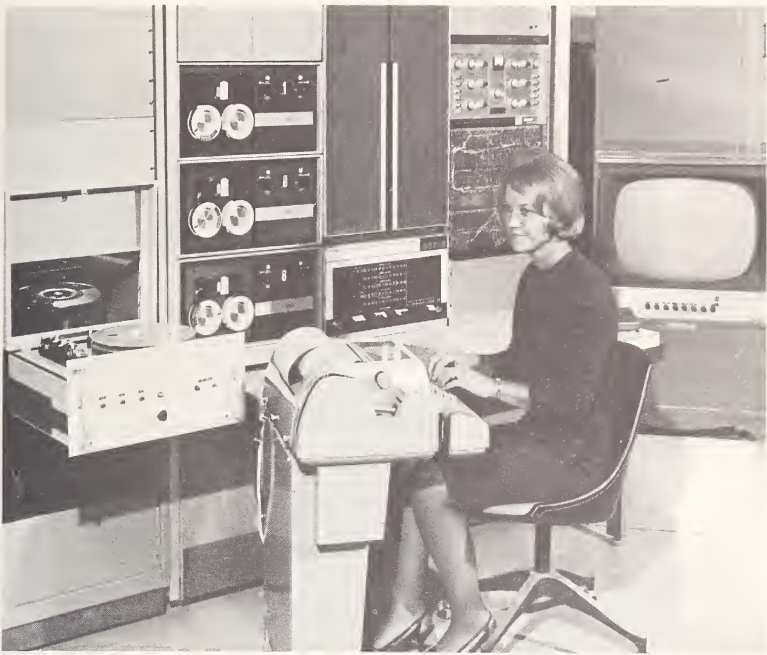
Figure 44.   Photograph of computer data system employing a PDP-8 computer, magnetic
tape transports, light pen, function box, and 21 in. display oscilloscope. System is
used both for data acquisition from nuclear ADC's and on-line data analysis.

digital-to-analog converter under control of a programmed sequence of
operations which may assume any form the user desires. It is this
versatility which makes a processor quite desirable for multiparameter
experiments and for multiple control of many ADCs sharing the common
memory of the processor. In the conventional "hard-wired" pulse height
analyzer, analysis of a pulse from the detector produces a number
corresponding to a particular address in the analyzer memory. This
address is uniquely defined by the memory control circuitry and the usual
procedure is to initiate a process which adds the number "one" to the
contents of that memory location. If this same address information is
entered into the accumulator of a digital processor, this information can
be used in many ways. For example, it might be stored in a number of
different locations for different purposes, or it might be modified to
change the gain of the spectrum, etc.

This circuitry required to connect a nuclear type of analog-to-digital
converter or any other external device to a digital processor can be
referred to as an interface. To provide some insight into the versatility
which can be achieved with such systems, let us examine a typical ADC
interface. Figure 46 illustrates a computer system designed for general

Figure 45.   Larger data system employing DEC PDP-9 computer, magnetic drum storage,
and sophisticated display system for on-line data analysis.

laboratory use as a single or multiparameter pulse height analyzer system.
This system utilizes a PDP-9 processor with 16K words of 18 bit
memory. As indicated in the figure, the processor is connected to four (4)
12 bit ADCs to provide input from four spectrometers. In most
processors, information from outside sources may be entered into the
computer memory by three different means:

1. Direct memory access — in this access mode, the address information
is entered directly into dedicated memory locations, identified by the
interface circuitry, much in the same fashion as in "hard-wired" pulse
height analyzers. The transfer and add-one operation, in this case, is
accomplished in one memory cycle (1 or 2 microseconds with most
machines) on what is known as a "cycle-stealing" basis. This implies that
entry of information from the external source is made by interrupting the
normal sequence of operation of the machine's resident program for only
one memory cycle, then returning control of the machine operation to the
resident program.

2. Program Interrupt — in this method of entry, the completion of a run-
down in the ADC causes a message to flow to the processor indicating
that input "X" has information which requires the attention of the

9-IOT's

Load X
Load Y

3-18 Bit Banks
Relay Drivers

3 Intensity Levels

Oscilloscope
(AC)

18 Bit
Register

Incremental
Tapedeck
Data Channel

ADC
No.1
12 Bit   12
Tag— 6

ADC
No.2   12
Tag— 6

ADC
No.3   12
Tag— 6

ADC
No.4   12
Tag— 6

Coincidence Circuitry

Multiplexer

Data
Channel
No.1

PDP-9
Processor

Dectape
Control

Data
Channel
No.2

Scaler
Input
(AC)

Real Time
Clock

Input From
3 Scalers
(Schmidt Triggers
Or Prescalers)

NOTE:

6 Bits Of Tag Information From Each
ADC Include One Bit For Coincidence,
1 Bit To Identify ADC, 1 Bit For Reject,
And 1 Bit For Clock.

INC-B-9102

Figure 46. Block diagram of typical interface between nuclear ADC's and digital computer illustrating versatility of data handling capability of such systems.

machine. The normal program in operation at that time is then interrupted, and a special program called to handle the information presented to the processor by the device which produced the "interrupt". This method of entry provides the ultimate in flexibility, but may result in a considerable increase in the time required to handle an event which has been analyzed and presented for storage.

3. 3-cycle data-break mode — The Digital Equipment Corp. machines such as the PDP-9, provide a special form of fast entry which makes it possible to handle data at very high rates, using a form of cycle stealing which permits the use of list techniques for handling data. A detailed description of this mode of entry is beyond the scope of this paper. Let it suffice to say, that it makes possible the handling of data at very high rates, with all of the combined advantages of direct memory access and interrupt modes.

Let us assume that we are using the interrupt mode of operation, for the sake of this discussion. As indicated in the figure, the input from each ADC is represented by an 18 bit register which provides for 12 bits of

data and 6 bits of tag information for each event. This additional 6 bits may be used to designate whether or not the event was one of a pair of coincidence events, which ADC produced the event, whether or not the pulse was from a pulse generator (for gain stabilization or live time measurement), and whether or not the pulse should be rejected for any reason designated by external pulse conditioning circuitry. In multiparameter operation, this information would serve to determine where the event should be stored, *i.e.*, which portion of the multidimensional array, singles, *etc*. Also, other information of interest can be stored for future reference (*e.g.* number of rejects, for what reason, singles, coincidences, and simultaneously a record of gain and zero stability, *etc.*).

Other peripherals identified in the figure include (1) three 18 bit relay operated voltage dividers for operating computer controlled pulse generators for gain and zero stabilization, checking instrumental linearity, and controlling other experimental parameters which require an analogue signal, (2) a tape deck, and (3) scaler inputs for gross indication of counting rates or other digitized information of interest, and (4) an oscilloscope display.

A point of general interest is to provide a response to the question: Should a processor system or "hard-wired" system be chosen for a particular application? Of course, no simple answer will suffice. The computer based system will require a definite commitment on the part of the user to become knowledgeable in the areas of digital logic and computer systems programming. We conservatively estimate that the cost of the total programing effort required to bring such a system on line is equal roughly to the capital investment in equipment.

C. Control Panel Concept

One of the greatest difficulties encountered in the use of digital processors for data acquisition results from the unfamiliarity of experimenters with such equipment. Normally, the only means for an experimenter to communicate with the processor is through a teletypewriter keyboard. This implies that the normal operations encountered in the use of a multichannel pulse-height analyzer must be accomplished through a very lengthy dialogue with the computer, using the keyboard. A concept which provides a satisfactory alternative is one which provides the user with a switch panel which may be identical in every respect to that which he normally uses in the operation of laboratory equipment. Figure 47 is a photograph of a control panel and oscilloscope display interfaced to a PDP-8 processor which simulates a multichannel pulse height analyzer. Such panels, which may be located remotely from the processor, provide the user with complete control of his experiment and require no knowledge of computer equipment.
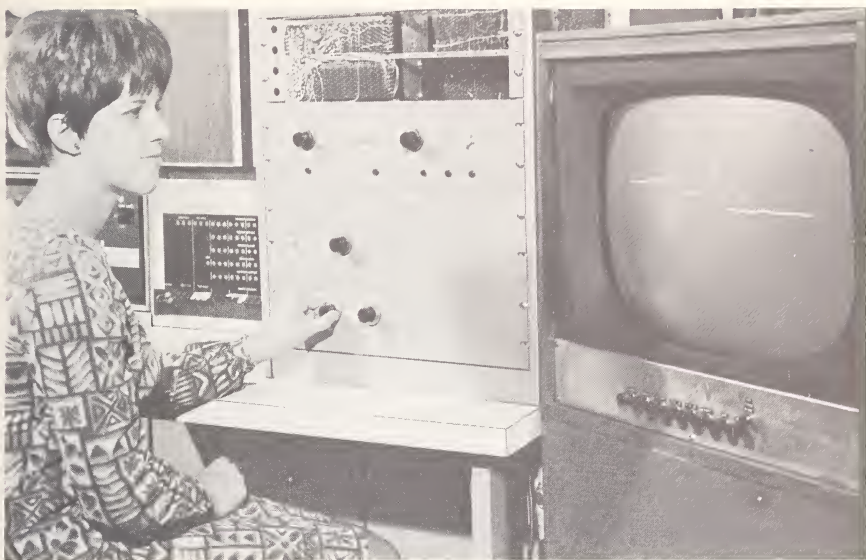
Figure 47.   Photograph illustrating use of "control panel" simulating hard-wired functions
of conventional multichannel pulse height analyzer.

The Digital Control Panel concept provides a simple solution to this important problem. The position of all switches on the panel are decoded and presented to the computer interface as the contents of a digital register which is examined periodically by the resident program in the computer that is controlling the experimental input. Hardware and software overhead for the use of this approach are minimal.

D.   GRAPHICAL DISPLAY DEVICES

A modern computer display system incorporates devices to supplement the cathode-ray tube which make it possible to achieve true interaction between the operator and the program being executed in the computer. The principle devices of interest are (1) the light pen, and (2) the function keyboard. The use of these two devices with a display oscilloscope are the basis of computer graphics as applied to techniques for on-line analysis of experimental data.

The light pen, illustrated in Figure 48, is an optical device which permits an operator to identify for the computer, points of reference from the material displayed on the oscilloscope screen, and subsequently to initiate operations of his choice. Then, based upon his own judgement he can view the result and repeat the operation or change the procedure if desired. A typical use of the light pen is illustrated by Figure 49. In Figure
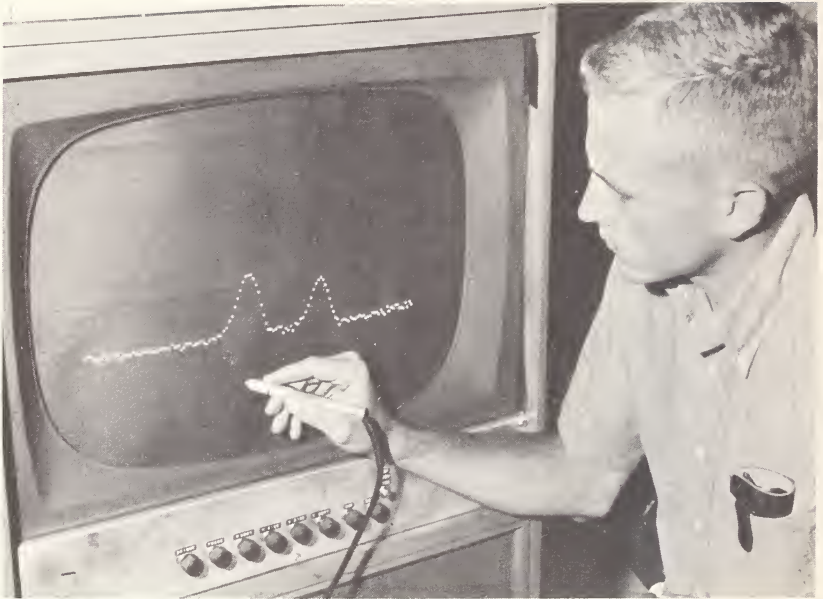
Figure 48.   Photograph of operator using light pen and large display oscilloscope to interact with computer system.

48 the operator is viewing a portion of a pulse height spectrum on the oscilloscope screen. Let us say that he desires to know the channel position of a peak in this spectrum. He might point the light pen at the dot representing the maximum y value for that peak. The result is shown in Figure 49. The point of interest has been intensified and the channel number associated with that peak displayed in the upper left-hand corner of the oscilloscope screen. This type of operation, which might be termed information retrieval, is considered to be the most effective use of the light pen, although it may also be used to insert subjective material, *e.g.*, to "draw in" estimates of background intensities on the screen for subsequent subtraction, *etc*.

The function keyboard is a simple device consisting of a small keyboard which is interfaced to the computer, generally through the interrupt structure of the machine. An interrupt "flag" is generated when a key is depressed, which causes the computer to interrogate the keyboard register to determine which key has been activated. This information can then be used to implement any program residing in the computer memory. An example of how these devices are used might be to describe a procedure used to analyze Ge(Li) spectra using graphical techniques [33,34]. Assuming that a portion (256 channels) of a 4096 channel pulse height spectrum is displayed on the large screen oscilloscope, as if one
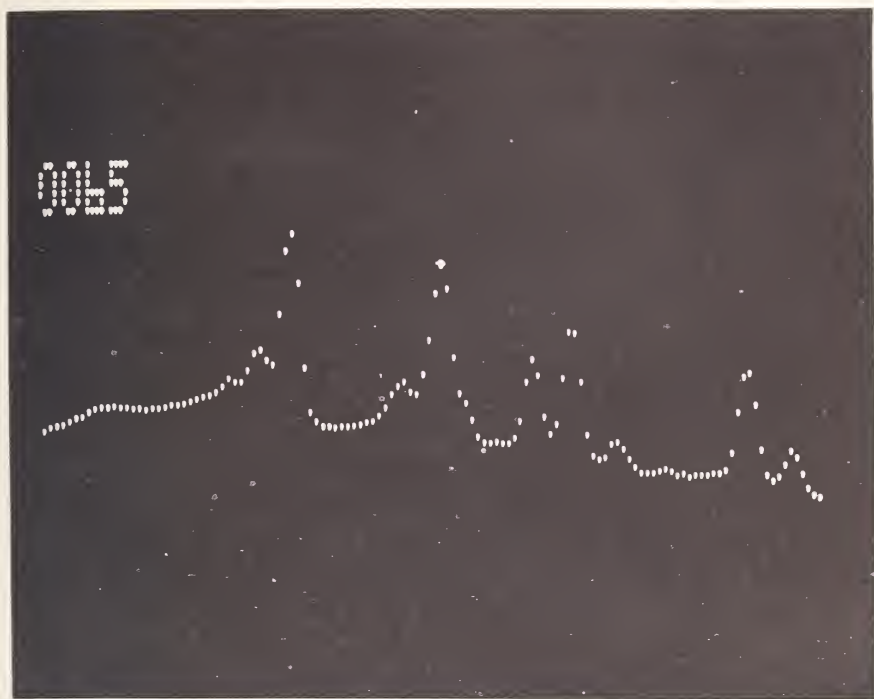
Figure 49. Display of oscilloscope screen showing concept of information retrieval using light pen. Intensified dot indicates which point was interrogated with light pen. Channel number retrieved is displayed in upper left hand corner of screen.

were viewing a portion of the surface of a rotating drum, one of the channels is intensified to provide a reference. The operator, by depressing keys on the function keyboard, may cause the spectrum to rotate past him from right to left or from left to right. During this process of rotation, the intensified point remains fixed in position, so that the reference point is changing. To determine the position (or energy) of a given peak in the spectrum, the operator chooses a point on the side of a given peak by rotating the spectrum until that point is intensified. He then depresses another key on the "function box" which activates a program which performs a fit to that peak and ultimately determines the energy, intensity, *etc.* Using similar techniques to extract information on the background, *etc.*, this procedure can be used to accomplish the entire analysis of a spectrum. Typically, an experienced user can analyze a 4096 channel pulse-height spectrum from a Ge(Li) spectrometer containing 50 to 100 peaks and determine energies and intensities in a few minutes. Normal techniques, employing plotting, card punching, and the use of large fitting routines in a normal batch mode with a large computer system, require from 1 to many days to analyze such a spectrum, depending on operator
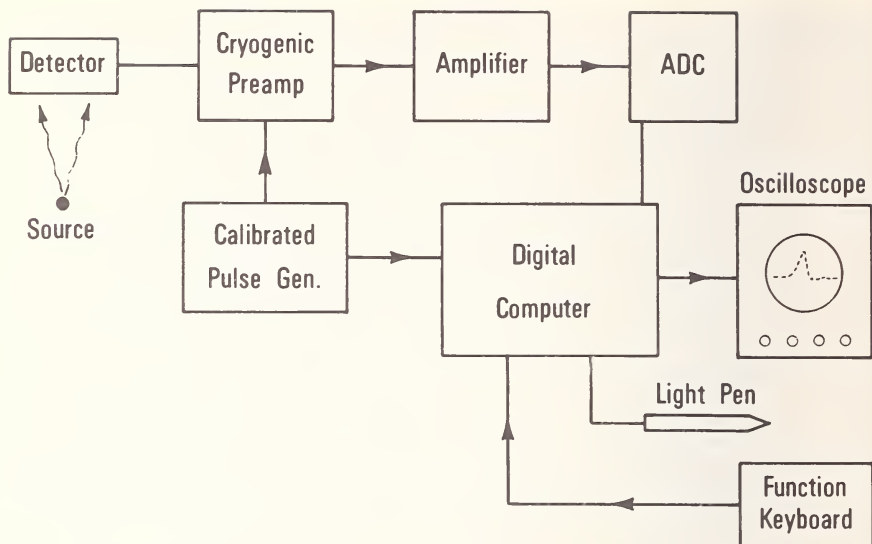
Figure 50.   Block diagram of automated analysis system for x-ray fluoresence applications which permit on-line qualitative elemental analysis.

accuracy in punching, etc. We feel that this accomplishment is an adequate demonstration of the power of graphical techniques for on-line data analysis.

Another example of the present capabilities of on-line data acquisition and analysis is illustrated by Figure 50. This figure represents a block diagram of an automated x-ray fluorescence analyzer which has been demonstrated in laboratory form. It incorporates a cryogenic Si(Li) high resolution x-ray spectrometer, ADC, and a digital computer with graphical display system. Using an ultra-stable pulse generator which is calibrated in terms of charge produced in the detector, the gain and zero reference of the ADC system is continuously determined by the digital computer. After the measurement of a sample is completed, the resultant spectrum is displayed on the oscilloscope screen. An operator may then interrogate this spectrum by the use of the light pen and function keyboard to determine the elemental composition of the material. This is accomplished by pointing the light pen at the highest channel of a peak in question. A program residing in computer core will then determine the position of this peak on the channel *vs* energy scale and calculate the energy corresponding to this position. By search and comparison with a reference library file of x-ray energies for each element, which are also residing in core, an elemental identification is made and the result displayed adjacent to the peak of the oscilloscope screen. Provision for including interferences may be included. The results of such analyses are shown by the two spectra in Figure 51. These results illustrate two
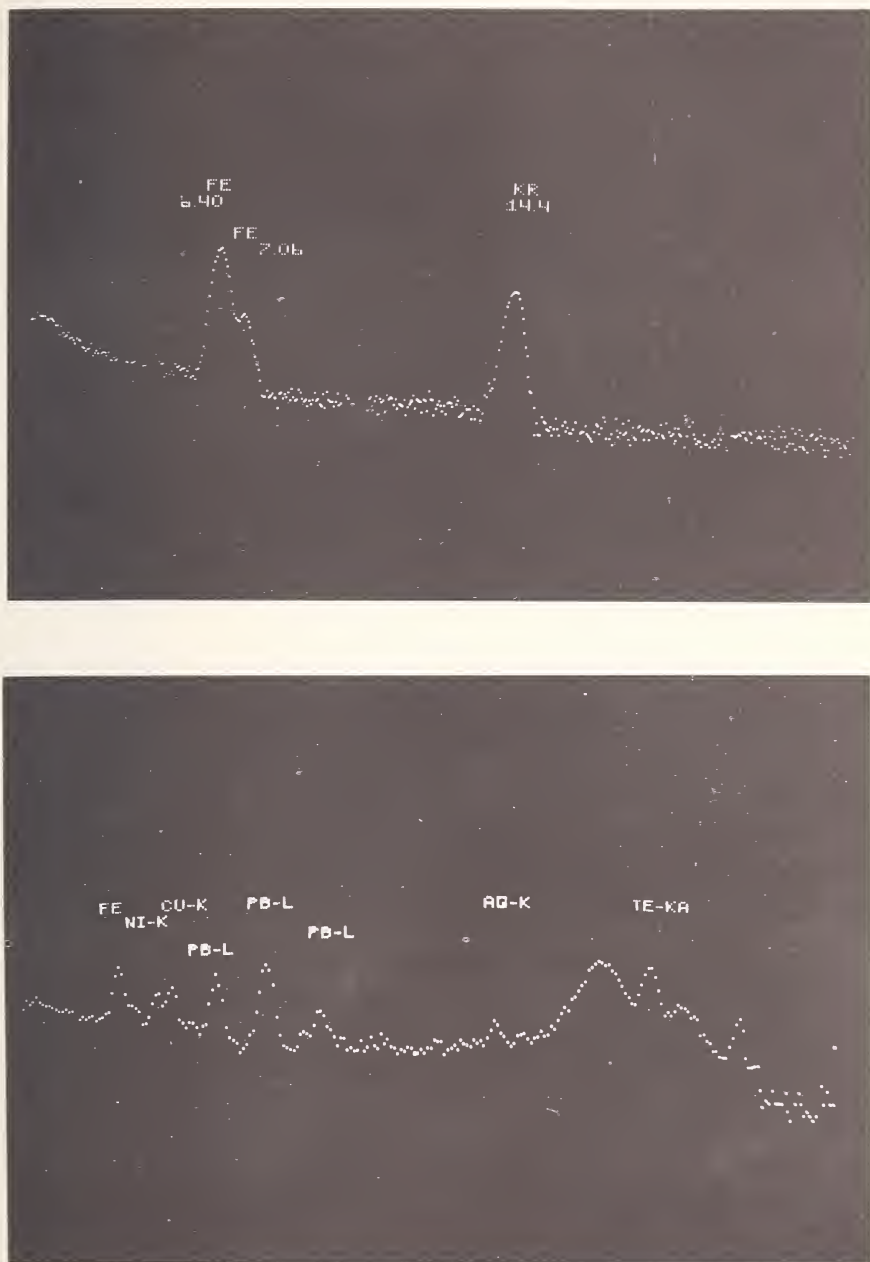
Figure 51. Oscilloscope display of qualitative analysis of two x-ray spectra using automated data system.

possible formats for the output of the results of the analysis. The important conclusion, since the techniques are quite straightforward, is that such automated analysis equipment, with the present state-of-the-art in microelectronic circuitry can be constructed in the form of a field instrument which would place the power of a very sophisticated laboratory technique in the hands of field geologists, metallurgists, *etc.* Read-only memories and other component developments which are presently available make the possibility of realizing a reliable system of this type appear quite attractive.

VII.   Summary

The advances made in the development of high resolution gamma-ray spectrometers and in the techniques for the use of digital processor systems for the acquisition and on-line analysis of pulse-height data offer many practical advantages for applications in the field of activation analysis. Reliability and cost of such sophisticated equipment are approaching the point where their economic use will soon become possible.

I believe that it is fair to state that the largest real cost incurred in practical activation analysis is connected with the process of data analysis. The development of graphical techniques which permit interactive dialogue between experienced operator and machine will greatly enhance the capability for the use of advanced and sophisticated techniques for data analysis. Up to the present time, the major limitation to extending the capabilities of laboratory techniques to routine analytical procedures has been the requirement for the input from experienced scientific personnel. The reduction of this process to one which will require little time per analysis will greatly simplify the process.

VIII.   Acknowledgments

IX. References

[1]   McKay, K. G., Phys. Rev. **84**, 829 (1951).
[2]   Meyer, J. W., J. Appl. Phys. **30**, 1937 (1959).
[3]   Walter, F. J., and Dabbs, J. W. T., AEC Report ORNL 2501, 73 (1958).
[4]   Goulding, F. S., Nucl. Instr. and Meth. **43**, 1 (1966).
[5]   Pell, E. M., J. Appl. Phys. **31**, 291, 1675 (1960).
[6]   Freck, D. V., and Wakefield, J., Nature **193**, 669 (1962).
[7]   Webb, P. P., and Williams, R. L., Nucl. Instr. and Meth. **22**, 361 (1963).
[8]   Tavendale, A. J., and Ewan, G. T., Nucl. Instr. and Meth. **25**, 185 (1963).
[9]   Tavendale, A. J., IEEE Trans. on Nucl. Science, **NS-11**, 3, 191 (1964).
[10]   Fano, V., Phys. Rev. **70**, 44 (1946).
[11]   Nybakken, T. W., and Vali, V., Nucl. Instr. and Meth. **32**, 121 (1965).
[12]   Elad, E., Nucl. Instr. and Meth. **37**, 327 (1965).
[13]   Radeka, V., IEEE Trans. on Nucl. Science, **NS-11**, No. 3, 358 (June 1964).
[14]   Smith, K. F., and Cline, J. E., IEEE Trans. on Nucl. Science, **NS-13**, 468 (June 1966).
[15]   Fairstein, E., and Hahn, J., "Nuclear Pulse Amplifiers — Fundamentals and Design Practice", Parts I – IV, Nucleonics, **23**, No. 7, 9, 11 (1965), and **24**, No. 1 (1966). (1966).
[16]   Crouch, D. F., and Heath, R. L., U.S. AEC Report IDO-16923 (1963).
[17]   Black, W. W., and Heath, R. L., IEEE Trans. on Nucl. Science, **NS-14**, No. 1, 591 (February 1967).
[18]   Black, W. W., Nucl. Instr. and Meth. **53**, No. 2, 249 (1967).
[19]   Knowlin, C. A., and Blankenship, J. L., Rev. Sci. Instr. **36**, 1830 (1965).
[20]   Robinson, L. B., Rev. Sci. Instr. **32**, 1057 (1961).
[21]   Chase, R. L., and Poulo, L. R., IEEE Trans. on Nucl. Science, **NS-14**, 83 (February 1967).
[22]   Gere, E. A., and Miller, G. L., IEEE Trans. on Nucl. Science, **NS-14**, 89 (February 1967).
[23]   Cline, J. E., and Johnson, L. O., (to be published).
[24]   Sakai, E., IEEE Trans. on Nucl. Science, **NS-15**, 310 (1968).
[25]   Johnson, L. O., and Heath, R. L., (to be published).
[26]   Helmer, R. G., Heath, R. L., Putnam, M., and Gipson, D. H., Nucl. Instr. and Meth. **57**, 46 (1967).
[27]   Helmer, R. G., U.S. AEC Report IN-1117, 32 (1967).
[28]   Seppi, E. J., Hendrikson, H., Boehm, F., and DuMond, J. W. M., Nucl. Instr. and Meth. **16**, 17 (1962).
[29]   Heath, R. L., "Scintillation Spectrometry Gamma-Ray Spectrum Catalogue", U.S. AEC Report IDO-16880 (1964).
[30]   Cline, J. E., IEEE Trans. on Nucl. Science, **NS-15**, 198 (1968).
[31]   Motz, H. T., Carter, R. E., and Barfield, W. D., Proceedings of a Symposium on Pile Neutron Physics, Vienna 1960 (IAEA 1962).
[32]   Hoogenboom, A. M., Nucl. Instr. **3**, 2, 1 (1958).
[33]   Black, W. W., and Heath, R. L., IEEE Trans. on Nucl. Science **NS-14**, No. 1, 591 (February 1967).
[34]   Richardson, C. W., Proceedings of DECUS Society (November 1967).

DETECTORS AND INSTRUMENTATION

Synopsis of Discussions

WILLIAM S. LYON

Oak Ridge National Laboratory
Oak Ridge, Tennessee

Our first paper established the usefulness and accuracy of spec-troscopy in applied activation analysis problems. At Iowa State, comparisons were made between NaI and Ge spectroscopy for trace determinations of potassium in potassium tungstate, lanthanum in lanthanum tungstate, and certain rare earth mixtures, Tb in Ho at various concentration levels, and Tb, Yb, Ho 1:1:1 mixtures. In all cases Ge shows less error than NaI, and seemed definitely superior. In the analysis of Ho for Tb, the NaI technique involved two gamma-ray peaks and with the germanium, eleven peaks. At Tb/Ho ratio of 1/100, 5 percent seems to be a reasonable error expectation. Where Tb-Yb-Ho was analyzed at 1:1:1 ratios ± 3% error was found. In the discussion period no clear error for the poorer showing of NaI was advanced. Data handling was performed by computer processing.

With these useful and interesting results fresh before us, the presentation of a method for measurement and comparison of detector efficiencies in Ge was pertinent and important. Because Ge detectors are produced in all sizes and forms, no standard method of comparison of detector efficiencies has yet been selected. The method presented here involves measurement of a standard source at 2 or more distances from the detector. The inverse square root of the count rate as a function of source-detector distance is plotted, and from this, the slope and distance intercept are obtained. From these two parameters, the detector efficiency can be calculated. During the discussion, several precautions were noted, particularly the requirement that distance be carefully measured, and that either a point source or point detector is assumed. The method holds considerable promise.

Since standard sources are so important in calibration and efficiency studies such as the one just mentioned, we were fortunate to learn from a representative of the National Bureau of Standards that standardized sources of ^{109}Cd and ^{228}Th are now available.

Our subject matter then became more complex as we heard reports on computerized systems and large anticoincidence or multidimensional

analyzer systems — some employing Ge, some NaI, and some with both, or with plastic scintillators. The point was made that in any of these systems, a reduction in the photopeak efficiency by *e.g.* a factor of 10, must be accompanied by a reduction in Compton background of 100. A study of one speaker indicates that two-thirds of the common nuclides encountered in activation analysis may be improved in detectability by use of an anticoincidence shielded germanium spectrometer. An interesting feature of these systems is that both coincidence and anticoincidence data are collected and stored; thus, one is able to take advantage of the unique properties of the several nuclides in the mixture. In discussion, a member of the audience described briefly a duode, *i.e.* a split Ge detector, that he has used for studies similar to those mentioned above. This duode should soon be commercially available. It was also brought out in the discussion that to reduce interference at the low energy end of the spectrum requires a greater amount of plastic or NaI in the shield than to accomplish this at higher energies.

Additional systems described in succeeding talks included a dual channel analyzer and coincidence system, a large NaI double crystal assembly that can be used with or without a germanium detector, and a Compton-suppressed coincidence gamma-ray scintillation spectrometer with a large NaI(Tl) crystal. The large NaI assembly when used with a 4π gamma counter of 13.5 in. diameter and 12 in. length provides for total interaction efficiencies ranging from 4π at low energy to ~0.84 at 2.0 MeV. It is most useful for positron emitters. The NaI can also be used for Compton suppression in Ge spectroscopy. The other large system has two subassemblies 13 1/2 in. long with a 6 1/2 in. diameter hole in the center. In the center hole is a 6 1/2 in. × 4 in. thick NaI crystal. Special matched photomultiplier tubes are used. Background and Compton suppression is quite good, but total efficiency is somewhat lower than with the other system.

Certain observations seem inescapable, and it is these that might prompt discussion and thought: (1) These large expensive systems are here, they are successful, and their use is increasing. Many of them, one suspects, were purchased as much for nonactivation programs as activation. Can a laboratory doing only activation analysis justify such devices? (2) With increasing sophistication of equipment, more and highly specialized technical manpower is needed. Can activation programs attract, utilize, and reimburse such people? What is the amount of down time with these machines? How many problems can be solved only by these means? (3) What does the future hold? Can the average laboratory afford to keep pace in their instrument race, or must the game go by default to the rich, rather than to the wise or the good?

In the plenary discussion, one European scientist voiced the opinion that probably 90 percent of the complex mixtures in his laboratory were

analyzed by Ge but where chemistry was indicated, NaI was preferred because of the much shorter counting time required. Long counting times cause a backlog of samples with the Ge systems. In Europe at present, there appear to be no large NaI or Ge complex systems such as described by American authors.

The cost of one such system was estimated at about $10,000 more than the required $30,000 for "state of the art" Ge assembly. Analyzers cost at least $25,000 – $30,000, and large NaI crystals can never be cheap. Probably, if one is able to operate a "state of the art" Ge system, one could also utilize one of these complex ones.

The importance of the improved sensitivity obtained by these large units should not be underestimated although it was conceded that chemistry might reduce the demand for complex instrumentation.

In another discussion the point was made that probably most of these systems had been purchased for purposes other than activation analysis, the complexity of electronics for NaI is in general less than for Ge, and that there may well be some intermediate ground between 3 in. × 3 in. NaI and the complex systems described above.

COMPARISON OF SOLID STATE AND SCINTILLATION GAMMA-RAY SPECTROMETRY IN ANALYSIS[1]

Adolf F. Voigt, Duane E. Becknell and Sr. Laurene Menapace

Institute for Atomic Research and Chemistry Department
Iowa State University, Ames, Iowa

I. Introduction

Although solid state detectors have been widely acclaimed as superior to scintillation detectors in almost every respect, actual comparisons of their behavior in analytical applications are conspicuously missing in the published literature.

The much better resolution of the solid state detector, referring exclusively to lithium-drifted germanium, may be offset by its lower efficiency. The higher atomic number of iodine gives the NaI(Tl) scintillation detector a considerably greater photoelectric efficiency at higher energies. The larger active volume of these counters also means that multiple Compton events can contribute appreciably to the counts within the full energy peak. The difference in efficiency as a function of energy for typical Ge(Li) and NaI(Tl) detectors is shown in Figure 1. For these measurements the standards were at the same distance, 10 cm, above a "20 cm³" Ge(Li) detector and a 10 cm NaI(Tl) well crystal.

It is difficult to disagree with the statement that the solid state detector is superior in application to qualitative or semi-quantitative analysis. In these cases its much better resolution outweighs any disadvantages. However, the situation may be different if the goal is the best precision available in activation analysis, or if the highest counter geometry and efficiency are needed, *e.g.* for an activity of very short half life. If the gamma rays from different components do not conflict, it is entirely possible that more precise results may be obtainable with a scintillation counter.

The purpose of these experiments was to compare the two detector systems in several analytical applications in which precision was the goal. These were the determination of several elements in the non-stoichiometric tungsten "bronzes" and the analysis of mixtures of rare earths.
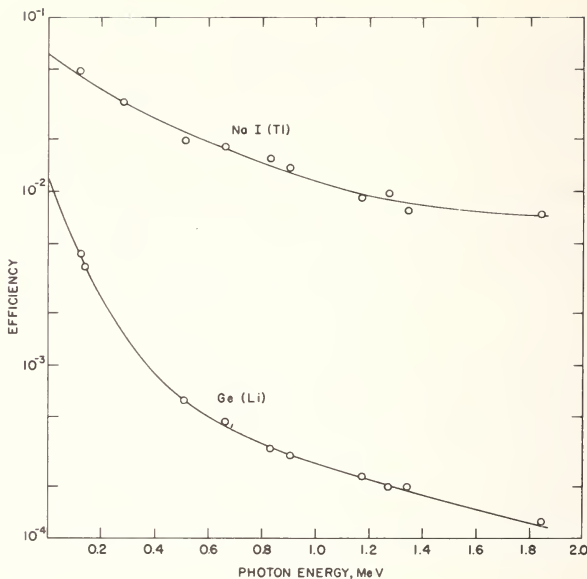
Figure 1.   Photopeak efficiency curves for NaI(Tl) and Ge(Li) detectors.

A.   Potassium-Tungsten Bronzes

Several methods are available for activation analysis of the compounds $K_xWO_3(0>x>1)$. The use of high energy photon activation has been published [1] but for routine work we have found that neutron activation followed by beta counting gives somewhat more reliable results. Scintillation counting of the gamma radiation has also been used with inconclusive results. In this case the low yield of the principal gamma ray (1.52 MeV) from ^{42}K presents a resolution problem even though its energy is well out of the range of the gamma rays from ^{187}W (0.48 to 0.878 MeV). This would appear to be a good case for scintillation counting, since there should be little interference and the greater efficiency of NaI at higher energies should be an advantage.

Various bronzes which had been analyzed by beta counting were irradiated using an internal standard method with K_2WO_4 as the comparison standard. Peak areas for potassium and tungsten were compared in both sample and standard and the analyses were based on these ratios. The accuracy thus depends on the assumption of a K/W ratio of exactly 2.00 in K_2WO_4. Other systematic and random errors are less than if an external standard is used. For each irradiation two samples and three K_2WO_4 standards sealed in polyethylene tubing were irradiated for 30 sec at a flux of $8 \times 10^{12} n \cdot cm^{-2} \cdot sec^{-1}$. Counting was done immediately after removal from the reactor. For the solid state counting the sample

was 3 cm from the detector and for scintillation counting 4 cm away with 1.6 cm of lead to depress the lower energy [187]W peaks. Solid state data were analyzed by a peak-finding program called ICPEAX. Direct comparison of the 1.52 MeV [42]K peak was made with each of five [187]W peaks at 0.480, 0.552, 0.619, 0.686 and 0.773 MeV and an x value was calculated from each comparison. These values were averaged for a single determination. The results represent the average of 5 or 6 such determinations with the error calculated from the deviation from this average.

Results in Table 1 show that the Ge(Li) data are much more precise than those from NaI(Tl) and that their differences from the beta counting method are considerably less. It would appear that greater reliance can be placed on the Ge(Li) data.

Table 1. Determination of K in $K_x WO_3$.

Sample	x value			Standard deviation (%)		
	Ge (Li)	NaI(Tl)	Beta	Ge (Li)	NaI(Tl)	Beta
K_2WO_4	2.00	2.00		0.8	4.3	
K9H	0.324	0.323	0.276	3.7	37.	4.4
K14K	0.296	0.416	0.312	0.7	3.8	3.2
K1B	0.309	0.403	0.284	2.3	3.7	4.2
K15H	0.282	0.323	0.302	1.7	5.8	4.0
K10A	0.298	0.343	0.304	0.7	15	5.9
Average				1.7	11.6	4.3

B. Lanthanum-Tungsten Bronzes

An external standard method has been published [2] for the analysis of the compounds $La_x WO_3$ in which a well-type NaI(Tl) crystal was used. The 1.6 MeV photopeak of [140]La and its sum peaks up to 2.25 MeV were counted in the sample and in a standard irradiated simultaneously.

We have now developed an internal standard method based on Ge(Li) detectors which involves the comparison of the 1.60 MeV [140]La peak and either the 480 or 686 keV [187]W peak. Choice between these depends on the method used. The 480 peak is ~50 times as intense as the 686 peak and is better for a computer-based calculation, while the 686 peak is more isolated and is better if a hand calculation is made. When the latest results were being calculated, the computer program was not operating properly and hand calculations were used.

Typical results of a computer calculation using the 480 keV peak are shown in Table 2. The deviation is about 5%. The expected value is an approximation based on stoichiometry.

Table 2. Analysis of La_xWO_3.

	Counting rates, c/m		Counting rate ratio W/La	La/W
	0.48 MeV	1.6 MeV		
Standard	1.02×10^5	9.98×10^2	1.02×10^2	0.153
Sample	7.87×10^4	1.18×10^2	6.69×10^2	
Standard	4.76×10^6	1.25×10^3	3.81×10^3	0.148
Sample	6.59×10^6	2.55×10^3	2.58×10^4	
Standard	9.26×10^5	1.37×10^3	6.76×10^2	0.163
Sample	1.20×10^6	2.90×10^2	4.14×10^3	
			Average	0.155
			Expected value	0.150

To test reproducibility with the 686 peak a series of 8-10 samples with a 1:1 La/W composition were prepared. One of these was used as a comparison standard and the counting rate ratios of the others were averaged and used to calculate a value of x. This value is listed in Table 3, with the error, σ_m, standard deviation of the mean value.

For the analysis of the bronzes the same procedure was used with each irradiation including five standards of the 1:1 La-W mixture, and three samples of the bronze. In this case also the errors listed in Table 3 are σ_m.

Table 3. Analysis of La_xWO_3.

W/La counting rate ratio, 686/1600

Nominal x value	Standard	Sample	x (La/W)
1.00	1.985	1.972 ± 0.012	1.007 ± 0.006
	2.099	2.095 ± 0.006	1.002 ± 0.003
0.15	1.232 ± 0.008	8.92 ± 0.18	0.1381 ± 0.0029
(0.150 ± 0.001)[a]	1.232 ± 0.008	8.93 ± 0.08	0.1380 ± 0.0015
	1.789 ± 0.013	12.88 ± 0.10	0.1389 ± 0.0015
	2.062 ± 0.017	15.05 ± 0.21	0.1370 ± 0.0022
0.015	1.881 ± 0.008	39.30 ± 0.76	0.0479 ± 0.0009
(0.068 ± 0.001)[a]			

[a] Previously determined by scintillation counting.

The values obtained for the 0.15 bronze are a bit lower than those observed with the 480 peak, but they are quite consistent. The results show that the nominal 0.015 bronze actually has an x value 3 times this large.

Comparison of these results with those from scintillation counting indicates that the solid state detector has a slight edge in reproducibility and, we now believe, in accuracy as well. The difference between the two methods is not great.

C. Rare Earth Mixtures

A problem to which we have given thought and experimentation for some time has been the analysis of rare earth mixtures, particularly for traces of rare earth impurities in a purified rare earth. This problem is essentially unapproachable by scintillation techniques, and even mixtures of similar concentrations are now analyzable by nondestructive methods.

The much greater selectivity of the solid state detector makes it seem feasible to try nondestructive methods for trace analysis. However, we felt it was necessary to demonstrate first that accurate results could be obtained by relatively large amounts of the rare earths in each other. The success of such a method appears to depend to a great degree on the resolution and reproducibility inherent in a particular detector and amplifier system.

Thus far we have applied the methods to several mixtures of terbium in holmium and a 1:1:1 mixture of terbium, ytterbium and holmium. In one set of experiments seven 1.00 mg samples of 1:1 mixture of Tb-Ho were irradiated with a 0.50 mg samples of Tb as an external standard. In the analysis by external standard the Tb peak areas in the samples were compared to the area of the same Tb peak in the standard. For the internal standard method the ratios Tb-x/Ho-1377 for six of the samples were compared to this ratio for sample 1, chosen arbitrarily as the standard. Typical calculations are shown in Table 4 for the 216 keV Tb peak. Similar data were obtained for eleven ^{160}Tb peaks with the Ge(Li) detector and two peaks, one of which was an unresolved doublet, with the scintillation detector. The results are listed in Table 5.

The determination by external standard using the 1115 keV Tb peak is obviously off by a large percentage; this was due to the measurement in the pure Tb standard. The total counts recorded under this peak were 1200 compared to 6000 to 50,000 for the other peaks. This measurement was discarded in computing the averages.

A similar analysis was made on a 1:10 Tb-Ho mixture. Solution samples with this Tb/Ho ratio were pipetted into polyethylene capsules, dried, sealed and irradiated with an integrated flux of 9×10^{15}n/cm^2. Spectra were accumulated for 45 min live time starting 12 hr after the

Table 4. Analysis of 1:1 Tb–Ho mixture using 216 keV Tb peak, 1380 keV Ho peak.

Sample	External standard			Internal standard	
	area	$\dfrac{\text{sample}}{\text{standard}}$		Tb/Ho	$\dfrac{(\text{Tb/Ho})n}{(\text{Tb/Ho})_1}$
Standard	73550				
1	57770	0.785		1.241	
2	97060	1.320		1.364	1.099
3	77850	1.058		1.352	1.089
4	69220	0.941		1.202	0.969
5	74970	1.019		1.302	1.049
6	74280	1.010		1.290	1.039
7	68060	0.925		1.182	0.952
Average		1.008			1.033
		± 0.062			± 0.025
Wt Tb (mg)		0.504			0.516
		± 0.031			± 0.012

Table 5. Analysis for terbium in holmium 1:1 mixture, expected value 0.500 mg.

	Tb peak (keV)	Ho peak, 1380 keV	
		External standard (mg)	Internal standard (mg)
NaI(Tl)	197 } 216 }	0.519 ± .015	0.494 ± .018
	298	0.523 ± .013	0.503 ± .014
	Average	0.521 ± .014 (.002)	0.499 ± .016 (.004)
Ge (Li)	197	0.565 ± .030	0.516 ± .031
	216	0.560 ± .023	0.504 ± .025
	299	0.540 ± .014	0.488 ± .015
	392	0.541 ± .022	0.433 ± .014
	879	0.539 ± .014	0.479 ± .014
	966	0.536 ± .014	0.482 ± .017
	1115	0.698 ± .024	0.464 ± .021
	1178	0.534 ± .014	0.481 ± .015
	1200	0.523 ± .012	0.482 ± .013
	1272	0.534 ± .014	0.487 ± .015
	1312	0.537 ± .020	0.495 ± .021
	Average (excl 1115)	0.541 ± .018 (.004)	0.485 ± .019 (.007)

irradiation. The computer method ICPEAX was used to resolve the spectra. A comparison standard of the same composition was used. Results are shown in Table 6 comparing the effectiveness of five Tb and three Ho peaks.

Table 6. Analysis of 1:10 Tb–Ho mixture Tb/Ho wt ratio $\times$ 10.

Tb peaks (keV)	Ho peaks, keV			
	673	706	1380	Average
216	1.13 ± 0.07	1.18 ± 0.13	1.06 ± 0.07	1.12 ± 0.09
298	1.05 ± 0.09	1.06 ± 0.06	0.97 ± 0.05	1.03 ± 0.07
879	1.01 ± 0.05	1.05 ± 0.07	0.93 ± 0.01	1.00 ± 0.05
962	1.02 ± 0.08	1.03 ± 0.08	0.94 ± 0.04	1.00 ± 0.07
1178	1.05 ± 0.09	1.05 ± 0.07	0.96 ± 0.04	1.02 ± 0.07
Average	1.05 ± 0.08	1.07 ± 0.09	0.97 ± 0.05	1.03 ± 0.07
	(0.05)	(0.06)	(0.05)	

σ_m = 0.017

The procedure was repeated for a 1:100 Tb-Ho mixture. In this case only the 216 keV Tb peak was large enough to be used. Results of internal standard comparison of these peak-ratios against a standard of the same composition are shown in Table 7. It appears that the method can be used at this level with no loss in accuracy. However, the 216 keV peak practically disappears at ratios much less than 1:100.

Table 7. Analysis of 1:100 Tb–Ho mixture Tb/Ho ratio $\times$ 100.

Ho peaks keV	Tb peak 216 keV
673	1.03 ± 0.03
706	0.999 ± 0.07
1380	0.997 ± 0.06
Average	1.009 ± 0.05
	(0.019)

The final study to be reported was on a ternary mixture of equal weights of terbium, ytterbium and holmium in which the Tb and Yb were determined. These results are shown in Table 8. The addition of a third' component has not created any difficulty in this case as the reproducibility and accuracy are as good as in the binary mixture. From

Table 8. Analysis for Tb and Yb in Ho 1:1:1 mixture,
expected value 1.00.

| Tb peaks (keV) | Ho peaks, keV | | Average |
	706	1380	
299	1.02 ± 0.09	0.98 ± 0.03	1.00 ± 0.07
879	1.01 ± 0.09	0.97 ± 0.03	0.99 ± 0.07
966	0.99 ± 0.10	0.95 ± 0.04	0.97 ± 0.07
1178	1.01 ± 0.15	0.96 ± 0.07	0.98 ± 0.12
Average	1.01 ± 0.11 (0.01)	0.96 ± 0.05 (0.01)	0.98 ± 0.08 (0.03)
Yb peaks			
251	1.08 ± 0.12	1.03 ± 0.04	1.05 ± 0.09
282	1.02 ± 0.10	0.98 ± 0.02	1.00 ± 0.07
396	0.99 ± 0.12	0.94 ± 0.05	0.97 ± 0.09
Average	1.03 ± 0.11 (0.03)	0.98 ± 0.04 (0.03)	1.007 ± 0.08 (0.03)

the large number of peaks seen in spectra of these mixtures, it appears clear that scintillation counting would be much less effective as the situation approaches this complexity.

II. Conclusions

The choice of solid state *vs* scintillation counters for quantitative analysis is not completely obvious. There appears to be situations in which better results are obtained by a scintillation counter, but this may be due to less than optimum use of the solid state detector. Improvement in reproducibility may come with improved circuitry following the solid state detector. On the other hand the greater efficiency of the scintillation detector may outweigh the resolution of the solid state detector for some applications, particularly if the amount of activity produced is less than optimum.

III. References

[1]   Wechter, M. A., and Voigt, A. F., Anal. Chem. **38**, 168 (1966).
[2]   Wechter, M. A., and Voigt, A. F., Anal. Chim. Acta **41**, 181 (1968).

MEASUREMENT AND COMPARISON OF DETECTOR EFFICIENCIES

John A. Dooley

Air Force Flight Dynamics Laboratory
Wright-Patterson AFB, Ohio 45433

I. Introduction

Recent detector studies [1,2] and manufacturers' literature [3] indicate that no standard method prevails for the measurement and comparison of detector efficiencies. Some of the problems, including influence of detector shape on the efficiency-energy dependency, have been pointed up by Sandborg and Orth [4]. Trends to report Ge(Li) detector efficiencies in terms of a standard sodium iodide configuration may lead to further difficulties.

With sodium iodide detectors, efficiencies can be related fairly easily. With such solid detectors most investigations are carried out on 2 in. × 2 in. or 3 in. × 3 in. cylindrical shapes. The detector can is a tight skin; the same applies to liquid scintillators. Larger detectors and well-counters pose special problems.

The advent of germanium and silicon detectors has brought dozens of new shapes and sizes. Each manufacturer has solved the cryogenic problem in his own way. The detector face, or more importantly, the effective center of detection, resides at some arbitrary distance from the outside face of the can.

It will be shown that appropriate usage of the inverse-square law allows for direct, accurate and relatable efficiency determinations. The method involves measurement of a standard source at two or more distances from the detector. A plot is made of the inverse square root of the count area as a function of source-detector distance. From this plot can be derived two quantities which give important information about the detector: (1) the slope, in conjunction with the source emission rate, gives an efficiency factor which is independent of measurement distances, of placement of the detector within the can and, to some extent, is independent of detector shape, (2) the distance intercept gives the distance of closest approach of a source to the effective center of detection, and consequently the maximum detector efficiency can be computed. Together, the two quantities allow computation of efficiency for any source-detector

distance, including the maximum efficiency attainable by the detector. Thus, the standardization for any detector system is based on easily obtained information relating to an effective center of detection rather than to an arbitrary container distance.

II. The Method: An Efficiency Factor

Standardization on an efficiency factor requires agreement on time and distance units. Table 1 presents a list of units and definitions implicit in the development. The graphical efficiency method is illustrated in Figure 1. The vertical axis represents the inverse square root of the count area: in the cases discussed here, the area under a photopeak. The horizontal

Table 1. Definitions and units.

Quantity	Units	Definition
G	$\sec^{-1}$	Source gamma emission rate
Q	$\sec^{1/2}$	Inverse square root of count rate
R	cm	Distance from can to source
S	$\sec^{1/2}\mathrm{cm}^{-1}$	Slope of inverse square root plot
R_o	cm	Distance intercept on plot
R'	cm	Distance from detection center to source
E(R')	none	Efficiency
E.F.	cm^2	Efficiency factor
T_c	sec	sec per count interval used for plot
D	cm	cm per unit of distance in plot

axis gives source distance from the detector can. Units are arbitrary if corrections are applied. A straight line is obtained with an equation

$$Q = SR + SR_o \qquad (1)$$

The distance of closest approach, R_o, can be read directly from the graph and the slope, S, is computed as indicated on the figure. A graphical fit on 10 in. $\times$ 15 in. graph paper yields about 5% precision (exclusive of data errors). Better precision can be obtained by a least square fit to a straight line.
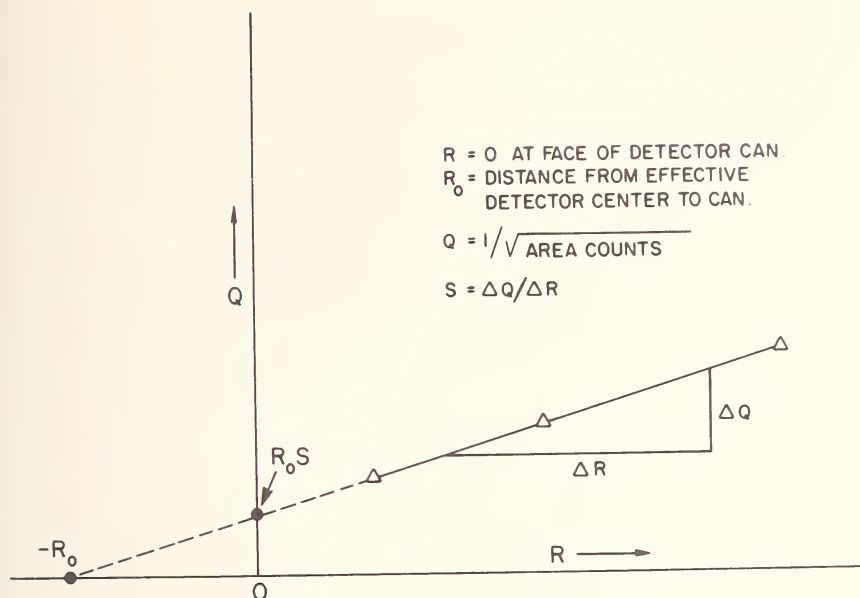
Figure 1.   Graphical efficiency method.

For the following three equations it is important to note that the distance reference for data analysis is the *effective detection center*, using R', which may or may not be the *detector geometric center*. The distance reference for measurement is the *detector container*, using R.

$$R'^2 E(R') = 1/GS^2 \qquad (2)$$

$$E.F. = 1/GS^2 \qquad (3)$$

$$E.F. = 1/GS^2 \cdot 1/T_c \cdot D^2. \qquad (4)$$

Equation (2) is the inverse-square law stated in terms of the quantities defined in Table 1. Equation (3) assumes units from Table 1 and shows that the efficiency factor, a constant, is exactly the extrapolated efficiency for a source distance of one cm from the effective detection center. Equation (4) indicates corrections to be applied for conversion of units.

Figure 2 shows data obtained on a 2 cm³ Ge(Li) system. The small range of distances used has introduced an error of about ± 1 mm in the extrapolated distance of closest approach, the average R_o being 1.39 cm for these data. Table 2 shows the tabulated analysis results for the detector. R_o, the distance of closest approach, was determined from the plots of Figure 2. The efficiency factors were computed from Equation (4). G, the source emission rates, are shown for reference. The sources, calibrated at the NBS, were corrected for decay.
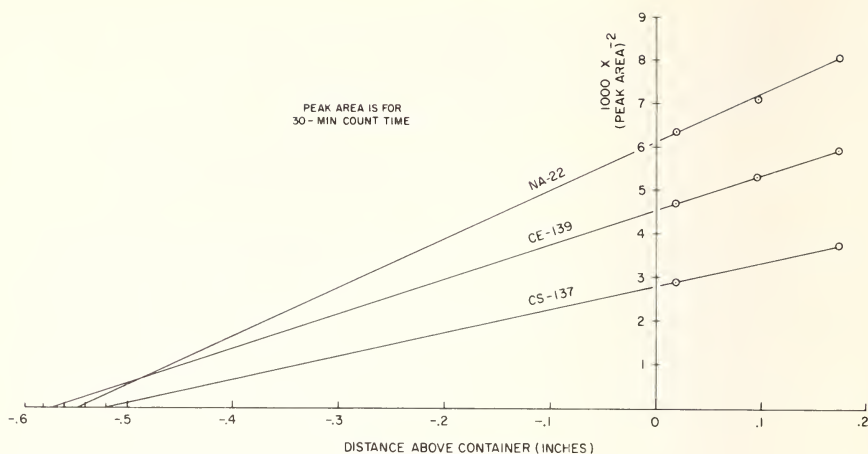
Figure 2. Inverse square root plot.

Table 2. Experimental efficiency parameters.

Energy (keV)	R_o (cm)	E.F. (cm^2)	G (sec^{-1})
166.	1.45	5.24×10^{-2}	1.085×10^3
662.	1.31	2.78×10^{-3}	4.48×10^4
1275.	1.39	9.76×10^{-4}	2.91×10^4

III. Efficiency Factors Compared

Efficiency measurements made on 2 cm³ detector systems illustrate the applicability of the method. All photopeak areas were converted to an effective source-detector distance of 1.00 cm. Figure 3 is a comparison of three such sets of efficiency factor determinations. Two of the sets of measurements were made on our system and the third at another laboratory. None of the curves were fitted by a function (cross section multiplied by exponential energy) of the sort used by Cothern and Tokcan [2] in recent measurements. Rather, smoothed connection lines were drawn to facilitate comparisons.

The five circles represent efficiency factors recently obtained at our laboratory [5] on a 4 cm² × .5 cm detector with photopeak areas computed on an IBM 7094 by our SPSA Computational System [6]. In this experiment the sources had individual source-center to detection-center distances varying from 1.40 to 1.86 cm. The dashed line connects hand-computed efficiency factor points previously obtained by Gorrell
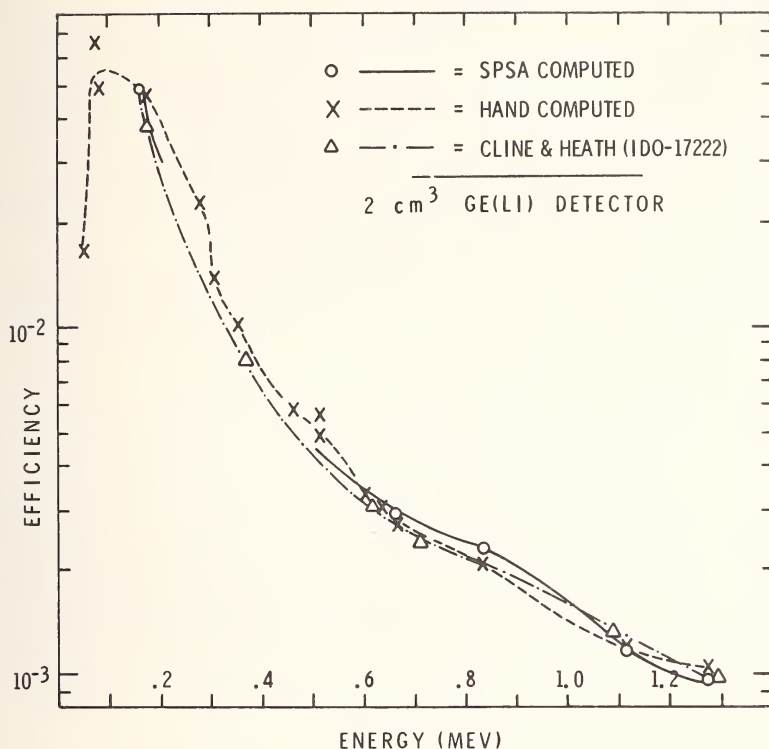
Figure 3.   Photopeak efficiency factors.

[7] and a student. They used a fixed center-to-center distance of 1.40 cm, which was with the source on the container.

The triangles represent efficiency factors calculated from Cline and Heath data [1]. They used a 2.5 $cm^2 \times .8$ cm detector with the sources 3 cm from the front face of the detector. For our calculations it was assumed that their effective center of detection was at the detector center. All three curves agree to within 10 to 15% from around 170 keV to 1300 keV.

IV. Discussion and Conclusions

For any given distance from detection center to source center, the measured efficiency ratio for two detectors will be the (constant) ratio of the two efficiency factors. For shallow (about 0.5 cm Ge) or diffuse detectors and with a source energy above 150 keV, or so, the detection center is the detector geometric center. As the detector is made deeper or the energy lower, the detection center shifts toward the source from the

geometric center, the bottom detector layers being less effective than the top. Also below about 150 keV the source, window or dead-layer thickness may partially nullify the increased photoelectric cross section. The efficiency factor will accordingly decrease at lower energies. Thus, for lower energies a higher efficiency factor is obtained with a more shallow detector (same volume) and a minimum dead thickness. The closest approach efficiency can be maximized in construction by placing the detector as close to the container lid as is feasible.

Above about 1500 keV for larger detectors the usual considerations obtain. The fewest photoelectrons escape from a minimum area detector (volume constant). In a cylindrical shape the diameter is equal to the depth.

It has been shown that the inverse-square law forms a practicable basis for determination of detector efficiencies. Using calibrated sources and straight line plots it is possible to directly determine standard and relatable efficiency factors without resorting to an intermediary sodium iodide measurement. It is felt that previous discrepancies in comparisons of detector efficiencies can be resolved by use of the efficiency factor method. The efficiency factor and the distance of closest approach for the energy region of interest should be the two parameters used in comparing efficiencies.

V. Acknowledgment

James H. Gorrell furnished data and calculations which were invaluable for the preparation of this paper.

The experimental portions of this work were performed at the Air Force Institute of Technology Nuclear Engineering Center.

VI. References

[1]   Cline, J. E., and Heath, R. L., "Annual Progress Report, Gamma-Ray Spectrometry of Neutron-Deficient Isotopes", Philips Petroleum Company Rept. IDO-17222 (1967).

[2]   Tokan, G., and Cothern, C. R., "Efficiency Determination for a Ge(Li) Detector" (paper delivered at Ohio Am. Phys. Soc. Meeting, April 1968).

[3]   "What's the Efficiency?", Ortec, Inc. Rept., News from Ortec (1968).

[4]   Sandborg, A., and Orth, J., "Relative Full Energy Efficiencies of Ge(Li) Detectors of Various Shapes and Volumes" (paper delivered at Chicago Nat'l Meeting of Soc. Appl. Spectry., 1968).

[5]   Dooley, J. A., Young, M., Gorrell, J. H., Polishuk, P., Singhal, N., and Thompson, J. M., "New Developments at W-PAFB in Computerized Spectral Analysis and Isotope Identification" (Abstract published in Trans. Am. Nucl. Soc. 11, 73 (1968)).

[6]   Dooley, J. A., Gorrell, J. H., Polishuk, P., and Young, M., "Computerized Quantitative Analysis of High-Resolution Spectra" (See this volume, p. 1090.)

[7]   Gorrell, J. H., AF Flight Dynamics Laboratory (Private Communication, 1968).

INSTRUMENTATION FOR COMPUTERIZED NEUTRON ACTIVATION ANALYSIS

D. D. Tunnicliff, R. C. Bowers and G. E. A. Wyld

Shell Development Company
Emeryville, California

I. Introduction

The efficient application of least squares computer calculations to neutron activation analysis makes some requirements on the instrumentation which are somewhat different from the usual requirements. Therefore, it is desirable to develop the instrumentation and the computer programs as parts of a complete system of analysis if optimum performance is to be achieved. The computer programs for this system are being described in a separate paper. This paper is concerned only with the instrumentation. Some of these special requirements and our solution for them are described below.

II. Nonlinear Energy Scale

Since the most significant features of the gamma-ray spectrum of some radioisotopes are found near 0.05 MeV and for others out near 3.0 MeV, it is highly desirable to be able to include data for this entire region in the calculations. The usual linear energy scale is unsatisfactory for use with a sodium iodide detector over such an energy range since it does not provide adequate dispersion for the low energy region. Ideally, the energy scale should provide a constant number of channels per bandwidth of resolution for the entire energy range of interest. This requires expanding the low energy region and compressing the high energy region.

A suitable nonlinear energy scale has been achieved by the use of a "log-compressor" which provides a logarithmic relation at the upper end of the scale and a linear relation at the lower end. With this device it is possible to cover the region from 0.04 to 3.0 MeV in 255 channels with a resolution for all peaks of 4-6 channels per half-bandwidth. Figure 1 shows the relation between energy and channel number. Figure 2 shows the sum of the separate spectra of tungsten and manganese each of which had been obtained using this energy scale. Figure 3 shows similar data obtained with a linear energy scale.
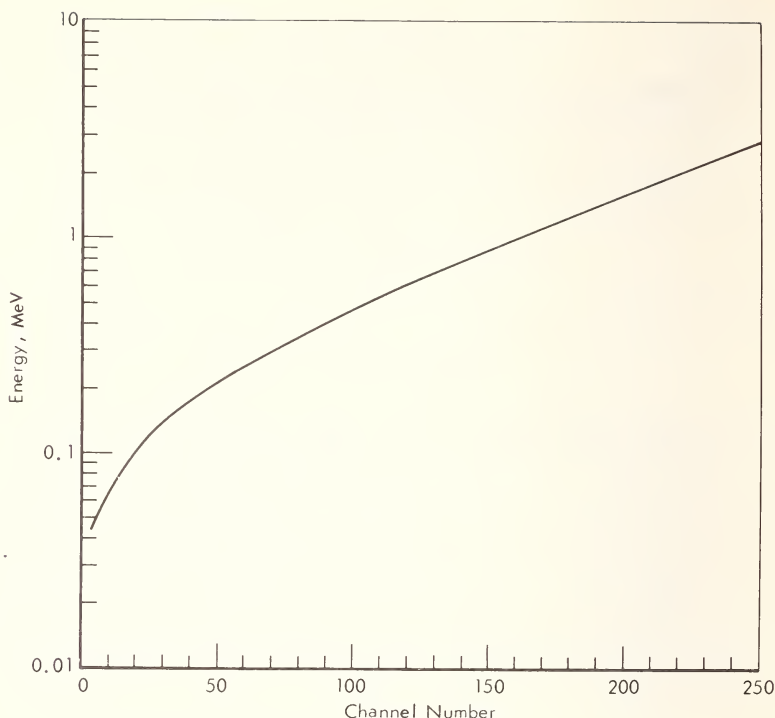
Figure 1.   Relation between energy and channel number.

This log-compressor is located in the circuit immediately following the usual linear amplifier. However, since the output voltage is only 0.1 volt for an input voltage of 10 volts, a second linear amplifier is required between the log compressor and the multichannel analyzer.

III. Stability

Since least squares computer calculations require a set of reference spectra for each of the radioisotopes involved, it is important that these reference spectra and the sample spectra be obtained under conditions which can be reproduced over long periods of time. Although it is a common practice to use either an automatic gain control to achieve reproducible conditions or to readjust the spectrum as part of the computer calculations, neither approach is completely satisfactory even for a linear energy scale and they are quite impractical for use with a nonlinear energy scale. The goal of the present design has been to achieve the desired stability by the careful selection of components and by thermostatting these components.

Three separate controls are used to determine the shape of the energy scale. These are the gain of the system preceding the log-compressor, the
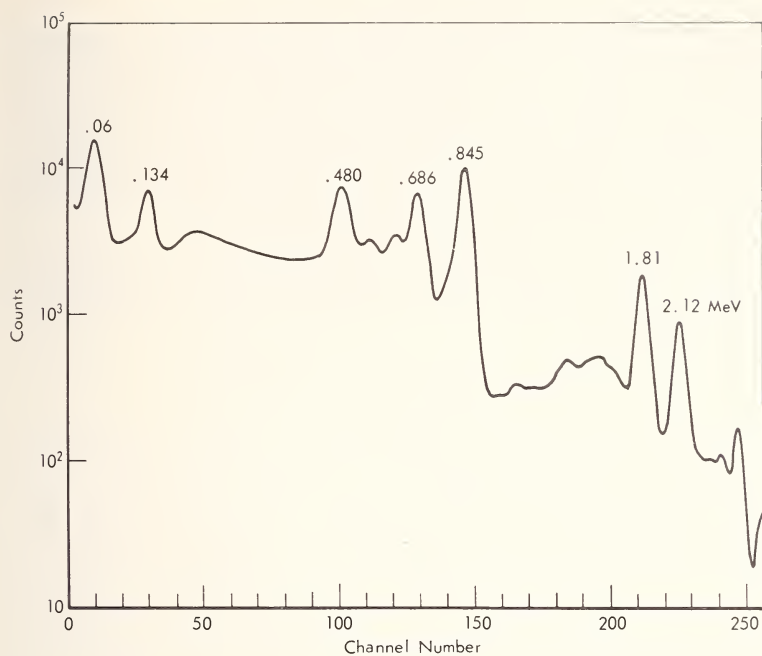
Figure 2.   Composite spectrum of tungsten and manganese, nonlinear scale.
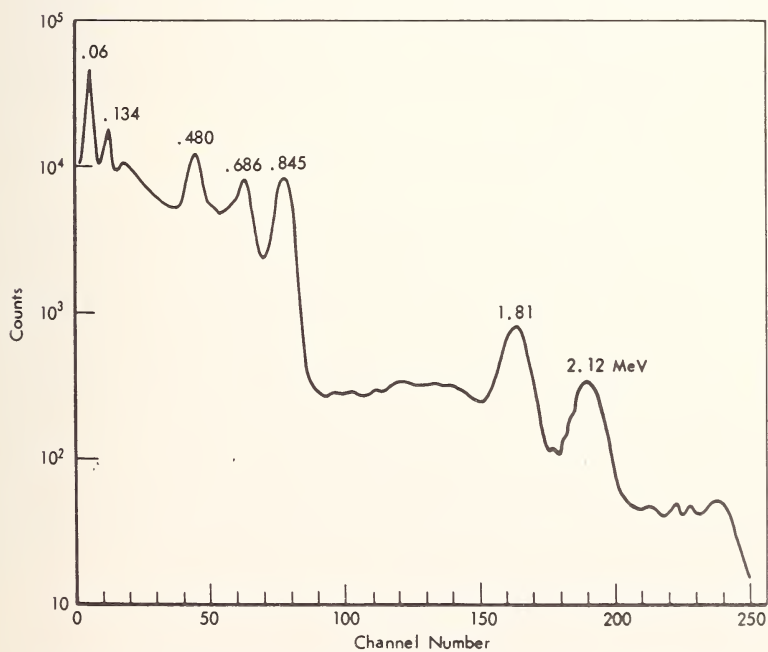
Figure 3.   Composite spectrum of tungsten and manganese, linear scale.

gain following the log-compressor, and the zero adjustment in the multi-channel analyzer. These three controls are used to maintain three locations on the energy scale. It is then assumed that if these three positions are held constant, intermediate positions will also be constant. The three reference peaks chosen for maintaining the scale are as follows: the ^{210}Pb peak at 0.045 MeV in channel 5, the ^{137}Cs peak at 0.661 MeV in channel 126 and the ^{24}Na peak at 2.75 MeV in channel 249.

It has been found that the energy scale can be maintained to about 0.1 channels over the entire region. This corresponds to about 2% of the half-width of an average peak.

IV. Detector and Counting Geometry

It is quite important that the shape of the spectra obtained from different regions in the sample do not differ significantly. This requirement essentially eliminates the use of a well-type detector since the spectrum obtained for a portion of the sample near the top of the well may differ considerably from the spectrum of a portion of the sample at the bottom of the well. This problem has been avoided by using a solid 3 in. × 3 in. thick thallium-activated sodium iodide detector and then mounting the sample beside it with the axis of the sample parallel to the axis of the detector. This geometry greatly reduces the effects of variations in the amount of sample in the sample container. The sample is rotated at 300 revolutions per minute (rpm) as it is being counted, as recommended by Anders and Briden [1], to minimize the effect of any inhomogeneity in the sample.

V. Data Readout System

Rapid readout of the spectral data in a form which can be easily input to a computer is essential. A magnetic tape recorder has been coupled to the multichannel analyzer so as to permit dumping 255 channels of spectral data directly onto a computer compatible magnetic tape. Since this operation requires only two seconds, there is essentially no delay between counting periods. A digital clock with a range of 9999 minutes and reading to 0.0001 minutes is a part of the unit. The time corresponding to the beginning and ending of each counting period is automatically recorded on the magnetic tape. These data are used as a measure of the decay time and the duration of each counting period. A counting period is terminated whenever the total counts or the length of the counting period exceeds preset values or by a manual push button.

Since one reel of magnetic tape may contain data for many samples, proper identification of all of the data is essential. A serial number is recorded on the magnetic tape for each set of data. The same serial

number is displayed on the panel of the unit and is written on an IBM typewriter at the same time as it is being written onto the magnetic tape. A code which defines the kind of data and the time in minutes is included with the typewriter record. These data together with appropriate notes added manually provide adequate information for the later identification of all the data for a given sample.

VI. References

[1]   Anders, O. U., and Briden, D. W., Anal. Chem. **36**, 287 (1964).

AN ANTICOINCIDENCE SHIELDED Ge(Li) GAMMA-RAY SPECTROMETER AND ITS APPLICATION TO NEUTRON ACTIVATION ANALYSIS[1]

J. A. Cooper, L. A. Rancitelli, R. W. Perkins, W. A. Haller and A. L. Jackson

Environmental and Life Science Division
Battelle Memorial Institute
Pacific Northwest Laboratory
Richland, Washington 99352

I. Introduction

The sensitivity of neutron activation analysis is strongly dependent on the sensitivity of the counting equipment used in measuring the product radionuclides. Although Ge(Li) gamma-ray spectrometers have greatly enhanced the selectivity and sensitivity, there still remain numerous cases where photopeaks from the less abundant radionuclides are obscured by the Compton distribution from the photopeaks of the major radionuclides produced.

In the past few years a large number of sophisticated Compton suppression spectrometers [1-14] have been developed to reduce this Compton interference. The all Ge Compton suppression spectrometers [10-14] utilize two Ge(Li) detectors which are operated in a sum coincidence mode. A major disadvantage of these spectrometers is their low photopeak efficiency. The Compton suppression spectrometers which utilize scintillators for anticoincidence shielding reject diode pulses resulting from gamma rays which have deposited a fraction of their energy in both the diode and scintillator. Many of the Compton suppression spectrometers of this type [1-4] have an inherent low efficiency because the source must be collimated and placed outside the anticoincidence shield, while those in which the sample is placed near the principal detector have not simultaneously provided high efficiency, good resolution and a high degree of Compton reduction [5-9]. This paper describes an anticoincidence shielded Ge(Li) gamma-ray spectrometer which was designed to provide a high degree of Compton reduction along with high efficiency and resolution, and illustrates its use in extending the applications of nondestructive activation analysis.

II. Experimental

The anticoincidence shielded spectrometer system is illustrated in Figure 1. The principal detector is a five-sided coaxial Ge(Li) diode [15] which is located near the center of a 26 in. diameter by 24 in. thick NE 102 plastic phosphor anticoincidence shield. It has a 3.25 in. diameter well which extends along its axis to the center and a 0.8 in. high by 2.6 in. wide sample insert port which extends horizontally from the phosphor edge to below the diode. The phosphor is viewed from each end by four 5 in. RCA 8055 photomultipliers.

ANTICOINCIDENCE SPECTROMETER SYSTEM
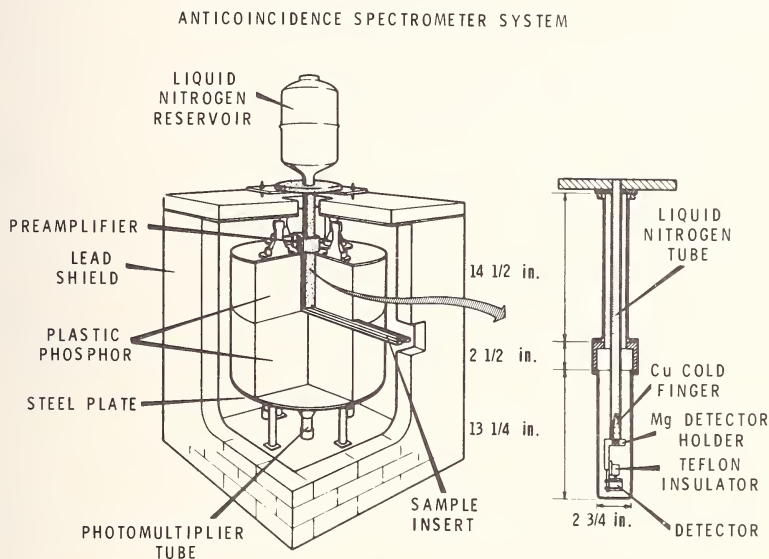
Figure 1.   Schematic diagram anticoincidence-shielded Ge(Li) gamma-ray spectrometer system.

In the design of the Ge(Li) spectrometer, emphasis was placed on minimizing the inactive volume of the diode and the cryostat mass near the diode. To minimize the inactive central core and maximize the efficiency and resolution, the Li was drifted in more than 11 mm from all five sides. In addition, the thickness of the doped surface layer was held at less than 1/2 mm. These specifications provided a 20 cm³ Ge(Li) diode with an active cross section of almost 11 cm² and with less than 10% inactive volume. The diode was mounted at the end of a 4 in. long magnesium cold finger which was attached through a copper cold finger to a stainless steel liquid nitrogen reservoir. The vacuum cap was made from 0.020 in. thick aluminum. The distance from the front face of the vacuum cap to the diode was 12 mm and its photopeak efficiency was 3.2% of that of a 3 in. diameter by 3 in. thick NaI(Tl) crystal. With the diode in the

phosphor the only inert material between it and the phosphor other than the vacuum cap and cold finger; was a 0.005 in. layer of light reflective paint on the phosphor.

To obtain a maximum counting efficiency the source is positioned against the front face of the diode vacuum cap. A characteristic of this close detector-sample arrangement inside the anticoincidence shield, is that where the decay of a radionuclide involves the emission of two or more gamma rays in cascade, a high probability exists for the detection of at least one of these in the plastic phosphor and the subsequent cancellation of the diode response to the coincident gamma ray. Therefore, to take full advantage of the information provided by the system, the spectrum of coincidence events between the diode and the phosphor is recorded in one-half of the 4096 channel memory while the anticoincidence events are stored in the second half of the memory. A block diagram of the electronics is shown in Figure 2. The pulse from the diode is fed first to a Canberra 1408C preamplifier and then is split and fed to an ORTEC 260 time pickoff and a Canberra 1416 amplifier. The 2.5 microsecond delayed unipolar pulse from the amplifier is delayed another 3 microseconds with a Canberra 1459 linear delay and then fed directly to the +10 volt input of the Nuclear Data 2200 analog to digital converter. The diode logic pulse from the ORTEC 403A time pickoff control is used to start the ORTEC 437 time to pulse height converter.

ELECTRONICS BLOCK DIAGRAM
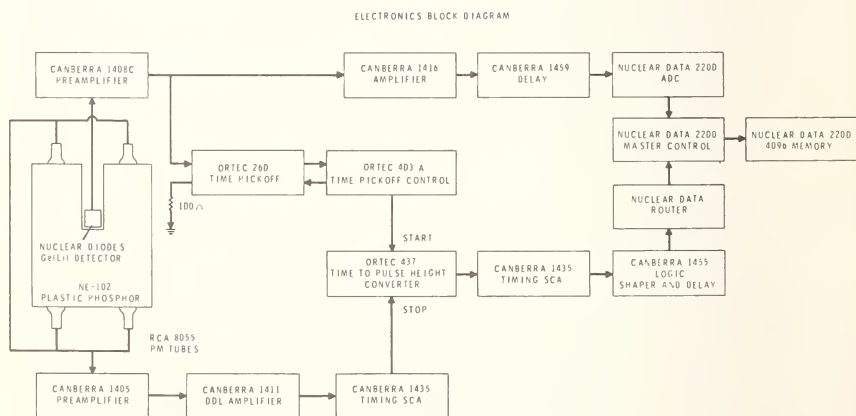
Figure 2.   Block diagram of electronics

The outputs from the phosphor phototubes are summed and amplified with a Canberra 1405 scintillation preamplifier and sent to a Canberra 1411 double delay line amplifier. The phosphor logic is then generated with a Canberra 1435 timing single channel analyzer from the zero crossover point and is used to stop the time to pulse height converter. The second timing single channel analyzer selects the resolving time (3

microseconds) and the logic shaper and delay adjusts the logic signal so it overlaps the linear pulse. The Nuclear Data router then directs the linear pulse to either the first half of the memory in the absence of a logic pulse or to the second half if a logic pulse is present.

III. Results and Discussion

A. RESULTS

The performance of the spectrometer is illustrated with the ^{137}Cs spectra shown in Figure 3. The Compton edge is reduced by a factor of 10 to provide a peak to Compton edge ratio of 245. The reduction in the photopeak efficiency accompanying this Compton reduction is less than 2%. However, where the decay of a radionuclide involves several
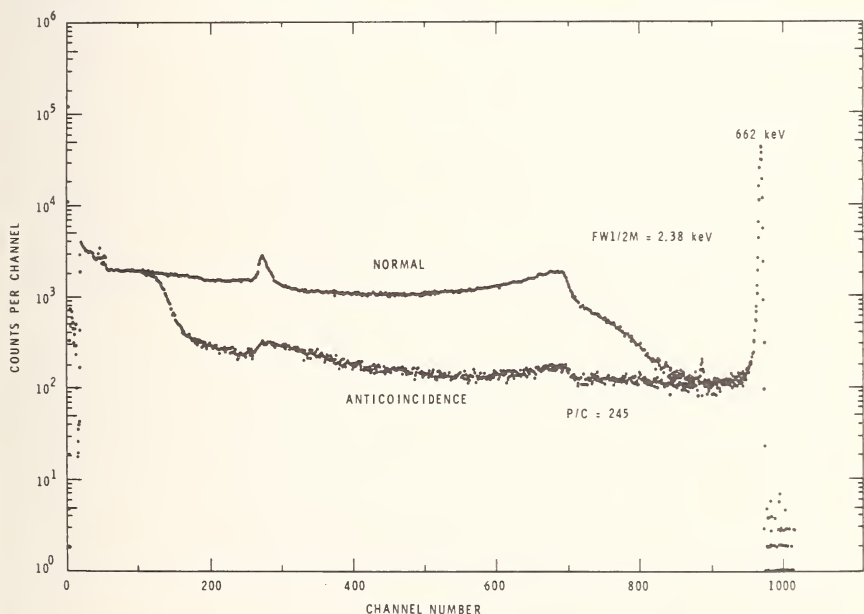
Figure 3. Gamma-ray spectra of ^{137}Cs recorded in the normal and anticoincidence modes.

coincidence transitions, the photopeak efficiencies have been reduced by as much as a factor of 65 in the anticoincidence spectrum. Since both the coincidence and anticoincidence spectra are stored simultaneously, there is no real loss in counting efficiency for any radionuclide. This large reduction factor is quite often an asset since the Compton continuum is reduced by an even larger factor. For example, the Compton edge for the ^{60}Co 1.33 MeV gamma ray is reduced by a factor of 45 and the ^{24}Na Compton edges from the 1.37 and 2.75 MeV gamma rays are reduced by

factors of 35 and 50. Shown in Figure 4 are the coincidence and anticoincidence gamma-ray spectra of a sample of muscle tissue from a tuna collected in the region of the Bikini atoll. In this sample ^{60}Co was by
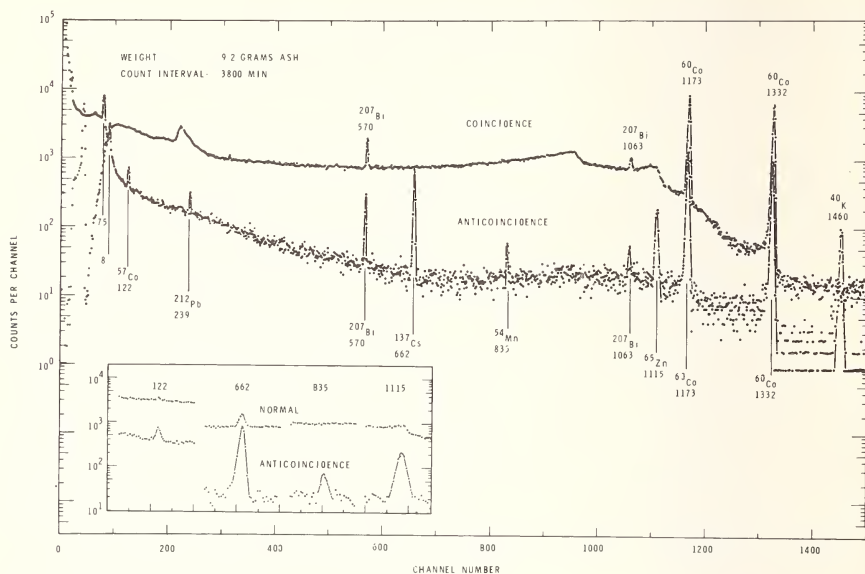
Figure 4.   Coincidence and anticoincidence gamma-ray spectra of a sample of muscle tissue from a tuna collected in the region of the Bikini atoll.

far the major constituent and the spectra clearly illustrate how a [60]Co Compton reduction of 40 or 50 enhances the sensitivity for the measurement of [54]Mn, [57]Co, [65]Zn and [137]Cs. In the determination of As in grains and in other produce by neutron activation analysis, the 559 keV line of [76]As is often obscured by the 554 keV line and the Compton continuum from higher energy lines in the more abundant [82]Br. Figure 5 shows a portion of the spectrum obtained by counting a [82]Br-[76]As source. In the anticoincidence spectrum the [82]Br interference at the [76]As 559 keV photopeak is reduced by a factor of 80 and the [76]As line made clearly discernible. It would be impossible to detect and measure [76]As in such a mixture from the normal spectrum.

The application of this system to other analyses of complex mixtures of radionuclides is illustrated in Figures 6 and 7. Figure 6 shows the spectra of proton activated basalt after a decay interval of two days. The Compton continuum has been reduced by a factor of 25 in the region of 1 MeV and has greatly enhanced the sensitivity for the measurement of ^{51}Cr, [87]Y, [7]Be, [54]Mn, [47]Ca and [42]K. The spectra of neutron activated WI standard rock, taken 20 days after irradiation are illustrated in Figure 7. The Compton continuum here is also reduced by a factor of about 25 and
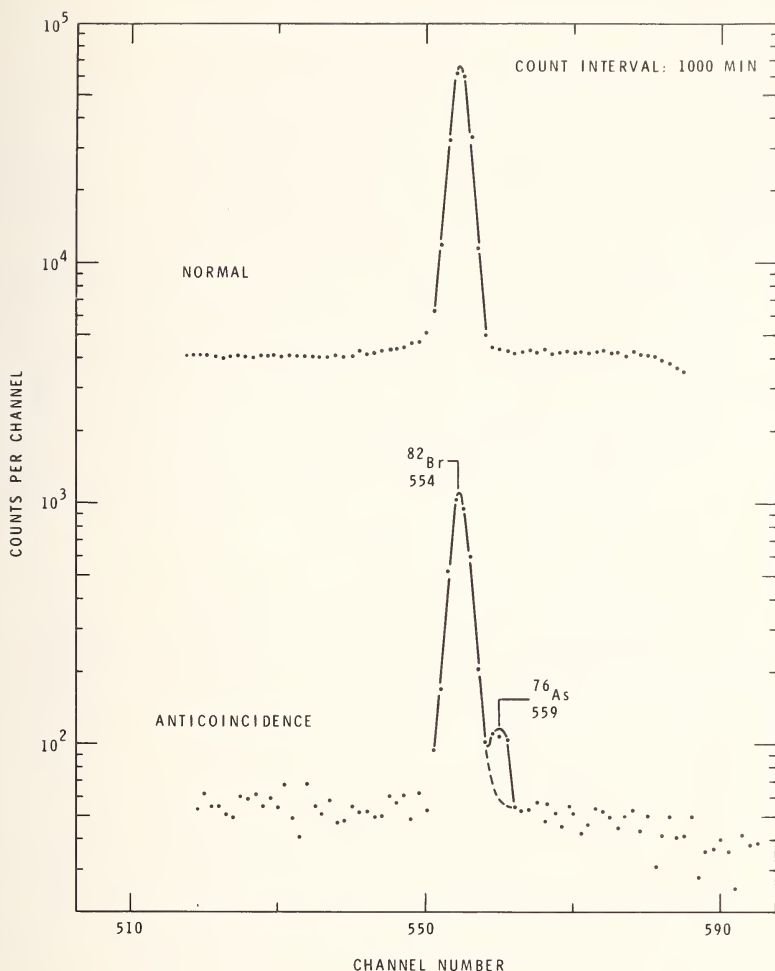
Figure 5.   Normal and anticoincidence spectra of a ^{82}Br-^{76}As source.

the standard deviations for ^{85}Sr, ^{65}Zn, ^{54}Mn and ^{86}Rb are reduced by
factors of from 4 to 2.5. These spectra were accumulated in 200 minute
counting periods and illustrate the quality of spectral definition which can
be achieved during such a period. The quantitative data obtained from
this system have been compared with those obtained with a normal diode
and a NaI(Tl) multidimensional analyzer. In most cases the agreement
has been excellent and always within the error limits. An additional
advantage resulting from the anticoincidence shielding is a substantially
reduced background in the anticoincidence mode which ranges from
about eightfold at 200 keV to tenfold at 1.5 MeV.

Figure 6.   Coincidence and anticoincidence spectra of proton activated basalt.

Figure 7.   Coincidence and anticoincidence spectra of neutron activated Wl standard rock.

B. DISCUSSION

The plastic phosphor anticoincidence shielding of a large high quality Ge(Li) diode provides a major improvement in the sensitivity for the measurement of many induced radionuclides in activated materials. Interference reductions of eighty fold have been achieved for some radionuclide measurements, and the very practical applicability of this instrumentation to a wide range of neutron activation and other radionuclide mixture analyses has been demonstrated. The simultaneous storage of both anticoincidence and coincidence spectra maintains a high detection efficiency for radionuclides with and without coincident gamma rays. The peak to Compton ratio of 245 to 1 for ^{137}Cs is the highest yet reported. However, this ratio is a function of detector resolution and efficiency as well as detector cladding and anticoincidence shielding, and it appears that peak to Compton ratios approaching 500 to 1 are within reach of the present technology.

IV. References

[1]   Kantele, J., and Suominen, P., Nucl. Instr. and Methods **41**, 41 (1966).
[2]   Michaelis, and Kupfer, H., Nucl. Instr. and Methods **56**, 181 (1967).
[3]   Orphan, V. J., and Rasmussen, N. C., Nucl. Instr. and Methods **48**, 282 (1967).
[4]   Camp, D. C., Lawrence Radiation Laboratory Report, UCRL 50156, p. 41 (March 3, 1967).
[5]   Cooper, R. D., and Brownell, G. L., Nucl. Instr. and Methods **51**, 72 (1967).
[6]   Anble, R. L., Berry, D. B., Berzins, G., Beyer, L. M., Etherton, R. C., Kelly, W. H., and Harris, Wm. C., Nucl. Instr. and Methods **51**, 61 (1967).
[7]   Sever, Y., and Lippert, J., Nucl. Instr. and Methods **33**, 347 (1965).
[8]   Hill, M. W., Nucl. Instr. and Methods **36**, 350 (1965).
[9]   Phelps, P. L., Hamby, K. O., Shore, B., and Potter, G. D., Lawrence Radiation Laboratory Report UCRL 50437 (May, 1968).
[10]   Kantele, J., and Suominen, P., Nucl. Instr. and Methods **56**, 351 (1967).
[11]   Gruhn, C. R., Kane, J. V., Kelley, W. H., Kuo, T., and Berzins, G., Nucl. Instr. and Methods **54**, 268 (1967).
[12]   Sayres, A. R., Baiker, J. A., IEEE Trans. Nucl. Sci., 11th Scintillation Semiconductor Counter Symp., (1968).
[13]   Palms, J. M., Wood, R. E., and Puckett, O. H., IEEE Trans. Nucl. Sci., 11th Scintillation Semiconductor Counter Symp., (1968).
[14]   Kraner, H. W., and Chase, R. L., IEEE Trans. Nucl. Sci., 11th Scintillation Semiconductor Counter Symp., (1968).
[15]   The coaxial detector used in this experiment was manufactured by Nuclear Diodes Inc., Prairie View, Illinois 60069.

A COINCIDENCE-ANTICOINCIDENCE SYSTEM FOR ACTIVATION ANALYSIS EMPLOYING A SPLIT NaI(Tl) ANNULUS AND A LARGE VOLUME Ge(Li) DETECTOR

R. L. Currie,[1] R. McPherson and G. H. Morrison

Cornell University
Ithaca, New York

I. Introduction

Most problems in activation analysis using gamma spectrometry can be laid to difficulty in quantitatively identifying a peak above a background Compton continuum. The excellent resolution of Ge(Li) detectors has significantly aided this quantification, but recent developments have suggested that further improvement would be possible using a surrounding shield to suppress Compton and pair escape events. Many such systems using plastic scintillators [1,2], NaI(Tl) [3-8], or both [9] have been developed, although most are used for structure spectroscopy with large source-detector distances. In this work, a large Ge(Li) detector with very good resolution and high peak-to-Compton ratio was inserted midway into the 3 in. diameter tunnel of an 8 in. diameter by 10 in. long NaI(Tl) annulus, and experiments were done with the source on the cryostat window for maximum sensitivity. This geometry also permits the use of the annulus in NaI(Tl)-Ge(Li) coincidence experiments on the source itself. A system was devised to permit several simultaneous experiments to be performed using the detector combination with a single multichannel analyzer.

II. Equipment

A. ANNULUS

The annulus is split lengthwise into halves, optically isolated by an internal septum, each viewed end-on by 3 RCA 6342A phototubes. Plug-on voltage dividers with focus and gain controls are used to match the outputs of the 6 tubes. The entire detector, a Harshaw Chemical Company "Matched Window" assembly, is surrounded on four sides by 4 in. of lead. We mix signals from the phototubes in the two groups of three

at the inputs of two emitter followers. The output of each of these emitter followers feeds a double-delay-line shaping amplifier with 1 μsec clipping time, and the two signals are added in a high level mixer for applications where the annulus is to be used as a single detector. The two separate halves and summed halves have resolutions at 662 keV of 11.3%, 11.2%, and 10.5% respectively.

B. Central Detector

The Ge(Li) detector of nominal 30 cm^3 volume was purchased from Nuclear Diodes, Inc. It is a five-side drifted, trapezoidal cross section coaxial detector with 10.6 cm^2 active area, 27.5 mm length, 11 mm drift depth, and 16.2 pF capacitance. The vacuum-cryostat assembly is made of low mass, low Z materials to give scattered gamma and pair production annihilation photons from the central detector the best possible chance to reach the surrounding annulus. The detector is mounted (see Figure 1) in a 6 in. long, 2 3/4 in. diameter, 0.5 mm thick vacuum cryostat. It is 15 mm from the end window of the cryostat, mounted with the p-core facing away from the window of an off-axis, 6 in. long aluminum (1100) cold finger. The aluminum finger attaches to a 1 in. diameter copper rod which extends down into the liquid nitrogen reservoir. The detector is cooled efficiently enough by this system so that at the operating bias of -1500 volts the leakage current is 0.9 nA. A Canberra Industries Model 1408A room temperature FET preamplifier is rigidly attached to the cryostat, and a single wire low capacitance vacuum feedthrough used to connect the detector. A Canberra Industries Model 1416 Gaussian shaping amplifier is the main amplifier; 2 μsec shaping constants are usually selected. The total system resolution is less than 2.8 keV full width at half maximum (FWHM) and the peak-to-Compton knee ratio is greater than 15:1 for the 1.33 MeV line of ^{60}Co.

C. Electronics

Figure 2 shows the typical electronic configuration for the entire system. An ORTEC Model 260-403 Time Pickoff Unit-Control is used to provide a leading edge time mark for all Ge(Li) detector pulses greater than 30 keV. The two halves of the annulus run into two separate single channel analyzers, usually set to detect 511 keV in each. The output of the summing amplifier is fed to an integral discriminator with low trigger level (30 keV), and can be fed to another single channel analyzer for energy discrimination of events in the annulus. Both the single channel analyzers and the integral discriminator are crossover timing devices. The various selected annulus events—any gamma interaction, 511 keV−511 keV coincidence between the halves, or some gamma in a selected energy
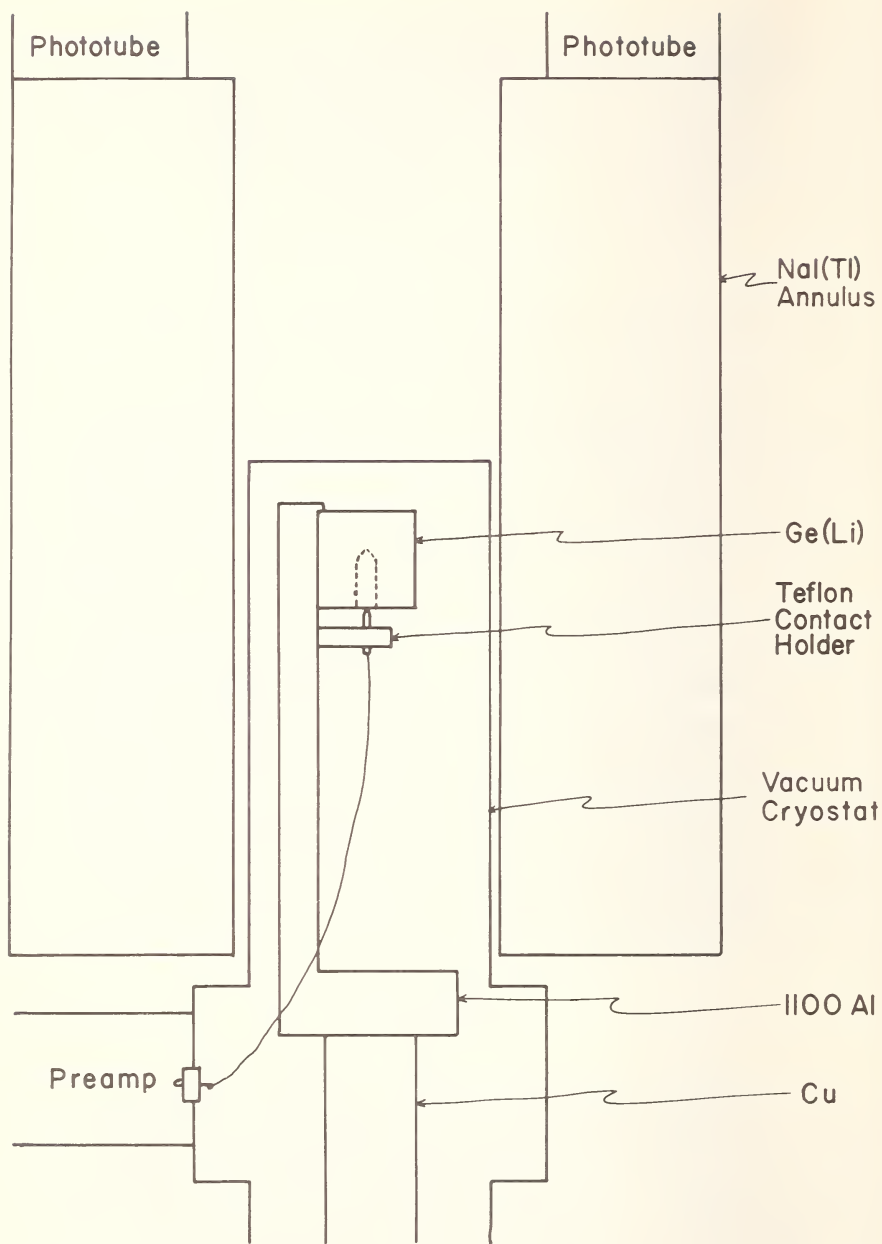
Figure 1.   Cross section view of detector system to scale showing relative position of components. Dimensions are included in the text.

window — are examined for coincidence with the time mark from the central detector with resolving time (2τ) of 300 nsec.

These coincidences are used as logic pulses for a router which provides the multiexperiment capability of this system. When the multichannel analyzer accepts a peak for analysis, a strobe signal is sent to the router which samples the status of the coincidence units. The router converts this information into binary signals to divide the analyzer's memory into quarters, and the accepted pulse is stored in the appropriate quarter according to the following scheme: the first quarter stores pulses for which no coincidence occurred; two quarters receive annulus-detector events of a selected particular nature — 511-511 coincidence, *etc.*; the remaining quarter stores all other pulses coincident with events in the annulus. Thus, no information is discarded, and by adding all four quarters together after the experiment the original, unsuppressed, central detector spectrum can be reconstructed. Provision has been made to store in halves of the memory so that, if only Compton suppression is desired, the "full energy" and "discarded" spectra can be spread over half the
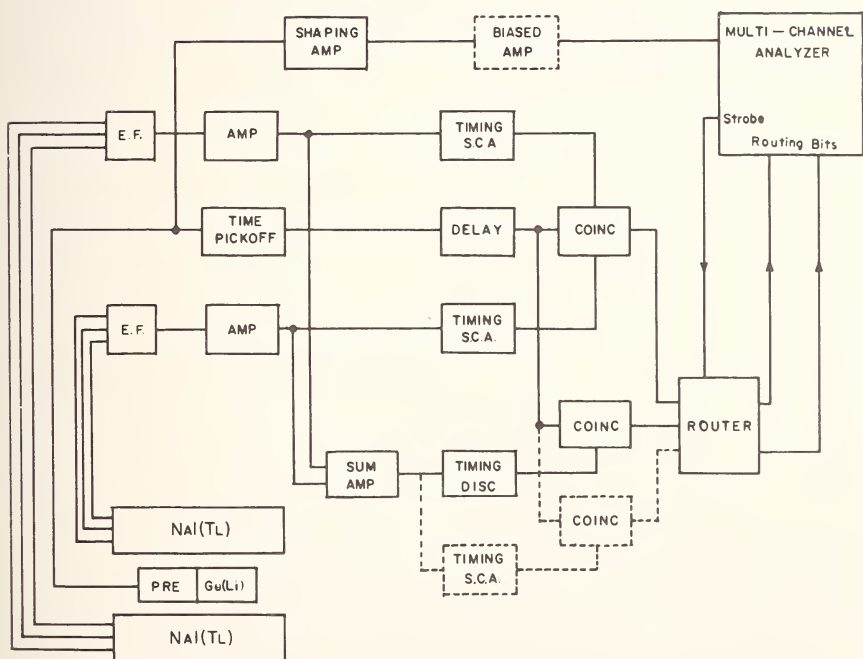
Figure 2. Block diagram of electronics. Notes: 1-dashed lines represent variation on the basic system; 2-arrows show direction of logic pulses around multichannel analyzer; 3-timing S.C.A.'s and Disc. have 0-2.2 μsec variable delays; 4-2 μ sec delay cables are between the coincidence units and the router.

memory of each. A biased amplifier is usually used to select an energy range of interest and provide good dispersion over this range.

III. Experimental

Figure 3 shows a logarithmic display of suppressed and unsuppressed spectra of a 0.1 μCi ^{137}Cs source on the face of the cryostat. Note the reduction in size and spread of the Compton knee and plateau. The knee is still present because these events are due to scattering at 180° which sends the scattered gamma out the hole in the annulus. For the same reason the forward scattered gamma-rays resulting from the low energy portion of the Compton distribution are not detected. The suppression factor defined as the ratio of counts in any given channel without suppression to counts with suppression therefore varies with energy. It is a maximum, 6.7, just below the knee, and approaches 1 as you go to lower energies; at the backscatter peak (~200 keV) it is still greater than 2. The peak to Compton knee ratio improves from 22:1 to 100:1 (improvement of 4.5); the plateau from 34:1 to 180:1 (improvement of 5.3).

Figure 4 illustrates a second type of situation — a source with coincident gamma rays. Here suppressed and unsuppressed spectra of a 0.05 μCi ^{60}Co source counted for the same length of time are displayed. The background is suppressed as before due to detection of Compton
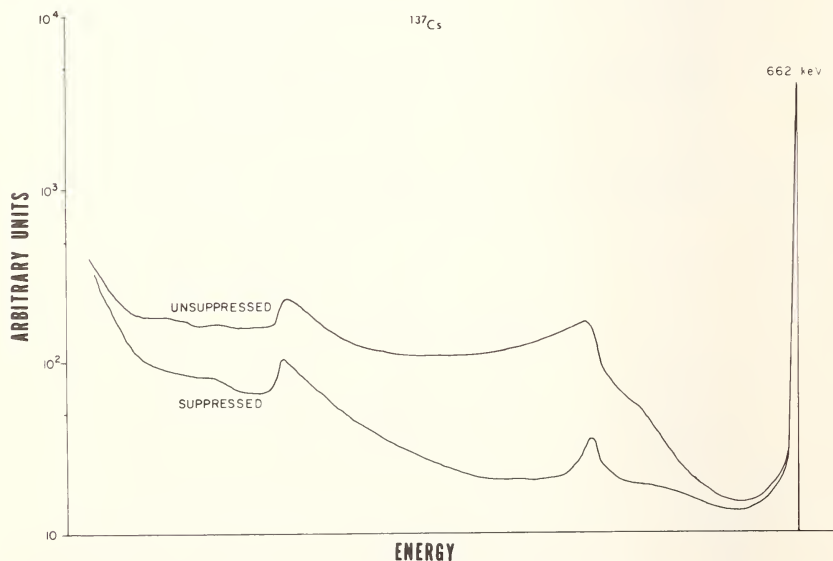
Figure 3.   Logarithmic display of suppressed and unsuppressed spectra of ^{137}Cs. FWHM at 662 keV is 2.5 keV.

scattered gamma-rays, but both peaks and background are suppressed due to detection of the coincident gamma-rays. The peak intensities are lower by a factor 3.3; the background is lower by a factor of 10.5 at the 1.33 MeV Compton knee, 15.0 between the two knees and at the 1.17 MeV knee, and 21.5 just below the 1.17 MeV knee. These figures yield peak to Compton improvements of 3.2, 4.5, and 6.5 in reasonable agreement with the ^{137}Cs results.

IV. Discussion

Let us consider the application of this system to activation analysis of complex samples, where the task is to identify peaks on a continuum due to other radioisotopes. An initial survey can be made using simple Compton and pair escape suppression, and the resulting spectra compared with the regenerated unsuppressed spectrum. Peaks appearing in the spectrum in coincidence with a 511 keV − 511 keV coincidence between the annulus halves are either pair escape peaks or gamma-rays associated with positron decay in the source. This information should permit quicker identification of the radioisotopes producing these peaks as well as improving their signal-to-background ratio.
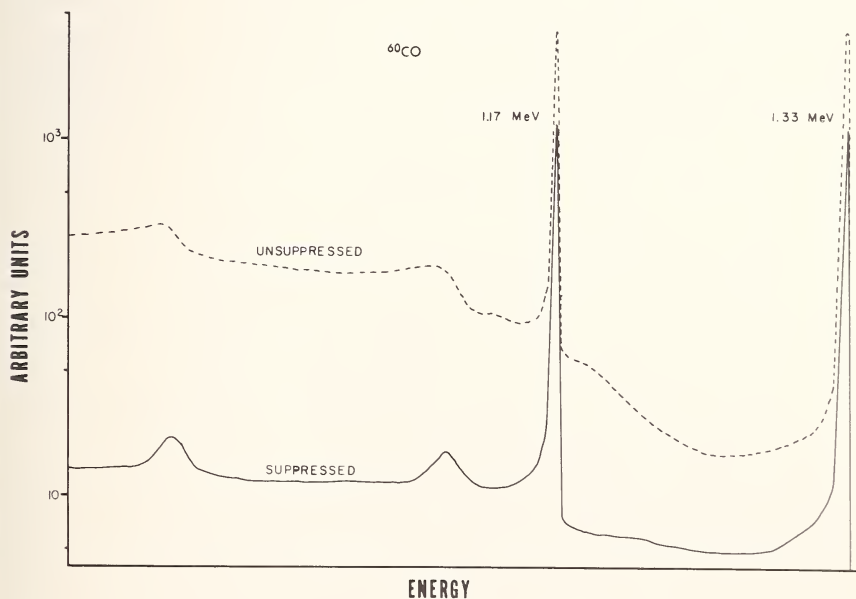
Figure 4.   Logarithmic display of suppressed and unsuppressed spectra of ^{60}Co above 900 keV. FWHM at 1.33 MeV is 2.7 keV.

Gamma rays in the Compton suppressed spectrum which have no reduction in peak height can be identified not only as having particular energy, but also as having no coincident gamma rays. Their peak-to-background ratio will be improved over the unsuppressed case. Gamma rays which are part of a cascade will be reduced in height from the unsuppressed to the suppressed spectrum. The approximate number of cascade gamma rays associated with such peaks can be estimated from the relative height in the two spectra. The importance of the capability of generating the unsuppressed spectrum in a complex situation is now obvious. Gamma rays from a cascade will be suppressed relative to background from non-cascade gamma rays or gamma rays from cascades with fewer members. Thus, their peak-to-background ratio may be worse as a result of suppression. This system, however, allows us to obtain the original spectrum and can never place us in a worse "signal to noise" condition than we started with, while still providing a maximum amount of additional information.

Once the statistically significant peaks in the spectra have been identified and integrated, the small marginal peaks can be examined and tentatively identified. If they are members of a cascade, the annulus can be used in a NaI(Tl)-Ge(Li) coincidence experiment with a single channel analyzer providing a routing signal, by the system outlined in dashed lines in Figure 2, to store a spectrum in coincidence with particular energy in the annulus. This should improve the peak-to-background ratio for that particular peak. If one is looking not for general, multielement capabilities, but rather for some particular element in a complex system, the annulus can be used in the NaI(Tl)-Ge(Li) coincidence mode to aid in the isolation of gamma rays which are members of a cascade.

V. References

[1]   Cooper, R. D., and Brownell, G. L., Nucl. Instr. and Meth. **51**, 72 (1967).
[2]   Hill, M. W., Nucl. Instr. and Meth. **36**, 350 (1965).
[3]   Kantele, J., and Suominen, P., Nucl. Instr. and Meth. **41**, 41 (1966).
[4]   Auble, R. L., Beery, D. B., Berzins, G., Beyer, L. M., Etherton, R. C., and Kelly, W. H., Nucl. Instr. and Meth. **51**, 61 (1967).
[5]   Sever, Y., and Lippert, J., Nucl. Instr. and Meth. **33**, 347 (1965).
[6]   Arnell, S. E., Hardell, R., Hasselgren, A., Jonsson, L., and Skeppstedt, O., Nucl. Instr. and Meth. **54**, 165 (1967).
[7]   Hinrichsen, P. F., private correspondence.
[8]   Camp, D. C., USAEC Report UCRL-50156 (1967).
[9]   Michaelis, W., and Kupfer, H., Nucl. Instr. and Meth. **56**, 181 (1967).

A DUAL CHANNEL ANALYZER AND EFFICIENT COINCIDENCE SYSTEMS FOR ACTIVATION ANALYSIS

Ralph A. Johnson

Shell Development Company
Emeryville, California

I. Introduction

Coincidence analysis improves the limits of detection and selectivity of many activation analyses involving emitters of positrons and cascade gamma rays. Positron-annihilation counting is especially well suited to coincidence analysis because of the high degree of energetic and angular symmetry of the two photons involved. The corresponding applications of coincidence analysis involving cascade photons are less favorable, and accordingly, are less frequently used. The reduced advantages are decreased efficiency and selectivity owing to the absence of the nice symmetries in photon energies and in emission angle which are characteristic of annihilation radiation.

The present study is oriented around systems involving single channel analyzers, coincidence gates, and scalers with readout suitable for data handling by computer. It is concerned with multichannel analyzers only for qualitative spectrum observation and as an aid in setting the single channel analyzers. The special instrumental approach taken in this study is an extension of concepts presented by the author in earlier reports [1,2]. In general, the instrumentation being described is intended to increase the versatility and effectiveness of the instrumentation prevailing in many activation analysis laboratories. In particular, modifications of a single channel analyzer are described which convert it into a dual channel analyzer. The objectives are economies in cost and space and the achievement of better stability.

The second objective of this study involves an analysis of the different kinds of coincidences encountered with two-photon cascade systems and their relationship to instrumental arrangements, selectivity, and counting efficiencies. Although a variety of electronic coincidence arrangements appear in the literature of activation analysis, there is little, if any, critical comment given by the authors on the reasons for their respective choices. This scarce coverage in the literature has prompted a more detailed treatment here of this paper's second objective.

II. The Dual Channel Analyzer

The dual channel analyzer is constructed by modification of a commercially produced, jitter-free, single channel analyzer. The modification consists of a supplementary circuit, including upper and lower level discriminators, an AND gate, and amplifier-shaper to output, as represented in the block diagram of Figure 1.
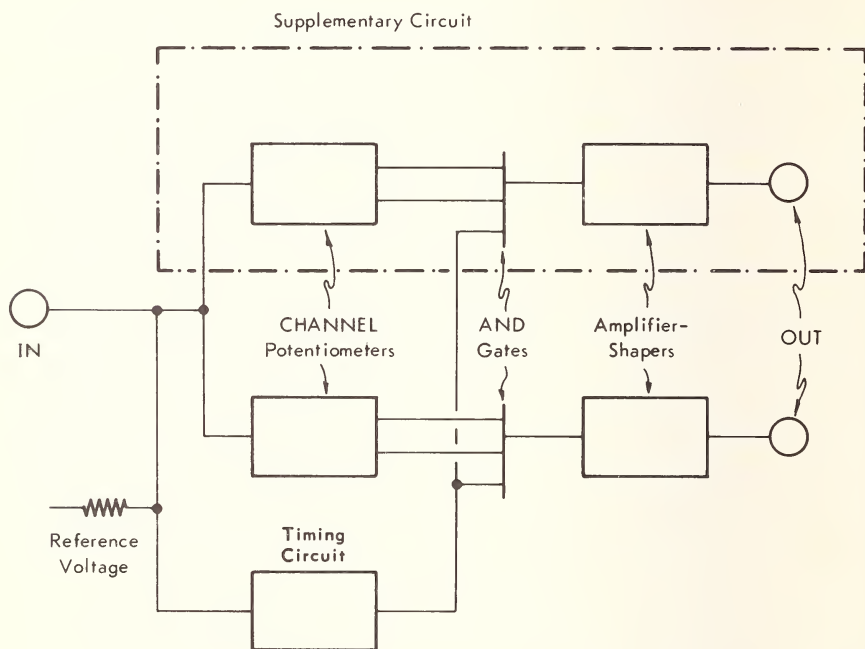
Figure 1.   Dual-channel analyzer

The dual channel analyzer yields output pulses corresponding to those photons included within either of two selected energy intervals, *i.e.,* channels. The supplementary circuit shares with the original channel, the input connection, the reference voltage, and the fast coincidence timing circuit.

In this laboratory, the dual channel analyzer is built into a supplementary module which also contains the channel selector, previously described. In this arrangement, the dual channel modification stands as an optional analyzer mode which may be switched in or out as needed.

III. Coincidence Systems for Cascade Photons

The types of coincident events which can be detected in a two photon cascade are represented in Figure 2. Photopeak-photopeak coincidences are represented by the diagonal bars. They are of two types, *viz* (1) the low energy peak from Channel I with the high energy peak from Channel II, and (2) the high energy peak from Channel I with the low energy peak from channel II; these are counterparts of the same basic event. Events of secondary importance are represented by the horizontal bars which correspond to the two counterparts of the coincidence of the low energy photopeak with the Compton pulses from the higher energy photon.

The systems of coincidence instrumentation for cascade gamma rays fall into three types:

A. The Two Channel System

With one channel set for the lower energy gamma from one detector and the other channel set for the higher energy gamma from the other detector, the events counted are those represented by one of the diagonal bars of Figure 2. The two channel system is that prevalent for positron annihilation coincidence counting except for the window settings.

B. The Four Channel System Based on Energy Levels (Figure 3)

This system differs most conspicuously from the preceding one by the addition of two analyzer channels. It differs from the following one, specifically, in that the low energy channels, one from each detector, feed
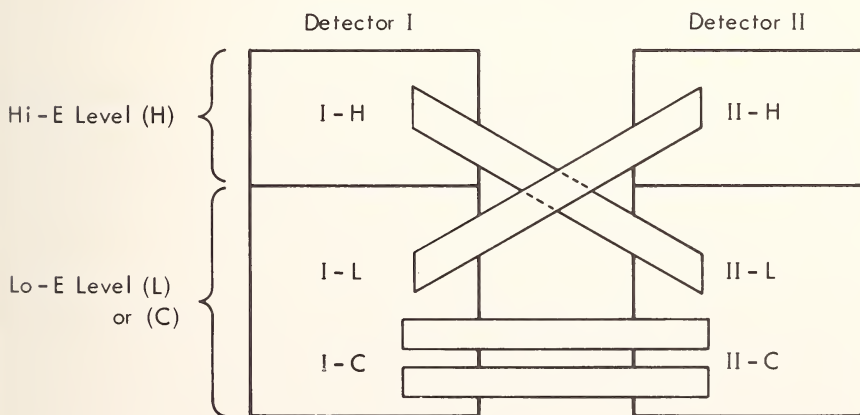
Figure 2.   Detector vs energy systems for coincidence counting. Diagonal bars represent photopeak-photopeak coincidences; horizontal bars represent photopeak-Compton coincidences.
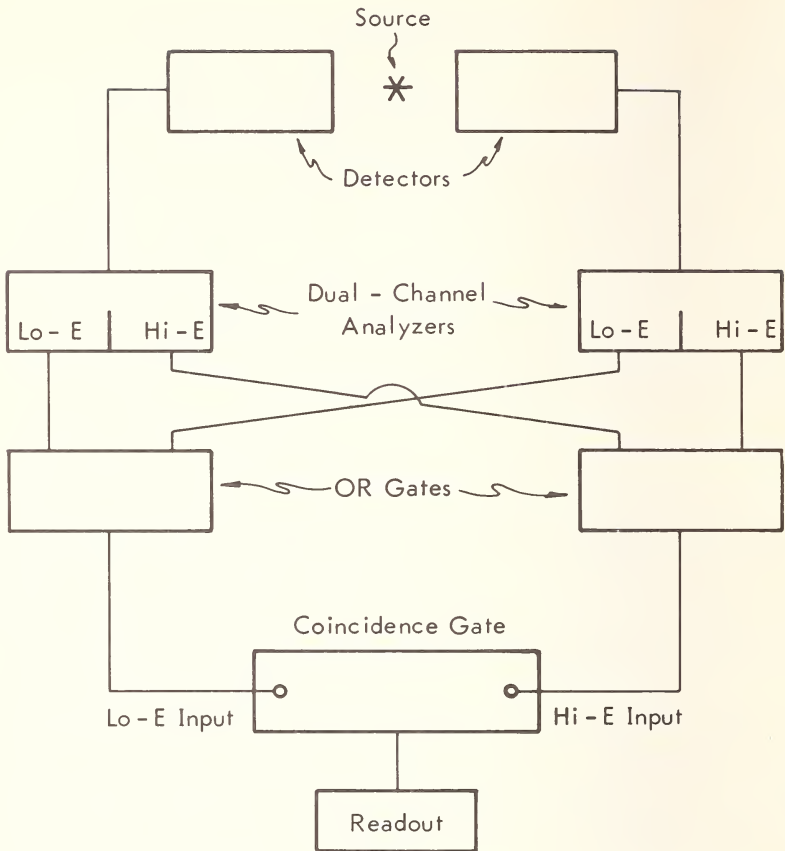
Figure 3.   Four-channel system with coincidences respective to energy levels.

a common coincidence input; correspondingly, the two high energy channels feed the other coincidence input. In this system the full capability for photopeak-photopeak coincidences is achieved, *i.e.,* the system counts events represented by both of the diagonals of Figure 2.

C. THE FOUR CHANNEL SYSTEM BASED ON DETECTORS (FIGURE 4).

In this variation, the high energy and low energy channels of each detector feed a common coincidence input; thus the coincidence is based on simultaneous events in two detectors rather than in two energy levels. With this arrangement the full capability for registering photopeak-photopeak coincidence is retained and the capability is added to count the secondary type of coincidences, *i.e.,* low energy photopeak with Compton from the high energy gamma ray.
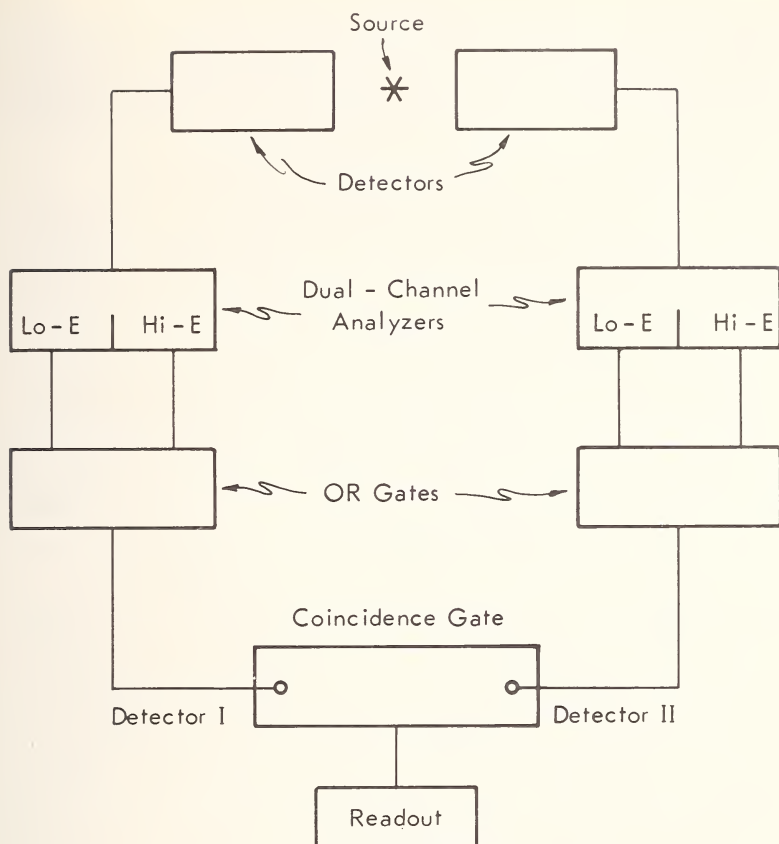
Figure 4.   Four-channel system with coincidences respective to detectors.

IV. Discussion and Conclusions

The two channel coincidence system offers full capability for counting positron-annihilation photons because of the favorable angular energetic symmetry involved. Furthermore, the same system approaches maximum capability for cascade decays in which the two gamma rays are similar in energy. (Cobalt-60 with gamma rays at 1.17 MeV and 1.33 MeV is a notable example).

For cascade gamma rays of more dissimilar energies, however, the two channel system is restricted to counting only one of the two possible photopeak-photopeak coincidences. Full capability for these coincidences is possible only if four channels are brought into play. With four channels, two coincidence systems are possible. If the channels are arranged to provide coincidence on the basis of energy levels, the

counting efficiency is doubled with no loss in selectivity. If the channels are arranged to yield coincidences on a detector-detector basis, a further increase in efficiency is obtained from coincidences of the low energy photopeak pulses with appropriate Compton pulses from the higher energy gamma ray.

The choice between the different four channel systems, *i.e.,* the one based on energy levels and the one based on detectors, is dependent on the kind of interference prevailing. For noncoincident interferences, either system is highly selective and the choice goes to the more efficient system, *i.e.* the one based on detectors. However, both systems will register any interfering pulses which are coincident and which fall into the appropriate energy levels. In general, the interfering events which happen most frequently are low energy:low energy events, *cf.,* the horizontal bar of Figure 2. Moreover, for the activity being determined, the efficiency for low energy: low energy events is much less than in the photopeak-photopeak mode. This adds up to inferior selectivity for the low energy: low energy events and points toward the use of coincidences based on energy levels when substantial amounts of coincident interferences exist.

The dual channel analyzer described above is especially well adapted to the four channel coincidence system. In comparison with a system of separate single channel analyzers, the dual channel analyzer, owing to a sharing of key electronic controls, *viz,* the reference voltage and the circuit, is more easily aligned and is more reliable. Moreover, it offers worthwhile economies in cost and space. (Aside from its aptitude for coincidence systems, the dual channel analyzer is useful for selecting counts from two photopeaks of a noncoincident, two gamma-ray emitter. A more detailed discussion of this instrument will be given elsewhere).

V. References

[1]   Johnson, R. A., Trans. Am. Nucl. Soc. **10,** (1), 86 (1967).
[2]   Johnson, R. A., and Blair, D. C., Anal. Chem. **39,** 1899-1900 (1967).

CHARACTERISTICS AND APPLICATIONS OF A LARGE SODIUM IODIDE DETECTOR ASSEMBLY[1]

Jack L. Parker, Dale M. Holm, and Barry K. Barnes

University of California
Los Alamos Scientific Laboratory
Los Alamos, New Mexico

I. Introduction

Response functions have been measured for a large sodium iodide double-crystal detector assembly. The assembly, used by itself and in conjunction with lithium-drifted germanium detectors, has been studied for applications in activation analysis and gamma-ray spectroscopy.

II. Physical Description

Figure 1 is a drawing of the detector assembly as mounted in its shield and being used in conjunction with a Ge(Li) detector. The two 6 in. thick, 13.5 in. diam NaI crystals are inside a single envelope and are optically isolated for coincidence counting. They may also be operated in parallel, in which case they form a cylindrical detector 13.5 in. in diam and 12 in. long with a well along a diameter through the center. The well allows a Ge(Li) high resolution detector to be placed at the center of the NaI assembly and a sample or a collimated beam of gamma rays to enter the assembly. The two holes of the well subtend at the assembly center only $\simeq 1\%$ of the total 4π steradians of solid angle. The large shield around the assembly is low background (Tadanac) lead and has a minimum thickness of 6 in.

III. Response Functions

Figure 2 shows spectra of the 662 keV gamma ray of ^{137}Cs from the individual NaI detectors and from the two detectors combined to form a 4π detector. For this energy, the assembly has a resolution of $\simeq 10\%$ and a full-energy peak-to-total ratio of 0.84. Note that this peak-to-total ratio for the 4π configuration is better than that for the individual 2π detectors (0.72). The improvement is due to full absorption in the 4π detector of Compton events which are only partially absorbed in the individual

---

GAMMA RAY SPECTROMETER
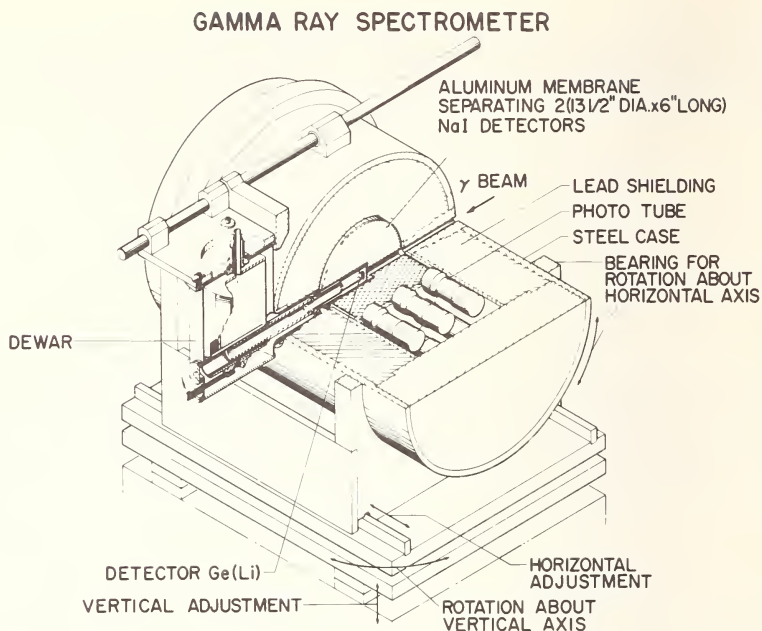
Figure 1.   The crystal assembly as mounted in its shield and being used in conjunction with a Ge(Li) detector.

crystals. This complete absorption of the energy of Compton-scattered gamma rays causes the Compton edges, clearly visible in the single crystal spectrum, to virtually disappear in the combined crystal spectrum.

Figure 3 presents the efficiency of the 4π detector as a function of gamma-ray energy. The curves extend to 2.0 MeV, the maximum energy of sources easily obtainable. For gamma-ray emitters with two or more simultaneous gamma rays, the assembly approaches 100% efficiency for detection.

The background of the whole detector assembly inside the large shield is about 650 events per second. Figure 4 shows a typical background spectrum. In addition to the normal monotonically decreasing background, there are peaks from ^{60}Co and another unidentified gamma ray, which probably comes from the steel lining in the lead shield. Because of the high efficiency of the large crystal assembly this background is unimportant for the proposed applications.

IV. Applications

A principal use of the assembly is to measure the decay curves of pure positron emitters formed in activation analysis with photons and charged
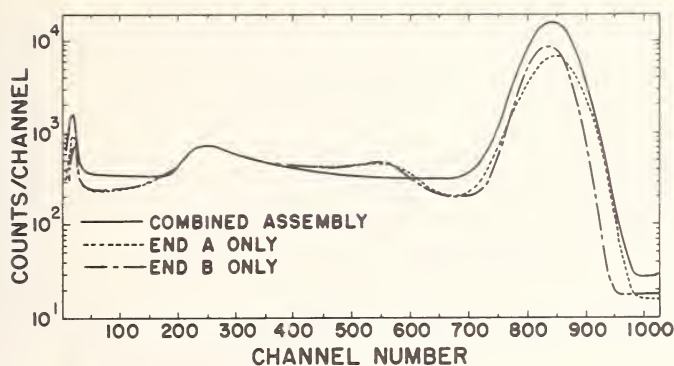
Figure 2. Spectra of the 662 keV gamma ray from ^{137}Cs for the individual NaI detectors and for the two detectors combined to form a 4π detector.
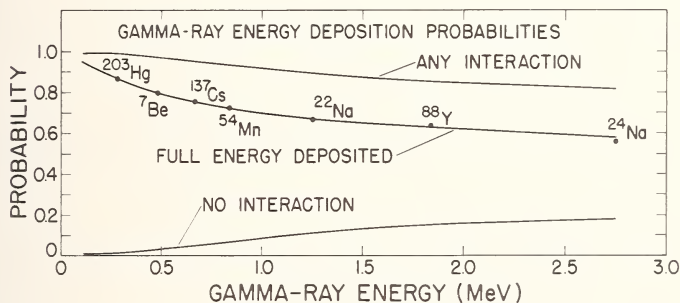
Figure 3. The efficiency of the 4π detector as a function of gamma-ray energy.

particles. From Figure 3 the probability of the 4π detector absorbing the full energy of a 0.51 MeV gamma ray is 0.79. Therefore, the probability of both 0.51 MeV photons from a positron annihilation being fully absorbed is ≈0.62, approximately 25 times the efficiency one would expect from two 3 in. by 3 in. NaI detectors separated by 6 cm. Many common interference reaction products are positron emitters which also emit a gamma ray in coincidence with the positron (^{22}Na for example, with a 1.28 MeV gamma ray). If the area of the 1.02 MeV peak (resulting from the full energy sum of both 0.511 MeV photons) is regarded as the true signal, it is evident that the high efficiency of the NaI assembly will remove many of the interference events from the signal channel. Most of the counts that are removed are recorded as a peak at higher energy (2.30 MeV in the case of ^{22}Na) and may be used to determine the number of interference counts in the signal channel. This feature is particularly useful in cases where the interference activity has a half life
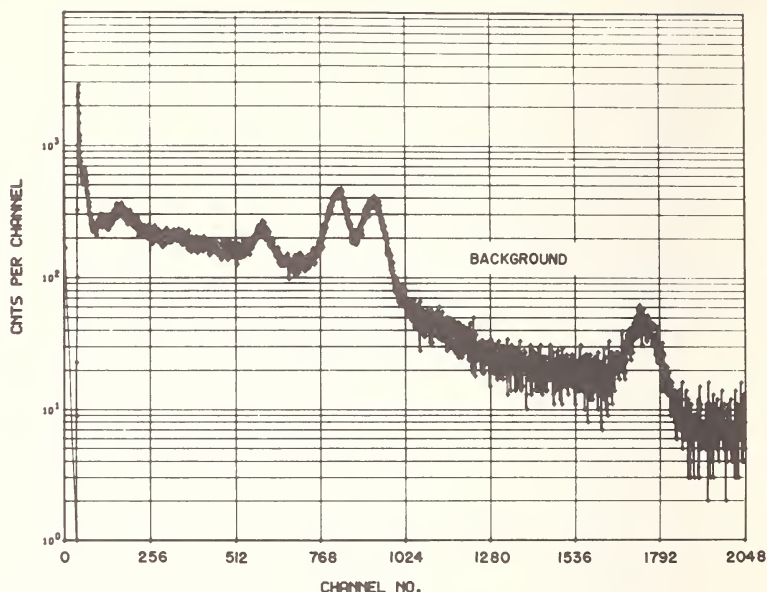
Figure 4.   An 8 min background spectrum from the NaI assembly connected to make a 4π detector.

approximately equal to one of the signal activities. Figure 5 is a ^{22}Na spectrum from the 4π detector. The number of counts in the 1.02 MeV peak is only $\simeq 10\%$ of what it would have been if ^{22}Na were a pure positron emitter. Therefore, the NaI assembly reduces the interference from ^{22}Na by $\simeq 90\%$.

For positron emitting activation products, we have found that gated single parameter operation is as useful as multiparameter operation. We require that 100 keV or more of energy be deposited in each half of the detector before the summed signal from them is stored. Requiring this coincidence as a prerequisite to storage reduces the background in the 1.02 MeV peak from 44 to 3.7 counts per second. Even greater background reduction can be obtained by moving the threshold up to 0.45 MeV, but 15% of the signal will be lost. This loss of signal is caused by one of the annihilation quanta scattering from one crystal into the other, depositing more than 0.51 MeV in one crystal and less than 0.51 MeV in the other. However, in most of these scatterings, more than 0.100 MeV is deposited in each of the detectors. Thus, in this mode of operation, the high efficiency of the system is fully utilized, but the background is reduced twelvefold.

The large NaI assembly is also an efficient device for suppressing the Compton distribution in Ge(Li) detector spectra. More than 90% of the
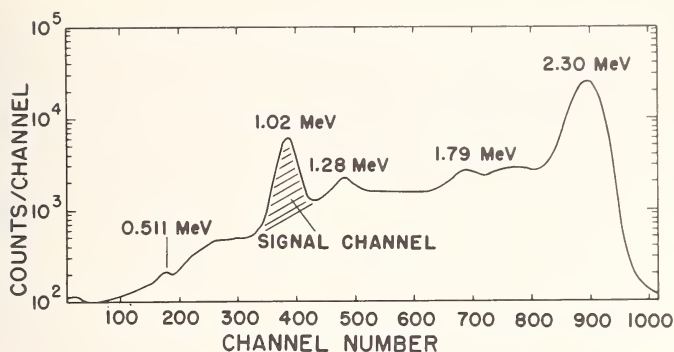
Figure 5.   A spectrum of ^{22}Na in gated single parameter mode.

Compton events in the Ge(Li) detector which result in a scattered photon entering the NaI may be eliminated from the spectrum. If the detector assembly were used only for Compton suppression, however, it would be unnecessarily large since a smaller anticoincidence annulus would be nearly as efficient for this purpose.

The Compton scattered photons entering the NaI assembly which correspond to the Compton edge in the Ge(Li) detector are of low energy (≈ 0.25 MeV). For these energies, a smaller thickness of NaI will approach 100% absorption. Thus, no significant differences between the Compton suppression of the 13.5 in. × 12 in. assembly and that of an 8 in. diam by 12 in. long annulus would be expected and none were found.

Because the NaI assembly consists of a pair of highly efficient 2π detectors, it may also be used in triple coincidence with a Ge(Li) detector to form a pair spectrometer of excellent resolution and optimum efficiency. The pair spectrometer mode is useful in identifying lines in complex spectra containing a number of gamma rays of energies greater than about two MeV.

Figure 6 shows the effectiveness of the NaI assembly in improving the quality and simplifying the structure of Ge(Li) gamma-ray spectra. The three spectra are of ^{24}Na (2.75 and 1.37 MeV gammas in cascade). The first spectrum was obtained with a bare 20 cm^3 five-sided-drift Ge(Li) detector. The second spectrum was obtained with the Ge(Li) detector operated in anticoincidence with the 13.5 in. × 12 in. NaI assembly. In the anticoincidence spectrum, the ratio of full energy peak amplitude to Compton edge amplitude is increased from 12:1 to 80:1, and the escape peaks from the 2.75 MeV gamma ray are largely suppressed. The third spectrum of Figure 6 is the triple coincidence spectrum of ^{24}Na in which all peaks but the double escape peaks are suppressed. The double escape peaks in the triple coincidence spectrum are $\approx 50\%$ of the amplitude of
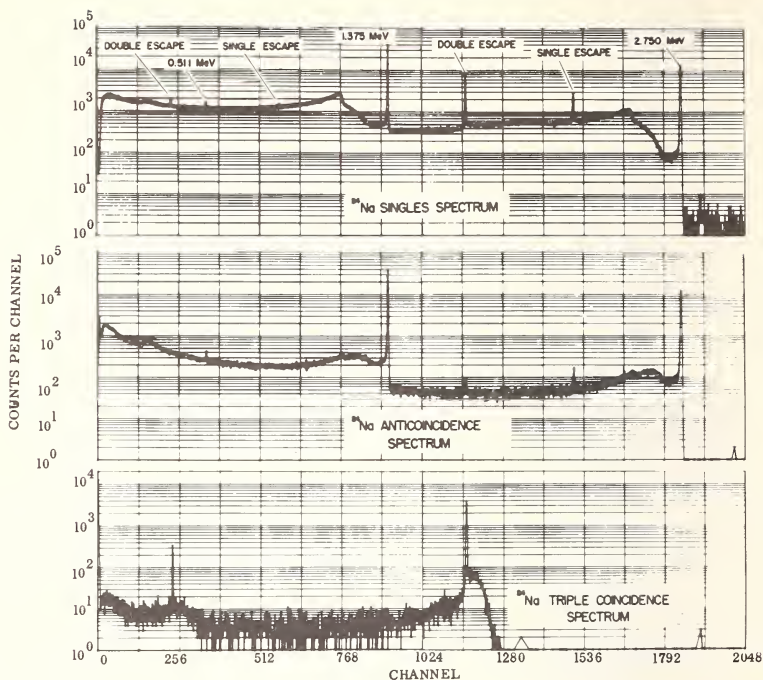
Figure 6.   Three ^{24}Na spectra taken with a Ge(Li) gamma-ray spectrometer.

those in the singles spectrum. The only difference in accumulating the three spectra was in the coincidence requirements for analyzing the Ge(Li) detector pulses.

Although we have stressed the applications for which the system was designed, the high efficiency and versatility of this system allow it to be used in many modes for varied purposes. For example, by placing a sample next to the Ge(Li) detector inside the NaI system, it is possible to emphasize or deemphasize cascade gamma rays. The uses are limited primarily by the imagination and ingenuity of the user.

A COMPTON-SUPPRESSED COINCIDENCE GAMMA-RAY SCINTILLATION SPECTROMETER WITH LARGE NaI (Tl) CRYSTALS

B. A. Euler, D. F. Covell and S. Yamamoto

*U.S. Naval Radiological Defense Laboratory
San Francisco, California 94135*

I. Introduction

A Compton-suppressed coincidence gamma-ray scintillation spectrometer has been assembled to obtain high sensitivity and selectivity in gamma-ray spectral measurements. The spectrometer is intended to satisfy requirements for the identification and estimation of low levels of gamma-ray radioactivity in a broad range of sample sizes and masses containing moderately complex mixtures of gamma-emitting radionuclides. The energy range of interest is 0-3 MeV. Several designs for a Compton-suppressed scintillation spectrometer have been proposed and evaluated by Perkins *et al* [1-3]. This spectrometer is similar in concept to an earlier design by R. W. Perkins, et al, but certain changes have been incorporated in the present design in order to: (1) eliminate deficiencies believed to exist in the earlier design, (2) satisfy particular requirements of the intended application, and (3) take advantage of recent improvements in the design and production of the various commercially available components.

II. Spectrometer Design

A. DETECTOR

The scintillation detector was chosen as the type of detector best suited to this application, particularly in view of the requirement for high sensitivity measurements on a variety of types and sizes of samples. The present detector shown in Figures 1 and 2, is constructed in two identical subassemblies. Each subassembly consists of a central crystal which has been packaged integrally with a Compton-suppression detector and photomultiplier assembly. These two subassemblies, one above the other, are placed face-to-face and spaced sufficiently far apart so that (1) an ample sample port is defined, and (2) any of several backscatter-suppression systems can be inserted between the two central crystals.

Each of the two subassemblies consists of an annular crystal, 13 1/2 inches in diameter by 6 1/2 inches in length, with a nominal 6 1/2 inch

ANNULAR NaI(Tl) COMPTON-
SUPPRESSION DETECTOR

UNACTIVATED NaI LIGHT PIPE

CENTRAL NaI(Tl) DETECTOR

NaI(Tl) BACKSCATTER-
SUPPRESSION DETECTOR

SAMPLE SLOT

CENTRAL NaI(Tl) DETECTOR

ANNULAR NaI(Tl) COMPTON-
SUPPRESSION DETECTOR

UNACTIVATED NaI LIGHT PIPE

PHOTOTUBES
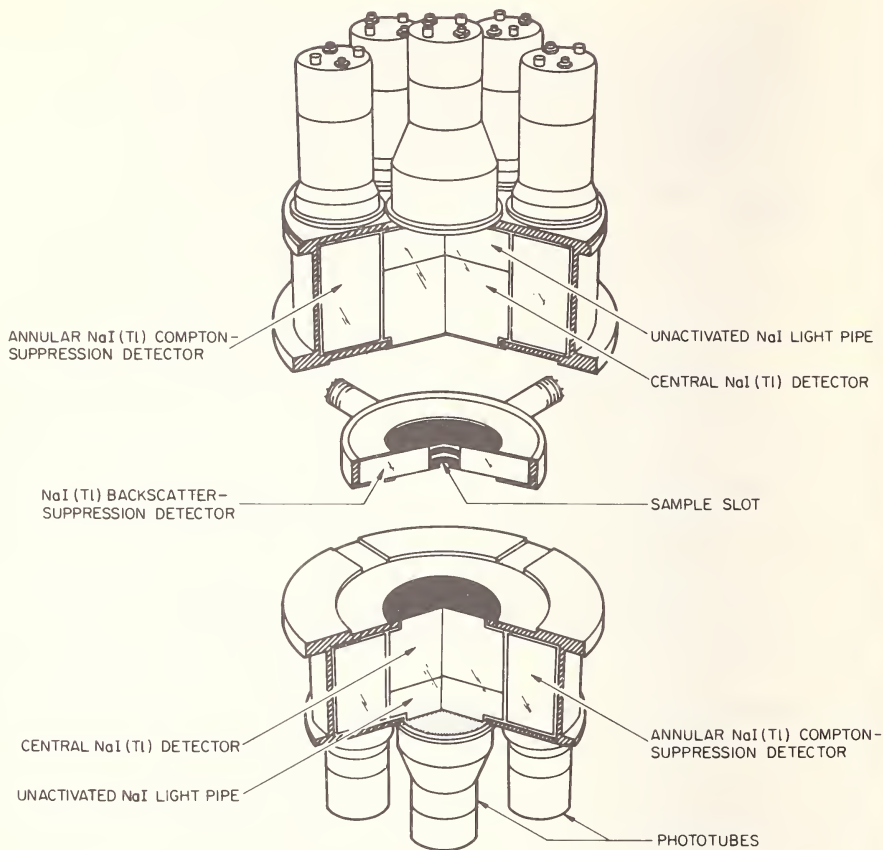
Figure 1.   Diagram of the Compton-suppressed coincidence detector system.

diameter hole through the center. A composite crystal, nominally 6 1/2 inches in diameter with a 4 inch thick crystal of NaI(Tl) optically coupled to a 2 inch thick crystal of unactivated sodium iodide (NaI) is contained permanently in the central hole. The exact diameters of the composite crystal and of the annular hole are such that a 3/32 inch space exists between the outer surface of the crystal and the adjacent surface of the annulus. This space is filled with magnesium oxide to decouple the two crystals optically and to provide maximum surface reflectance within each crystal.

A backscatter-suppression crystal can be optionally included as part of this detection system. This crystal consists of a "wafer" of NaI(Tl), 9 inches in diameter by 1 3/4 inches thick. A clear-through hole, 1 1/2 inches in diameter, is cut through the center of this crystal. A rectangular sample slot, 1 1/2 inches wide by 3/8 inches high extends from the edge of
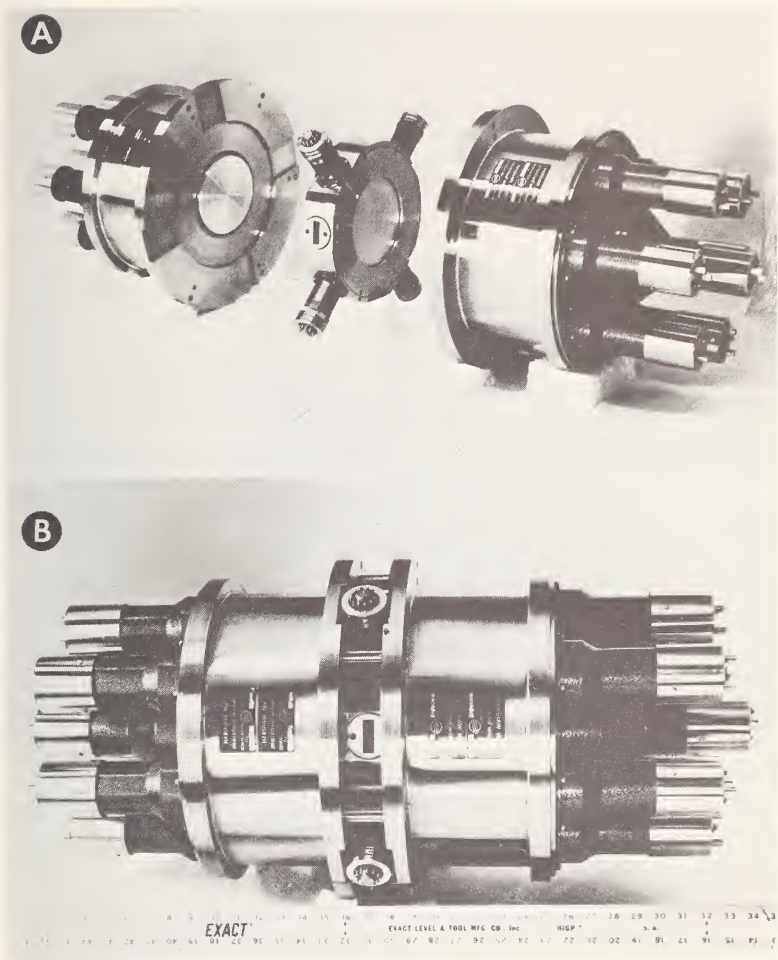
Figure 2. Completed assembly of the Compton-suppressed coincidence detector: (A) exploded view; (B) assembled view.

this crystal to the central hole. This slot which defines a precise sample geometry limits the sample size and shape, but the entire wafer can be removed to accommodate bulky samples.

B. Photomultipliers

The problem of tube selection was believed to be simplified by specification of a single 5 inch phototube on each of the two central crystals. Matched phototubes were specified so that optimum performance could more easily be achieved. For the Compton-

suppression detectors six matched 3-inch phototubes were specified for each of the two subassemblies. The wafer crystal was to be edge viewed, and four 1 1/2-inch phototubes were specified without a requirement for matching. Stable venetian-blind type photomultiplier tubes were specified. These tubes are available with a transit time spread of approximately 18 nanoseconds.

C. Detector Mount and Shield

A mobile carriage provides shock mounted mobile support for the detector assembly. The two subassemblies are mounted with their common axis oriented vertically. The carriage has hydraulically retractable casters and a 2-inch thick circular lead bottom plate which serves: (1) as the bottom portion of the detector shield, (2) to lower the carriage center of gravity in order to achieve increased stability, and (3) to enhance the shock absorption (mass inertia) characteristics of the carriage. A crystal lifting mechanism was designed to raise the upper crystal in a continuous motion up to six and one half inches above the lower crystal. This intercrystal spacing permits the easy insertion and removal of the wafer crystal and makes it possible to count samples of a variety of sizes and shapes. Three lifting screws support the upper crystal and are driven by a common manually operated drive chain. A calibrated odometer is attached to the drive chain and makes possible an accurately resettable counting geometry.

Interchangeable lead half-rings are stacked around the detector to form the shield. Each half-ring is 2 inches in height by 4 inches thick and weighs 120 pounds. The weight of the assembled shield is approximately 9,200 pounds.

D. Amplification and Gating Circuitry

Commercially available modules are used to achieve the required amplification and gating functions. Double-delay-line pulse shaping and zero-crossover coincidence and anticoincidence time marking techniques are used. Variable and fixed-time delays are incorporated and make possible (1) compensation of amplifier and detector timing differences, and (2) convenient determination of accidentals rates. Coincidence resolving time is continuously adjustable from 5 to 150 nanoseconds.

E. Pulse Height Analyzer

The pulse-height analyzer used with this system is a 4096 channel instrument built by Technical Measurement Corporation (TMC). This instrument makes possible either single-parameter or two-parameter pulse height measurement. Real time, delayed time, or simultaneous

real/delayed time totalizing data accumulation modes are possible. With additional input units the analyzer can provide up to ten-parameter measurement in the delayed-time totalizing mode. Each measurement parameter is capable of 1024 channels of digital resolution (ten-binary-digit resolution). Accessory components include: (1) a cathode ray tube display oscilloscope, (2) a fast digital printer, (3) a computer compatible magnetic tape system with read-in/read-out and file search capability, and (4) a tag (identification) word unit which inserts seven prespecified tag words onto each magnetic tape record.

III. Detector Response

Four modes of operation were defined for this spectrometer as follows: (1) gamma sum, in which the output signals from each of the two central crystals are linearly summed, (2) gamma-gamma coincidence, in which only those signals from the central crystals which are in coincidence are accepted, (3) gamma-gamma coincidence sum in which only those signals from the central crystals which are in coincidence are linearly summed, and (4) beta-gated gamma sum, in which signals from the central crystals are selected on the condition of a coincident beta ray (detected in a small auxilliary beta detector) and the selected signals are then linearly summed. In each mode the resultant pulse heights are measured.

The following qualities of the spectrometer were evaluated: (1) resolution, (2) background, (3) degree of Compton suppression, (4) efficiency, and (5) relative sensitivity.

A. Resolution

The resolution of the two central crystals as measured with a ^{137}Cs source ($E_\gamma = 0.662$ MeV) is 9.5% and 9.8% full width at half maximum (FWHM). The resolution of each annular crystal is 10.5% and the resolution of the wafer crystal is 27%.

B. Background

Background figures are integral counts over the equivalent gamma-ray energy range of 0.1-3.0 MeV.

The minimum background achievable (with the backscatter-suppression crystal removed) was 610 counts per minute in the gamma sum mode, 28 counts per minute in both the gamma-gamma coincidence and the gamma-gamma coincidence sum modes, and 0.14 counts per minute in the beta-gated gamma sum mode.

C. Compton Suppression

Under the most favorable conditions of Compton suppression, *i.e.* with the backscatter-suppression crystal installed, there was achieved a

reduction factor of approximately 3 over the Compton continuum and of approximately 6 in the backscatter region of representative pulse-height spectra.

D. DETECTION EFFICIENCY

Total-absorption-peak detection efficiency was measured in the gamma sum mode by use of a series of encapsulated point source standards. With the crystal assemblies spaced 1.800 inches apart and the samples placed midway between the two central crystals, the curve representing total absorption peak efficiency rises from approximately 50% at an energy of 100 keV to a broad maximum of 58% at 250 keV and falls to approximately 27% at 1.25 MeV. The drop-off at low energies is believed to be due primarily to: (1) attenuation in the encapsulation material of the standards, and (2) attenuation in the aluminum-magnesium oxide windows of the central detectors.

E. RELATIVE SENSITIVITY

One criterion for the selection of an appropriate operating mode for the measurement of a specific radionuclide is the relative sensitivity for the radionuclide in the various operating modes. Relative sensitivity is defined as follows:

$$\text{Relative Sensitivity} = \frac{\text{Photopeak Efficiency}}{\sqrt{\text{Photopeak Background}}}$$

In this equation, photopeak efficiency is defined as the ratio of the integral counting rate in the photopeak to the gamma emission rate of the radionuclide. In Table 1 are shown relative sensitivity values for ^{60}Co and for ^{137}Cs. Calculations were made for each mode by summing the counts in the region of the sum peak for the respective radionuclides, with the exception of the value for ^{60}Co in the gamma-gamma coincidence mode. This value was calculated by summation of the counts in the regions of

Table 1. Relative sensitivity for ^{60}Co and for ^{137}Cs for various operating modes.

Mode	Relative sensitivity	
	^{60}Co	^{137}Cs
Gamma sum	0.044	0.063
Gamma-gamma coincidence	0.074	– – –
Gamma-gamma coincidence sum	0.069	0.022
Beta-gated gamma sum	0.982	– – –

the two peaks observed in a two-parameter data field. Based on the relative sensitivity criterion, a most appropriate mode for a given radionuclide would be selected as the one which would yield the highest relative sensitivity. It should be noted that not all operating modes can be used in the measurement of all radionuclides. In the decay of ^{137}Cs, for example, the absence of a gamma-gamma cascade and the absence of a prompt beta-gamma coincidence preclude the use of the gamma-gamma coincidence mode and the beta-gated gamma sum mode. From Table 1 it is seen that, of the various modes evaluated, the relative sensitivity is highest in the beta-gated gamma sum mode for ^{60}Co and in the gamma sum mode for ^{137}Cs.

IV. Utility

The detection system described herein, when combined with single parameter and two parameter pulse height analyzers, provides an excellent facility for the identification and estimation of low levels of gamma-ray radioactivity in a variety of types and sizes of samples which contain moderately complex mixtures of gamma-emitting radionuclides. The detector has been in operation for two years and the qualities which have proven most valuable include: (1) versatility, which accrues from the range of operating modes which are possible; (2) sensitivity, which results from the high efficiency and low background that have been achieved; (3) selectivity, which is the result of the combination of resolution and the suppression of nonessential features of the pulse-height spectrum; (4) compactness, which results from the use of high density material (*i.e.,* NaI(Tl)) in the annuli; and (5) a high degree of stability in the system response.

V. References

[1] Perkins, R. W., Nucl. Instr. and Meth. **33,** 71 (1965).
[2] Perkins, R. W., and Robertson, D. E., Proc. 1965 International Conference Modern Trends in Activation Analysis, Texas A&M University, College Station, Texas, 1965, p. 48.
[3] Wogman, N. A., Robertson, D. E., and Perkins, R. W., Nucl. Instr. and Meth. **50,** 1 (1967).

DATA HANDLING

Synopsis of Discussions

J. I. TROMBKA, *Chairman*

Goddard Space Flight Center
Greenbelt, Maryland

The discussion on data handling reflected the radical change occurring in the field of pulse height analyzers (hard wire computers) and the incorporation of dynamic programable computers. The change has been forced by such problems as the incorporation of high resolution detectors, multiple detector set-ups, and the requirements of process control and batch processing of large amounts of data. The data handling problem essentially involves four phases, the housekeeping (*i.e.* identification of experiment, environmental corrections and control), data acquisition, data analysis, and interpretation and data display. Therefore, the radical changes that were considered involved determining how to combine these four factors most efficiently with the least expense.

Economics also influence this change. That is because of the number of multichannel analyzers required in a given laboratory. Would not the investment in a moderate size data processing computer designed to handle the input from a number of sensors be cheaper in the long run than investing in the individual pulse height analyzer?

Our session was fortunate in having a keynote speaker who put the data handling problem in proper perspective. We started with a place for the humanization of the data handling problem. Further, in the development of data handling systems, one must differentiate between automation and augmentation. The difference lies in the degree of human involvement and control of the data handling system. The era in which we now find ourselves and the era reflected by the majority of papers presented, is mainly typified by augmentation types of data handling systems. We are in the "learning how to do" part of development of systems at this time.

The papers presented described data handling and an analytic system for handling a myriad of problems from the simple (*i.e.* area integration, background subtraction, *etc.*) to complex (*i.e.* least square analysis, electronic and process control etc.). The size of computers considered ranged from the PDP8s to the on-line time sharing IBM360. Single and multisensor, multiparameter machines were considered.

During the presentation by Pierce *et al*, major problem areas emerged. First, how does one decide upon the computer and computer system to be used? Furthermore, there was interest by a number of groups in attaining the results of other persons' experiences in the development of data handling systems. The cost in both time and money is great and if previous experiences could be used, such costs could be greatly reduced. This concern was reflected in such questions as; how long did it take an individual group to develop their system? The answers indicated that it takes a minimum of one year for the simplest system and much longer for complex systems.

The above problem concerned itself with hardware, the next question asked concerned itself with software. That is, is there a central depository for the various computer programs developed? The answer is that there is not. Furthermore, even if such a depository was available, could the programs themselves be useful, because of the myriad of languages used in their construction? Thus the final question which arises is, how does one report these computer programs so as to make them understandable and useable by others?

During the discussion it was also pointed out that the analytic problems considered, herein are similar in nature and resolution to problems that have been considered by spectroscopists outside of the field of neutron activation and gamma ray spectrometry, one should not try to reinvent the wheel.

The majority of papers presented can be summarized as data handling systems which can be divided into three parts of utilization:

1. The data processor is used as a multichannel analyzer with controls for handling single or multicycle sensor systems. Housekeeping controls would also be exercised.

2. Single data acquisition and processing would be performed (*i.e.* display, integration, least square analysis, *etc.*).

3. The data are displayed either as new data or as analyzed data. The investigation could then use the information as needed or make a decision on further analysis to be performed.

Finally, because of the concern by the participants in this session for attaining information concerning both the software and hardware for data handling systems, it is suggested that this conference or other organization such as the National Bureau of Standards and/or the Atomic Energy Commission consider methods by which such information can be made generally available.

COMPUTERIZED QUANTITATIVE ANALYSIS OF HIGH-RESOLUTION SPECTRA

John A. Dooley, James H. Gorrell and Paul Polishuk

Air Force Flight Dynamics Laboratory
Wright-Patterson Air Force Base, Ohio 45433

Myron Young

Louisiana State University
Baton Rouge, Louisiana 70808

I. Introduction

In the field of neutron activation analysis at the Wright-Patterson AFB Nuclear Engineering Center, studies are being made on ear-bone samples, blood samples, and hydraulic fluid contaminants. In all the programs there is a requirement for an initial "quick look" followed by more detailed analysis. Ge(Li) detectors and 4096 channel analyzers brought resolutions improved by more than a factor of ten over sodium iodide systems.

A computer program is essential for the data reduction of this high resolution spectral detail. Because of core storage limitations, it was not feasible to extend the total spectrum, least square stripping methods commonly used with sodium iodide spectroscopy to 4096 channel data. Rather, the more simple approach of basing the analysis on photopeak information has been accepted; no prior detailed knowledge of spectral shapes is involved.

The Spectral Peak Search and Analysis Computational System (SPSA) was constructed especially to satisfy the requirements of flexible and convenient input for 4096 channels, location and analysis of peaks, automatic energy calibration, and formatted output including on-line plotted and printed data and analysis. SPSA places no special requirement on the experimenter with regard to his choice of amplifier gains, detection geometry or other set-up conditions. Other investigators have undertaken to develop such computer methods [1-6]. Some of this development was concurrent with our own.

For use in conjunction with SPSA, the computerized Isotope Library Identification Program (ILIP) was developed and is discussed elsewhere [7,8]. Combined usage of the two systems allows fast and accurate translation of high resolution spectral photopeak information into quantitative determination of isotope identities.

1090

II. Description of SPSA Computational System

Major analysis and computational blocks of SPSA are shown in Figure 1. Currently, the spectrum inputs originate in punched card, paper tape or magnetic tapes from five different analyzer systems: Nuclear Data and TMC 4096 channel, TMC 1024 channel, and RIDL and Packard 400 channel systems. The exact energy calibration information can be entered on cards and SPSA will proceed directly to analyze the first sample. Usually the first spectrum read in, or first two spectra, are from a calibration run on standard isotopes. The exact energies and approximate keV per channel are entered on cards along with other program-control parameters. SPSA locates and analyzes the calibration photopeaks, matching exact peak center in channels with the input energies. A precise energy calibration curve is obtained which is used throughout subsequent sample analyses. New calibration spectra can be entered as often as dictated by equipment stability and desired accuracy in analysis.
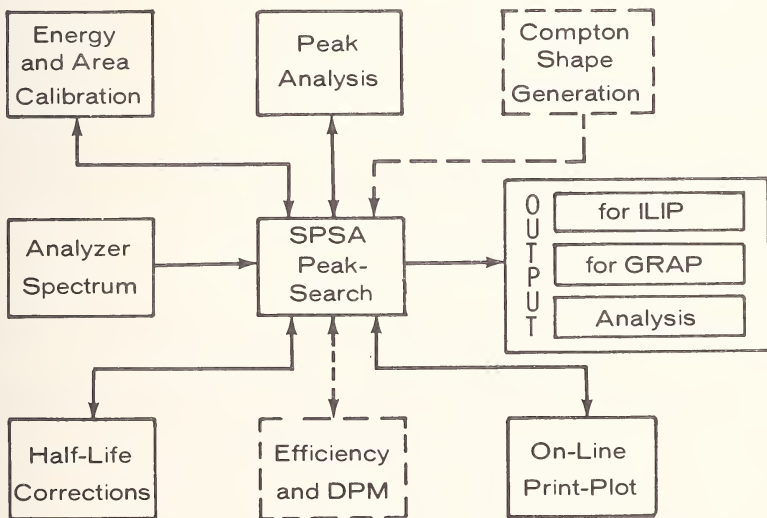
Figure 1.   SPSA spectral computation system.

SPSA next reads in an entire sample spectrum. Presmoothing of the data is performed, and linear or semilog print- plots are available. Figure 2 shows such a plot for a sample containing five isotopes. Starting at the low energy side, SPSA begins its search for peaks by looking for count

increases in adjacent channel groups. The required size of the increase is on the order of the square root of the counts and is derived from input parameters. Similarly, the program locates the right side of the peak. The peak analysis block of Figure 1 becomes fully operational. The baseline external to the photopeak, with a straight line under the peak temporarily assumed, is fitted to give an interpolated baseline. This interpolated baseline is subtracted channel-by-channel from the data counts to give a corrected photopeak. The fractional channel of highest counts, the corresponding energy, the full-width-at-half-maximum (FWHM), and the area for the transposed peak are determined. If Compton suppression has been requested, a peak is rejected if it does not meet certain photopeak shape requirements.
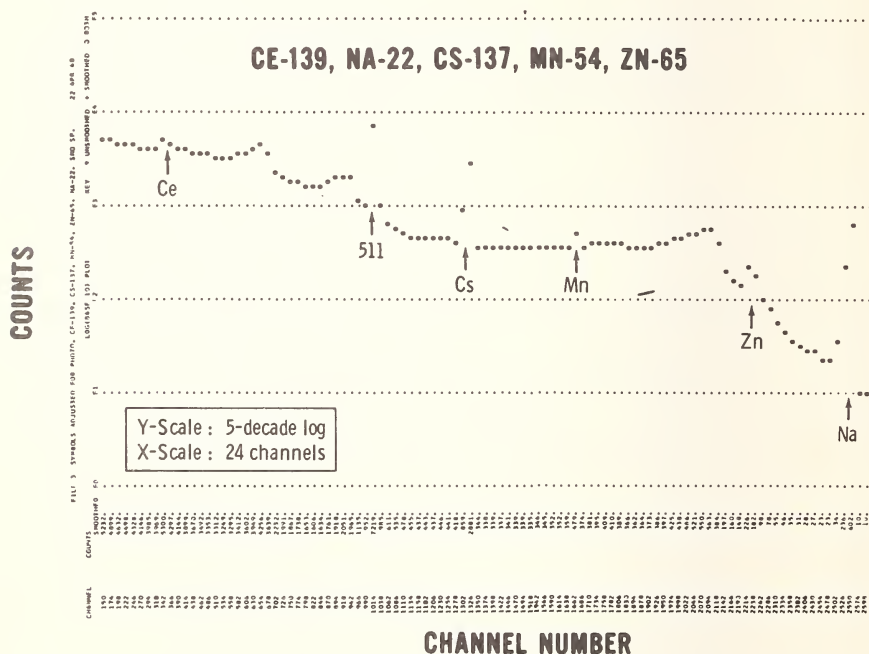
Figure 2.   Log spectrum plot.

In this way SPSA proceeds along a spectrum until the highest energy is reached. Each peak is analyzed in turn with a line of print-out, a punched card of results of analysis, and a scaled plot of the photopeak region including the interpolated baseline. Such a plot is shown in Figure 3 for the sodium-22 photopeak region. At the conclusion of the spectral analysis a summary table is printed. The punched cards, originally intended for input to ILIP and Gamma-Ray Analysis Program (GRAP) [1], have turned out to be extremely useful in another way. The summary

output can be reprinted as often as necessary from the cards. The cards can be automatically sorted to pick a common peak of interest contained in several spectra. In short, the punched card output allows arbitrary and fast reordering of the analysis results for the many spectra constituting a computer run and can relate results from one run to another.
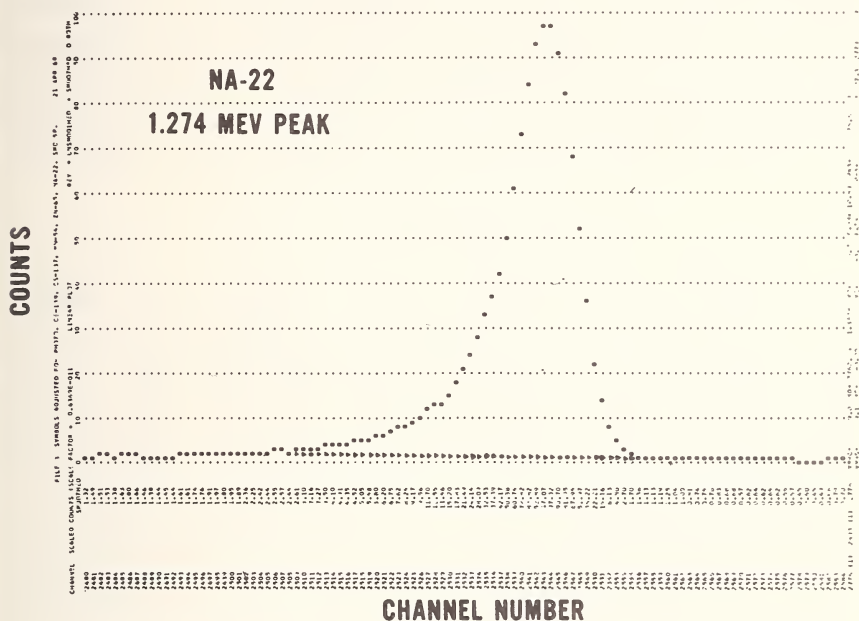
Figure 3.   Linear region plot.

Other special features built into SPSA include the capability of comparing photopeak parameters from as many as three consecutive spectra. An experimenter can discover low intensity peaks by repeating data accumulation for the same sample. With the SPSA search parameters set for high sensitivity this "unanimous vote" feature will distinguish between baseline noise and a genuine but small peak.

Half life decay corrections are made for the count period, prior waiting time and for infinite reactor irradiation. Additionally, the statistical uncertainty in each peak area is computed.

III. Experimental Results

A 4096 channel analyzer was used with a 2 cm³ Ge(Li) detector system set for an inverse gain of about 0.5 keV per channel. Five NBS calibrated point sources of cerium-139, cesium-137, manganese-54, zinc-65 and sodium-22 were counted singly and for all 32 possible combinations.

Since the sources were close to the detector, the counting geometries were carefully tended. SPSA was used to compute the photopeak parameters for five groups of 16 spectra. Each group comprised all spectra which contained a given isotope. For convenience, the 5-isotope composites were used as SPSA calibration spectra. Table 1 shows the results of the study. Column 1 lists the isotope name. Column 2 indicates the exact energy given to SPSA for calibration. The next three pairs of columns display energy, area and FWHM. The left column of each pair gives the value for the single isotope. To its right is the value of the parameter averaged for the 16 spectra which contain that isotope. Experimental standard deviations are associated with each average value.

Table 1. SPSA analysis results.

Isotope	Photopeak energy (keV)	Peak energy (keV)		Peak area (counts)		FWHM (keV)	
		Single	Composite average	Single	Composite average	Single	Composite average
Ce−139	166.0	165.8	165.9 ± 0.2	31863	30525 ± 1890	3.04	$3.08 \pm .10$
Cs−137	661.2	661.4	661.2 ± 0.5	71403	72029 ± 1010	4.06	$4.10 \pm .08$
Mn−54	835.0	833.5	834.3 ± 0.3	3051	3282 ± 266	4.41	$4.37 \pm .32$
Zn−65	1114.0	1116.2	1115.3 ± 0.8	3857	4110 ± 254	4.51	$4.79 \pm .32$
Na−22	1274.0	1273.6	1273.1 ± 0.8	19163	19481 ± 430	5.22	$5.36 \pm .39$

The deviations from the average peak energies ranged from 0.2 to 0.8 keV. The differences of the averages from exact energies ranged from 0 to 1.3 keV. More than half of the residual energy error can be attributed to two causes: (1) to uncertainties in the "exact" values and their not forming a smooth set, (2) equipment gain instabilities not fully corrected by SPSA.

The peak areas (counts for 30 min) varied in error from 1.4% to 8%. The largest deviations occurred for the peaks with the largest statistical uncertainties in the counts. Part of the error is due to the increased statistical uncertainty in the small difference of two large numbers; the rest of the error is due to baseline distortion resulting from Compton pile-up.

The FWHM values have deviations and errors under 0.4 keV. This kind of accuracy is, perhaps, to be expected since FWHM is a differential quantity. Short-term gain instabilities tend to be equal from measurement to measurement. Long-term instabilities which might affect the peak center reproducibility need not affect the FWHM.

IV. Summary

A computer computational system has been constructed in compatible Fortran-IV language. The system will fit into 32K core storage and only

the tape control section is peculiar to the direct-coupled IBM-7094, for which SPSA was designed. SPSA meets the initial objectives of maximum flexibility in experimental calibration, data input and types of program output. A novel parameter card arrangement has been designed to minimize user error. No library of isotope spectra is required. Very rough estimates of the measurement conditions, along with exact calibration energies, suffice for SPSA to establish an energy calibration which allows peak energies to be routinely measured with an accuracy of 1 keV, or better. Photopeak area determination is dependent upon statistical uncertainty in the peak counts and in the baseline which is interpolated for subtraction from the data counts. Error in area is typically under 10% even for extreme instances of Compton pile-up.

V. Acknowledgments

Without the support and assistance from the technical and management staffs of the Deputy for Engineering Digital Computation Division, the SPSA computational system would have fallen short of completion by many hundreds of computer shots. In particular, the willing and capable help in analysis and programming by James P. Hudson and James M. Thompson is acknowledged.

The highest praise goes to Mrs. Adelle B. McLean of Systems Research Laboratories, Inc., for her participation in so many phases of this work.

The experimental portions of this work were performed at the Air Force Institute of Technology Nuclear Engineering Center.

VI. References

[1] Harvey, J. A., and Stevens, J. M., "Analysis of High-Resolution Gamma-Ray Spectra", ORNL Phys. Div. Ann. Prog. Rpt., ORNL-4082, Oak Ridge National Laboratory, Oak Ridge, Tennessee 1967.
[2] Spink, P., and Erskine, J. R., "A Computer Program for Automatic Decomposition of Spectra from Charged-Particle Reactions", ANL Rpt, PHY-1965B, Argonne National Laboratory, Argonne, Illinois, 1956.
[3] Tepel, J. W., "A Computer Program for the Analysis of Time-of-Flight Spectra", Nucl. Instr. Methods 40, 100 (1966).
[4] Mariscotti, M. A., "A Method for Automatic Identification of Peaks in the Presence of Background and Its Application to Spectrum Analysis", BNL Rpt 10441, Brookhaven National Laboratory, Upton, New York, 1967.
[5] Yule, H. P., "Mathematical Smoothing of Gamma Ray Spectra", Nucl. Instr. Methods 54, 61 (1967).
[6] Murphy, H. M., "PPA, A Computer Program for Photopeak Analysis", AFWL-TR-65-111, Kirtland Air Force Base, 1966.
[7] Dooley, J. A., Gorrell, J. H., Thompson, J. M., and Hoffman, E., "Computerized Identification of Reactor-Produced Isotopes" (See this volume, p. 1148.)

[8]   Dooley, J. A., Young, M., Gorrell, J. H., Polishuk, P., Singhal, N., and Thompson, J. M., "Computer Program Development for Processing of Activation Analysis Data", (Paper delivered at Seventh National Meeting of the Society for Applied Spectroscopy, Chicago 1967; submitted for publication in Advancements in Appl. Spectry., 1968).

ON-LINE DATA ANALYSIS OF DIGITAL PULSE-HEIGHT SPECTRA

Part I - Analytical Structure

J. I. Trombka

Part II - Operational Computer Systems

R. L. Schmadeback

Goddard Space Flight Center
Greenbelt, Maryland

Part I - Analytical Structure

A number of analytical instrumental methods have been studied at our laboratory to obtain geochemical information concerning planetary surfaces. Neutron-gamma, x-ray fluorescence, and mass spectroscopic techniques have been considered. In all of these cases digital spectra are obtained. These spectra are characteristic of the interaction of the incident radiation flux with the detector. In order to obtain the desired geochemical information from the digital spectra, these spectra must be either unfolded in order to eliminate detector response or compared with standard spectra. A general on-line data analysis system is now being developed at our laboratory to handle such problems.

As a first step in understanding the total system, the following outline is presented in order to describe both the conceptual design and information flow pattern.

On-Line Digital Spectra Analysis System

   I. Method of sampling
  II. Raw data acquisition and display
    A. Real time
    B. Card input
    C. Magnetic tape
    D. Display
       1. Semi-log
       2. Linear
    E. Printed output
    F. Card output
    G. Plotted output

III. Library preparation
    A. Measured standard spectra
        1. Compensation for detector and electronic drift to obtain internal constancy
           a. Gain compensation
           b. Zero shift compensation
        2. Set pulse height or energy region for analysis
           a. Shift to common energy scale
           b. Resolution change
IV. Data preparation
    A. Data compression
    B. Background compensation
    C. Component subtraction
    D. Compensation for detector and electronic drift
        1. Gain
        2. Zero drift
    E. Range of analysis on scale calibration
    F. Data smoothing
    G. Calculation of statistical weight
V. Data analysis
    A. Raw data analysis
        1. Least square
        2. Area integration
        3. Pattern recognition
        4. Differentiation
        5. Preparation of output V–C
    B. Error analysis
        1. Statistical variance
        2. Chi-square
        3. Correlation and interference
        4. Prepare for output V–C
    C. Data interpretation

The above outlined program has been implemented for use on the CDC 3200 and details of the programming procedure are included in the second part of this paper. In this section a summary of the data analysis flow will be included to clarify the application of the program.

At Step I outlined above, calculations of the proper gain and number of digital channels needed in order to obtain unique solutions or maximum information from the measurement can be carried out. These parameters are determined primarily from a consideration of the detector resolution. Next the digitized pulse-height spectrum is obtained with a pulse-height analyzer and is transmitted to the computer in a number of ways as outlined in Section II. Real time transmission indicates a direct telephone line from the multi-channel analyzer's memory to the computer. Once the

raw data are obtained it can be displayed on a cathode ray tube, and compared with other raw data spectra or standard spectra. Other methods of outputting the raw data are available as indicated.

The numerical data analysis methods developed in this program require comparison and utilization of standard or library spectra. In Section III various methods for obtaining such standard spectra are available. Further preliminary adjustment of these spectra to more closely correspond to the energy scale and resolution of the detector can be made. Once the standards are prepared, we look again at the raw data, Section IV. A number of options are now available to the analyst. The data can be compressed by integration or possibly by obtaining some function of the data (*e.g.* The logarithm of data is of interest in utilizing the neutron die away technique.). Next compensation for background can now be made. Also a method for stripping a single component or groups of components is available. Corrections of gain and zero drifts are then made. If necessary, data smoothing can be performed. Finally calculation of statistical variance for each channel is carried out.

The data are now ready for analysis. The various analytic procedures are outlined in Section V and will be detailed in the presentation. Once an analysis has been obtained statistical error calculations are carried out to determine the validity of results.

By optimal use of the investigator, analyst, and the computer, the general analytic program described above has been made possible. We believe the on-line computer capability will allow for handling a great variety of problems, and furthermore, greatly simplify the application to a variety of sophisticated analytic procedures in the analysis of digital pulse-height spectra.

Solutions of a number of problems will be described at the presentation in order to clarify the application of this system. The next section describes the actual computer program design and implementation in greater detail.

Part II - Operational Computer Systems

The on-line computer program is an improved version of the "Linear Least Squares Analysis of Radiation Spectra" computer program [1] developed at Goddard for the IBM 7094. The on-line program is presently being run on a CDC 3200 computer with a memory core of 16,384 words of 24 bits per word. Because of the small memory size the program has been recorded on magnetic tape using an overlay technique. The program is a self teaching program which requires only 30 minutes of training for the first introduction to the computer.

The overlay technique [2,3] assumes that the computer program is composed of a series of independent subprograms which can be stored on

a magnetic tape (*i.e.* overlay tape) and called into memory only when required for actual computation overlaying the subprogram which was previously stored in that memory area. Control of the programs residing in memory at any one time is done by use of the main program. Data are made accessible to all of the subprograms by being stored in a common data area. Flow diagrams of the program will be presented.

Experiments are presently being conducted in an effort to optimize the man-machine interface. Figure 1 shows the present configuration of the analytical system. The system uses three inputs in an effort to keep the program as flexible as possible so that problems in nondispersive x-ray analysis as well as neutron activation can be done. The punched card input allows us to use data sent to us from other sources outside our laboratory. The magnetic tape input allows us to store large amounts of data in a limited area. Finally the data link input allows data to be transmitted to the computer from a remote sensor. The data transmission is presently being done using a data quality telephone line. The display unit allows the investigator to compare the input spectrum with his library or previous spectra in order to decide which data option should be used in the program. Since the investigator is remote from the sensor unit the display also allows him to have a real-time display of the data that he has just finished accumulating. After the data have been analyzed, the display is again used to display the results so that decision can be made as to the
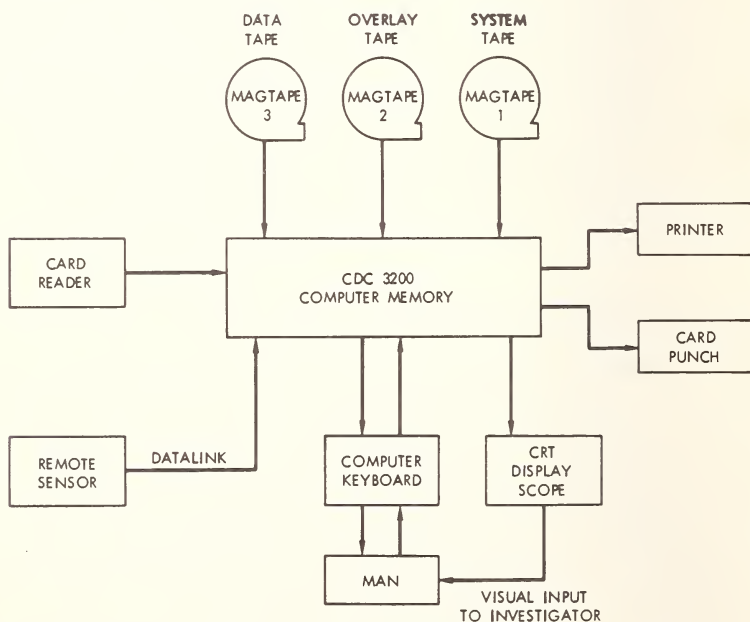
Figure 1.   On-line analytical system.

path to take during the next analysis. The card punch is used as an output for the real-time spectra received *via* the data link to preserve the original data. The results of the analysis are printed on the line printer so a hard copy will be available for future use.

The typewriter is used as an input from the man to the computer and an output to the man from the computer. The program is written so that the options available to the investigator are typed out each time a decision needs to be made. He then enters his choice by name using the typewriter as the input. By using this method the investigator actually becomes involved in the data analysis process and therefore is able to better obtain meaningful results.

An example of data reduction of a gamma-ray spectrum obtained by neutron activation will be presented and the operation of the computer in the on-line mode will be demonstrated.

III. References

[1] Trombka, J. I., and Schmadebeck, R. L., A Numerical Least-Square Method for Resolving Complex Pulse Height Spectra, NASA SP-3044.

[2] Computer Systems Fortran Reference Manual, Control Data Corporation, August 1966, Pub. #60057600.

[3] Computer Systems Real-Time Scope Reference Manual, Control Data Corporation, Oct. 1966, Pub. #60172500.

SPECTRAL DATA HANDLING SYSTEMS

F. P. Brauer and J. E. Schlosser

Battelle Memorial Institute[1]
Pacific Northwest Laboratory
Richland, Washington

I. Introduction

Gamma-ray spectrometry is frequently used to identify and estimate radionuclides in neutron activated samples. Spectra observed at different times after neutron exposure are often accumulated on a single sample in order to obtain half life as well as energy information; and thus estimate both long and short-lived nuclides.

The use of multidimensional detector configurations [1] or Ge(Li) detectors can result in up to 4000 channel spectra. The quantity and complexity of the data is further increased when the laboratory has a variety of different detector systems and analytical requirements. Electronic data processing techniques can be used to handle the large data volumes associated with modern instrumental activation analysis and are essential in some multiplex analyzer configurations. Several data processing systems utilizing large digital computing center facilities have been developed by our laboratory for the assembly of spectra files, analysis of the spectra, and storage and retrieval of the analytical results.

II. Description

A. HARDWARE

Gamma energy spectra are obtained at our laboratory with NaI(Tl) detectors and Ge(Li) detectors coupled to 400 channel or 4096 channel analyzers [2-4]. The larger analyzers are used with multidimensional NaI(Tl) detector systems or Ge(Li) detectors. Coincidence and multiplex logic are used with many of the systems. The 400 channel systems may be used to accumulate one to eight spectra of 50 to 400 channels in length. The 4096 channel analyzers are used to accumulate one 4096 channel spectrum or several shorter spectra.

A 4096 channel multiparameter analyzer will accumulate a 64×64 channel spectrum. No significant data will be stored above the $X + Y =$

64 diagonal if the maximum energy of interest is adjusted to be below channel sixty-four. When two similar detectors are used as the detection system, the spectrum is symmetrical on each side of the $X = Y$ diagonal. Thus if the spectrum is folded on the $X = Y$ diagonal only 25 percent of the channels are required to store the multiparameter spectrum. Multiplex logic circuits have been developed at our laboratory to store four multiparameter spectra in a 4096 channel memory [5]. Since the axis or noncoincident events often require more than 64 channel resolution, the analyzer memory is further split to allow storage of 240 channels of axis data per spectrum. The resulting four spectra array presented in 64×64 channel format is illustrated in Figure 1.
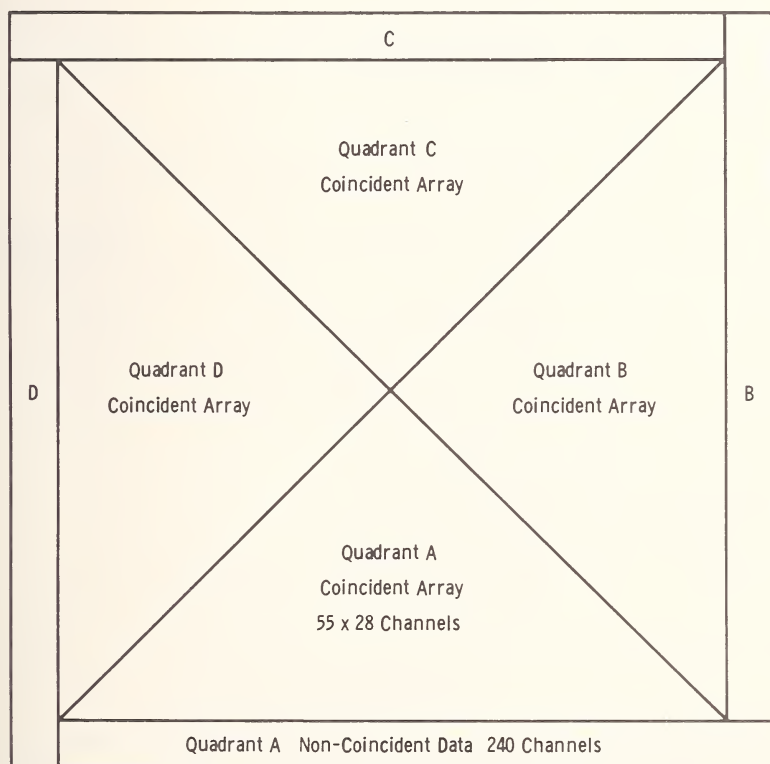
Figure 1. Multiplexed 4096 channel array.

Punched paper tape is used to transfer experimental data from the multichannel analyzers to the data processing center. A "Serial Number Device" (SND) automatically records time and identification information on paper tape prior to each readout of the multichannel analyzer's memory [5]. The contents of the "Serial Number" are listed on Table 1.

The time is clock controlled and the rest of the information is set up using ten-position thumb wheel switches.

Table 1. Serial number contents.

Decimal digits	Description	
1	Start of data character	
4	Live time in tenths of minutes	
2	Analyzer number	400 Channel Analyzers
1	Selector switch position	
8	Time at end of count in 10^{-4} days	
2	Detector number	
2	Counting mode code	
5	Analysis number	
1	End of serial number character	

Repeated up to 8 times depending on number of detectors (for rows: Detector number, Counting mode code, Analysis number)

Decimal digits	Description	
1	Start of data character	
5	Live time in tenths of minutes	
2	Analyzer number	
1	Number of detectors	
8	Time at end of count in 10^{-4} days	4096 Channel Analyzers
2	Array code	
1	Display and dump selector	
4	First channel number on readout	
4	Last channel number on readout	
1	Binary scale factor for axis data	
8	Geometry codes	
2	Detector number	
2	Counting mode code	
5	Analysis number	
1	End of serial number character	

Repeated up to 4 times depending on number of detectors (for rows: Detector number, Counting mode code, Analysis number)

B. SOFTWARE

Several software systems have been developed for storage and processing of spectral data. The various systems are designed to allow for different spectral formats and permit different degrees of automation and versatility. In all the systems, sample spectra, background spectra and empirical standards are maintained on magnetic tape spectra files and are supplied as needed to the calculation program (GEM) which uses a weighted least squares method to obtain nuclide estimates [6]. The more automated systems have less flexibility but can efficiently process large volumes of data for samples of quite similar characteristics. The more

versatile and less automated systems consist of two logical functional operations, (1) file maintenance and (2) file usage for calculation or plotting. The calculation and plotting operations use input cards to specify the data required from the spectra file and to control program operations. The spectral information input to all systems is presently in the form of punched paper tape.

The systems have been coded in FORTRAN IV for an IBM 7090 and a Univac 1108.

The following describes the plotting capabilities of one or more of the various systems that have been implemented:

a. Plotting of single parameter spectra with or without background correction.

b. Plotting of decaying single parameter spectra on one plot with or without background correction.

c. Plotting of the sums or differences of several single parameter spectra.

d. Plotting of decay curves for selected energy ranges.

e. Multidimensional displays of multiparameter spectra.

f. Plotting of slices through multidimensional spectra.

The following describes the calculation capabilities of various versions of GEM program:

a. High speed search of file for desired spectra.

b. Up to 40 nuclides per sample.

c. Up to 50 spectra per sample.

d. Background chi square computation for consistency checks.

e. Limit on maximum precision of data.

f. Limit on minimum standard spectra probabilities.

g. Automatic decay and sample size corrections.

h. Normalized chi square computations for reliability check.

i. Automatic model selection and reduction.

j. Error estimates computed for each nuclide.

Some of the program features which make the calculational programs especially user-oriented are the following:

a. Little order is required in the input.

b. Only changed quantities need be entered on subsequent cases.

c. No counts of spectra, nuclides, *etc.*, need to be furnished.

d. Input data is extensively edited.

e. When necessary, additional output is provided to aid in diagnosing errors, and estimating correlations.

f. Input card listing with appended edit messages for ease of data error correction.

g. Output of nuclide estimates on cards or magnetic tape for storage file.

h. Output of nuclide estimates from comparator standards stored, for associated samples.

i. Optional simplified peak area and nuclide estimating procedure for use with high resolution spectra.

Radionuclide results obtained from the spectra analysis program are stored on a magnetic tape master data file. This file is also used to store other sample information such as size and history which are entered by card input. The desired analytical estimates are calculated from the nuclide estimates and other required data, and stored on the file during the file maintenance processing. The master data file can be used to generate summary reports and plots using versatile selection and sorting logic included in a retrieval program. Figure 2 is a simplified flow chart of the system.
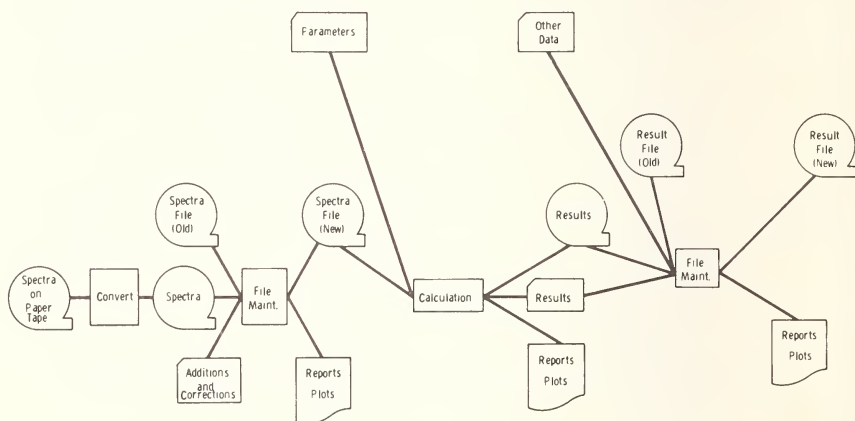
Figure 2.   Data handling system.

III. Discussion

The use of computer maintained files has been found essential to the accurate handling of large numbers of radionuclide spectra. The major problems are associated with transfer of the data from the multichannel analyzers to the computer. Equipment malfunctions associated with reading and writing punched paper tape have presented serious problems but can be controlled by careful selection of equipment, a good routine maintenance program, and software edit routines. Identification and time information not normally available in the analyzer memory can be conveniently attached to the spectra tape. The use of multiplexing techniques can reduce the number of channels to be processed and equipment requirements. The searching of magnetic tapes is rather

expensive when only small volumes of data are processed with large files. This problem can be minimized by maintaining several short files rather than a single multiple reel file. With adequate scheduling and organization the computing facilities can be used to free the scientist of much detailed tabulating, plotting, and calculating. The system described can be used with most spectral data and is not limited to gamma spectrometry data.

IV. References

[1]   Perkins, R. W., and Robertson, D. E., Proc. 1965 Int. Conf. Modern Trends in Activation Analysis (1965).
[2]   Brauer, F. P., and Connally, R. E., HW-SA-2932 (1963).
[3]   Brauer, F. P., Connally, R. E., Kaye, J. H., and Schlosser, J. E., BNSA-121 (1965).
[4]   Brauer, F. P., Kaye, J. H., and Connally, R. E., BNWL-SA-1381 (1968).
[5]   Connally, R. E., and Mitzlaff, W. A., to be published.
[6]   Nicholson, W. L., Schlosser, J. E., and Brauer, F. P., Nuclear Instruments and Methods **25,** 45 (1963).

"HEVESY", A COMPUTER PROGRAM FOR ANALYSIS OF ACTIVATION ANALYSIS GAMMA-RAY SPECTRA

Herbert P. Yule

Activation Analysis Research Laboratory
Texas A & M University
College Station, Texas 77843

I. Introduction

Interpretation of activation analysis NaI(Tl) or Ge(Li) gamma-ray spectra typically involves location of peaks in the spectra, determination of peak energies, measurement of peak intensities, and calculation of concentrations of the elements from which the gamma ray emitters were formed. If more than a few spectra are to be processed, the most economical and accurate way to process the data is with a computer, provided input errors can be overcome and the spectra can be obtained in computer compatible form.

Incorrect input data often present unrecognizable data to the computer resulting in job termination before all the data are processed. Thus, processing several hundred spectra can take many computer runs over a number of days or weeks. Incorrect input data may also result in computation of wrong answers. This paper describes the Texas A&M general purpose activation analysis computer program, named "HEVESY" after the founder of activation analysis.

II. Description of the Program

Data on punched cards in several formats of computer compatible magnetic tape are read and edited prior to computation. The editing feature takes care of incorrectly punched cards, missing cards, and extraneous cards. Occasionally, data cannot be edited because of very serious errors in the data. In this case, the program simply abandons that spectrum and searches for one that is error free or able to be edited.

For valid or corrected data, the program searches the spectrum for peaks, rejecting meaningless statistical fluctuations, Compton edges, and backscatter peaks. For each peak, the program lists the peak energy, the net peak area, the base area, the channels at the extreme right and left sides of the peak, peak width, and standard deviation of the peak area. If the input instructions on punched cards request it, concentrations of

1108

various elements are calculated using the peak area method. The program can be requested to compute amounts of elements present in a completely automatic mode. For example, by punching one two digit number, the analyst can request the amount of chromium in a sample to be computed based on the thermal neutron product, ^{51}Cr. The program knows that ^{51}Cr has a half life of 27.8 days, a prominent peak at 320 keV, and the yield of ^{51}Cr under standard conditions. It checks the spectrum to be sure there is a peak at 320 keV, computes the peak, and the amount of chromium present, relative either to the known yield or a comparator standard. The program contains similar pertinent information on 129 reactor neutron induced radioactivities.

Throughout the calculation, the program continually tests its results for errors. The program has performed very satisfactorily for a number of months. Several tens of thousand of spectra have been processed, and many of the computed results have been very carefully scrutinized for errors in either the input data or the results. No errors in the results have been observed, although numerous invalid data sets have been rejected by the program. Other data sets with minor errors have been computed for those results which could be obtained correctly, omitting computation of results which would be incorrect.

The ability of the program to bypass invalid data sets without ceasing execution has been very advantageous. Without this feature, it is clear that it would not be practical to compute the large volume of data generated in our laboratory. To take an extreme example, suppose each of the first four spectra in a group of several hundred are sufficiently incorrect to cause termination. On the first computer run, the reading of the first data set ends the computation. No results are obtained. Assuming the experimenter makes correct repairs to the first set, the second run gives results for the first spectrum, but terminates while reading the second. Thus, it takes at least five computer runs to get all the results if there are no other invalid data sets. As much as a week may be lost in this way, and the addition of new, possibly invalid, data sets complicates the situation. As it is written, the program avoids all this trouble, and eliminates the need for first running the data through the computer with an editing program.

In searching a spectrum for peaks, net peak areas are computed using the smoothed first derivative method [1]. For the quantitation part of the calculation, this method is also used unless the analyst used the option to implement Covell's method [2].

The present program is unique in a number of respects: (1) the relatively fast and very accurate peak location by the derivative sign change method, without input information on approximate location, (2) the ability to extract some correct information from data sets containing invalid information (3) the automatic concentration calculation freeing the

analyst from punching half lives, peak locations, peak boundary locations, and so on.

III. References

[1]   Yule, H. P., Anal. Chem. (in press).
[2]   Covell, D. F., Anal. Chem. **31,** 1785 (1959).

DEVELOPMENT OF A DIRECT CONNECTION BETWEEN AN ACTIVATION ANALYSIS LABORATORY AND AN IBM 360/65 COMPUTER

F. Girardi, G. Guzzi, G. Di Cola,
W. Becker and A. Termanini

C.C.R.
Ispra, Italy

I. Introduction

Processing of gamma spectrometric data by means of electronic computers (IBM 7090 and IBM 360/65) has been carried out in our laboratory since 1962. The output of the gamma spectrometers are punched tapes, which are processed "batchwise", with delay times of the order of one day. Although this delay is acceptable for much routine work, there are applications for which a faster answer would be desirable. Furthermore, if the delay time could be kept within one minute or two, it is believed by minimizing useless countings, the overall productivity of the counting equipment could be increased considerably.

To reach this goal the Activation Analysis Laboratory, the Electronic Instrumentation Section and the Scientific Data Processing Center (CETIS) of the Joint Nuclear Research Center of Euratom at Ispra are cooperating to set up a teleprocessing system between the activation analysis laboratory and the IBM 360/65 of CETIS as a first step toward a more complete teleprocessing network between laboratories and a centralized computer.

II. Description of System

The installation (which is expected to be fully operating by the end of the year) is basically composed of an IBM 1070 Telecommunication System installed in the counting room and connected by a coaxial cable (to meet future requirements in bandwidth) to the main computer. An interface, a digital entry device and an electronic clock complete the system.

Figure 1 shows a schematic drawing of the equipment installed in the counting room. Two 512 channel analyzers and the necessary control units were assembled into a single unit which can be controlled and used by an operator at the front desk. Two pneumatic sample changers are included for sending specimens to the detectors. The system can already
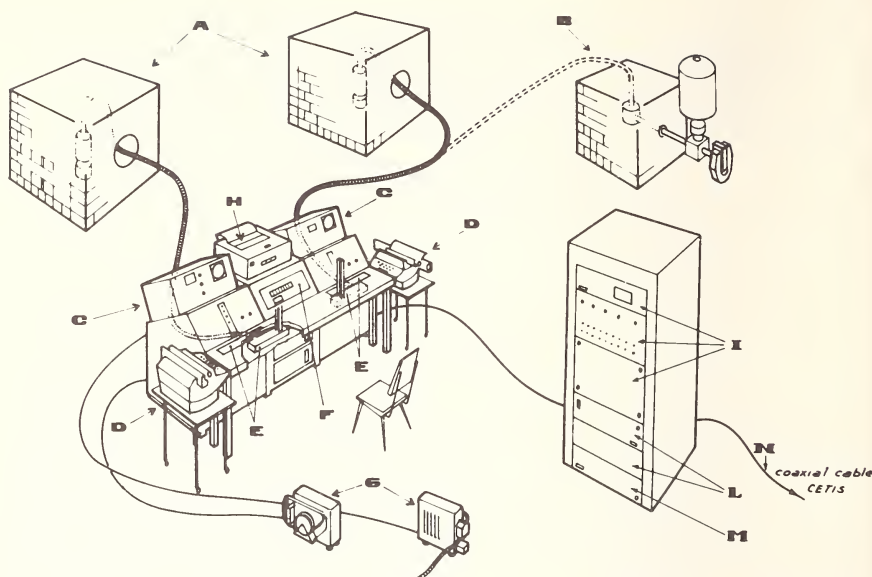
Figure 1.   Teleprocessing of gamma spectrometric data. Schematic view of the counting and teleprocessing equipment. A — 3 in. × 3 in. NaI(Tl) scintillators; B — 47 cm³ Ge(Li) detectors; C — 512 channels analyzers; D — Typewriters; E — Sample changers; F — Digital input; G — Tape punchers; H — IBM 1053 printer; I — IBM 1070 process communication system; L — Interface; M — Modem; N — Coaxial cable.

work automatically with punched tape read-out without operator control on a series of samples, as is frequently done during lunch breaks or night periods.

Figure 2 shows a block diagram of the hardware for on-line data processing. The two gamma spectrometric systems work independently, and they can work simultaneously if required. The detectors can be chosen as desired among two 3 in. × 3 in. scintillators and a 47 cm³ Ge(Li) semiconductor. The control units can easily be switched from the "tape punch" mode to the "transmission" mode by the operator. Once the output mode has been chosen, the operator will work on the operating switches of the multichannel analyzers as done with conventional read-out systems.

III. Operation of the System

Without entering into details which in part are not yet finally established, the system should operate as follows:

(1) Once the operator has switched the system to transmission mode (presumably at the beginning of the working day), spectra will be recorded
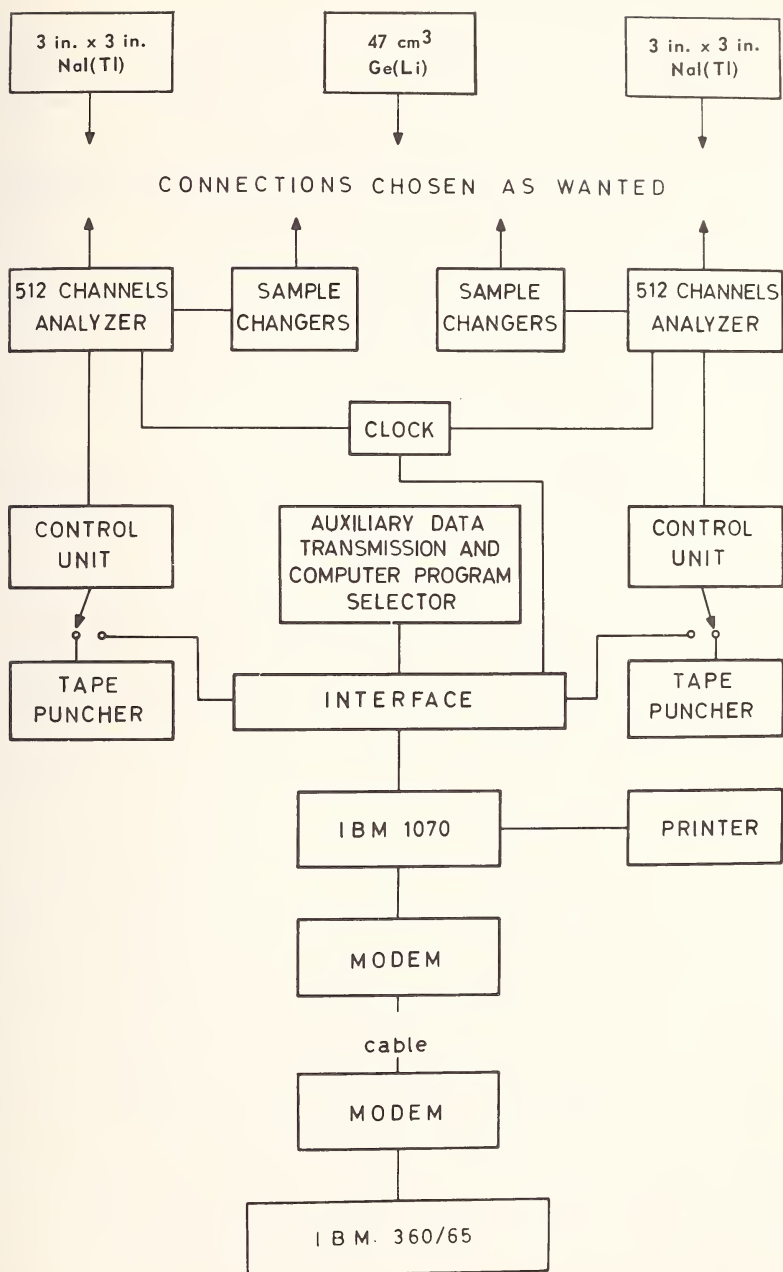
Figure 2. Teleprocessing of gamma spectrometric data. Block diagram of the equipment.

in the usual way. While the radioactive specimen is being counted, the operator will send to the computer through a digital input device, a code number by which he refers to a certain experimental set up and gives instructions on the kind of calculation requested.

(2) At the end of the counting period the interface switches itself to a "ready" position, and awaits the interrogation of the computer, which will be done at fixed times (presumably each minute).

(3) When the computer is ready for data acquisition, the content of the analyzer memory will be transmitted at the rate of 100-130 characters per second; 12-30 seconds are required for a complete spectrum (256 or 512 channels). At the end of the transmission the analyzer is ready for another counting sequence which will start automatically if the sample changer is used.

(4) The treatment of the data will start immediately. The computation time for a complete processing of a spectrum should be limited to 1-2 seconds according to a preliminary evaluation done on the basis of the existing programs.

(5) Once the results have been obtained, they are immediately transferred back to the laboratory at a rate of 13 characters per second. The essential information required to evaluate the results including a few necessary control data are estimated to be less than 130 characters (one typewriter line) or 10 seconds.

The logical flow of the computer program for data processing, which is presently being prepared on the basis of existing programs, is shown in Figure 3.

In order to occupy only a minor part of the computer memory devoted to teleprocessing users, the computer program is divided into sections. The main program, which will coordinate the different parts, should be resident in the memory of the computer and will transfer the control to the various segments of the program, according to the coded instructions received. Optionally it will be possible to store on disk the spectra received during a working period and process them later, batchwise. A preliminary version of the operating program for teleprocessing is being prepared, but at least two or three months are required to have it ready for full test.

Plans for future development include a faster transmission rate and a partial transfer of the analyzer's controls to the computer itself.
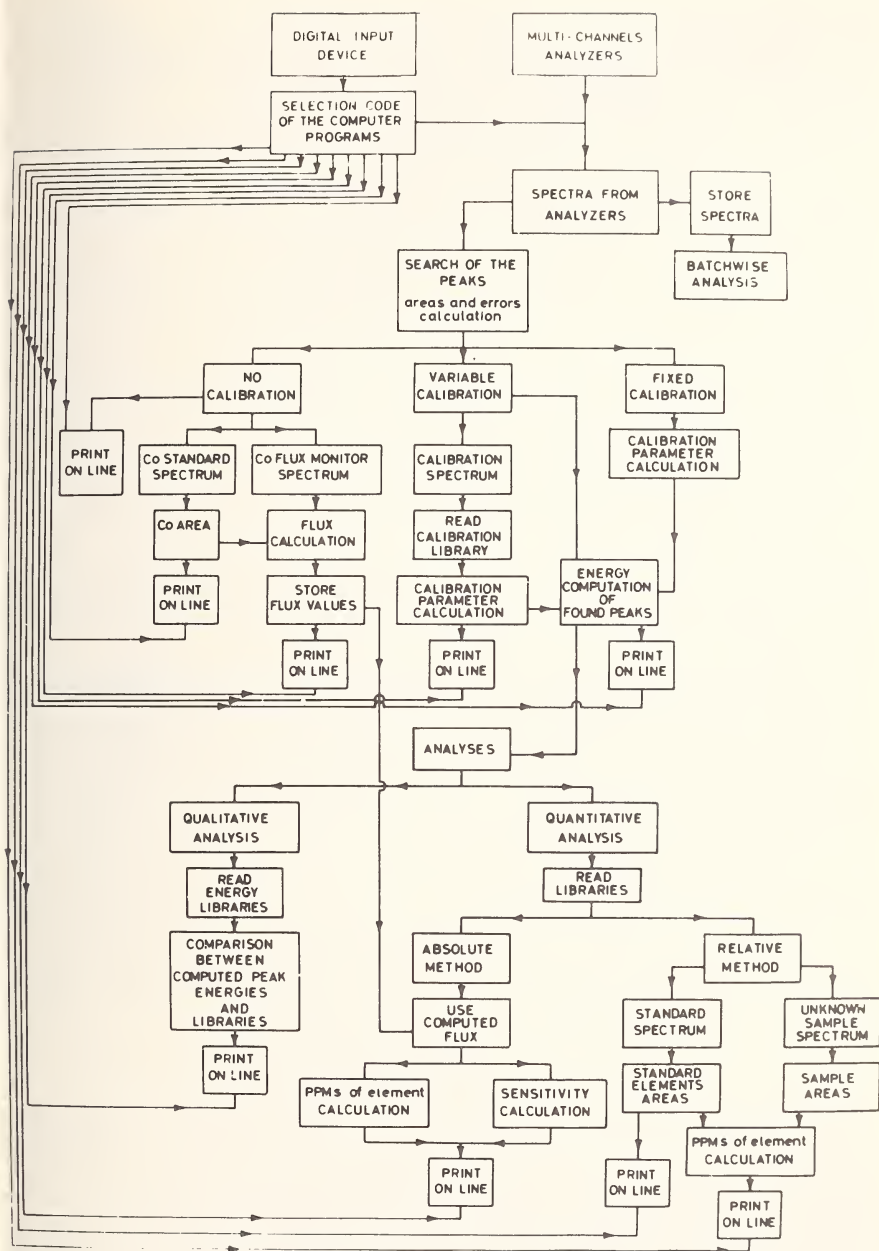
Figure 3. Teleprocessing of gamma spectrometric data. Flow sheet of the data processing program.

DEVELOPMENTS IN THE USE OF SMALL DIGITAL COMPUTERS IN ACTIVATION ANALYSIS SYSTEMS

T. B. Pierce, R. K. Webster, R. Hallett and D. Mapper

Analytical Sciences Division
A.E.R.E., Harwell, England

I. Introduction

Small digital computers with substantial technical capabilities are now readily available at relatively low cost and have many potential uses in an activation analysis laboratory. They may find application (1) as an integral part of some analytical instrument for direct data acquisition, *e.g.* as a gamma spectrometer, (2) as units for on-line control of other analytical instrumentation, *e.g.* a neutron generator, (3) for intermediate data storage and processing between measuring instrumentation and a central large-scale computer, and (4) as a computer for calculation in its own right.

A particular advantage of an activation analysis system incorporating a computer over those based on special-purpose pulse amplitude analyzer, is the speed and ease with which the function of the machine may be changed merely by altering the computer program. This versatility is of particular value in a laboratory concerned with a variety of different applications, and we describe here the uses to which a small computer has been applied for activation analysis. It will be seen that experience has so far been gained in using a PDP-8 computer as a gamma spectrometer, and for processing data for neutron and charged particle activation, *i.e.* categories (1) and (4) above, and that work is in hand to develop systems operating in modes (2) and (3).

II. Equipment

The computer used for this work is a PDP 8 (Digital Equipment Corporation, Maynard, Mass.); 2 magnetic (DEC) tape units provide increased storage capacity. The machine itself is a 12 bit, fixed word length, parallel computer with a 4096 word random access store and a cycle time of 1.5μsec. The tape system stores a maximum of 1474 blocks of data, each block containing 128 words at fixed positions on the tape. This system enables blocks of data to be easily retrieved or updated without disturbing information which has been previously recorded.

Electronic units connected to the PDP 8 are all of Harwell design and with the exception of the gamma-ray spectrometer control panel are modular units either of the 2000 or IANUS series. A 30 cm³ coaxial Ge(Li) detector coupled with a room temperature field effect transistor (FET) preamplifier provides an overall resolution of 5 keV (^{60}Co, 1.33 MeV, FWHM) for gamma spectrometry.

The above system is being used extensively for reactor activation analysis. A second PDP 8 is also used to process data obtained from experiments with a sealed tube neutron generator (Elliot Electronic Tubes Ltd.) or one of the Harwell electrostatic generators. Data are normally accumulated at the site of the experiment and then transferred to the PDP 8 on punched paper tape.

III. Applications

A. Use of Computer as a Gamma-Ray Spectrometer

The original intention in adapting the PDP 8 computer for operation as a gamma-ray spectrometer was to provide a system capable of performing the functions normally expected of a "fixed wire" multichannel analyzer while exploiting the additional capability of a program computer. The initial modes of operation required from the spectrometer were specified by the Analytical Sciences Division, A.E.R.E., Harwell; the subsequent design and construction of interfaces was carried out by Electronics and Applied Physics Division [1]. The basic system consists of an analogue to digital converter (ADC) interfaces to connect the ADC to the computer and the computer itself. In addition, a special control panel provides easy control of routine operations such as the start of counting the display of spectra *etc.*, and can be disabled when the computer is employed for uses other than that of a gamma-ray spectrometer.

The ADC is a Harwell series 2110 modified to a pulse rate of 8 MHz giving a maximum dead time of 300 μsec. Pulses from the ADC are transferred to the data store of the PDP 8 *via* an interface constructed from Harwell IANUS modules; data transfers are initiated by program interrupt giving a dead time of about 70 μsec. Timing pulses (1, 10, 100 and 1000 msec) from a clock-pulse generator are stored during a count cycle so that a live or real time can be preset.

The following operations are controlled from the settings of the control panel: count, clear, store, set limits to terminate the count, display spectra, select data storage area and nature of output.

Display during counting is on a 19 in. cathode ray tube (CRT) with a choice of linear, logarithmic or square root presentations. A second display permits comparison of the accumulating spectrum with any other portion of stored data. The time displays can be superimposed if desired.

The data store is divided into 16 sections of 128 channels, each of which can be used individually or in any combination of adjacent blocks to give 256, 512, 1024 or 2048 channels. A live display on the panel indicates the counting data area being used. Output may be typed, punched on paper tape or written on to magnetic tape. In all cases the universal time, live time and real time, together with selected auxiliary data, such as the total count output from the ADC can be printed out if required. An additional facility is provided by the "charge-parameter" control which enables any selected gamma-ray spectrum stored on magnetic tape to be brought into store and displayed.

A maximum count of 2^{18} can be recorded in each of 2000 channels by using 1 1/2 computer words per channel. This avoids the limitation set by the 12 bit word length of the PDP 8, but leaves only 1000 bits of storage for program. Consequently, those routines not permanently required to operate the data accumulation programs are stored on magnetic tape and called into memory as required.

This system has now been employed for the intact analysis by reactor neutron activation of a variety of samples such as steels, alloys, and geochemical materials. For this purpose, data from the gamma-ray spectrometer are stored on magnetic tape and transferred into the central IBM 360/65 computer through a second PDP 8 which is part of the central computer complex. In addition to sample and standard spectra required for subsequent least squares procedures, background information, universal real and live times are recorded on the tape together with weights of sample and standard and appropriate half lives.

As a result of experience gained with the gamma-ray spectrometer, further programs are being written to extend the scope and usefulness of the instrument. For example, an energy calibration program has been developed which permits rapid identification of the energies of peaks in an unknown spectrum, and an associative store program and interface are also available for conversion of the instrument for multiparameter analysis.

B. Use of the Computer as a Data Processor

A large computer may not always be available or for that matter may not be required for mathematical operations needed to evaluate experimental information from certain activation procedures. This could occur, for example, in relatively small-scale field activation analysis installations based on irradiation with a neutron generator. Consequently, two programs have been written to evaluate the potentialities of the PDP 8 for carrying out calculations likely to be required for activation determinations. The first is a modification of the least-squares program used on the IBM 360/65; the second consists solely of totalling counts

over significant energy regions of the sample and standard spectra and subsequently solving a set of simultaneous equations. The least squares program clearly provides the more powerful approach to spectral analyses, but requires substantially more computer time. Both programs have been successfully applied to the determination of a number of elements in steels and alloys by fast neutron activation analysis.

As part of a program of charged particle activation analyses, the variation in composition of surfaces is examined by raster scanning with microbeams of charged particles, measuring either the prompt gamma-radiation or the charged particles emitted during the irradiations. In order to obtain a rapid initial representation of the sample surfaces to permit subsequent, more refined irradiations to be carried out, data representing counts emitted from each volume of the irradiated surface sample are fed into the PDP 8 and presented in 3 ways. Hard copy is obtained as a number pattern on the teletype; an isometric CRT display is available for examination of the counts from simple samples, and a contour display program has also been written which is used for the more complex samples. Facilities are available for photographing different contour displays from the same sample and printing them in different colors on the same print for a permanent record.

Many other programs have been written which find regular use in activation analysis. Operations carried out include spectrum stripping, calculation of activities, peak areas, capture gamma-ray yields, elastic scattering yield with angle and decay corrections.

IV. Future Developments

Experience with sealed tube generators have shown these instruments to be reliable and easy to operate. It is therefore reasonable to suppose that such a generator might be run automatically and unattended under computer control.

Plans are in hand to interface a PDP 8 to a new, high output sealed tube neutron generator (neutron output 10^{11} n/sec total) with the ultimate aim that the computer will perform the operations of (a) control of generator, sample transfer system, count and irradiation times, (b) gamma-ray spectrometry, and (c) reduction and calculation of experimental data to provide a completely integrated system.

In the work described so far, each computer has been used for a single purpose at any one time but for certain applications it is more economical to time share a large general purpose computer between several instruments. Two Honeywell DDP 516 computers will be installed in the Analytical Sciences Division within the next 2-3 months to operate on this basis.

One of these machines is not for activation work but will be used for data collection from a range of analytical instruments such as NMR, ESR and mass spectrometers. However the second of these will be interfaced to 4 radiation detectors and provide for simultaneous accumulation of gamma spectra, and for data-processing either in the machine itself or in the central IBM 360/65 computer to which it will be connected by a fast data link.

V. Reference

[1] Lewis, A., A Multichannel Analyzer Application for a Small Computer, A.E.R.E. Report R 5844.

ON-LINE ACTIVATION ANALYSIS
WITH A PDP-9 COMPUTER

C. J. Thompson

Atomic Energy of Canada Limited
Commercial Products
Ottawa, Canada

I. Introduction

This paper will describe the operation of an activation analysis system set up at Atomic Energy of Canada Limited, Commercial Products. The basic elements of the system are, (1) an antimony beryllium thermal neutron source with a flux of up to 7×10^8 n·cm^{-2}·sec^{-1}, (2) a PDP-9 computer which is used to acquire and analyze the spectra, and (3) a fast pneumatic sample changing system. The system has been designed for routine quantitative measurements of a few elements in many samples on a continuous basis, and for rapidly analyzing complex spectra to find the elements present in "unknown" samples. To this end we have obtained the spectra from chemically pure elements under standard conditions and these spectra are stored on magnetic tape.

The antimony-beryllium neutron source has been described previously [1,2,5]. I will describe it briefly but concentrate on the data handling techniques used by the computer to analyze the gamma-ray spectra.

II. Description of the System

A. NEUTRON SOURCE

The antimony-beryllium neutron source provides a very uniform, accurately known, flux of pure thermal neutrons. These features give uniform neutron flux throughout large sample volumes. Lack of fast neutron reactions usually simplifies the interpretation of spectra from many-element compounds.

The neutron source has five sample positions and has room for up to eight 3000 curie ^{124}Sb sources. The neutron flux is between 1 and 7×10^8 thermal n·cm^{-2}·sec^{-1}. Pneumatic transfer tubes from 2 of the sample positions terminate in facilities controlled by the PDP-9 computer.

B. DETECTORS

The complex spectra produced by most materials as a result of neutron activation are usually best analyzed by germanium detectors. We have

1121

three such detectors with active volumes of 7, 30 and 35 cm³. The largest is in a cylindrical chamber opposite a 4 in. × 4 in. NaI detector. These detectors are surrounded by 4 inches of lead. The low background system, in which both the detectors can be used individually or in coincidence, can be used for analyzing the most complex spectra.

C. Computer Hardware

The PDP-9 computer has 8192 words of memory, a fast arithmetic unit, 2 Dectape transports and a Calcomp plotter all supplied by the Digital Equipment Corporation. In addition we have interfaced a Hewlett-Packard 5415A, 100 MHz ADC, a special purpose ADC, a display, and sample changer interface which have been designed and built by the users.
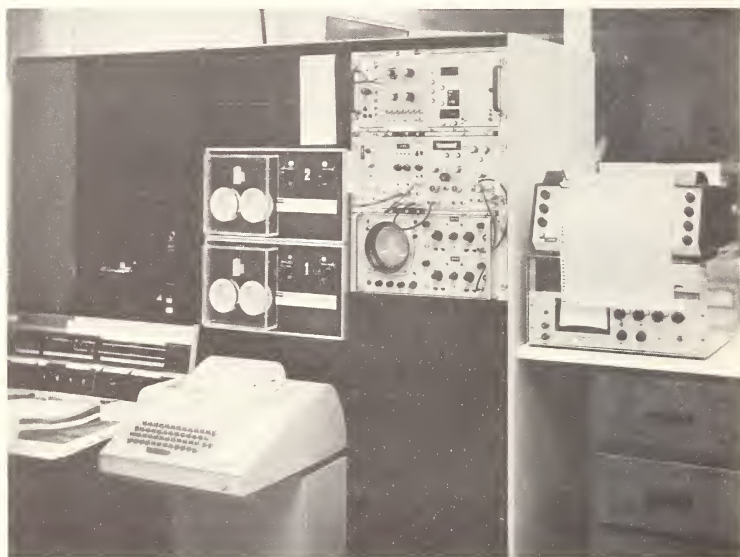
Figure 1.   Photograph of PDP-9 "Spectrum Analyzer".

D. Computer Software

In writing the software for this system the goal has been to do as much data reduction on the spectrum as possible with a single resident program. To this end the program occupies the entire lower half of the memory with the upper half used for storing four 1024 channel spectra. This approach in the software has several advantages. One, if the computer is used to collect spectra, except when the data rate is very high, it is idle most of the time. Some of this time can be used to process the data from the previous

measurement. Two, the computer makes good use of all the hardware since spectra can be stored on "Dectape", plotted, displayed and various peak areas measured at the same time. Three, there is no need to wait for results, since the same program provides most of the required information about peak areas and energies immediately.

Table 1 is a list of the 26 basic commands for the "Spectrum 40" spectrum analysis program. By typing the letter specified and some

Table 1.   Command letters used with the "Spectrum–40" Spectrum Analysis Program.

INPUT
           D — Disable encoder or time delay
           E — Enable encoder or time analysis
           R — Read spectrum from paper tape
           Y — Irradiate sample in neutron pool

DISPLAY
           K — Kill display
           L — Logarithmic display
           V — Linear display
           Q — Calibrate display with halo generator

DATA REDUCTION
           A — Add two spectra or correct for live time
           H — Do nothing
           I — Integrate "total counts"
           J — Integrate "Photopeak"
           M — Subtract one spectrum from another
           S — Search for peak channel
           U — Store sequence of experimental results
           W — Measure width of peak
           X — Execute sequence of commands

OUTPUT
           P — Punch spectra on paper tape
           T — Type out spectrum
           Z — Compressed spectrum punch
           & — Plot spectrum being displayed

DECTAPE
           B — Bring experiment from dectape
           F — Find names of experiment on dectape
           G — Give notes of experiment on dectape
           N — New experiment onto dectape
           O — Erase experiment from dectape

numbers, the function alongside the letter is executed. The first group of commands deals with the flow of samples to and from the neutron cell and the activation time, delay time (if any) and measurement time. The second group sets the display in log or linear mode. The third group of commands allows the addition and subtraction of any fraction or multiple of any spectrum from itself or another spectrum. These are used for adding elemental spectra to simulate complex spectra, correction for live time, spectrum stripping and background subtraction. The system can also be calibrated in keV per channel so that when a peak is integrated its energy is also given. Both "total count" and "photopeak" integrations (with the area below the photopeak subtracted away) are possible. The location of a peak can be found and the detector energy resolution can be measured in either percent or keV. The last two groups of commands to put spectra on Dectape and retrieve them, and to output spectra on punched tape and the teletype. Spectra can also be plotted on the "Calcomp" plotter. In addition to the teletype the operator may use the display [3] to identify peaks. The "Halo generator" on the display allows the operator to turn any point on the spectrum into a circle of light 1/4″ in diameter. When he has identified a particular peak, the operator pushes a button which causes a typeout of the photopeak area and the energy in keV.

III. Operation of the System

A. COMMAND SEQUENCES

Almost all of the above commands can be assembled into a "micro program". A typical example might include the following steps.
1.   Activate the sample for 2 minutes and count it for 2 minutes.
2.   Correct for live time and subtract background.
3.   Display a section of the spectrum and plot it.
4.   Measure the area and energy of 5 photopeaks of interest.
5.   Store the experiment, (spectrum and all typed results) on Dectape.
6.   Repeat the sequence for 30 more samples.
In such a sequence the computer can run unattended and perform all the routine activation analysis work over night. Table 2 is a typical printout from the sequence outlined above (for one sample).

This system has been under development for over a year and has been in routine use with the above features for several months. During that time it has been used to measure gold and uranium in rock samples, components of steel samples [4], traces (30 parts per million (ppm)) of hafnium in zirconium compounds and in many other applications.

As an example of the method of data presentation, Figure 2 shows a semi-logarithmic plot of the spectrum of a steel sample after a 2 minute irradiation and measurement. This was one of many measured with the

Table 2. Typical computer printout giving the areas and energies of 5 photopeaks present in a spectrum, the measurement time, display calibration scales and total counts in the spectrum.

```
REAL TIME:   2M      ·00S
LIVE TIME:   1M   25 ·52SRATIO:    1·40
100   CHANS· PER DIV· HORIZ·    6400= COUNTS PER DIV· VERT·
  1   15354 PHOTO PEAK COUNTS AT  842·46 KEV·
  1   34623 PHOTO PEAK COUNTS AT 1426·66 KEV·
  1    1185 PHOTO PEAK COUNTS AT 1767·02 KEV·
  1    1392 PHOTO PEAK COUNTS AT 1797·50 KEV·
  1     774 PHOTO PEAK COUNTS AT 2092·14 KEV·
 10X 122005 TOTAL COUNTS
```

sequence of commands described above. Table 2 shows the computer output from this measurement. The five peaks listed are from ^{56}Mn (.845, 1.81, and 2.11 MeV) ^{51}V (1.43 MeV) and ^{28}Al (1.78 MeV).
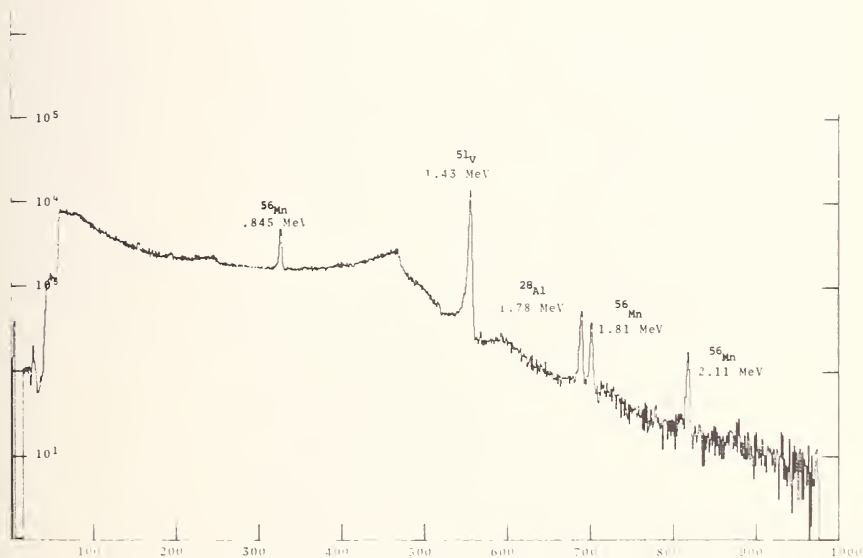
Figure 2. Computer plot of typical spectrum from a steel sample containing manganese, vanadium and aluminum.

The system has proven to be a great improvement over a conventional multichannel analyzer and is in use continuously in both developing new measurement techniques and in routine activation analysis.

IV. References

[1]   Churchill, T. R., Proceedings IAEA Symposium on Radioisotope Tracers in Industry and Geophysics, Vienna 1967, Vol. II. p. 271.
[2]   Courtemanche, R., and Kushneriak, S. A., Canadian Nuclear Technology, March-April, Vol. V, No. 2 (1966) pp. 32-34.
[3]   Thompson, C. J., Proceedings of the DECUS Fall 1967 Symposium, p. 177.
[4]   Churchill, T. R., Transactions of the American Nuclear Society and Canadian Nuclear Association, June 1968, pp. 94-95.
[5]   Downs, W. E., Nuclear Applications 5, No. 8, 55-61 (1968).

MAN-MACHINE INTERACTION IN ANALYSIS
OF PULSE-HEIGHT SPECTRA

Walter R. Burrus

Tennecomp, Inc.
Box J
Oak Ridge, Tennessee 37830

There are two basic approaches to processing the increasing mass of data produced by modern nuclear data acquisition equipment. The first is through "automation" and aims to replace as many human decisions as possible by computational decisions motivated by the desire to achieve unattended error free analysis. What actually happens is that the human subjective interaction occurs at the time the program is written and debugged. The numerical and physical intuition of the programmer is built in and frozen. The second approach is through "augmentation" and aims to augment the human operator by doing the repetitive and tedious arithmetic and bookkeeping functions but leaving the subjective decisions fluid and at the disposal of the operator. A relatively unskilled technician has a much more powerful pattern recognition capability than large scale digital computers. Thus the augmentation approach is sometimes superior in problems which involve the analysis of graphical patterns. The automation approach is often superior if only a very few types of patterns can occur. Several typical nuclear data analysis tasks are reviewed from the "automation" and the "augmentation" viewpoints. Among these are "unfolding" of scintillation spectra, identification of small peaks obscured by statistical "noise" and the extraction of areas and centroids of multipeaked data.

PANEL DISCUSSION ON INFORMATION RETRIEVAL

THE NBS AUTOMATED ACTIVATION ANALYSIS INFORMATION RETRIEVAL SYSTEM

G. J. Lutz, R. J. Boreni, R. S. Maddock and W. W. Meinke

National Bureau of Standards
Washington, D.C.

I. Introduction

The Analytical Chemistry Division of the National Bureau of Standards maintains a file on the literature of activation analysis. For several years the indices of the file were kept manually on punched cards by two of the authors (W.W.M. and R.S.M.). In 1964, as the number of items approached 2000, it became apparent that computer methods would greatly facilitate the storage and retrieval of information contained in the file. The Control Data Corporation was contracted to modify their INFOL system to accommodate the deep indexing that was desired for flexibility and ease of retrieval. All of the items in the file were indexed to those categories that were considered to be of interest to anyone searching the activation analysis literature.

II. Indexing

Each item in the file is coded to each (if appropriate) of the following five main categories.
    I Element Determined
    II Matrix Analyzed
    III Technique Used
    IV Nature of Publication, Language and Country of Origin
    V Scope of Publication

A. ELEMENT DETERMINED

Since activation analysis is an elemental method, a listing of all of the elements will suffice for this category. In addition, the rare earths as a group are in this key.

B. MATRIX ANALYZED

There are 105 subcategories in this key. They include general categories such as minerals and drugs, twelve categories of biological

matrices and five categories of forensic matrices. In addition there are categories for specific elements and groups of elements, their compounds and alloys. The breakdown in this category has been made partially on the basis of frequency or analyses of sample but also on the basis of particular problems associated with specific samples. As an example, lithium, its compounds and alloys has a category alone, while the rest of the alkali metals, their alloys and compounds share a key number.

C. Technique Used

The components of this category may be considered to belong to one of the following groups:

    I Radiation Source
    II Chemistry Used (or Nondestructive)
    III Radiation Detector
    IV Errors and Corrections Associated with Activation Analysis
    V Other

Just as Element Determined, Matrix Analyzed and Technique Used specify an activation analysis, so do the first three groups above specify technique used. In general, items describing a specific analysis are coded to the appropriate key of these first three groups.

The specific items under Radiation Source include reactor (n,γ), reactor-epithermal, reactor-fast, neutron generator, accelerator, photon activation and charged particle activation. Chemistry Used includes the usual separation methods in activation analysis as well as keys for dissolution technique, automated chemistry and group separations. The Radiation Detector category includes gamma spectrometry, beta and alpha spectrometry, coincidence counting, nondiscriminatory counting, neutron counting and prompt gamma counting.

Group IV, Errors and Corrections, includes flux determination as well as self-shielding for each of neutrons, charged particles and photons, and also includes interfering nuclear reactions, other errors associated with irradiation, and counting errors. Group V, Other, includes sensitivity tables, discussions of precision and accuracy, techniques, facilities, computer applicators, data handling systems and electronics.

D. Nature of Publication, Language and Country of Origin

In this category, the item is keyed as to whether it is an abstract, bibliography, book, conference proceedings, institute or course notes, professional journal article, trade journal article, patent, press release, report or thesis. In addition it is coded to the language of the item and its country of origin.

E. Scope of Publication

In this category, an effort is made to classify the item with respect to emphasis and content. Among the classifications in this key are broad critical technical review and extremely detailed and thorough treatment for specific element, or specific matrix, or specific technique.

III. Storage and Retrieval

When indexing of an item has been completed, its accession number, authors, literature citation, year of publication and the keys of classification are punched on paper tape for storage on magnetic tape. Subsequently, searches may be made on the basis of the classification, authors and year of publication. Any desired specificity may be obtained in the search. Although most users specify a given element or elements in a given matrix it is entirely practical to do a search for example for oxygen as the element to be determined in all matrices by all techniques other than neutron generator.

IV. Discussion

Prior to publication of the bibliography to be presented to the attendees of this conference, the system had only "in house" usage. Over the past three years it has proven very useful in the solution of specific problems as well as in maintaining state-of-the-art awareness of categories of interest to the Activation Analysis Section.

The editors intend to periodically update the bibliography and would welcome suggestions from the activation analysis community as to desired types of bibliographic break-down which might appear either as division reports or in the open literature.

V. Acknowledgments

We wish to thank the members of the Activation Analysis Section for their assistance in keying and their many imaginative suggestions for improving the utility of the system.

EDGE-PUNCHED CARD LITERATURE RETRIEVAL SYSTEM FOR ACTIVATION ANALYSIS

T. Braun

Institute of Inorganic and Analytical Chemistry
L. Eotvos University
Budapest, Hungary

E. Bujdoso and M. Miskei

Research Institute for Non-Ferrous Metals
Budapest, Hungary

I. Introduction

Studying the literature is an important duty for every professional. However, the rapidly increasing number of scientific publications presents an increasing problem that research workers have to solve. Many well-known difficulties can be overcome by means of appropriate bibliographic compositions, minimizing the time required for literature searches. Recently, a number of professional fields have published data and bibliography collections accessible for the majority of interested users. These systems represent, essentially, a compromise between the vast quantity of details the researcher is interested in, and the generalizing efforts of systematization. The system may be considered as satisfactory if the development of the field concerned and the detailed problems of the individual authors can be continuously incorporated and covered.

The increasingly extensive acceptance of activation analysis made the elaboration of such a documentation system most urgent. The approximately 5000 publications issued so far and the annual increment of 600 to 800 additional papers published, fully confirm the above statement. The situation is further complicated by the fact that these publications use several languages. A documentation system using a single language, preferably English, would render further assistance.

The present authors, having dealt with the documentation problems of the activation analysis for many years [1], set up a working group for the elaboration of a generally adaptable system. The literature research for this system is carried on by the Activation Analytical Documentation Service within one of the institutions of the Hungarian Academy of Sciences. For an up-to-date scientific literature and data filing method,

the punch card system was selected since this had been successfully used for similar purposes in a number of fields [2-7]. Our system was designed to satisfy above all the requirements of individual research workers and laboratories and, therefore, the employment of manual edge-punched cards was decided upon, since these necessitate only very simple means directly usable on site by any researcher. By having all the explications printed on each card, our punch cards make the use of both master cards and a separate code book or special code instructions superfluous.

II. The Activation Analysis Literature Card System (AALC)

The documentation of an activation analytical work makes use of an A-5 size double-row edge-punched card (Figures 1 and 2). Coding must meet two main requirements: (1) All the data necessary for the identification and retrieval of the publication must be indicated. (2) As many data on the contents of the publication should be presented as possible with, however, easy handling and review maintained, and adequate possibilities provided for expansion in conformity with the expected further development of the scientific field in question.

Figure 1.   Front side of the AALC card.

Figure 2. Back side of the AALC card.

A. Identification and Retrieval

For identification and retrieval purposes, the following items were considered sufficient:

1. Name of the author(s).
2. Title of the paper; place and year of publication; precise references.
3. Type and character of the publication.
4. True presentation of its abstract published in reference periodicals.

B. Contents

For the contents indication of the following notions was considered necessary:

1. The matrix (matrices) tested.
2. The element(s) determined.
3. Type of irradiation.
4. Some important features of the activation process (such as self-shielding, sensitivity, principles, radiochemical measurement methods, equipment, *etc.*).
5. Major fields using activation analysis.

The items listed above were coded onto the edge-punched card in the following manner:

C. DESIGN OF THE PUNCHED CARD

The name of authors, title of the work and precise references are printed onto the front side of the card. Of these data the first three letters of the surname of the first two authors are indicated by two triangles (Figures 2-a and 2-b) and one double row (Figure 2-c) codes, with deep punching for the first and shallow punching for the second author. Indication of the first and third letters has the entire alphabet available whereas for the second letter it is sufficient to use only the 5 vowels [5], with a single hole only to mark the rest of the letters. The 3 letters can be registered by 5 simultaneous needle holes. At the triangle codes, the name of the second author is shallow punched. Now the first authors having identical three first letters and representing a weight due to the coincidence of other deep punching will fall out.

For the indication of more than two authors a pair of classification holes was introduced (Figure 2-d) whereby papers of one, two, or more authors can be readily sorted. When information is wanted on the activity of a given author at world level, the needles are inserted to the external rows of the fields (Figures 2-a and 2-b). Thus only such papers will be omitted where the author sought for is the third or fourth, *etc.* Such cases amount, however, to only a small percentage of the papers searched for.

The last two digits of the year of publication are registered by two decimal codes (Figure 2-e) which make classification by years possible, with 2-4 needles used simultaneously. Papers are distinguished, furthermore, by publication types as well (periodical, report, conference proceeding, *etc.*), with shallow punched direct codes (Figure 2-f) suitable for combination with the previous punchings.

The content abstract of the publication is not presented on the card but there is sufficient space provided for on the back side where the user may record his own annotations. In order to facilitate quick searching for the content abstracts, the references of all the review periodicals (Nuclear Science Abstracts, Chemical Abstracts, Referativnyi Zhurnal, *etc.*) were registered.

The other code systems enable the content classification of the papers concerned. Two direct codes serve the selection of review articles (Figure 1-g) and bibliographies (Figure 1-h) by shallow punching. The field in question and the characteristic items are indicated by a double-row triangle code system (Figure 1-i) using the combination of shallow and deep punchings. This, in turn, can be combined again with the previous codes (Figures 1-g and 1-h).

The immense number of matrices had to be reduced. Mainly the periodic system was relied upon (triangle code, Figure 1-j) where the elements could be indicated by deep and their compounds by shallow

cutouts. When searching for compounds, shallow punchings discard the respective elements as well which can be separated, however, by further deep needle sorting.

Since triangle code permits the unequivocal indication of only a single information, publications involving the analysis of two or more elements or compounds are punched at the rare earth, semiconductors, noble metals, or other metals places.

In addition to the elements of the periodic system and their compounds, the materials tested most frequently are indicated by a double-row direct code (Figure 1-k). Separation of the titles in the external and internal row, respectively, is done by two consecutive needle holes again. Materials not to be indicated in either the Figure 1-j or the Figure 1-k field are shallow punched at the title "others". This code (Figure 1-k) makes possible the indication of several simultaneous matrices, if they are adjacent and not superimposed.

D. CODES

Figure 1-g, 1-k combined permit precise selection. When designing the code of the elements analyzed, it must be taken into account that the publications rarely deal with the determination of only one of the 90 elements. Based upon earlier bibliographies [1] the 54 elements determined most frequently were selected and arranged into a double row direct code system (Figure 1-1) in such a manner that the deep punching of the superimposed pairs were most frequent. This is in order to minimize the number of data lost in the external row. The superimposed elements can be separated by consecutive needle holes and the remainder is arranged into groups I-V (see Figure 1). Another hole indicates if the paper concerns the determination of more than ten elements (Figure 1-VI.).

A double row direct code makes possible the classification of the type of irradiation (Figure 2-m) where the superimposed types can be separated by two successive sortings.

E. FIELDS

Figure 1-i,j and k include vacant places where either the user may program in new data or it may be used by the designers for extension in conformity with the development of the subject matter.

F. EXAMPLES

The application of the AALC system will be illustrated by means of a simple and a complex example:

1. Let us search the publications dealing with Cu determination in aluminum. Two needles are introduced to the field marked j of the lower longitudinal edge of the card, into the second and third holes of the inside row, whereby the Al-metal matrix is fixed. In order to make the information thus obtained complete, the other metals are similarly tested, that is, holes 38 and 49 are punched. Now the inside hole of the upper longitudinal edge of each fall-out card is punched (Figure 1-1) and, thereby, every paper discussing the determination of Cu in aluminum metal will be discovered (the cards caught by the needle indicate the papers dealing with the above topic).

2. Papers published in 1967 and dealing with oxygen determination in steel by fast neutron irradiation are looked for. One needle is inserted to marks 4 and 2, each, in the first part of field Figure 1-e (outside row) because two figures must be added up, and similarly to the inside row of mark 7 in the second part. This completes the selection of the papers published in 1967. Then, on these cards, mark "fast n" of the outside row in the field Figure 2-m is punched whereby the publications involving neutron irradiation are separated. Inserting the needle to the inside "slow n" legend of the same field separates fast and slow neutrons as all the cards on the latter subject will fall out.

Inserting the needle now to holes 8 and 10 of the field Figure 1-j (inside row) on the cards thus selected will give the Fe matrices, and to the 0 legend of field Figure 1-1 will lead to the desired cards among those dropped.

III. Conclusions

The bibliography composed on the basis of the system described above is suitable to render information rapidly and accurately on the following problem types:

1. Activation analytical determination of certain element(s), in general (examples: copper, cadmium, iodine, *etc.*).

2. Activation analytical determination of certain element(s) in a given matrix (examples: copper in aluminum, cadmium in plants, *etc.*).

3. Activation analytical publications in a given field (examples: agriculture, medicine, *etc.*).

4. Selection of activation analytical publications by authors.

5. Selection of activation analytical publications by year.

6. Selection of activation analytical publications by paper type (examples: periodical, book, conference proceedings, *etc.*).

7. Selection of activation analytical processes by irradiating particles.

8. Selection of the publications on some major technical topics of activation analysis problems (examples: nuclear data, sensitivity, self-shielding, *etc.*).

The first approximately 5000 coded cards will be issued during 1969.

IV. References

[1] Bujdoso, E., and Toth, L., Activation Analysis, Bibliography I, Nuklearis Dok. Szolgalat **3**, 81 (1961). Bujdoso, E., Miskei, M., Ormos, G., Activation Analysis, Bibliography II, Atomtechn. Tajekoztato **6**, 87 (1963). Bujdoso, E., Miskei, M., and Ormos, G., Activation Analysis, Bibliography III, OAB Izotopalkalmazasi Szakbizottsag Kiadvanya, Budapest, 148 (1966).

[2] "Documentation in Molecular Spectroscopy" published in collaboration with Institut fur Spektrochemie und Angewandte Spektroskopie, Dortmund and the DMS Scientific Advisory Board, London. Verlag Chemie, Weinheim and Butterworth and Co., London.

[3] "Kunststoff Dokumentum", Dorec Verlags AG, Luzern.

[4] "Bibliography on Electron Microscopy on Keysort Cards", New York Society of Electron Microscopists, New York 21.

[5] Casey, R. S., Perry, J.W., Berry, M. M., and Kent, A., Punched Cards, Reinhold, New York, 1958.

[6] Scheele, M., Punch-Card Methods in Research and Documentation, Interscience, New York, 1961.

[7] Bourne, C. P., Methods of Information Handling, John Wiley, New York, 1963.

ISOTOPES INFORMATION CENTER

P. S. Baker

Oak Ridge National Laboratory
Oak Ridge, Tennessee

I. Introduction

The ORNL Isotopes Information Center was conceived by the Division of Isotopes Development of the U.S. Atomic Energy Commission in early 1962. In cooperation with the AEC's Division of Technical Information a program was funded (1) to establish and staff an information center and (2) to publish a technical progress review, subsequently entitled "Isotopes and Radiation Technology". Since its start, the Center has been growing slowly through addition of qualified staff and the acquiring, indexing, and storing of appropriate material; in March, 1966 it "became of age" and officially opened its doors for business.

Although the Isotopes Information Center is applications oriented, its scope includes much material related to the nuclear field in general, and we feel that in one way or another it offers potential service to almost everyone dealing with isotopes.

II. Scope

The broad scope of the Center includes anything that has to do with the production and use of isotopes. Specifically, the present areas are delineated somewhat more precisely, with strong emphasis on applications in industry and research, and current awareness of related applications in biology, medicine, agriculture, and education.

In general, reports dealing with strictly *routine* production methods or applications are not accessioned; however, incorporation of a new isotope in a routine use is included. The "rule of thumb" scope of the Center presupposes serving *any* needs in the isotopes field which are not satisfied elsewhere. Appendix I lists the general in-scope subject headings.

III. Operations Methodology

A. INPUT

Input to the Center to date has consisted entirely of complete copy, with most documents being stored as microfiche in order to reduce our

1138

storage problem without sacrificing utility. The Center itself subscribes to approximately 30 "fertile" journals, most of which are foreign, and scans, either directly or indirectly, about 650 more.

Preliminary scanning of publications identifies in-scope articles, which are then either copied or ordered. Each document is studied and indexed by a staff member under a system organized in such a fashion as to permit retrieval of *information*, as well as documents. During this process, appropriate keywords or categorizing terms are assigned to the document. These are chosen from a list that includes about 350 isotopes, ~100 elements, ~75 uses or methods, ~55 users, ~30 methods or preparation, and ~20 miscellaneous items such as the year of publication, and whether the entry is a patent, textbook, or bibliography (Appendix I). In all, there are nearly 700 terms in the thesaurus. Accession cards are prepared next, and on these are typed the keywords as well as the necessary descriptive cataloging material.

Since the operating success of any information center depends upon its ability to retrieve accessioned information, considerable thought has gone into this problem. The Termatrex system, a random-access, visual system based on a plastic card "memory", is used to retrieve documents. In this system, each 9 1/2 in. × 11 in. card is assigned a specific indexing term, for example, "Chemistry, Analytical", "Phosphorus-32", or "Tracer". Ten thousand "address" holes can be punched in each card in a precise 100 × 100 hole pattern. If there is any information in a document which can be identified by a keyword, the document accession number is punched into the appropriate card. A punch in a specific location indicates that there is information on that subject in the document having that accession number. If several cards are superimposed and put on a light box, a beam of light will come through at the document numbers that contain information on all the subjects chosen. In our operations a complete card set includes ~700 cards and will permit up to 10 thousand accessions. Several sets can be used, however.

For example, an article entitled "Determination of Oxygen in Steel by Activation Analysis" would show the important descriptors, "Oxygen", "Industry, Primary Metal", "Activation Analysis", and "Fluorine-19" (since ^{19}F was the activated radioproduct in this article). The individual cards with these terms are "pulled" from the file, stacked together, and the address of the new article is punched in the cards. The cards are now returned to the file rack. At a later date, retrieval involves assembling cards representing the key terms in a query on a reader. Lights appear at those addresses which are "hits" and which show relevant articles − *i.e.*, a bibliography.

B. OUTPUT

Output from the Center includes several general categories:

1.   State-of-the-art reviews of various areas of isotope applications. Many of these summary articles are included in the previously mentioned quarterly review, "Isotopes and Radiation Technology".

2.   Writing *critical evaluations* of the state of the art in various areas, with particular reference to the worldwide situation and including suggested programs for long-range research and development (to be sponsored, for example, by the AEC). The emphasis here is on the word "critical".

3.   Making replies to written, telephone, and personal requests for information. These may emphasize bibliographies and usually include appropriate reprints from "Isotopes and Radiation Technology", when available.

4.   Publication of revised editions of "Special Sources of Information on Isotopes", "Radioisotopes in World Industry", and "Isotope Developments" fliers; compiling and publishing data related to particular programs.

5.   Occasional writing of special brochures; for example, "Radioisotopes in Industry", one of the AEC "Understanding the Atom" series. The Center has also recently completed the translation of a Russian book on food irradiation.

6.   Distribution of information on isotope uses in conjunction with the USAEC Neutron Activation Exhibit, which is usually manned by IIC personnel.

APPENDIX I

Subject Headings

I. PREPARATION OF ISOTOPES
    A. Preparation of Radioisotopes
        1. Activation
        2. Fission products
        3. Chemical or physical separations of radioisotopes
    B. Separation of Stable Isotopes
        1. Electromagnetic process and equipment
        2. Thermal diffusion
        3. Other stable isotope separation methods
    C. Sources (includes information on preparation of sources and
        other information on sources)

1. Alpha
2. Beta
3. Gamma (including characteristic x-ray sources and bremsstrahlung sources)
4. Neutron (includes generator and isotope sources)

D. Target Preparation
   1. Radioactive
   2. Stable

E. Irradiator Design

F. Transmutation Doping (includes conversion of one stable element to another by nuclear reactor in order to change properties of the original element)

II. ISOTOPE USERS

A. Agriculture

B. Education (includes information intended mainly for teaching, especially student and lecture experiments)

C. Forensic Investigations (investigation of crime)

D. Industry

   1. Building industry
   2. Chemical industries (other than drugs, plastics, petro-chemicals, and rubber industries)
   3. Electric and gas industries
   4. Electronics industry
   5. Fabricated metal industry
   6. Food industry
   7. Machine industry
   8. Mining industry (does not include petroleum and natural gas but does include prospecting)
   9. Paper industry
   10. Petroleum and natural gas industries
   11. Petroleum refining and related industries
   12. Pharmaceuticals industry
   13. Plastics industry
   14. Primary metal industry
   15. Rubber industry
   16. Stone, clay, and glass industries
   17. Textile industry
   18. Tobacco industry
   19. Transportation industry

E. Life Science

   1. Anatomy
   2. Biochemistry
   3. Biophysics
   4. Botany
   5. Cytology
   6. Ecology
   7. Entomology
   8. Genetics
   9. Hematology
   10. Microbiology
   11. Nucleic acid studies
   12. Nutrition and metabolism
   13. Pathology
   14. Pharmacology
   15. Photosynthesis
   16. Physiology
   17. Radiation biology
   18. Zoology

F. Medicine (includes medical diagnosis, therapy, and research: but should not include animal research unless it is specifically directed to medical goals)

G. Physical Science

    1. Analytical chemistry
    2. Geophysics
    3. Hydrology
    4. Inorganic chemistry

    5. Metallurgy
    6. Organic chemistry
    7. Physical chemistry
    8. Physics

H. Space

III. ISOTOPE USES

A. Effect of Materials on Radiation

    1. Measurement and control systems

        a. Density gages
        b. Level gages
        c. Neutron gages
        d. Thickness gages

    2. Radiation absorptiometry
    3. Radiography (industrial or medical)
    4. Secondary radiation effects (includes Compton effect or scattering, and bremsstrahlung)

B. Effect of Radiation on Materials

    1. Catalysis
    2. Fiber modification
    3. Fission-energy-induced reactions
    4. Food preservation (includes pasteurization and sterilization)
    5. Growth acceleration
    6. Growth inhibition
    7. Insect control
    8. Luminescence

    9. Mossbauer effect
    10. Polymer modification
    11. Polymerization
    12. Radiolysis
    13. Seed mutation
    14. Static elimination
    15. Sterilization of pharmaceuticals and medical equipment
    16. Synthesis
    17. Therapy
    18. X-ray fluorescence

C. Heat Sources

    1. Diagnostics
    2. Flow measurement
    3. Friction and wear
    4. Isotope dilution
    5. Labeled reagent

    6. Material tracking (labeled tracers)
    7. Preparation of tagged materials
    8. Radiometric analysis
    9. Reaction mechanism
    10. Separation

IV. ISOTOPE METHODS

A. Activation Analysis
B. Chromatography
C. Dating
D. Electrolysis
E. Hot Laboratories
F. Ion Exchange

G. Isotope Generators (milkers)
H. Precipitation
I. Recoil (Szilard-Chalmers reaction)
J. Safety
K. Solvent Extraction
L. Volatilization

V. ISOTOPE PROPERTIES

A. Cross Section and Yields
B. Energy Levels
C. Isotope Abundance

D. Moments and Spins
E. Nuclear Reactions
F. Radioactive Decay

VI. ISOTOPE DETECTION AND DETERMINATION

A. Autoradiography
B. Calorimetry
C. Counting
D. Dosimetry

E. Isotope Scanning
F. Isotopic Analysis
G. Radiochemistry
H. Spectrometry (α, β, or γ)

CATALOGUE OF GAMMA RAYS EMITTED BY RADIONUCLIDES[1]

M. A. Wakat

Savannah River Laboratory
E. I. du Pont de Nemours and Co.
Aiken, South Carolina 29801

I. Introduction

Identification of the observed lines in a gamma spectrum has always been a time consuming process. This task has become more difficult with the advent of semiconductor detectors which can produce a single gamma-ray spectrum with greater than one hundred resolved gamma lines.

Not only can lithium drifted germanium Ge(Li) detectors resolve large numbers of gamma photopeaks in a spectrum, but the energies of these photopeaks can be measured to within ±1 keV routinely and to within ±0.1 keV with careful analysis. This has produced a wealth of new information on the exact energies of gamma radiations. To utilize the information contained in a gamma spectrum, some convenient way is needed to quickly compare the measured energies with the current values for known gamma rays. A number of listings of gamma rays ranked by energy [1-7] have been used extensively. However, these listings are all based on data obtained prior to extensive publication of Ge(Li) energy assignments. A catalogue that will include all measured gamma rays emitted by radioactive nuclei and the new energy information provided by Ge(Li) spectroscopy is being compiled at the Savannah River Laboratory, and will be issued before the end of 1968. This compilation can be useful to those laboratories developing computer programs for data reduction of Ge(Li) spectra [8-10] by providing needed library information for comparisons.

II. Presentation of the Data

The content and format of this tabulation have been chosen to give as much information as possible which would be of value in analytical applications. The format is illustrated in Figure 1.

ENERGY (MEV)		NUCLIDE	ABUNDANCE	HALF LIFE	PRODUCTION MODE	ASSOCIATED GAMMA RADIATIONS				
						ENERGY 1	ABUNDANCE 1	*	ENERGY 2	ABUNDANCE 2
.284		CU 61	.12	3.32H	CP	.655	.11	*	1.19	.05
.296		GA 67	.22	77.9 H	CP	.093	.40	*	.184	.24
.302		BA 133	.14	7.2 Y	NG,PN	.356	.69	*	.107	.40
.343		CU 59	.05	81.5 S	CP	1.305	.11	*	.872	.09
.356		BA 133	.69	7.2 Y	NG,PN	.107	.40	*	.081	.30
.368		NI 65	.045	2.56H	NG	1.481	.25	*	1.115	.16
.371		CU 61	.03	3.32H	CP	.284	.12	*	.655	.11
.373		BA 131	.13	12.0 D	NG	.496	.48	*	.124	.28
.382		BA 133	.08	7.2 Y	NG,PN	.356	.69	*	.107	.40
.386	D	BA 126	.38	97 M	CP	.23	1.00	*	.70	.33
.398		GA 67	.07	77.9 H	CP	.093	.40	*	.184	.24
.39		ZN 71	.013	13.8 H	NG	.510	.13	*	.92	.03
.41		CO 54	1.00	1.5 M	PN	1.14	1.00	*	1.41	1.00
.439		ZN 69M	.95	13.8 H	NG	.0086	*	*	*	*
.441	D	BA 128	.27	2.4 D	CP	.134	U	*	.278	U
.463		CU 59	.05	81.5 S	CP	1.305	.11	*	.872	.09
.472		NI 56	.35	6. D	CP	.163	.99	*	.812	.85
.48		ZN 61	.11	1.48M	CP	1.64	.06	*	.98	.03
.490		CO 55	.12	18.2 H	CP	.930	.80	*	1.41	.13
.496		BA 131	.48	12.0 D	NG	.124	.28	*	.216	.19

Figure 1. Format of the Gamma Ray Catalogue.

The sources of nuclear data used in the compilation are the "Table of Isotopes" 6th Edition by Lederer, Hollander, and Perlman [11] and the volumes of Nuclear Data published from February 1966 to March 1968 [12]. The compilation includes all gamma transitions that have been reported and included in the nuclide decay schemes of either of these two data sources.

The energies of the gamma rays are listed to 0.1 keV if reported to this level of precision. The number of significant figures listed is selected to indicate the precision of the reported energy. For this reason the energies are listed in MeV.

To facilitate identification of a nuclide which is sustained by a parent nuclide with a half life greater than twice that of its daughter, all gamma radiations from these daughter nuclides are listed with both the daughter and parent nuclides. When listed under a parent nuclide, these radiations are indicated by the symbol D following the energy listing. Because many parent-daughter relationships in the three natural radioactive decay chains are complex, shorter half-life daughter radiations are not included for nuclides with atomic numbers greater than 83.

If x-rays are prominent in the photon spectrum of a nuclide, the $K_{\alpha 1}$ energy is included in the gamma-ray listing of the nuclide, and will be identified by the symbol X following the energy listing. If K x-rays are not emitted because of low energy of the gamma transition, the $L_{\alpha 1}$ x-ray energy is listed. Abundances are not included for these x-rays because their principal purpose is to remind the user of the possibilities of x-rays in a region when searching for the identification of a low energy gamma ray.

Annihilation radiation from positron emitters is listed for pure positron emitters only because this radiation has limited value for identification. The 511 keV annihilation radiation is listed under associated gamma radiations if there are no other gamma radiations which would be more

distinctive of the nuclide. Whenever an annihilation radiation is listed, it is indicated by the sumbol A following the 511 keV energy.

Abundances are listed as photons per disintegration where such information is available. Abundances followed by an asterisk indicate relative intensity values. Whenever a gamma ray has been reported, but an intensity value has not been assigned, it is indicated by "S" for a strong but quantitatively unknown transition, by "W" for a weak but quantitatively unknown transition, or by "U" when no information is available as to intensity.

In order to assist in the identification when some history of the unknown gamma emitting sample is known, a listing of up to three possible modes of production for each nuclide is given. The modes and their abbreviations are given in Table 1.

Table 1. Identification of possible methods of production of nuclides.

NG	=	(n, γ) reactions	AN	=	(α, n) reaction
NO	=	naturally occurring	AP	=	(α, p) reaction
FP	=	fission product	N2	=	$(n, 2n)$ or (γ, n) reactions
BD	=	beta decay	NP	=	(n, p) reaction
AD	=	alpha decay	MN	=	multiple neutron capture
PN	=	(p, n) reaction	CP	=	other charged particle reactions

To aid in the identification, up to two other gamma rays are listed under associated gamma rays that would also be observed in the spectrum of the nuclide. These are either the most intense gammas in the spectrum or those abundant transitions with the best known energies. When there are no other gamma rays associated with the nuclide, a 511 keV annihilation radiation or an x-ray may be listed.

Subtables of the gamma rays according to the mode of production and half life ranges have also been included for those instances in which information is available. The subtables are given in Table 2.

III. Preparation of the Tabulation

The information necessary for each gamma ray is stored on punched cards with one card for each gamma ray. The cards are kept together under each nuclide and are kept in order of mass rather than energy. This facilitates updating for each nuclide or mass chain as new nuclear data become available.

Table 2. Subtables of the gamma ray catalogue.

A. According to Half–Life   B. According to Mode of Production

    1. less than one hour   1. (n, γ) reactions

    2. one hour to one day   2. fission products

    3. one day to ten days   3. naturally occurring

    4. greater than ten days

The mechanics of the tabulation using the IBM 360 computer for a list processing procedure are simple enough to allow frequent updating. Thus any group wishing to maintain a current catalogue of gamma ray information could use this compilation as a foundation for such a program. The gamma rays may be easily sorted for any special subtable which might be useful for other specific applications.

IV. References

[1] Crouthamel, C. E., Applied Gamma Ray Spectrometry, Pergamon Press, New York, 1960.

[2] Hawkings, R. C., Edwards, W. J., and McLeod, E. M., Tables of Gamma Rays from the Decay of Radionuclides, CRDC-1007, (1961).

[3] Heath, R. L., Scintillation Spectrometry-Gamma Ray Spectrum Catalogue, IDO-16880-1 (1964).

[4] Mateosian, E. der, and McKeown, M., Table of Gamma-Rays Emitted by Radioactive Nuclei Arranged in Order of Increasing Energy, BNL-605 (1960).

[5] Rackow, A., Tabelle zur Identifizierung Unbekannter Gammaspektren. Karl Thiemig KG, Munich (1962).

[6] Rousseau, A., Study of Fission Product Gamma Spectra in the Band 0-500 keV, CEA-1202 (1959).

[7] Smith, G. W., and Farmelo, D. R., Nucleonics **16**, No. 2, 80 (1958).

[8] Barnes, V., IEEE Trans. Nucl. Sci. **15**, No. 2, 437 (1968).

[9] Gunnink, R., Levy, H. B., and Niday, J. B., Identification and Determination of Gamma Emitters by Computer Analysis of Ge(Li) Spectra, UCID-15140 (1967).

[10] Helmer, R. G., Heath, R. L., Schmittroth, L. A., Jayne, G. A., and Wagner, L. M., Nucl. Instrum. Methods **47**, 305 (1967).

[11] Lederer, C. M., Hollander, J. M., and Perlman, I., Table of Isotopes, 6th ed., John Wiley, New York, 1967.

[12] Nuclear Data, Section B, **1**, No. 1 to **2**, No. 5 (February 1966 to March 1968).

COMPUTERIZED IDENTIFICATION OF REACTOR-PRODUCED ISOTOPES

John A. Dooley and James H. Gorrell

Air Force Flight Dynamics Laboratory
Wright-Patterson Air Force Base, Ohio 45433

James M. Thompson

Deputy for Engineering Digital Computation Division
Wright-Patterson Air Force Base, Ohio 45433

Edward Hoffman

University of Dayton
Dayton, Ohio 45409

I. Introduction

In the course of attempting to analyze unknown samples using reactor activation analysis at the AFIT Nuclear Engineering Center, the problem frequently arose as to what major and contaminant constituents were in the samples. It was necessary to answer this question before quantitative determinations could be made.

To minimize the amount of work in this type of qualitative identification, a Fortran-IV computational system was developed which uses the photopeak energies found in an unknown spectrum and logically determines which isotopes are present. The photopeak energies from a spectrum are compared to an energy-isotope list. There is an initial tabulation of all isotopes which could have emitted each gamma ray present in the sample spectrum. Those isotopes which emit gamma rays not present in the spectrum are rejected. Output includes several lists of varying certainty of identification, including annihilation, sum peaks and escape peaks. Accuracy and speed of analysis to a considerable extent are controlled by the detection system resolution and compatible energy calibration. Thus, there is considerable advantage in using a high resolution detector system to obtain the spectrum. System operation and results are illustrated using a composite spectrum of five isotopes.

1148

II. ILIP

A. ANALYSIS SYSTEM

The ILIP Analysis System comprises the card library, two tape-generating programs and the Isotope Library Identification Program (ILIP). Figure 1 depicts the major blocks of the analysis system. At the top is seen the block for the isotope library on cards. For each isotope there is a header card with atomic name, number, weight, half life, production reaction and type of decay. Following the header there is one card for each gamma ray with its intensity ratio and energy. These cards are read as input to the program Library Isotope List (LIL). As desired a duplicate deck can be punched, an isotope list with a special format printed, and a mag tape library created. Limited error checking and totalling is performed. At present, our card library contains 1200 gamma rays for 200 isotopes.
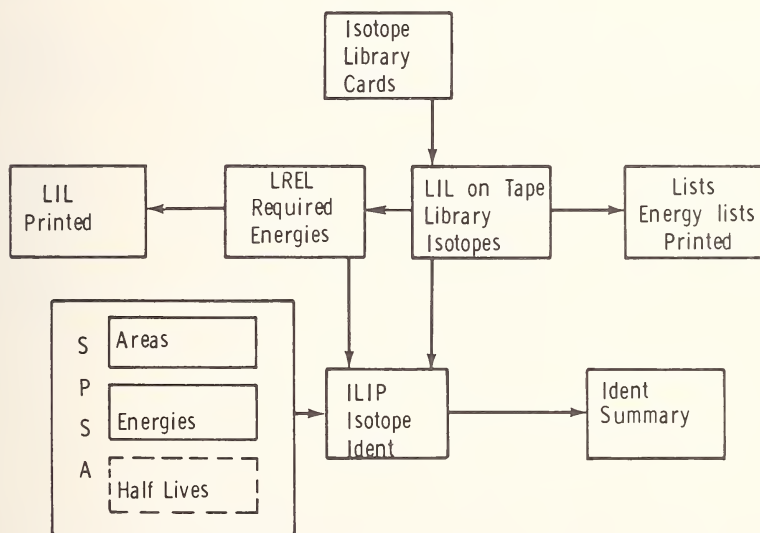
Figure 1. ILIP analysis system.

The output tape from LIL is used as input to the program Library Required Energy List (LREL). Similar output options are available, including an energy-isotope tape. Three lists are generated with the energies in ascending order: nonrequired energies, required, and both. All three lists can be printed but only the required-energy list is put on the LREL output tape. If a gamma ray has a relative intensity of less than 10%, it is considered nonrequired for identification. Any such gamma found in a spectrum is processed, nevertheless.

The LIL and LREL tapes and a list of spectrum energies constitute the input to ILIP. The spectral energies can be obtained manually or by some computerized method such as the Spectral Peak Search and Analysis Program (SPSA) [1-3]. The dimensions in ILIP are consistent with a maximum of 100 peaks per spectrum. Several control parameters are entered, including a comparison tolerance in keV. Two energies whose difference is not greater than the tolerance are considered to be matched.

B. Output Lists

In the course of its logic, ILIP generates nine output lists following a table of contents and a list of the input energies. Each output list has a sample identification list number, short title, list symbol, description and headings for the output. The first three items for each of the nine lists are shown in Table 1 as they appear on the computer run.

Table 1. Output lists.

OUTPUT LIST 1.   PRELIMINARY IDENTIFICATION LIST (PIL).
OUTPUT LIST 2.   UNIDENTIFIED ENERGY LIST (UEL).
OUTPUT LIST 3.   ACCEPTED ISOTOPE LIST (AIL).
OUTPUT LIST 4.   ISOTOPE INCLUSION LIST (IIL).
OUTPUT LIST 5.   TENTATIVE ACCEPTED ISOTOPE LIST (TAIL).
OUTPUT LIST 6.   REJECTED ISOTOPE LIST (RIL).
OUTPUT LIST 7   UNIDENTIFIED ENERGY LIST 1 (UEL 1).
OUTPUT LIST 8.   NON–REQUIRED ESCAPE SUM IDENTIFICATION
                   LIST (NESIL).
OUTPUT LIST 9.   UNIDENTIFIED ENERGY LIST 2 (UEL 2).

In the computer output, List 1 prints the results of a comparison of the input energies with all required energies in the library. Lists 2, 7 and 9 print energies which are not identified for a given state of the analysis, List 9 being a terminal list of energies which have defied complete identification. List 3 gives fully identified isotopes, List 5 partially identified isotopes, and List 6 possible isotopes which were logically eliminated. List 8 tabulates energy identification in terms of fully identified isotopes. Energies which represent nonrequired peaks, single and double escape peaks or sum peaks are printed there. List 4 is a convenience feature which summarizes energy identification redundancy by listing accepted isotopes which include the same observed energies.

An energy within tolerance of 511 keV is given special handling to minimize confusion between annihilations and gamma-ray transitions. Thus, all annihilation gamma rays are treated as nonrequired and appear

in List 8 if identified. If any energies remain unidentified in List 9, the program starts again from the beginning with the tolerance doubled.

C. Analysis of a Composite Sample

To test the analysis features of ILIP, a composite sample was constructed using NBS standard isotopes of cerium-139, cesium-137, manganese-54, zinc-65 and sodium-22. The spectrum energies determined by SPSA were used as input to ILIP: 166.08, 510.77, 661.57, 834.32, 1114.98 and 1273.50 keV. The tolerance for identification was set at 2.5 keV.

List 1 printed 18 isotopes as candidates for identification. List 2 showed that no energies were left without at least tentative identification. The results of List 3, as taken from the computer run, are shown in Table 2.

Table 2. Isotope identification.

OUTPUT LIST 3.   ACCEPTED ISOTOPE LIST (AIL).   A POSITIVE IDENTIFICATION HAS BEEN MADE.   ALL REQUIRED ENERGIES FOR THE ISOTOPE MATCH AN OBSERVED ENERGY.

ISOTOPE	KEV REQUIRED	KEV OBSERVED	DELTA KEV
XE–131M	163.9	166.1	−2.2
BA–139	166.0	166.1	−0.1
CE–139	166.0	166.1	−0.1
C S–137	661.6	661.6	0.0
BA–137M	661.6	661.6	0.0
MN–054	835.0	834.3	0.7
ZN–065	1114.0	1115.0	−1.0
NA–022	1276.0	1273.5	2.5

List 4 reminds us that xenon-131m, barium-139 and cerium-139 are equivalent analysis results. For these, the experimenter can rule out the 11.8-day xenon-131m gas and the 83-minute barium-139. Similarly, the equivalence of cesium-137 and barium-137m can be resolved; the barium-137m level is populated by cesium-137 decay. This version of ILIP does not use the half life information which is available on the LIL tape. Eventually, it is planned to build half life logic into ILIP.

List 5 contained four isotopes which had transition energies of about 511 keV but other required energies were not present. List 6 printed six isotopes which were definitely eliminated. List 7 indicated that an energy of around 511 keV had still not been satisfactorily identified. List 8 showed that the 511 keV gamma ray was due to zinc-65 and sodium-22,

thus completing the identification. This fact was confirmed in List 9 which stated that there were no unidentified energies.

If List 9 had not been empty, the program would have doubled the tolerance to 5.0 keV and started over with the analysis. In this case, it would have found a preliminary match with 29 isotopes instead of 18 isotopes. The accepted isotope list would have contained 11 entries instead of the eight found at 2.5 keV tolerance.

III. Summary and Discussion

A computerized, qualitative analysis system has been constructed. All subroutines are available in Fortran-IV coding and should run on any machine which uses this language.

The present tape library includes primarily reactor produced isotopes, but the method can be extended for use with charged particles and high energy neutrons. The library cards are coded for the type of reaction which produces the isotope. The computer times need not be excessive since only the appropriate library need be put on tape. Alternatively, with a composite library, the program can be set to utilize only the appropriately coded isotopes.

Operation of the system, including updating the library tapes, is simple and the runs are fast. Each single-tolerance run on a six-energy spectrum at 2.5 keV tolerance takes about 30 seconds on an IBM-7094. A 26 energy spectrum with 10 keV tolerance takes about five minutes to run. No information gained by the program is lost to the user. The results of each major decision are printed.

ILIP can best do its job, which is to minimize the analysis effort of the experimenter, when a high-resolution detection system is used. Present day Ge(Li) detectors with 4096 channel analyzers have resolutions on the order of 3 keV for the cesium-137 photopeak. With only reasonable attention, ILIP tolerances on the order of 3 to 5 keV are possible. With careful energy calibrations and small adjustments to the isotope library energies, tolerances from 1 to 3 keV, or better, can be used in ILIP.

IV. Acknowledgments

V. References

[1] Dooley, J. A., Young, M., Gorrell, J. H., Polishuk, P., Singhal, N., and Thompson, J. M., "Computer Program Development for Processing of Activation Analysis Data", Developments in Appl. Spectry. (in press, 1968).

[2] Dooley, J. A., Young, M., Gorrell, J. H., Polishuk, P., Singhal, N., and Thompson, J. M., "New Developments at W-PAFB in Computerized Spectral Analysis and Isotope Identification" (Abstract published in Trans. Am. Nucl. Soc. **11**, 73 (1968).

[3] Dooley, J. A., Gorrell, J. H., Polishuk, P., and Young, M., "Computerized Quantitative Analysis of High-Resolution Spectra", (See this volume, p. 1090).

COMPUTATION OF EXPERIMENTAL RESULTS IN ACTIVATION ANALYSIS

Plenary Lecture by HERBERT P. YULE

Activation Analysis Research Laboratory
Texas A&M University
College Station, Texas 77843

I. Introduction

The introduction sets the frame of reference for discussion in the remainder of the lecture. It is necessary to set forth some preliminary considerations which have strong implications regarding the method by which results are computed and the degree of effort required to produce an accurate result. Subsequently, it is germane to review, briefly, experimental procedures which might be used, for the result-computation method is a strong function of the procedure which led to and produced the counting data. A number of ways in which counting data are treated are then described. Preliminary remarks on the processing of large numbers of samples including ramifications of data processing will then be made.

Section II traces the early history of activation analysis, showing the development of computation methods as new instrumentation has emerged. Section II is not only a review, but describes in considerable detail the computation methods appearing prior to 1962.

Section III contains detailed descriptions of today's most prevalent computation methods. For each method, we have tried to indicate how various researchers have improved the accuracy of the computed results. We have, therefore, relied on an evolutionary approach.

Section IV presents the present author's critiques of the methods discussed in Section III, including comments on accuracy, errors, and outright failures of an individual method.

Section V is devoted to crystal ball gazing.

A. PRELIMINARY CONSIDERATIONS

1. *Routine and Nonroutine Activation Analysis*

For the purposes of the data computation, routine activation analysis involves the analysis of a large number of samples of similar composition.

1155

Analysis with 14 MeV neutrons, of oxygen in metals may be routine, if the metal does not activate too much and there is enough oxygen to be measured readily. In this case, the experimenter might need only the count rate of the 6.1 MeV gamma rays emitted by ^{16}N and a neutron flux monitor. Depending on experimental procedure, the result could be given by the product of the ratio of the count rate of the unknown to that of a standard and a flux normalizing factor. The analysis would be routine — the result computation is easy and straightforward, and requires little or no subjective judgment. Errors in the computation of the results are primarily due to human errors in the mechanics of the calculation. The most significant feature of routine data computations is that they need very little judgment in the result-computation process.

By nonroutine activation analysis is meant the analysis of samples having composition about which little is known. For example, the analyst may be required to analyze a commercial product about which he can learn little from the manufacturer. If the analysis is done with reactor neutrons. Those radioisotopes making observable contributions to the data must be identified before quantitation is attempted. This identification process may be trivial, or it may be very difficult. Thus, nonroutine activation analysis may require a great deal of judgment in interpretation of the data, and the interpretation may be quite time consuming.

In routine activation analysis, then, result-computation is a simple, straightforward matter. On the other hand, result-computation in nonroutine analysis frequently requires a great deal of study.

2. The Activation Method and its Relation to Result-Computation

The activation method will clearly influence the degree of complexity of result-computation. If samples are irradiated with a relatively low intensity source, such as neutrons from a radioactivity source, the analysis of the data will be quite simple. The experimenter will only observe radiations from those elements having large macroscopic cross sections. He will observe, therefore, major constituents and/or those having sizable activation cross sections. The number of elements in this category is not large, and thus identification of radioactivity isotopes observed is relatively simple. Quantitation with such data is typically simple also. With reactor neutron activation, however, many radioisotopes may be formed during activation. Interpretation of these data can be very difficult. Over 100 radioactive species are formed from the stable elements in the periodic chart, and positive identification of species contributing to an observed spectrum may be very complex even with high resolution gamma-ray spectrometers. Interferences among

contributors which have been identified can present problems in obtaining accurate and precise quantitative results.

Charged particle activation analysis typically generates data on the decay of one more positron emitters which are usually identified from the decay curve. Subsequently, the decay is resolved to obtain quantitative results.

In addition to the activation method, other important considerations are the detection systems, sample transfer, sample size, irradiation and decay times, and radiochemistry. All these factors influence the capability of the experiment to yield the desired results.

3. Analytical Goals and Data Interpretation

Analysis of experimental data must conform to the goals of a particular analysis. For example, if one is analyzing an ore, the desired information may be the economic feasibility of mining a vein. A very accurate result may be important only if the metal content of the ore sought indicates borderline economic feasibility; otherwise, the results indicate feasible or unfeasible mining prospects.

In other experiments, the content of an element in a particular matrix may be important at any level. Even if no signal from a given element is observed, the analyst may wish to compute an upper limit for the elemental content.

Some analyses are of an exploratory nature so that any information of either qualitative or quantitative nature is useful.

Thus, the goals of an experiment have an important influence on the result-computation. Knowledge that a certain element (or group of elements) is present or absent may suffice, or, to the contrary, very accurate measurement of contents may be required.

B. Experimental Procedure

1. Sample Preparation

The first step in preparing for an analysis is sample preparation. The sample is placed in some sort of device to hold it in place during irradiation. In reactor neutron activation analysis, the sample is often encapsulated in a small polyethylene vial, and it is not unusual to place this vial inside of another vial to prevent contamination of the sample container. Sample weight is often measured during the encapsulation procedure. For other types of activation, more elaborate sample preparation techniques may be necessary.

2.   Irradiation

The next step is the irradiation with reactor neutrons, 14 MeV neutrons, charged particles, etc. Subsequently, the sample may be counted, it may be transferred to a fresh, unirradiated container and then counted, or it may be subjected to radiochemical purification prior to counting.

3.   Accumulation of Counting Data

Radiations emitted during radioactive decay are detected with counting systems sensitive to beta particles, gamma rays, or both. The complexity of such systems ranges from the relatively simple beta detector coupled to a scaler to elaborate gamma-ray spectrometers with anti-Compton mantles or special coincidence counting arrangements. A large fraction of activation analysis data collection is performed with NaI(Tl) or Ge(Li) detectors coupled to multichannel analyzers. Data accumulated with this type of system will be the major concern of the present chapter. The primary emphasis here will be on the analysis of pulse-height spectra, but there will also be some discussion about the analysis of decay curves such as are obtained when the analyzer is used in the multiscaler mode. Analysis of data taken with relatively complex experimental arrangements such as coincidence experiments, multidimensional experiments, time-of-flight analyses, and other rather unusual systems is considered outside the scope of this lecture.

4.   Analysis of Counting Data

The analysis of data is a two step process, the qualitative analysis of the data followed by the quantitative analysis of the data. In the first step, contributors to the observed data are identified, and in the second step the quantitative results are computed. Qualitative analysis often consists, with nonroutine analyses, in identifying those radioactive isotopes making observable contributions to the experimental data. In routine analyses, however, the analyst knows what the contributors are from previous experience with similar samples, because the qualitative analysis was performed before the analysis became routine. Quantitative analysis may then be completed by decay curve analysis, or analysis of the pulse-height spectrum.

The qualitative and quantitative analysis of activation analysis data are the subject of the remainder of this lecture. As mentioned above, only NaI(Tl) and Ge(Li) gamma-ray spectrometer data are discussed. Thus, positron emitters are not excluded from discussion because of the annihilation quanta they generate. Activation analysis with beta particle detectors is largely excluded because of the lack of specificity of energy of

emitted particles, and hence analysis with isotopes emitting only the beta particles is not discussed in any detail. Analysis featuring alpha particle detection is not included because it is not generally applicable to samples of finite thickness.

C.   General Considerations in the Counting and Interpretation of Data

1.   The Simplest Case

In a simplified way, the activation analysis equation may be stated as

$$A \sim w \qquad (1)$$

where w is the weight of a specific element, X, in a sample and A is the observed, measured, interference-free signal proportional to the radioactivity generated by irradiation of the sample. For the purposes of the present discussion, such important factors as decay corrections, saturation factors, and others, are omitted in order to emphasize the difficult part of the computation. Equation (1) says that if we can measure A directly and determine the proportionality constant implied in the equation, then we can compute the amount w of element X present in the sample. The proportionality constant may be determined by irradiating a comparator standard of known w, or it may be assumed to have a known value determined in previously performed experiments. Other considerations such as flux variation, counting geometry variation, decay factors, and various sources of error may have to be considered but if the analysis can be arranged so that Equation (1) holds, it is a rather simple analysis. Very often, however, A cannot be obtained without some computational manipulation, and the more general case is that in which several radioisotopes are observed simultaneously. It must be emphasized that A is a measured quantity which is obtained directly from the counting system without any computation.

2.   The More Complex Case – Several Observable Isotopes

If one could always arrange his experiment so that his data could be analyzed using Equation (1), there would be little to discuss in the interpretation of activation analysis data. In many analyses, however, one obtains several radioactivities which are observed simultaneously:

$$A_{\mathrm{obs}} = \sum_i A_i \qquad (2)$$

In Equation (2), there are i component radioactivities observed by the detection system. The observed quantity is A_{obs}, the sum of the individual components. If one can somehow compute an A_i free of contributions from the other components, one can then obtain the desired weight of the

ith component, W_i, as indicated in the preceding section. This is the essence of the activation analysis computation, *i.e.* the retrieval of an A_i, having no appreciable contributions from other radioisotopes, or at least an A_i for which the contributions can be estimated at a tolerable level. Methods of computing each A_i are reviewed below in the introduction and discussed at length in the body of the lecture.

3.   A Basic Problem in Resolving Complex Cases

In general, the computation of A_i is complicated by two types of interference in varying degrees.

One type of interference may be called the gamma-ray interference. When using gamma-ray pulse height analysis, the analyst may find that he is unable to use the peak area method to obtain A_i because of an interference from an extraneous gamma ray appearing in the same region of the spectrum. He will then try to remove the interference by resorting to spectrum stripping, least squares analysis, or some other, possibly improvised, method. If none of these succeeds, perhaps because his result computation is essentially the subtraction of two large numbers with an error much larger than the result itself, he will have to try a different activation method, different analytical chemical technique, resort to radiochemistry, or abandon the analysis.

In the preceding example, the desired gamma-ray peak was more-or-less observable in spite of the interference. In another type of gamma-ray interference, the interfering gamma rays are sufficiently intense that they or their Compton continua completely obscure the gamma radiations from the isotope of interest. For this type of interference, no meaningful result is calculable except possibly an upper limit. To get an answer more definitive than an upper limit, a change of experimental technique is also indicated.

The second type of interference may be called "nuclear reaction interference". One way it is manifested is in the production of the same radioisotope from more than one element. Equation (1) could be written

$$A_i \sim N_i \qquad\qquad (3)$$

where N_i is the number of atoms of the stable element in the sample — that is, the radioactivity of type i is proportional to the amount, or number of atoms, of an element present in the sample. Clearly, if the radioactivity, A_i, is produced from more than one element, a computed value of A_i will probably not yield an accurate computed amount of the element in the sample. As an example, consider the measurement of the sodium content of very pure aluminum foil by activation analysis with reactor neutrons. The ^{24}Na produced by thermal neutron capture in

sodium would have an interference from ^{24}Na produced by the fast neutron reaction ^{27}Al(n,α)^{24}Na. The yield of the capture reaction is several orders of magnitude larger than that of the fast reaction. In pure aluminum, the amount of sodium present may be orders of magnitude less than the amount of aluminum in the sample, and the ^{24}Na produced from the aluminum may be a significant fraction of that produced from the sodium. The analyst must determine whether or not the interference is serious before an accurate sodium content may be quoted. The severity of the interference could be computed based upon known yields, or it may be measured by irradiation of the same sample again, after the ^{24}Na produced in the first irradiation has largely decayed away. In the second irradiation, a thermal neutron shield such as a cadmium foil wrapper would be used to reduce the thermal neutron product yield relative to the fast neutron product yield.

Another type of "nuclear reaction interference" occurs in reactor activation analysis, sometimes, with two elements having adjacent positions in the periodic chart. If the element with the larger atomic number is being measured, the analyst must be aware that, for specific pairs of elements, such as osmium and iridium, some of the thermal neutron product radioactivity may have been produced from the decay of an isotope produced by thermal neutron capture in the element with the lower atomic number.

4. Qualitative Analysis of Counting Data

In a typical case several radioactivities are generated during irradiation and subsequently detected. Unless contributors to the spectra are known in advance, the analyst must first identify them. For gamma-ray spectra, taken with NaI(Tl) or Ge(Li) detectors, the first step in spectrum interpretation is generally the listing of possible isotopes which could be contributing to the observed spectral peaks. Subsequently, some of the possible contributors are removed from the list using various criteria such as half life, or comparison to the known shape of the spectrum of a possible contributor.

If the raw data are accumulated with a beta particle detector or in the multiscaler mode with a gamma-ray detector, the analyst identifies components from their half lives and, in the former case, the maximum beta particle energy if needed. In the latter case adjustment of the electronics may also supply information since the analyst can select an energy region to count.

Radiochemical separations can be of great assistance in qualitative analysis of data. Very often the separation is so successful that a glance at the counting data is sufficient to show either than the desired radioisotope is present or absent. In separations which provide less decontamination,

one expects to find elements with similar chemical properties carried along. In thermal neutron activation analysis with radiochemical separation of chlorine, for example, one is not surprised to find ^{80}Br and ^{82}Br contamination. Nevertheless, radiochemistry is a very powerful technique in qualitative analysis of data.

5. Quantitative Analysis of Counting Data

Once the contributors to the counting data have been identified, quantitative analysis is begun. As in the preceding section, it is assumed that the counting data contain contributions from several radioisotopes.

For beta particle counting or gamma-ray counting in the multiscaler mode, the quantitation process usually involves decay curve resolution. This computation may be performed by successive subtractions of long-lived components until the decay curve of the individual isotope is obtained, or more elaborate computer methods may be employed. In any case, the analysis of the data should yield an interference-free activity which is then converted to the weight of the element as described above.

In the analysis of gamma spectra, several methods of quantitation are available. The first of these is the peak area method in which the area of a spectral peak is computed so as to exclude the Compton continuum upon which it rests. This area may then be converted to the weight of an element (see Fig. 1). Spectrum stripping is a means of analysis which subtracts out interfering components from the observed spectrum until A_i is free of interference. Figure 2 shows a peak before and after component subtraction although stripping is really unnecessary for the peak in Figure 2 since it has no appreciable interference which would prevent accurate peak area calculation. The least squares analysis of spectral data synthesizes a spectrum which approximates the observed spectrum. Using the least squares criterion, spectra of individual components are added together to give a "best fit" to the observed data. The activity of each component in the synthetic spectrum, relative to a reference spectrum of that isotope, is obtained from the least squares computation. Figure 3 shows portions of spectra of ^{59}Fe and ^{60}Co, each counted by itself, and of the two sources counted together. The difference between the least squares synthetic spectrum, a linear combination of the ^{59}Fe and ^{60}Co spectra, and the observed mixture is plotted at the top of the figure.

Other methods of quantitative analysis include linear programming, analog computation techniques, and methods which are tailored to individual situations.

6. Activation Analysis of Large Numbers of Samples

When large numbers of samples are to be analyzed, it is advantageous to employ digital computers to obtain computed results. A good
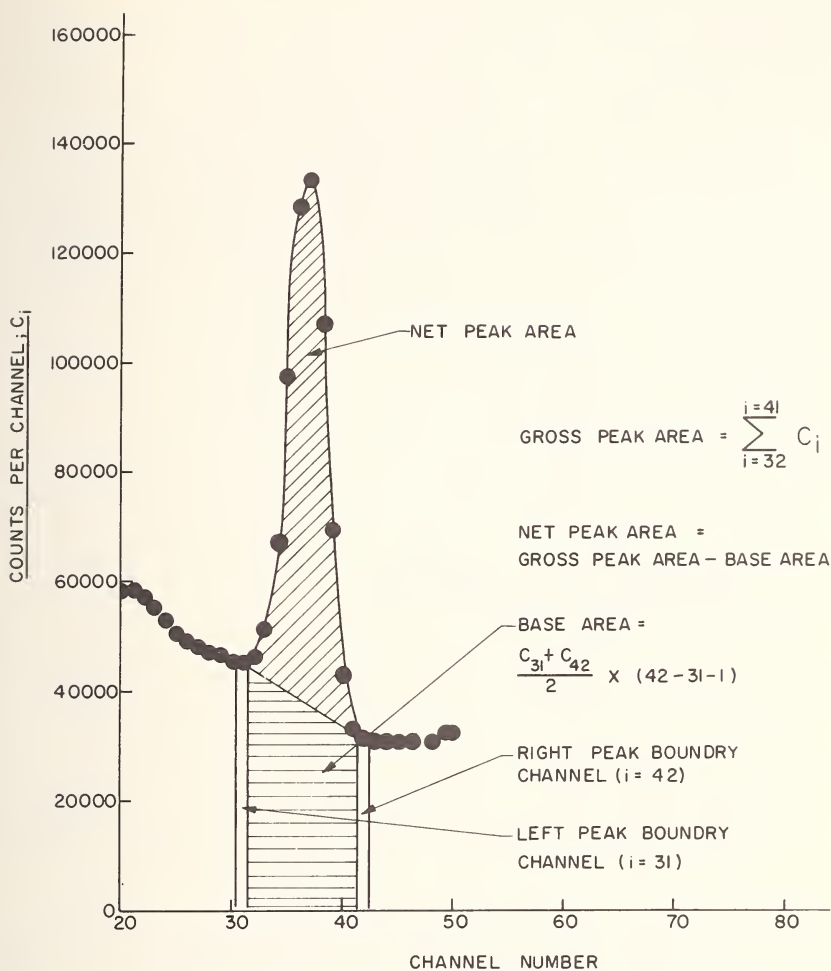
Figure 1.   The classical peak area method for complicated measurement of the total absorption peak.

illustration of a computer application is the analysis of similar samples. As an example consider the thermal neutron activation of biological tissue for sodium content in cystic fibrosis detection. Quantitation could be based on computation of the areas of the 1.368 MeV and/or 2.75 MeV peaks. Using the computer, one can check for the existence of peaks at these energies, compute their areas and compute the sodium content of the samples. For a simple error check, the ratio of the areas of the two peaks may be compared against a known value of the ratio.

A modification of the above procedure is adaptable for semi-routine activation analysis. In this type of analysis, samples are being examined
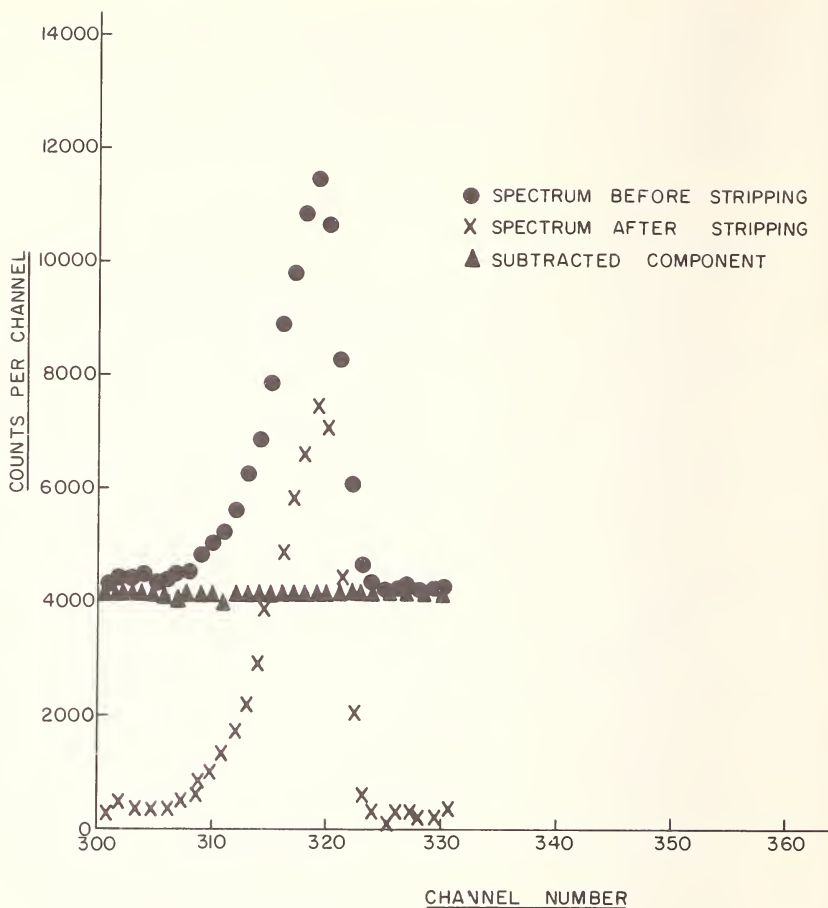
Figure 2.   Subtraction of interferences under a total absorption peak by spectrum stripping.

for the presence or absence of certain radioactivities. Examples of this type of analysis are the study of material flow through a manufacturing plant using cold tracers or the determination of retention and excretion of trace elements added to the diet. Following irradiation, spectra of the samples may be checked for peaks from the element of interest. If the presence of the element is established, its activity may be determined by one of the methods listed in the preceding section. If no evidence for the peak is found, no computation of weight is made, or an upper limit is computed.

Computer processing of nonroutine activation analysis samples is considerably more difficult than the processing of routine or semiroutine samples. In the latter cases quantitation is based on prior knowledge of
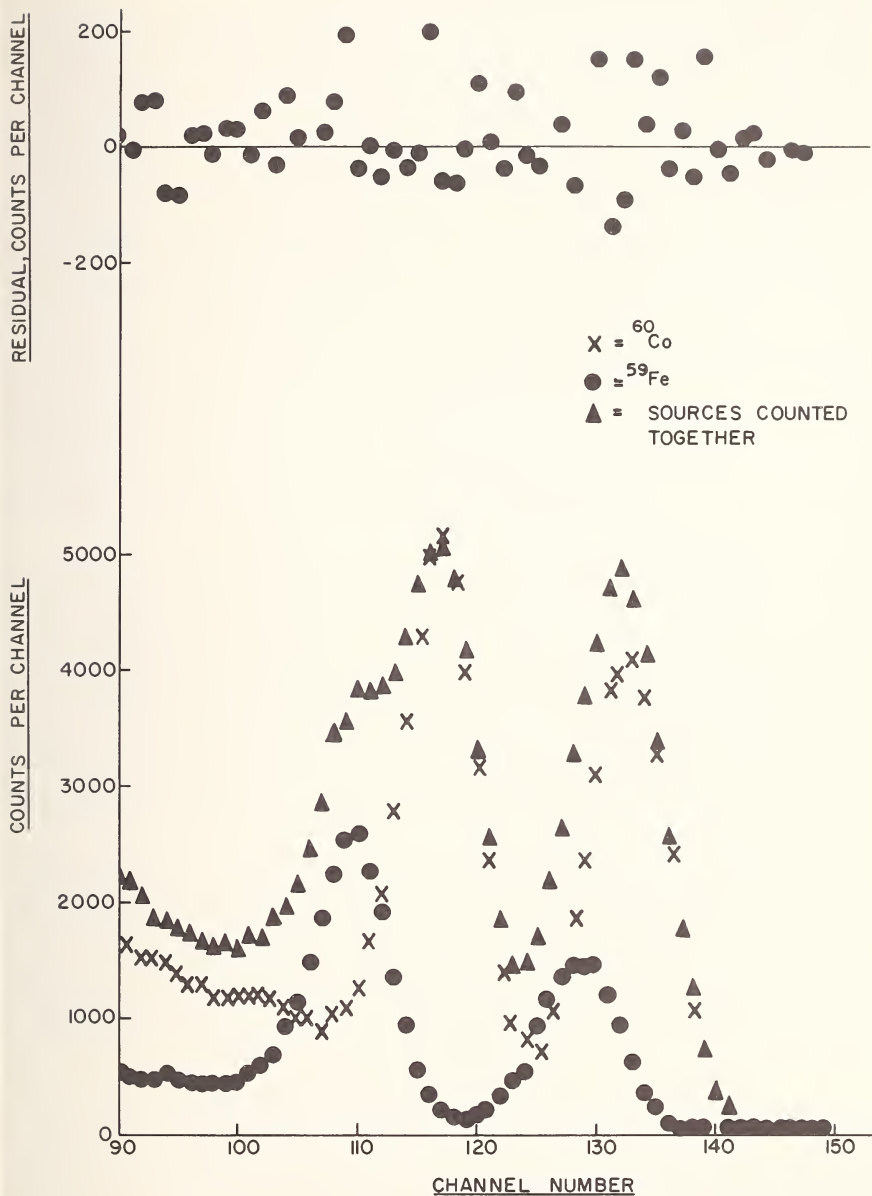
Figure 3. Least squares analysis of a mixture of cobalt-60 and iron-59.

component radioisotopes, while in the former case no such knowledge is available by definition. The computer program must first determine which isotopes are present, and this is not necessarily an easy chore. The number of possible contributing isotopes may be quite large; in reactor

neutron work there are well over 100 possible contributing isotopes, not counting fission products. The decision as to which isotopes are present and which are not, often requires a great deal of skill and judgment. Some computer programs have been written for this purpose, but their accuracies seem somewhat limited. (Several papers presented at this conference show that considerable progress is being achieved in this area, however).

For routine or semiroutine analysis, skillful programming is necessary if large volumes of data are to be processed. Editing of the data is very important to overcome such problems as incorrect data deck arrangement, invalid punches on the data cards, illegal or extraneous characters on magnetic tape, and so forth. Editing may be completed before data are submitted to the computer for result computation, or the data may be edited as they are read for computation. The latter method is clearly preferable since accurate manual correction of all the mistakes on cards is tedious and difficult. A self editing program must be able to skip over or correct bad data.

Another important feature of programming to handle a large volume of data is checking of incorrectly computed numbers obtained in the course of a calculation. Intermediate numbers (*i.e.* decay factors, saturation factors, *etc.*) are frequently omitted from the final printing of results, and it is important to check many of these numbers during the computation to determine whether they are in an acceptable range. For example, peak areas may be checked for negative values which can result from incorrect data deck set-up, incorrect data, incorrect programming, or the absence of a peak in the spectrum.

Drift control too is important in processing a large volume of data. In addition to its importance in least squares calculations, drift control is important for peak area computations, for, if a peak drifts more than a few channels, the computer must be able to decide whether the peak has merely drifted or there is an interfering nearby peak. This decision can be a difficult one for an experienced analyst or for a machine devoid of judgment.

II.   Historical Review: The Pre-1962 Period

This section contains brief descriptions of the highlights of some published articles containing information pertinent to mathematical computations in activation analysis. The review covers the period from the beginning of activation analysis over thirty years ago and ends with 1961. During that period, the development of new radiation detection systems appeared, and appropriate calculation methods were devised for these systems. Accordingly, a review of these methods is well suited to chronological presentation.

By 1962, most of the computation methods currently in use had been published, and much effort has subsequently gone into refining existing methods. Section III, therefore, is devoted to describing current (and nearly current) methods. Within each computation type, the presentation is intended to show evolutionary improvements.

Some of the articles reviewed here and in section III are activation analysis papers in which the mathematical computations are secondary to the purpose of the work described, but these computations are deemed significant in the development of activation analysis computation methods, thus serving the primary purpose of the present review. Other papers reviewed are directly concerned with resolution of observed data into individual components. These papers are not concerned with activation analysis, but their contents bear directly on the computation problems of activation analysis.

The first activation analysis was performed in the 1930's by Hevesy and Levi [1-3]. They irradiated an yttrium sample with neutrons from a radium-beryllium source and determined the impurity, dysprosium, which constituted about one percent of the sample. Identification of the dysprosium was made using the half life of the dysprosium activity. The samples were counted with a Geiger-Muller (GM) tube. The detection limit for dysprosium was estimated at one milligram.

In 1938, Seaborg and Livingood [4] published their study on impurities in iron. They bombarded iron with deutrons from the cyclotron and observed radioactivities produced by the (d,p) reaction. The beta particles emitted by these isotopes were detected by a Lauritsen electroscope. Identification of gallium isotopes was obtained through radiochemical separations and the half lives of the product isotopes, ^{70}Ga and ^{72}Ga. The authors estimated the gallium in the iron at 6 ppm, pointing out that 0.6 ppm of gallium would have been well above the detection limit. Their computational procedure was to convert the electroscope reading to the end of bombardment and then to saturation. This result was compared with a theoretical result which yielded the 6 ppm figure. They also pointed out that decay curve resolution could be applied to a composite decay curve taken with no radiochemical separations, and they were able to measure copper in neutron irradiated beryllium using the ^{64}Cu and ^{66}Cu activities.

In 1952, Smales [5] reported on determination of uranium in rocks by activation analysis employing radiochemical separations and beta particle counting. Identification of radioisotopes was accomplished using half lives and the maximum energies of the beta particles. Atchison and Beamer [6], also in 1952, reported measurements of trace impurities in magnesium by activation analysis using GM counters.

Leddicotte *et al* [7,8], in 1953, reviewed early activation analysis studies by several groups of workers, and discussed the potential of

activation analysis for a wide variety of applications, listing computed sensitivities for many elements. They pointed out that a typical analysis would be performed with radiochemical separations and beta particle counting.

The NaI(Tl) scintillation counter was a great boon to activation analysis because it provided so much information not previously available without much tedious study. In 1953, Connally and Leboeuf [9] published their study on analysis of radionuclide mixtures with a gamma-beta scintillation detector. They used the maximum beta particle energy as an identification aid, but indicated that gamma-ray energy was of considerable value in identifying radioisotopes contributing to their spectra. Quantitation was performed by estimating the total peak area after subtraction of the Compton continua from higher energy gamma rays. The peak was assumed to be Gaussian in shape with the peak parameters related by the expression

$$A = 1.07 \, hW \tag{4}$$

where A is the computed peak area, h the maximum peak height, and W is the full width at half maximum. Figure 4 indicates some of the difficulties in obtaining an accurate area by the present method (a Gaussian plotted on semilog paper has the shape of an inverted parabola). The parabola fits the observed points well at the tip of the peak but poorly at the bottom of the peak, since the background was not subtracted prior to fitting the Gaussian. Even then the fit on the left side would not be a good one. In the same year Kahn and Lyon [10] pointed out the usefulness of the NaI(Tl) spectrometer as an aid in identification of activation products.

In 1955, Lyon and Reynolds [11] identified ^{24}Na, ^{27}Mg, and ^{28}Al using gamma-ray spectrometry applied to reactor cooling water. Peak areas were obtained by graphical integration. In the same year, Morrison and Cosgrove (12) reported an activation analysis study of trace impurities in silicon using scintillation counters. They computed peak areas in a manner quite similar to that of Connally and Leboeuf [9]. Upson, Connally, and Leboeuf [13] described in 1955 a method for electronic spectrum stripping to analyze for low energy gamma-ray emitters in radionuclide mixtures. An exhaustive treatment of the statistics of scintillation spectrometers was published in the same year by Breitenburger [14].

In 1956, Connally [15] published further studies of instrumental gamma-ray spectrometry omitting the counting of beta particles described earlier [9].

In 1957, Putman and Taylor [16] described spectrum stripping for activation analysis, and C. S. Cook [17] mentions both spectrum stripping and peak area computation in a review article on gamma-ray
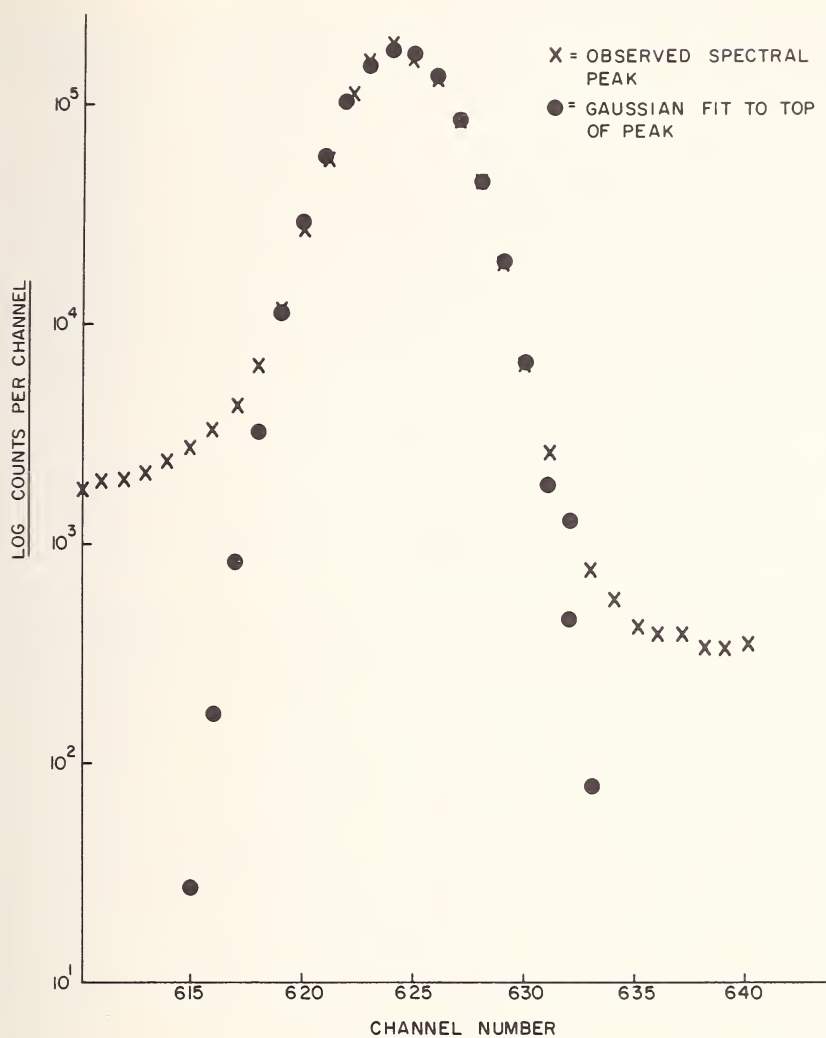
Figure 4. Fitting a Gaussian function to a total absorption peak.

spectrometry. Cosgrove and Morrison [18] pointed out the vast potential for neutron activation analysis employing gamma-ray spectrometry.

Most of the above mentioned studies which utilized scintillation counters accumulated data with single channel analyzers. However, Lyon and Reynolds [11], employed a 40 channel analyzer as early as 1955. Thus the instrumentation to achieve full utilization of the scintillation counter data for activation analysis made its appearance.

The year 1957 also saw the appearance of R. L. Heath's "Scintillation Spectrometry Gamma-Ray Spectrum Catalogue" [19]. In addition to the

high quality spectra of gamma rays of individual isotopes, the catalog contained much useful information on detector and shield construction.

In 1958, Halfhill anticipated the future need for reading out pulse-height spectra in computer compatible form on magnetic tape [20].

By 1959, methods of computation especially tailored for pulse-height spectra accumulated with multichannel analyzers began to appear in the literature. Covell's peak area computation method [21] provided an elegant, simple way to compute quantitative radioisotope contributions to spectra of mixtures of several radionuclides. His method was readily and quickly performed with an adding machine or mechanical calculator, and was far easier than the earlier method of computing the area under the Gaussian shaped peak. Figure 5 indicates the Covell concept. The area is computed by summing the channels in the range $I-\Delta I$ to $I+\Delta I$ and subtracting the trapezoidal base area. Covell showed that by comparing areas computed with the same ΔI, he could accurately compute the contribution of an isotope to a spectrum. Accurate results were obtained for varying ΔI values as long as the same ΔI was used in comparing two spectra.

Lee [22], using a 256 channel analyzer to accumulate spectra, described the complement method for analysis of radionuclide mixtures.

NET PEAK AREA =
$$a_0 + \sum_1^3 a_i + \sum_1^3 b_i$$
$$- (3+3+1/2)(a_3 + b_3)$$
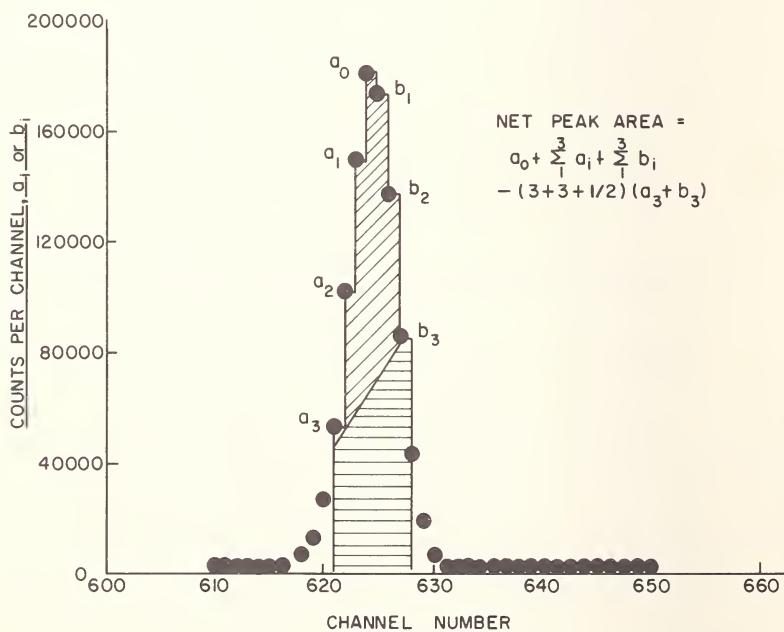
Figure 5. An example of quantitative measurement of total absorption peak area using the Covell method.

Similar to spectrum stripping, the procedure was to store the mixture spectrum containing contributions from several radionuclides, and then, in effect, remove the contribution of one of the components by counting a source containing only that component until its contribution vanished. In practice, this was done by complementing the mixture spectrum, and then counting the known source — the effect was to subtract the known source spectrum from the mixture spectrum. The lengths of the counts for the mixture and the known source could be used to compute the contribution of the known source to the mixture.

Bate and Leddicotte applied the complement subtraction method to the activation analysis of six components in tobacco [23]. The tobacco samples were irradiated for 155 hours at 7×10^{11} n·cm^{-2}·sec^{-1}, and counted 60 days after irradiation using commercially available 200 channel analyzers. L. Salmon presented tabulations, specifically for activation analysis, on isotopes produced by (n,γ) activation, including information on their half lives, energies, and relative intensities [24]. Gardner *et al* described a method of decay curve analysis using Fourier transforms [25].

In 1960, Kuykendall, Wainerdi, and associates described "Computer Coupled Activation Analysis" [26]. The pulse-height spectra were readout onto punched paper tape, converted to punched cards by a tape-to-card converter, and the cards submitted to the computer for qualitative and quantitative analysis. The computer program identified spectral components by searching for the highest energy, statistically significant, peak in a spectrum, and determining its half life from other spectra of the same sample. Knowing the energy and half life of the peak made identification possible by comparing against known energies and half lives of (n,γ) activation products. Once identified, the amount of element present was computed by the peak area method. Then this component was stripped out using a "library" spectrum of the pure component. The entire process was repeated until all peaks had been examined. In addition to the above digital computer program, they also described an analog computer approach to analyze the spectra by energy and decay.

While the Texas A&M group were establishing the importance of computer data processing in activation analysis, physicists were studying mathematical methods of gamma-ray spectrum analysis. Chester and Burrus' idea was to convert the observed spectrum into an ideal one, having one peak of infinitesinal width for each energy gamma ray emitted by the source [27]. For ^{137}Cs, for example, an observed spectrum containing the 662 keV full energy peak, Compton edge, Compton continuum, and backscatter peak would be reduced to a single very narrow peak at 662 keV. The remaining parts of the spectrum, which are artifacts of the detection system were thus removed. They tried both

matrix inversion techniques and linear programming on synthetic spectra, concluding that the latter approach gave better results which were less susceptible to problems caused by statistical fluctuation.

Westermark and Sjostrand, in performing activation analysis for mercury [28], computed net peak areas by arbitrarily drawing in a straight baseline tangent to either side of the 77 keV peak. This method of peak area calculation is considerably different from that of Covell [21]. Because it is an important method of computation which needs a name to distinguish it from Covell's method, we shall refer to it as the classical peak area method, for this intuitive method has been used in many regions of science for many years. Later in the present chapter we shall compare accuracies of the two methods. Westermark and Sjostrand demonstrated the accuracy of classical method for their activation analysis work.

Other important developments in 1960 include the development of the method of compensation for dead time losses in pulse height analyzers by Covell [29]. Guinn and Wagner [30] summed up the state of activation analysis instrumentation in their article on instrumental activation analysis featuring thermal neutron activation, NaI(Tl) detectors, and multichannel analyzers, although no mention is made of computer usage. With such instrumentation, radiochemical separations would be less frequently required. Hence, many activation analyses are purely instrumental, involving (perhaps) sample transfer to eliminate activities generated in the vial itself and in the air or other gas inside the vial; but utilizing no radiochemical separations. They mentioned the importance of peak area and peak height computations, and listed sensitivities for many elements. C. W. Gilbert described a method of simultaneous estimation of different radioisotopes by the unique technique of using sets of detectors with different sensitivities for different elements [31]. The very useful text, "Applied Gamma-ray Spectrometry", edited by C. E. Crouthamel [32] also appeared in 1960. Among its contents are an extensive description of activation analysis, a fine catalog of NaI(Tl) spectra of many radioactive isotopes, tables of counting efficiencies and geometries, and exhaustive tables of gamma rays arranged by isotope, energy, and half life.

In the following year (1961) instrumental activation analysis was discussed by Anders and Beamer [33] who viewed their work as an extension of that of Guinn and Wagner [30]. Their extension was to get the maximum information from their gamma-ray spectra. For that purpose. Anders [34] using thermalized 6 MeV neutrons, generated activities, and catalogued spectra of the most of the stable naturally-occurring elements. Computer preparation of data for the catalog included (1) reduction of the number of channels of data by combining data in adjacent pairs of channels in order to smooth the spectra and reduce statistical

scatter, (2) correcting for counting losses caused by dead time, (3) converting the spectra from counts per channel to counts per channel per minute, (4) subtraction of background, (5) normalization to a "standard" flux, and (6) preparing a semi-log plot of the spectrum. Analysis of unknowns [33] was then begun by visual identification of spectral components using the catalog. Computation of the total peak area for the component having the highest energy gamma-ray peak was used for quantitative result computation for the element from which the gamma-ray emitter was formed. No attempt was made to compute the net peak area above some assumed baseline — the total area is the sum of all the counts in the region of the peak, since background has been subtracted. The catalogued spectrum of the component is then stripped out, and the entire process repeated. In the case of interferences for which more than one radioisotope contributed to peak, the authors pointed out that it was often possible to overcome computational problems by waiting for the shorter lived interfering activity to decay away.

In describing activation analysis with short-lived isotopes, Anders [35], pointed out that a convenient way to obtain the spectrum of the short-lived isotope free of contributions from other longer-lived isotopes was to count the sample very soon after irradiation and then recount it later when the short-lived activity has decayed away. Using a computer to strip out the later count, the resultant spectrum could be processed as indicated by Anders and Beamer [33]. A similar computation technique was reported in the course of a study on "Methodical Improvement in Activation Analysis", by W. Bock-Werthmann and W. Schulze [36].

Fite, Gibbons, and Wainerdi [37] reported their studies on "Computer Coupled Automatic Activation Analysis" at the second Texas A&M computer program for activation analysis. Their first program [26] identified spectral components, and then evaluated peak areas to obtain quantitative results. The newer program assumed that larger numbers of similar samples could be processed by the computer in one computer run, and that these spectra were linear combinations of spectra of individual isotopes which could be resolved by a set of simultaneous equations. A pulse height spectrum is a one dimensional array, and we may write U (for unknown) for the spectrum of sample containing quantities of radioisotopes which are to be determined. Similarly, a spectrum of an isotope formed from a known quantity of element may be defined as S (for standard). Since it is likely that U contains contributions from several isotopes, it is likely that we shall require a standard for each one, and it becomes necessary to distinguish between standards. Thus, S_i is the spectrum of the ith standard. If we describe the contents of a spectrum one channel at a time rather than collectively, the symbols become U_j and S_{ji} where j is the channel number. The mixture spectrum, U, contains

contributions of several gamma ray emitting isotopes, and thus for any channel

$$U_j = \sum_{i=1}^{i=p} \alpha_i \, S_{ji} \tag{5}$$

for contributing isotopes numbered one to p. The coefficient α_i is the ratio of the intensity in channel j for the ith isotope in the unknown spectrum to the intensity in the standard spectrum. For example, if the height of a given peak in the unknown spectrum is 8000 counts and 80000 counts in the standard, $\alpha = 0.1$ (assuming no other contributors to the peak). The method employed by Fite *et al* [37] to obtain numerical values for α_i was to measure the height of the spectrum at different channel numbers, say j, k, . . n:

$$U_j = \sum_{i=1}^{p} \alpha_i \, S_{ki} \tag{6}$$

$$U_k = \sum_{i=1}^{p} \alpha_i \quad S_{ki}$$

$$
\begin{array}{cccc}
. & . & . & . \\
. & . & . & . \\
. & . & . & .
\end{array} \tag{6a}
$$

$$U_n = \sum_{i=1}^{p} \alpha \quad S_{ni}$$

and then solve the simultaneous equations for the values of α_i. Clearly, to solve these equations one needs to choose one value of U_j for each component. A two component mixture would require solution of two equations, three components, three equations, and so on.

Ehmann [38] presented a variation on the classical peak area method by using a curved baseline rather than the straight baseline used in the classical and Covell methods [21].

L. Salmon presented the method analysis of gamma-ray spectra by the least squares technique [39]. In this method of analysis the identities of isotopes contributing to the unknown spectrum, U, were assumed to be known, and the solution to the least squares equations gave the relative intensities of each contributor. The least squares approach can be formulated using the terms developed above

$$\sum_{j=k}^{j=n} w_j \left(U_j - \sum_{i=1}^{i=p} \alpha_i S_{ij} \right)^2 = M \tag{7}$$

The term W_j is a weighing factor, and M is the quantity to be minimized, and the analysis is performed using data in channels k to n. In essence, the least squares technique forms a synthetic spectrum, the right hand

term in the parentheses, by adjusting the α coefficients to minimize the weighted square of the difference between the observed and synthetic spectra. Salmon prepared and tested a computed program to solve the least squares equations, and clearly demonstrated the power of least squares gamma-ray spectrum resolution.

When gamma-ray spectra are analyzed by mathematical techniques which, in effect, combine standard spectra to form synthetic spectra which approximate a spectrum of unknown quantitative composition, it is important to avoid complications due to gain shifts and baseline shifts. A gain shift is a shift in the amplification of the detection system; a gain shift which increased the amplification of the system by one percent would shift a peak in channel 100 to channel 101, and a peak in 200 would move to 202. (It is assumed here that channel zero corresponds to zero energy). A baseline shift translates the entire spectrum to the left or right by a fixed number of channels. Clearly, a significant shift in the spectrum of an isotope between the time it is recorded as a standard and as a component of a mixture spectrum will result in incorrect values of α in either the least squares spectrum analysis (Salmon [39]) or the simultaneous equation method (Fite *et al* [37]). Covell and Euler [40] found that gain shift was a function of counting rate and of the photomultiplier tube type. To eliminate these shifts, a system was built to control both gain and baseline shift in scintillation spectrometers and was reported by Fite, Gibbons and Wainerdi [41]. Gain shift control was achieved by continuously monitoring the position of a reference peak in the spectrum. A slight shift in position of this peak resulted in correction voltage being generated and applied to the phototube to restore the peak to its assigned position. The reference peak was produced by a plutonium alpha emitter embedded in the scintillation crystal. By comparing peak positions with drift control operating and not operating, the authors were able to demonstrate that their system worked very well.

A number of other significant papers on the analysis of spectra appeared in 1961. De Soete and Hoste reported results of studies of computations for adjacent peaks, including problems of resolution of adjacent peaks and determination of their energies and peak areas [42]. W. R. Morgan [43] wrote a computer program to strip out interfering activities, fit a Gaussian curve to the full energy peak, and compute the peak area by integrating under the curve.

W. Zimmerman described a simple, elegant way to determine exact peak position and width without elaborate fitting of a Gaussian peak to the data [44]. R. L. Heath [45] demonstrated an empirical method of prediction of spectrum shape which worked very well for monoenergetic gamma rays. With a knowledge of decay schemes more complex spectra were predictable.

A. Savitzky, in an article entitled "Data Processing in Analytical Chemistry" [46], foresaw a "computer revolution" which would "lead to development of new instruments which yield only partially processed data and which will rely on computers to make final computations". He also pointed out the importance of the first and second derivatives for the analysis of spectral data.

To summarize the era from Hevesy's first experiments in the 30's until 1961, the most rapid progress for activation analysis followed the introduction of the NaI(Tl) scintillation counter and the multichannel analyzer. Three major types of calculations were devised: (1) peak area, (2) spectrum stripping and (3) spectrum syntheses. Peak areas were computed in various ways so as to obtain the total area, the net area above a baseline, or the area defined in any one of several other ways. Spectrum synthesis features combining reference spectra to obtain an approximate facsimile of the spectrum being analyzed. The combination was achieved by solving a set of linear equations or by the least squares technique.

III.   Description of Current Methods of Computation

In 1962, a symposium entitled "Applications of Computers to Nuclear and Radiochemistry" was held at Gatlinburg, Tennessee in October [47]. Included in the proceedings (published in 1963) are papers on decay curve analysis, unfolding of pulse height spectra, least squares analysis of beta-ray spectra and of gamma-ray spectra, programs to obtain quantitative results from activation analysis spectra, and many others. Of particular interest is Appendix II by R. H. Moore on "chi-square" and curve fitting. In the remainder of this section, we shall mention several of these papers, but the serious student of computation methods for nuclear counting data is advised to consult the symposium proceedings.

Section III of the present lecture contains subsections on the peak area method, least squares analysis of pulse height spectra, spectrum stripping, smoothing and differentiation of spectra, decay curve analysis, and miscellaneous topics.

A.   COMPUTATION OF NET PEAK AREAS

In 1963, Lightowlers [48] performed activation analysis on diamonds for manganese, sodium, and copper using the classical peak area method, indicating concern about the accuracy of the method. Decat, Van Zanten and Leliart [49] used the Covell method, apparently without similar concern.

Borella and Guzzi, in 1964, reported a computer program for activation analysis [50]. Peak areas were determined by comparison of unknown and library spectra, summing the counts in the peak, and subtracting the

base area which was computed as the product of the number of channels times the number of "background" counts per channel on the right side of the peak. This was a variation on the classical method in that it uses only the right hand peak boundary to estimate the base area. Wainerdi *et al* [51] reported a general activation analysis computer program to allow the analyst the choice among the peak area methods, least squares fitting, or quadratic fitting.

Choy and Schmitt reported their peak area computer program, in 1965, featuring fitting of specified functions at the right hand and left hand boundaries of the peak to select the peak boundary channels [52]. This method of selection overcomes statistical scatter, automatically selecting the minimum on the left and fitting a tangent on the right.

Plantin [53] reported his peak area program which first smoothed the NaI(Tl) spectra, located peaks, determined boundary channels, and computed net peak areas by the classical method. Methods of peak location and peak boundary selection are discussed below.

Mundschenk in 1966 discussed the problems of complex (or overlapping) photopeaks when determining exact peak positions [54] and calculating intensities of individual components [55]. The present author described a computer routine for peak location, boundary channel selection, and peak area measurement by the classical method [56].

In 1967, Mariscotti reported a computer program using the second derivative to locate peaks and then to determine peak intensities by fitting a Gaussian function to the peaks [57]. Girardi *et al* [58, 59] reported an activation analysis program featuring peak location and the classical peak area method. Heath and co-workers [60] discussed their thorough photopeak analysis program for the determination of peak position, area, and width; input information included the number of channels to be fit by one or more Gaussians and their energies.

The present author studied the classical peak area method for Ge(Li) detector spectra and compared the classical and Covell methods [61]. This study resulted from the suggestion that peak area measurements using Covell's method [21] gave incorrect results at moderate and high counting rates. It was shown that resolution losses caused difficulties in peak area computation with Covell's method unless great care was exercised in selection of peak boundaries. However, with proper boundaries the method is very accurate. The classical method, which selects boundary channels where the peak becomes indistinguishable from background or the Compton continuum from a higher energy gamma ray is just as accurate and considerably easier to implement. Recently, Schmitt [62] has pointed out the efficacy of a baseline restorer module in reducing peak shape distortion. Addition of a restorer will probably make the application of Covell's method easier.

B.   METHODS OF PEAK LOCATION AND BOUNDARY CHANNEL SELECTION

Computer location of peaks without prior knowledge of their positions in NaI(Tl) or Ge(Li) spectra has been described by many authors [26,50,53,56,57,58,59,61]. Most of these methods depend on finding a group of adjacent channels which was significantly more counts than the channels on either side of the group [26,53,58,59]. One way to implement this approach is to compare the sum of the counts in a selected number of channels (e.g. three channels with three channel sums on either side) [53]. Plantin found it advantageous to smooth his spectra before searching for peaks. Using some statistical criterion to test whether number of counts in the central group of channels is significantly greater than those on either side establishes the presence or absence of a peak.

The smoothed first derivative furnishes another means of peak location [56,61]. Figure 6 shows a peak and the smoothed first and second derivatives. In this method, the derivative attains a maximum positive value at about half maximum height as the left side of a peak, then smoothly decreases toward zero as the channel number increases, becomes negative at the peak center, and reaches a minimum value at half height on the right side of the peak. Thus, a change in sign of the derivative from one channel to the next indicates the presence of a peak.

Because of the short radius of curvature which exists at the tops of Ge(Li) detector peaks, the smoothed second derivative exhibits rather deep, negative minima. By searching for these minima, peaks can be located [57].

Earlier, the use of the smoothed second derivative to locate peaks in NaI(Tl) spectra was examined, but discarded in favor of the first derivative method, described above [56].

Once peaks have been identified, peak boundary channels must be selected. This may be accomplished by referring to previously established boundaries for the specific peak being examined [50]. Since the boundaries depend, to some extent, on various experimental parameters, most analysts have preferred to determine the boundaries from the spectrum itself. For NaI(Tl) spectra above several hundred keV, the left boundary is typically taken at the minimum below the peak. Identification of the channel with the minimum number of counts is often complicated by statistical scatter. Choy and Schmitt [52] solved this problem by finding the minimum in a function fitted to the data in several channels about the minimum. Others use the minimum from a mathematically smoothed spectrum [53,61]. Girardi *et al* [58,59] chose left and right boundaries at the channels for which the decrease in counts per channel is no longer statistically significant. Right hand boundary channels are selected at the minimum on the right side of a peak [53] where the
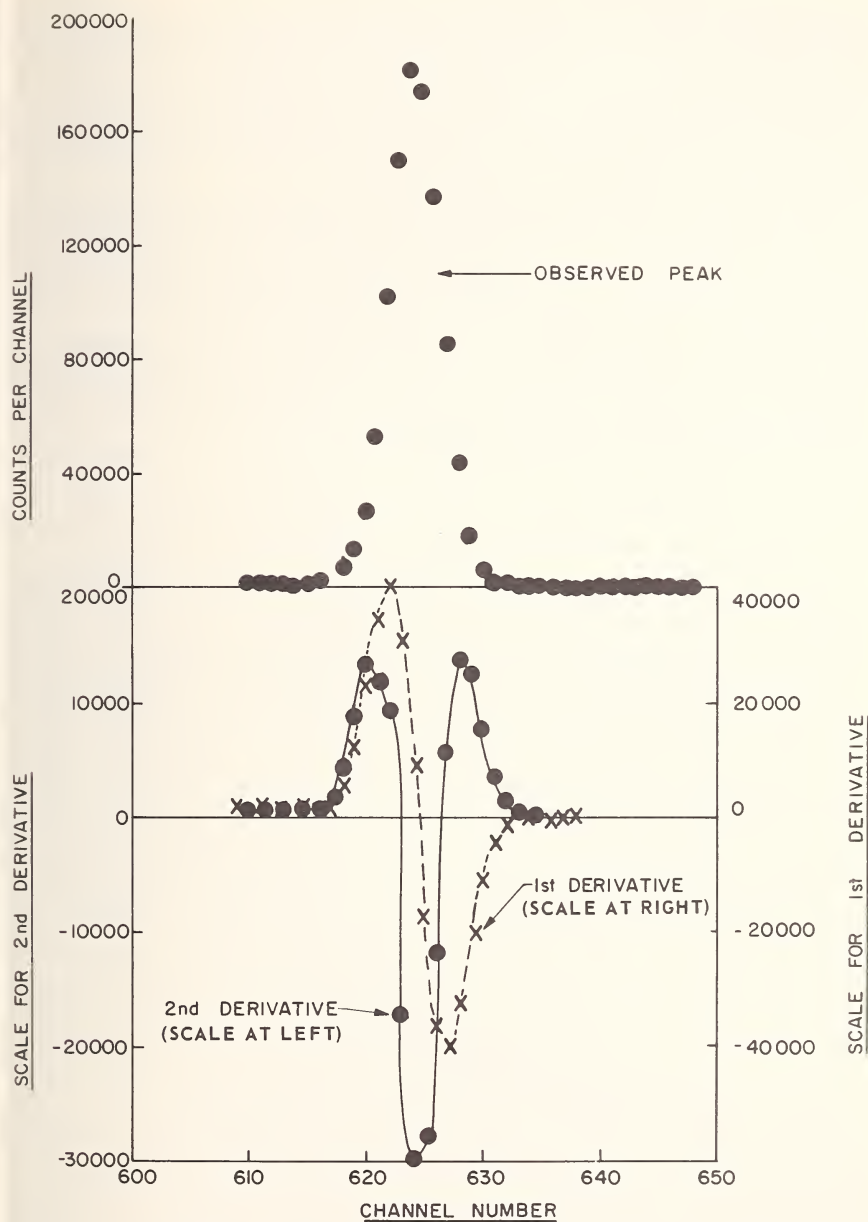
Figure 6. Example of the smoothed first and second derivatives of a total absorption peak.

derivative becomes positive, or where a line drawn through the spectrum at the left boundary is tangent to the spectrum on the right hand side [53,56,61]. Boundaries found using the tangent are often fewer channels

away from the peak channel than those found using the minimum. In this event, a line drawn through the spectrum at the minimum on the left and right sides of the peak would actually pass above the spectrum near the right boundary, and hence be an inaccurate representation of the tops of the base area (see Fig. 7). The boundary determined by the tangent would be far superior in this case.

The above discussion applies primarily to NaI(Tl) spectra, but for peak location with spectra taken on Ge(Li) detectors is similar, except that it is sometimes necessary to fit a tangent to the left side of the peak, (a mirror image) similar to the tangent fitting described above [61].

Peak areas are computed by summing the spectrum between the boundary channels and subtracting the base area. It is then necessary with most methods to test for certainty that the net peak area is statistically significant relative to the base area.

C.   LEAST SQUARES ANALYSIS OF PULSE HEIGHT SPECTRA

Analysis of gamma-ray spectra obtained with NaI(Tl) detectors by means of the least squares technique has proven very popular. The principle of the method has been described above but it seems reasonable to describe it again here in a somewhat different way. Consider a simple example of a spectrum containing a mixture of ^{24}Na and ^{56}Mn gamma rays. We have on hand two reference spectra, often called libraries or standards; one of these contains contributions from ^{24}Na only, and the other, ^{56}Mn only. If we multiply the number of counts per channel in the ^{24}Na by a relative intensity factor and add to it the ^{56}Mn multiplied by another factor, the resultant spectrum will be a very good approximation of the observed mixture spectrum. Because of statistical scatter in the number of counts per channel, the mixture and synthetic spectra will never be identical. Equation (7) describes the least squares equation where the relative intensity factors (α) are obtained. As mentioned earlier, L. Salmon [39] demonstrated (in 1961) the power of the technique. Comparing results of least squares computations on known mixtures, he demonstrated the general superiority of the technique over results obtained from spectrum stripping. At low counting rates, where stripping gave poor results, the results quoted by Salmon are very impressive. In analyzing a three component spectrum with large statistical variations he found percentage errors to be roughly a factor of ten smaller as obtained with the least squares fit as compared to those obtained by stripping.

At the Gatlinburg Conference [47] Salmon discussed further studies of the least squares method [63], including general validity of the method, accuracy and sensitivity of the method, and sources of errors. The problem of overlapping peaks may limit with the sensitivity of the
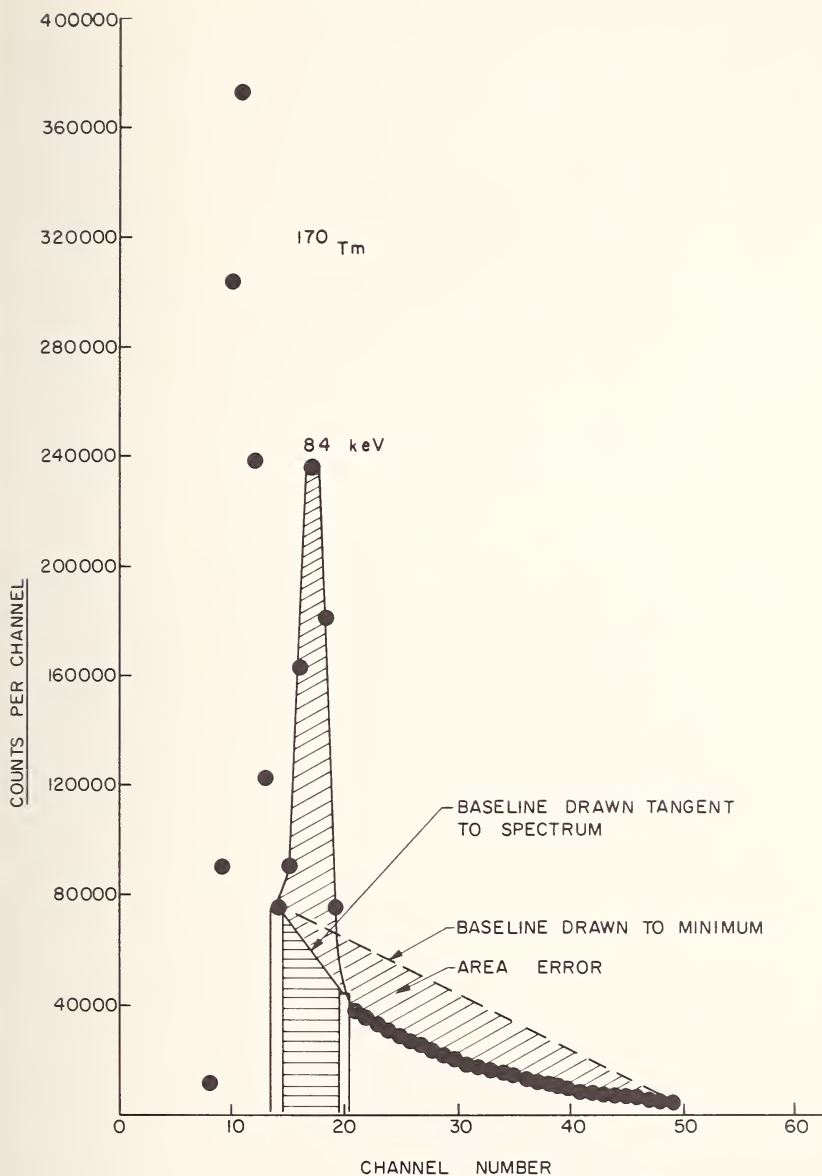
Figure 7. Illustration of inaccuracies associated with improper selection of boundary channels around the total absorption peak.

method, but Salmon was able to resolve detected peaks with NaI(Tl) at 0.51 and 0.52 MeV quite effectively. A primary source of error in the least squares analysis occurs from gain shift, and the need for gain

stabilized spectra is mentioned, although he points out that the computer could sometimes transpose a spectrum to form one free of gain shift. Another source of error is unpredicted nuclides which make significant contributions to the composite spectrum. In this event no reference spectrum would be used in the fitting procedure, and the results would probably be inaccurate. Presumably, application of the chi-squared statistic to the result would indicate an unsatisfactory solution warning the analyst not to accept the results.

Other least squares procedures were presented at Gatlinburg. Drew, Fite, and Wainerdi [64] presented their least squares program and gave results. Their program was tailored specifically for activation analysis. Nicholson, Schlosser, and Brauer present their elaborate technique [65]; a revised version was published subsequently, in 1963 [66]. Trombka, in his paper [67], paid special attention to off diagonal elements and their bearing on the problems of interferences. He found backgrounds troublesome to solve for analytically, and concluded that the best procedure was to subtract it before attempting to fit the data. He also observed that the least squares technique sometimes gives negative results (*i.e.* negative contributions of one or more reference isotopes), and postulated that these isotopes were probably not present in the mixture and should be eliminated from the reference spectra used in fitting.

Parr and Lucas, in 1964, presented the results of their solution to problems of gain and baseline shifts [68]. They pointed out the severity of the shift problem, especially for low activity samples requiring counting times of several minutes or hours. Their technique was to count a thorium ore source before or after each count on a mixture spectrum, using the 0.24 MeV and 3.2 MeV peaks to determine both gain shift and baseline shift. Using the known amounts of shifts, the mixture spectrum was transformed so as to eliminate them, and then the fit was performed. In testing their procedures, they counted ten different sources (^{22}Na, ^{54}Mn, ^{65}Zn, ^{95}Zr-^{95}Nb, ^{90}Sr, ^{106}Ru, ^{125}Sb, ^{137}Cs, ^{144}Ce, and ^{228}Th) individually and together. When counted together, deliberate gain and baseline shifts were introduced — — 1.5 percent and 1.0 channels, respectively. Analysis of the spectra without compensation for shifts gave poor results; for example, the count rate of ^{24}Na was 68 percent of its known value; ^{54}Mn, 65 percent; ^{65}Zn, 84 percent; ^{95}Zr-^{95}Nb, 120 percent, ^{90}Sr, 167 percent, etc. After correction for shifts, these results became 99.5, 95.4, 98.5, 99.0, and 99.0 percent respectively, clearly a dramatic improvement. All results were within one or two standard deviations of the correct result, 100 percent. Perhaps even more astounding is that they were able to determine ^{90}Sr in Alaskan caribou bone correctly, as determined by radiochemical analysis, even though ^{90}Sr made no observable contribution to the spectrum.

A number of other groups presented least squares gamma-ray spectrum resolution programs. Helmer *et al* [69] described a linear least squares program including gain shift correction capability. Munzel reported a least squares program for an activation analysis [70]. Salmon discussed his general computer program for analysis of gamma-ray spectra including least squares and gain shift capabilities [71]. Wainerdi *et al* [52] described their automated system for counting large numbers of samples, recording counting times, sample number, and spectra in computer compatible format, and performing least squares analyses on the data. The present author discussed analysis of spectra by least squares for obscure radioactivities in the presence of severe gain and baseline shifts [72].

Pasternack and Liuzzi, in 1965, presented their studies of residuals in evaluation of results of least squares computations [73]. Residuals are the difference between the observed and synthetic, computed, spectrum:

$$R_i = C_i - S_i \tag{8}$$

where R_i is the residual in channel i, and C_i and S_i have the meanings defined above. Taking the statistician's viewpoint, they were able to derive a single statistic which indicated, by its numeric value, whether or not residuals behaved randomly as they should when the solution is valid. Schonfeld [74] reported a method for obtaining improved accuracy with fast decaying isotopes. He used two approaches to minimize errors: (1) selection of optimum counting conditions, and (2) accumulation of several spectra during the decay of the isotope and fitting the least squares results to a decay curve.

Blackburn, in 1965, described a least squares spectrum resolution method in which the solution was obtained by the method of determinant algebra [75]. Wohlberg [76] presented a detailed look at the least squares technique for gamma-ray spectrometry with emphasis on sources of error. Emery *et al* [77] evaluated several different computer programs from the standpoints of cost, input effort required, and gain shift capability. They found, briefly, that each program gave about the same result except that one of them gave no result for several elements.

In 1966, Schonfeld, Kibbey, and Davis described their program featuring gain-shift and baseline-shift correction capabilities [78]. Their results very clearly demonstrate the need for those corrections, for they were able to obtain very accurate results using the corrections. Their illustration of the dependence of "chi-square" on these shifts is excellent.

In 1967, Schonfeld brought out a considerably improved least squares program, "Alpha-M", [79] as compared to earlier versions, "Alpha" [74,79]. Some of the improvements need not be mentioned here because they are mainly concerned with programming features. However, he

demonstrated that, at low count rates, weighting factors based on calculated counts rather than observed counts, produced dramatically better results. In one instance, use of weighting factors based on actual counts gave a result known to be 40 percent in error; with Schonfeld's new method this dropped to less than one percent. This is perhaps an extreme example, but clearly shows the superiority of the new method. Another improvement in accuracy results from optional subtraction of background from low count rate spectra, and comparing fits with or without subtraction to determine whether changes in background counting rate during sample counting makes the subtraction introduce large errors.

Other articles of interest appearing in 1967 include further studies by Pasternack and Liuzzi on the application of statistics for evaluating fits using residuals [80,81]. Helmer, Heath, *et al* [84] published several of their computer programs for analysis of spectra by isotope or by single gamma-ray components; these programs are very thorough and exhaustive in their treatment of the problem.

Finally, in 1968, Trombka and Schmadebeck [83] reported their method, which featured gain and baseline shift corrections and careful attention to interferences. They point out that the least squares technique sometimes gives negative results, and indicates that negative components may sometimes be correctly set to zero contribution. Great caution is required in doing so, however.

D.   Spectrum Stripping

Spectrum stripping is often inaccurate due to inherent compounding of statistical errors by successive subtractions. It is not surprising that the least squares technique has been more widely used, for it does not suffer from this limitation. Occasionally, however, successful application of stripping has been reported.

In 1963, Bailey and Ross[84] used stripping to obtain the intensity of a ^{18}F peak at 0.51 MeV, in spite of a very much more intense 0.56 MeV ^{76}As peak. They measured the oxygen content of gallium arsenide utilizing the reaction $^{16}O(t,n)^{18}F$.

Computerized spectrum stripping was reported by Blotcky, Watson, and Ogborn at Gatlinburg (published in 1963) [85], and by Salmon [71] in 1964.

Menon and Berry [86] used stripping in the analysis of pesticide residues in grain samples. Their program included spectrum smoothing, weighting of the data, and gain shift correction of the data. Components were subtracted beginning with the highest energy peak.

E.   Spectrum Smoothing

Typical activation analysis gamma-ray spectra frequently contain fewer counts, and hence greater statistical scatter, than the analyst would like. The desired peaks may be due to a short lived activity, and counting longer might result in the desired activity being overwhelmed by some longer-lived species. Or, the analyst may have to process a large number of samples in the time allotted by a counting schedule or an irradiation facility schedule. In any case, the analyst is often confronted with considerable scatter in his spectra, and the determination of peak energies, peak widths, and net peak areas is complicated considerably by the scatter. If he wishes to process his data with the computers, he will frequently find computer programs can handle smoothed data much more readily.

For these reasons, Gibbons and Shanks at Texas A&M made a thorough study of spectrum smoothing in 1962 [87]. Their first effort was to smooth the data by fitting a third order polynomial to five channels of data using the method of least squares. The equation used was

$$D_i = \frac{1}{35} \left[-3C_{i-2} + 12C_{i-1} + 17C_i + 12C_{i+1} - 3C_{i-2} \right] \tag{9}$$

where C_i was the observed number of counts in channel i and D_i is the smoothed number of counts in channel i.

While the new spectrum D was effectively smoothed, they chose to examine additional methods. Their second method involved Fourier transforms and mathematical low pass filters; the result was a very smooth spectrum, but unfortunately contained additional small peaks introduced by the smoothing process.

Filters for the detection of radar pulses in the presence of noise were used in developing their third method. The filtering function derived was

$$H(t) = \frac{1}{\sigma \sqrt{2\pi}} \, e^{-\frac{1}{2}\left(\frac{t}{\sigma}\right)^2} \tag{10}$$

where t was time, σ the half width at half maximum, and $H(t)$ the function. Substituting channel number for time permits application of the filter to spectra. Interestingly, this filter had a Gaussian shape, identical to the shape of the described spectral peaks.

To test the various smoothing methods, they used a computer program to estimate the amount of ^{24}Na activity in a series of low activity counts. The known amount was computed from a long count. By far the best results were achieved using the Gaussian filter described in the preceding paragraph.

In 1964, Savitzky and Golay [88] published a general paper on smoothing and differentiation of data by the least squares technique. They pointed up the advantages of smoothing the data to remove statistical

fluctuation, and indicated that smoothing is frequently mandatory in computer data reduction. As an example, consider a peak having a moderate amount of statistical scatter. To determine the peak position one needs a smooth curve through the points, since the channel with the largest number of counts very well may not be at the actual center of the peak. Figure 8 shows the efficiency of smoothing a small peak with considerable scatter in the data. Determination of peak position without the smoothed data is difficult, but it is easy with the smoothed data.

Savitzky and Golay [88] presented the "Simplified Least Squares" technique for smoothing. The basic assumptions they used are: (1) small regions of a spectrum may be represented by power functions of order two or greater, (2) observations on the energy (or time) axis are made at equal intervals (*i.e.* all channels have the same width), and (3) all fluctuations and errors are found in measured spectral values (*i.e.* counts/channel - all channel widths are the same). The least squares fit of
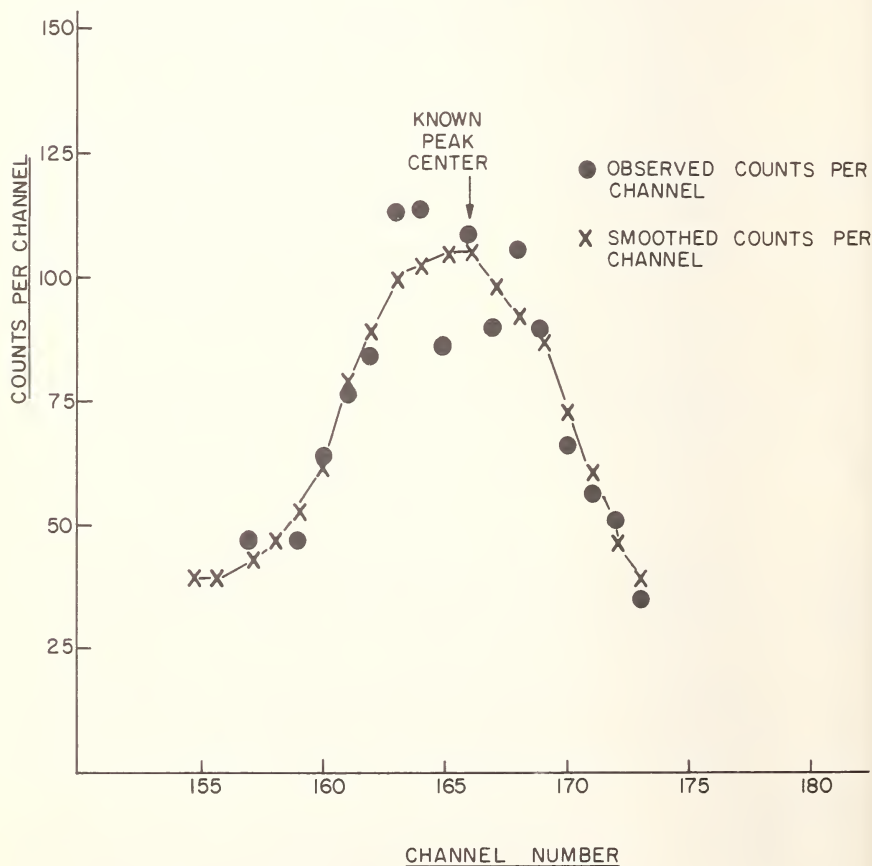
Figure 8.   Smoothing of very small total absorption peaks.

the power function is made in a general way once, and the results are integer constants which may be used for the actual smoothing.

Actually, smoothing is a special case of the more general term convolution. Using the derived integers, one can smooth a spectrum or smooth and differentiate it simultaneously. Consider a region of a spectrum containing five adjacent channels, and assume we wish to convolute the region with 3rd order polynomials. The convolution for smoothing is

$$D_i = \frac{1}{35} \left[-3C_{i-2} + 12C_{i-1} + 17C_i + 12C_{i+1} - 3C_{i+2} \right] \tag{11}$$

where C, and D, and i are the observed counts per channel, the smoothed counts per channel, and the channel number, respectively. The convolution to give the smoothed first derivative (E_i) is

$$E_i = \frac{1}{10} \left[-2C_{i-2} - C_{i-1} + C_{i+1} + 2C_{i+2} \right] \tag{12}$$

and the second derivative, F_i

$$F_i = \frac{1}{7} \left[2C_{i-2} - C_{i-1} - 2C_i - C_{i+1} + 2C_{i+2} \right] \tag{13}$$

and the third, G_i.

$$G_i = \frac{1}{2} \left[-C_{i-2} + 2C_{i-1} - 2C_{i+1} + C_{i+2} \right] \tag{14}$$

Figure 9 shows the behavior of the third derivative in the vicinity of a peak. See Figure 6 for the first and second derivatives.

This technique of data convolution is clearly a very simple and rapid one. For small amounts of data, hand computation is feasible, and for large amounts of data high speed digital computation is easy to program and takes little computer time.

In 1965, Blackburn [75] applied the smoothing technique to remove scatter in his reference spectra before applying the least squares method of spectral resolution. In this way, he attempted to reduce the statistical uncertainties with which his program had to contend.

In 1966, the present author presented his application of data convolution to the location of peaks in NaI(Tl) spectra [56]. The essence of the method is based on the fact that the smoothed first derivative changes from positive to negative, with increasing i, at the top of a peak. Using a computer routine to search for pairs of adjacent channels with $E_i > 0$ and $E_{i+1} < 0$ or by locating three channel such that $E_i > 0$, $E_{i+1} = 0$, and $E_{i+2} < 0$, the routine quickly locates peaks. Each "peak" is then tested for statistical significance. Of course, Compton edges and backscatter peaks are also located in this way, and it is important to have the program eliminate these artifact peaks.

The above method of peak location ran very fast on the computer, and demonstrated the ability to select peaks very successfully. Small, wide
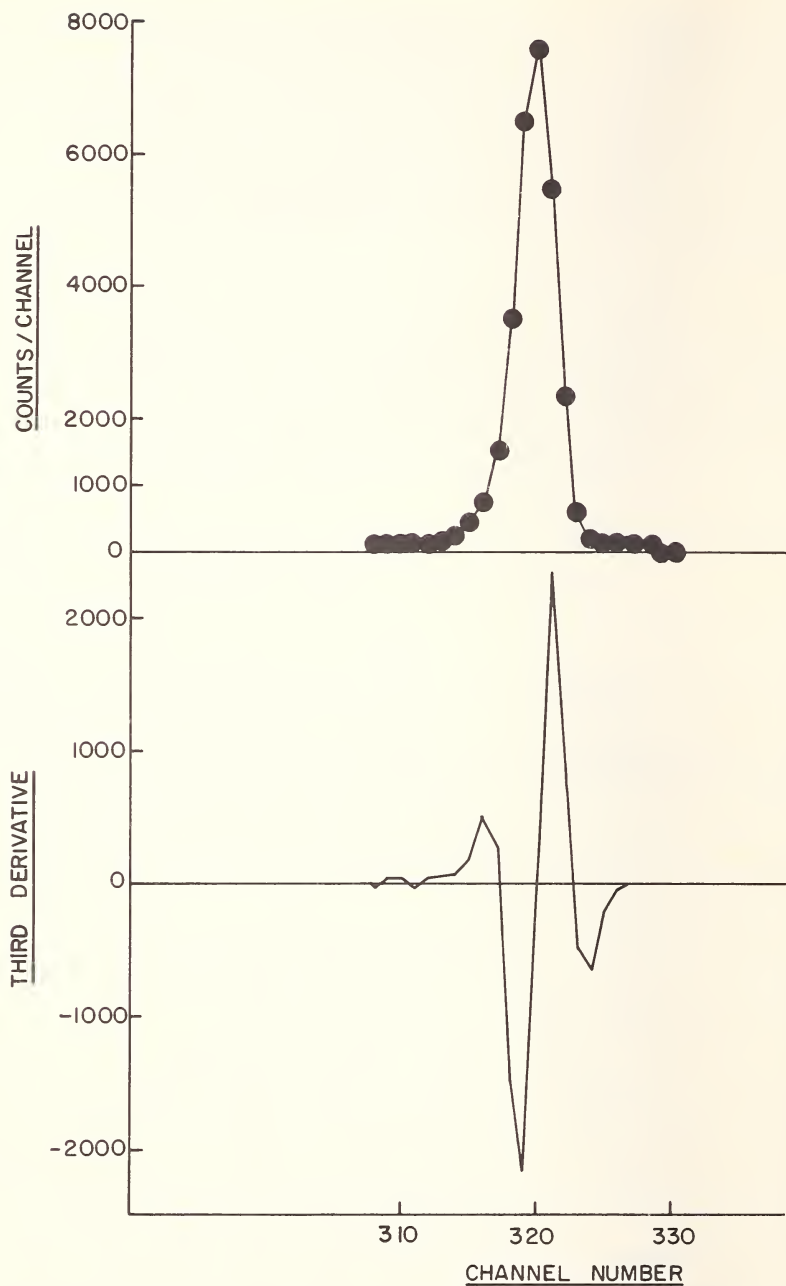
Figure 9.   Behavior of the smoothed third derivative of a total absorption peak.

peaks were sometimes overlooked, however, and this led to the investigation of proper interval width selection. That is, was the convolution using five channels of data the best choice, or should seven, nine, eleven, or more channels be used? After trying various methods of selecting proper widths, it was concluded that the number of channels used should be about the same as the calculated detector resolution at that energy [89]. Thus, in convoluting a spectrum taken on an NaI(Tl) detector, several interval widths would be used for different parts of the spectrum; narrow widths would be used in the low end of the spectra where peaks are narrow, and increasingly wider intervals would be used as energy, channel number, and resolution increase (See Fig. 12).

Applications of convolution to Ge(Li) detector peak location and net area computation are described in an article by the present author, published in 1968 [61].

A general discussion on peak location with digital computer techniques was given in 1968 by Morrey [90]. Extensive use of first through fourth derivatives permitted resolution of many adjacent peaks in an absorption spectrum of $\Phi_4 As UCl_6$.

F.   Decay Curve Analysis

Decay curve analysis is of interest to activation analysts who must resolve beta decay curves. Also those activating with for example, the (γ,n) reaction often must resolve a number of different positron emitters, all having their most prominent peak at 511 keV.

Several authors presented papers on decay curve analysis at Gatlinburg: Cumming [91], Gardner and Gardner [92], Nervik [93], and Shafer [95]. Subsequently, Munzel [70] presented his activation analysis decay curve program. Least squares resolution was used by Cumming, Nervik, and Munzel, while the method Fourier transforms was used by the Gardners and by Shafer. One example of each technique should suffice for the present purposes. Since the present author is familiar with Cumming's program, having used it on several occasions [95], that paper is chosen for presentation. The Gardners' paper is also briefly described since it is closer to the subject of this chapter, on data computation; the Shafer paper is more theoretical and is recommended to those concerned with the theoretical aspects of data reduction.

The least squares formulation [91] begins with a set of n measurements of counting rates f_i of the sample at times t_i.

$$f_i = \sum_{j=1}^{m} x_j \exp\ (-\lambda_j t_i) + v_i \tag{15}$$

Here x_j is the activity at $t=0$ of component j, and v_i is the residual which is

composed of statistical fluctuations and experimental errors. The least squares analysis then minimizes

$$\sum_{i=1}^{n} (v_i^2/\sigma_i^2)$$

where σ_i is the standard deviation of f_i. The results listed include the values of x_j and their standard deviations and other pertinent information. The program has an option to allow half lives to vary in an attempt to obtain a better fit. This option may be used to study half lives [91], and was so employed by the present author [95], although considerable care and judgment are required because the program was not specifically intended for this purpose.

The Gardners begin in a similar fashion

$$f(t) = \sum_{j=1}^{n} N_i^0 \exp (-\lambda_j t) \tag{16}$$

Here $f(t)$ is the observed activity at time t and N_j^0 the activity of the jth component when $t=0$. They state that an exponential series may be represented by a Laplace integral equation

$$f(t) = \sum_{j=1}^{n} N_j^0 \exp (-\lambda_j t) = \int_0^\infty g(\lambda) \exp (-\lambda t) d\lambda \tag{17}$$

where $g(\lambda)$ is a sum of delta functions. Further mathematical development need not be given here, but several advantages over the least squares method are stated by the authors. This method can handle growth and decay chains as well as decay only. No initial estimates of half lives are required, as they are with least squares methods, and the number of components comes out of the analysis, unlike the least squares method.

G.   MISCELLANEOUS TOPICS OF INTEREST

A number of interesting articles have appeared in the literature, and they are rather unique in their approach to the problems of data reduction and/or activation analysis. This section briefly mentions these varied, unrelated articles or topics. The only ordering in this section has been to list the activation analysis oriented articles first.

As part of their general activation analysis program containing peak area and least squares pulse height spectrum resolution capabilities, Wainerdi *et al* [51] 1964 reported the quadratic fitting technique. Very similar to the least squares technique, the quadratic technique also obtains the minimum sum of the squares of the differences between synthetic and observed spectra. However, the mathematics of the quadratic fitting yield non-negative or zero results, and the method is not plagued by negative results, unlike the least squares method.

Several papers on electric spectrum stabilization have appeared. Guinn and Lasch, at Gatlinburg, pointed out the difficulties gain and baseline shifts introduced into spectrum stripping calculations [96]. In 1964, Dudley and ben Haim reported a system for stabilizing both gain and baseline parameters for NaI(Tl) counters without adding any counts to the spectrum---most gain stabilizers need a spectral peak to fix on [97]. J. M. Ferguson, in 1968, reported on statistics of stablizing devices [98].

Resolution of gamma-ray spectra may be performed with a set of linear equations which express, in a straightforward way, the fact that one can add together spectra of individual isotopes to form a composite which is (approximately) identical with observed mixture. Such solutions were given at Gatlinburg by Blotcky, Watson, and Ogborn [85] and by Drew, Fite, and Wainerdi [64].

Computer programs to predict optimum experimental procedures prior to actual analysis have been given by Isenhour, Morrison, and Evans [99,100].

In the analysis of gamma-ray spectra, the analyst typically tries to obtain elemental contents of observed components. Computer programs for estimating upper limits for all elements making no observable contributions have been reported by Girardi *et al* [101] and the present author [102]. Very small upper limits (less than one ppm) were frequently obtained.

Hull and Gilmore [103], in 1964, described programs for activation analysis of lubricating oils. Picking energy bands, the program essentially performed a least squares decay curve analysis on each energy band.

In 1966, F. J. Kerrigan [104] published his linear programming method for activation analysis gamma-ray spectra. This approach minimizes the sum of residuals as opposed to the least squares technique which essentially minimizes the sum of the squares of the residuals. The computer searches for the minimum in the present method, while the least squares method solves a set of equations for the minimum. The present author feels that the least squares technique should consume only a small fraction of the computer time required for linear programming solutions on the same problem. Comparison of results by the two methods would be interesting.

In 1965, M. D. Cohan [105] discussed the application of on-line computers to activation analysis. A small digital computer served to collect data from several different analog to digital converters (*i.e.* serves as memories of several analyzers) and performed some control functions and was able to do simple calculations. The advantage of such a system is that answers are available quite soon after data collection is complete — no long turn around times occur, as happens with off-line computers for which data are converted to computer format, carried to the computer with a suitable program, and returned to the analyst hours later.

Activation analysts typically think of resolving spectra into individual isotopic components. It is also possible to analyze spectra for the intensity of each gamma ray, although this usually requires a great deal of computer time per spectrum. Programs accomplishing resolution have been published by Graber and Watson [106], in 1966, and Heath *et al* [107], in 1967.

Transformation of observed spectra to what would be observed with an ideal detector (Fig. 10) is known as the unfolding technique. Scofield described an unfolding technique at Gatlinburg [108], and Young and Burrus described a fine unfolding program in 1968 [109]. It is unfortunate that the technique is so time consuming.
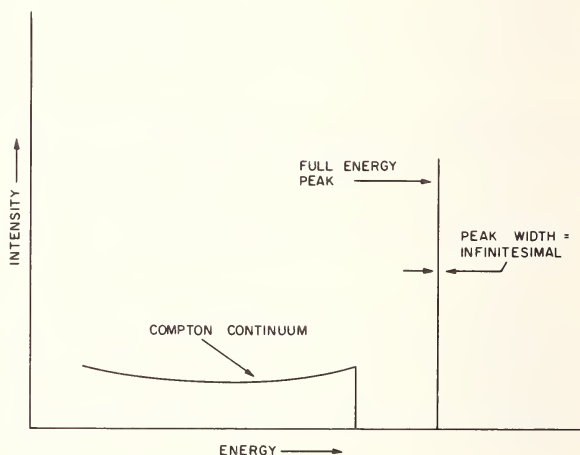
Figure 10. Representation of gamma-ray spectrum using an ideal detector.

Blackburn [110], in 1967, presented his studies of errors introduced in spectrum analysis by mathematical shifting of the spectra by nonintegral channel amounts.

Kowalski and Isenhour [111] describe their program for inputing an observed spectrum to the computer and obtaining a continuous, differentiable analytical function as a result.

Suppression of Compton continua by coincidence techniques has been studied by Galloway [112] with the interesting conclusion that little or no benefit is all that one should anticipate in many instances.

Carnahan, in his spectral resolution program, treated the spectra as histograms [113], 1964.

Gunnink, Levy, and Niday, in 1967, reported a computer program for the identification of isotopes contributing to Ge(Li) detector spectra by

comparing observed peaks against tabulated information on energies of gammas emitted by isotopes and their half lives [114].

IV.   Discussion of the Different Computation Methods

In the present section, many of the computation methods mentioned in Sections II and III are discussed. I shall try to indicate which techniques are currently in rather general use, and which are not, and the reasons they are or are not used. I shall also discuss, when appropriate, such topics as accuracy, precision, usefulness, speed and ease of computation, ease of putting information into the computer, and last, but very important, failures of each method.

In discussing these topics, it is logical and convenient to organize the present section to parallel the preceeding section, and discuss the computation of net peak areas, peak location, least squares, spectrum stripping, spectrum smoothing, and differentiation decay curve analysis, and miscellaneous topics.

A.   Net Peak Area Computation

The three main ways to estimate net peak areas are the classical, Covell, and Gaussian methods. The Gaussian method appeared shortly after the appearance of the NaI(Tl) detector, and was first used with data obtained on single channel analyzers. The Gaussian method was a long, tedious procedure for manual calculation, and when multichannel analyzers became available the complement subtraction method [22,13,23] greatly simplified the task of estimating the intensity of the gamma rays from the components of the observed spectrum. This technique, however, imposed rather severe restrictions on the experimental procedure since it was necessary to have available several sources of activity and count them as needed for the subtraction.

When Covell [21] demonstrated the applicability and the accuracy of his method, the estimation procedure became markedly simpler, for the procedure reduced to counting the unknown and a standard and computing net peak areas using Covell's quick and easy method. Subsequently, Westermark and Sjostrand [28] demonstrated the accuracy of the classical method for activation analysis.

At the present time, the Covell and classical methods are widely used in activation analysis calculations. They are clearly the simplest, most direct way to utilize the information provided by gamma-ray spectrometers. Accuracies of the two methods have been discussed by Bowen and Gibbons in their text on activation analysis [115]. They pointed out that the two methods have comparable accuracy under most circumstances, but the Covell method is more accurate for small peaks resting on relatively large Compton continua.

Two factors to be considered in discussing accuracy are peak shape change and peak position change. If either change occurs, then the Covell method may become quite inaccurate unless great care is used in choosing the channels to use as peak boundaries. On the other hand, the classical method is not sensitive to these changes since it includes the entire peak area. In the classical method, the analyst seeks to compute the net peak area so as to include as much of the peak as possible by selecting peak boundary channels where the peak becomes indistinguishable from the continuum or background upon which it rests. If one chooses the Covell boundaries similarly, then comparable accuracy is obtained.

Proper selection of peak boundary channels for Ge(Li) detector showing considerable peak shape change has recently been discussed by the present author [61]. Considerable resolution loss was found at moderate and high counting rates as well as long term variations in peak positions (but see the comments at the end of Section III,A,5, however). It was found that the classical method showed little sensitivity to these changes, and that the Covell method would too, if boundary channels were suitably chosen to include the whole peak.

The peak area method generally works very well unless there are interfering peaks. This point has been discussed in detail by Plantin [53] who illustrated the resultant inaccuracies in the classical method very clearly. It seems apparent that proper implementation of the Covell method would clearly give a considerably more accurate result in instances where the position of the interfering peak was at the side of the peak of interest. Covell boundaries could be chosen to minimize the effect of the interference.

To summarize the peak area method, it may be stated that both the Covell and classical methods are widely used and generally give accurate results provided there are no interfering peaks. Each method is quick and easy to compute by hand or by computer.

B.   Peak Location

The location of spectral peaks by computer relieves the analyst of considerable tedium. As early as 1960, Kuykendall and Wainerdi used a computer program to locate peaks in their studies of automated activation analysis [26]. Subsequently, others have reported peak location programs [50,26,57,53,56,61]. It is presumed that most of these methods are still in use at these authors' laboratories, although Kuykendall's program was abandoned in favor of the more general programs developed by Wainerdi and co-workers [51].

The accuracy of a peak location program may be measured by its success in locating spectral peaks. There is little information on this point in the literature, so the author will comment on his own program's

accuracy [61]. This program locates a peak by first finding sign changes in the smoothed first derivative as has been discussed earlier. For NaI(Tl) spectra, it incorporates the concepts developed in reference [116], that the smoothing interval width must be changes so as to account for resolution change. For example, if the spectrometer is calibrated so that, for example, the ^{51}Cr peak (320 keV) is channel 32 and the ^{60}Co peaks (1173 and 1333 keV) are in channels 117 and 133, respectively, the smoothing interval widths used are: 5 channels from channels 21 to 59, 7 from 60 to 115, 9 from 116 to 190, 11 from 191 to 285, and 13 from 286 to 384.

For our Ge(Li) detectors, we use a five channel interval width and a gain calibration of 1.0 keV/channel. Thus, 1600 channels covers the energy range $0-1.6$ MeV and 3200 channels $0-3.2$ MeV. In practice, the 1600 channel spectrum is sufficient for most of our purposes.

With these experimental arrangements, the program very seldom misses a peak. Missed peaks are typically very small, less than 20 counts high, and peaks this small are of little use for activation analysis The program occasionally has trouble with complex peaks, although the smoothed third derivative is presently being investigated as a remedy for this problem; this topic is discussed in another paper at the present conference [116]. In favor of the program, it must be stated that it is considerably more accurate at peak location than all but the most careful analyst.

Peak location programs should also be able to compute accurate net peak areas which means they must determine peak boundary channels correctly. The data in [61] show the efficacy of our boundary channel selection method; this point is covered in Section A, above.

C. Least Squares

The power of the least squares technique for gamma-ray spectrum resolution was demonstrated in 1961 by Salmon [39]. In the ensuing years, numerous workers published their versions, as we have enumerated in Section III. In the absence of extremely stable counting systems (*i.e.* those systems having electronic gain and baseline stabilization) gain and baseline shifts frequently resulted in grossly inaccurate answers. Consider, for example, the fitting of a ^{64}Cu peak (511 keV), found in channel 51 in the reference spectrum to a ^{64}Cu peak which has shifted to channel 52 in the mixture spectrum. The answer will be seriously in error, and will probably be underestimated.

Parr and Lucas [68], in 1964, published their very effective method of coping with these shifts by measuring them and using the computer to correct their data. Subsequently, Schonfeld has programmed the

computer to relieve the analyst of the chore of measuring the shifts [78], and has achieved vastly better accuracy at low counting rates [79].

Typical least squares programs require carefully prepared reference spectra as input information to the program, and they may be quite some trouble to prepare. In this sense, least squares programs are somewhat troublesome to use.

In using least squares programs, it is important to know which isotopes contribute to the observed spectra, and also which ones do not. Poor results are obtained when a reference isotope makes no contribution to the mixture spectrum or when the mixture contains an isotope not included in the reference spectra. Usually, the program will notify the analyst that the fit is poor, and he must repeat the fit with a different set of spectra. Sometimes, examination of the residuals provides a clue as to the missing reference spectrum, if their is only one missing. What happens to the residuals when more complicated problems arise depends on the individual case.

Of course, if the analyst has many complex spectra to analyze and they are all quite similar in that the same isotopes contribute to each, the least squares technique may very well be the best approach, particularly if overlapping peaks cause problems with peak area measurements.

D.   Spectrum Stripping

This method of analysis has largely been abandoned because of the greater accuracy of the least squares technique or the greater resolution of the Ge(Li) detectors. Further discussion is not necessary.

E.   Spectrum Smoothing and Differentiation

Spectrum smoothing is a mathematical technique which filters out much of the statistical scatter occurring in pulse height spectra. Smoothed spectra are frequently useful for the determination of peak energy, net peak area, and in area computations following spectrum stripping. Smoothed derivatives are useful for computer peak location, peak boundary channel location, and for studies of compound peaks. The efficacy of smoothing was clearly demonstrated by Gibbons [87], as indicated in section III.

It is interesting to test the smoothing and differentiating technique by applying it to a smooth function, $y = x^3$. We compute the value of y at intervals of $\Delta x = 1$, then insert these y values into the equations given in section III,E and compute the smoothed values of y and the smoothed derivatives. Table 1 shows the results for all these computations, omitting the first two and last two numbers since it is not possible to smooth all the values. In a 400 channel spectrum, for example, channels 1, 2, 399, and

Table 1. Examples of data convolution on a smooth set of data.

x	$y = x^3$	Moving average	Smoothed curve	First derivative		Second derivative	
				Computed	Smoothed	Computed	Smoothed
-3	- 27	---	---	---	---	---	---
-2	- 8	---	---	---	---	---	---
-1	- 1.0	- 7.0	- 1.0	+ 3.0	+ 6.4	-6.0	-6.0
0	0.0	0.0	0.0	0.0	3.4	0.0	0.0
1	1.0	7.0	1.0	3.0	6.4	+ 6.0	+ 6.0
2	8.0	20.0	8.0	12.0	15.4	12.0	12.0
3	27.0	45.0	27.0	27.0	30.4	18.0	18.0
4	64.0	88.0	64.0	48.0	51.4	24.0	24.0
5	125.0	155.0	125.0	75.0	78.4	30.0	30.0
6	216.0	252.0	216.0	108.0	111.4	36.0	36.0
7	343.0	---	---	---	---	---	---
8	512.0	---	---	---	---	---	---

400 cannot be smoothed since data in channels -1, 0, 401, and 402 would be required by the equations above. Column 2 in the Table gives the computed y value and column 3 the moving average computed over a five point interval. Column 4 gives the smoothed y values computed over a five point interval by simplified least squares calculation. The smoothed and computed y values are identical while moving average only poorly approximates the correct y values. The computed and smoothed derivatives agree almost identically with the sole exception of the first derivative at $x = 0$. Presumably, the inflection in the curve is responsible for this minor error.

Application of the smoothed third derivative to complex peak studies is shown in Figure 11 [116]. The most important consideration in applying this technique is to use a smoothing interval which contains roughly the same number of channels as would be spanned by the full width at half maximum, changing the interval width when necessitated by the characteristics of Ge(Li) or NaI(Tl) detectors [89].

An example of a smoothed spectrum is shown in Figure 12 which shows a ^{60}Co spectrum accumulated at 4.0 keV/channel. The smoothed spectrum is indicated by the line segments joining the values of D_i, and the raw data are the points. The smoothing interval was 19 channels wide. Note how well the smoothed spectrum removes the statistical scatter, accurately pinpoints the center of the peak (and hence its energy), and gives a good indication of the peak width.

The smoothed first derivative, computed from the data points illustrated in Figure 10 is shown in Figure 13. The derivative is positive on the left hand side of the peak and negative on the right. The sign change in the derivative is the basis of a convenient method of locating peaks in a spectrum [56,61]. In computing the peak area above a baseline
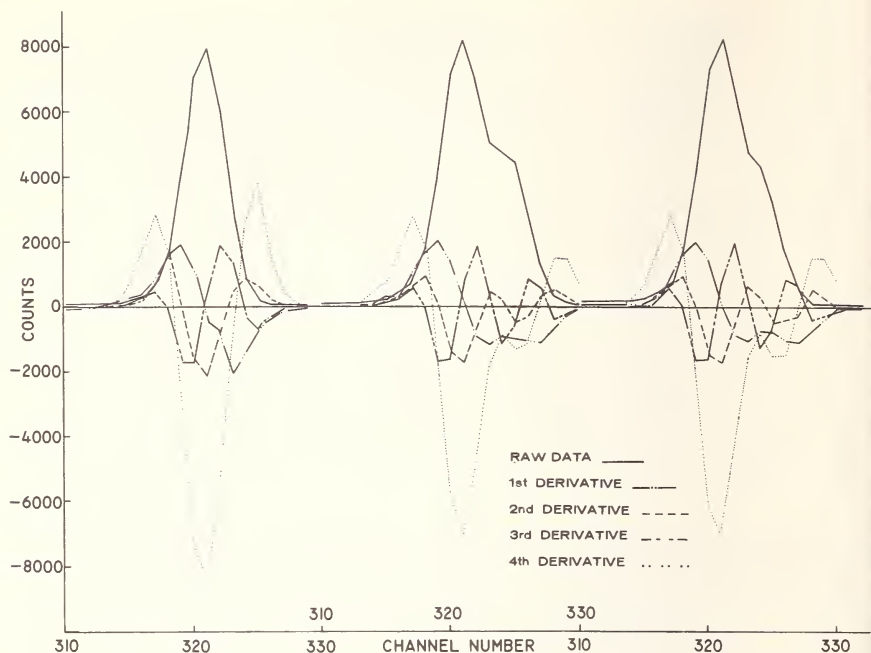
Figure 11. The left hand peak is a simple peak ^{51}Cr observed with a Ge(Li) detector. Observed data points are connected by straight line segments. The remaining two peaks are composites of two ^{51}Cr peaks observed with slightly different analyzer baseline settings and different live times.

drawn intersecting the spectrum at the sides of a peak, the smoothed first derivative is used to locate these intersections. The right hand boundary channel is located where the derivative changes from negative to positive, for example. Comparison of the slope of the baseline with the smoothed derivative (which is another way of computing the slope) is a convenient way of establishing boundary channels for unsymmetrical peaks.

The smoothed second derivative provides another way of locating peaks [57,89]. It forms deep, negative minima at the peak locations. The sign change in the first derivative is easier to implement, however.

The smoothed third derivative is useful in studying compound peaks which are combinations of two or more peaks. The behavior of the smoothed third derivative at a single peak is shown in Figure 9. The derivative is essentially zero until well up the left side of the peak, then rises to a small positive value, quickly descends to a large negative value, very rapidly swings to a large positive value near the top, and descends to a small negative value on the right side of the peak. The most significant aspect of the third derivative is its sensitivity to the central part of the peak. This behavior and the use of the third derivative for studying
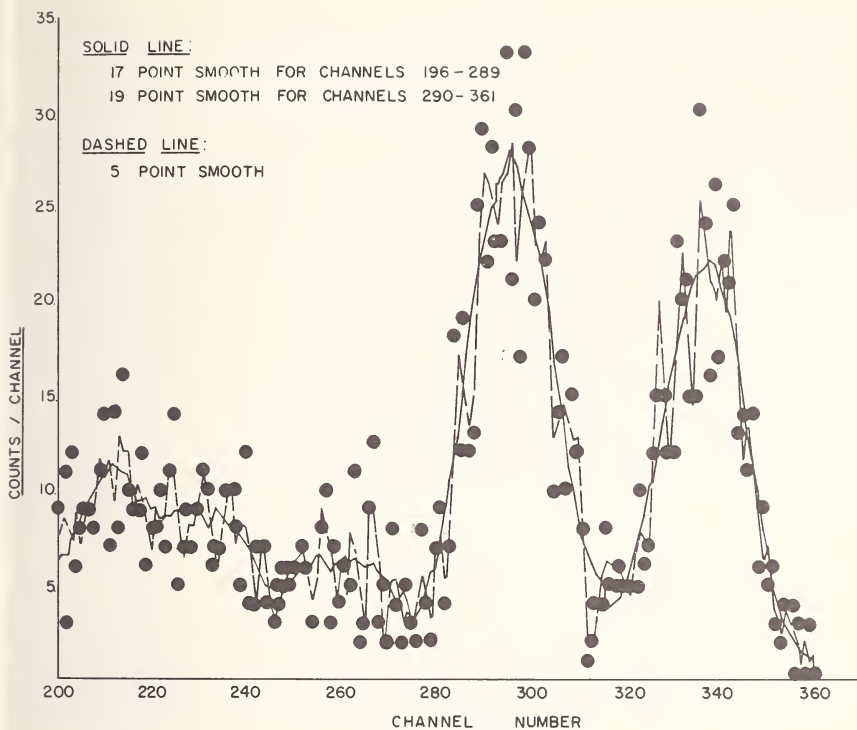
Figure 12. An example of a smoothed cobalt-60 gamma-ray system. Note how effectively the 17- and 19-point smoothings remove statistical scatter in spite of the very low number of counts and large amount of scatter.

compound peaks was recently pointed out by Morrey [90]. Application of the third derivative, Figure 12, to a compound peak clearly indicates that the peak is compound. The smoothed spectrum also shows two peaks, but the smoothed first derivative does not. While it is perfectly clear to the eye that the peak in Figure 12 is compound, a computer could easily fail to recognize that fact.

V. The Future

The future may be predicted on the basis of past experience. As anyone who has purchased common stocks knows, this is risky business. One can easily predict better detectors with larger geometries and sharper resolution, better computation techniques, and improved experimental techniques. Clearly, improved resolution will make life easier in some respects, but will 4000 channels be sufficient to take advantage of this resolution? In some instances, they surely will not, and while the data are simpler to interpret in any region of the spectrum, the larger number of
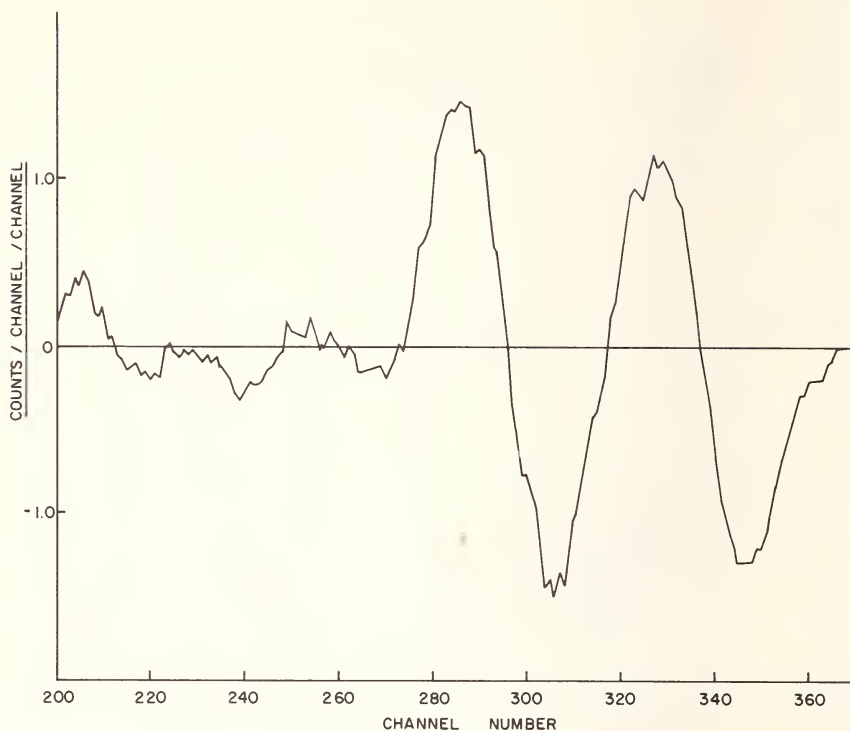
Figure 13.　The smoothed first derivative of the gamma-ray spectrum in Figure 12.

channels will be more work to interpret, and the computer techniques will be relatively more important.

Another way of predicting the future is to imagine the combination of two or more apparently unrelated fields, namely, activation analysis and cybernetics. This combination led to the "grand scheme" which was originally conceived by R. E. Wainerdi and D. Gibbons at Texas A&M, and has subsequently received additional ideas by the present author. Basically, the idea is to feed into a computer enormous quantities of information on various analytical chemical techniques of all types. When considering an analysis, the analyst would supply the computer with the available information on the material under consideration together with information on the facilities at his disposal. The computer would consult its data bank and respond with some text such as, "Determination of gold in these samples at the ppb level is definitely feasible in samples of the specified composition. Irradiate with thermal neutrons for three hours at standard flux, wait 10 days for ^{24}Na to decay, and count on NaI(Tl) spectrometer". Or, the answer might be to use atomic absorption, gas chromatography, etc. Upon submission of the experimental data to the

computer, exhaustive checks of the resultant computation would be made using information from the data bank.

We shall close this discussion of the future with our own favorite concept, Interactive Activation Analysis. The first word, *interactive* (please note we did not write *iterative*), means interaction between man, spectrometer, and computer. The computer would continually monitor the output of the spectrometer, computing and evaluating while the counting is in progress. The computer could control the counting time so that the sample is counted just long enough to get the desired statistical accuracy and then request the system to change samples. Computed final results would, of course, be available within seconds of count completion. Optimization of counting techniques would be implemented by allowing the computer to adjust the spectrometer. Computer results could be tabulated when all counting is completed, and the results could be collated with results of previous runs. The computer could even keep track of your samples and spectra.

VI. References

[1]   de Hevesy, G., "Radiochemical Methods of Analysis", Vol. I, IAEA, Vienna, 1965, p. 3.

[2]   de Hevesy, G., K. danske vidensk. Sels. Mat. fys. Medd. **14**, 5 (1936).

[3]   de Hevesy, G., "Adventures in Radioisotope Research", Pergamon Press, New York, 1962, Vol. I, p. 60.

[4]   Seaborg, G. T., and Livingood, J. J., J. Amer. Chem. Soc. **60**, 1784 (1938).

[5]   Smales, A. A., Analyst **77**, 778 (1952).

[6]   Atchison, G. J., and Beamer, W. H., Anal. Chem. **24**, 1813 (1952).

[7]   Leddicotte, G. W., and Reynolds, S. A., ASTM Bulletin, 188, 29 (1953).

[8]   Brooksbank, W. A., Leddicotte, G. W., and Mahlman, H. A., J. Phys. Chem. **57**, 815 (1953).

[9]   Connally, R. E., and Leboeuf, M. B., Anal. Chem. **25**, 1095 (1953).

[10] Kahn, B., and Lyon, W. S., Nucleonics **11**, No. 11, 61 (1953).

[11] Lyon, W. S., and Reynolds, S. A., Nucleonics **13**, No. 10, 61 (1955).

[12] Morrison, G. H., and Cosgrove, J. F., Anal. Chem. **27**, 811 (1955).

[13] Upson, U. L., Connally, R. E., and Leboeuf, M. B., Nucleonics **13**, No. 4, 39 (1955).

[14] Breitenberger, E., Progr. in Nuclear Phys. **4**, 56 (1955).

[15] Connally, R. E., Anal. Chem. **28**, 1847 (1956).

[16] Putnam, J. L., and Taylor, W. H., Int. J. Appl. Radiat. Isotopes **1**, 315 (1957).

[17] Cook, C. S., American Scientist **45**, 245 (1957).

[18] Cosgrove, J. F., and Morrison, G. H., Anal. Chem. **29**, 1017 (1957).

[19] Heath, R. L., IDO-16408 (1957).

[20] Halfhill, D. W., Nucleonics **16**, No. 12, 55 (1958).

[21] Covell, D. F., Anal. Chem. **31**, 1785 (1959).

[22] Lee, W., Anal. Chem. **31**, 800 (1959).

[23] Bate, L. C., and Leddicotte, G. W., ORNL-2866, p. 33, 1959.

[24] Salmon, L., Analytical Abstracts 6, No. 3352 (1959).

[25] Gardner, D. G., Gardner, J. C., Lausch, G., and Meinke, W. W., Rev. Sci. Ins. **31**, 978 (1959).

[26] Kuykendall, W. E., and Wainerdi, R. E., *et al*, Proceedings, IAEA Conf. "The Uses of Radioisotopes in Phys. Sci. & Industry", Copenhagen, Denmark, 1960.

[27] Chester, R. O., and Burrus, W. R., ORNL-3016, 249 (1960).

[28] Westermark, T., and Sjostrand, B., Int. J. Applied Radist. Isotopes, **9**, 1 (1960).

[29] Covell, D. F., Anal. Chem. **32**, 1086 (1960).

[30] Guinn, V. P., and Wagner, C. D., Anal. Chem. **32**, 317 (1960).

[31] Gilbert, C. W., Int. J. Appl. Radiat. Isotopes **8**, 230 (1960).

[32] Crouthamel, C. E., "Applied Gamma-Ray Spectrometry", Pergamon Press, New York, 1960.

[33] Anders, O. U., and Beamer, W. H., Anal. Chem. **33**, 226 (1961).

[34] Anders, O. U., Dow Chemical Co. publication (1961).

[35] Anders, O. U., Anal. Chem. **33**, 1706 (1961).

[36] Bock-Werthmann, W., and Schulze, W., Proceedings, 1961 Intl. Conf. "Modern Trends in Activation Analysis", College Station, Texas, Dec. 1961, p. 145.

[37] Fite, L. E., Gibbons, D., and Wainerdi, R. E., TEES-2671-1 (1961).

[38] Ehmann, W. D., Proceedings, 1961 Intl. Conf. "Modern Trends in Activation Analysis", College Station, Texas, Dec. 1961, p. 41.

[39] Salmon, L., AERE-R 3640, published without appendix in Nucl. Instrum. Methods **14**, 193 (1961).

[40] Covell, D. F., and Euler, B. A., Proceedings, 1961 Intl. Conf., "Modern Trends in Activation Analysis", College Station, Texas, Dec. 1961, p. 12.

[41] Fite, L. E., Gibbons, D., and Wainerdi, R. E., Proceedings, 1961 Intl. Conf., "Modern Trends in Activation Analysis", College Station, Texas, Dec. 1961, p. 102.

[42] DeSoete, D., and Hoste, J., Proceedings, 1961 Intl. Conf., "Modern Trends in Activation Analysis", College Station, Texas, Dec. 1961, p. 59.

[43] Morgan, W. R., Proceedings, 1961 Intl. Conf., "Modern Trends in Activation Analysis", College Station, Texas, Dec. 1961, p. 16.

[44] Zimmerman, W., Rev. Sci. Instrum. **32**, 1063 (1961).

[45] Heath, R. L., Proceedings, 1961 Intl. Conf., "Modern Trends in Activation Analysis", College Station, Texas, Dec. 1961, p. 155.

[46] Savitzky, A., Anal. Chem. **33**, 25A (1961).

[47] O'Kelley, G. D., NAS-NS-3107 (1963).

[48] Lightowlers, E. C., Anal. Chem. **35**, 1285 (1963).

[49] Decat, D., Van Zanter, B., and Leliaert, G., Anal. Chem. **35**, 845 (1963).

[50] Borella, A., and Guzzi, G., EUR 531e (1964).

[51] Wainerdi, R. E., Fite, L. E., Gibbons, D., Wilkins, W. W., Jimenez, P., and Drew, D., Symposium on Radiochemical Methods of Analysis, Salzburg, Austria, Vol. II, (1964), p. 149.

[52] Choy, S. C., and Schmitt, R. A., Nature **205**, No. 4973, 758 (1965).

[53] Plantin, L., Proceedings, 1965 Intl. Conf., "Modern Trends in Activation Analysis", College Station, Texas, April 1965, p. 91.

[54] Mundschenk, H., Nucl. Instrum. Methods **44**, 325 (1966).

[55] Mundschenk, H., Nucl. Instrum. Methods **45**, 77 (1966).

[56] Yule, H. P., Anal. Chem. **38**, 103 (1966).

[57] Mariscotti, M. A., Nucl. Instrum. Methods **50**, 309 (1967).

[58] Guzzi, G., Pauly, J., Girardi, F., and Dorpema, B., EUR 3469e (1967).

[59] Girardi, F., Guzzi, G., and Pauly, J., Radiochim. Acta. **7**, 202 (1967).

[60] Helmer, R. G., Heath, R. L., Putnam, M., and Gipson, D. H., Nucl. Instrum. Methods **57**, 46 (1967).

[61] Yule, H. P., Anal. Chem. **40**, 1480 (1968).

[62] Schmitt, R. A., private communication, 1968.
[63] Salmon, L., NAS-NS-3107, (1963), p. 165.
[64] Drew, P. D., Fite, L. E., and Wainerdi, R. E., NAS-NS-3107, p. 237 (1963).
[65] Nicholson, W. L., Schlosser, J. E., and Brauer, F. P., NAS-NS-3107, (1963), p. 254.
[66] Nicholson, W. L., Schlosser, J. E., and Brauer, F. P., Nucl. Instrum. Methods 25, 45 (1963).
[67] Trombka, J. I., NAS-NS-3107, (1963), p. 183.
[68] Parr, R. M., and Lucas, H. F., Jr., IEEE Trans. Nucl. Sciences, NS-11 No. 3, 349 (1964).
[69] Helmer, R. G., Metcalf, D. D., Heath, R. L., and Cazier, G. A., IDO-17015 (1964).
[70] Munzel, H., Symposium on Radiochemical Methods of Analysis, Salzburg, Austria, 1964, Vol. II, p. 141.
[71] Salmon, L., Symposium of "Radiochemical Methods of Analysis", Salzburg, Austria, Vol. II, (1964), p. 125.
[72] Yule, H. P., Invited Paper at Conf. on Spectroscopy, Instrumentation and Chemistry, San Francisco, (1964).
[73] Pasternack, B., and Liuzzi, A., Technometrics 7, 603 (1965).
[74] Schonfeld, E., Proceedings, 1965 Intl. Conf. "Modern Trends in Activation Analysis", College Station, Texas, April 1965, p. 279.
[75] Blackburn, J. A., Anal. Chem. 38, No. 8, 1000 (1965).
[76] Wohlberg, J. R., Proceedings, 1965 Intl. Conf., "Modern Trends in Activation Analysis", College Station, Texas, April 1965, p. 13.
[77] Emery, J. F., Dyer, F. F., Alexander, T., and Schonfeld, E., ORNL-P-1127.
[78] Schonfeld, E., Kibbey, A. H., and Davis, W., Jr., Nucl. Instrum. Methods 45, 1 (1966).
[79] Schonfeld, E., Nucl. Instrum. Methods 52, 177 (1967).
[80] Pasternack, B. S., and Liuzzi, A., invited paper, 126th Annual Meeting of Amer. Statistical Association, Los Angeles, 8-15, 1966.
[81] Liuzzi, A., and Pasternack, B. S., Nucl. Instrum. Methods 57, 229 (1967).
[82] Helmer, R. G., Heath, R. L., Schmittroth, L. A., Jayne, G. A., and Wagner, L. M., Nucl. Instrum. Methods 47, 305 (1967).
[83] Trombka, J. I., and Schmadebeck, R. L., Nucl. Instrum. Methods 62, 253 (1968).
[84] Bailey, R. F., and Ross, D. A., Anal. Chem. 35, 791 (1963).
[85] Blotcky, A. J., Watson, B. T., and Ogborn, R. E., NAS-NS-3107, p. 276 (1963).
[86] Menon, M. P., and Berry, D. W., Anal. Chim. Acta 38, 349 (1967).
[87] Gibbons, D., and Shanks, J., in Fite, L. E., et al TEES-2671-2, 1962, p. 5-27.
[88] Savitzky, A., and Golay, M. J. E., Anal. Chem. 36, No. 8, 1627 (1964).
[89] Yule, H. P., Nucl. Instrum. Methods 54, 61 (1967).
[90] Morrey, J. R., Anal. Chem. 40, 905 (1968).
[91] Cumming, J. B., BNL-6470.
[92] Gardner, D. G., and Gardner, J. C., NAS-NS-3107, p. 33 (1963).
[93] Nervik, W. E., NAS-NS-3107, p. 9 (1963).
[94] Shafer, R. E., NAS-NS-3107, p. 41 (1963).
[95] Yule, H. P., Nucl. Phys. A94, 442 (1967).
[96] Guinn, V. P., and Lasch, J. E., NAS-NS-3107, p. 243 (1963).
[97] Dudley, R. A., and ben Haim, A., Symposium on Radiochemical Methods of Analysis, Salzburg, Austria, 1964, Vol. II, p. 69.
[98] Ferguson, J. M., Nucl. Instrum. Methods 58, 318 (1968).
[99] Isenhour, T. L., and Morrison, G. H., Anal. Chem. 36, No. 6, 1089 (1964).
[100] Isenhour, T. L., Evans, C. A., Jr., and Morrison, G. H., Proceedings, 1965 Intl. Conf., "Modern Trends in Activation Analysis", College Station, Texas, April 1965, p. 123.

[101]   Pauly, J., Guzzi, G., Girardi, F., and Borella, A., Nucl. Instrum. Methods **42**, 15 (1966).
[102]   Yule, H. P., Anal. Chem. **38**, 818 (1966).
[103]   Hull, D. E., and Gillmore, J. T., Anal. Chem. **36**, No. 11, 2073 (1964).
[104]   Kerrigan, F. J., Anal. Chem. **38**, No. 12, 1677 (1966).
[105]   Cohan, M. D., Proceedings, 1965 Intl. Conf., "Modern Trends in Activation Analysis", College Station, Texas, April 1965, p. 157.
[106]   Graber, H. D., and Watson, D. D., Nucl. Instrum. Methods **43**, 355 (1966).
[107]   Heath, R. L., Helmer, R. G., Schmittroth, L. A., and Cazier, G. A., Nucl. Instrum. Methods **47**, 281 (1967).
[108]   Scofield, N. E., NAS-NS-3107, p. 108 (1963).
[109]   Young, M. H., and Burrus, W. R., Nucl. Instrum. Methods **62**, 82 (1968).
[110]   Blackburn, J. A., Anal. Chem. **39**, 100 (1967).
[111]   Kowalski, B. R., and Isenhour, T. L., Anal. Chem. **40**, 1186 (1968).
[112]   Galloway, R. B., Nucl. Instrum. Methods **55**, 29 (1967).
[113]   Carnahan, C. L., Nucl. Instrum. Methods **30**, No. 2, 165 (1964).
[114]   Gunnink, R., Levy, H. B., and Niday, J. B., UCID-15140 (1967).
[115]   Bowen, H. J. M., and Gibbons, D., Oxford at the Clarendon Press, 1963.
[116]   Yule, H. P. (See this volume, p. 1256).

COMPUTATION TECHNIQUES

Synopsis of Discussions

WERNER SCHULZE, *Chairman*

Institute for Inorganic Chemistry
Free University
Berlin, Germany

The session on Computation Techniques overlaps partially with Session 15 on Data Handling. The 9 papers presented during the session give new details on the evaluation of the gamma-ray spectra. Two of the papers (35,87) gave a complete activation analysis system. In the first one, the observed gamma-ray spectrum is built-up stepwise from a library of observed spectra until no better representation of the experimental data can be found. The constancy of the magnitude and spectrum of neutrons has been assumed. The inclusion of data for different decay times greatly increases the power of the method. The multitude of equations can be reduced by considering elements instead of radio-isotopes for calculation. Pasternak takes into account possible variations in gain and/or baseline shift. For each reference spectrum two additional parameters are added. For goodness of fit the residuals are not used directly. The ratio of the sum of squares of successive differences in the residuals and the sum of squared residuals provides a better indicator. The success of this procedure was demonstrated on experimental data of total body counting, analyzing for Ra-226, K-40 and Cs-137.

The necessity of having a gain-changing computer program (rather than an electronic device) is recognized by Steyn. This program has been made extremely simple by first using for an enlargement reduction of the spectrum to a smaller size and then interpolating the missing channel-values necessary at enlargement by Aitken's method. The method simultaneously provides some smoothing and therefore must be handled carefully to avoid losses in fine structure. Application of this technique seems to be very useful for finding the Compton continuum that corresponds to an intermediate peak energy. From the several possibilities of errors which are stressed by Lucas, I wish to mention the handling of channels with zero counts. The proposal of assigning to all these channels a variance of 1 seems one suitable possible way to overcome this difficulty. That geometrical effects, *i.e.* variations in sample height (of $\pm 5\%$) can affect strongly the Compton region and also

the width of a peak is well known, but it is often not recognized that a missing nuclide can give the same effect in the residuals and therefore can lead to unexpected errors. Duc *et al.* show that evaluation of residuals only is insufficient if trace amounts have to be considered. Instead of this, the examination of the correlation coefficient of any trace component is very useful as is demonstrated with a model sample containing Cu-64, Na-22 and Mn-54. The work previously reviewed considers spectra from NaI scintillators. New problems arise with Ge(Li) detectors, because of their good resolution. It turned out in discussion that some 20 elements can be determined with germanium detectors instead of only 10 elements using NaI crystals, but the success depends of course upon the matrix. Two papers gave useful procedures for finding qualitative and quantitative composition of a mixture. The method of Gunnink relies upon information from a library of decay schemes instead of standard spectra and is highly recommended as a comparison to the method of working with spectral standards. Ralston *et al.* give a method for evaluation of peak areas in Ge(Li) gamma-ray spectra. First, a baseline is constructed by averaging and replacing cycles with the experimental data. Then the peaks can be evaluated by integration.

The necessity of resolving double-peaks is recognized by Yule, in which the second and third derivatives of the peak are used. The method works at high counts/channel but has increasing limitations with small peaks.

A manual resolution method of complex peaks is given by Lukens, using the information of the normal error curve. It is demonstrated that this procedure gives good results.

COMPUTER ANALYSIS OF GAMMA-RAY SPECTRA: VALIDITY OF THE RESULTS[1]

Henry F. Lucas, Jr., and David N. Edgington

Radiological Physics Division
Argonne National Laboratory
Argonne, Illinois 60439

I. Introduction

The mathematical treatment used for computer analysis of gamma-ray spectra obtained from NaI(Tl) crystals and multichannel analyzers has assumed many forms [1,2,3]. Some methods were developed from previously used manual methods of calculations, while others attempted to use statistical evaluation techniques. In all cases, non-random instrumental effects, such as channel dropout and pulse pileup were evident.

Large numbers of computer programs have been written and perhaps now it is high time that we consider whether we are asking the computer the correct questions concerning the input data and the results. This paper will consider several questions which have not been generally recognized and others which are well-known.

II. Method

Gamma-ray spectra were obtained with a 4 in. × 2 in. NaI(Tl) crystal with 6% resolution for ^{137}Cs. The spectra were accumulated in 511 channels with a ND-120 multichannel analyzer over the energy range 0.06 to 3.2 MeV. All instrumentation was located in an underground counting room in which ^{222}Rn was controlled and was always less than 0.01 pCi/liter. In addition line voltage was regulated to ± 0.3V, and the temperature to ± 0.1 °C. The background counting rate of 108 counts/min (cpm) was always stable within counting statistics of a 200 minute count. All spectra were accumulated on paper tape or computer-compatible 1/2 in. wide magnetic tape. All samples are counted in a highly reproducible geometrical configuration and are 10.0 ± 0.2 ml in volume.

All calculations were performed with an iterative weighted linear least squares program on a CDC-3600 computer [1]. This computer program corrects for shifts in zero energy intercept and in gain. It also accurately

estimates variance in the sample and background spectra, compensates for correlation introduced by the shift and stretch correction and includes the variance from the library of standard spectra. Up to 20 nuclides may be determined in a single sample. There is no restriction in the number of data spectra or in the number of library standard spectra since they are stored on magnetic tape and are obtained as required. Typically, analysis is performed over all channels from 10 to 500 with no restriction on total counting rate below 100,000 counts per minute, *i.e.* zero counts per channel is acceptable. Only one input data control card is required per case except for establishing the initial list of nuclides which requires two more. The validity of the calculations is obtained from the two goodness of fit parameters, χ_F and S, the ratio of δ/σ for each channel, and the total counts assigned to each nuclide where:

$$\chi_F^2 = \left(\sum_j \omega_j \delta_j^2 / \text{variance } (\delta_j) \right) / F \tag{1}$$

(ω_j is a weighting factor depending on the variance, δ_j is the difference between observed and calculated count rate in channel j, and F is the number of degrees of freedom) and

$$S = (2\chi_F^2)^{1/2} - (2F - 1)^{1/2}. \tag{2}$$

Most errors or omissions in the input data cards or in the data are recognized by the computer program.

II.   Discussion

A.   EVALUATION OF ERRORS IN INPUT DATA

These errors are instrumental in nature and occur at time of accumulation in the multichannel analyzer during readout or during transcription into the computer input form. Typically, these are observable as extra or lost digits in any individual channel. Errors of this type are readily detected by comparison with adjacent channels. A less obvious and equally frequent problem is the random dropout of a particular digit in the output media. These can only be detected by a careful statistical analysis which involves the point-by-point comparison of the variance of the counts recorded and the deviation from a least squares polynomial fit.

B.   ZERO COUNTS IN A CHANNEL

Statisticians are unanimous in stating that this situation should be avoided! However, this situation frequently arises and any computer program must compensate for this effect, otherwise the results will be heavily biased due to the incorrect computation of variance. This is

because the weighting factor in the least squares is calculated from the variance, and zero variance will give an effective infinite value for this factor. There are two general methods for dealing with this problem: (1) assign an arbitrary variance to all channels with zero counts or (2) limit the least squares analysis to those channels containing a finite number of counts. We have found, however, that only a moderate bias is introduced into the goodness of fit parameters (χ_F and S) if a variance of 1 is assigned to all channels with zero counts and the number of degrees of freedom is reduced by the number of channels so changed.

C.   EVALUATION OF RESIDUALS

A plot of the residual in each channel gives very little information because the individual count rates may differ by several orders of magnitude. However, if this residual is normalized by dividing by the standard deviation of that channel (δ_j/σ_j), the value obtained has units of sigma (σ) and for pure random statistical data should be normally distributed with zero mean and unit variance (*i.e.*, 99% of all normalized deviations should be within the range of $\pm$ 2). All non-statistical and instrumental effects are immediately apparent and recognizable. In particular, one can distinguish (1) improperly compensated changes in zero-energy intercept and/or gain due to electronic variations or count rate, (2) missing nuclides, and (3) uncorrected errors in data. Furthermore, by excluding a minor component from the analysis, its significance may be tested.

The effect of small errors in peak positions is illustrated in Figure 1. The gamma-ray spectrum from 0 to 3.2 MeV (the energy range of all spectra shown in the figures) obtained for a mixed standard containing 95,000 cpm ^{24}Na, 4320 cpm ^{60}Co, 585 cpm ^{99}Mo, 5,475 cpm ^{233}Pa, 7,332 cpm ^{56}Mn, 440 cpm ^{65}Zn, 1,361 cpm ^{69}An, 43,992 cpm ^{64}Cu, 2,022 cpm ^{115}Cd and 503 cpm ^{51}Cr is shown in Figure 1A. The normalized residual for each channel is plotted in Figure 1B. The sigmoid shaped curve between channels 50 and 100 is a unique characteristic for small errors in peak position. Since this curve is only associated with the photopeak from ^{64}Cu, this library spectrum is the one in error. The error in peak position is less than 0.1 channel and is only apparent when the variance in each channel of the photopeak is small compared to the deviation for the 0.1 channel shift. This occurs when the total counts for the ^{64}Cu is greater than 200,000 and will be different for other nuclides.

The effect of missing nuclides on the least squares analysis is summarized in Table 1 and illustrated in Figure 2A. When this sample was first analyzed ^{82}Br and ^{47}Sc were not available in the library of standard spectra and the residual shown in Figure 2B was obtained. The positive
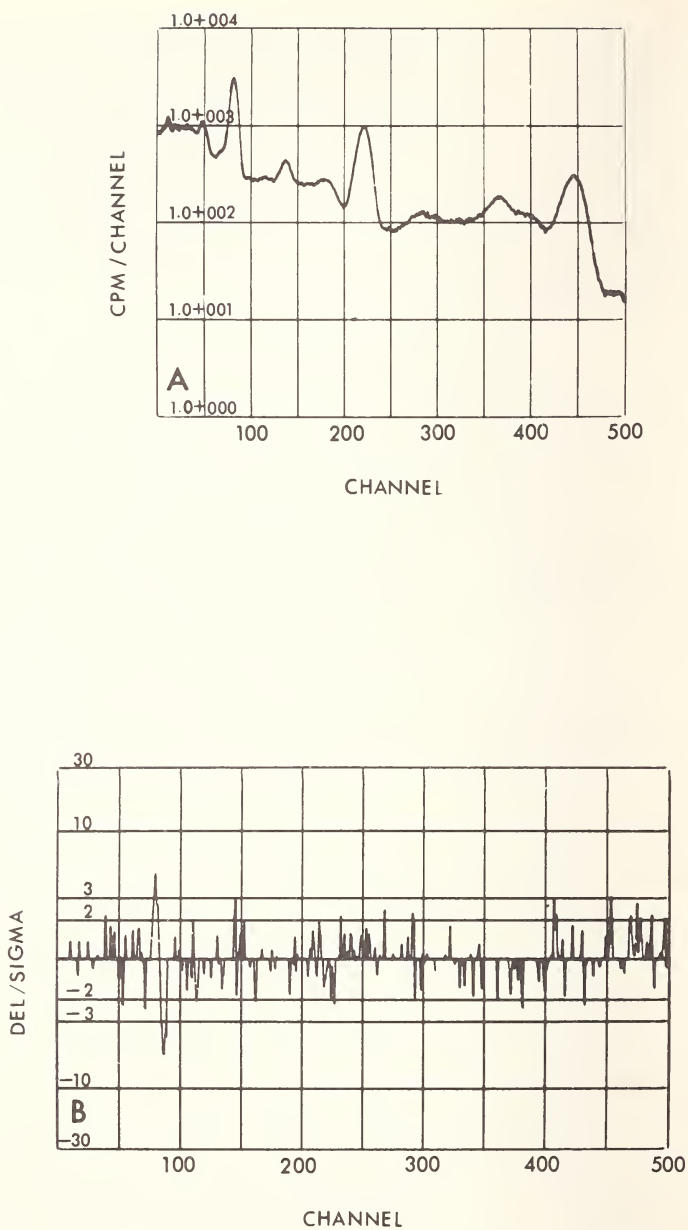
Figure 1. (A) Gamma-ray spectrum from mixed standards. (B) Plot of δ/σ from least square analysis of sample given in (A).

Table 1. Effect of missing nuclide on least squares analysis.

Counts per minute

Number	^{24}Na	^{42}K	^{40}La	^{64}Cu	^{82}Br	^{47}Sc	χ^2_F	S
1	40 ± 7	57 ± 10	118 ± 14	186 ± 10	N.A.[a]	N.A.[a]	33.5	148.3
2	9.3 ± 1.7	<6	12.1 ± 3.4	125 ± 3	408 ± 5	N.A.[a]	2.06	13.5
3	9.7 ± 1.2	<4	11.6 ± 2.4	122 ± 2	399 ± 4	16.2 ± 0.8	1.06	1.00

[a]N.A. = Not available for least squares analysis.
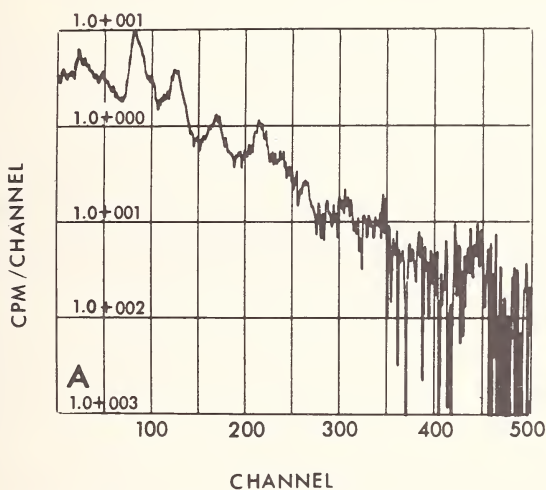
Figure 2A. Gamma-ray spectrum of a fraction separated by anion exchange from irradiated caribou bone.

peaks correspond to photopeaks of missing nuclides and may be used for identification purposes while negative peaks correspond to overcompensation for those nuclides present. In this case the peaks observed were found to correspond to those expected from ^{82}Br. When this nuclide was added to the library and the analysis rerun the residual shown in Figure 2C was obtained. The positive peak here was identified as ^{47}Sc and when this was added to the list of nuclides in the library the residual shown in Figure 2D was obtained. This residual is acceptable and this is further confirmed by the concomitant changes in χ_F and S to approach their normal values.

The significance of a minor component is illustrated in Figure 3. In this example the total count rate was 11,800 cpm and the sample was counted
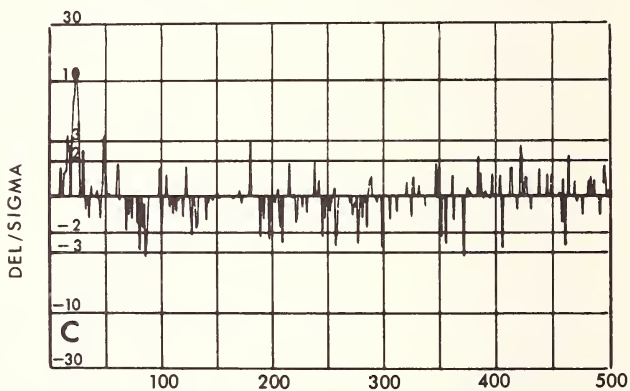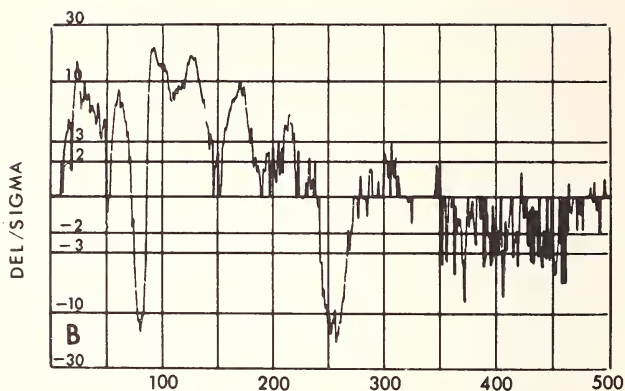
Figure 2B and 2C.   Normalized residuals obtained and used to identify ^{82}Br and ^{47}Sc, respectively.
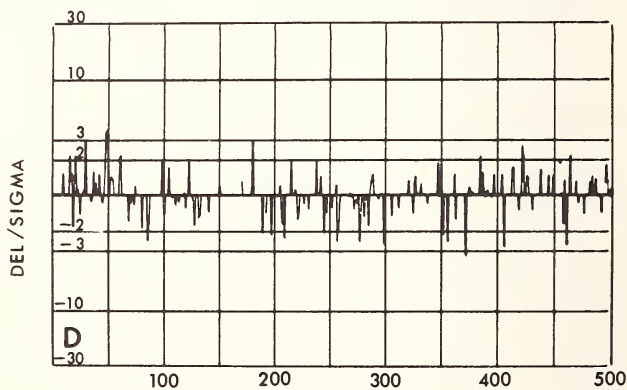
Figure 2D.   Normalized residual for final analysis.
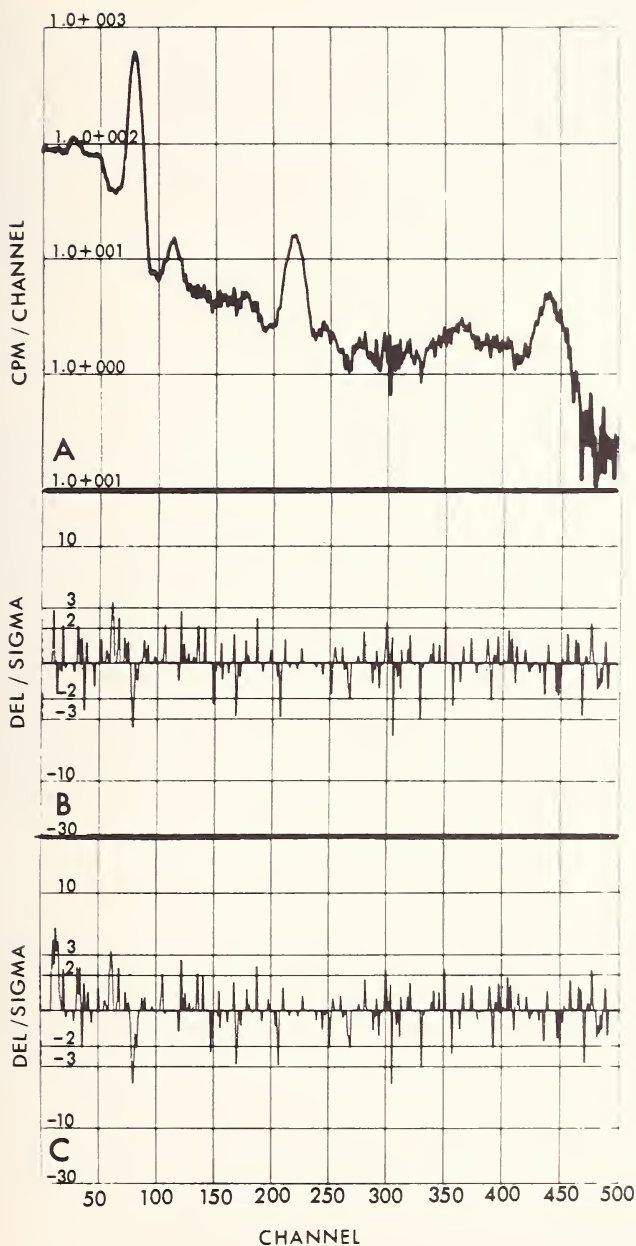
Figure 3.   A. Gamma-ray spectrum of the fraction believed to contain neptunium (from irradiated uranium) separated by anion exchange [4] from the irradiated lymph nodes of a miner. Normalized residuals obtained in the analysis as described in text with minor component ^{239}Np present B. and absent C.

for 20 minutes. The major components are ^{24}Na and ^{64}Cu. The normalized residual for the analysis of this spectrum is shown in Figure 3B in which ^{239}Np is included in the library. The activity assigned to ^{239}Np was 99 cpm (or 0.83% of the total) and the values of χ_F and S were 1.107 and 1.64, respectively. If the contribution due to ^{239}Np is removed, the residual shown in Figure 3C is obtained. A peak is observed in channel 14 which corresponds to the 106 keV x-ray associated with this nuclide. In addition, the values of χ_F and S increase to 1.272 and 4.01, respectively.

D.   GEOMETRICAL EFFECTS

Variations in the height or volume of a sample are usually only expected to affect the geometrical efficiency. While this may be essentially true for very large detectors or for samples at a large distance from the detector, significant changes in spectral shape also occur. These changes are easily observable by the least squares method. Variations in sample height of $\pm$ 5% affect both the width of the photopeak and the intensity of the scattered Compton region of the spectrum. For analysis of a simple mixture of nuclides by the least squares method this spectral change will give the same form of residual as that obtained when a nuclide is missing. The errors introduced by small variations in sample volume or height are dependent on the particular nuclides in the mixture. For instance, ^{60}Co emits its two gamma rays in cascade so that the effects will be greater than for ^{85}Sr. The effect will also be more important for two nuclides whose spectra are highly correlated as, for instance, ^{64}Cu and ^{76}As.

IV.   References

[1]   Parr, R. M., and Lucas, H. F., Jr., IEEE Trans. Nucl. Sci., NS-11 (3), 349 (1964).
[2]   Helmer, R. G., Heath, R. L., Schmittroth, L. A., Jayne, G. A., and Wagner, L. M., Nucl. Instr. Methods 47, 305 (1967).
[3]   Schonfeld, E., Kibbey, A. H., Davis, W., Jr., Nucl. Instr. Methods 45, 1 (1966).
[4]   Edgington, D. N., Int. J. App. Rad. and Isotopes 18, 11 (1967).

THE DISCOVERY OF ERRORS IN THE DETECTION OF TRACE COMPONENTS IN GAMMA SPECTRAL ANALYSIS

Lloyd A. Currie

National Bureau of Standards
Washington, D.C.

I. Introduction

Least squares solutions to over-determined systems in physical science generally provide parameter estimates, their standard errors, and various measures of the quality of the fit of the set of observations to the model. Such an approach has been applied for a number of years for the estimation of individual radionuclide contributions to an observed composite gamma-ray spectrum [1]. Perhaps the most popular indicators for misfit of the observations to the assumed model are the resulting series of normalized residuals and the statistic, χ^2, which is derived from this residual set. Too large a value for χ^2 is indicative of trouble, while a plot of the residuals may often pinpoint the source of trouble. Errors which are frequently uncovered in the process include missing components, shifts in peak position (gain, zero), and gross, isolated mistakes (dropped channels).

That errors may not always be directly located by the residuals, however, is illustrated in Figure 1. This figure resulted from the least squares analysis of a mixture of background, ^{22}Na, and ^{54}Mn. The negative (^{22}Na) peak and positive (^{54}Mn) peak in the residual plot clearly indicate the presence of trouble, but they do not directly point to its origin. In fact, the (unintentional) mistakes occurred in the standard spectrum for ^{54}Mn in channels 62, 65 and 67.

A more subtle kind of error-detection problem may arise when one or more components are present at "trace" levels—*i.e.,* if they are scarcely detectable. In order to examine this problem we must first discuss the question of detection limits as related to the least squares approach.

II. Detection Limits in Overdetermined Systems

The general problem of limits for decision, detection, and determination has been discussed previously for the one component situation [2]. For
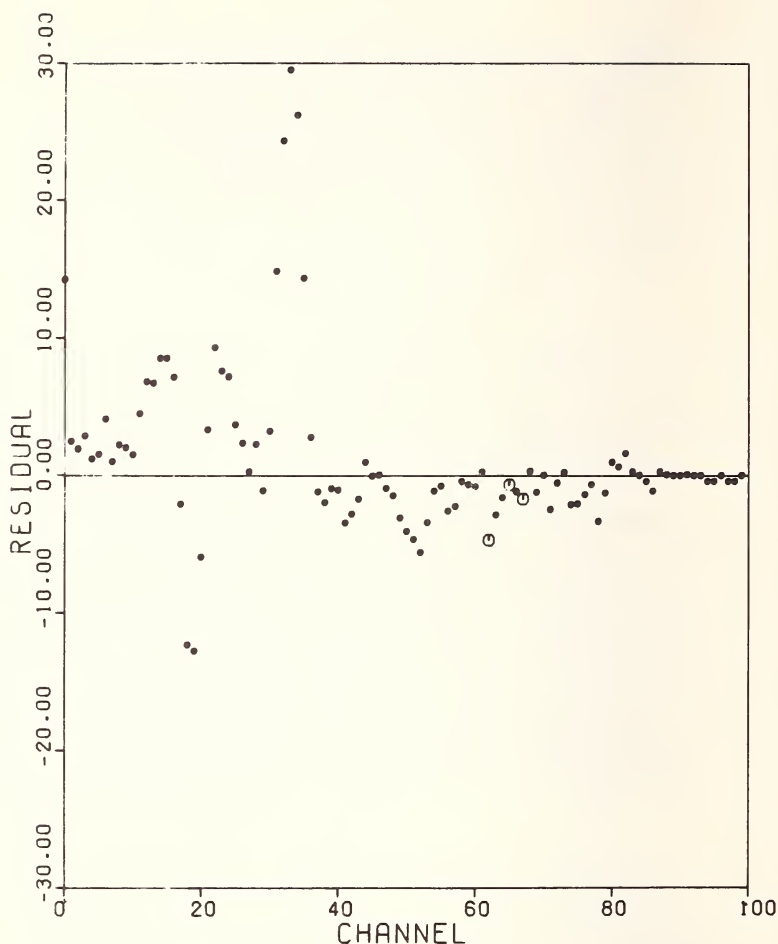
Figure 1.   Plot of normalized residuals from the least squares analysis of ^{22}Na, ^{54}Mn, and background. Channel zero is the timing channel, and the enlarged points refer to channels containing systematic errors.

the particular case of radioactivity (Poisson distribution) the "critical level" was seen to be,

$$L_C = k_\alpha \sigma_o \qquad (1)$$

and the "detection limit",

$$L_D = L_C + k_\beta \sigma_D \qquad (2)$$

where: σ_o, σ_D represent the standard deviation when the component of interest is absent, and present at its detection limit, respectively, and k_α, k_β

represent the values of the standardized normal variate corresponding to the selected limits for the errors of the first and second kinds, respectively. In the limit of large numbers of counts (>100), $\sigma_o \sim \sigma_D$, and $L_D \sim 2\,L_C$. Thus, for example, if the two types of error are each set at 5%, $k_\alpha = k_\beta = 1.645$, and the relative standard deviation at the critical level equals .608, while that at the detection limit equals .304. (Note that L_C is to be used for making *a posteriori* decisions regarding detection, whereas L_D is used to assess *a priori* detectability).

Equations (1) and (2) have been applied to the measurement process in which estimation is carried out by means of least squares. The method of solution is iterative in nature in that σ_o must first be calculated from a model containing the component of interest at level, zero; then the level is adjusted until equation (2) is satisfied. The results of such calculations are presented in Table 1. The reference levels for the standards and

Table 1. Detection limits for ^{22}Na in various radionuclide mixtures.[a]

No. of components	$L_D(^{22}\text{Na})$[b]	Component—J	Level—J[b]	Correlation coefficient (Na, J)
1	.00012[c]	—	—	—
	.0053	—	—	—
2	.0147	^{64}Cu	0	−.92
	.0062	^{54}Mn	0	−.50
	.0104	^{54}Mn	1.	−.59
	.0260	^{54}Mn	10.	−.61
3	.0291	^{64}Cu	$L_D(.284)$	−.93
		^{54}Mn	1.	−.62

[a] Number of observations equals 6.
[b] Levels refer to the respective standards as unity.
[c] Background = 0.

background used in deriving the detection limits in Table 1 were as follows:

Background	28000 total counts
^{22}Na	69000 total counts
^{64}Cu	4400 total counts
^{54}Mn	44000 total counts

The detection limit is thus seen to depend both upon the levels of interfering components (and background) and the magnitude of the correlation coefficient. If the model includes ^{54}Mn or ^{64}Cu, even at level zero, the detection limit for ^{22}Na exceeds its value in the one-component model. Variation with level of interference is rather complex; when one interfering component overwhelms all others, the variation approaches the "square root" relationship discussed in reference [2].

III. Model Errors

When one or more of the components in a mixture lies below its detection limit there exists a significant chance of missing such a component (by definition). It therefore becomes extremely important to consider the effects of such a nondetected component upon the estimates of the remaining components. If the model is correct — *i.e.,* includes the trace component, "A" — the remaining estimates are unbiased and no difficulties arise. On the other hand, if the model does not include "A", either because of ignorance or because of model simplification, the results are necessarily biased. The signs and magnitudes of the normalized biases are dependent upon the actual magnitude of "A" and the respective correlation coefficients. More seriously, it can be shown that neither χ^2 nor the magnitudes of the residuals may indicate the presence of trouble, if "A" lies below its detection limit.

Errors of the type just discussed may have especial significance in the evaluation of several trace components in the same sample. For example, in the Standard Reference Materials program at the National Bureau of Standards, we are concerned with certifying specific materials (including high-purity materials) with respect to their trace constituents. It is quite . likely if an incomplete model is used that, besides the systematic errors induced in macro-constituents, trace components may be "seen" when they are absent and/or missed when they are present. The probability of such mistakes can become quite large when large (positive or negative) correlation coefficients are involved, as the following example demonstrates.

Table 2 is based upon least squares analyses of a gamma-ray spectrum constructed from ^{64}Cu, ^{22}Na, and ^{54}Mn at levels: L_C (.142 0, and 1, respectively). (Levels are given in terms of the "standards" as stated earlier). Since ^{64}Cu was present at its critical level it will be missed with a probability of 50%. It may be seen that the effect of the incomplete model on the macro-constituent, ^{54}Mn, is a slight reduction in the standard error estimate and the introduction of a serious, negative, systematic error. The effect on the trace constituent, ^{22}Na — which is, in fact absent — is profound! A rather large decrease in the standard error estimate (and critical level) is accompanied by a large positive systematic error which

Table 2. Effects of model errors on the mixture ^{64}Cu, ^{22}Na, and ^{54}Mn.

Model	^{22}Na Errors ($\rho = -.93$)			^{54}Mn Errors ($\rho = +.46$)	
	Systematic	Random (σ)	L_C	Systematic	Random (σ)
Correct (Includes ^{64}Cu)	0	.0088	.0145	0	.0082
Incorrect (Excludes ^{64}Cu)	+.0137	.0032	.0052	−.0063	.0072

causes the absent component to be "detected". It was observed that neither the magnitude of the residuals (extreme=−1.4) nor the value of χ^2 ($P_x^2=.72$) were indicative of misfit. A miniature Monte Carlo experiment was performed with the same system and it was observed: that χ^2 exceeded its .975 limit only one time out of six; that ^{22}Na was detected every time; and that the most serious error in the ^{22}Na estimate was equal to 6.05 times its standard error — an event which would be expected, by chance, with a probability of 2×10^{-7}.

The conclusions are, perhaps, obvious. When dealing with trace analysis one must be extremely cautious in using too simple a model, as the systematic errors can be enormous, while the popular fit-statistics may appear perfectly satisfactory. The probability of such pitfalls can be assessed rigorously, but this subject will be discussed elsewhere. A principal caution to be taken, however, is to examine the correlation coefficients of any trace components which are possible but which are being considered for exclusion. If these coefficients exceed ~ 0.4 it would be wise either to include such components in the model or to "orthogonalize" by means of chemistry, coincidence methods, mass separation, etc.

IV. References

[1]   Nicholson, W. L., Schlosser, J. E., and Brauer, F. P., Nucl. Inst. Meth. 25, 45 (1963). Pasternack, B., and Liuzzi, A., Biometrices 24, 353 (1968). Parr, R. M., and Lucas, H. F., Jr., Proc. Ninth Scint. Semicond. Sympos., IEEE Trans. Nucl. Sci. NS-11, 349 (1964). Trombka, J. I., NAS-NS-3107, 183 (1963).

[2]   Currie, L. A., Anal. Chem. 40, 586 (1968). See also references given in the above publication.

REGRESSION ANALYSIS OF GAMMA-RAY SPECTROMETER DATA WITH AN APPLICATION TO THE ASSAY OF HUMAN RADIOACTIVITY BURDENS[1]

Bernard Pasternack and Naomi Harley

Institute of Environmental Medicine
New York University Medical Center
New York, New York

I. Introduction

A standard technique for estimating radionuclide concentrations from gamma-ray spectrometer data (when the half lives of the nuclides concerned are long relative to the time of counting and the identity of the nuclides is known) is the method of weighted least squares [1-10]. Recently, Liuzzi and Pasternack [11] presented a modified (*i.e.* non-linear) regression method which permits correction for gain and baseline discrepancies between the reference and mixture pulse-height distributions. The method is based upon iteratively transforming reference pulse-height distributions until a best least squares regression fit is obtained.

This procedure requires a gain and baseline compatible set of reference spectra since, in effect, the set is made gain and baseline compatible with the pulse-height distribution of the mixture. The least squares solution then yields the appropriate nuclide quantity estimates. In this regard, a method was proposed for obtaining a library of reference spectra which would be internally consistent in gain and baseline. However, as an alternative, a simple modification in the compensation technique was suggested which allows the reference spectra to be individually transformed in any given analysis.

The basic statistical model is that a background corrected pulse-height distribution for a mixture of nuclides is equal to some linear combination of individual characteristic distributions for the constituent nuclides (plus superimposed statistical variations); it is assumed that counts in the pulse-height channels are statistically independent. Since concentrations of the constituents in a mixture are represented by coefficients in this linear combination, estimation of these coefficients is equivalent to estimation of these concentrations. Figure 1 contains typical characteristic (or reference) pulse-height distributions for ^{65}Zn, ^{137}Cs, ^{106}Ru and an arbitrary mixture of these nuclides.
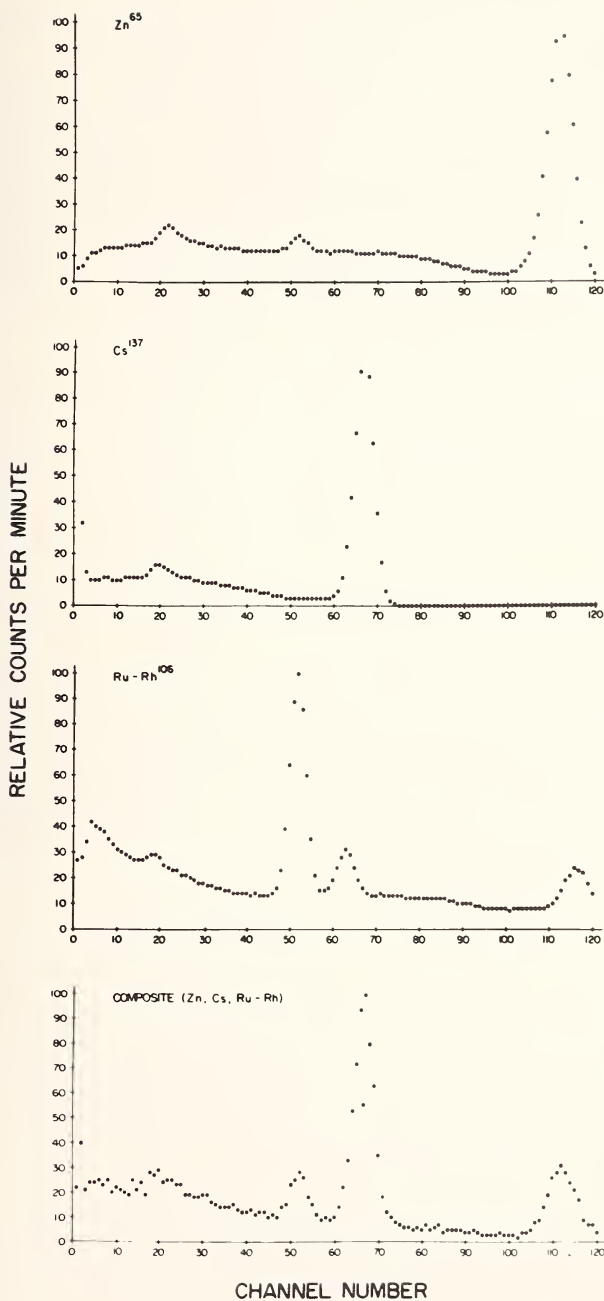
Figure 1. Typical pulse-height distributions taken from plots made by an IBM 1401 printer.

The weighted least squares solution essentially involves obtaining values for the nuclide concentration coefficients $\underline{\theta}' = (\theta_1 \theta_2 \ldots \theta_m)$ — prime denotes transpose — such that the sum of squares of the weighted differences between corresponding channel counts of the observed pulse-height distribution and the indicated linear combination of reference pulse-height distributions is a minimum. Thus consider a background corrected pulse-height distribution over n channels obtained after counting a mixture of $m(< n)$ distinct radionuclides for a period of time t. Denote this distribution by the row vector $\underline{x}' = (x_1 x_2 \ldots x_n)$. The weighted least squares solution [5] is given by

$$\hat{\underline{\theta}} = (AW^{-1}A')^{-1}AW^{-1}\underline{x} \tag{1}$$

where the matrix

$$A = \begin{bmatrix} a_{11} & a_{12} & \cdots & a_{1n} \\ a_{21} & a_{22} & \cdots & a_{2n} \\ \cdot & \cdot & \cdot & \cdot \\ \cdot & \cdot & \cdot & \cdot \\ \cdot & \cdot & \cdot & \cdot \\ a_{m1} & a_{m2} & \cdots & a_{mn} \end{bmatrix} \tag{2}$$

is called a calibration matrix and represents the set of reference spectra to be used in an analysis with W as an appropriate weighting matrix.

Standard errors for the nuclide quantity estimates are given by the square root of the diagonal elements of $(AW^{-1}A')s^2$ where s^2 is the normalized residual mean square statistic

$$s^2 = (n-m)^{-1}[\underline{x} - A'\hat{\underline{\theta}}]'W^{-1}[\underline{x} - A'\hat{\underline{\theta}}]. \tag{3}$$

Residuals represent the scattering of the observed mixture pulse-height data about the estimated average pulse-height distribution indicated by the least squares solution. A compatible set of nuclide estimates should result in a random display of residuals when plotted against channel number. On the other hand inadequacies in a calculation would result in systematic patterns (*i.e.* poor fit) in the residual plot. Figure 2 contains plots of normalized residuals resulting from analyses under various model conditions.

Rather than use s^2 as an index of goodness to fit, Pasternack and Liuzzi [5] have elected to use a statistic which more directly reflects the configuration of residuals. This statistic is based upon the ratio of the sum of squared successive differences in the residuals and the sum of squared residuals. This ratio can be used to perform a convenient statistical test for estimate credibility (*i.e.* goodness of fit) since its statistical properties
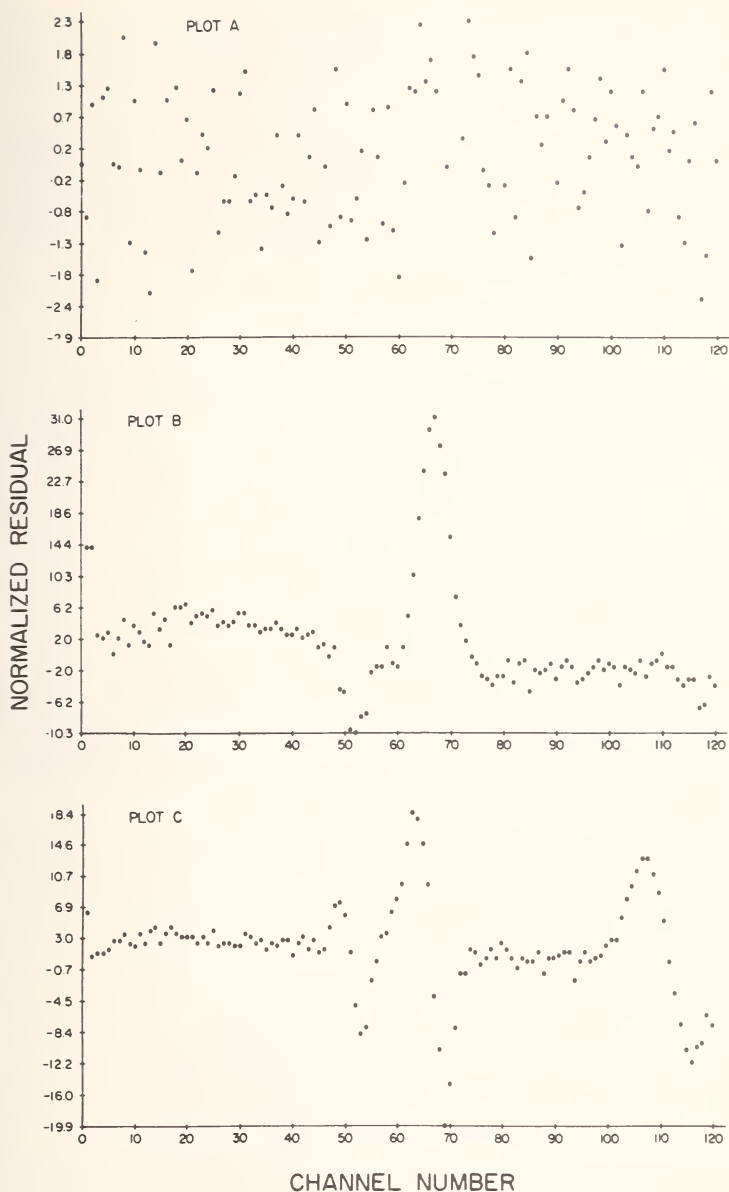
Figure 2. Plots of normalized residuals resulting from the analyses, under various model conditions, of pulse-height distributions for a mock sample. Plot A: adequate model; Plot B: incomplete nuclide set model inadequacy; Plot C: gain inconsistency model inadequacy.

have been evaluated [12,13]. Under ideal conditions for least squares analysis the ratio statistic has an expected value of unity; deviations from ideal conditions result in lower values for the ratio.

Let $\phi_i(v)$ denote the expected count rate in the voltage interval $(v, v + dv)$ when counting a unit amount of the ith nuclide — where $\phi_i(v)$ is defined over an arbitrary voltage scale such that a channel number corre-corresponds to the upper voltage bound of that channel. The jth spectral coefficient of the ith nuclide is then simply

$$a_{ij} = \int_{j-1}^{j} \phi_i(v)\, dv. \tag{4}$$

A change in baseline (α) and gain (β) of the counting system corresponds to a linear transformation of the pulse-height channel scale; *viz.* $v = \alpha + (1 + \beta)v^*$ or $v^* = (v - \alpha)/(1 + \beta)$. The new set of spectral coefficients (a^*_{ij}) corresponding to a change in baseline and gain, in terms of $\phi_i(v)$, is thus

$$a_{ij}^* = \int_{\alpha+(j-1)(1+\beta)}^{\alpha+j(1+\beta)} \phi_i(v)\, dv. \tag{5}$$

In order to effect the transformation indicated by equation (5), $\phi_i(v)$ is approximated (locally) by a second order polynomial allowing the shifted A matrix (A^*) to be expressed as a somewhat complex transformation of the original (observed) A matrix with the transformation depending on α and β.

The computer programmed compensation technique [11] introduces for each of the m reference spectra to be used in an analysis, two additional parameters to account for the alteration in voltage scale; these $2m$ parameters are estimated by the least squares fitting procedure by minimizing (based on a preselected convergence criterion), with respect to the compensation parameters, the function

$$s^2 = \frac{1}{n-m} [\underline{x} - A^{*\prime}\hat{\underline{\theta}}]'\, W^{-1}\, [\underline{x} - A^{*\prime}\hat{\underline{\theta}}] \tag{6}$$

where

$$\hat{\underline{\theta}} = [A^*W^{-1}A^{*\prime}]^{-1} A^*W^{-1}\underline{x}. \tag{7}$$

Figure 3 contains plots of two reference spectra of ^{137}Cs. Plot A is an untransformed ^{137}Cs spectrum; Plot B contains the spectrum resulting from the transformation of the spectrum in Plot A corresponding to a $+10\%$ change in gain by the procedure just described.
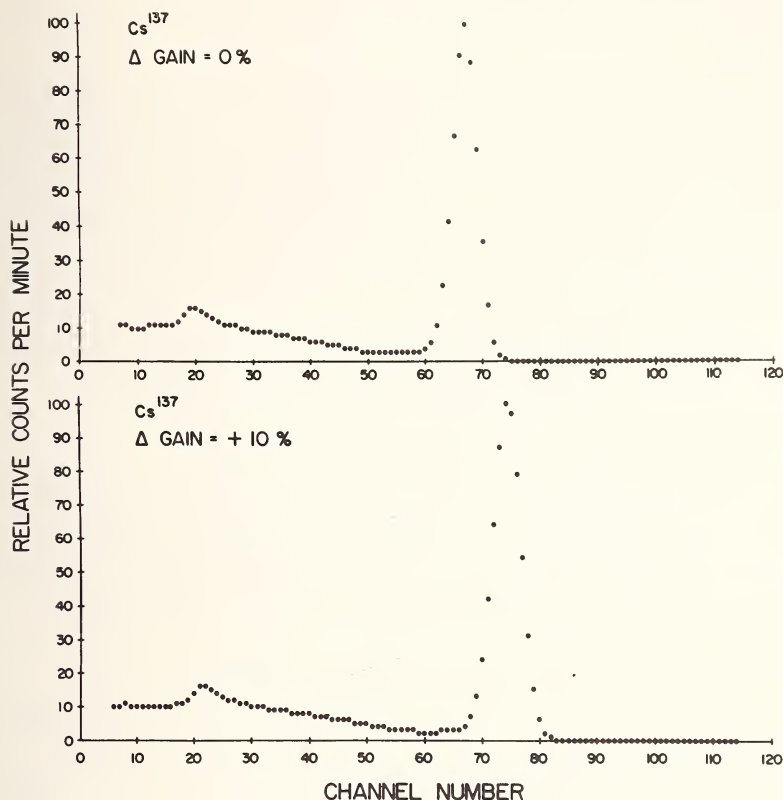
Figure 3. Pulse-height distributions for ^{137}Cs. Plot A: untransformed; Plot B: 10% increase in gain ($\beta = +0.1$).

II. Experimental

Environmental samples have been extensively assayed by the method described above. Experimental sampling studies have also been performed confirming the validity of the statistical methodology applied [12,13]. Also, possibilities of *in vivo* neutron activation analysis have been discussed by Palmer *et al* [15]. Here, we will describe a recent application to total body counting.

For this study a woman who had been a radium dial painter fifty years ago was counted on four separate occasions. Total body counting is performed with the individual seated, using an 8 in. × 4 in. NaI(Tl) detector positioned so that the body geometry is approximately a 1/2 meter arc. The counting data are collected using 200 channels of a Victoreen 400-channel analyzer which is calibrated for approximately 10 keV/channel. The detector and chair are housed in a steel room whose

dimensions are approximately 5 ft. × 6 ft. × 7 ft. The walls are 7 in. thick.

The "calibration phantom" consists of two 10 liter rectangular plastic carboys, each filled with 8 liters of dilute HCl and the standard or reference nuclide. Two 10 liter carboys are prepared for each calibration standard and each contains half the reference activity. The carboys are prepared to contain approximately 1 μCi radium-226, 1 μCi cesium-137 and 140 grams of potassium. The carboys are placed base to base in the chair for calibration, one in the chair seat and the other against the chair back. The calibration carboys thus approximate a thorax and thigh geometry. The patient, as well as all calibration carboys, is counted for 30 minutes and an overnight background measurement is obtained.

III. Results and Discussion

Table 1 shows the results of the computer analysis for radium-226, potassium-40 and cesium-137 when the analysis is performed over channels 10-190. In all cases, the computed values of s^2 and the ratio statistic are beyond their respective one-tailed 5% critical values.

Table 1. Analysis of total body counting data.[a]

Date	Run No.	Ra-226(nCi)	K(g)[b]	Cs-137(nCi)	α	β	s^2 (critical s^2 5%)	Ratio (critical ratio 5%)
2/9/68	I	29.75 ± .44	60.39 ± 6.74	2.83 ± 1.10	−0.1634	1.0028(Ra)	2.58	0.409
					−0.0033	1.0044(K)	(1.18)	(0.880)
					+0.0228	1.0240(Cs)		
	II	30.37 ± .45	60.14 ± 7.00	2.92 ± 1.15	−0.0011	1.0029(Ra)	2.76	0.438
					−0.0279	1.0121(K)	(1.18)	(0.880)
					+0.0367	1.0246(Cs)		
3/1/68	III	30.17 ± .54	58.62 ± 8.22	3.88 ± 1.33	+0.0351	0.9994(Ra)	3.77	0.301
					−0.0161	1.0029(K)	(1.18)	(0.879)
					−0.2162	1.0333(Cs)		
	IV	28.97 ± .53	73.42 ± 8.00	5.46 ± 1.42	+0.0091	0.9967(Ra)	3.46	0.322
					−0.0138	1.0044(K)	(1.18)	(0.879)
					−0.2210	1.0102(Cs)		

[a] Case 5025 (0.10–1.90 MeV)

[b] Expected K burden 65.2 g [16].

Figure 4 shows for one of the analyses a plot of the background corrected total body spectrum along with the fitted spectrum and the normalized residuals. A pattern below channel 30 is clearly evident. To minimize the effects of differential scattering, the data were reanalyzed over channels 45-190 and are shown in Table 2. The near unity values of the ratio statistic, in this case, indicates that the normalized residuals are, in fact, randomly distributed above about 0.4 MeV. The background
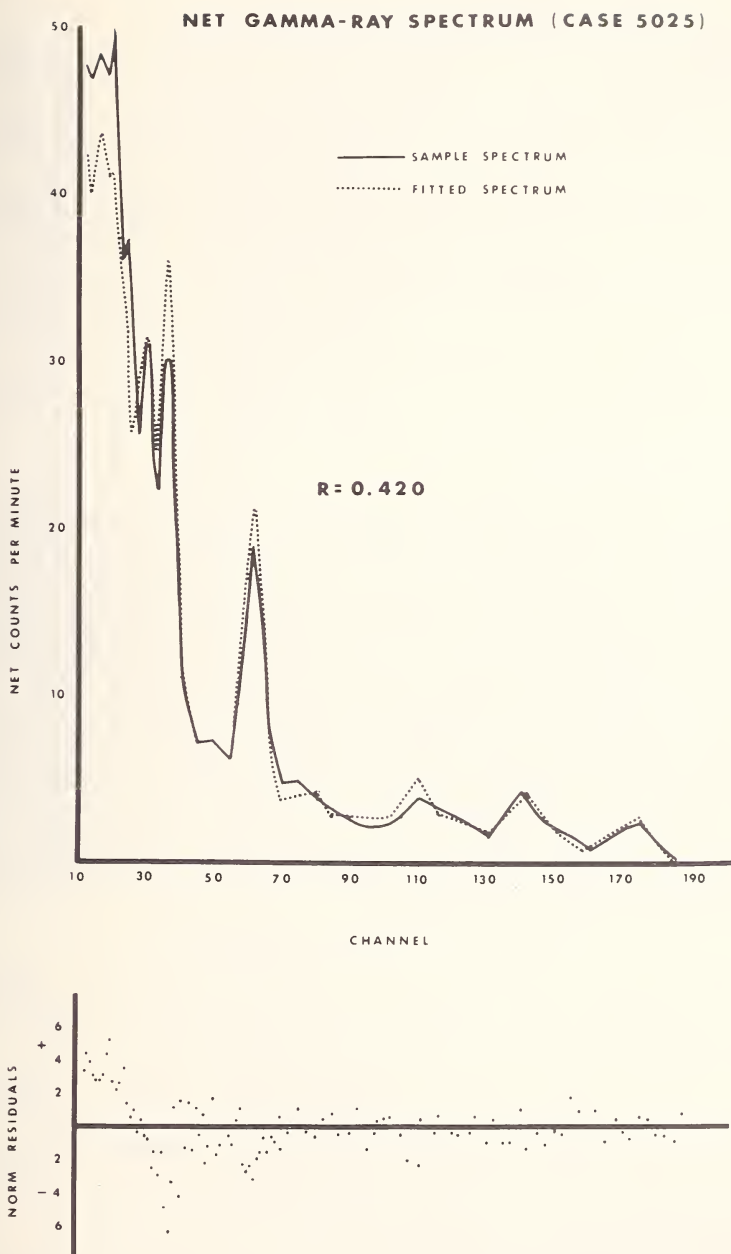
Figure 4. Observed and fitted total body pulse-height distributions for a former radium dial painter (0.10-1.90 MeV) including a plot of normalized residuals.

ACTIVATION ANALYSIS

Table 2. Analysis of total body counting data.[a]

Date	Run No.	Ra-226(nCi)	K(g)[b]	Cs-137(nCi)	α	β	s^2 (critical s^2 5%)	Ratio (critical ratio 5%)
2/9/68	I	27.66 ± .41	58.42 ± 4.00	2.27 ± .62	−0.5447	1.0087(Ra)	0.848	0.958
					−0.0201	1.0062(K)	(1.200)	(0.869)
					−0.0377	1.0338(Cs)		
	II	28.07 ± .46	59.03 ± 4.52	1.99 ± .70	−0.0092	1.0361(Ra)	1.070	0.992
					−0.0001	1.0056(K)	(1.200)	(0.869)
					+0.0275	1.0121(Cs)		
3/1/68	III	27.89 ± .46	58.61 ± 4.59	2.97 ± .71	−0.5390	1.0072(Ra)	1.101	0.837
					−0.0141	1.0036(K)	(1.200)	(0.869)
					+0.2508	1.0359(Cs)		
	IV	27.47 ± .49	72.39 ± 4.87	3.61 ± .80	−0.0352	1.0020(Ra)	1.200	0.879
					−0.0149	1.0044(K)	(1.200)	(0.867)
					+0.4334	1.0137(Cs)		

[a] Case 5025 (0.45–1.90 MeV)

[b] Expected K burden 65.2 g [16].

corrected total body spectrum along with the fitted spectrum and the normalized residuals, plotted over channels 45-190 are shown in Figure 5.

Although the need for baseline and gain compensation between standard and sample measurements on a given date is dubious, there was a visible shift (approximately two channels) in the instrument calibration between the two measurement dates. To illustrate the utility of the method for individually shifting reference spectra, the data of February 9th were reanalyzed from 0.45-1.90 MeV using the standardization measurements of March 1st. These data are shown in Table 3 and indicate the expected greater values of α and β. Even with noticeable compensation, near unity values of the ratio statistic have been maintained. Note, by contrast, the poor results obtained when the data were analyzed without compensation.

Table 3. Analysis of total body counting data.[a]

Date	Run No.	Ra-226(nCi)	K(g)[b]	Cs-137(nCi)	α	β	s^2 (critical s^2 5%)	Ratio (critical ratio 5%)
WITH COMPENSATION								
2/9/68	I	27.07 ± .42	60.21 ± 4.22	1.91 ± .63	−0.1100	0.9800(Ra)	0.924	0.931
					+0.0176	0.9675(K)	(1.200)	(0.865)
					+0.4836	1.0138(Cs)		
	II	27.51 ± .46	60.96 ± 4.60	2.03 ± .69	−0.0848	0.9818(Ra)	1.092	0.954
					+0.0261	0.9785(K)	(1.200)	(0.865)
					+0.6734	1.0102(Cs)		
WITHOUT COMPENSATION								
2/9/68	I	27.58 ± .81	40.01 ± 7.29	−2.62 ± 1.33	− − −	− − −	3.269	0.310
					− − −	− − −	(1.200)	(0.855)
	II	28.10 ± .78	49.62 ± 7.06	−2.21 ± 1.28	− − −	− − −	2.938	0.444
					− − −	− − −	(1.200)	(0.855)

[a] Case 5025 (0.45–1.90 MeV) − − March 1 standards used for February 9 data.

[b] Expected K burden 65.2 g [16].
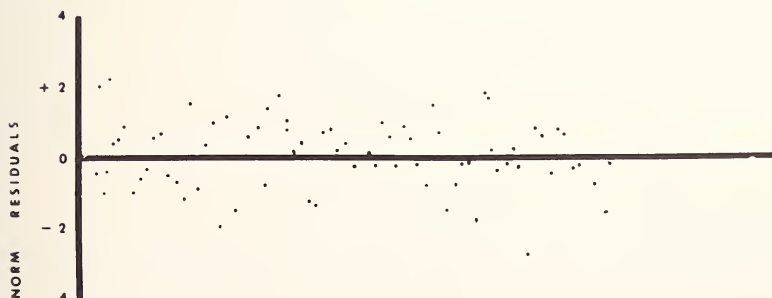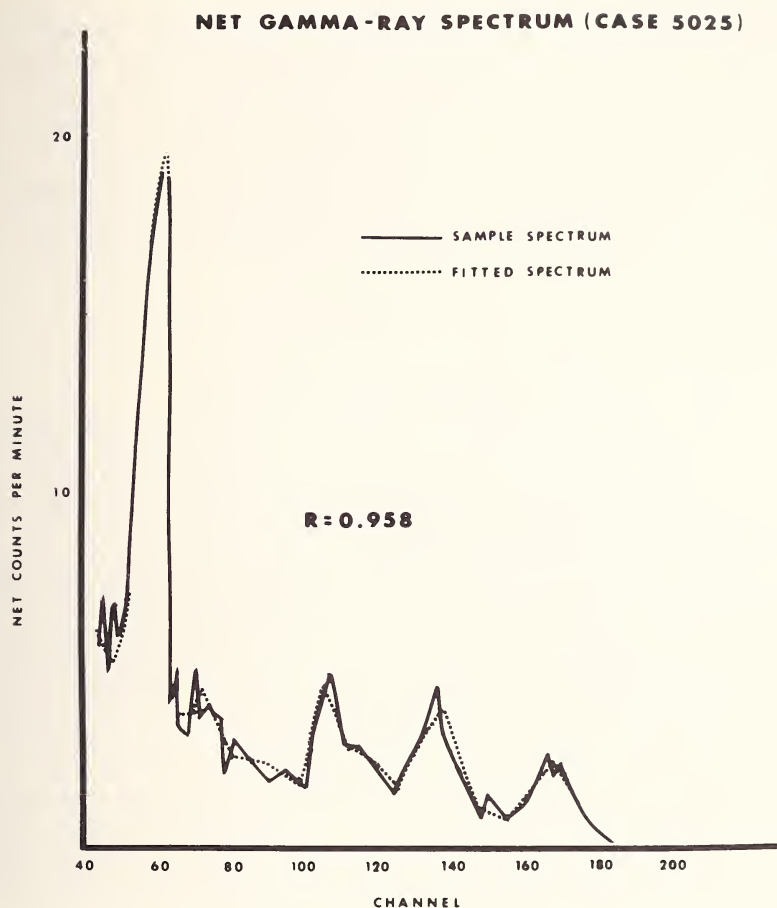
Figure 5.   Observed and fitted total body pulse-height distributions for a former radium dial painter (0.45-1.90 MeV) including a plot of normalized residuals.

Yamamoto [14] recently extended the work of Nicholson *et al* [3] to allow for least squares analysis of several time-dependent pulse-height spectra, with correction for instrumental shifts in gain and baseline using the method of Covell [6]. We have also extended our technique to include decay constants as input information in the analysis of such spectra. Application to the study of ^{198}Au salt pharmacodynamics in rheumatoid arthritis patients *via* total body gamma-ray spectrometer data analysis is currently underway and will be reported upon elsewhere.

IV. References

[1]   Pasternack, B. S., Technometrics **4**, 565 (1962).
[2]   Salmon, L., USAEC Monograph NAS-NS 3107, 165 (1963).
[3]   Nicholson, W. L., Schlosser, J. E., and Brauer, F. P., Nucl. Instr. and Meth. **25**, 45 (1963).
[4]   Parr, R. M., and Lucas, H. F., Jr., IRE Trans. Nucl. Sci. NS-11, 349 (1964).
[5]   Pasternack, B. S., and Liuzzi, A., Technometrics **7**, 603 (1965).
[6]   Covell, D. F., Nucl. Instr. and Meth. **36**, 229 (1965).
[7]   Heath, R. L., Nucl. Instr. and Meth. **43**, 209 (1966).
[8]   Schonfeld, E., Kibbey, A. H., and Davis, W., Jr., Nucl. Instr. and Meth. **45**, 1 (1966).
[9]   Brown, J. E., and Hatch, E. N., Nucl. Instr. and Meth. **47**, 185 (1967).
[10]   Helmer, R. G., Heath, R. L., Schmittroth, L. A., Jayne, G. A., and Wagner, L. M., Nucl. Instr. and Meth. **47**, 305 (1967).
[11]   Liuzzi, A., and Pasternack, B. S., Nucl. Instr. and Meth. **57**, 229 (1967).
[12]   Pasternack, B. S., and Liuzzi, A., Biometrics **23**, 11 (1967).
[13]   Pasternack, B. S., and Liuzzi, A., Biometrics **24**, 353 (1968).
[14]   Yamamoto, S., Nucl. Instr. and Meth. **52**, 245 (1967).
[15]   Palmer, H. E., Nelp, W. B., Murano, R., and Rich, C., Phys. Med. Biol. **13**, 269 (1968).
[16]   Report of the United Nations Scientific Committee on the Effects of Atomic Radiation, Supplement No. 16 (A/5216) (1962).

COMPUTER GAIN CHANGING OF SCINTILLATION SPECTRA

J. J. Steyn

NUS Corporation, Washington, D.C.

D. G. Andrews

University of Toronto, Toronto, Canada

I. Introduction

There are advantages in having available a technique for digital-computer gain changing of pulse-height spectra as opposed to electronic gain changing. A number of computer gain changing codes have been reported in recent years. Two of these are basically similar in that they apply the method of quadratic fitting to groups of three channels and determine the gain changed spectrum after appropriate scaling of the computed coefficients [1,2]. A third, employs the method of linear search and extrapolation [3], while a fourth, relying on the mass (channel count) conservation method is somewhat limited with respect to the amount of gain change [4,5].

A gain changing computer code identified as GANE and described below, was developed during the course of an experimental research into gamma photon backscattering as an aid in the computer analysis of spectra [6]. It is designed primarily around a sequence of logical steps, *viz.* an algorithm. It has been extensively tested over the past four years in a variety of applications and has been found to be accurate as well as versatile and computer time-saving.

II. Algorithm Description

A gain decreasing algorithm was developed to numerically redistribute a histogram spectrum,

$$y_i \,; i = 1, 2, 3, ..., n. \tag{1}$$

of n channels measured at a gain of g_1 to appear as if measured at a gain of g_2 and having m channels, *i.e.*, as

$$z_j \,; j = 1, 2, 3, ..., m. \tag{2}$$

1231

A histogram of gain, g_1 is reduced to a gain of g_2 by application of the algorithm as expressed by flow diagram of Figure 1. The ratio g_1/g_2 represents the electronic equivalent gain change, and

$$\sum_{i=1}^{n} y_i = \sum_{j=1}^{m} z_i \tag{3}$$

expresses the conservation of the before and after integral spectrum count. Small differences in this equality occur in practice since the gain change ratio chosen may be such that channel m will not contain a full count complement. In this instance, m, would be replaced by $m - 1$.

In order to increase spectral gain g_1 to g_2, the histogram is first reduced to exactly $g_2/2$. The elements of this temporarily reduced histogram

$$y_i \; ; i = 1, 2, 3, ..., m/2 \tag{4}$$
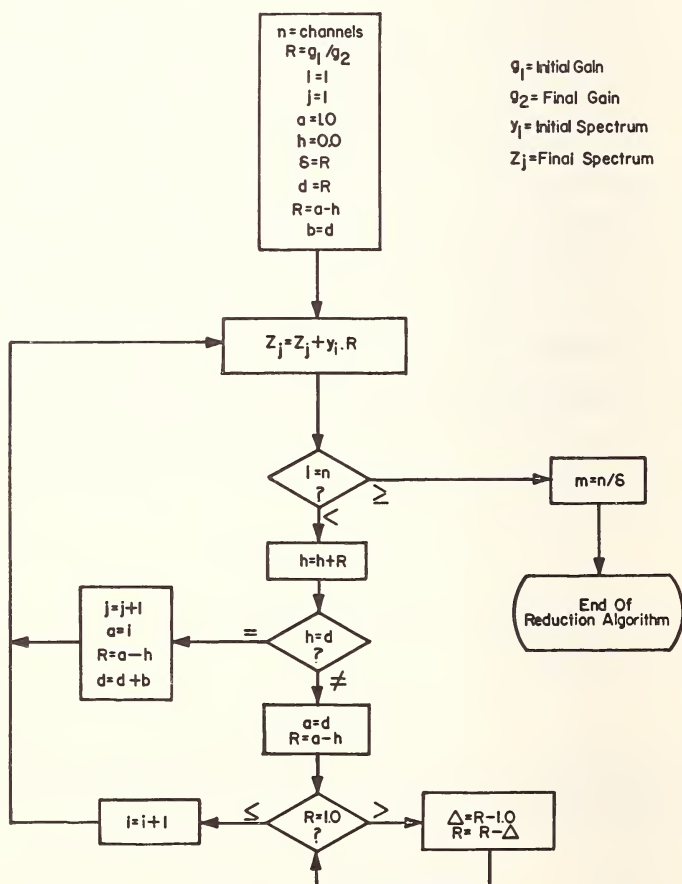
Figure 1.　Flow diagram of gain reduction algorithm.

are stored in

$$z_j \; ; j = 1, 3, 5, ..., m \tag{5}$$

The elements

$$z_j \; ; j = 2, 4, 6, ..., m - 1 \tag{6}$$

are determined from an interpolation relationship for equal-width X-axis intervals

$$z_{j+1} = \tfrac{1}{8} \left(3z_j + 6z_{j+2} - z_{j+4} \right) \tag{7}$$

which is based on Aitken's interpolation method [7]. The new histogram is then shifted a half channel and scaled, to produce the desired increased-gain spectrum of m channels and gain g_2, as

$$z_j \; ; j = 1, 2, 3, ..., m. \tag{8}$$

Again, as in gain decreasing

$$\sum_{i=1}^{n} Y_i = \sum_{j=1}^{m} z_j \tag{9}$$

Code GANE, written around the above logic includes two optional features, namely: a true zero shift capability and a spectral smoothing sequence. The zero shifting is carried out either positively or negatively in two steps. This provides for economy when only an integer channel shift is required. The smoothing option used the reduction algorithm to obtain "improved" statistics by a sequence of halving and doubling. As in any smoothing technique it must be employed with caution if loss or smearing of valuable fine structure is to be avoided.

The code, written in a general FORTRAN language, is readily usable on most computers without modification, *e.g.* IBM-7090, -7094, -1620, CDC-3600, GE-235, *etc.* It is called by a main program and is designed to return with "up-to-date" argument values. The preparation of arguments prior to calling is generally trivial and often unnecessary.

III. Results and Discussion

Figure 2 shows the 0.6616 MeV photopeak of a gain changed ^{137}Cs pulse-height analyzer spectrum, plotted at $g_2 = 74.5$ and 149.5 corresponding to 75 and 150 PHA channels. The 0.5 channel apparent difference is due to PHA channel counts being actually located at channel mid-points. The spectrum was experimentally measured for $g_1 = 111.27$, where g_1 was determined by subsequent regression analysis. It can be seen that even in this region of maximum spectral curvature combined
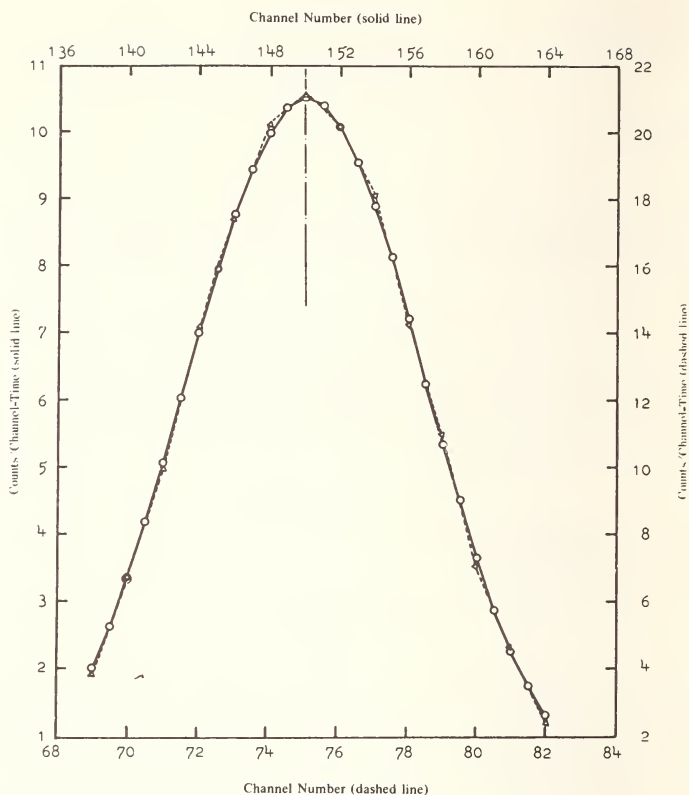
Figure 2. ^{137}Cs photopeak pulse height measured at channel 111.27 gain changed to channel 75.0 and 150.0 by subprogram GANE.

with relatively large gain change, the agreement is as good as the regression analysis allowed. Figure 3 shows the same results for the entire spectrum.

Figure 4 illustrates the advantages of a gain changing code in generating standard Compton continua from standard radioisotope spectra. In this particular figure the 0.51 MeV component of ^{65}Zn was evaluated and subtracted using the spectrum of ^{85}Sr. The standard spectra were measured experimentally without concern for the photopeak pulse height, since it was to be computer evaluated.

Figure 5 gives another example of usage of the gain changing technique. In this case the standard Compton continua of which Figure 4 is typical, were used to interpolate a Compton continuum at an intermediate energy with the aid of the gain changing technique. The interpolation was carried out after changing the standards in overlapping parts and such that
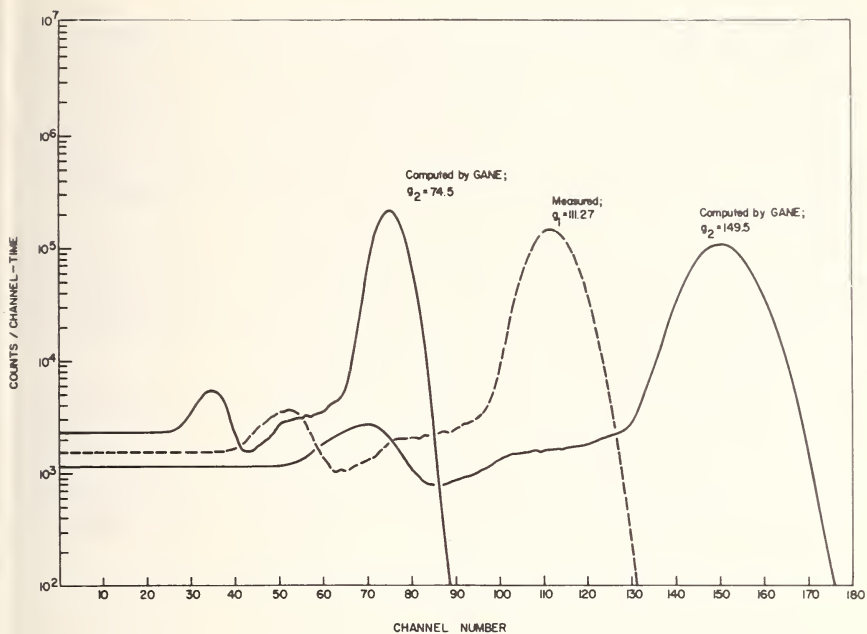
Figure 3. Example of code gain changing a ^{137}Cs spectrum.
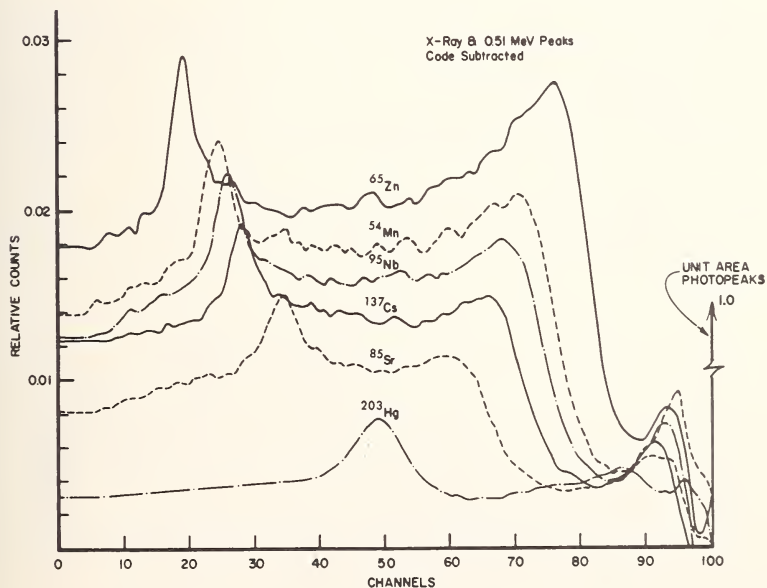
Figure 4. Compton continua normalized to a unit area photopeak in channel 100.

backscatter and Compton edge were pulse-height aligned. The interpolated spectrum was then un-aligned "by parts" using the gain changing technique, to yield the interpolated continuum. The extrapolated continuum in Figure 5 was determined similarly for the purpose of analyzing a ^{60}Co spectrum. The experimental spectra of Figures 4 and 5 were obtained from NASA-Goddard Space Flight Center [8].

Figure 6 gives an example of the smoothing achievable with code GANE. The smoothed spectrum, obtained by a single halving and doubling, *i.e.*, single degree, clearly improves the poor spectral statistics. Second degree smoothing was generally unnecessary.

It was found that gain decrease operations did not lead to integral count differences other than the omission of the count in the fractionally loaded highest channel. Large gain decrease operations noticeably smoothened spectra with poor statistics, in agreement with the result that would have been obtained by actual electronic gain reduction. On the other hand, gain
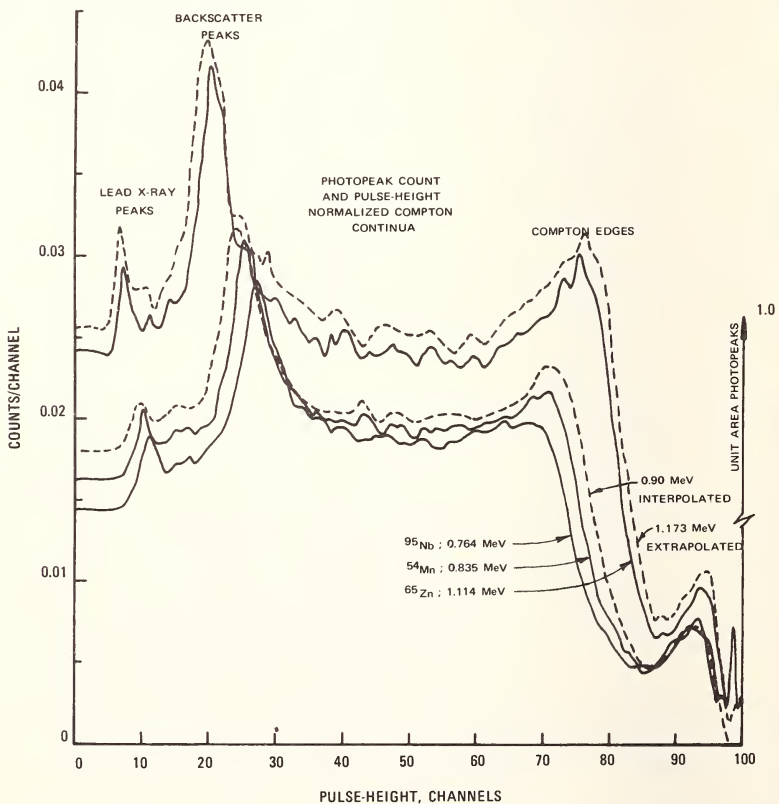
Figure 5.   NaI(Tl) response function continua determined using code GANE.
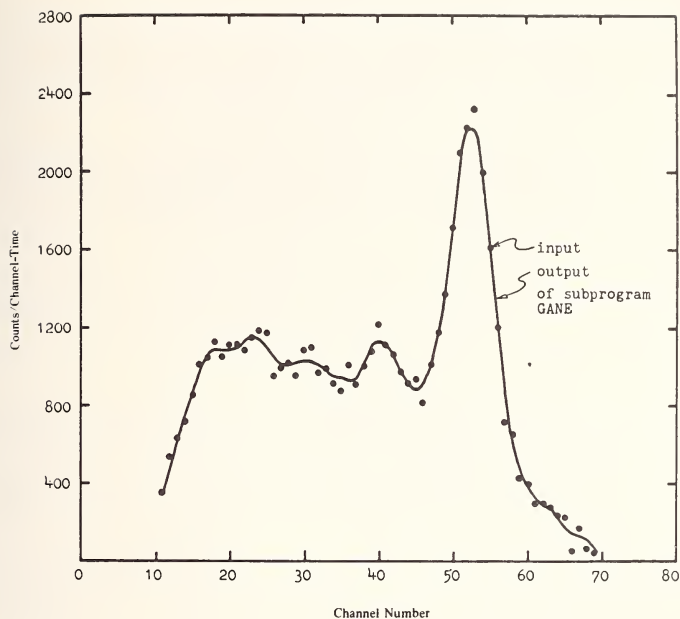
Figure 6.   Example of backscattering spectrum smoothed by subprogram GANE.

increase operations gave results statistically better than those that might have been electronically obtained. This is so for two reasons: (1) the gain increase procedure has a partial reliance on interpolation, and (2) although it is possible to predict a statistically improved gain reduced spectrum from a measured spectrum, it is not possible to predict the reverse.

In actual operation the program has represented expected spectral shape with gratifying accuracy and speed, as evidenced by the figures.

IV. References

[1]   Heath, R. L., Helmer, R. G., Schmittroth, L. A., and Cazier, F. A., IDO-17017 (1965).

[2]   Jarrard, J. D., Reactor Code Abstract Number 131, Argonne National Laboratory Code Center (1963).

[3]   Trombka, J. I., and Schmadebeck, R. L., Nucl. Instr. & Meth. **62**, 253 (1968).

[4]   Paatero, P., Nucl. Instr. & Meth. **31**, 360 (1964).

[5]   Paatero, P., University of Helsinki, Private Communication (1966).

[6]   Steyn, J. J., Ph.D. Thesis, University of Toronto (1965).

[7]   Ledley, R. S., "Digital Computer and Control Engineering," McGraw-Hill Company, Inc. (1960).

[8]   Harris, D. W., NASA-Goddard Space Flight Center, Private Communication (1967).

A COMPUTER METHOD OF PEAK AREA DETERMINATIONS FROM Ge(Li) GAMMA SPECTRA[1]

H. Robert Ralston, Bio-Medical Division
George E. Wilcox, Computation Division

Lawrence Radiation Laboratory
University of California
Livermore, California

I. Introduction

The development of Ge(Li) gamma detectors has made high resolution gamma spectrometry a readily usable laboratory tool. The resolutions which are routinely achieved have brought about a simplification in the problems of peak identification and at the same time posed problems of peak area integration.

Since the resolution is of the order of 3 keV, full width half maximum (FWHM) the number of points representing a peak on an analyzer with even 4096 channels is quite small for a spectrometer set to 2 or more MeV full scale. The peak area is determined by adding the counts in each channel within the peak and subtracting that portion which is contributed by the Compton effect from higher energy peaks. This calculation requires that the limits of the peak be defined and that the amplitude of the Compton continuum at the location of the peak be known.

This task of determining an appropriate base line (Compton level) from which to begin and end the integration of a peak area appears easy when calculations are being done by hand and subjective judgment is exercised on each peak. When computer methods are used the problem becomes one of translating a subjective evaluation into a computer program which will give consistent and accurate results.

A program which defines the baseline and limits of integration is shown in the flow chart (Fig. 1). The computational method is as follows: A spectrum is generated by replacing the counts in any given channel of original data by the average of the original point plus $n/2$ points on each side. The generated spectrum is now compared to the original data point by point. If the original data exceed the averaged data by more than k standard deviations, the original data is replaced by the averaged data at that point. The alternating process of averaging and replacing is continued with ever decreasing values of k down to 0.2. Each step of this process

---

reduces the contribution of peaks whose significance is defined by the then current k.
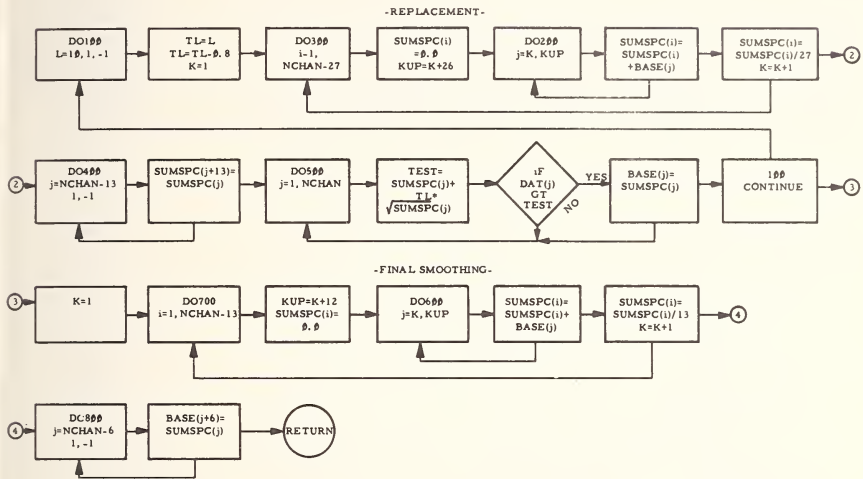
Figure 1.   Flow chart of basic program.

This repetitive process reduces the significance of all peaks until the data at previous peak locations has no more significance than the random scatter of the Compton continuum data points. Thus the final averaging represents the average of the Compton continuum with no superimposed photopeaks. The alternating process is repeated ten times. The resulting spectrum is the base.

The base is now used in conjunction with the original raw data as a basis for defining and integrating significant peaks. The portions of spectra which can cause problems are the ends and regions of sharp changes in slope. The selection of n (the number of points in the averaging process) is dependent on the number of points in the spectrum, the resolution of the system, and the conversion gain. For 2048 channels at 1.0 keV per channel, values of 27 for n give satisfactory results for a 3 keV (FWHM 1332 keV) detector. The value of k is generally set at 9.2 and reduced by 1.0 for each pass until the value is 0.2.

II. Experimental

A quantitative evaluation of the program was obtained by the use of a pulser. The pulse was injected into the preamplifier at the point where the Ge(Li) diode signal appears. The resolution was about 0.5 keV better than measured with diode pulses.

A series of pulses was placed at regular intervals along the energy axis of a ^{60}Co spectrum. The pulser was timed so that the same number of pulses was injected into the preamplifier for each position. The spectrum was then processed and the areas from each pulser peak integrated. Figure 2 shows the results of this test. The ^{60}Co spectrum was counted for 10 minutes, and in a second run, for 100 minutes. The pulses were paired in some portions of the spectrum so that it would be possible to determine in effects of peak separations. The separation of the peaks was varied.
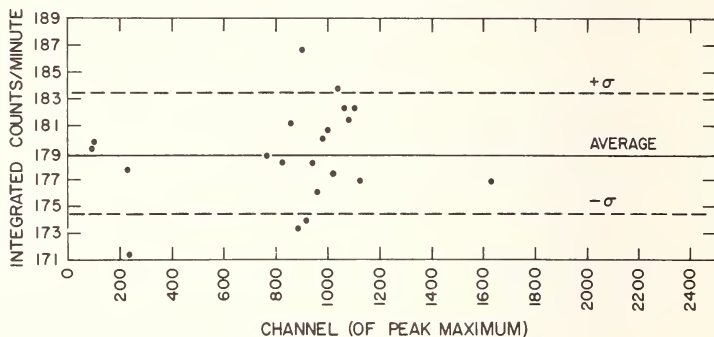
Figure 2.   Scatter of peak area pulser generated peaks superimposed on a ^{60}Co spectrum.

A second series of pulser runs was done in which successive peaks were decreased in amplitude relative to the preceding peak. In this way it was possible to determine a lower limit of peak height upon which the program will operate to distinguish the peak. It was also possible to determine how well the peak was integrated. Table 1 shows the results of these checks. The ^{60}Co spectrum was run for 10 and 150 minutes. Figure 3 shows a portion of the spectrum with pulser peaks superimposed.

III. Results and Discussion

The pulser tests, the results of which are shown in Table 1 and Figures 2 and 3 show that the peaks can be located and quantitated to levels approaching 2 standard deviations from the averaged Compton background (base line). The determinations of peak areas is consistent in most cases with the calculated standard deviations and the uncertainties of gating the pulser on and off.

The program functions satisfactorily for most spectra with well defined peaks. It fails to quantitate two peaks which are not separated by having a low point between them less than $k\sigma$ above the base line. This is an inherent limitation on a generalized single pass program. "Double" peaks are identified. Although such peaks are not quantitated, all pertinent
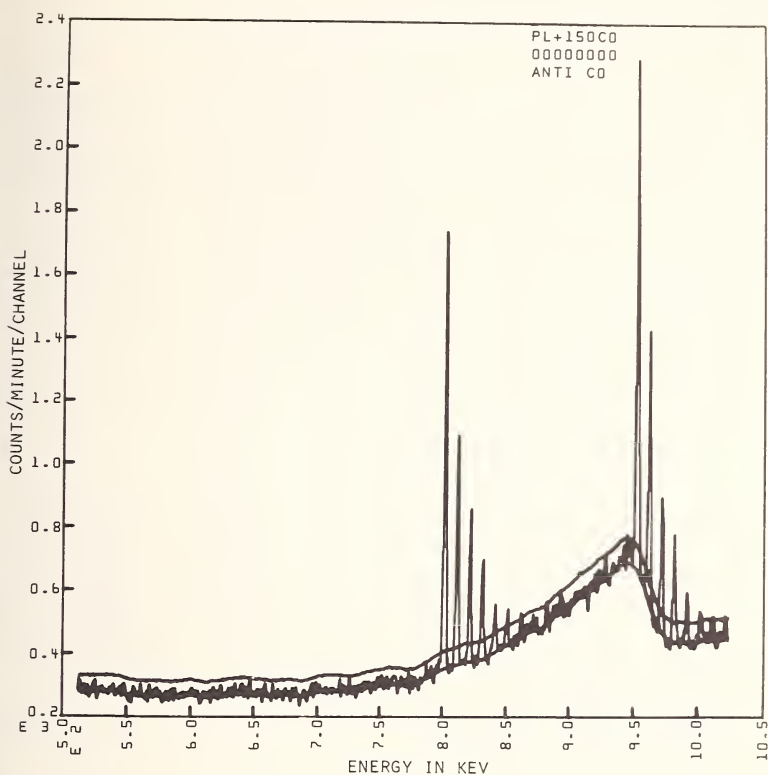
Figure 3. Pulser produced peaks superimposed on the Compton edge of a ^{60}Co spectrum. The lower line is the generated base and the upper line is the 2σ level.

parameters are saved. A later subroutine will be required to resolve these "doubles."

Peaks which are on a Compton edge are readily identified and quantitated down to levels approaching twice the background under the peak.

Figure 4 is a portion of a mixed gamma spectrum. The peaks at the 520 keV region were identified by the program as separate peaks and satisfactorily quantitated. The peak at 720 keV was identified as a single peak. The peaks at 750 to 760 keV were identified as a triple peak. The program identified the step on the leading edge of the 750 keV peak as a maximum with a subsequent minimum greater than the 2σ level. The peak area reported was for all three peaks combined. The peaks at 810 keV and 865 keV were identified and quantitated.

The triple peak can be resolved into its separate components by raising the $k\sigma$ level above $k = 2$ so that the minima are below the $k\sigma$ line.

The Fortran 400 listing of this program is available upon request.

Table 1. Integrated peak areas for pulser generated peaks.[a]

Location (channel) number)	Pulser peaks only (no Compton)	FSD	Peaks + 10 min ^{60}Co spect.	FSD calc by computer program	Actual deviation from original value	Peaks + 150 min ^{60}Co spect.	FSD calc by computer program	Actual deviation from original value
300	3581	.017	3540	.018	.012	3516	.025	.018
310	1802	.024	1756	.026	.026	1902	.038	.053
320	1068	.031	1060	.035	.007	1031	.063	.034
330	718	.038	701	.043	.024	795	.078	.032
340	368	.053	357	.066	.030	262.3	.158	.287
350	191	.074	146	.108	.236	—	—	—
360	154	.082	128	.118	.169	168.1	.254	.092
370	126.5	.091	96.4	.144	.238	—	—	
380	84.2	.111	90.9	.165	.080	—	—	—
390	57.4	.136	49.0	.236	.146	—	—	—
800	3601	.017	3589	.017	.003	3528	.025	.020
810	1794	.024	1760	.026	.019	1750	.039	.025
820	1082	.031	1050	.035	.030	975	.058	.099
830	737	.037	700	.044	.050	662	.083	.102
840	369	.053	354	.068	.040	333	.159	.098
850	202	.072	182.3	.105	.098	182	.239	.099
860	162	.079	185.6	.112	.146	—	—	—
870	124.9	.090	93.6	.158	.250	—	—	—
880	90.6	.107	—	—	—	145	.316	.600
890	67.3	.123	53.7	.265	.200	—	—	—
950	3587	.017	3585	.018	.0006	4100	.026	.143
960	1792	.024	1781	.026	.006	1932	.045	.078
970	1085	.031	1043	.035	.039	926	.067	.147
980	721	.038	680	.045	.057	727	.090	.008
990	367	.053	335.5	.068	.086	279	.161	.240
1000	190	.074	189.2	.111	.004	258.3	.209	.360
1010	148.3	.084	120	.131	.190	141.3	.311	.047
1020	106.7	.099	86.7	.169	.187	—	—	—
1030	100.6	.101	64.5	.214	.360	—	—	—
1040	57.4	.133	—	—	—	—	—	—

[a] Column 2 shows the calculated peak areas without any Compton continuum.

Column 4 shows the peak areas as calculated after a ^{60}Co source was counted for 10 minutes to give a relatively low Compton continuum.

Column 7 shows the peak areas as calculated after a ^{60}Co source was counted for 150 minutes.

The fractional standard deviations (FSD) were calculated by the Computer program. Actual deviations from the original peak areas are shown for comparison.
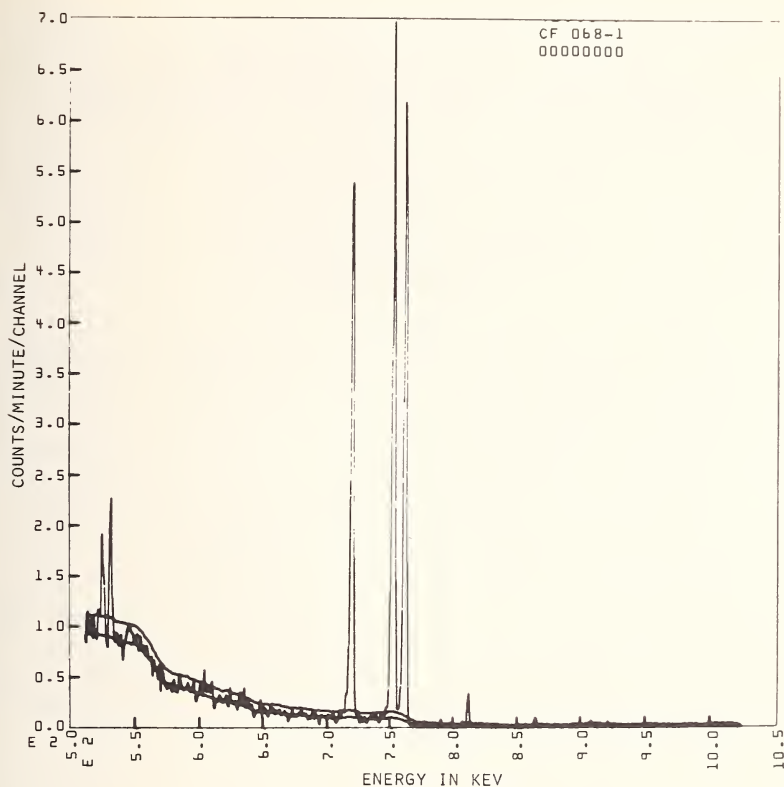
Figure 4. Portion of mixed gamma spectrum showing the generated base line and the 2σ line.

QUANTITATIVE ANALYSIS OF UNKNOWN MIXTURES BY COMPUTER REDUCTION OF Ge(Li) SPECTRA[1]

Ray Gunnink and J. B. Niday

Lawrence Radiation Laboratory
University of California
Livermore, California

The extensive use at this laboratory of Ge(Li) gamma-ray detector systems as nondestructive analytical instruments has necessitated the development of computer programs capable of accurate reduction and interpretation of the spectral data. This need resulted not only from the large number of data channels typically used but also from the complexity of the spectra. We have written and previously reported [1] on a code which has given us over two years of valuable service in analyzing samples containing mixtures of fission and activation products. With the experience gained we have been able to make several improvements in the analyses performed by the operating program. This paper will emphasize a recent major change in the treatment of unresolved peak interferences in the final calculation of the disintegration rates of the various components.

A summary of the data reduction sequence used by the program is as follows. First, the significant peaks in the spectrum are found by examining the change in slopes between data points, a process which takes into consideration the statistical uncertainty of the channel counts involved. After finding the exact position of the beginning and ending channels, and the background for each peak, the net peak areas are determined by simple integration. Some special provisions are made for assessing the areas of partially resolved multiplets. Next, an energy scale is calculated from input data and is used to determine the precise energy of all the peaks found in the spectrum. Also, the gamma-ray intensities are calculated from the peak areas using data on geometry, sample parameters, and detector efficiency.

At this point the spectral data have been reduced but not interpreted in the analytic sense. The method we have adopted involves identifying the most probable source for each peak individually by use of appropriate decay scheme information. A previously prepared library tape provides organized and cross-indexed data on half lives, parent-daughter

---

relationships, exact gamma-ray energies and branching intensities, and selected associative relationships.

First, all known gamma rays whose energy is within a specified tolerance of the measured value for the peak are considered as possible sources. Discrimination between these is based on a series of mathematically formulated tests which evaluate the agreement of the energies, and the energy and intensity relationships of one or two gamma rays which should be found in association with the peak, and also consider the half life of the candidate in relation to the age of the radioactive sample. After all the peaks have been assigned to various nuclides (with alternate choices retained in some cases), our procedure has been to calculate separately the disintegration rate corresponding to the total count under each peak assigned to a given nuclide and to report a weighted average along with the individual results. Even with present day high-resolution equipment, complex spectra contain unresolved peak interferences which result in the calculation of high values and some potential loss of information. It has been essential, therefore, that a careful selection be made from the computer-printed results by a knowledgable experimenter.

In attempting to solve this problem, we have written a computer routine which uses the method of least squares to solve a set of linear equations describing the spectral information. This procedure assumes that the observed peak intensities are due to a linear combination of one or more components. The contribution of a component to a particular peak is determined by its branching intensity for that gamma ray and by its disintegration rate which is the value we wish to determine. An ordered array is first prepared with one column for each identified species (or alternate) and one row for each identified peak. The entries in this matrix of coefficients are the appropriate gamma-branching probabilities obtained from the library tape. From this array, the sets of nuclides with one or more interferences each can be selected and appropriate matrices constructed for analysis by the linear least-squares routine [2] in use at our computation center. We have found that for a complex spectrum of fission products, the "chain reaction" of interferences is such as to draw nearly all the components into a single matrix.

The results thus far on this new approach have been very encouraging. The procedure used in setting up the matrix arrays for calculation, some of the problems encountered, and results of typical analyses will be presented.

I. References

[1]   Gunnink, R., Levy, H. B., and Niday, J. B., American Chemical Society Symposium
        on Nuclear Methods of Chemical Analysis, April 10-14, 1967.
[2]   This routine was written by von Holdt, R. E., Computations Division, LRL,
        Livermore, California.

A COMPUTER-BASED SYSTEM FOR NEUTRON ACTIVATION ANALYSIS

D. D. Tunnicliff and G. E. A. Wyld

Shell Development Company
Emeryville, California

I. Introduction

The calculation of the composition of a complex sample from an analysis of the spectral data obtained from neutron activation and subsequent counting with a multichannel analyzer is usually complicated by the interference of each element on the determination of other elements. If the reference spectrum of each radioisotope present in the sample is available, and if it can be assumed that the observed sample spectra are a linear combination of these individual spectra with suitable decay factors, then the composition of the sample can be determined by standard least squares calculations. The most accurate results can be obtained by solving for only the radioisotopes present in the sample. Including components not present decreases the size of the determinant, and thus increases the probable errors in the calculations. Since samples being analyzed often contain unexpected components, some method of determining both the qualitative and the quantitative composition is desirable. The stepwise regression program described by Efroymson [1] has been very successful in our laboratory [2] for the simultaneous determination of both the qualitative and the quantitative determination of the composition of samples using mass spectrometric data. This same approach has now been applied to processing data from neutron activation analysis. The application of this stepwise regression program to data obtained for a single decay time has been described by Shumway [3] and by Young and Singhal [4]. The present program simultaneously makes use of spectral data for as many as 6 decay times. Including data for several different decay times greatly increases the power of the method.

II. Mathematical Basis

The basic equation used for these calculations is as follows:

$$C_i = \phi \left[\frac{T_L}{T_2 - T_1} \right] \sum_{j=1}^{n} W_j \, A_{ij} \left[\frac{e^{-\lambda_j T_1} - e^{-\lambda_j T_2}}{\lambda_j} \right] [1 - e^{-\lambda_j T_0}] \tag{1}$$

1246

where

C_i = observed counts in channel i
ϕ = neutron flux
T_1 = decay time to start of counting period
T_2 = decay time to end of counting period
T_L = live time of counting
T_0 = length of the irradiation
W_j = weight of radioisotope j (or the element) in the sample
A_{ij} = specific activity for radioisotope j at channel i
λ_j = decay factor for radioisotope j $(.69315/T_{0.5})$.

The principal assumptions of the above equation are that the number of counts observed for any component is directly proportional to the amount of the component present; the spectra are additive; the flux remains constant during the irradiation; and the "dead time" of the analyzer does not change during any counting period. With these reservations, equation (1) must hold for all channels and all decay times. This results in a set of equations equal in number to the product of the number of channels and the number of counting periods. If the specific activities, A_{ij}, have been determined by prior calibration, then this set of equations can be solved for the unknown weights, W_j, using least squares techniques. The proper significance of each equation is preserved by dividing all terms in each equation by the square root of the observed number of counts.

Equation (1) must, of course, include terms for every significant radioisotope for each element to be considered. However, if the isotopic distribution for each element can be considered to be constant, the specific activities can be expressed in terms of the weight of the element instead of the weight of the isotope, and then the computed terms for all radioisotopes of a given element for a given channel and decay time can be added together before starting the regression calculations. This permits using these calculations to determine elements rather than just isotopes.

The stepwise regression procedure is a mathematical method of choosing from among a large library of reference spectra the smallest subset of spectra which can be combined together so as to best match the observed sample spectra. The calculations proceed in a stepwise fashion choosing at each step a new component which will give the greatest improvement in the fit of the calculated spectra to the observed spectra. The concentration for each component previously chosen is recomputed for each step. A component previously chosen may be rejected at any later step if the fit between the calculated and the observed spectrum is not unduly increased. This stepwise procedure continues until either: (1) No additional significant components can be found; (2) An adequate fit has been obtained; (3) No further significant improvement in the fit can be obtained.

The above approach is quite general in application. No special development is required for a new mixture provided all the necessary reference spectra are available and the assumptions on which equation (1) is based remain valid.

III. Use of Internal Standard

One of the problems of activation analysis is to provide some means of securing an adequate measure of the neutron flux. Another problem is to adequately correct for the effects of variations in sample size, shape and position with reference to the detector. The usual practice of analyzing a standard for each element of interest is quite undesirable for complex samples since it greatly increases the cost of the analysis, particularly when a wide variety of samples are being analyzed. The ability of a computer program to simultaneously analyze for several components makes the use of an internal standard an attractive solution to the above problems. This computer program is designed to permit the use of any element as an internal standard. The ratio of the true to computed weights of the standard is used to adjust the weights of all the other components.

IV. Reference Spectra

The library of reference spectra used for these calculations must include the spectrum of every significant radioisotope present in the sample. These spectra must be obtained using the same detector and, at least approximately, the same counting geometry as will be used for counting the samples. A separate computer program has been developed for computing these reference spectra using data obtained for either a single radioisotope or for a mixture.

If the data for a single channel and a single decay time for an element which forms several radioisotopes are substituted into equation (1), the only unknowns will be the specific activities, A_{ij}. If the sample is counted for a number of decay times equal to, or preferably greater than, the number of unknowns, then this set of equations can be solved for each of the specific activities for that particular channel. The complete spectrum of each radioisotope is obtained by repeating this process for each channel.

This program also includes, as an option, an iterative procedure to determine the half life of each radioisotope which gives the best fit of the computed spectra to the observed spectra. Data for up to 20 different decay times can be used in the calculations. When the half lives are to be determined, the decay times must be chosen so as to reflect the effect of these half lives on the observed spectra. Several trial calculations are required with some elements so as to ascertain just which radioisotopes are significant.

When the analysis program is to be used for the determination of elements and not isotopes the only requirement of these calculations is to resolve the observed spectrum of the element into a sufficient number of individual spectra which can be used later to compute an adequate representation of the spectrum of the element for any specified irradiation and counting conditions. This greatly reduces the requirements as to the accuracy of the individual spectrum.

V. Comments

The optimum use of least squares computer techniques impose some rather severe requirements on the experimental conditions used in making the measurements. The computer program and the instrumentation must be developed together if the best results are to be achieved. The instrumentation developed for use with this program is being described in a separate paper.

The program includes many options and special features. Provision has been included for modifying equation (1) to handle radioisotopes resulting from a series decay. Correction for bremsstrahlung is included as part of the calculation. Since the calculations give both the concentrations and the probable error in the concentration of each component, it has been possible to include a procedure which automatically rounds off the final concentrations to a number of significant figures consistent with the computed errors. It is also possible to force an element present only in trace amounts to enter the regression and thus calculate a probable error for the concentration of this component. This value can be used to derive an estimate of the detection limit of the component in this particular sample.

These programs have so far been applied only to samples irradiated with thermal neutrons. However, the same programs and procedures should be applicable to samples irradiated with fast neutrons.

VI. References

[1]   Efroymson, M. A., "Multiple Regression Analysis", in "Mathematical Methods for Digital Computers", Ralston, A., and Wilf, H. S., eds., Wiley, New York 1960.
[2]   Tunnicliff, D. D., and Wadsworth, P. A., Anal. Chem. **37**, 1082 (1965).
[3]   Shumway, R. H., Public Health Service, Publ. No. 999-R-5 (1963).
[4]   Young, M. H., and Singhal, N. S., Nucl. Instr. and Meth. **45**, 287 (1966).

RAPID MANUAL RESOLUTION OF
MULTI-COMPONENT GAMMA-RAY PHOTOPEAKS

H. R. Lukens

Gulf General Atomic Incorporated
San Diego, California

I. Introduction

Numerous computer programs have been devised in recent years as aids for the analysis of complex spectra *e.g.*, O'Kelley [1], Trombka [2], Schonfeld, Kibbey, and Davis [3], and Yule [4]. By contrast, little attention has been given to manual methods for resolving multi-component photopeaks. Carnahan has described an excellent detailed procedure for this purpose [5]; however, it requires the computation of a minimum of 22 quantities in its application.

The method presented here for manually resolving overlapping peaks is analogous to that of Carnahan insofar as the histogram nature of the data is recognized, and a normal probability of distribution is assumed. However, the present method features a truly simple calculation that involves only one basic equation and the Table of the Normal Curve of Error (TNCE) [6].

Briefly, given that the, full width half maximum (FWHM) resolution of a multichannel analyzer system has been calibrated, the resolution of a photopeak may be expressed in units of s per channel, S, for a particular conversion gain setting:

$$S = 2.356 \, \sigma/n, \qquad (1)$$

where n is the number of channels at FWHM, and σ is the standard deviation of the normal curve of error.

The fraction, F_m, of N total net photopeak counts (in a single-component photopeak) that will fall in m channels to one side of the peak's centerline can be found in TNCE by looking up the area corresponding to t, where $t = mS$. Then, if G_m total gross counts are in m channels, and the average peak baseline value is B counts per channel,

$$G_m - mB = F_m N, \qquad (2)$$

Where the shape of the baseline under a composite photopeak is in doubt, but can be assumed to be reasonably linear over a small number of

1250

channels, equation (2) may be set up for each of two values of m, and the simultaneous solution of the two equations will be independent of the actual value of B.

Variations of the method permit one to test an unknown photopeak for spectral purity (where the instrument resolution is known), or to determine the FWHM of the photopeak of a standard source. In one variation, TNCE if not required.

II. Experimental

A. APPARATUS

The following radionuclides were used: ^{69m}Zn, ^{22}Na, ^{64}Cu, ^{124}Sb, ^{134}Cs, and ^{137}Cs.

Two multichannel gamma-ray spectrometers each equipped with a 3-inch by 3-inch solid NaI(Tl) detector, were used: (1) a 400 channel system with 8.83% FWHM resolution at 0.605 MeV, and (2) a 100 channel system with resolutions of 8.35% at 0.603 MeV and 8.00% at 0.662 MeV.

B. PROCEDURE

Three basic experiments were carried out.

Experiment 1. The following spectra were obtained with the 100 channel system at a conversion gain of 15.0 keV per channel: (1) ^{137}Cs, counted for 2 minutes, (2) a composite of the first spectrum and that of ^{124}Sb, counted for 3 minutes, and (3) ^{124}Sb, counted for 3 minutes.

Experiment 2. The following spectra were obtained with the 100 channel system at a conversion gain of 14.6 keV per channel: (1) ^{22}Na, counted for 4 minutes, (2) ^{64}Cu, counted for 10 minutes, and (3) ^{64}Cu plus ^{69m}Zn, counted for 10 minutes.

Experiment 3. The ^{134}Cs source was counted for 40 minutes with the 400 channel system at a conversion gain of 15.4 keV per channel.

III. Results and Discussion

A. RESULTS

Experiment 1. The net photopeak counts obtained from counting the two sources alone, plus added relevant information, are given in Table 1. Gross counts in the composite spectrum over the region of interest are given in Table 2. The average baseline value, B, under the composite peak was 365 counts per channel.

Computation of the ^{137}Cs contribution to the composite spectrum based on B and the gross counts in channel 45 was carried out as follows. With the peak centerline at channel 44.0, $t = 1.5 S$ (channels 45 plus one-half of

Table 1. Individual ^{137}Cs and ^{124}Sb spectra, relevant data.

Radionuclide	Eγ MeV	Photo-peak channel	Resolution FWHM channels	Resolution S, σ per channel	Time (min)	Net photo-peak counts[a]
^{137}Cs	0.662	44.0	3.52	0.668	2	11,855 ± 116
^{124}Sb	0.603	40.8	3.41	0.690	3	11,346 ± 135[b]

[a] Plus—or—minus values are one standard deviation based on counting statistics.

[b] The 0.603 and 0.72 MeV photopeaks of ^{124}Sb had 13,102 ± 147 net counts combined.

Table 2. Composite ^{137}Cs and ^{124}Sb photopeak, raw data (^{137}Cs — 2 min, plus ^{124}Sb — 3 min), over region of interest.

Channel	Gross counts	Channel	Gross counts	Channel	Gross counts
34	625	42	3360	49	415
35	611	43	3445	50	302
36	677	44	3733	51	183
37	927	45	2952	52	190
38	1605	46	1732	53	121
39	2688	47	989	54	100
40	3630	48	644	55	115
41	3744				

channel 44) corresponds in TNCE to $F_m = 0.3418$; and t = 0.5 S (one-half of channel 44) corresponds to $F_m = 0.1308$. Therefore, in channel 45, F_m = 0.3418 − 0.1308 = 0.2110. By equation (2), 2952 − 365 = 0.2110 N, and N = 12,380 ±320 net counts, where ±320 is one standard deviation based on counting statistics.

The simultaneous equation method was also used to compute the ^{137}Cs contribution to the composite spectrum. With $t = 2.5$ S (channels 45, 46, and one half of channel 44) corresponding to $F_m = 0.4525$, the value for F_m in channel 46 was 0.4525 less 0.3418, or 0.1107. The equations obtained were:

$$2952 - 365 = 0.2110\,N$$
$$1732 - 365 = 0.1107\,N.$$

The solution found for N was 12,200 ±680 net ^{137}Cs counts.

The total ^{124}Sb contribution to the total of 25,011 ±193 net counts in the composite photopeak was calculated to be 12,811 ±374 net counts by subtracting the computed ^{137}Cs contribution from the total. The net counts contributed by the 0.603 MeV ^{124}Sb gamma ray were computed by the simultaneous equation method using channels 37 and 38 (fractional peak area = 0.0622 and gross counts = 2532) in one equation, and channels 39 and 40 (fractional peak area= 0.3810 and gross counts = 6318) in the other equation; the computed value was 11,850 ± 450 net counts.

Experiment 2. The 0.511 MeV photopeak of ^{22}Na was found to have 75% of the total net counts in channels 34 through 36. Of the 53,287 ± 242 net counts in the composite photopeak, 33,834 ± 196 net counts were estimated to be in channels 34 through 36. Thus, the ^{64}Cu contribution was estimated, by 33,834/0.75, to be 45,100 ± 261 net counts.

The net counts in the 0.511 MeV photopeak of the individual spectrum of ^{64}Cu were found to be 45,451 ± 239.

Experiment 3. The ^{134}Cs photopeak, given over the region of interest in Table 3, contained 91,319 ± 390 net counts, and the peak centerline fell at channel 39.4. The FWHM appeared to be 10.9%, when computed by Eq. (2) and TNCE. Since the system resolution was known to be 8.83% for 0.605 MeV gamma rays, it was apparent that the photopeak contained more than one component.

Table 3. ^{134}Cs spectrum, over region of interest.

Channel	Gross counts	Channel	Gross counts	Channel	Gross counts
30	4690	36	8846	42	7797
31	4619	37	12887	43	3129
32	4582	38	18121	44	1560
33	4662	39	22661	45	1313
34	4943	40	22217	46	1300
35	6154	41	15464	47	1419

Since the true channel widths were known to be 0.676 σ/channel, the contribution of the 0.605 MeV gamma ray was calculated from the 19,127 ± 158 net counts in channel 40. Channel 40 theoretically contained 0.108 (from 0.4 × 0.676 σ) plus 0.158 (from 0.6 × 0.676 σ), or 0.266 of the net counts; therefore, the 0.605 MeV component was computed to be 72,000 ± 600 net counts.

B. Discussion

Table 4 summarizes the results of the experiments, and demonstrates that the computational method herein described gives good agreement with true values (within counting statistics).

Table 4. Summary of results.

Experiment	Radionuclide	Gamma ray MeV	Net contribution, counts Experimental[a]	Computed[b]
1	^{137}Cs	0.662	$11,855 \pm 116$	$12,280 \pm 320$
				$12,200 \pm 680$
	^{124}Sb	0.603	$11,346 \pm 135$	$11,850 \pm 450$
2	^{64}Cu	0.511	$45,451 \pm 239$	$45,100 \pm 261$
3	^{134}Cs	0.605	$74,000 \pm 1450^{c}$	$72,000 \pm 600$

[a] Determined from single isotope spectra, per described experiments.[c]

[b] Determined from multi-component spectra, per described experiments.

[c] Based on data of Brown and Ewan[7], who found $81 \pm 1.6\%$ of the ^{134}Cs gamma rays at 0.605 MeV.

The simplicity and ease with which single components of composite photopeaks may be obtained by either the single equation or simultaneous-equations method was demonstrated in Experiment 1. Experiment 2 illustrates a variation in which TNCE is not required, and Experiment 3 illustrates the analysis of a peak that might appear to have only one component.

While the various facets of the method have long been known, their formulation in the present form for the rapid and reasonably accurate manual resolution of multicomponent gamma-ray photopeaks has not to the author's knowledge been previously enunciated.

IV. References

[1] O'Kelley, G. D., Editor, "Application of Computers to Nuclear and Radiochemistry", NAS–NS3107 (1962). Available from Office of Technical Services, U.S. Dept. of Commerce, Washington, D.C.

[2] Trombka, J. I., Tech. Report No. 32–373 (1962), Jet Propulsion Laboratory, Calif. Inst. of Technology, Pasadena, Calif.

[3] Schonfeld, E., Kibbey, A. H., and Davis, W., Jr., Report ORNL–3744 (1965). Oak Ridge Natl. Laboratory, Oak Ridge, Tenn.

[4] Yule, H. P., Anal. Chem. **38**, 103 (1966).

[5] Carnahan, C. L., Nucl. Instr. and Meth. **30**, 165 (1964).

[6] Weast, R. C., Editor in Chief, "Handbook of Chemistry and Physics", 45th Edition (1964), pp. A106–A109. Chemical Rubber Co., Cleveland, Ohio.

[7] Brown, R. A., and Ewan, G. T., Nucl. Phys. **68**, 325 (1965).

COMPUTER STUDIES OF COMPLEX FULL ENERGY PEAKS USING SECOND AND THIRD DERIVATIVES

Herbert P. Yule

Activation Analysis Research Laboratory
Texas A&M University
College Station, Texas 77843

Interpretation of gamma-ray spectra obtained in activation analysis frequently requires location of spectrum peaks as a first step. Once located, the peaks may be used to obtain further information of a qualitative and quantitative nature. Locating peaks with a computer program not only relieves the analyst of tedious work but usually provides more reliable results.

There are three general types of computer routines for studying spectrum peaks. The first kind searches the spectrum for peaks channel by channel, looking for parts of the spectrum which have significantly more counts than the adjacent regions on either side. Programs which operate in this way have been published by Kuykendall *et al* [1], Plantin [2], Choy and Schmitt [3], and Girardi *et al*[4]. The second method employs the smoothed first (or second) derivative, making use of the fact that the first derivative is positive on the left hand side of a peak and negative on the right. Peaks are located by searching for sign changes in the first derivative (Yule [5,6]). Alternatively, the second derivative may be examined for pronounced minima (Yule [5], Mariscotti [7]). The third type is typically used by the physicists in making detailed studies of individual peaks (Heath [8]), and fits one or more modified Gaussians to designated peaks. While this method provides extremely accurate results on designated peaks, it does not in many cases satisfy the requirements of activation analysis. Typically, what the analyst needs from the computer is a list of peak locations and intensities, and these should be obtained without having to input detailed information on peaks to be studied and detector resolution.

Methods one and two are not, however, especially well suited for the determination of locations and intensities of complex peaks, while method three was specially designed for such situations. A complex peak is one which has significant contributions from two gamma rays of different energy. Visual examination of a plot of the peak will usually permit a quick decision on whether it is complex, but programming the computer

to detect complex peaks quickly and without *a priori* information on complexity is quite difficult. A detailed evaluation of peak resolution is often useful in this regard, but may not be useful due to the limitations of method three.

Recently, Morrey [9] pointed out applications of third derivatives to the determination of peak complexity. The present paper reports the adaptation of the simplified least squares data convolution technique to studies of complex Ge(Li) detector peaks with the smoothed second and third derivatives [10].

Complex spectra were generated in the laboratory by counting a ^{51}Cr source (gamma-ray energy, 320 keV) at various settings of the "slope/intercept" potentiometer which translates the energy axis without changing channel widths. Thus, it was possible to move the ^{51}Cr peak from its usual position, centered about at channel 321, to another channel of our choice. Complex peaks were generated by accumulating a peak, changing the potentiometer, and without erasing the first spectrum, taking another count. By varying counting periods it was possible to mix peaks of different size.

Figure 1a shows a simple ^{51}Cr peak, taken with the slope intercept in its normal setting. The solid line joins points in the observed spectrum; the broken lines represent the various derivatives, as indicated in the legend. The first derivative's behavior is as explained above, positive below channel 321, and negative above. The second derivative forms a deep minimum at channel 321 because of the short radius of curvature at the top of the peak. The third derivative exhibits most interesting behavior. Approaching the peak from the left, it rises slowly, to a small maximum to the left of channel 321, descends rapidly to a pronounced minimum, very rapidly rises to a pronounced maximum, and descends less rapidly to a minor minimum. The violent behavior of the third derivative near the peak channel can be used to detect complex peaks. In Figure 1a, the third derivative exhibits three roots in the region near the center of the peak.

Figure 1b shows a complex peak composed of two peaks of relative intensity two to one. The first derivative is negative from channel 321 to 330, and its slightly erratic behavior gives an indication of the complexity. The second derivative quickly swings positive at channel 323, becoming negative again by channel 325. The third derivative has an even more pronounced reaction, exhibiting five roots rather than three as in Figure 1a. Both the second and third derivatives clearly show the complexity of the peak, with the third derivative demonstrating a more sensitive response.

Figure 1c illustrates a more subtle case in which the two peaks are closer together than those in Figure 1b. However, both the second and third derivatives clearly indicate the complexity of the peaks.
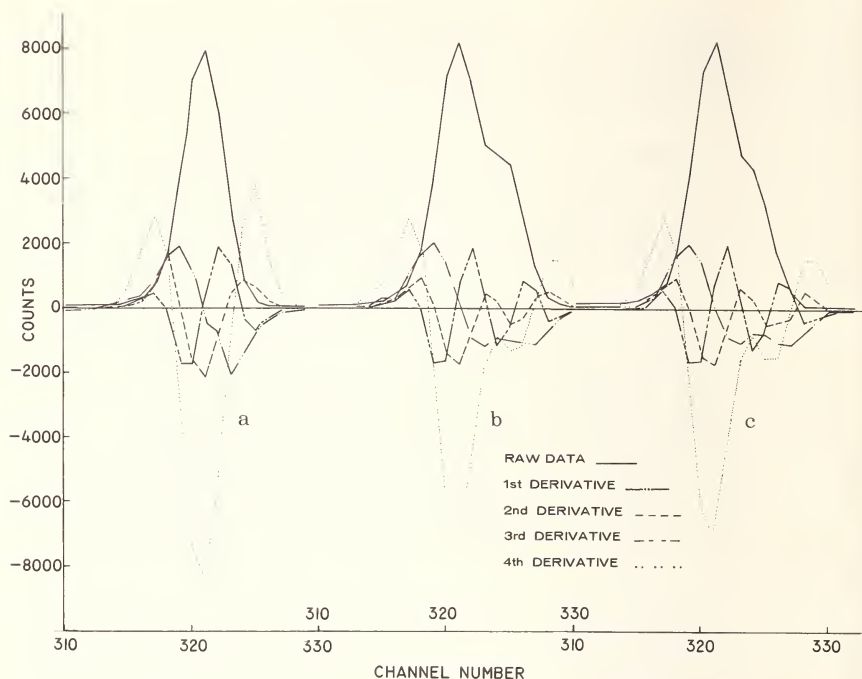
Figure 1.   a. Simple ^{51}Cr peak and first, second, third, and fourth derivatives; b. Complex peak composed of two peaks with relative intensities of two to one; c. Complex peak composed of two peaks with relative intensities of two to one.

A number of questions remain about the application of this method of detecting complex peaks. How does the implementation of the smoothing-differentiating computation affect the results? How sensitive is the method for small contributors to large peaks? How reliable is the method for small complex peaks? What is the role of statistical fluctuations in terms of reliability and sensitivity? These questions are currently under study in our laboratory.

I. References

[1]   Kuykendall, W. E., Wainerdi, R. E., "An Investigation of Automated Activation Analysis", presented at the International Atomic Energy Agency Conference on "The Use of Radioisotopes in the Physical Sciences and Industry", Copenhagen, Denmark, Sept. 6-18, 1960.

[2]   Plantin, L. O., Proceedings, 1965, International Conference on "Modern Trends in Activation Analysis", College Station, Texas, 1965, p. 91.

[3]   Choy, S. C., and Schmitt, R. A., Nature **205**, 758 (1965).

[4]   Girardi, F., Guzzi, G., and Pauly, J., Radiochimica Acta 7, 202 (1967).

[5]   Yule, H. P., Anal. Chem. **38**, 103 (1966).

[6]   Yule, H. P., Anal. Chem. **40,** 1480 (1968).
[7]   Mariscotti, M. A., Nucl. Instr. Methods **50,** 309 (1967).
[8]   Helmer, R. G., Heath, R. L., Putnam, M., Gipson, D. H., Nucl. Instr. Methods **57,** 46 (1967).
[9]   Morrey, J. R., Anal. Chem. **40,** 905 (1968).
[10]   Savitzky, A., and Golay, M. J. E., Anal. Chem. **36,** 1627 (1964).

ACCURACY, PRECISION AND STANDARDS

Synopsis of Discussions

DEREK GIBBONS, *Chairman*

Wantage Research Laboratory (AERE)
Wantage, Berkshire, England

The majority of discussion for this session was concerned with questions of homogeneity—or lack of it. This was particularly important in the provision of Standard Reference Materials since there is little point in attempting to improve the accuracy or precision of a technique if it is already better than the homogeneity (including unavoidable contamination errors) of the material on which it is being tested or of the samples to which it is being applied. The homogeneity of Standard Reference Materials must be established, not only in the general sense, but ideally for each element of potential interest. In favorable cases, where two or more elements are known to behave in a similar metallurgical or chemical way, the established homogeneity of one can at least be indicative of the homogeneity of others. However, since at present the homogeneity of Standard Reference Materials cannot be guaranteed right up to their very surface, they cannot easily be used for charged particle analysis. Even for bulk analysis a recommended post-irradiation etching procedure must be followed since too deep an etch, which can concentrate an element onto the remaining material, may be as inadequate as no etch at all.

In neutron generator analysis it was pointed out that where a sample is being analyzed as representative of bulk material, steps taken to minimize errors due to inhomogeneity within the actual sample (such as in-irradiation rotation, *etc.*) may not in fact be justified. Dual analysis of each side of a sample, by demonstrating the existence of inhomogeneity may indicate possible errors in the sampling technique. On the other hand, where a sample is a complete unique entity, and the total quantity of an element is required, then all possible steps to minimize these errors and others due to flux gradients must be adopted.

The relative merits of sodium iodide and germanium detectors was again discussed. Ignoring questions of cost differences which are a matter for the individual, it is important that these detectors be examined on a comparable and practical basis. Both detectors can vary considerably in size, and sodium iodide detectors of improved resolution are now

available. Comparisons in terms of photopeak efficiency are not necessarily adequate, since in the "least squares" interpretation of sodium iodide data, more information is used than that contained solely in the peak. The effective efficiency for a given statistical accuracy is therefore weighted even further in favor of sodium iodide. The time required to achieve a given statistical accuracy must also be considered, especially when dealing with radioactivities of relatively short half life. For nonroutine and qualitative work, the germanium detector is obviously superior in its ability to identify simultaneously such a large number of components, but where there is no fundamental objection, the use of radiochemistry coupled with sodium iodide measurements and least squares data treatment when appropriate, still gives the best results in terms of precision and sensitivity and is becoming increasingly attractive with the development of automated group separation schemes.

Finally, when considering the precision and detection limit of a technique, it is essential to provide some common and acceptable criteria of comparison, both for comparison of different activation analysis approaches and for inter-comparison of different analytical techniques. For example, there is often confusion in the literature between the error associated with the mean of a series of measurements on the same material, and that associated with a single measurement, and the relevant confidence limits are frequently omitted. However, although activation analysis may sometimes be less precise than other techniques it is usually inherently more accurate. Consequently, although it may appear unattractive on the basis of single measurements it has obvious advantages in establishing reliable analyses for reference materials.

THE PRECISION OF MULTI-ELEMENT TECHNIQUES IN ACTIVATION ANALYSIS

R. F. Coleman

*UKAEA, Atomic Weapons Research Establishment,
Aldermaston, Berkshire, England*

I. Introduction

There is an increasing need for the development and use of multi-element techniques in order to reduce the cost of analysis when the estimation of a large number of elements in a particular sample is required. The purpose of analysis is frequently to detect or monitor changes in the composition of materials, and it is the precision of the analytical method which often controls the minimum detectable difference. Activation analysis has found applications in this field, particularly in the estimation of trace elements in a sample; however, from the published literature it is difficult to assess the precision of the various methods used. In this paper, the precision of analysis of known mixtures has been determined by three activation methods and also by a more practical test involving the analysis of a glass sample with more than 20 detectable components.

II. Experimental

Since suitable samples of known composition were not available, a preliminary comparison of methods was made with artificial mixtures. 10-100 mg of chromium, zinc, silver, cobalt, tantalum metals, scandium oxide and caesium nitrate were irradiated for 12 hours in a flux of $3 \times 10^{12} n \cdot cm^{-2} \cdot sec^{-1}$. The choice of elements was dictated by the need for activation products with a single, fairly long, half life; the basic nuclear properties are listed in Table 1. Stock solutions were prepared, contained in polythene ampoules, and stored in air saturated with water vapor. From dilutions of the stock solutions, pure standards of known weight and mixtures containing varying known proportions of each element were prepared.

For the more practical test small pieces of glass, 2-12 mg in weight were irradiated for 5 days in a flux of $3 \times 10^{12} n \cdot cm^{-2} \cdot sec^{-1}$, then counted on suitable later occasions and compared with standards prepared from pure materials irradiated in similar conditions.

The artificial mixtures and the glass samples were analyzed in three ways.

Table 1. Nuclear properties of the artificial mixture.

Nuclide	Half life	Principle gamma energies (MeV)
^{46}Sc	84 d	0.889, 1.120
^{51}Cr	28 d	0.320
^{60}Co	5.2 y	1,173, 1.332
^{65}Zn	245 d	0.511, 1.115
^{110}Ag	260 d	0.658, 0.68, 0.706, 0.764 0.818, 0.885, 0.937, 1.384, 1.505
^{134}Ca	2.2 y	0.57, 0.605, 0.796, 1.038 1.168, 1.365
^{181}Ta	115 d	0.100, 0.15, 0.22, 1.12, 1.22

A. GAMMA SPECTROMETRY WITH SODIUM IODIDE DETECTOR

Direct estimation of the activities by peak area measurement was impossible in this case, because for most elements there was considerable interference from overlapping photopeaks. The spectra were resolved into the component parts by least squares analysis using a computer program based on the principle of automatic gain and threshold shifting proposed by Schonfeld *et al* [1]. It is worth emphasizing that a gamma-spectrometric system must have either a reliable stabilizing system for both gain and threshold, or alternatively, a mathematical treatment allowing for variations in these parameters if least squares methods of data analysis are used. Otherwise, large errors will result in the estimation of minor components in the spectra.

B. GAMMA SPECTROMETRY WITH GERMANIUM DETECTORS

A 20 cm³ germanium detector (full width at half maximum (FWHM), 7.0 keV for 1.33 MeV cobalt − 60 peak) was used for the measurement of activity. In this case because of the superior resolution compared with sodium iodide, some nuclides could be determined by peak area measurement with reasonable precision. Analysis of the spectra of the artificial mixtures was also performed by least squares. This method was not applied to glass samples because of the large number of components, and the number of channels necessary for data collection results in a prohibitive cost.

C. Gamma Spectrometry after Automatic Group Separation

A group separation scheme involving the sequential extraction of metal complexes by thenoyl-trifluoroacetone (TTA) and diethylammonium-diethyldithiocarbamate (DDDC) from aqueous solutions of different pH into six fractions of carbon tetrachloride has been developed. The sample is dissolved and transferred to the apparatus; all subsequent operations, such as the addition of reagents, stirring, and separation of organic phase, are performed automatically, controlled by a program previously recorded on magnetic tape. The activity of each fraction is counted in a gamma spectrometer, and the spectra resolved by least squares analysis as above.

III. Results and Discussion

A. Analysis of the Artificial Mixtures

The gamma spectra from a minimum of four different mixtures were analyzed by the different methods described, and a summary of the results are presented in Table 2. As is expected the precision varies depending on the contribution of the particular nuclide to the total activity. The method of measurement with the best precision used a sodium iodide crystal and spectrum analysis by least squares; the coefficient of variation ranging from 1% for major constituents to nearly 5% for minor components. The radiochemical group separation also had satisfactory precision of 2-3% for major constituents but rose to 25% for minor contributors. The measurement of peak areas in spectra from a germanium detector was less satisfactory; 5-9% for three of the major

Table 2. Precision of the measurement of mixed activities.

Element	NaI (least squares)			Ge (least squares)			Ge (peak area)			Radiochemical separation		
	(a)	(b)	(c)	(a)	(b)	(c)	(a)	(b)	(c)	(a)	(b)	(c)
Tantalum	35	1.0	0.4	29	3.3	1.0	29	5.6	1.6	18	[a]	[a]
Scandium	25	0.8	0.2	21	3.2	0.7	21	70[b]	14.7[b]	23	2.3	0.5
Cobalt	16	1.5	0.3	23	6.0	2.6	23	6	1.4	21	3.1	0.6
Silver	13	1.6	0.2	16	0.9	0.1	16	8.7	1.4	10	1.9	0.2
Cesium	6	2.2	0.2	9	17.1	1.5	9	14	1.3	7	8.9	0.6
Chromium	3.5	3.0	0.1	0.5	14.0	0.1	0.5	22	0.1	2	25.6	0.5
Zinc	1.5	4.5	0.1	1.5	3.3	0.1	1.5	ND[c]	ND[c]	19	2.8	0.5

Notes: (a) Proportion of total activity %.
        (b) Coefficient of Variation %.
        (c) Standard deviation as percentage of total activity.

[a] — 50% Ta lost by hydrolysis.

[b] Contamination from Ag and Ta.

[c] ND = Not Detected.

components but for the fourth [46]Sc there was serious interference from [110]Ag and [181]Ta. The [65]Zn photopeaks could not be detected in the spectra. Using the least squares method of analysis for the spectra from a germanium detector improved the precision, considerably.

B. Analysis of the Glass Sample

The results for the trace elements detected in glass are presented in Table 3 and show the mean value for more than 20 elements as well as the coefficient of variation of replicate measurements by each method. For the majority of elements, the mean values are in reasonable agreement. When this is not the case, comparison with other techniques would be required if absolute measurements are of prime importance. Since it is

Table 3. Analysis of glass sample (ppm).

Element	NaI detector		Group separation		Ge detector	
	Mean	C of V[a]	Mean	C of V[a]	Mean	C of V[a]
Barium			173	10	D[b]	
Cerium	7.7	12	8.7	10	D	
Cobalt	1.8	22	1.0	10	0.5	
Cesium	0.91	11	0.56	10	D	
Chromium	ND[c]		0.48	14	ND	
Copper	ND		0.21	24	ND	
Europium	0.41	9.0	0.21	18	D	
Iron	920	18	1120	7.3	1300	30
Hafnium	1.47	6.7	1.22	4.6	1.6	22
Lanthanum	3.7	8.9	3.69	1.5	D	
Lutetium	0.06	22	0.04	11	D	
Neodymium	6.9	11	6.7	12	D	
Rubidium	32	7.2	19.8	1.5	D	
Antimony	0.52	9.9	0.33	23	D	
Scandium	0.55	3.0	0.51	1.7	0.56	6.5
Samarium	1.13	4.6	0.70	1.8	D	
Tantalum	0.33	23	0.11	12	ND	
Thorium	1.34	4.5	1.12	3.0	1.4	14
Uranium	1.75	4.9	0.77	7.3	ND	
Ytterbium	0.34	26	0.22	5.8	D	
Zinc	ND		30	15	ND	

[a] Coefficient of variation (%).
[b] D = Detected in large sample (87 mg).
[c] ND = Not detected.

precision about which this paper is mainly concerned, this has not been done except in one case, uranium, in which the measurement following group separation was confirmed.

In the analysis of the glass, the group separation method has the best precision with 5 elements better than 3% and 13 better than 10%, compared with 1 and 9 respectively for direct gamma spectrometry by sodium iodide. In this test, the precision of measurement by germanium detector is poor, this is partly due to the poor efficiency of the detector. By counting 10 samples together, a total sample weight of 87 mg, gamma rays from 16 elements could be detected but the precision is not as good as that of the other methods.

C. GENERAL DISCUSSION

It is necessary to be cautious in drawing general conclusions from the limited data presented in this paper. Nevertheless, the particular experiment is in agreement with the normal experience in this laboratory. It should be emphasized that it is not possible to obtain good precision for a large number of elements without some careful developmental work which can usually only be justified if a large number of similar samples are to be analyzed.

The excellent precision of least square methods of analysis of gamma spectra for artificial mixtures always deteriorates to some extent in practical situations, because it is rarely possible to include all the standards required in the correct form for the analysis of unknown spectra. The problem is minimized by the prior radiochemical separation of selected groups of elements before spectrum analysis, and this accounts for the approximately similar behavior of the method for artificial mixtures and the glass sample. The least squares method of analysis of spectra both with and without group separation is often better for measuring small concentrations of nuclides, *e.g.* zinc in the artificial mixtures, than the peak area method with germanium detectors, because despite the better resolution of the latter, some photopeaks are not completely separated or may be lost in the Compton continuum.

The germanium detectors presently available are of limited size and inferior sensitivity compared with sodium iodide. Also, to take advantage of the resolution, it is necessary to spread the spectra over about 10 times as many channels. As a result, longer counting times and larger samples are necessary to accumulate sufficient counts/channel to minimize statistical errors. This seriously restricts their use in activation analysis at the present time. Their main value is in my opinion as a diagnostic tool in quickly detecting the presence of unsuspected gamma-emitters. This information can be used to advantage to produce more accurate data by other methods.

It is concluded that the use of group separations which can now be readily automated as described above is the best compromise available, permitting multi-element analysis of a wide variety of samples with good precision.

IV. Acknowledgments

I wish to thank Mr. G. C. Goode and Mr. J. R. Goodchild for assistance during these experiments.

V. Reference

[1]   Schonfeld, E., Kibbey, A. H., and Davis, W., U.S. A.E.C. Report ORNL 3744.

CONTRIBUTION TO IMPROVEMENTS IN ACCURACY AND REPRODUCIBILITY OF ROUTINE ACTIVATION ANALYSIS

F. Dugain

Centre de Recherches du Groupe Pechiney
38 – Voreppe – France

I. Introduction

In certain conditions activation analysis may be considered as a method in which systematic errors are of very little importance. For this reason we use it for the routine determination of small amounts (*i.e.* some parts per million) of impurities in our reference materials. Studies were made that demonstrate the accuracy of the figures obtained but we have sometimes observed variations up to 10 or 15% in a series. We had then to make a great number of analyses since precise results were needed. In order to avoid this loss of time we studied some factors which appeared to be related to random errors.

Let us consider the calculation of a result

$$X_{\mathrm{ppm}} = \frac{C_x}{C_s} \quad \frac{M_s(\mu\mathrm{g})}{M_x(\mathrm{g})} \tag{1}$$

C_x, C_s being the counting rates of unknown and standard in the same conditions (geometry, decay, *etc.*).

The error on the weight of the sample is negligible but not on the weight of the standard which is subject to a random error, and also to a systematic one, if, as usual, it is arising from a solution. Moreover, the activity ratio C_x/C_s supposes that sample and standard received the same flux during irradiation; it is well known that this is not the case in a pool reactor.

We will describe in this paper two attempts to get (1) the maximum of certitude about the value of each standard used in routine, and (2) an estimation of the flux depression, and the practical way to compensate its effect.

II. Experimental

A. Apparatus and Reagents

Irradiations are made in a pool reactor, in a flux of 10^{13} n·cm^{-2}·sec^{-1} with 12 to 15% fast neutrons. Radiochemical separations are carried out

1268

on anion exchange resins Dowex 1. A 400 channel analyzer with a 3 in. ×
3 in. NaI crystal is used for counting. Standards are prepared from pure
metals (3 N or 4 N) solution and stocked in silica tubes.

B. Procedure

1. Standards Preparation and Control

Two or three hundred composite standards are prepared at the same
time. Calculated amounts of pure metals are accurately weighed and
dissolved in concentrated hydrochloric acid. After addition of an
appropriate quantity of ^{22}Na tracer to get a sufficient activity, the solution
of metals is adjusted to volume. By the mean of a micropipette, a volume
of 50 μl is dropped into each silica tube. After evaporation at 70 °C, the
tubes are sealed. Then the activity of ^{22}Na is counted for each tube with a
precision of ± 0.6% (100,000 counts). It is then possible to draw the
distribution of the values and consequently to eliminate any tube that
would be situated out of a given limit of deviation.

In order to check the accuracy of the mean value, we pick up 10 tubes
in the middle class after dissolution of the dry deposit and adjust to
volume in a polyethylene flask. The average activity is compared to that
of 10 other solutions obtained by accurate macro-dilution of the original
solution.

2. Estimation of Flux Depression

Using selected standards we arrange seven of them in the irradiation
can as shown in Figure 1. After irradiation and dissolution in acid, the
elements are separated on resin [1]. In the given example, the standards
contained zinc, chromium, nickel, and cobalt. The reproducibility of
chemical separations on resin is excellent and introduces practically no
error [2]. It is possible then to get more data in one irradiation. The
eluates are counted in 30 ml polyethylene flasks. All the activities are
compared to the activity of the O tube taken equal to 100.

III. Results and Discussion

A. Results

1. Standards Control

Table 1 gives the figures obtained with 3 different micropipettes. As
shown in Figure 2, a series of 200 pieces can be normally distributed
within a range of ± 2.5% from the mean value. Routinely, two pieces are
taken from two symmetrical classes in order to avoid any correction. The
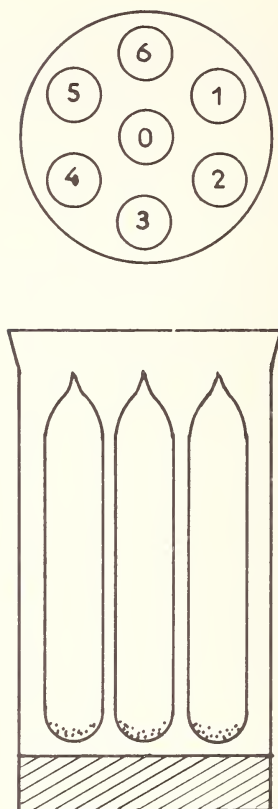
Figure 1.   Arrangement of standards in the irradiation can for flux depression studies.

Table 1. Comparison between three micropipettes
for 50 μl volumes.

Instrument	Activity (mean of 9 values)
1	$137,500 \pm 300$
2	$137,100 \pm 300$
3	$137,300 \pm 300$

Note: The differences are not significant.

average of the two values is very close to the mean value of the population. When testing the accuracy of the mean value by comparison with macro-dilution, no significant difference was found. For example,
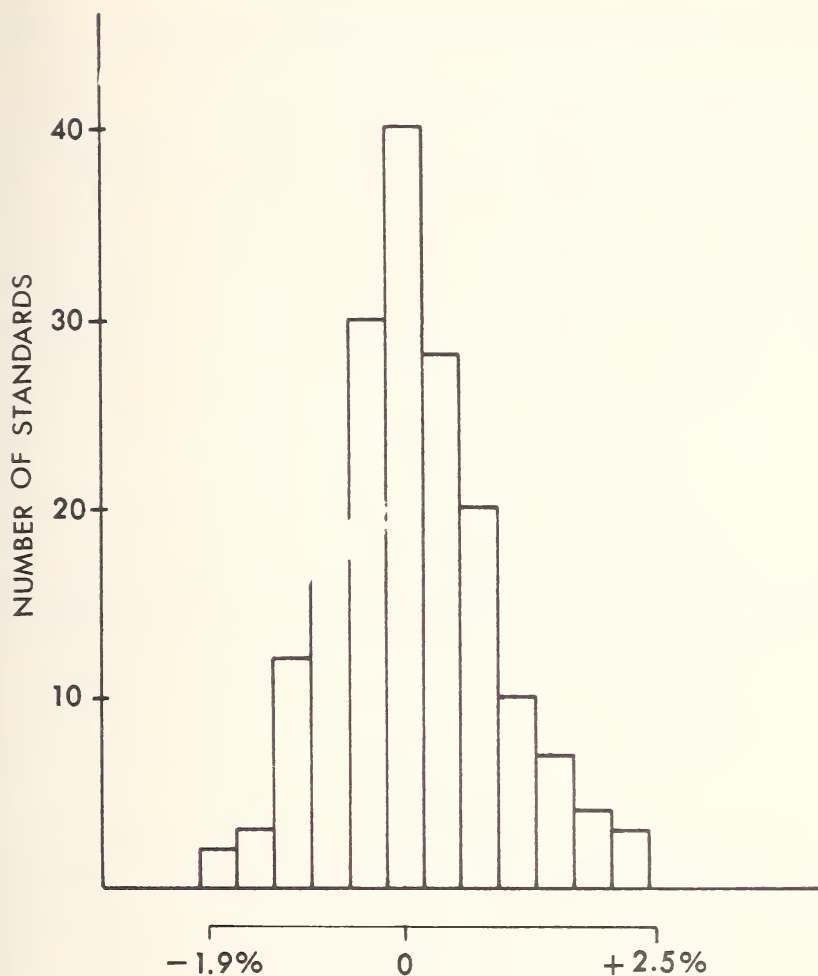
Figure 2. Distribution of 180 standards after counting the activity of ^{22}Na added. Precision on each value is $\pm 0.6\%$.

mean value for standards, $105,970 \pm 370$; mean value for comparators, $106,470 \pm 180$. The difference of 500 counts (0.5%) is not significant.

2. Flux Depression Effect

Table 2 gives the complete results of the experiment. From these figures we can evaluate the error arising from the flux according to the arrangement of sample and standard in the can.

Table 2. Effect of flux depression in a pool reactor.

		Activities (corrected from ^{22}Na value)			
Tube No.[a]	Activity ^{22}Na	^{65}Zn (n, γ)	^{51}Cr (n, γ)	^{60}Co (n, γ)	^{58}Co (n, p)
0 (central)	100	100	100	100	100
1	100.7	96.8	98.8	98.4	93.2
2	100.9	97.9	99.7	99.0	95.8
3	100.7	101.3	100.7	100.1	103.0
4	100.1	101.3	101.8	101.4	106.7
5	98.9	101.1	102.3	102.7	104.9
6	99.9	101.0	101.5	102.4	98.1

[a] See Figure 1. Tube 1 received less neutrons than the others. Flux depression for rapid neutrons appears to be much higher than for thermal ones (last column of the table).
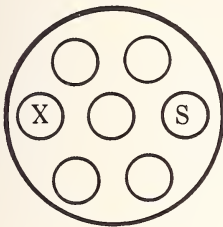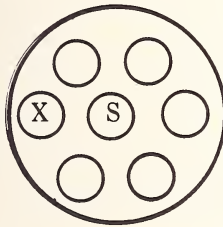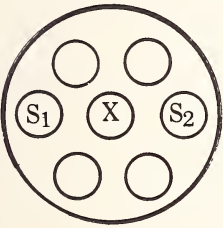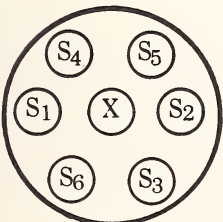
B. DISCUSSION

The mean value of the standards is supposed to be exact as we have seen above, and on eleven measurements concerning two irradiations the standard deviation was found equal to 0.9%. As previously stated two standards are used in our routine analysis, so the deviation of their mean value can be at the maximum 1.6% of the exact value. As observed in Table 3 (first line), if no care is taken about the arrangement of sample (X) and standard (S), the difference of the activities can be 4.5% for the (n,γ) reactions and 13.5 for the (n,p) reaction.

The third arrangement (that we have adopted) makes sure that the maximum difference between the mean value of the two standards and the sample is lower than 2%. Measurements on 21 pairs of standards such as S_1-S_2 compared with the O tube show that the difference due to the flux in these conditions is equal on the average to 0.75% (Figure 3). The extreme value of this difference would be 1.98% (*i.e.* 2%).

Considering equation (1), it appears that the error due to the above factors (standards and flux) can be calculated using regular statistics, that is to say by way of the square sum. In order to estimate the overall error on a result, we must add in the same way the error due to the chemical

Table 3. Maximum of flux depression according to the relative position in the can.[a]

Various arrangements in the can	Maximum difference between	Effect of flux depression in percent			
		^{65}Zn	^{51}Cr	^{60}Co	^{58}Co
1	X and S	4.5	3.5	4.3	13.5
2	X and S	3.2	2.3	2.7	6.7
3	X and $\dfrac{S_1 + S_2}{2}$	1.2	1.1	1.2	0.6
4	X and $\dfrac{S_1 + \cdots + S_6}{6}$	0.1	0.8	0.7	0.3

[a] Maximum effect of flux depression according to the relative position of the sample (X) and the standard (S). Arrangement No. 3 is usually taken for our analyses.
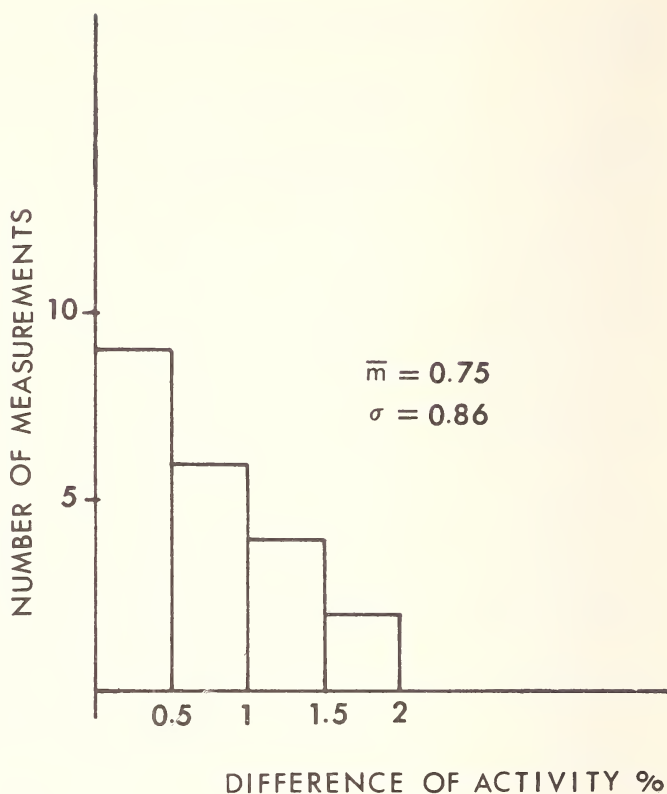
Figure 3.   Flux effect. Differences between the 0 tube and the mean value of two standards as shown in Table 3 (line 3).

separations on the resins. We said that it is very small and our experiments indicate that it is smaller than 1%. But we must take into account the possible error in counting rates. At 40,000 counts (*i.e.* ± 1%) for the sample and 250,000 counts (*i.e.* ± 0.4%) for the standard, the deviation of the activities ratio is about 1.1%. Finally, the overall error must be calculated as follows:

$$e^2 = (1.6)^2 + (2)^2 + (1)^2 + (1.1)^2 = 8.76 \ [3].\ \ \ \ \ \ \ \ (2)$$

The overall error appears to be very close to 3%. Of course the statistical treatment is neither complete nor rigorous but we think it gives a good idea of the maximum error for a single result.

C. Applications

Some examples are given which seem to confirm our conclusions concerning either accuracy or reproducibility.

1. Table 4 gives the figures for an aluminum powder considered as a reference material. Although the concentrations of some of the impurities were not in the usual range, the figures are in good agreement with our conclusions.

2. Table 5 gives the figures obtained before the application of our new method and at the present time. Accuracy seems to be satisfactory, and the precision has been obviously improved. Table 6 gives complete results for 5 irradiations in copper determination.

3. Table 7 shows the results obtained for 3 samples of aluminum (7 elements determined in each sample; two runs for each sample).

Table 4. Analysis of a powder aluminum sample.

	Other analytical methods	Our method		
		Single values	Mean	Δ (%)
Fe %	0.424	. 0.418 0.432	0.425	1.7
Ni %	2.00	1.86 2.00	1.93	3.5
Zn ppm	—	721 752	737	2.0
Co ppm	—	19.1 19.7	19.4	1.5
Cr ppm		76.6 77.3	77.0	0.5

Note: The figures in the last column agree with our calculation con-
cerning reproducibility.

Table 5. Copper in aluminum.[a]

	Cu in aluminum[b]	Δ for a single result	Δ(%)
Usual method	3.73	0.5	13
New method	3.66	0.14	4

[a] Reproducibility is improved. There is no significant difference between the two mean values.

[b] Results of 6 determinations.

Table 6. Deviation observed in copper determination on two samples, five runs each sample.[a]

	Copper, ppm	
Irradiation	Aluminum 1	Aluminum 2
1	3.64	3.82
2	3.60	3.84
3	3.67	3.82
4	3.74	3.86
5	3.68	3.88
$\bar{m}$	3.66	3.84
σ	0.052	0.027
Δ max	0.135	0.07
Δ max%	3.7	1.8

[a] Δ max $= \sigma t$

IV. Conclusion

The described procedure concerning standards control and symmetrical irradiation improves considerably the confidence in a single result when making routine analyses.

V. Acknowledgment

Table 7. Deviation observed in duplicate runs for the determination of seven elements in three aluminum samples.

Samples	781 Results (ppm)	$\bar{m} \pm \Delta$	$\Delta\%$	783 Results (ppm)	$\bar{m} \pm \Delta$	$\Delta\%$	784 Results (ppm)	$\bar{m} \pm \Delta$	$\Delta\%$
Copper	580 588	584±4	0.7	198 204	201±3	1.5	81.0 81.0	81.0±0	0.
Gallium	87 90	88±2	2.3	55.4 55.8	55.6±0.2	0.4	28.5 28.1	28.3±0.2	0.7
Chromium	109 112	110±2	1.8	37.0 36.7	36.8±0.2	0.5	13.1 13.3	13.2±0.1	0.8
Nickel	90 98	94±4	4.3	36.4 41.1	36.7±0.4	1.1	13.0 12.6	12.8±0.2	1.6
Iron	2380 2440	2410±30	1.3	1740 1690	1715±25	1.5	930 970	950±20	2.1
Zinc	950 940	945±5	0.5	341 351	346±5	1.5	128 134	131±3	2.3
Cobalt	2.05 1.95	2.00±0.05	2.5	0.91 0.95	0.93±0.02	2.0	0.385 0.410	0.400±0.15	3.7

VI. References

[1]   Laverlochere, J., and Aubouin, G., Rapport CEA No. 23-59, 1963.
[2]   Dugain, F., Anal. Chim. Acta **42**, 39-50 (1968).
[3]   Lyon, W. S., Guide to Activation Analysis, D. Van Nostrand, Princeton, 1964, pp.
        72-79.

PRECISION IN THE NEUTRON ACTIVATION ANALYSIS FOR GOLD IN STANDARD ROCKS G-1 AND W-1

K. Fritze and R. Robertson

Department of Chemistry
McMaster University
Hamilton, Ontario

I. Introduction

The concentration of gold in standard rocks, G-1 and W-1, has been determined by a number of analysts and their results are shown in Table 1. An inspection of the data indicates a generally poor agreement in particular for G-1 and also that the same authors appear to obtain a better precision for W-1 than for G-1. In spite of the fact that there are specific difficulties in the activation analysis for gold related to the preparation of the standards and in some cases to the exchange between carrier and radioactive gold, it would seem that these sources of errors cannot account for such large discrepancies. This leads to the conclusion that the data variations are at least in part due to the samples themselves. The purpose of this work, therefore, is to investigate whether or not gold is homogeneously distributed in G-1 and W-1.

II. Experimental

A. Apparatus and Reagents

Irradiations were carried out at a flux of $1.6 \times 10^{13} \text{n} \cdot \text{cm}^{-2} \cdot \text{sec}^{-1}$ in the McMaster reactor. The gamma spectra of all samples were recorded using a 12 cm³ coaxial Ge(Li) detector [5] and a Series 2000 Nuclear Data 1024 channel analyzer. Some samples were also measured with a 7.5 × 7.5 cm NaI(Tl) crystal and a Nuclear Data 256 channel analyzer. All reagents used were analytical grade.

B. Procedure

One sample each of about 200 mg of G-1 and W-1 were irradiated in quartz containers for 7 days. After a three day cooling period, eight small "aliquots" were taken from each sample and weighed accurately. Each of these was transferred into a 100 ml Teflon beaker and 5 ml of a standardized gold carrier solution were added. This solution contained

Table 1. Literature values for the gold content of G–1 and W–1.

Authors	Gold content G–1 (ppb)	Gold content W–1 (ppb)
Vincent and Crocket [1]	4.3	8.5
	4.6	8.3
Shcherbakov and Perezhogin [2]	4.6 ± 0.8 (2σ)	5.0 ± 0.6 (2σ)
Baedecker and Ehmann [3]	2	4
	2.0	4.8
		4.9
Keays and Crocket [4]	3.3 ± 0.9 (σ)	5.8 ± 0.7 (σ)

4.239 mg/ml of Au and was ~6 N in HCl and ~1 N in HNO_3. Approximately 1 ml of 48% hydrofluoric acid was then added and the solution taken to dryness. Another 1 ml of hydrofluoric acid and also a few drops of concentrated sulfuric acid were added to the residue. After evaporating to SO_3 fumes, the sample was boiled with 10 ml concentrated hydrochloric acid containing a few drops of nitric acid. The resulting clear solution was filtered through Whatman 42 paper, and gold was precipitated as the metal from the filtrate using sodium sulfite. The gold was collected on a glass fiber filter disc (sample ϕ, 6 mm), washed with hydrochloric acid and alcohol, dried, weighed and counted for 2000 seconds using the Ge(Li) detector.

The reproducibility of sample preparation was checked with aliquots of a [198]Au solution containing carrier and a standard deviation of 0.7% was obtained for seven samples using NaI(Tl) counting.

The filtrates of the gold precipitations were collected quantitatively and their gamma spectra were also recorded after adjustment to a standard volume.

III. Results and Discussion

A. RESULTS

The results of the experiments are shown in Table 2 for G-1 and Table 3 for W-1. The second column gives the values for the specific activity of [198]Au (counts per 2000 sec in the 412 keV photopeak per mg rock). The counting of one set of eight samples extended over about five hours and the data were corrected for the decay during this period. All chemical yields were between 80 and 90%. The third column gives an estimate of the actual gold contents. These were arrived at by counting one sample of each set for ten minutes using the NaI detector. From the count rate and

the decay scheme for ^{198}Au, the disintegration rate was calculated using the methods described by Heath [6]. This value in turn was used together with the irradiation and decay data to estimate the amount of gold in the sample. The main purpose of this exercise was merely to show that there is general agreement with values obtained by others. They are not meant to indicate an actual analysis. The fourth column shows a relative measure for the sodium concentrations in each sample (counts per 200 sec on the 2754 keV photopeak).

Table 2. The relative gold content of G–1.

Sample	Weight (mg)	Spec. activity ^{198}Au counts/(2000 sec · mg)	Gold content[a] (ppb)	Spec. activity ^{24}Na counts/(200 sec · mg)
1	14.74	48	(3.7)	181
2	21.03	28	(2.2)	172
3	22.46	42	(3.2)	170
4	17.91	29	(2.2)	179
5	18.11	65	(5.0)	177
6	25.74	156	(12)	175
7	26.27	26	(2.0)	170
8	22.48	26	(2.0)	179

[a] See text for the method used to estimate the gold content.

Table 3. The relative gold content of W–1.

Sample	Weight (mg)	Spec. activity ^{198}Au counts/(2000 sec · mg)	Gold content[a] (ppb)	Spec. activity ^{24}Na counts/(200 sec · mg)
1	17.05	90	(6.2)	160
2	16.00	66	(4.5)	165
3	28.50	70	(4.8)	154
4	21.96	56	(3.9)	159
5	22.10	67	(4.6)	160
6	15.28	57	(3.9)	163
7	16.87	71	(4.9)	158
8	28.02	57	(3.9)	159

[a] See text for the method used to estimate the gold content.

B.   DISCUSSION

It is clearly evident from the data presented here that the trace quantities of gold in G-1 and W-1 are not homogeneously distributed in the two rock samples. This effect is much stronger in the case of G-1. On the other hand the data for sodium which is expected to be evenly distributed, are consistent within the limits of the analytical method. The discrepancies in the results for gold of other analysts and the better precision obtained previously for W-1 in comparison to G-1 can be explained entirely by the observations reported here.

Inspecting the data in more detail, one notices that the minimum value for the gold concentration appears in four out of eight samples in the case of G-1, and in three out of eight samples in W-1. Within these selected groups, the agreement between individual data is as close as can be expected from the analytical method. It is inviting to speculate on the reason for this observation. It could be that the rock samples contain one particular mineral which is homogeneously distributed in the powdered rock samples and which contains a relatively constant amount of gold. This phase would be responsible for the minimum gold content. In addition, there exist one or more gold containing minerals which show a strong tendency towards segregation. To firmly establish the existence of these minimum values, a much larger number of analyses is required, and this work is now in progress. It is also intended to attempt a mineral separation after the irradiation in order to obtain more specific information.

The heterogeneity of trace element distribution in standard rocks poses some problems. Materials of this type are obviously not very useful as standards which are used by analysts to show that a particular analytical method gives satisfactory results. The second difficulty relates specifically to neutron activation analysis. During this investigation it was found that the activated gold can be almost completely (>95%) extracted from the rock powder with aqua regia. The same was found to be true for lanthanum in G-1 whereas the extraction of sodium amounted to only ~1%. If one takes this observation as evidence for the existence of a specific acid soluble rare earth mineral present in individual particles, it appears possible that results for these elements might be low on account of self-shielding effects.

IV.   Acknowledgments

V. References

[1] Vincent, E. A. and Crocket, J. H., Geochim. et Cosmochim. Acta 1, 143 (1960).
[2] Shcherbakov, Yu. G., and Perezhogin, G. A., Geokhimiya 6, 518 (1964).
[3] Baedecker, P. A., and Ehmann, W. D., Geochim. et Cosmochim. Acta 29, 329 (1965).
[4] Keays, R. R., and Crocket, J. H., J. Radioanal. Chem. in press 1968.
[5] Fiedler, H. J., Hughes, L. B., Kennett, T. J., Prestwich, W. V., Wall, B. J., Nucl. Inst. Meth. 40, 229 (1966).
[6] Heath, R. L., Scintillation Spectrometry, Vol. 1, AEC Report IOD-16880-1 (1964).

HIGH PRECISION ACTIVATION ANALYSIS OF SODIUM USING AN INTERNAL STANDARD TECHNIQUE

R. H. Marsh and W. Allie, Jr.

Ford Motor Company
Scientific Research Staff
Dearborn, Michigan

I. Introduction

Many workers have used activation analysis to determine sodium in a variety of materials employing radiochemical separations. Reuland and Voigt [1] analyzed tungsten bronzes for sodium nondestructively, using coincident gamma counting. Lightowlers [2] determined sodium in a diamond using a pulse-height analyzer. Schroeder and Winchester [3] determined sodium in silicate rocks nondestructively by discriminating against gamma rays having energies less than 2.6 MeV, and using sodium carbonate as a standard. Kawashima [4] determined dyprosium in yttrium oxide using the yttrium as an internal standard. Standard deviation for a single determination was about 10%. Recently Lutz and DeSoete [5] employed sodium as an internal standard for the determination of carbon in sodium by photon activation analysis.

The problem under consideration here was that of the determination of macro amounts of sodium in a material which could only be readily solubilized by a basic fusion. Because of the possibility of contamination, loss of sample, dilution error, *etc.,* to which the usual methods used for the determination of sodium can be subjected, it was decided to attempt to develop a neutron activation technique which would be highly precise and accurate. Although neutron activation is usually thought of as a trace method, proper care should allow the technique to be used for macro quantities.

One of the severest limitations to the precision of activation analysis is nonuniform neutron fluxes which are found in reactors and which require flux mapping in order to apply corrections. Also, the maintenance of strictly uniform irradiation and counting geometry is difficult. The use of an internal standard obviates the necessity of mapping neutron fluxes in reactors and maintaining strictly uniform counting geometry.

1284

II. Experimental

A. APPARATUS AND REAGENTS

The following special equipment and reagents were used: a cooled, lithium-drifted germanium detector and 400 channel analyzer having a resolution of 5-6 keV full width at half maximum (FWHM) for cobalt-60 radiation, and a lithium-drifted germanium detector and 2048 channel analyzer with a digital spectrum stabilizer having a resolution of 3.5 keV FWHM. Potassium carbonate containing less than 2 parts per million of sodium, obtained from United Mineral and Chemical Corporation. All other materials used are common to an analytical laboratory.

B. PROCEDURE

Approximately 10 mg of As_2O_3 and 20 mg of Na_2CO_3 were accurately weighed into a series of 1 cm long polyethylene vials. The powders were mixed thoroughly, and the stirring rod and walls of the vial were washed down with anhydrous diethyl ether which had been saturated with polystyrene. The polystyrene pins the powders down and prevents losses in subsequent operations. The ether was evaporated and the vial filled with molten polyethylene.

The sealing operation was best done by melting low-melt index polyethylene (available from Union Carbide Corporation) in a beaker which was heated carefully over a burner or on a hot plate.   The polyethylene was poured into the vial while the vial was held in a dish of water and allowed to remain in the water until the polyethylene had set. The vials were then cut down to size for convenience and used as standards. The samples were prepared in the same manner, weighing out enough sample to obtain approximately 20 mg of sodium. Pure arsenic and sodium background blanks were prepared similarly.

The standards and ceramic samples are then irradiated for four minutes in the pneumatic tube of the reactor and cooled overnight to allow any short-lived activities and trapped argon-41 to decay. Each vial was then counted for a sufficient time to provide good counting statistics, *i.e.*, $\sigma = 0.7\%$ or better. Clock times must be recorded accurately for decay corrections. Results were obtained by plotting out the spectra, subtracting out the background blanks, correcting for decay, and calculating the percent sodium oxide. The percent sodium oxide was calculated as follows:

$$Na_2O = \frac{YN_2W_1GF}{N_1W_2} \times 100 \tag{1}$$

where

$Y=$ Average ratio of corrected counts per gram of arsenic to corrected counts per gram of sodium in the standards.

$N_1=$ Corrected counts of arsenic.

$N_2=$ Corrected counts of sodium.

$W_1=$ Weight of arsenic.

$W_2=$ Weight of sample.

$GF=$ Combined gravimetric factors.

III. Results and Discussion

During the experimental work two major sources of error became apparent. In the first place, the ability of the technique to be independent of flux variations depends on the materials being very thoroughly mixed. Merely shaking them in a vibrator for a while is not enough. With the powder spread over the inside walls of the vial, various portions would experience widely varying fluxes. Any inhomogeneities would readily be detected. If the samples were only fairly well mixed but confined to one small location, they would experience a more uniform flux and inhomogeneities would be less conspicuous. This was accomplished by mixing the material in the open vial with a quartz stirring rod. The rod and sides of the vial were then washed down with ether, the ether evaporated and the vial partially filled with molten polyethylene. The vial was cut down, producing a fairly small, sealed standard sample. This provided two other advantageous results. Practically all the air (and argon) is excluded so a twenty-hour "cooling" period is eliminated, and a fairly large number of specimens can be irradiated in the pneumatic tubes at the reactor at the same time, gaining in convenience (no sodium-24 from the pool water to wash off), as well as subjecting the specimens to a more thermalized flux.

A well thermalized flux is important because of the epithermal neutron absorption resonance peaks of arsenic. Experiments run where the samples were irradiated in the core where the flux contains a noticeably larger portion of epithermal neutrons than in the pneumatic tubes gave results which were considerably less precise.

The second major source of error was in subtracting out the pure sodium and arsenic background blanks. Attempts to reproduce the data obtained from the visual comparison gave deviations of the same order as previously mentioned. A better method is to analyze the data by computer. The method is as follows:

$$A'a = Aa - Rs\,Ba$$
$$A's = As - Ra\,Bs \tag{2}$$

where

$Aa =$ Area of the arsenic sample peak.

$As =$ Area of the sodium sample peak.

$Ra =$ Ratio of the area of the arsenic sample peak to the background blank peak.

$Rs =$ Ratio of the area of the sodium sample peak to the area of the sodium background blank peak.

$Ba =$ Area under the sodium background blank spectrum corresponding to the position of the arsenic peak.

$Bs =$ Area under the arsenic background blank spectrum corresponding to the position of the sodium peak.

Thus, two values, corrected for contributions from the other nuclide, are obtained for the sample arsenic and sodium peak areas. The values are only an improved approximation, however, since the original values used to obtain the ratio of sample peak area to background peak area were not corrected. The accuracy of the correction is improved to the limit of the accuracy of the data by repeating the process using the new values obtained until there is no observable change in value.

The final values are then corrected for decay during the individual count;

$$X = \frac{\gamma \Lambda t}{1 - \exp(-\Lambda t)} \qquad (3)$$

and for decay back to the start of the first count;

$$Z = X \exp(\Lambda t) \qquad (4)$$

The percent sodium oxide is then calculated as in (1). To test the accuracy of the method, samples which had been analyzed by atomic absorption spectroscopy were run by this method. The results are shown in Table 1.

In order to see if the method could be used for trace analysis, an attempt was made to analyze similar material which had been deposited on quartz slides. The sample weights were of the order of ten micrograms and were supposed to be identical, having been made at the same time. Standards were prepared, and internal standards were added by the evaporation of solutions. Krylon clear plastic spray was used as a protective cover. The samples were irradiated for one hour at a flux of 1.5 $\times 10^{13}$n·cm^{-2}·sec^{-1} and counted. The data were handled as before and the results are given in Table 2. The precision is thought to be as good as the ability to produce identical samples.

All the results presented so far were from data taken with the 400 channel analyzer. Peaks consisted of three or four channels. The computer program employed required data from the three highest channels in each peak. Because of this limitation, the precision of the method is reduced by shifts in the spectrum caused by gain and zero drift

Table 1. Comparison of neutron activation and atomic absorption results.

| Percent Na_2O | Neutron activation analysis | | |
	Average	Standard deviation	Average deviation percent
8.10	8.07.	0.075	0.74
7.99			
8.16			
8.03			
8.0691	8.01	0.05	0.48
7.9940			
7.9724			
7.9801	8.00	0.14	0.19
7.8943			
7.9729			
8.0894			
	Atomic absorption spectroscopy		
8.12	8.01	0.089	0.087
7.93			
8.03			
7.94			

Table 2. Na_2O in alumina on thin films.

cpg[a] As/cpg Na	Average	Standard deviation	Average deviation percent
4.1427	4.20	0.06	1.03
4.1948			
4.2659			
Percent Na_2O			
8.49	7.86	0.57	5.3
7.37			
7.72			

[a] cpg = counts per gram.

during and between measurements. This difficulty can be overcome by using a pulse-height analyzer having more channels and a digital spectrum stabilizer. By integrating the entire peak area, the counting statistics can be improved without resorting to long counting times. The stabilizer insures reproducible peak shapes and the integration can be carried out with a digital computer. An example of the precision which can be obtained is shown in Table 3. The standards were prepared by the evaporation of solutions to reduce weighing errors.

Table 3. The analysis of ceramic samples employing a 2048–channel analyzer with a digital spectrum stabilizer.

cpg[a] As/cpg Na	Average	Standard deviation	Average deviation percent
5.200	5.205	0.0069	0.100
5.202			
5.213			
Percent Na_2O			
8.166	8.157	0.012	0.109
8.154			
8.152			

[a] cpg = counts per gram.

The primary sources of error in the method are weighing errors which, when weighing into polyethylene vials, can be significant unless care is taken to avoid static charge build up; gain and zero drift in the electronics which can be eliminated or compensated by a digital spectrum stabilizer and total peak integration; the presence of epithermal neutrons in the flux; improper mixing of sample and standard; and ability to collect sufficient data to obtain good counting statistics. The major contributions to the error of the results presented in Table 3 are probably random counting errors and small weighing errors.

Ceramic samples have been analyzed on a routine basis using this method but without a digital spectrum stabilizer or total peak integration. The standard deviations for a single determination have been consistently within 1.5 percent (Table 4).

More recent work indicates that a similar weight of copper can be substituted for arsenic to eliminate the need for well thermalized fluxes.

Table 4. Analysis of ceramic.

cpg[a] As/cpg Na	Average	Standard deviation	Average deviation percent
2.8996	2.89	0.039	0.97
2.8501			
2.9267			
Percent Na_2O			
9.31	9.44	0.18	1.4
9.34			
9.64			
cpg[a] As/cpg Na			
2.7888	2.77	0.032	0.87
2.7261			
2.7983			
2.7646			
Percent Na_2O			
8.10	8.07	0.075	0.74
7.99			
8.16			
8.03			

[a] cpg = counts per gram

IV. References

[1]   Reuland, R. J., and Voigt, A. F., Anal. Chem. **35**, 1263-67 (1963).
[2]   Lightowlers, E. C., Anal. Chem. **35**, 1285-90 (1963).
[3]   Schroeder, G. L., and Winchester, J. W., Anal. Chem. **34**, 96-99 (1962).
[4]   Kawashima, Toshi, Denki Tsushin Kenkyusho Kenkya Jitsuyoka Hokoku **13**, 1835-
            43 (1964).
[5]   Lutz, G. J., and DeSoete, D. A., Anal. Chem. **40**, 818 (1968).

NBS STANDARD REFERENCE MATERIALS AVAILABLE FOR ACTIVATION ANALYSIS

W. Wayne Meinke and J. Paul Cali

Office of Standard Reference Materials
National Bureau of Standards
Washington, D. C. 20234

Considerable work has been done at NBS over the past four years to test the homogeneity of several NBS—Standard Reference Materials (SRM). Two methods have been used extensively—electron microprobe analysis and residual resistivity ratio techniques. With the former method homogeneity at a spatial resolution to a few microns is possible, and it appears that several NBS—SRM's now available as stock items are eminently suitable as round-robin standards for activation analysis. The second method mentioned above provides homogeneity information for *only* electrically active elements, but since these are generally the metallic elements, it can be shown that several very high purity SRM's are suitably homogeneous for many elements of interest.

A. STEELS AND BRASSES

NBS—SRM 461, a low alloy steel, has been carefully studied by electron microprobe and by quantitative metallographic techniques. This work is reported in NBS Miscellaneous Publication 260-3, Metallographic Characterization of an NBS Spectrometric Low-Alloy Steel Standard, R. E. Michaelis, *et al.*

The report concludes "that NBS-461 steel is sufficiently homogeneous that any present microanalytical technique can be carried out with little chance of inaccuracy due to inhomogeneity." Nickel at 1.73% was studied in detail, but other elements such as copper, 0.34%, chromium, 0.43%, and molybdenum, 0.30%, are also suitable elements for analysis. The actual certified values are given on the Certificate of Analysis which accompanies the material.

NBS Miscellaneous Publication 260-10, Homogeneity Characterization of NBS Spectrometric Standards II: Cartridge Brass and Low-Alloy Steel, H. Yakowitz, *et al* is a continuation of the work reported in NBS MP 260-3. SRM's 1102 and C1102 are cartridge brass materials in wrought and chill-cast form, respectively. Both copper, 72.85%, and zinc, 27.10% are homogeneous at micron spatial resolution. As is shown on the Certificate of Analysis, issued with the materials many elements of

interest, *e.g.,* iron, tin, nickel, aluminum, antimony, arsenic, *etc.* are present in the 7-110 ppm range. As in the case of SRM 461, the quoted statement given above concerning homogeneity, applies to this SRM also.

The SRM 463 steel, also covered in this report can be used for copper, nickel, and silicon.

Because SRM's 461-468, inclusive, were prepared as a series there is no reason to believe that any member of the series could not be used. Of all the members in this series, perhaps SRM 467 should be dismissed from consideration, because of relatively large amounts of W, Nb, Ta, and Zr being present which might cause homogeneity problems.

For the SRM's discussed thus far, it can be said generally that those elements which form continuous solid solutions with the matrix can be expected to be homogeneously distributed, even when small sample sizes are taken for analysis.

B. NEUTRON FLUX WIRES

Within the next four months, NBS will have available a Cobalt in Aluminum SRM in wire form. The cobalt will be at the 0.1% ppm level. The homogeneity of the cobalt is being measured with an accuracy of 0.1% of the amount present by the residual resistivity ratio (RRR) method. Homgeneity of this order will be available over selected, relatively short pieces of wire, while homogeneity at a 0.3% level can be guaranteed for several hundred foot lengths. This SRM should be ideally suited both from a matrix point of view, as well as the simplicity of the gamma activity induced.

C. HIGH PURITY METAL SRM's

Two SRM's have just recently been made available which are suitable for activation standards. These are SRM 682, High Purity Zinc, and SRM 683, Zinc Metal. The elements certified, together with information concerning the preparation and homogeneity are given on the Certificates of Analysis and the technical announcements. Although homogeneity for elements at the part per billion level could not be guaranteed over the entire lot of zinc (several hundreds of pounds), it can be reasonably expected that material selected from adjoining portions of the zinc bars will be suitably homogeneous at the 10 milligram sample size for elements such as copper, cadmium, iron, silver, and tin which form continuous solid solutions with the zinc. Lead, bismuth and thallium are known to be somewhat inhomogeneously distributed at the 20-50 mg level.

Both high purity and doped platinum SRM's 680 and 681, respectively, are also now available. Twelve elements are certified at the 10^2-10^4 part per billion level. For selected lots of these SRM's homogeneity is

expected to be high. Exact etching procedures to minimize plating effects and/or differential etching should be emphasized. This holds true for all these high-purity SRM's. The Certificates of Analysis and Technical Announcement give details.

Similar to the two platinum SRM's is a high-purity gold SRM just released. It may be an interesting material for use in the investigation of systematic sources of error due to flux perturbation effects and self-shielding.

The last material to be discussed is high-purity aluminum. Unfortunately, this material has not, as yet, been certified for composition. It is, however, based on RRR methods, perhaps the most highly homogeneous solid material which has ever been produced. Three grades are available for use. They are: (1) a 'so-called' 6-9's purity aluminum having a $R_{273}/R_4 = 1000\text{-}3000$, in the form of 20 mil diameter wire; (2) a single crystalline aluminum, about 1 1/2 inch in diameter by 2 inches long, called cryogenic aluminum whose RRR = 15,000; and (3) a kilogram sample prepared (partially) in Germany using a process where the aluminum is precipitated from an organic medium and then subsequently zone-refined. The RRR for this very high-purity aluminum is an amazing 45,000. For this latter material, homogeneity is expected to be very high. It should be noted that CNRS, Saclay is producing a graded chromium doped aluminum series (using the base material as in 3, above) ranging from 1-1000 ppm of chromium.

THE ROLE OF ACTIVATION ANALYSIS IN THE NBS STANDARD REFERENCE MATERIAL PROGRAM

J. Paul Cali

Office of Standard Reference Materials
National Bureau of Standards
Washington, D.C.

I. Introduction

The past twenty years has seen the foundation of entirely new technologies based on the ability of man to produce, measure, and control highly pure materials. The entire electronics industry has been revolutionized with the advent of new materials of high purity, such as silicon and germanium. In the medical, biological, and botanical fields much recent work has been undertaken to measure, discover, and explain the role of trace elements in biological and botanical processes.

The National Bureau of Standards through its Standard Reference Material (SRM) program is responsive to these new thrusts in industry and science. New SRMs of high purity materials and/or SRMs certified for trace elements are now available or are in process to enable the analyst, materials engineer, and quality control engineer to measure and control the production of these new materials. At NBS, activation analysis has already made significant contributions to this program, and will be used even more fully in the future.

II. Discussion

A. General Philosophy and Definitions

There are available to the SRM program more than 18 analytical techniques capable of measuring trace quantities at the part per million and lower level (Table 1). It is the purpose of this paper to assess the uniqueness, utility, advantages, and drawbacks of activation analysis when considered in competition with these other methods. In order to assess these qualities, however, it is first necessary to examine the SRM program in terms of its requirements and goals.

An SRM is any well-characterized material, produced in quantity, that can be used to calibrate a measurement system, or to produce scientific data that can readily be referred to a common base.

Table 1. Techniques available to SRM program for measurement of traces.

Conductimetry	Coulometry
Polarography	Potentiometry
Stripping Voltommetry	Gas Mass Spectrometry
Isotope Dilution Mass Spectrometry	Spark Source Mass Spectrometry
Ultra Micro Chemistry	Electron Microscopy
Activation Analysis – fast neutron	Activation Analysis – LINAC
Activation Analysis – thermal neutron	Fission Track Techniques
Atomic Absorption and Fluorescence	Flame Emission Spectrometry
Optical Emission Spectrometry	Fluorimetry

First, it should be emphasized that "well-characterized" does not mean, necessarily, completely characterized. Any particular SRM is always only characterized for those properties necessary for its intended end use. Implicit in this statement is also the fact that the accuracy of the certified value should be no greater than necessary.

The term "produced in quantity" means that relatively large amounts of material are processed (*e.g.* up to 10 tons for some of the steel SRMs). The homogeneity testing of such quantities is difficult, and techniques useful for this aspect of certification are in demand.

Inherent in the term "to calibrate a measurement system" is the recognition of the fact that ideally SRMs are to be certified whenever technically feasible on an absolute basis. The inherent limitations basic to any particular analytical technique must then be recognized when work is assigned.

Finally, there are certain practical considerations which enter into the decisions made in the technical management of this program. Whether to request the assignment of a particular analytical technique of an operating division will depend in part on factors such as cost, time of analysis, availability of alternative methods, difficulty of analysis, and acceptance of the technique.

With this background, the fair assessment and role of activation analysis, relative to the factors stated in the first paragraph, can now be placed in proper perspective.

B. Assessment of the Activation Analysis Technique

1. Uniqueness

The fact that there is often no analytical reagent blank associated with this method provides an opportunity, given the right SRM, to check blank values for competitive and alternate methods of analysis. The appearance

of a sodium induced activity as shown in a gamma spectrum of a high purity zinc SRM lead to a reanalysis and subsequent reevaluation of the sodium content provided by another technique. When the value of the blank is of the same order of magnitude as the trace level element being sought, then activation analysis is often without peer.

2. Utility

Whenever high purity SRMs are involved, it is usually necessary to perform a multielement analysis. Activation analysis, for many matrices, is ideally suited in this regard. When the trace elements are present at the sub-part per million (ppm) level, then the only alternate technique is spark source mass spectrometry. By judicious preplanning it is often possible for the two techniques to complement each other, each doing those elements best suited for the particular matrix on hand. Very often serious interferences in one of the techniques are of no consequence to the other.

A second area where activation analysis is useful is in the homogeneity testing required to prove the acceptability of large lots of material prior to the measurement of the elements being certified. The ability of the method to provide relative values of several elements, quickly and nondestructively, is appropriate to this aspect of SRM production.

3. Advantages

Activation analysis is, of course, well known for its ability to detect traces at extremely low levels. In many of the high purity SRMs now in process, this is in fact the only technique capable of assigning values at the part per billion level.

A second advantage, but one which other analysts must be convinced of, is the inherent lack of serious systematic errors in the method, at least when a nondestructive comparative technique is used. It will be to the advantage of all sensitive techniques to compare results on homogeneous SRMs with the view to searching out systematic errors. Because referee methods do not exist at the ppm level and below, activation analysis will play a leading role in this area of research.

Finally, light element analysis, at low levels especially, is difficult and alternate methods are few. Yet the determination of oxygen, nitrogen, and carbon is extremely important for whole classes of SRMs. Here photon and fast neutron activation analysis is leading the way.

4. Disadvantages

Activation analysis is, of course, no cure-all. Certain matrices are very difficult to handle by this technique, especially those of high capture cross

section. Problems of induced activity at high dosage rates and serious flux perturbation problems must be recognized. Not every analysis is best suited to this technique.

Random systematic errors when chemical manipulations are required, as opposed to nondestructive techniques, may be large. Additional study is definitely required in this area. Correction for chemical yield should be kept as small as possible; indeed the philosophy being used here at NBS is to make chemical manipulations as quantitative as possible in order to minimize both random and possible systematic errors.

Finally, the factor of the acceptance of a technique must be recognized. Surprisingly, it is this aspect which produces as much discussion as any other point raised. While other analysts are convinced of the detection sensitivity of activation analysis, they are not persuaded of the inherent accuracy of the method especially when performed using nondestructive comparative techniques. Somewhat bolstering this view, not unexpectedly, the literature on the accuracy of the activation analysis method is indeed sparse.

III. Conclusions

The past contributions by activation analysis to the SRM program have been significant. In the certification of two recent SRMs — high purity zinc and platinum — several elements on the certificate of analysis could not have been listed had not activation been available. The oxygen content in several metal SRMs was determined by fast neutron activation and provided an alternate analysis to vacuum fusion determinations. Certification on an absolute basis thus became feasible. In addition, the major constituents of several metallo-organic SRMs have been successfully measured and the values certified by 14 MeV neutron activation.

The real test of this technique in terms of increased accuracy of analysis and also in volume of work completed lies, however, in the immediate future. Well over 17 distinct SRM projects now in process will draw heavily on this method for the certification of a wide variety of elemental determinations covering the entire periodic table.

AN OXYGEN STANDARD FOR THE DETERMINATION OF OXYGEN IN STEEL BY 14 MeV NEUTRON ACTIVATION ANALYSIS

R. Gijbels,[1] A, Speecke,[1] and J. Hoste

Institute for Nuclear Sciences
Ghent University, Proeftuinstratt
Ghent, Belgium

I. Introduction

For the determination of oxygen in steel *via* the reaction $^{16}O(n,p)^{16}N$ by means of 14 MeV neutrons, a relative method was adopted, measuring the oxygen content of the sample by comparison with a standard of known oxygen content. Since the present method was developed for industrial application (actually 1000 irradiations per week, using 35 g steel samples, for routine analysis and extensive steel studies), the system had to be as simple and as reliable as possible and the samples easy and fast to prepare from the frusto-conical-shaped bomb samples which are now adopted in European steel plants [1]. Hence, a rotating sample assembly has not been considered.

II. Experimental

A. APPARATUS

A transport system with aluminum tubes of rectangular section (26.5 mm × 9.5 mm) was used. Sample and standard (disks 26 mm × 9 mm) were irradiated behind each other. Thus, they necessarily present the same face to the neutron generator and to the detector (Fig. 1). The samples are transported without a container and can be analyzed on both sides, allowing in this way the detection of asymmetric oxygen inclusions [2].

The sample is closest to the target and consequently is subjected to the highest neutron flux. Flux gradients, geometry factors, neutron and gamma-ray absorption must be considered (see below). The activities of samples and standards are measured simultaneously during 30 sec with two separate but nearly identical detector systems. Duplication of transport and counting equipment is fully compensated by minimization of the standardization errors and the simplicity of automatic computation of the results.

---

[1]Research associate of the I.I.K.W.
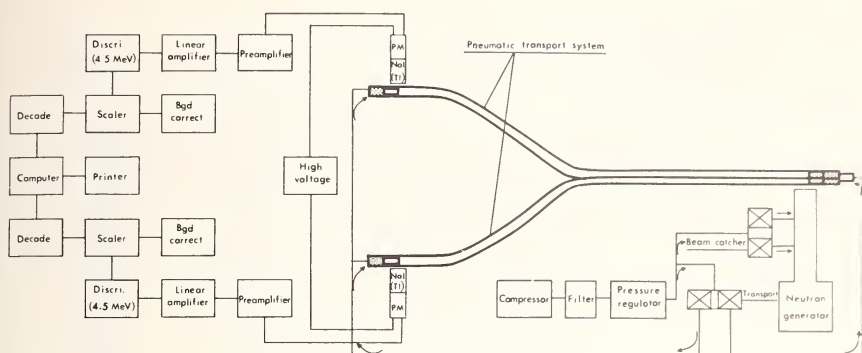
Figure 1. General design of the system.

The neutron generator was a SAMES, Type J, 150 kV, 1.5 mA accelerator with an 80 MHz-60 W rf ion source and a constant field acceleration tube (10 electrodes) using targets with a useful diameter of 18 mm.

B. Standards

The standards were cylindrical capsules in ordinary steel, machined to the following dimension (see Fig. 2): internal diameter 22.00 ±0.02 mm; external diameter 26.0 mm; internal thickness 7.00 ±0.02 mm; external thickness 9.00 ±0.02 mm; wall thickness of bottom and cover 1.00 ±0.01 mm. These tolerances must be kept as strictly as possible.

The capsules are filled with a mixture of spectrographic pure graphite (3/4) + Fe_2O_3 p.a. (1/4). Fe_2O_3 was checked for purity and the mixture for homogeneity. This mixture is pressed into the capsule at 1000 psi in 7 portions. The box contains then 4.92 g of the mixture, *i.e.* 394 mg of oxygen. The blank value, b, of the box, filled with a pure graphite pellet was 4.3-4.5 mg of oxygen as determined by activation analysis.

To be of practical value a standard must be completely symmetrical; moreover, two identical standards should be available (see below). From Table 1, it appears that the standards are identical and symmetrical; hence, they are completely interchangeable and reversible.

III. Theoretical Considerations

A. Calibration of the System ("Determination of k")

At the end of irradiation, the measured ^{16}N activity for a standard, irradiated in position 1 (nearest to the target), is given by

$$A_s(1) = \sigma[\bar{\phi}_1] w_s \theta N_0 S c_s c_1 / M \qquad (1)$$
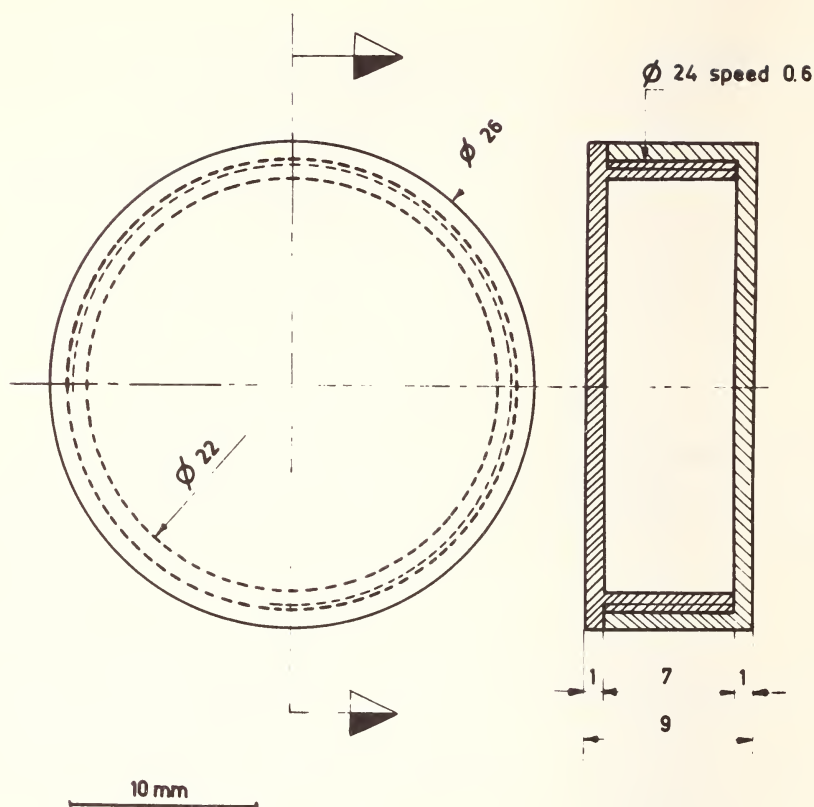
Figure 2.   Standard capsule.

Table 1.   Comparison of two oxygen standards.

Position 1	Position 2	k[a]
Standard 1[b]	Standard 2[b]	4.00 ± 0.04[c]
" 1[b]	" 2[d]	4.00 ± 0.04[c]
" 2[d]	" 1[d]	4.00 ± 0.04[c]

[a] k = ratio of measured ^{16}N activities;

[b] cover side facing the tritium target;

[c] average value of 20 determinations; the reproducibility is expressed in terms of the standard deviation for a single determination;

[d] bottom side facing the tritium target.

where

σ = 14 MeV cross section of the reaction $^{16}O(n,p)^{16}N$;

θ = isotopic abundance of ^{16}O;

M = atomic weight of ^{16}O;

N_0 = Avogadro's number;

S = saturation factor;

$[\bar{\phi}_1]$ = average 14 MeV neutron flux in the capsule at position 1 (diameter 22 mm, thickness 7 mm);

c_1 = detection efficiency, including the setting of the discriminator and the detection efficiency of the detector for the gamma rays of interest at measuring station 1;

c_s = "transmittance factor", which takes into account the absorption of neutrons in the standard during activation and the self-absorption of gamma rays during the counting [3].

The measured activity for a standard in position 2 is given by

$$A_s(2) = \sigma[\bar{\phi}_2]w_s\theta N_0 S c_s c_2 \exp(-\Sigma_s d)/M \tag{2}$$

where $\exp(-\Sigma_s d)$ takes into account the 14 MeV neutron removal by the standard, which is simultaneously irradiated in position 1.

The measured activity ratio k is given by

$$k = \frac{A_s(1)}{A_s(2)} = \frac{[\bar{\phi}_1]c_1}{[\bar{\phi}_2]c_2 \exp(-\Sigma_s d)} \tag{3}$$

B. OXYGEN ANALYSIS IN STEEL

The measured ^{16}N activity induced in a steel sample, irradiated in position 1, is given by

$$A_{Fe}(1) = \sigma\bar{\phi}_1 w_x\theta N_0 S c_{Fe}c_1/M \tag{4}$$

where:

$\bar{\phi}_1$ = average 14 MeV flux in a cylinder of 9 mm thickness and 26 mm diameter (steel sample);

c_{Fe} = the "transmittance factor" for steel.

For the standard, which is irradiated simultaneously in position 2, one can write

$$A_s(2) = \sigma[\bar{\phi}_2]w_s\theta N_0 S c_s c_2 \exp(-\Sigma_{Fe}d)/M \tag{5}$$

since the standard is shielded by a steel sample. Σ_{Fe} is the macroscopic fast neutron removal cross section for iron; $d = 9$ mm.

From equations (4) and (5) follows:

$$\frac{A_{Fe}(1)}{A_s(2)} = \frac{\bar{\phi}_1 w_x c_1 c_{Fe}}{[\bar{\phi}_2]w_s c_2 c_s \exp(-\Sigma_{Fe}d)} \tag{6}$$

After substituting equation (3) into equation (6) one finds:

$$w_x = \frac{w_s}{k} \frac{A_{\mathrm{Fe}}(1)}{A_s(2)} \frac{c_s}{c_{\mathrm{Fe}}} \frac{\exp(-\Sigma_{\mathrm{Fe}}d)}{\exp(-\Sigma_s d)} \frac{[\bar{\phi}_1]}{\bar{\phi}_1} \qquad (7)$$

where k is determined in A; $A_{Fe}(1)$ and $A_s(2)$ are determined experimentally in B; w_s is known (394 mg of oxygen), not including the blank value. Hence w_x can be calculated if the ratios c_s/c_{Fe}, $\exp(-\Sigma_{Fe}d)/\exp(-\Sigma_s d)$ and $[\bar{\phi}_1]/\bar{\phi}_1$ are known.

Since calculations yield only approximate results, these ratios have been determined experimentally. The procedure will be described elsewhere [4].

IV. Results and Discussion

A. RESULTS

1. Correction Factors

The following results were obtained

$$\exp(-\Sigma_{Fe}d)/\exp(-\Sigma_s d) = 0.949 \pm 0.006$$

$$c_s/c_{Fe} = 1/0.939 \pm 0.005$$

$$[\bar{\phi}_1]/\bar{\phi}_1 = (0.974 \pm 0.001)(1.070 \pm 0.005)$$

where the factor 0.974 takes into account the decrease in thickness of the oxygen layer in the standards as compared to the samples (9 mm-7 mm), and the factor 1.070 the decrease in radius (13 mm-11 mm).
Hence equation (7) becomes:

$$w_x = \frac{(1.053\, w_s + b)}{k} \frac{A_{\mathrm{Fe}}(1)}{A_s(2)} \qquad (8)$$

The calculations for routine analyses are performed using a small ratio computer [2]. The relative error on the correction factor 1.053 is ~1%. The accuracy is estimated to be within the same limits.

2. Accuracy Tests

The results of activation analysis were compared with those obtained by reducing fusion analysis in 3 or 4 selected laboratories of the E.S.C.C. High Authority [5]. The agreement is satisfactory although the results of activation analysis tend to be higher (see Table 2, samples 1 and 2).

3. Long-term Reproducibility

A non-killed chromium-manganese steel has been analyzed over a period of 6 months using the same oxygen standards. From Table 3 it

appears that essentially the same result is found, the average value being 941 parts per million (ppm).

Table 2. Comparison between A.A. and R.F.A. (results in ppm oxygen).

	R.F.A. average value for			R.F.A. overall average (a)	A.A. average (a)	A.A. − R.F.A. (ppm)
Sample	Lab. I	Lab. A	Lab. E	Lab. M			
1	269	265	254	—	263 ± 8	285 ± 17	+ 22
2	169	145	149	—	154 ± 13	183 ± 12	+ 29
3	146	144	137	—	142 ± 7	148 ± 7	+ 6
4	322	329	301	—	317 ± 25	316 ± 15	− 1
57	943	910	952	901	929 ± 27	935 ± 25	+ 6
68	1230	1205	1275	1233	1240 ± 35	1253 ± 40	+ 13

(a) Standard deviation for a single determination.

Table 3. Long term reproducibility (results for sample 57 − front side).

Date	Oxygen (ppm)	Date	Oxygen (ppm)
30−06−67	933 ± 13	09−11−67	936 ± 21
03−07−67	943 ± 36	09−11−67	936 ± 13
04−07−67	929 ± 27	17−11−67	944 ± 45
04−10−67	951 ± 22	23−11−67	946 ± 35
10−10−67	950 ± 20	23−11−67	934 ± 35
25−10−67	944 ± 15	07−12−67	915 ± 47
25−10−67	944 ± 15	07−12−67	944 ± 45
27−10−67	936 ± 40	08−12−67	949 ± 26
27−10−67	931 ± 37	13−12−67	934 ± 43
30−10−67	934 ± 17	14−12−67	945 ± 55

Mean long-term standard deviation: ± 30 ppm (± 3.2%)

Lowest value ± 13 ppm (± 1.4%)

Highest value ± 55 ppm (± 5.8%)

4. Influence of Beam Defocalization and Distance of Sample to Target

Although beam control is rather limited, different diaphragm currents have been used without influencing the analytical result. Even if the target to sample distance is increased from 9 mm (normal) to 15 mm, no special effect was observed (see Table 4). This means that the standard in position 2 monitors the flux in position 1 rather accurately.

Table 4. Influence of beam defocalization and distance of sample to tritium target on analytical result.

Date	Diaphragm current	Distance to target as compared with normal position	Oxygen in sample 57 (ppm)
10–10–67	normal (< 5 μ A)	+ 1.8 mm	953 ± 5
			943 ± 47
09–11–67	15–25 μ A	normal	926 ± 10
			944 ± 39
09–11–67	normal (< 5 μ A)	+ 6.0 mm	921 ± 16
			936 ± 39
09–11–67	15–25 μ A	+ 6.0 mm	959 ± 23
			949 ± 20
17–11–67	15–25 μ A	normal	944 ± 20
17–11–67	10–20 μ A	+ 3.5 mm	939 ± 12
			930 ± 26
			951 ± 19

B. Discussion

The standards and system described above have been used in the Seraing LD Steel Plant of S.A. Cockerill-Ougree-Providence (Liege, Belgium, since February 1967 [1]. The results obtained during this period are sufficiently reproducible to warrant their metallurgical use. In addition, the rapidity of the method has been amply demonstrated; the preparation of the specimen from the frusto-conical-shaped bomb sample can be effected within 35 sec using an automatic lathe [6]. Irradiation and counting time are 5 and 30 sec respectively; the results are computed automatically. The results of activation analysis agree satisfactorily with these obtained by various carburizing fusion methods. The standardization of the system is very simple. The preparation of the oxygen standard poses no special problems. Correction for differences in

geometry and in neutron and gamma-ray absorption is more complicated but must only be carried out once.

V. References

[1] Hans, A., Tyou, Ph., Lacomble, M., and Collette, F; C.N.R.M., No. 18, 37 (December 1967).
[2] De Soete, D., Hoste, J., and Speecke, A.; EUR 3656e, Euratom Brussels (1967).
[3] Fujii, I., Miyoshi, K., Muto, H., and Shimura, K.; Anal. Chim. Acta 34, 146 (1966).
[4] Gijbels, R., Speecke, A., and Hoste, J.; Anal. Chim. Acta, in press.
[5] International Committee for the Study and Rationalization of the Methods of Gas Determination in Iron and Steel, Subcommittee Oxygen. Comparison of activation analysis and reducing fusion, O.C.T. 198 (January 1968).
[6] Lacomble, M., Collette, F., Hans, A., and Tyou, Ph.; C.N.R.M., No. 13, 33 (December 1967).

A HIGH PURITY CELLULOSE AS A POSSIBLE BIOLOGICAL REFERENCE MATERIAL[1]

L. A. Rancitelli, T. M. Tanner and W. A. Haller

Battelle Memorial Institute
Pacific Northwest Laboratory
Richland, Washington 99352

I. Introduction

The increased interest in the trace element analysis of biological materials has pointed out the need for suitable comparative biological standards similar to the U.S. Geological Survey's geological standards, W-1 and G-1. Recognizing this need, Bowen [1] prepared a dry kale powder and provided samples to a number of laboratories for trace element characterization and homogeneity tests. Additional reference materials have since been prepared by other workers from alfalfa, blood, kidney powder, beef liver, orchard leaf and oak leaf [2]. A second type of standard reference material which is needed to insure precision in very low level trace element analysis is an ultrapure substance with the basic chemical and structural characteristics of biological material (a carbon, oxygen, hydrogen, nitrogen substance) with a trace element content of 1 to 2 orders of magnitude lower for determining the limitations of a procedure. It could also serve as a reference blank in assessing the level of inherent background contamination associated with an analytical procedure and would be a suitable matrix for the addition of known amounts of stable elements to produce "test samples" for use in evaluating the accuracy of a procedure at higher trace element levels.

This communication describes a material which fulfills the above criteria and has been used in this capacity in our laboratory for the past year. The material, a high purity cellulose filter (IPC No. 1478), is commercially available from Knowlton Brothers, Watertown, New York, in a 38-inch by 100-foot roll.

A trace element analysis by direct instrumental neutron activation is presented to demonstrate the homogeneity and purity of the material. For these measurements an analytical technique is described which permits trace element measurements at these very low concentrations with good precision.

II. Experimental

A. Apparatus and Reagents

Two irradiation facilities were employed in this investigation. The first, the heavy water moderated Plutonium Recycle Test Reactor (PRTR), has a rabbit system with a delivery time of about 10 seconds, and a neutron flux of about 2×10^{13} n·cm^{-2}·sec^{-1} with a cadmium ratio in excess of 100. The second facility was a graphite moderated Hanford plutonium reactor with its characteristic high, well-thermalized neutron flux.

The gamma-ray spectrometric analysis of neutron activated samples was performed with two detector systems. The first consisted of a high resolution five-sided coaxial Ge(Li) detector with an active volume of 20 cm^3 [3]. The second detector system was an anticoincidence shielded, gamma-gamma coincidence multidimensional analyzer employing NaI(Tl) crystals [4].

Two rolls of IPC filter material were sampled, one of untreated material and the second treated with Kronisol (di-butoxyethylphthalate) as a part of the manufacturing process. Clean sections consisting of about 2 sq. ft. of these IPC materials were placed in a clean laminar flow hood (Agnew-Higgins work station) and six random 0.5 gram samples were taken with a tubular quartz cutter. Each sample was placed in a clean polyethylene vial and freeze dried in a Thermovac freeze dryer for about 12 hours. The quartz cutter and polyethylene vials used in this procedure were thoroughly cleaned prior to use by leaching in double distilled nitric acid and rinsing with double distilled water. After freeze drying, the sample containers were sealed with plastic tape and wrapped in 1 mil aluminum foil to prevent in-reactor contamination.

Appropriate flux monitor standards were prepared for each set of samples. Aqueous solutions ($\sim 10^{-8}$ g/ml) of each element of interest were prepared and sealed in quartz ampoules 4 mm i.d. by 4 cm long which had been cleaned prior to use by boiling in nitric acid. Earlier work has shown that a negligible amount of contamination of the aqueous solutions results from leaching the ampoules [3]. Sets of standards were sealed in aluminum cans for irradiation with each set of samples.

B. Procedure

Each set of samples with its standards was irradiated in a graphite moderated Hanford production reactor to an integrated thermal neutron flux of about 10^{17} n/cm^2. The flux in the neutron irradiation region of the reactor is highly thermalized with a flux gradient of less than 5% over all irradiation positions. After a suitable decay period (2-3 days) the

aluminum foil was removed and the polyethylene containers were heavily lacquered to prevent transfer of external contamination to the sample. The plastic tape was then removed and the container lacquered. Following removal of the samples from their irradiation containers, the thread backing which gives structural support to the filter medium was removed and discarded, the edges of the samples trimmed to eliminate any possible contamination by the quartz cutter, and the samples were weighed.

Due to radiation damage, the samples were in a friable condition and could be readily pulverized to provide a homogeneous dispersion. They were evenly distributed in a hot 2% agar solution and placed in 1/2 in. by 2 in. rings to provide a standard counting geometry. The ampoules containing the aqueous standards were rinsed in nitric acid and distilled water to eliminate any external contamination, then opened and a 50 μl aliquot of each prepared in the standard geometry described for the samples.

Immediately after mounting, the samples were counted in an anticoincidence shielded multidimensional gamma-ray spectrometer to obtain the activity of the neutron induced ^{24}Na and ^{82}Br. After a decay period of several weeks to eliminate the ^{24}Na and ^{82}Br activities, the samples were again counted for 1000 minutes in the multidimensional gamma-ray spectrometer to determine the activation products ^{46}Sc, ^{51}Cr, ^{59}Fe, ^{60}Co, ^{65}Zn, ^{110m}Ag, ^{124}Sb and ^{140}Ba-La from U fission, The observed radionuclide concentrations in the samples and the standards were decay corrected to a standard counting time and the elemental contents of the samples were calculated from a comparison of their induced radioactivity with the specific activity of the standards.

Two samples of untreated IPC material, together with the appropriate standard solutions were irradiated in the rabbit facility of the heavy water moderated Plutonium Recycle Test Reactor to an integrated neutron exposure of 10^{15} n/cm^2. Several gamma-ray spectra of the sample and standards were taken with a 20 cm^3 Ge(Li) detector system to determine the neutron induced activities ^{24}Na, ^{28}Al, ^{38}Cl, ^{42}K and ^{56}Mn. A comparison of these activities after applying the appropriate decay corrections [5], with those of the standards yielded the concentrations of sodium, aluminum, chlorine, potassium and manganese.

III. Results and Discussion

A. RESULTS

The average concentrations of several trace elements found in treated and untreated filter material are presented in Table 1 together with the standard deviation of the average and the number of analyses.

Table 1. Trace element content of IPC filter material as measured by neutron activation analysis.

Element (conc.)	Untreated	Untreated	Treated with kronisol	Bowen's kale average (7)	Estimated experimental error (%)
Na (ppm)	72 ± 2	74 ± 5	83 ± 2	2,600	5
Fe "	5.7 ± 0.1	---	3.7 ± 0.3	120	10
Mn "	---	1.2 ± 0.1	---	15	10
K "	---	<20	---	24,600	10
Cl "	---	38 ± 3	---	3,300	5
Al "	---	4.6 ± 0.4	---	6.4–80	10
Zn "	0.64 ± 0.03	---	0.53 ± 0.04	32	5
Br "	0.16 ± 0.02	---	---	24	15
Cr "	0.13 ± 0.06	---	0.16 ± 0.04	0.33	25
Co (ppb)	2.6 ± 0.1	---	2.1 ± 0.4	56	5
Cs "	0.30 ± 0.04	---	0.06 ± 0.02	69	25
Sb "	1.5 ± 0.2	---	3.0 ± 0.2	65	10
Sc "	0.40 ± 0.1	---	0.45 ± 0.02	8.4	10
Ag "	<1	---	<1	30–50	15
U "	<1	---	<1	-----	15
Number of analyses	5	2	6		

An estimate of the total experimental error based upon counting statistics, self-shielding errors, side reactions, source inhomogeneity, and contamination is also presented in Table 1 for each element. Counting statistics generally accounted for the major portion of the error except in the case of scandium.

It is evident from Table 1 that small differences do exist in the trace element content of the treated and untreated filter material. However, each material is rather uniform and ultrapure with respect to the elements considered. The concentrations of many elements are well below the detection limits of most analytical procedures but are obtainable by careful activation analysis. An analysis of Bowen's kale [7] is included in Table 1 to provide a comparison of trace element levels in kale with this very pure cellulose material. Not only the trace elements but the more abundant constituents: potassium, sodium and chlorine, which are typically high in biological tissue, are extremely low in the IPC filter material.

B. Discussion

The properties of IPC filter material make it a very desirable substitute to serve as a biological reference. It does fill the need of a very high purity material which is essential where the merits of an activation analysis procedure for minor constituents must be tested. It is recommended that any organization which assumes the responsibility of providing biological reference materials consider this or a similar material which would allow the critical evaluation of analytical procedures at levels comparable to the lowest expected in biological materials.

IV. References

[1]   Bowen, H. J. M., Analyst **92**, 124 (1967).
[2]   Smith, G. W., and Becker, D. A., Proceedings of the Symposium on Nuclear Activation Techniques in the Life Sciences, Amsterdam, May 1967, paper SM-91/61.
[3]   Rancitelli, L. A., Haller, W. A., and Cooper, J. A., "Instrumental Neutron Activation Analysis of Biological Tissue", to be published in Physical Sciences Annual Report for 1967.
[4]   Perkins, R. W., and Robertson, D. E., Proceedings of the 1965 International Conference: "Modern Trends in Activation Analysis", College Station, Texas, p. 48, 1965.
[5]   Hoffman, B. W., and Van Camerik, S. B., Anal. Chem. **39**, 1198 (1967).
[6]   Friedlander, G., Kennedy, J. W., and Miller, J. M., "Nuclear and Radiochemistry", John Wiley and Sons, Inc., New York, Chapter 6 (1964).
[7]   Girardi, F., Pauly, J., Sabbioni, E., and Vos, G., Proceedings of the Symposium on Nuclear Activation Techniques in the Life Sciences, Amsterdam, May 1967, paper SM-91/10.

MICROSTANDARDS FOR ACTIVATION ANALYSIS

David H. Freeman

Analytical Chemistry Division
National Bureau of Standards
Washington, D. C. 20234

I. Introduction

A single ion exchange bead is ideally suited for the encapsulation of a precisely defined quantity of matter [1]. The amount may well be below the limits of weighability. The aspect of precision has two origins, as follows: (1) Ion exchange resin can be prepared under suspension conditions that can yield extremely spherical particles. This geometry uniquely permits the "weighing" of a bead in terms of diameter measurement using precise microscopic techniques [2]. (2) Ion exchange beads are available as highly homogeneous entities providing appropriate care is taken [3]; otherwise, they tend to exhibit the effects of uncontrolled factors that cause heterogeneity [4].

For spherical and homogeneous resin particles then, the bead mass m is given by

$$m = \rho v \tag{1}$$

as the product of density ρ and volume $v = \pi d^3/6$.

Ion exchange beads possess an important flexibility for variable composition. In the first case, the ion exchange sites may be saturated with a single element. Second, a mixture of two or more counterions can be prepared. The mixture is a solid solution and there is no reported evidence of departure from random counterion mixing. The first case permits exchange site saturation. The second permits controlled dilutions of different ions so that a trace loaded bead may be prepared, and many possible combinations of elements or isotopes are easily recognized.

For exchange site saturation, it is helpful to recall the conventional ion exchange capacity C(meq/g) of carefully dried resin. If the resin is in the hydrogen form, the equivalent weight of the network E_N and of the hydrogen ion E_H ($E_H = 1.008$) are related:

$$\frac{1000}{C_H} = E_N + E_H = E_{RH} \tag{2}$$

where E_{RH} is the resin equivalent weight including the exchange site structure. For any counterion, the weight fraction f^* of the element with equivalent weight E^* in the saturated bead is given by

$$f^* = \frac{E^*}{E_N + E^*} \tag{3}$$

Thus, equation (1) can be modified

$$m^* = f^* \rho v \tag{4}$$

so that it now refers to the particular element carried by the counterion.

One feature of ion exchange resin network structure is so obvious that it is easily overlooked. Each counterion is attached to an exchange site of which varied types ($-SO_3H$, $-COOH$, $-PO_3H$, *etc.*) are possible. In the case of the sulfonate, exchange site saturation requires that the number of counterions per sulfur atom approach unity. Thus, a saturated resin bead is required to carry its own internal standard, in this case sulfur. Similarly, a mixture of counterions can be devised to include an additional exchangeable reference standard.

II. Microstandard Preparation

The chemical and physical homogeneity of ion exchange particles depends upon control of the basic steps of preparation:

$$\begin{array}{cccc} \text{I} & & \text{II} & \text{III} \\ \text{MONOMERS} \rightarrow & \text{COPOLYMER} \rightarrow & \text{RESIN} \rightarrow & \text{MICROSTANDARDS} \end{array}$$
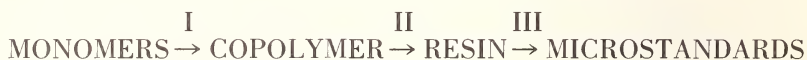
Step I is subject to requirements for optical and mechanical perfection of the copolymer beads. Step II must introduce no radial gradient of exchange site concentration within a bead, and no difference in that concentration among different beads. This respectively implies intra-particle and inter-particle homogeneity. Step III is subject to the same specification as it refers to the distributed counterions. It goes without elaboration that a microstandard bead is prone to ion-exchange loss that would be caused by inadvertant introduction of electrolytic contamination. The use of specialized procedures and reagent purity is an obvious necessity. In certain cases, it may be possible to obtain direct synthesis of the microstandard by covalent coupling of the desired atom or group onto the copolymer matrix.

While the foregoing requirements are merely outlined here, there are exhaustive experimental criteria available for testing these requirements. The same tests have been used to demonstrate the failure to achieve these properties when the proper precautions are omitted [4].

III. Evaluation of a Microstandard

There are several useful metrological features of homogeneous and spherical particles. This discussion will be restricted to one direct experimental test of equation 4 in which counterion content is related to the diameter of the individual bead. Precise light microscopy is available so that bead diameter can be obtained correctly to within 0.1 μm [2]. For a ten micron bead, this would imply a volume relative error of 3%. A factor of ten less has been obtained with larger beads [5].

The accuracy of equation 4 assumes a small degree of inter-bead heterogeneity. Activation analysis permits a direct test of the associated maximum error. In such measurements, a bulk resin sample is irradiated. For a model, it is assumed that each individual particle will yield radioactivity a_i^* (at reference time) in proportion to counterion mass. Thus, assume $m_i^* = ka_i$. The deviation is then defined:

$$\delta_i = m_i^* - ka_i^* \tag{4a}$$

Measurements of ρ and f^* describe the corresponding particle-average properties. It follows that inter-particle heterogeneity can be expressed in terms of fluctuations in the single particle measurements. Accordingly, we require that $\Sigma\delta_i = O$. Then, the specific radioactivity is obtained on the basis of an additive internal standard for the specific radioactivity: $k = \Sigma m_i^*/\Sigma a_i^*$. It follows by substitution:

$$k = \frac{\pi\rho f^* \Sigma d_i^3}{6\Sigma a_i^*} \tag{4b}$$

The relative inter-particle heterogeneity Δ is now obtained for a given particle:

$$\Delta = 1 - \frac{\pi\rho f^* d_i^3}{6ka_i^*} \tag{5}$$

For a series of measurements, the average value of Δ tends to describe the heterogeneity property of the sample.

The results of several experiments with neutron activation and analysis of single sodium loaded beads are shown in Figure 1. The 16 measurements at the far right were obtained with bead immersion in an inert hydrocarbon so that the exclusion of atmospheric moisture is maximum. The remaining points represent a series of less precise measurements that were designed to test the sensitivity of using beta-gamma-gamma coincidence counting [6] with approximately one count per hour background. It is clear that such measurements extend to nearly picogram quantities of sodium, and this implies the feasibility for

evaluating resin heterogeneity corresponding to twenty billion exchange sites. Second, it is equally clear that an improvement in measurement precision is desirable and efforts are being made to refine the experimental procedures.
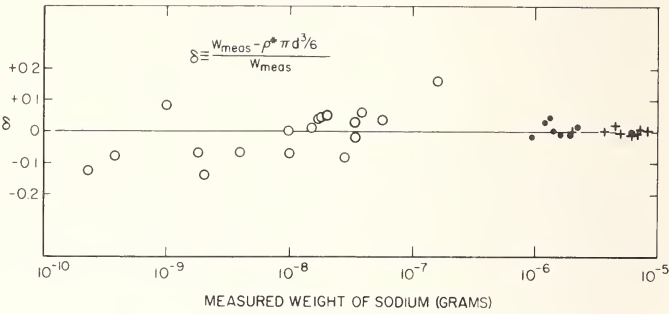
Figure 1.   Activation analysis of single ion exchange beads plotted to show bead capacity departures from a constant value.

IV.   Range of Applicability

Any ionic species that is stable in a polar solvent can be loaded onto an ion exchange bead. The periodic table shown in Figure 2 is an indication
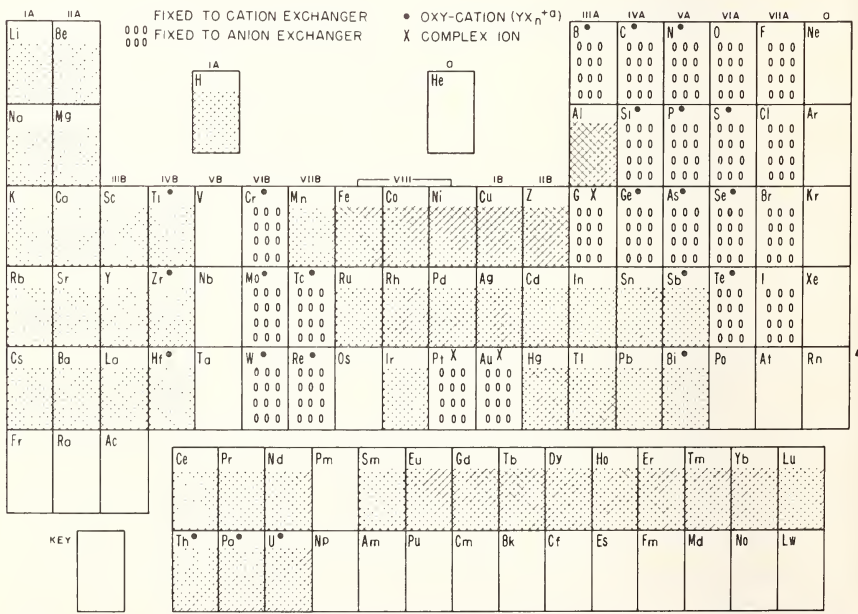
Figure 2.   A periodic table showing the broad range of possibilities for loading elements unto anion or cation exchange resin beads for subsequent use of microstandards.

of the wide range of possibilities for loading elements onto cation or anion exchange resin beads. There is no restriction to inorganic ions so that various organic or organometal ions are also possible.

The mass range is very wide. Ion exchange beads occur in varying sizes from over a millimeter to less than one micrometer in diameter. The corresponding mass ranges from a milligram to less than a picogram. If counterion mixtures are used, it should be possible to place just a few atoms of a given element on a single bead. Experiments involving just a few thousand counterion molecules are now in progress. To assist in making estimates for possible application of microstandards, it is helpful to use the nomograph shown in Figure 3. The center line permits varied loading under fractional loading where the partial density ρf^* is a maximum for a given counterion, or under partial saturation where the partial density is allowed to range to small values.
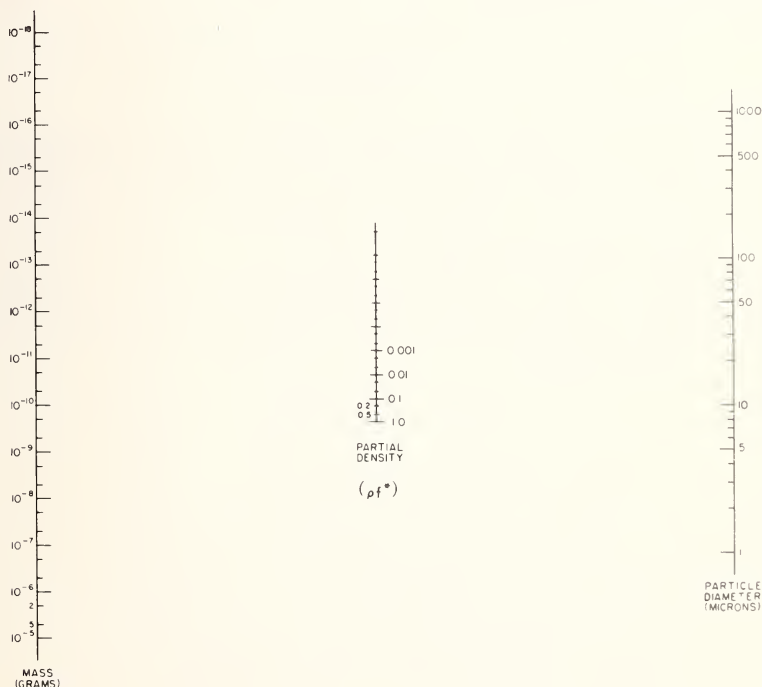
Figure 3.   Nomogram for determining mass of counterion as a function of particle size and of specific counterion density (g/ml).

One can visualize a rather extensive array of possible applications for the carefully prepared resin microstandards. (1) The ion exchange matrix is ideally suited for activation analysis in that it involves a relatively inert

network structure containing carbon and hydrogen, with functional groups that add sulfur and oxygen for cation exchange, or nitrogen for anion exchange. These elements are difficult to activate with neutrons. (2) The dry resin beads are known to be relatively inert to massive doses of nuclear radiation. When activated, the radioactive beads can be used as point sources that are far more "point-like" than is usually obtained. Roughly, a 0.1 mm bead will contain 10^{-7} grams of counterion with a mass attenuation of 0.01 g/cm^2. (3) The use of radioactive beads should permit measurement of absolute counting geometry. Similarly, the measurement of relative geometry for different detectors should be particularly easy to obtain. (4) Beads containing known amounts of matter can be used as flux monitors for virtually any required mass of interest to activation analysis.

The important conclusion is that the beads are emerging with precisely demonstrable homogeneity, and they are providing new capabilities for precise microstandardization.

V. References

[1]   Freeman, D. H., and Paulson, R. A., Nature **218,** 563 (1968).
[2]   Freeman, D. H., "Precise Studies of Ion Exchange Systems Using Microscopy" (Chap. 5) in "Ion Exchange" Vol. I, J. A. Marinsky, Ed., Marcel Dekker, Inc., (New York, 1966).
[3]   Wiley, R. H., Allen, J. K., Chang, S. P., Mussleman, K. E., and Venkatachalam, T. K., J. Phys. Chem. **68,** 1776 (1964).
[4]   Freeman, D. H., Patel, V. C., and Hood, M. E., J. Polymer Sci. (a) **3,** 3893 (1965).
[5]   Freeman, D. H., and Scatchard, G., J. Phys. Chem. **69,** 70 (1965).
[6]   Connally, R. E., Rev. Sci. Instr. **24,** 458 (1953), DeVoe, J. R., NBS Technical Note No. 276, Jan (1966).

1968 INTERNATIONAL CONFERENCE ON MODERN TRENDS IN ACTIVATION ANALYSIS

JAMES R. DEVOE, *General Chairman*
PHILIP D. LAFLEUR, *Assistant General Chairman*
SAM S. NARGOLWALLA, *Treasurer*

Program Committee

JAMES R. DEVOE, *Chairman*
PHILIP D. LAFLEUR
GEORGE J. LUTZ
W. WAYNE MEINKE
SAM S. NARGOLWALLA

Arrangements Committee

P. D. LAFLEUR, *Chairman*
B. A. THOMPSON — *Housing*
W. P. REED, W. D. KINARD — *Food*
D. A. BECKER — *Transportation*
B. A. THOMPSON — *Registration*
T. E. GILLS — *Tours*
L. W. MASTERS — *Social*
F. A. LUNDGREN — *Audio-Visual*
H. L. FRUSH — *Ladies Program*

SUBJECT INDEX

AUTHOR INDEX